16 June 2006 | $10

Science

AAAS

Suddenly the idea hit us... Cold Expression

Introducing ArcticExpress™ Competent Cells – cold-adaptive protein expression technology by Stratagene.

Cross the protein solubility barrier with our new ArcticExpress™ Competent Cells*, featuring cold-adapted technology. Lower growth temperatures (11-13°C) and protein folding chaperonins provided by the Antarctic isolate *Oleispira antarctica* allow these cells to properly process your insoluble proteins without fusion tags or complicated refolding methods.

- **Low growth temperatures (11-13°C) enhance protein folding and solubility**
- **Contains chaperonins Cpn60 and Cpn10 from psychrophilic bacterium, *Oleispira antarctica***
- **Correct for codon bias and enhance solubility at the same time**

Need More Information? Give Us A Call:

Stratagene US and Canada
Order: 800-424-5444 x3
Technical Service: 800-894-1304 x2

Stratagene Japan K.K.
Order: 3-5821-8077
Technical Service: 3-5821-8076

Stratagene Europe
Order: 00800-7000-7000
Technical Service: 00800-7400-7400

www.stratagene.com

Ask us about these great products:

ArcticExpress™ (DE3) Competent Cells	10 x 0.1 ml	230192
ArcticExpress™ (DE3)RIL Competent Cells	10 x 0.1 ml	230193
ArcticExpress™ (DE3)RP Competent Cells	10 x 0.1 ml	230194
ArcticExpress™ Competent Cells	10 x 0.1 ml	230191
ArcticExpress™ RIL Competent Cells	10 x 0.1 ml	230195
ArcticExpress™ RP Competent Cells	10 x 0.1 ml	230196

*Patent pending.

STRATAGENE

LESS HASSLE. MORE HELPFUL.

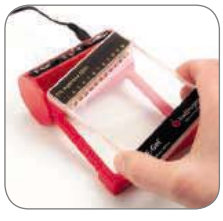

E-Gel® Pre-Cast Gels for Nucleic Acid Analysis deliver fast, convenient, and easy electrophoresis.

Imagine excellent resolution in as little as 12 minutes. No mess. No pouring. No liquid. No waiting. And, Invitrogen's self-contained bufferless agarose gels are available in the widest variety of precast formats and percentages anywhere for consistent, high-resolution results. Every time. Every throughput. From 12-well to automated 96-well gels.

See them in action at www.invitrogen.com/egels.

invitrogen™

© 2006 Invitrogen Corporation. All rights reserved. These products may be covered by one or more Limited Use Label Licenses (see the Invitrogen catalog or our website, www.invitrogen.com).

GE Healthcare

www.dowellstubbs.com

Faster protein purification? It's not rocket science.

HiTrap™ columns give you pure proteins with less effort. They come prepacked with the widest choice of media, ensuring results you can depend on in a broad range of applications, and the highest level of convenience.

But we're never content to stand still. We constantly strive for new innovations for tomorrow's research and drug development. And thanks to our technological achievements and global presence, we're able to help you turn your scientific ideas into reality – bringing science to life and helping transform healthcare.

We call it Life Science Re-imagined.

Discover how HiTrap columns can help power your protein purification.
Visit www.gehealthcare.com/life

imagination at work

GE Healthcare Bio-Sciences AB, a General Electric Company.
Björkgatan 30, 751 84 Uppsala, Sweden.
© 2006 General Electric Company - All rights reserved.

GE05-06

Volume 312, Issue 5780

COVER

Bacterial mats growing around a subaquatic spring in Lake Cadagno, Switzerland. The sulfate-rich water from these springs flows to the bottom of the lake, where bacterial activity produces hydrogen sulfide, leading to permanent anoxia. A general mechanism for the enhanced preservation of organic molecules under such sulfide-rich conditions is described on page 1627.

Image: Mauro and Franca Bernasconi

DEPARTMENTS

EDITORIAL

NEWS OF THE WEEK

NEWS FOCUS

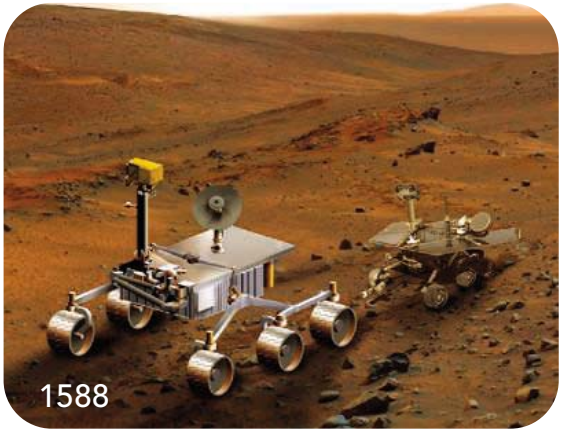
1588

LETTERS

BOOKS *ET AL.*


1608

POLICY FORUM

PERSPECTIVES

CONTENTS continued **>>**

Systems Biology — RNAi and Gene Expression Analysis

GeneGlobe — the world's largest database of matching siRNAs and RT-PCR assays

New

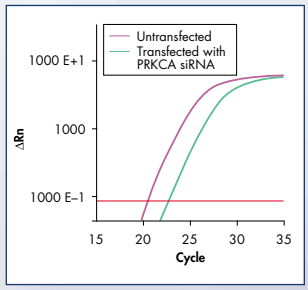

Reliable quantification after knockdown

Visit www.qiagen.com/GeneGlobe

Enter the world of reliable gene silencing and gene expression analysis!

Genomewide solutions from QIAGEN include potent, specific siRNAs and matching, ready-to-use, validated primer sets for SYBR® Green based real-time RT-PCR assays. Benefits include:

- Easy online access to RNAi and gene expression solutions at GeneGlobe
- siRNAs and RT-PCR assays for the entire human, mouse, and rat genomes
- RT-PCR assays for arabidopsis, drosophila, dog, and chicken

For matched siRNAs and real-time RT-PCR assays you can rely on, go to www.qiagen.com/GeneGlobe !

QIAGEN

For up-to-date trademarks and disclaimers, see www.qiagen.com . RNAiGEXGeneGlobe0106S1WW © 2006 QIAGEN, all rights reserved.

Qs & AAAs

www.sciencedigital.org/subscribe

For just US$99, you can join AAAS TODAY and start receiving *Science* Digital Edition immediately!

Qs & AAAs

www.sciencedigital.org/subscribe

For just US$99, you can join AAAS TODAY and start receiving *Science* Digital Edition immediately!

Science

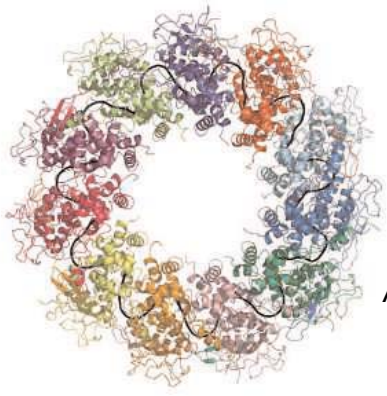

ALBERTINI *et al.*

SCIENCE EXPRESS

www.sciencexpress.org

MOLECULAR BIOLOGY

Characterization of the piRNA Complex from Rat Testes
N. C. Lau et al.
A class of noncoding RNAs, about eight nucleotides longer than siRNA or miRNA, assemble into complexes that probably participate in gene silencing.
10.1126/science.1130164

STRUCTURAL BIOLOGY

Structure of the Vesicular Stomatitis Virus Nucleoprotein-RNA Complex
T. J. Green, X. Zhang, G. W. Wertz, M. Luo
10.1126/science.1126953

Crystal Structure of the Rabies Virus Nucleoprotein-RNA Complex
A. A. V. Albertini et al.
Two viruses sequester their RNA genome within nucleoprotein to protect it from the host immune response but can expose it for transcription and replication.
10.1126/science.1125280

PLANETARY SCIENCE

A Thick Cloud of Neptune Trojans and Their Colors
S. S. Sheppard and C. A. Trujillo
The dynamics and red color of a group of asteroids that co-orbit with Neptune indicate that they may have been captured during the early outward migration of the giant planets.
10.1126/science.1127173

PERSPECTIVE: Puzzling Neptune Trojans
F. Marzari
10.1126/science.1129458

REVIEW

BREVIA

1621

RESEARCH ARTICLES

REPORTS

CONTENTS continued **>>**

www.roche-applied-science.com

LightCycler® 480 Real-Time PCR System

Rapid by nature, *accurate by design*

LightCycler® 480 Block Cycler Unit for 96 or 384 wells, easily exchanged by users within minutes.

For years, Roche has provided real-time automated PCR solutions you can count on. Now, you can obtain the proven performance and benefits of the original LightCycler® System in a 96- or 384-well instrument platform for high-throughput applications – the new **LightCycler® 480 Real-Time PCR System**.

Speed – Save time without sacrificing the quality of your results – precise, high-speed temperature changes maximize specificity and yield.

Accuracy – Benefit from our novel thermal block cycler and data-capture technologies to minimize edge-effects for outstanding accuracy and precision.

Versatility – Combine 5 excitation and 6 detection channels, multiple probe formats, proven analysis software, and true master mix reagents to meet your specific application needs.

Compatibility – Take advantage of the instrument's automation and LIMS capabilities to interface with your current systems and future workflows.

Visit ***www.roche-applied-science.com/lightcycler480*** for more information.

Roche Diagnostics

Roche Diagnostics GmbH
Roche Applied Science
68298 Mannheim
Germany

For general laboratory use. Not for use in diagnostic procedures.

This LightCycler® 480 Real-Time PCR System is licensed under U.S. Patent No. 6,814,934 and corresponding claims in its non-U.S. counterparts and under one or more of U.S. Patents Nos. 5,038,852, 5,656,493, 5,333,675, or corresponding claims in their non-U.S. counterparts, for use in life science research. It is also an Authorized Thermal Cycler. Purchase and use of this LightCycler® Instrument, in conjunction with Authorized Reagents, provides a limited license for use of the PCR process in life science research. No rights are conveyed expressly, by implication or by estoppel under any other patent claims or for any other application.

LIGHTCYCLER is a trademark of Roche.

The technology used for the LightCycler® System is licensed from Idaho Technology, Inc., Salt Lake City, UT, USA.

The product is covered in-part by US 5,871,908, co-exclusively licensed from Evotec OAI AG.

© 2006 Roche Diagnostics GmbH. All rights reserved.

Science

REPORTS *CONTINUED...*

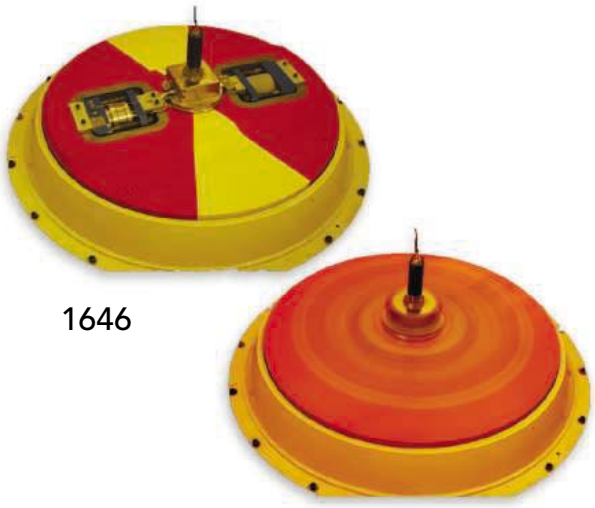

1646

AAAS
ADVANCING SCIENCE, SERVING SOCIETY

SCIENCE (ISSN 0036-8075) is published weekly on Friday, except the last week in December, by the American Association for the Advancement of Science, 1200 New York Avenue, NW, Washington, DC 20005. Periodicals Mail postage (publication No. 484460) paid at Washington, DC, and additional mailing offices. Copyright © 2006 by the American Association for the Advancement of Science. The title SCIENCE is a registered trademark of the AAAS. Domestic individual membership and subscription (51 issues): $139 ($74 allocated to subscription). Domestic institutional subscription (51 issues): $650; Foreign postage extra: Mexico, Caribbean (surface mail) $55; other countries (air assist delivery) $85. First class, airmail, student, and emeritus rates on request. Canadian rates with GST available upon request, GST #1254 88122. Publications Mail Agreement Number 1069624. **Printed in the U.S.A.**

Change of address: Allow 4 weeks, giving old and new addresses and 8-digit account number. **Postmaster:** Send change of address to AAAS, P.O. Box 96178, Washington, DC 20090–6178. **Single-copy sales:** $10.00 current issue, $15.00 back issue prepaid includes surface postage; bulk rates on request. **Authorization to photocopy** material for internal or personal use under circumstances not falling within the fair use provisions of the Copyright Act is granted by AAAS to libraries and other users registered with the Copyright Clearance Center (CCC) Transactional Reporting Service, provided that $18.00 per article is paid directly to CCC, 222 Rosewood Drive, Danvers, MA 01923. The identification code for *Science* is 0036-8075. *Science* is indexed in the *Reader's Guide to Periodical Literature* and in several specialized indexes.

CONTENTS continued **>>**

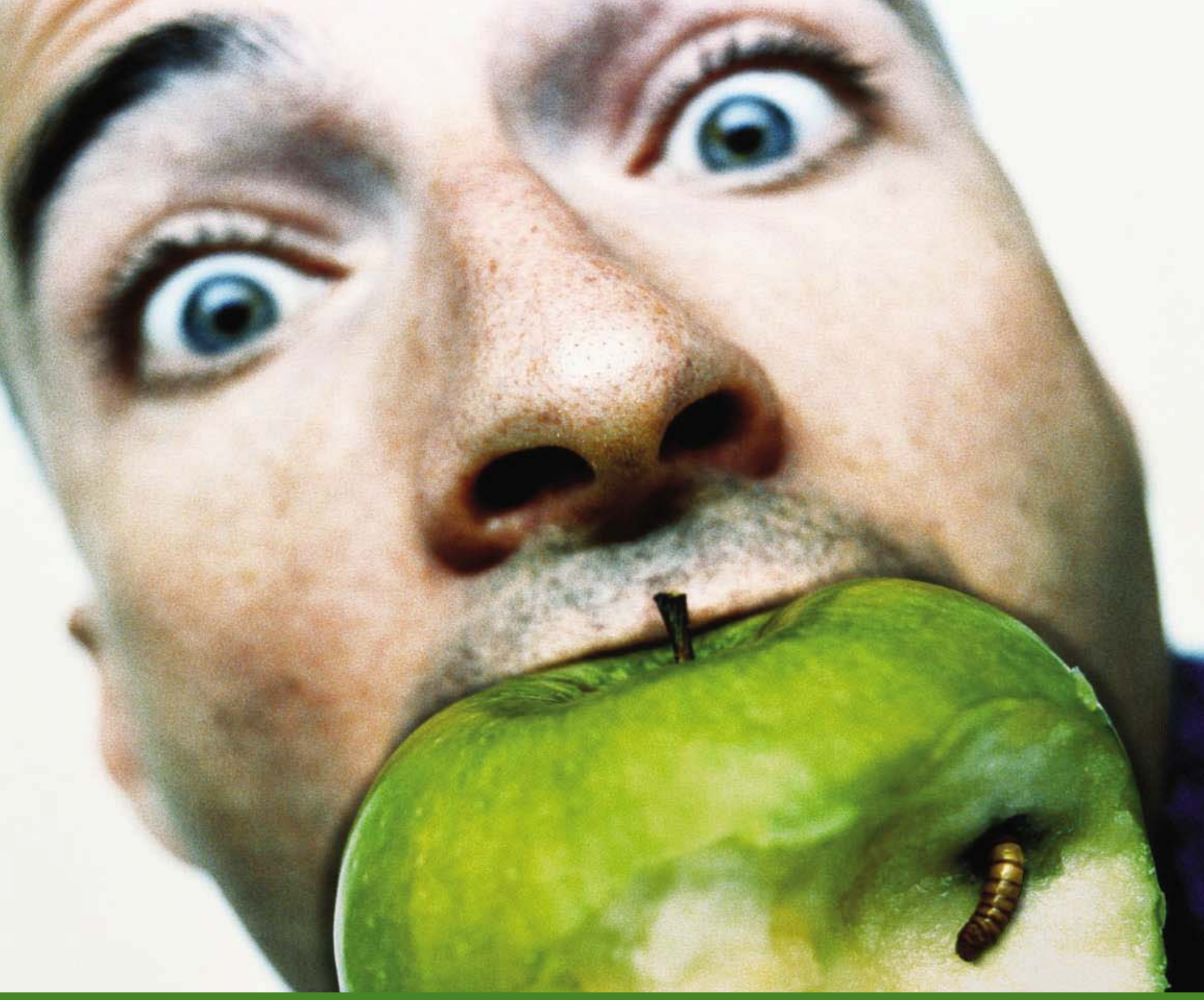

Is unexpected DNA worming its way into your RNA?

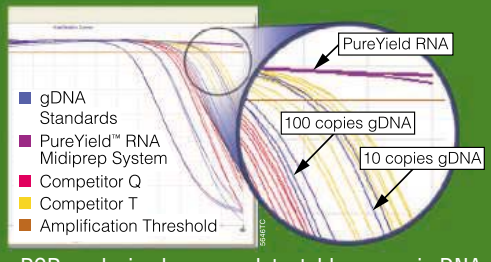

qPCR analysis shows no detectable genomic DNA contamination in PureYield™ RNA samples.

The PureYield™ RNA Midiprep System uses a novel, non-DNase method to remove genomic DNA prior to RNA isolation. PureYield reduces your chances of inaccurate results by eliminating DNA from your RNA preps. You get pure, total RNA with no detectable genomic DNA contamination. No surprises. No starting over.

Request a FREE sample* at: **www.promega.com/rna**

*Samples to qualified customers where available, while supplies last.

©2006 Promega Corporation. 13386-AD-MD

PROMEGA CORPORATION • www.promega.com

Promega

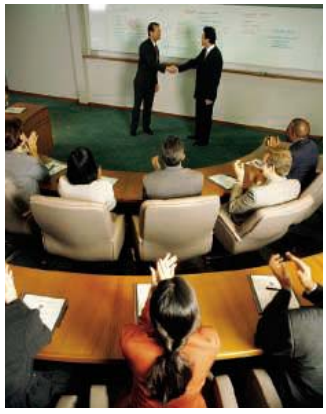

Meetings for cell signaling researchers.

SCIENCE'S **STKE**

www.stke.org SIGNAL TRANSDUCTION KNOWLEDGE ENVIRONMENT

PERSPECTIVE: "Bits" and Pieces
M. B. Yaffe
A combination of comparative genomics and experimental analysis allows discovery of new protein-interaction motifs.

EVENTS
Find more than 40 meetings with signaling sessions or themes, including 18 new listings.

GUENTER ROSSENBACH/ZEFA/CORBIS

A systems viewpoint on aging from Palermo, Italy.

SCIENCE'S **SAGE KE**

www.sageke.org SCIENCE OF AGING KNOWLEDGE ENVIRONMENT

PERSPECTIVE: Aging at the Interface of Stem Cell Renewal, Apoptosis, Senescence, and Cancer
A. Nebel, E. Schaffitzel, M. Hertweck
Scientists apply systems biology approaches to the field of aging-related research.

CLASSIC PAPER: Pleiotropy, Natural Selection, and the Evolution of Senescence
G. C. Williams
The author discusses his theory of senescence; *Evolution* **11**, 398 (1957).

SCIENCE**NOW**

www.sciencenow.org DAILY NEWS COVERAGE

On Mars, No One Can Hear You Scream
Sound travels much shorter distances on Red Planet than on Earth.

Turning a Tumor's Lights Off
Blocking key enzyme in energy-producing pathway slows cancer growth.

Another Cup of Joe, Bartender
Coffee protects liver from damage due to alcohol.

Budget cuts hit future workforce.

SCIENCE **CAREERS**

www.sciencecareers.org CAREER RESOURCES FOR SCIENTISTS

US: Cutbacks Cause Uncertainty Among Space Researchers
A. Fazekas
NASA budget cuts are jeopardizing space science and its future workforce.

US: Tooling Up—Salary Negotiation, Part 1
D. Jensen
Once a company makes you an offer, they want to close the deal.

UK: Just Do It
A. Forde
Nanotechnologist Jeremy Baumberg says that the key to success is finding the right environment.

EUROPE: Brewing a Career in the Chemical Industry
E. Pain
Dutch biochemist Jeroen van Roon started building strong ties with a specialty chemicals company early in his training.

Separate individual or institutional subscriptions to these products may be required for full-text access.

Imagination will often carry us to worlds that never were. But without it we go nowhere.

Carl Sagan

American astronomer, novelist (1934-1996)

Our core strengths include not only technologies that support superior products and services, but also the spark of ideas that lights the way to a brighter future. Shimadzu believes in the value of science to transform society for the better. For more than a century, we have led the way in the development of cutting-edge technology to help measure, analyze, diagnose and solve problems. The solutions we develop find applications in areas ranging from life sciences and medicine to flat-panel displays. We have learned much in the past hundred years. Expect a lot more.

www.shimadzu.com

SHIMADZU

EDITED BY STELLA HURTLEY AND PHIL SZUROMI

The Early Bird…and Snail

Because many of the earliest well-described birds are from extinct lineages, it has been difficult to resolve the early evolution of the lineage that led to modern birds. An early ornithuran bird, *Gansus yumenensis*, has been known only from fragmentary fossils. **You *et al.*** (p. 1640) now describe several fossils which show that this Early Cretaceous bird has many derived features. It was also well adapted for an aquatic-amphibian lifestyle—the fossils even show what appears to be webbing in the feet. The early embryos of some animals, such as mollusks, develop through the formation and cleavage of polar lobes to form functionally specific cells. **Chen *et al.*** (p. 1644 please see the news story by Unger) describe fossils of what appear to be polar-lobed embryos in rocks dated to the Late Precambrian in China. This developmental strategy originated near the time that the first animals appeared.

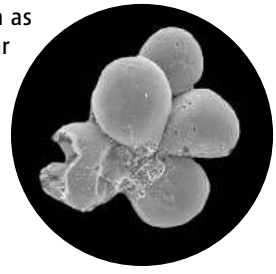

Community Standards Needed

Until very recently, the study of natural selection has been largely restricted to examining individual candidate genes in comparison to theoretical expectations. Large, genome-wide data sets represent resources that are fundamentally changing the way selection can be studied. **Sabeti *et al.*** (p. 1614) describe key genetic indicators of selection and critically review statistical tests and candidate loci in the human genome and suggest that community standards are needed for the field to move forward.

Inorganic Chemistry of Oil

The reduction reactions that organic carbon underwent during its initial low-temperature preservation on the way to petroleum have been obscure (other than that the process retained distinct biomarkers of the original source that have proven highly useful in paleoecology). The reactions, which saturate double bonds, have long been thought to be the work of bacteria. **Hebting *et al.*** (p. 1627, published online 11 May; see the cover and the Perspective by **Hayes**) now show through both laboratory experiments and field studies that the major reactions proceeded inorganically and involved hydrogen sulfide and other sulfur species.

Counting Electrons Coming and Going

As electronic devices shrink, the flow of electrons through the device can become quantized. For metrology and noise-measurement applications, it is crucial to be able to determine how the electrons flow through the device. Single electrons can be counted in one direction, but scattering and back flow occur that can affect the statistics and transport parameters. Using a pair of coupled quantum dots, **Fujisawa *et al.*** (p. 1634) counted electrons flowing through their device in either direction. They see the expected antibunching behavior of electron flow and show that the device can operate as a sensitive ammeter in the attoampere regime.

Balance of Forces in Emulsions

When a sand pile is compacted, not all of the grains are in close contact; the forces are actually transmitted through chains of connected particles. **Zhou *et al.*** (p. 1631) show that this phenomenon also occurs between liquid droplets in concentrated emulsions. High-resolution confocal fluorescence microscopy was used to measure contact areas between droplets, from which the forces that create the deformation regions could be calculated. The chains arise because the largest forces on a drop tend to be directed opposite to one another. Thus, the net force on each drop is zero when the system is mechanically stable.

Centrifuging Mineral Melts

Trace elements can be used to infer the history of magmas if their partitioning between crystals that may remain in the magma's source region and the resulting melts is understood. Although data on the fractionation between crystals and melts can be obtained in conventional experiments, it has been difficult to assess the effect of melt composition, which requires separation of the melts at high temperatures and pressures in an experimental charge for analysis. **Schmidt *et al.*** (p. 1646) spun a high-pressure piston-cylinder apparatus rapidly enough to create a giant centrifuge reaching accelerations of 3000*g*. The data allow development of a theory incorporating melt composition into fractionation factors.

Together, We Are Strong

Although cortical neurons respond reliably to thalamic inputs, the proportion of thalamic synapses on cortical neurons is quite small. Previous studies suggested that thalamocortical responses are reliable because the synapses transmit more efficiently than others. **Bruno and Sakmann** (p. 1622; see the Perspective by **Alonso**) developed a technique for studying individual synaptic connections in the intact brain that allowed paired recordings to be made in living animals. In the intact animal, the relia-

Continued on page 1571

CREDITS (TOP TO BOTTOM): YOU *ET AL.*; CHEN *ET AL.*; ZHOU *ET AL.*

PIERCE

The Protein People™

Assay Development

"Oh ELISA, now that you have 16 new coated plates, I'll never leave you!"

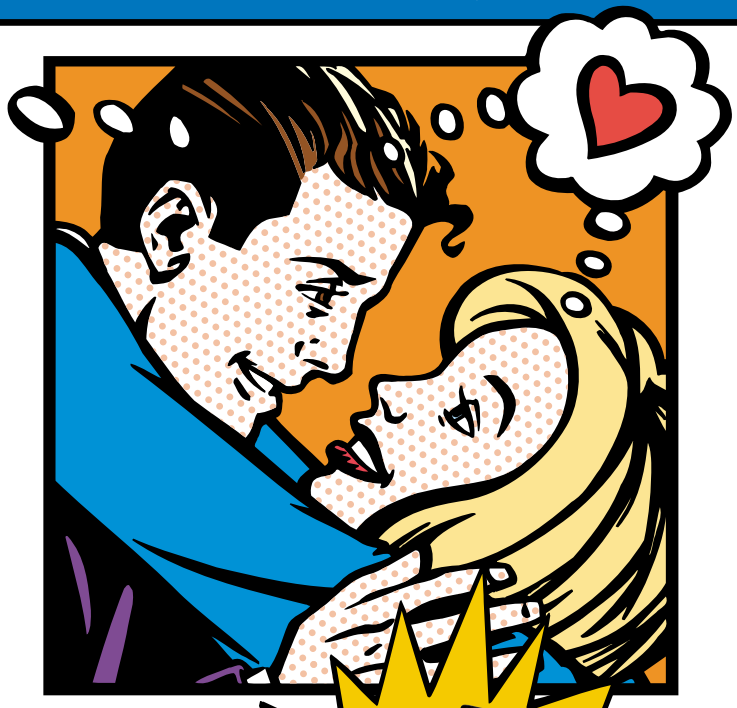

Now there's more to love about ELISA products from Pierce.

Our complete line of products for ELISAs includes precoated microwell plates. We've added 16 new coated plates for fluorescent and chemiluminescent detection, including Streptavidin, NeutrAvidin™, Protein A, Protein G, Anti-mouse IgG, Anti-rabbit IgG, Amine-binding Maleic Anhydride and Sulfhydryl-binding Maleimide coatings on both black and white plates

Blocking buffers include SuperBlock®, StartingBlock™ and SEA BLOCK Buffers and the new Protein-Free Blocking Buffers (Product #s 37570, 37571, 37572 and 37573)

Detergents and wash buffers include our ultrapure Surfact-Amps® Detergents and our BupH™ Pack Pre-formulated Binding and Wash Buffers

Detection probes include a complete line of secondary antibodies labeled with HRP, AP, biotin, fluorescein, rhodamine and the new DyLight™ Fluors. Labeled Protein A & G and Streptavidin, Avidin and NeutrAvidin™ Biotin-Binding Protein are also available

Enzyme substrates include patented SuperSignal® Chemiluminescent Substrates; QuantaBlu™ Chemifluorescent Substrates; and TMB, ABTS, OPD and PNPP Substrates for colorimetric detection

Go to ***www.piercenet.com*** for a complete list of Pierce products to make your ELISAs perform better, faster and more economically than ever before.

Pierce Coated Plates are available in **large-volume quantities** for manufacturing applications. **Custom microplate-coating services** are also available for assay product development (IVD) or screening (HTS) applications.

www.piercenet.com

PIERCE

Tel: 815-968-0747 or 800-874-3723 • Fax: 815-968-7316
Customer Assistance E-mail: CS@piercenet.com

© Pierce Biotechnology, Inc., 2006. Pierce products are supplied for laboratory or manufacturing applications only.
NeutrAvidin™, QuantaBlu™, StartingBlock™, SuperBlock®, Surfact-Amps® and SuperSignal® are trademarks of Pierce Biotechnology, Inc.
*SuperSignal® Technology is protected by U.S. Patent #6,432,662. Tween®, Triton®, and Brij® are registered trademarks of ICI Americas.

For distributors outside the U.S. and Europe, visit www.piercenet.com

For European offices and distributors, visit www.perbio.com

PERBIO

Continued from page 1569

bility and amplitude of synaptic transmission were as low as had been estimated previously for intracortical connections. However, the strong synchrony of thalamic neurons maintained substantial activation of cortical neurons without any need for further intrinsic cortical amplification.

Running on Empty

Cancer cells often change their mode of energy production from aerobic respiration to glycolysis. **Matoba *et al.*** (p. 1650, published online 25 May) now link this switch to mutations in the tumor suppressor gene, p53. p53 controls the expression of a factor that is needed to assemble the cytochrome c oxidase complex, a major site of oxygen consumption in mitochondria. When p53 is inactivated, as it is in many cancers, respiration decreases and alters cellular metabolism.

Metabolic Information Highway

The several distinct tissues that contribute to the maintenance of energy balance in mammals must somehow communicate with one another. For example, the liver sends metabolic signals to peripheral adipose tissue, but the underlying mechanisms are poorly understood. Studying a mouse model, **Uno *et al.*** (p. 1656) found that these tissues communicate by means of a neuronal pathway consisting of the afferent vagus nerve from the liver and efferent sympathetic nerves to adipose tissues. This pathway is involved in the regulation of energy expenditure, systemic insulin sensitivity, glucose metabolism, and fat distribution between the liver and periphery, and it may also help protect the animal from the metabolic disturbances that are set in motion by excess fat storage.

Passing Through

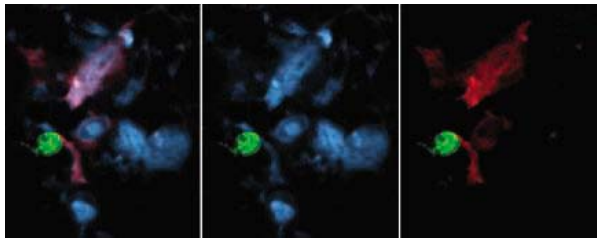

In the immune system, B cells and T cells both recognize antigen and thought to do so by distinct means. T cells require specialized antigen-presenting cells, called dendritic cells (DCs), to pick up protein at peripheral tissues, which they then process and present as peptides to T cells within the organized lymphoid tissues. Using intravital imaging in mice, **Qi *et al.*** (p. 1672) reveal that some B cells encounter antigen in a rather similar way on DCs as they exit from the blood and before they migrate to the specialized B cell regions of the lymph nodes, called follicles. B cells that recognized antigen in this way started to show signs of activation and slowed down their migratory behavior within T cell–rich areas. Such slow-moving, activated B cells would increase their chances of garnering the critical help of T cells required for them to produce antibodies.

CREDIT: QI *ET AL.*

Inflammation, Amplification, and Aggravation

Many details of how inflammatory pain is amplified at the spinal dorsal horn have been uncovered in recent years, but a unifying cellular model is still missing. **Ikeda *et al.*** (p. 1659) identified a synaptic pain amplifier that is turned on by low-frequency conditioning stimulation and by natural noxious stimulation. In vivo, a low-frequency afferent barrage can raise Ca^{2+} concentration in nociceptive spinal cord neurons sufficiently to induce long-term potentiation. This process causes amplification of pain-related information at the first synapse in pain pathways.

Brainy Birds

Do animals have "theory-of-mind," that is, the ability to understand that other animals have thoughts and feelings? **Dally *et al.*** (p. 1662, published online 18 May) provide evidence that western scrub-jays might attribute different knowledge states to specific individuals. When it comes to protecting their hidden caches of food, scrub-jays keep track of precisely who was watching and when, and use this information to combat the threat that particular individuals pose to their caches.

Announcing New *Science* Online Seminars.

We hope you enjoy the show.

Now you can have your very own personal presentation of the latest breakthrough papers in *Science*, presented by the authors, with our new *Science* Online Seminars.

Powered by Biocompare, *Science* Online Seminars give you a web-based audio and visual presentation of an author discussing and showing the application of the research and/or methods and protocol. Best of all, you can access these Seminars whenever you want.

Sound like a good idea? Then why not go and try it now. Go to: **www.sciencemag.org/onlineseminars**

Science
AAAS

Science Online Seminars are produced by the Office of Publishing and Member Services

Sometimes, even flies dangle their legs.

Just let the world's best motorized fluorescence stereomicroscope work for you: with precision, quiet and fast. You determine the sequence of your fluorescence experiments. Everything else - from filter and zoom change up to digital recording of z-stacks - is done computer-controlled by your Leica MZ16 FA and it even offers top performance: 16:1 zoom, maximum magnification of 920x, resolution of 840 lp/mm/1500 lp/mm, finest visible structure width of 0.3 µm / 0.6 µm.

Automated performance guarantees higher productivity and better results in industry and laboratory environments, and ultimately safeguards the future of your business.

The Leica MZ16FA can be individually expanded up with the Leica LAS software and Leica digital cameras to a complete system for perfect documentation and analysis.

Leica

MICROSYSTEMS

www.leica-microsystems.com/**MZ16FA**

Donald Kennedy is Editor-in-Chief of *Science*

A Welcome New Look

THERE HAS LONG BEEN AN UNCOMFORTABLE RELATIONSHIP BETWEEN THE SCIENTIFIC COMMUNITY in the United States and the regulations of its government regarding exports. In the early 1980s, that conflict flared up in protests against restrictions on the publication of basic research findings and on the admission of foreign nationals to seminars or symposia in the United States. The issue is of increasing international concern, not only because it hampers useful transnational collaboration, but because restrictions have been applied to exports that might improve other nations' economic competitiveness with the United States, as well as to those with potential military applications.

The anxiety among scientists and academic administrators has returned, and once again its major source has been the application of certain regulations to basic research findings. ITAR (International Traffic in Arms Regulations) control the export of military data and defense services; EAR (Export Administration Regulations) are managed by the Department of Commerce and address security concerns regarding dual-use technologies. Both raise a similar problem: Regulations have been applied to scientific information as well as to technology, military devices, and supporting data.

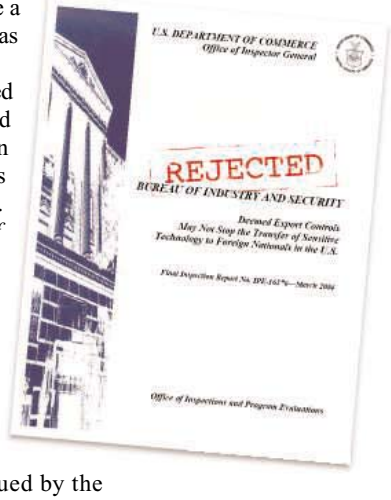

Further difficulties arise because there is a subcategory under EAR called "deemed exports." An export is "deemed" to occur if a scientist in the United States has given information to a foreign national that would be considered an export had it actually been sent abroad. New worries arose when Commerce's Office of the Inspector General (OIG) issued a scary report in 2004. Ominously entitled *Deemed Export Controls May Not Stop the Transfer of Sensitive Technology to Foreign Nationals in the U.S.*, the proposal could have made U.S. universities responsible for obtaining licenses for thousands of visiting researchers and raised a significant bar to scientific exchanges. Furthermore, it said that the licensing of a foreign national to receive a deemed export should be based on their nation of origin rather than citizenship! Suppose your collaborator was born in Iran, left in 1972 while the Shah was still in charge, and has lived as a British citizen ever since. He's a security risk? Give us a break.

Well, an Advance Notice of Proposed Rulemaking was then issued by the Department of Commerce's Bureau of Industry and Security, setting forth the OIG's report and asking for public comment. A few weeks ago, Commerce addressed those comments, and in an almost wholesale rejection of the OIG's report, it withdrew the previous Notice. The outcome is that foreign nationals are to be identified by citizenship, not country of origin. It also maintains more limited licensing requirements and relieves academic institutions by reinforcing the exclusion of fundamental research from EAR.

The news gets better. Last month, at a meeting at the Massachusetts Institute of Technology that was sponsored by the U.S. National Academies' Committee on a New Government-University Partnership for Science and Security, speakers from the government security community expressed skepticism about how well export regulations are working. And yet another Federal Register notice just issued by Commerce has announced that a new Advisory Committee will review and provide recommendations to Commerce on the deemed export policy.

It is clear that this change in position has resulted from the yearlong dialogue of thoughtful conversations between university presidents, scientists, and officials of the Department of Commerce. According to the participants, much of the credit for this move to step back and take a careful look at the problem belongs to David McCormick, the Under Secretary of Commerce for Industry and Security.

McCormick clearly deserves praise. The OIG created an unfair and unworkable definition of a foreign national. The EAR have had deeper problems, dating back to the first years of the Reagan administration. Now there is reason to hope that the "use" definition will continue to carve out an exemption for the results of basic research. After all, the result of that 1980s controversy was National Security Defense Directive 189, signed by President Reagan, which states that there will be no restrictions on fundamental research except for classification. That's still in effect, and these recent actions are consistent with it in ensuring that EAR won't resume their role as a barrier to international scientific cooperation. Hope springs eternal.

– Donald Kennedy

10.1126/science.1130850

EDITED BY GILBERT CHIN AND JAKE YESTON

CELL BIOLOGY

A Blight Upon Malaria

Many pathogens, whether of plants or animals, export their own proteins in order to modify their local environment and to disable host defenses. Channeling secretory proteins into the molecular machines that allow them to cross membranes generally relies on short amino acid sequence motifs. Oomycetes are deep-branching eukaryotes that include the notorious *Phytophthora*, which causes devastating diseases such as potato late blight and sudden oak death. *Phytophthora* colonizes plants by establishing and residing within a membrane-bounded haustorium inside cells.

Bhattacharjee *et al*. show that *Plasmodium* and *Phytophthora*, phylogenetically distant eukaryotic pathogens, use similar host-targeting motifs. *Plasmodium* has a host-targeting motif that is linked to over 400 virulence factors, which make up the "secretome." *Phytophthora* possesses virulence determinants that are recognized by plant hosts and, like *Plasmodium,* the highly conserved leader sequence motif RxLR along with a nearby acidic domain can be found in multiple effectors that are delivered into the host cell cytoplasm. — CA

PloS Pathol. **2**, e50 (2006).

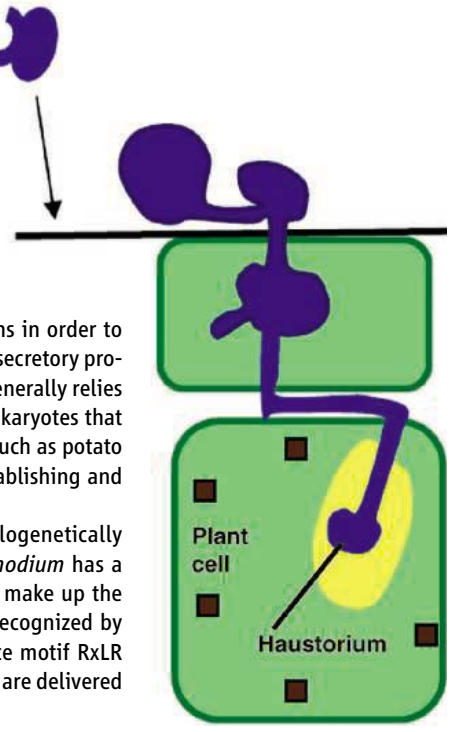

Schematic of *Phytophthora* invasion.

ASTROPHYSICS

Imaging a Quasar Jet

The first quasar to be discovered, 3C273, hosts a prominent and narrow jet of relativistic particles emitted from its galactic core. Detailed pictures of the jet show that it glows from radio to x-ray frequencies and, unusually, can even be seen in visible light. Physical models of the jet have tried to explain how it forms and retains its tight columnar shape despite traveling far beyond its parent galaxy.

Uchiyama *et al.* have examined mid-infrared images acquired with the Spitzer Space Telescope and find that the jet changes color abruptly in the middle. They attribute the long-wavelength (radio to infrared) radiation from the outer part of the jet to the synchrotron emission of charged particles moving at relativistic speeds along the jet in a strong magnetic field. In contrast, the inner part appears to be dominated by a high-energy component that exudes both x-rays and visible light. This short-wavelength emission could arise either from synchrotron radiation by a second population of electrons or protons—an explanation supported by current polarization data—or else from inverse Compton scattering of photons by jet particles. This result runs counter to prior theories that tied the origin of the optical light to the radio emission mechanism, and it suggests that optical emission may yet be detected in quasars with x-ray jets. — JB

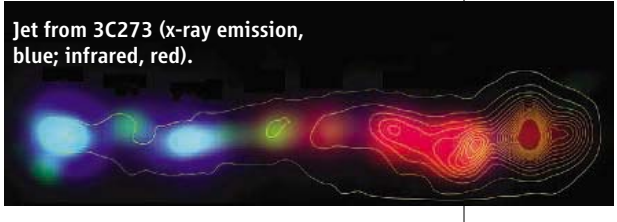

Jet from 3C273 (x-ray emission, blue; infrared, red).

Astrophys. J. astro-ph/0605530 (2006).

COMPUTER SCIENCE

Better Technology via Hacking

In the public mind, the term "hacker" has nothing but negative connotations, conjuring up images of subversive outcasts writing illicit computer viruses, breaking into bank accounts, or scrambling Pentagon databases. But the epithet originally meant someone adept at taking technology intended for one purpose and retooling it, often in startlingly creative and unexpected ways; and the global community of information technologists who tweak software and hardware outside normal channels still exists.

Conti, a professor of computer science at the United States Military Academy, takes the position that mainstream computer scientists could learn some lessons from the unconventional thinking in the hacker community. In a special issue on hacking and innovation, he points out that hackers are passionate about technology, unconstrained by traditional methods, and often years ahead of their academic and corporate counterparts. Hackers publish journals and present their work at well-attended technical conferences, but live in a parallel universe apart from better-known professionals. Other articles in the issue explore how hackers help pinpoint security flaws in wireless networks and identify Internet vulnerabilities, and discuss some of the legal issues surrounding nontraditional technology experimentation. — DV

Commun. ACM **49**, 33 (2006).

GENETICS

Mighty Meaty miRNAs

The Texel breed of sheep sports a pronounced musculature, which makes it economically important for the agricultural industry. To establish the basis of the Texel phenotype, Clop *et al.* have used quantitative genetics to map the genomic region responsible, initially to the second chromosome and then, using finer quantitative trait loci mapping, to the myostatin gene; mutations in this gene are known to increase muscle mass in mice and humans. Of the 20 single-nucleotide polymorphisms identified, two track the Texel phenotype closely. One of these is located in the 3′ untranslated sequence of the myostatin gene. The G-to-A change creates an octamer sequence that inadvertently corresponds to the seed, a critical specificity determinant, of the micro (mi) RNAs *miR-1* and *miR-206*, both of which are expressed at high levels in sheep muscle. Analysis of myostatin levels revealed a marked reduction in Texel sheep and is consistent with the role of miRNAs in repressing the translation of target genes. In a bioinformatic analysis of the human and mouse genomes, the authors locate hundreds of poly-

CREDITS (TOP TO BOTTOM): BHATTACHARJEE *ET AL.*, *PLOS PATHOL.* **2**, 5 (2006); Y. UCHIYAMA *ET AL.*, *ASTROPHYS. J.* (2006)

morphisms that have the potential to create or destroy targets of miRNA seed sequences, and hence to influence gene expression in a fashion analogous to that seen in sheep. — GR

Nat. Genet. 10.1038/ng1810 (2006).

BIOCHEMISTRY

A Party of 10, Again

Applying proteomic technologies has made it possible to catalog the complement of proteins expressed in a cell or a tissue, and experimental and computational analyses have coupled proteins to their partners in social networks of metabolic and regulatory connectedness—an interactome. Partying (multiple contacts simultaneously) and dating (one at a time) have been proposed as classifying behaviors, and probing the interaction surfaces may help sort out which is which.

Hernández *et al.* have used tandem affinity purification and mass spectrometry to map the 10 distinct subunits of the yeast exosome, a complex involved in RNA processing. Of the three subunits with RNA-binding motifs (Csl4, Rrp40, and Rrp4), Csl4 showed up in substoichiometric quantities and hence was tagged so as to pull out only the complete 10-subunit species. Destabilizing the intraexosome interactions with dimethylsulfoxide, followed by mass spectrometry, established the composition and neighbor relationships for the six-subunit ring; likewise, all three RNA-binding proteins could be placed on the same face of the ring, with the largest subunit, the Dis3 RNase, on the other side. — GJC

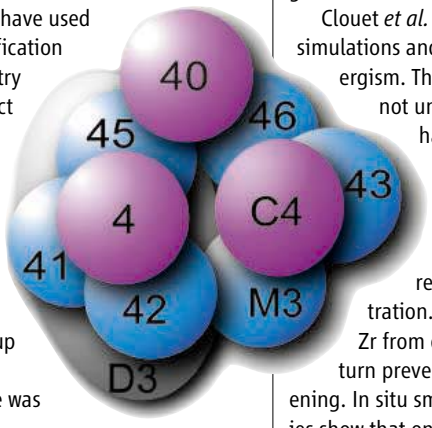

Schematic of the yeast exosome (ring subunits in magenta, RNA-binding subunits in blue).

EMBO Rep. 10.1038/sj.embor.7400702 (2006).

MATERIALS SCIENCE

Synergistic Alloying

Impurities are often empirically added to a metal to improve its properties through the formation of second-phase precipitates; however, understanding and predicting the performance of different impurities can be complex. Zirconium (Zr) and scandium (Sc), for example, individually form alloys with aluminum that enhance strength and resistance to recrystallization. When Zr and Sc are added together, the net effect is significantly greater than the impact of either one alone.

Clouet *et al.* use a combination of atomic simulations and experiments to explain this synergism. They find that the precipitates are not uniform in composition but instead have a Sc-rich core surrounded by a Zr-rich shell. Sc diffuses more rapidly than Zr within the solid solutions and thus begins to form precipitates first, until reaching an equilibrium concentration. Lattice thermodynamics inhibit Zr from diffusing into the core, which in turn prevents the precipitates from coarsening. In situ small-angle x-ray scattering studies show that once enough Zr reaches the shell, an Al_3Zr composition results that is resistant to further annealing. Overall, these effects lead to a higher concentration of smaller precipitates, enhancing the nucleation of the aluminum and thereby creating a stronger alloy. — MSL

Nat. Mater. **5**, 482 (2006).

Science stke AAAS

www.stke.org

<< Promoting Central Regeneration

In general, neurons in the mature vertebrate central nervous system fail to regenerate after injury. Intriguingly, however, activation of macrophages in the eye after damage to the optic nerve stimulates the regeneration of retinal ganglion cells (RGCs), so that their axons grow beyond the site of injury. Yin *et al.*, who previously determined that macrophage-secreted proteins less than 20 kD in size promoted axon regeneration, used mass spectrometry of a prominent component and identified oncomodulin, a calcium-binding protein that has been found in tumors. Although inactive on its own, oncomodulin potentiated the ability of mannose plus forskolin (which elevates cAMP levels) to promote axon outgrowth in cultured RGCs. Pharmacological analysis indicated that oncomodulin activity depended on Ca^{2+}/calmodulin–dependent kinase II and on gene transcription. Delivery of oncomodulin and a cAMP analog into the vitreous promoted optic nerve regeneration in vivo. Thus, oncomodulin appears to represent a previously unidentified macrophage-derived trophic factor capable of promoting axonal regeneration in at least some central neurons. — EMA

Nat. Neurosci. **9**, 843 (2006).

Q

Who's cultivating tomorrow's scientific geniuses?

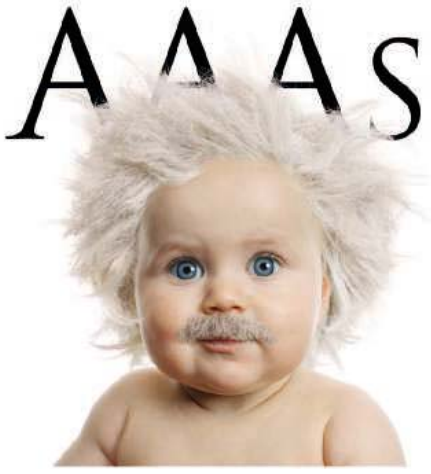

Questions and Answers.

Some particularly gifted children might be able to make quantum leaps in their education and find science a relatively easy subject to comprehend. Others may need a little more help and encouragement at an early age. Helping develop that interest and provide the learning tools necessary is something we at AAAS care passionately about. It's a big part of the very reason we exist.

Our educational programs provide after-school activities such as the Kinetic City web-based science adventure game, based on the Peabody Award winning Kinetic City radio show; *Science* Netlinks, with over 400 science lessons available on the Internet; and Project 2061, which provides teaching benchmarks to foster an improved understanding of science and technology in K-12 classrooms.

AAAS has been helping to answer the questions of science and scientists since 1848, and today is the world's largest multidisciplinary, nonprofit membership association for science related professionals. We work hard at advancing science and serving society – by supporting improved science education, sound science policy, and international cooperation.

So, if your question is how do I become a member, here's the answer. Simply go to our website at www.aaas.org/join, or in the U.S. call 202 326 6417, or internationally call +44 (0) 1223 326 515.

Join AAAS today and you'll discover the answers are all on the inside.

AAAS

ADVANCING SCIENCE, SERVING SOCIETY

www.aaas.org/join

CREDIT: HERNÁNDEZ *ET AL.*, *EMBO REP.* **7**, 605 (2006)

www.sciencemag.org

Science

1200 New York Avenue, NW
Washington, DC 20005
Editorial: 202-326-6550, FAX 202-289-7562
News: 202-326-6500, FAX 202-371-9227

Bateman House, 82-88 Hills Road
Cambridge, UK CB2 1LQ
+44 (0) 1223 326500, FAX +44 (0) 1223 326501

Subscription Services For change of address, missing issues, new orders and renewals, and payment questions: 866-434-AAAS (2227) or 202-326-6417, FAX 202-842-1065. Mailing addresses: AAAS, P.O. Box 96178, Washington, DC 20090-6178 or AAAS Member Services, 1200 New York Avenue, NW, Washington, DC 20005

Institutional Site Licenses please call 202-326-6755 for any questions or information

Reprints: Author Inquiries 800-635-7181
Commercial Inquiries 803-359-4578
Corrections 202-326-6501

Permissions 202-326-7074, FAX 202-682-0816

Member Benefits Bookstore: AAAS/BarnesandNoble.com bookstore www.aaas.org/bn; Car purchase discount: Subaru VIP Program 202-326-6417; Credit Card: MBNA 800-847-7378; Car Rentals: Hertz 800-654-2200 CDP#343457, Dollar 800-800-4000 #AA1115; AAAS Travels: Betchart Expeditions 800-252-4910; Life Insurance: Seabury & Smith 800-424-9883; Other Benefits: AAAS Member Services 202-326-6417 or www.aaasmember.org.

science_editors@aaas.org	(for general editorial queries)
science_letters@aaas.org	(for queries about letters)
science_reviews@aaas.org	(for returning manuscript reviews)
science_bookrevs@aaas.org	(for book review queries)

Published by the American Association for the Advancement of Science (AAAS), *Science* serves its readers as a forum for the presentation and discussion of important issues related to the advancement of science, including the presentation of minority or conflicting points of view, rather than by publishing only material on which a consensus has been reached. Accordingly, all articles published in *Science*—including editorials, news and comment, and book reviews—are signed and reflect the individual views of the authors and not official points of view adopted by the AAAS or the institutions with which the authors are affiliated.

AAAS was founded in 1848 and incorporated in 1874. Its mission is to advance science and innovation throughout the world for the benefit of all people. The goals of the association are to: foster communication among scientists, engineers and the public; enhance international cooperation in science and its applications; promote the responsible conduct and use of science and technology; foster education in science and technology for everyone; enhance the science and technology workforce and infrastructure; increase public understanding and appreciation of science and technology; and strengthen support for the science and technology enterprise.

Information for Contributors

See pages 102 and 103 of the 6 January 2006 issue or access www.sciencemag.org/feature/contribinfo/home.shtml

EDITOR-IN-CHIEF **Donald Kennedy**
EXECUTIVE EDITOR **Monica M. Bradford**
DEPUTY EDITORS **R. Brooks Hanson, Katrina L. Kelner**
NEWS EDITOR **Colin Norman**

Editorial supervisory senior editors Barbara Jasny, Phillip D. Szuromi; **senior editor/perspectives** Lisa D. Chong; **senior editors** Gilbert J. Chin, Pamela J. Hines, Paula A. Kiberstis (Boston), Marc S. Lavine (Toronto), Beverly A. Purnell, L. Bryan Ray, Guy Riddihough (Manila), H. Jesse Smith, Valda Vinson, David Voss; **associate editors** Jake S. Yeston, Laura M. Zahn; **online editor** Stewart Wills; **associate online editor** Tara S. Marathe; **book review editor** Sherman J. Suter; **associate letters editor** Etta Kavanagh; **information specialist** Janet Kegg; **editorial manager** Cara Tate; **senior copy editors** Jeffrey E. Cook, Cynthia Howe, Harry Jach, Barbara P. Ordway, Jennifer Sills, Trista Wagoner; **copy editor** Peter Mooreside; **editorial coordinators** Carolyn Kyle, Beverly Shields; **publication assistants** Ramatoulaye Diop, Chris Filiatreau, Joi S. Granger, Jeffrey Hearn, Lisa Johnson, Scott Miller, Jerry Richardson, Brian White, Anita Wynn; **editorial assistants** Lauren Kmec, Patricia M. Moore, Brendan Nardozzi, Michael Rodewald; **executive assistant** Sylvia S. Kihara

News senior correspondent Jean Marx; **deputy news editors** Robert Coontz, Jeffrey Mervis, Leslie Roberts, John Travis; **contributing editors** Elizabeth Culotta, Polly Shulman; **news writers** Yudhijit Bhattacharjee, Adrian Cho, Jennifer Couzin, David Grimm, Constance Holden, Jocelyn Kaiser, Richard A. Kerr, Eli Kintisch, Andrew Lawler (New England), Greg Miller, Elizabeth Pennisi, Robert F. Service (Pacific NW), Erik Stokstad; Katherine Unger (intern); **contributing correspondents** Barry A. Cipra, Jon Cohen (San Diego, CA), Daniel Ferber, Ann Gibbons, Robert Irion, Mitch Leslie (NetWatch), Charles C. Mann, Evelyn Strauss, Gary Taubes, Ingrid Wickelgren; **copy editors** Linda B. Felaco, Rachel Curran, Sean Richardson; **administrative support** Scherraine Mack, Fannie Groom **bureaus:** Berkeley, CA: 510-652-0302, FAX 510-652-1867, New England: 207-549-7755, San Diego, CA: 760-942-3252, FAX 760-942-4979, Pacific Northwest: 503-963-1940

Production director James Landry; **senior manager** Wendy K. Shank; **assistant manager** Rebecca Doshi; **senior specialists** Jay Covert, Chris Redwood; **specialist** Steve Forrester **Preflight director** David M. Tompkins; **manager** Marcus Spiegler; **specialist** Jessie Mudjitaba

Art director Joshua Moglia; **associate art director** Kelly Buckheit; **illustrators** Chris Bickel, Katharine Sutliff; **senior art associates** Holly Bishop, Laura Creveling, Preston Huey; **associate** Nayomi Kevitiyagala; **photo editor** Leslie Blizard

***Science* International**

Europe (science@science-int.co.uk) **editorial: international managing editor** Andrew M. Sugden; **senior editor/perspectives** Julia Fahrenkamp-Uppenbrink; **senior editors** Caroline Ash (Geneva: +41 (0) 222 346 3106), Stella M. Hurtley, Ian S. Osborne, Stephen J. Simpson, Peter Stern; **associate editor** Joanne Baker **editorial support** Alice Whaley; Deborah Dennison **administrative support** Janet Clements, Phil Marlow, Jill White; **news: international news editor** Eliot Marshall **deputy news editor** Daniel Clery; **correspondent** Gretchen Vogel (Berlin: +49 (0) 30 2809 3902, FAX +49 (0) 30 2809 8365); **contributing correspondents** Michael Balter (Paris), Martin Enserink (Amsterdam and Paris), John Bohannon (Berlin); **intern** Laura Blackburn

Asia Japan Office: Asca Corporation, Eiko Ishioka, Fusako Tamura, 1-8-13, Hirano-cho, Chuo-ku, Osaka-shi, Osaka, 541-0046 Japan; +81 (0) 6 6202 6272, FAX +81 (0) 6 6202 6271; asca@os.gulf.or.jp; **asia news editor** Richard Stone +66 2 662 5818 (rstone@aaas.org) **japan news bureau** Dennis Normile (contributing correspondent, +81 (0) 3 3391 0630, FAX 81 (0) 3 5936 3531; dnormile@gol.com); **china representative** Hao Xin, + 86 (0) 10 6307 4439 or 6307 3676, FAX +86 (0) 10 6307 4358; haoxin@earthlink.net; **south asia** Pallava Bagla (contributing correspondent +91 (0) 11 2271 2896; pbagla@vsnl.com) **Africa** Robert Koenig (contributing correspondent, rob.koenig@gmail.com)

EXECUTIVE PUBLISHER **Alan I. Leshner**
PUBLISHER **Beth Rosner**

Fulfillment & Membership Services (membership@aaas.org) **director** Marlene Zendell; **manager** Waylon Butler; **systems specialist** Andrew Vargo; **customer service supervisor** Pat Butler; **specialists** Laurie Baker, Tamara Alfson, Karena Smith, Vicki Linton; **circulation associate** Christopher Refice; **data entry supervisor** Cynthia Johnson

Business Operations and Administration director Deborah Rivera-Wienhold; **business manager** Randy Yi; **senior business analyst** Lisa Donovan; **business analyst** Jessica Tierney; **financial analyst** Michael LoBue, Farida Yeasmin; **rights and permissions: administrator** Emilie David; **associate** Elizabeth Sandler; **marketing: director** John Meyers; **marketing managers** Darryl Walter, Allison Pritchard; **marketing associates** Julianne Wielga, Mary Ellen Crowley, Catherine Featherston, Alison Chandler, Lauren Lamoureux; **international marketing manager** Wendy Sturley; **marketing/member services executive:** Linda Rusk; **japan sales** Jason Hannaford; **site license sales: director** Tom Ryan; **sales and customer service** Mehan Dossani, Kiki Forsythe, Catherine Holland, Wendy Wise; **electronic media: manager** Lizabeth Harman; **production associates** Sheila Mackall, Amanda K. Skelton, Lisa Stanford, Nichele Johnston; **applications developer** Carl Saffell

Advertising director worldwide ad sales Bill Moran

Product (science_advertising@aaas.org); **midwest** Rick Bongiovanni: 330-405-7080, FAX 330-405-7081 • **west coast/w. canada** Teola Young: 650-964-2266 **east coast/e. canada** Christopher Breslin: 443-512-0330, FAX 443-512-0331 • **uk/europe/asia** Tracey Peers (Associate Director): +44 (0) 1782 752530, FAX +44 (0) 1782 752531 **japan** Mashy Yoshikawa: +81 (0) 33235 5961, FAX +81 (0) 33235 5852 **traffic manager** Carol Maddox; **sales coordinator** Deiandra Simms

Classified (advertise@sciencecareers.org); **u.s.: sales director** Gabrielle Boguslawski: 718-491-1607, FAX 202-289-6742; **inside sales manager** Daryl Anderson: 202-326-6543; **west coast/midwest** Kristine von Zedlitz: 415-956-2531; **east coast** Jill Downing: 631-580-2445; **canada, meetings and announcements** Kathleen Clark: 510-271-8349; **line ad sales** Emnet Tesfaye: 202-326-6740; **sales coordinators** Erika Bryant; Rohan Edmonson Christopher Normile, Joyce Scott, Shirley Young; **international: sales manager** Tracy Holmes: +44 (0) 1223 326525, FAX +44 (0) 1223 326532; **sales** Christina Harrison, Svitlana Barnes; **sales assistant** Helen Moroney; **japan:** Jason Hannaford: +81 (0) 52 789 1860, FAX +81 (0) 52 789 1861; **production: manager** Jennifer Rankin; **assistant manager** Deborah Tompkins; **associates** Christine Hall; Amy Hardcastle; **publications assistants** Robert Buck; Mary Lagnaoui

AAAS Board of Directors retiring president, chair Gilbert S. Omenn; **president** John P. Holdren; **president-elect** David Baltimore; **treasurer** David E. Shaw; **chief executive officer** Alan I. Leshner; **board** Rosina M. Bierbaum; John E. Dowling; Lynn W. Enquist; Susan M. Fitzpatrick; Alice Gast; Thomas Pollard; Peter J. Stang; Kathryn D. Sullivan

AAAS
ADVANCING SCIENCE, SERVING SOCIETY

Senior Editorial Board

John I. Brauman, *Chair, Stanford Univ.*
Richard Losick, *Harvard Univ.*
Robert May, *Univ. of Oxford*
Marcia McNutt, *Monterey Bay Aquarium Research Inst.*
Linda Partridge, *Univ. College London*
Vera C. Rubin, *Carnegie Institution of Washington*
Christopher R. Somerville, *Carnegie Institution*
George M. Whitesides, *Harvard University*

Board of Reviewing Editors

Joanna Aizenberg, *Bell Labs/Lucent*
R. McNeill Alexander, *Leeds Univ.*
David Altshuler, *Broad Institute*
Arturo Alvarez-Buylla, *Univ. of California, San Francisco*
Richard Amasino, *Univ. of Wisconsin, Madison*
Meinrat O. Andreae, *Max Planck Inst., Mainz*
Kristi S. Anseth, *Univ. of Colorado*
Cornelia I. Bargmann, *Rockefeller Univ.*
Brenda Bass, *Univ. of Utah*
Ray H. Baughman, *Univ. of Texas, Dallas*
Stephen J. Benkovic, *Pennsylvania St. Univ.*
Michael J. Bevan, *Univ. of Washington*
Ton Bisseling, *Wageningen Univ.*
Mina Bissell, *Lawrence Berkeley National Lab*
Peer Bork, *EMBL*
Dennis Bray, *Univ. of Cambridge*
Stephen Buratowski, *Harvard Medical School*
Jillian M. Buriak, *Univ. of Alberta*
Joseph A. Burns, *Cornell Univ.*
William P. Butz, *Population Reference Bureau*
Doreen Cantrell, *Univ. of Dundee*
Peter Carmeliet, *Univ. of Leuven, VIB*
Gerbrand Ceder, *MIT*
Mildred Cho, *Stanford Univ.*
David Clapham, *Children's Hospital, Boston*
David Clary, *Oxford University*
J. M. Claverie, *CNRS, Marseille*
Jonathan D. Cohen, *Princeton Univ.*
F. Fleming Crim, *Univ. of Wisconsin*
William Cumberland, *UCLA*
George Q. Daley, *Children's Hospital, Boston*
Caroline Dean, *John Innes Centre*
Judy DeLoache, *Univ. of Virginia*
Edward DeLong, *MIT*
Robert Desimone, *MIT*
Dennis Discher, *Univ. of Pennsylvania*
Julian Downward, *Cancer Research UK*
Denis Duboule, *Univ. of Geneva*
Christopher Dye, *WHO*
Richard Ellis, *Cal Tech*
Gerhard Ertl, *Fritz-Haber-Institut, Berlin*
Douglas H. Erwin, *Smithsonian Institution*
Barry Everitt, *Univ. of Cambridge*
Paul G. Falkowski, *Rutgers Univ.*
Ernst Fehr, *Univ. of Zurich*
Tom Fenchel, *Univ. of Copenhagen*
Alain Fischer, *INSERM*
Jeffrey S. Flier, *Harvard Medical School*
Chris D. Frith, *Univ. College London*
R. Gadagkar, *Indian Inst. of Science*
John Gearhart, *Johns Hopkins Univ.*
Jennifer M. Graves, *Australian National Univ.*
Christian Haass, *Ludwig Maximilians Univ.*
Dennis L. Hartmann, *Univ. of Washington*
Chris Hawkesworth, *Univ. of Bristol*
Martin Heimann, *Max Planck Inst., Jena*
James A. Hendler, *Univ. of Maryland*
Ary A. Hoffmann, *La Trobe Univ.*
Evelyn L. Hu, *Univ. of California, SB*
Olli Ikkala, *Helsinki Univ. of Technology*
Meyer B. Jackson, *Univ. of Wisconsin Med. School*
Stephen Jackson, *Univ. of Cambridge*
Daniel Kahne, *Harvard Univ.*
Bernhard Keimer, *Max Planck Inst., Stuttgart*
Elizabeth A. Kellog, *Univ. of Missouri, St. Louis*
Alan B. Krueger, *Princeton Univ.*
Lee Kump, *Penn State*
Virginia Lee, *Univ. of Pennsylvania*
Anthony J. Leggett, *Univ. of Illinois, Urbana-Champaign*
Michael J. Lenardo, *NIAID, NIH*
Norman L. Letvin, *Beth Israel Deaconess Medical Center*
Olle Lindvall, *Univ. Hospital, Lund*
Richard Losick, *Harvard Univ.*
Ke Lu, *Chinese Acad. of Sciences*
Andrew P. MacKenzie, *Univ. of St. Andrews*
Raul Madariaga, *École Normale Supérieure, Paris*
Rick Maizels, *Univ. of Edinburgh*
Michael Malim, *King's College, London*
Eve Marder, *Brandeis Univ.*
George M. Martin, *Univ. of Washington*
William McGinnis, *Univ. of California, San Diego*
Virginia Miller, *Washington Univ.*
H. Yasushi Miyashita, *Univ. of Tokyo*
Edvard Moser, *Norwegian Univ. of Science and Technology*
Andrew Murray, *Harvard Univ.*
Naoto Nagaosa, *Univ. of Tokyo*
James Nelson, *Stanford Univ. School of Med.*
Roeland Nolte, *Univ. of Nijmegen*
Helga Nowotny, *European Research Advisory Board*
Eric N. Olson, *Univ. of Texas, SW*
Erin O'Shea, *Univ. of California, SF*
Elinor Ostrom, *Indiana Univ.*
Jonathan T. Overpeck, *Univ. of Arizona*
John Pendry, *Imperial College*
Philippe Poulin, *CNRS*
Mary Power, *Univ. of California, Berkeley*
David J. Read, *Univ. of Sheffield*
Les Real, *Emory Univ.*
Colin Renfrew, *Univ. of Cambridge*
Trevor Robbins, *Univ. of Cambridge*
Nancy Ross, *Virginia Tech*
Edward M. Rubin, *Lawrence Berkeley National Labs*
Gary Ruvkun, *Mass. General Hospital*
J. Roy Sambles, *Univ. of Exeter*
David S. Schimel, *National Center for Atmospheric Research*
Georg Schulz, *Albert-Ludwigs-Universität*
Paul Schulze-Lefert, *Max Planck Inst., Cologne*
Terrence J. Sejnowski, *The Salk Institute*
David Sibley, *Washington Univ.*
George Somero, *Stanford Univ.*
Christopher R. Somerville, *Carnegie Institution*
Joan Steitz, *Yale Univ.*
Edward I. Stiefel, *Princeton Univ.*
Thomas Stocker, *Univ. of Bern*
Jerome Strauss, *Univ. of Pennsylvania Med. Center*
Tomoyuki Takahashi, *Univ. of Tokyo*
Marc Tatar, *Brown Univ.*
Glenn Telling, *Univ. of Kentucky*
Marc Tessier-Lavigne, *Genentech*
Craig B. Thompson, *Univ. of Pennsylvania*
Michiel van der Klis, *Astronomical Inst. of Amsterdam*
Derek van der Kooy, *Univ. of Toronto*
Bert Vogelstein, *Johns Hopkins*
Christopher A. Walsh, *Harvard Medical School*
Christopher T. Walsh, *Harvard Medical School*
Graham Warren, *Yale Univ. School of Med.*
Colin Watts, *Univ. of Dundee*
Julia R. Weertman, *Northwestern Univ.*
Daniel M. Wegner, *Harvard University*
Ellen D. Williams, *Univ. of Maryland*
R. Sanders Williams, *Duke University*
Ian A. Wilson, *The Scripps Res. Inst.*
Jerry Workman, *Stowers Inst. for Medical Research*
John R. Yates III, *The Scripps Res. Inst.*
Martin Zatz, *NIMH, NIH*
Walter Zieglgänsberger, *Max Planck Inst., Munich*
Huda Zoghbi, *Baylor College of Medicine*
Maria Zuber, *MIT*

Book Review Board

John Aldrich, *Duke Univ.*
David Bloom, *Harvard Univ.*
Londa Schiebinger, *Stanford Univ.*
Richard Shweder, *Univ. of Chicago*
Ed Wasserman, *DuPont*
Lewis Wolpert, *Univ. College, London*

IMAGES

DOCUMENTING THE BIG MELT

For dramatic illustrations of how much Alaska's glaciers have shrunk in the last century, take a gander at this new gallery from the National Snow and Ice Data Center in Boulder, Colorado. Displayed are 14 pairs of photos taken from the same locations as much as 104 years apart. For example, Muir Glacier dominated this 1941 shot of what is now Glacier Bay National Park (below). By 2004, the ice had dwindled into the background (above). Curators plan to post more photos. >> nsidc.org/data/glacier_photo/special_collection.html

RESOURCES

Fire Lookout

Brush and forest fires transform habitats and pour pollutants and carbon dioxide into the air. Researchers studying fire's impact on atmospheric chemistry, land use, or related subjects can pinpoint burns at the World Fire Atlas from the European Space Agency. Satellite images updated about every 6 hours and other data let visitors identify new hot spots and track existing ones. Free registration provides access to an archive of fire maps that date back to 1995. This summary chart (above), for example, shows the locations of 2005's blazes. >> dup.esrin.esa.int/ionia/wfa/index.asp

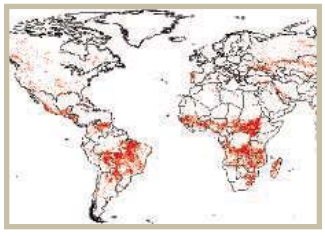

DATABASE

Building Blood Cells

Determining which genes coax immature red blood cells to grow up could help researchers devise new treatments for anemia and counter the side effects of chemotherapy. To find out which genes switch on as red blood cells mature, visit the Hembase database from the National Institute of Diabetes and Digestive and Kidney Diseases. Scientists there combined their measurements of messenger RNA levels with results from previous studies on gene expression in blood cell precursors. You can track down active genes by chromosome location or by whether they take part in tasks such as defining the blood group. >> hembase.niddk.nih.gov

TOOLS

That Shouldn't Be Turning Blue

Chemical rections don't always turn out, spawning unanticipated products or fizzling altogether. Although these flops rarely end up in papers, they can be instructive for other researchers attempting to duplicate a synthesis. That's the rationale behind the Chemistry Unpublished Papers Forum from the University of Pisa in Italy. The new site lets chemists report reactions that unexpectedly faltered or that released surprising products. After completing the free registration, visitors can post their lab woes or join discussions of more than a dozen troublesome reactions, such as copper nanoparticles' failure as catalysts. In the "Fake Chemistry" section, users can identify papers that they think show suspiciously high yields. >> www.chemunpub.it

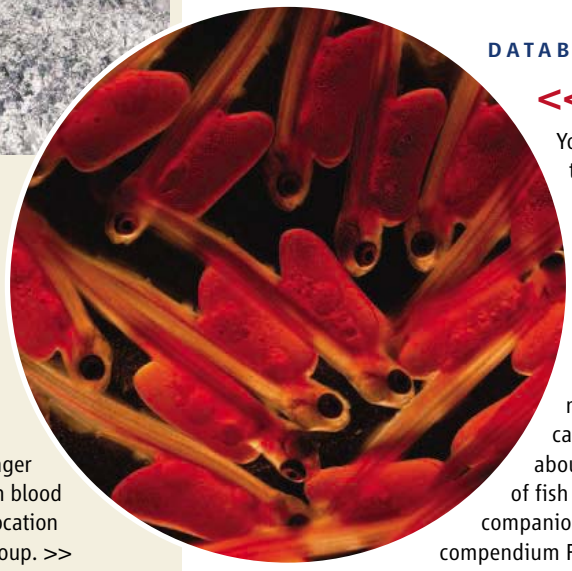

DATABASE

<< Fish Fry

Young fish such as these Atlantic salmon (*Salmo salar*; left) often frequent different habitats than do their parents and swallow different foods. Researchers, fisheries managers, and others can reel in information about the early stages of fish life at LarvalBase, a companion to the ichthyology compendium FishBase (NetWatch, 24 December 1999, p. 2423). Supervised by Bernd Ueberschaer of the Leibniz Institute of Marine Science in Kiel, Germany, LarvalBase houses data on juvenile fishes compiled from papers, books, reports, and unpublished "gray" literature. You'll find listings for nearly 2200 species that are important for fisheries and aquaculture. The information includes egg hatching times, charts that compare the anatomy of larval stages, roundups of larval diet, and rearing instructions for some well-studied species. You can also take a larva identification quiz. >> www.larvalbase.org

Send site suggestions to >>
netwatch@aaas.org
Archive: www.sciencemag.org/netwatch

CREDITS (TOP TO BOTTOM): WILLIAM FIELD AND BRUCE MOLNIA/USGS; EUROPEAN SPACE AGENCY; GETTY IMAGES/NGS


L'ORÉAL-UNESCO Awards 2006
FOR WOMEN IN SCIENCE
Science needs women.
Thank you, Dr Pamela BJORKMAN
California Institute of Technology, USA
Laureate for North America, for her discoveries related to the three-dimensional structures of human leukocyte antigens and how the immune system recognizes targets.
L'ORÉAL
UNESCO
for Women in Science
pour les Femmes et la Science
Four other women scientists are receiving the L'ORÉAL-UNESCO Awards in 2006.
www.lorealusa.com/forwomeninscience
© L'ORÉAL-UNESCO Photos "Micheline Pelletier/Gamma"

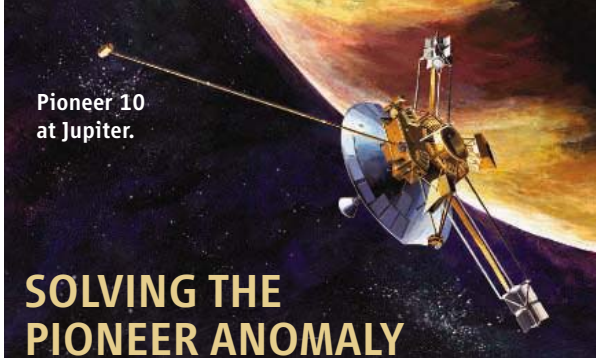

Pioneer 10 at Jupiter.

SOLVING THE PIONEER ANOMALY

A new effort has been launched to explain the mysterious slowdown of two NASA spacecraft. Pioneer 10 and 11 left Earth more than 30 years ago to explore the outer solar system, and over the past 11 years, Doppler radar data have shown that they are slowing down slightly more than would be expected from the sun's gravity alone. Right now, as the pair approach the edge of the solar system, the two spacecraft are almost 400,000 kilometers closer to the sun than scientists predicted.

This "Pioneer anomaly" has sparked an array of possible explanations, from dark matter to a flaw in our current understanding of gravity. NASA said it didn't have the budget to look into the question, so the Planetary Society, a private group of space buffs based in Pasadena, California, staged a fund drive to get things moving. With a grant from the society of more than $100,000, physicist Slava G. Turyshev of NASA's Jet Propulsion Laboratory in Pasadena is leading a project to recover 20 years of early Pioneer data from old magnetic tapes and convert the information to modern media for analysis.

Turyshev, who believes there will be an engineering explanation for the anomaly, hopes to precisely detect the direction in which the decelerating force is operating. Physicist Orfeu Bertolami of the Technical University in Lisbon, Portugal, agrees that older Pioneer data should be analyzed and suggests that the results could be used to decide whether a new space mission should be launched to investigate the anomaly.

White Wine After Death?

Drinking fine wine is part of the good life. In ancient Egypt, wine was also essential for a good afterlife because it symbolized rebirth. Yet Egyptian texts mention only red wine, leaving archaeologists to wonder whether whites were also on the menu.

Spanish researchers have now analyzed residues in amphorae from the tomb of King Tutankhamun and concluded that the young monarch was sent to the afterlife with both red and white wines. Egyptologist Maria Rosa Guasch-Jané and food scientist Rosa Lamuela-Raventós of the University of Barcelona examined 12 amphorae from Cairo's Egyptian Museum that were excavated from the tomb in 1922. Extracting dry residues from six of the vessels, the team analyzed the samples with a methodology they developed using liquid chromatography and mass spectrometry. All contained tartaric acid, a marker for grape wine. But two also had syringic acid, a breakdown product from red grape pigment. The researchers conclude in the August issue of the *Journal of Archaeological Science* that the other four probably contained white wine.

Regarding the two amphorae flanking Tut's sarcophagus, one apparently held white wine and bore an inscription from the "Estate-of-Tutankhamun." The other held red wine and was from the "Estate-of-Aton."

Carl Heron, an archaeologist at the University of Bradford in the U.K., says the team's claim that this represents the first evidence that white wine was drunk in ancient Egypt is plausible but needs confirmation.

HORSE TALK

In the interest of interspecies communication, two researchers have broken down the components of a horse's whinny.

David Browning, an acoustician at the University of Rhode Island, Kingston, noticed that whereas the cow "moo" has a straightforward acoustic spectrum like that of a party horn, equines—including horses, donkeys, and zebras—express themselves using a wider bandwidth and a more variable frequency.

An initial acoustic analysis conducted by Browning and bioacoustician Peter Scheifele of the University of Connecticut, Storrs, has now revealed two major components to the whinny. One, involving an upward shift in frequency, corresponds to a heightened emotional state—as when a stallion is chasing a mare. The other, a "tremolo," modulates the sound, such as when the whinny is a greeting. Hunger or other stresses also change the frequency of the whinny, the two reported last week at the Acoustical Society of America meeting in Providence, Rhode Island.

By monitoring whinnies, "we'd like to be able to identify stress and its causes earlier," says Scheifele. Animal behaviorist Steven Hopp of Emory and Henry College in Emory, Virginia, notes that horse stress levels might be hard to quantify but says a comparison of the sounds of equine species could yield intriguing results. That's coming: Browning and Scheifele have already studied the donkey "heehaw," and they plan to record and study three zebra species that respectively yip, bray, and whinny.

Canada's Heritage

A 4-year, $52 million "Renewal Project" was launched last week at the Museum of Anthropology, on the University of British Columbia campus in Vancouver. The museum features one of the world's largest collections of totem poles. One part of the project will be a new digital Reciprocal Research Network to facilitate collaboration among 12 institutions worldwide that have collections of indigenous North American artifacts. Three "First Nation" communities will be involved in helping make it accessible to tribal groups. "Eighty percent of the heritage" of people from the Northwest coast is in museums, notes a museum spokesperson.

CREDITS (TOP TO BOTTOM): NASA; UBC MUSEUM OF ANTHROPOLOGY/PHOTO: BILL MCLENNAN; GETTY IMAGES/DIGITAL VISION

Jeremy Rifkin's new cause
1586

Early fossils from China
1587

ENVIRONMENTAL SCIENCE

Climate Sensors Dropped From U.S. Weather Satellite Package

5 June was the day the music died for geographer Anne Nolin of Oregon State University, Corvallis. That's when the U.S. government decided to strip several climate instruments off a suite of polar-orbiting satellites intended to provide the next generation of weather and climate-monitoring data for military, civilian, and scientific users (*Science*, 2 June, p. 1296).

Nolin, who uses passive microwave imaging to study snow and ice at the poles, is one of a legion of climate scientists distraught by the reduced capacity, rising costs, and launch delays in the National Polar-Orbiting Operational Environmental Satellite System (NPOESS) program. And they aren't alone: Last week, members of the House Science Committee excoriated the heads of three government agencies for what they see as a decade of management missteps.

Weathering a storm. From left, NOAA's Conrad Lautenbacher, NASA's Michael Griffin, and the Air Force's Ronald Sega field tough questions on NPOESS from the House Science Committee.

NPOESS was conceived in 1994 as a joint project of the Department of Defense and the National Oceanic and Atmospheric Administration (NOAA), each of which operates its own polar satellites, with NASA as a junior partner. The government said that NPOESS, in addition to saving money, would provide the nation with an enhanced capability to wage war, track storms, and study a host of climate variables, from electron density in space to solar irradiance to sea-surface interactions. For climate scientists, the alliance would combine NASA's expertise in building and flying high-quality research payloads with NOAA's commitment to operational satellites.

The payoff was to be a more robust longitudinal record of an ever-changing Earth. But that promise hasn't been realized—and there's a chance it may never come to pass. "We're seeing a disintegration of the U.S. environmental satellite system," says Richard Anthes, head of the organization that manages the National Center for Atmospheric Research in Boulder, Colorado, and co-chair of an almost-completed U.S. National Academies' exercise to lay out long-range research priorities for the field.

Geoscientists who rely on space-based observations of Earth regard the downsizing of NPOESS as a serious blow to their discipline. "Essentially, NPOESS is saying NOAA won't be doing climate," says Kathie Kelly, who studies atmosphere-ocean coupling at the University of Washington's Applied Physics Laboratory in Seattle. "Basically, no one is going to do climate."

Last week's hearing was a chance for officials from the three relevant agencies—Air Force Under Secretary Ronald Sega, NASA Administrator Michael Griffin, and NOAA head Conrad Lautenbacher—to explain a 5 June decision that was mandated by the program's budget overruns. The original $6.5 billion plan for NPOESS called for a fleet of six satellites (up to three in orbit at any one time), with nine instruments collecting data on 55 environmental elements. A preparatory satellite would be launched in 2006, and the final one a decade later. The new $11.5 billion plan promises only four satellites (two at one time), bearing only three of those nine instruments. The first launch would be in 2009 and the final one in 2022.

Key instruments that have been discarded include the Conical Scanning Microwave Imager/Sounder (CMIS) that Nolin was counting on; the Total Solar Irradiance Sensor; the Aerosol Polarimetry Sensor; the Earth Radiation Budget Sensor suite; the Space Environment Sensor suite; and one of two Ozone Mapping and Profiler suite. Those instruments lost out in a competition that gave priority to weather forecasting.

NPOESS officials told the committee that the new configuration will still be equipped to monitor weather and collect climate information. Lautenbacher said the government will build a smaller and less capable CMIS with the $265 million that remains in CMIS's initial budget of $465 million, and the Navy is studying how to replace an altimeter that would have monitored sea surface height and wave characteristics. Instruments on other missions can take up some of the slack, the agency officials assured legislators, although the sensors may be less capable. "Instead of gold fixtures and marble countertops, we may have to settle for chrome and Formica," Lautenbacher explained after the hearing. "But we can still get what we need."

Legislators aren't nearly as optimistic. "Twelve years into the program, and 3 years before the first launch, we are at a critical point where there is little room left to recover from further missteps," noted Representative Vern Ehlers (R–MI), chair of the panel's environmental subcommittee, who intoned that "today is not a happy occasion." The chair, Representative Sherwood Boehlert (R–NY), was even less politic. "How the hell can we do our job without sufficient information?" he exclaimed, joining with ranking Democrat Representative Bart Gordon (D–TN) in a full-throated attack on what they see as the Bush Administration's refusal to explain its latest decision.

Pressed by Ehlers on what might be added back if more money became available, Griffin pointed to the academies' forthcoming decadal study. But Anthes says the panel didn't expect NPOESS to be cut back so severely and that the report, due out in December, will make a case for a "balanced strategy for all of the earth sciences … and for the importance of the science."

–JEFFREY MERVIS

CREDIT: BILL INGALLS/NASA

INFECTIOUS DISEASE

Polio Experts Strive to Understand a Puzzling Outbreak

Health authorities in Namibia are scrambling to vaccinate the entire population, some 2 million people, against poliovirus, which has resurfaced after a 10-year absence in a highly unusual—and deadly—outbreak. Unlike most outbreaks, this one is targeting adults rather than young children. Outbreaks among adults are "as rare as hen's teeth," says Bruce Aylward, who directs the global campaign to eradicate polio from World Health Organization (WHO) headquarters in Geneva, Switzerland, because adults usually have acquired immunity either through vaccination or exposure to infected children. But when an adult in infected, the disease tends to be much more severe.

As *Science* went to press, at least 47 suspected cases were under investigation in Namibia, and wild poliovirus type one had been confirmed in four. Seven people had died, and several others were critically ill. Shipments of vaccine were en route to Namibia for the first of at least three emergency campaigns, and officials were bracing for yet more cases before the virus can be contained.

Although the latest outbreak is yet another blow to the global campaign to eradicate polio, WHO officials say they are optimistic that the Namibian government can quash it. But the outbreak remains puzzling. A team of epidemiologists has rushed in to investigate, while others have been scouring the genetic sequence of the virus for clues. Genetic evidence suggests that the virus originated in India, one of four countries where polio is endemic, and that it recently jumped across the border from Angola into Namibia. Angola had interrupted transmission of wild poliovirus in 2001 but was reinfected with an Indian virus last year; only a handful of new cases have been reported there.

When it reached Namibia, the virus found fertile soil. Why is not clear, but the prevailing assumption is that the afflicted adults were not immunized as children. Namibia didn't offer routine vaccinations until the early 1990s, but once the country began polio immunization in earnest, the last case of indigenous poliovirus was reported in 1996. One puzzle, says Aylward, is how the affected adults apparently escaped exposure to the circulating virus before then. In other adult outbreaks, for instance in Albania in 1996 or Cape Verde in 2000, the populations were either culturally or geographically isolated, he notes.

The first case identified in Namibia was a 39-year-old farmer from Aranos, about 150 kilometers from the capital of Windhoek. He went to Windhoek for gall bladder surgery and became ill, with sudden paralysis, about 2 weeks later on 8 May. He is now on a respirator. Within days, other cases were reported around Windhoek, mostly among adults between age 20 and 40. Health authorities initially thought they might be dealing with Guillain-Barre syndrome, an autoimmune disorder that may be triggered by infections. But on 2 June, a WHO-accredited laboratory in South Africa confirmed wild poliovirus.

Index case? Namibia's outbreak has been traced to a virus that came from India via Angola. Top: A child in Angola receives polio vaccine.

So far, epidemiologists don't know where the farmer picked up the virus or even whether he is the first in the chain of transmission, says David L. Heymann, the WHO director general's representative for polio eradication. Investigators are looking for any connection among the suspected cases. "We may never know," says Heymann, who notes that many of the victims are unable to talk because they are on respirators. Investigators are also trying to determine whether a cluster of Guillain-Barre cases reported in April may have been polio as well, he adds.

A shipment of monovalent oral polio vaccine is scheduled to arrive in Namibia this week. In the first campaign, slated to begin 21 June, and a second scheduled for late July, the government hopes to reach every person in the country, adults and children alike. The age group to be targeted in subsequent campaigns has yet to be determined. "I am very confident [Namibia] will be able to [control the outbreak]," says Heymann. He lauds Namibia's rapid response and says the campaign will also benefit from the country's sparse population and the onset of winter.

A bigger challenge may be knocking out polio next door in Angola, says Heymann. The last reported case of polio in Angola was in November 2005, but last month, wild poliovirus from Angola also resurfaced in the Democratic Republic of Congo (DRC), which abuts Angola to the north. "They are clearly not doing enough to stop transmission," says Heymann. New sequencing data from Angola, the DRC, and Namibia suggest that the virus was introduced into one of these countries a year ago and has been circulating in all three.

Although the new outbreaks are troubling, WHO officials say the most serious threat to polio eradication remains the densely populated states of northern Nigeria, where there has been intense opposition to vaccination and an epidemic is raging out of control. Already, 438 cases have been reported this year, nearly triple the number at the same time last year.

To Ellie Ehrenfeld, a polio biologist at the U.S. National Institutes of Health, the Namibian outbreak provides yet more evidence that "the world cannot be left unimmunized." Even if the eradication campaign succeeds, she warns, "the potential for a hideous, hideous outcome is really there."

–LESLIE ROBERTS

CREDIT: POLIOERADICATION.ORG

eppendorf® is a registered trademark.

get*real*speed

Real-time PCR system Mastercycler® ep *realplex*

Innovative technology meets ultimate speed with the new, space-saving Mastercycler® ep *realplex* real-time PCR system.

Mastercycler ep *realplex* features high ramping speeds and short detection times, so you can complete more experiments each day—on even the tightest lab bench.

Eppendorf Mastercycler® ep *realplex*:

- High speed real-time PCR in <30 minutes
- Use reagent kits and consumables of your choice
- Intuitive software
- Modular concept provides ultimate flexibility
- Highly sensitive optical system

For more information visit
www.eppendorf.com/realplex

eppendorf

In touch with life

www.eppendorf.com · Email: info@eppendorf.com · Application support: 516-515-2258
In the U.S.: Eppendorf North America, Inc. 800-645-3050 · In Canada: Eppendorf Canada Ltd. 800-263-8715
Your local distributor: www.eppendorf.com/worldwide · Application support: Phone +49 180 366 67 89

Practice of the patented polymerase chain reaction (PCR) process requires a license. The Eppendorf [or appropriate trademark] Thermal Cycler is an Authorized Thermal Cycler and may be used with PCR licenses available from Applied Biosystems. Its use with Authorized Reagents also provides a limited PCR license in accordance with the label rights accompanying such reagents. This is a Licensed Real-Time Thermal Cycler under Applera's United States Patent No. 6,814,934 and corresponding claims in non-U.S. counterparts thereof, for use in research and for all other applied fields except human in vitro diagnostics. No right is conveyed expressly, by implication or by estoppel under any other patent claim.

REPRODUCTION

Bone Marrow Fails to Produce Oocytes

It was a controversial idea from the start: Last year, researchers suggested that cells in the bone marrow can travel through the circulatory system to the ovaries and become oocytes. If true, the discovery might lead to new fertility and menopause treatments. And it would have meant that women receiving bone marrow transplants could give birth to genetically unrelated children. But a paper in this week's issue of *Nature* should put that particular worry to rest. In a series of mouse experiments, the authors find no evidence that bone marrow cells become mature oocytes.

The new results "raise a serious rebuttal to the hypothesis that you could restore someone's fertility by giving them a bone marrow transplant," says Louis De Paolo of the National Institute of Child Health and Human Development in Bethesda, Maryland.

Standard textbooks explain that shortly after birth, a female's ovaries have all the potential egg cells she will ever have. But in the past 2 years, a group has claimed that the textbooks may be wrong. In a 2004 *Nature* paper, Josh Johnson and Jonathan Tilly of Harvard Medical School in Boston and their colleagues presented evidence that new oocytes can develop in adult mice (*Science*, 12 March 2004, p. 1593). Then, based on experiments in which seemingly sterilized mice appeared to produce new oocytes after a bone marrow transplant, they concluded in *Cell* last year that the eggs might be derived from bone marrow cells that had migrated to the ovaries (*Science*, 29 July 2005, p. 678).

These results were met with skepticism, and to date no other group has reported similar findings. Instead, in the new *Nature* paper, Amy Wagers of the Joslin Diabetes Center in Boston and her colleagues challenge Johnson and Tilly's second claim.

Wagers and her colleagues created pairs of parabiotic mice: mice with their skin sewn together between the front and hind legs so that they have a shared circulatory system. Parabiotic pairs can live for more than a year, eating and moving relatively normally. In Wagers's experiments, one parabiotic mouse was normal, and the other came from a strain genetically engineered to express green fluorescent protein (GFP) in all its tissues. The researchers reasoned that if circulating bone marrow cells contribute to oocyte development, they should find GFP-expressing oocytes in the normal mouse and nonfluorescent ones in the mutant. However, even after 8 months of sharing blood, the mice only produced oocytes that matched their own genotype.

Wagers and her colleagues also checked whether bone marrow cells help repair the damage done to ovaries by chemotherapy drugs, one of the claims that Tilly and his colleagues made. The Joslin team gave doses of two ovary-damaging drugs to a normal mouse and then joined it to a mouse expressing GFP. But again, they found no fluorescent oocytes in the normal mice. The team did find GFP-expressing cells near mature oocytes in those rodents' ovaries, but they were immune-system cells. "We looked at hundreds of oocytes and never saw one that was partner- or donor-derived," Wagers says.

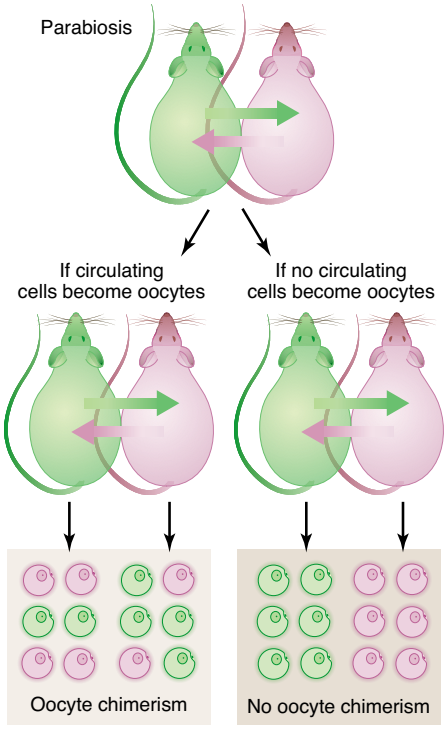

Green eggs. Shared circulation between a normal mouse and one expressing green fluorescent protein reveals whether bone marrow spawns oocytes.

But Tilly says the paper does not directly contradict his group's observations. His team reported evidence of immature oocytes, he says, which might help support ovarian function even if they never mature into fertilizable eggs. The new paper "has raised an important issue about the mature egg population, but it in no way addresses seeding of the ovary," he says, because Wagers's group only examined ovulated oocytes.

Although Wagers's team doesn't address the still-contentious issue of whether adult mammals keep producing new oocytes, David Albertini of the University of Kansas Medical Center in Kansas City says their data clearly answer the key question of whether bone marrow cells are a source of any such fresh eggs. "The nice thing about these experiments is that a very simple question was asked, and a very clear result was obtained," he says. **–GRETCHEN VOGEL**

CREDITS: ADAPTED FROM K. EGGAN *ET AL.*, *NATURE*, ADVANCED ONLINE PUBLICATION; (ILLUSTRATION: K. SUTLIFF/*SCIENCE*)

Coral Reefs to Get Protection

Environmentalists are cheering a Bush Administration decision to phase out commercial fishing around one of the most remote and undisturbed coral reefs in the world. The Northwestern Hawaiian Islands Coral Reef Ecosystem Reserve's 348,550 square kilometers is home to a rich diversity of fish, turtles, and mammals. Two decades of exploitation, halted in 2000, wiped out the reef's native lobsters.

Last fall, the governor of Hawaii banned fishing within state waters. The new management plan, expected to be announced this week, would eventually extend the ban to federal waters, 80 kilometers offshore. Although reef fishing generates revenues of only about $1 million a year, Pew Charitable Trusts' Environment Program Director Joshua Reichert calls the new plan a "significant policy achievement." There will be 60 days for public comment to the National Oceanic and Atmospheric Administration. **–ERIK STOKSTAD**

Start-Up Center Starting Up

BEIJING—China hopes to seed its biotechnology industry with a national incubation center in Beijing.

Last week, officials announced that the Beijing International Trust and Investment Co. Ltd. would invest $160 million over 3 years to create the China National Academic Center for Biotechnology. The center, whose goal will be nurturing 100 companies and up to 500 research labs, will focus on the start-up and development phase of companies created to exploit Chinese technologies. Zhu Zhen, an expert in plant genetics engineering with the Chinese Academy of Sciences, says the Beijing center is well-positioned to help scientists overcome traditional obstacles to turning their discoveries into products. **–GONG YIDONG**

Global Health a Taxing Problem

PARIS—Passengers departing from French airports will pay a new tax starting next month that will help buy drugs for the world's poorest nations. The campaign, dubbed UNITAID, is expected to raise $250 million annually. Thirteen other nations worldwide have promised to follow suit with similar fees.

Surcharges range from $1.25 for economy flights to a whopping $50 for first-class intercontinental tickets. Global health advocates applaud the plan, long championed by French President Jacques Chirac, as needed support for a new International Drug Purchase Facility that will negotiate low prices for drugs to combat diseases affecting the developing world.

–MARTIN ENSERINK

GENETICS

U.S. Hospital Launches Large Biobank of Children's DNA

Joining a growing list of "biobank" projects around the world that aim to link genes and common diseases, researchers in Philadelphia, Pennsylvania, last week announced a plan to collect DNA from 100,000 people. This new project comes with a youthful twist: "The focus here is entirely on children," says study leader Hakon Hakonarson of the Children's Hospital in Philadelphia (CHOP).

Ethical questions already swirl around existing biobanks, and the storage of children's DNA could raise new issues, notes pediatrician and medical ethicist Jeffrey Botkin of the University of Utah School of Medicine in Salt Lake City. For example, whether to permit DNA to be used for unspecified future projects is "always more ethically sensitive" when decided by parents for their children, he says. However, birth defects researcher Jeffrey Murray of the University of Iowa in Iowa City, who is not connected with the project, contends that a large children's DNA bank is needed and can be operated ethically and safely. "We'd be letting children down by not doing this," he adds.

According to its plan, CHOP will spend $40 million from private sources over the next 3 years to analyze DNA from 100,000 children and begin searching for links to childhood diseases such as asthma, diabetes, and obesity. The core population will be drawn "relatively randomly" from the hospital's 1 million patient base, says Hakonarson, a former CHOP staffer who recently returned from working at deCODE Genetics Inc., the Icelandic company that has paved the way for population biobanks (*Science*, 8 November 2002, p. 1158). The hospital also plans to collaborate with outside groups to recruit youngsters with rarer diseases, such as neuroblastoma, a childhood cancer.

Each child's DNA will be scanned for some 550,000 common markers. To address privacy concerns, these data will be combined with medical records in a triple-encrypted database that leaves researchers with no way to identify participants, says Hakonarson. He adds that the parents also agree that they won't have access to their child's results, as the DNA scan is only for research purposes. Ultimately, CHOP hopes the project leads to new diagnostics and treatments tailored to a child's genetic makeup.

Some large epidemiology studies of children in Europe and the United States have collected DNA but have likely not begun comprehensive genotyping, says Murray. Another proposed U.S. effort, the National Children's Study (see p. 1585), would also enroll 100,000 children and store ▶

Banking on DNA. Researchers hope that a new DNA database on children will uncover genes involved in diseases such as asthma and will lead to better treatments.

CREDIT: GETTY IMAGES

STEM CELL RESEARCH

Harvard Cloners Get OK to Proceed With Caution

Harvard University researchers last week were given the go-ahead to use cloning to create disease-specific lines of human embryonic stem cells. The approval makes Harvard the second U.S. academic institution, after the University of California, San Francisco (UCSF), to use research cloning—known as somatic cell nuclear transfer (SCNT)—as a tool for studying diseases such as diabetes and Parkinson's.

"I'm very happy to hear" the Harvard news, says Arnold Kriegstein, head of UCSF's new Stem Cell Institute. "The more people who are working on this, the more likely that it will succeed."

Scientists described their plans to use the technology at a 6 June press conference at Harvard, noting that five institutions and eight Institutional Review Boards spent 2 years reviewing the arrangement before giving their approval. It's been a "Herculean effort," said researcher George Daley of Children's Hospital Boston, referring to the ethical, logistical, legal, and financial matters that had to be resolved. Some states have banned the technique because it involves creating and destroying fertilized eggs, and there are no reports of success with SCNT, the procedure Korean scientist Woo Suk Hwang used in now-discredited research (*Science*, 2 June, p. 1298).

One major issue that Harvard has addressed involves egg donation procedures. The researchers plan to recruit local "compassionate" donors, who will not be paid anything beyond expenses. To avoid medical problems that have reportedly plagued women who donated eggs for Hwang's research, Kevin Eggan of the Harvard Stem Cell Institute said there will be limits on blood levels of estradiol resulting from hormonal stimulation. He said no more than 8 to 10 eggs will be taken from any individual. Potential donors will be given a 25-page booklet informing them of every conceivable risk.

All financial backing for the research will be privately donated, in keeping with the federal prohibitions on funding such work. And it's not just scrupulous accounting that will be necessary; Harvard provost Steven Hyman told the *Harvard Crimson* that rules extend even to what scientists can and cannot touch. In keeping with the extreme caution surrounding the enterprise, Harvard spokesperson B. D. Colen says all the researchers involved will stay mum until the first results are published.

Several projects now have the green light. Eggan and colleague Douglas Melton are cultivating skin cells from diabetics to insert their nuclei into enucleated eggs. Their goal is disease-specific stem cell lines—moving the study of disease "from patients to a petri dish," as Melton put it. Eggan also intends to use the technique to study neurodegenerative diseases such as amyotrophic lateral sclerosis. Daley, meanwhile, plans to create customized cell lines using skin biopsies from patients with sickle cell anemia and other blood diseases.

Last month, UCSF researcher Renee Reijo Pera got permission to attempt nuclear transfer using "failed-to-fertilize" eggs from fertility clinics. Harvard now has the only group in the world with permission to work with fresh donor eggs. **–CONSTANCE HOLDEN**

their DNA but would focus initially on environmental disease factors.

Botkin says institutional review boards (IRBs) evaluating DNA banks vary on whether to allow open-ended consent for studies that could include, for example, identifying genes affecting behavior. The CHOP project will give parents a choice: They can check a box allowing analysis of their child's DNA for specific diseases, or one permitting future studies on unspecified topics. Hakonarson says the biobank approach has been "well-received" by CHOP's IRB. But Botkin, who offered ethics advice to the National Children's Study, says he prefers an "intermediate level of specificity," such as limiting the studies to cancer research.

Another issue that troubles some researchers, including Murray, is that CHOP expects to partner with drug companies and patent discoveries. Without intellectual property rights, firms are unlikely to be interested in following up on a promising lead, explains CHOP Chief Scientific Officer Philip Johnson. He adds that after a delay, the database will be open to other investigators: "Our goal is to make all of the information publicly available." **–JOCELYN KAISER**

U.S. 2007 BUDGET

NIH Gets Off to a Slow Start

A House spending panel last week endorsed a flat budget for the National Institutes of Health (NIH)—but told the agency to make room for a $3.2 billion children's health study that NIH says it cannot afford. Legislators also want NIH to make mandatory a voluntary program in which grantees submit their accepted manuscripts to a free online archive.

The legislation, a first step toward approving a 2007 budget, essentially matches President George W. Bush's $28.3 billion request for agency programs under the panel's jurisdiction. If the Senate isn't more generous, it would mean the third straight year at that level. Like Bush's request, the House bill would give the NIH director's office a $140 million boost, mainly for biodefense countermeasures and the trans-NIH Roadmap. Most of NIH's 27 individual institutes and centers would suffer cuts of about 0.5% to 0.8%.

"No question, we're extremely disappointed" by the NIH levels, says Jon Retzlaff, director of legislative relations for the Federation of American Societies for Experimental Biology. NIH expects to fund 656 fewer research grants in 2007 than this year.

Legislators went against the Administration's wish to cancel the National Children's Study by ordering the National Institute of Child Health and Human Development to spent $69 million of its $1.26 billion budget on preparing to track 100,000 children from birth to age 21. A report accompanying the bill says the committee is "very disappointed" that the president's budget does not explain why it proposed eliminating the study, which is already funding seven "vanguard" centers. Advocates say NIH needs new money to fund the study, and they are hoping that the Senate will be more generous.

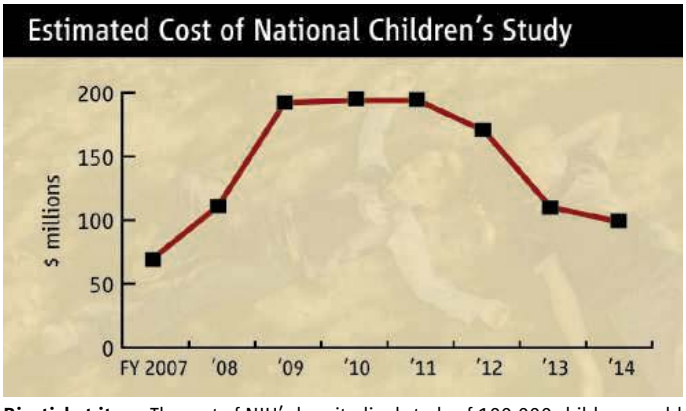

Big-ticket item. The cost of NIH's longitudinal study of 100,000 children would peak during enrollment and then level off at $99 million a year after 2014.

The spending bill would also require researchers to post a copy of every manuscript they generate using NIH funds in the agency's free, full-text PubMed Central archive within 12 months after publication in a journal. The committee resisted calls from open-access advocates to require posting within 6 months, which many scientific societies fear could bankrupt journals that provide funds for their other activities. "The 12 months is a positive step," says Martin Frank, executive director of the American Physiological Society.

The bill moves to the floor later this month and then to the Senate, which in March voted to give appropriators an extra $7 billion partly to boost NIH. "Senator [Arlen] Specter (R–PA) feels very strongly about NIH," says Representative Ralph Regula (R–OH), chair of the spending panel. "So it's very possible that the numbers could change before we're done." **–JOCELYN KAISER**

CREDITS (TOP TO BOTTOM) PHOTOS.COM; SOURCE: NIH

Transgenics Make Progress

The first medicine developed using transgenic biotechnology could soon hit European hospitals. Amid controversy, the European Medicines Agency (EMEA) found earlier this month that ATryn, which contains recombinant human anticlotting proteins extracted from the milk of transgenic goats, is fit for public use. If the European Commission agrees, patients with congenital antithrombin deficiency, a clotting disorder, may soon receive the drug.

Produced by U.S. company GTC Biotherapeutics Inc., the drug initially received a no-go from EMEA because the study's sample size was too small. At the company's request, EMEA reconsidered and accepted data from previously excluded trial patients. EMEA declared on 1 June that the benefits of ATryn outweighed the risks, and the final go-ahead is expected in 3 months. But some researchers have expressed concern about the scanty data offered to support the decision. **–ELISABETH PAIN**

House Panel to Bush: Math Later

A new $250 million push by the White House to strengthen mathematics for elementary and middle school students appears doomed this year after a House panel zeroed it out of a 2007 spending bill for the Department of Education (ED).

Dubbed Math Now, the initiative was to be the centerpiece of a $412 million request to improve math and science education that is part of the president's broader American Competitiveness Initiative. But legislators decided to put off the program while an ED-funded panel, launched last month, studies the effectiveness of various math curricula (*Science*, 19 May, p. 982). "It made more sense to wait until the panel has finished," says a congressional aide. The spending panel provided only $97 million for ED's share of the competitiveness initiative.

Education lobbyists don't expect any more support in the Senate. "I got the sense several weeks ago that it was a lost cause this year," says Ken Krehbiel of the National Council of Teachers of Mathematics. At the same time, however, legislators added $42 million to the president's $183 million request for the Mathematics and Science Partnerships, a state block-grant program for precollege math and science education. **–JEFFREY MERVIS**

AGRICULTURE

A Kinder, Gentler Jeremy Rifkin Endorses Biotech, or Does He?

For years, activist Jeremy Rifkin was the bête noire of biotechnology. Beginning in 1983, he filed several lawsuits to block field trials of genetically modified (GM) organisms and grabbed headlines around the world. Rifkin, an economist who runs the nonprofit Foundation on Economic Trends in Washington, D.C., said such actions were necessary to force an insulated research world to confront pressing ethical questions. To many in the scientific community, however, Rifkin was simply fanning irrational fears about biotechnology. A headline of a 1989 *Time* magazine profile called him "The Most Hated Man in Science" and captured the prevailing sentiment.

After a decade and a half of protests and campaigns to ban GM crops, Rifkin largely moved on to other topics, such as commerce, European politics, and hydrogen fuel. But now Rifkin, 61, is jumping back into agricultural biotech—this time, as a promoter. "This is an amazing twist for Jeremy Rifkin," says Susan McCouch, a rice geneticist at Cornell University. "I've never seen the man come out in favor of anything." But, like many others, she doubts his support will make much difference, as he is endorsing a biotech approach, known as marker-assisted selection (MAS), that is already well accepted.

In a white paper posted to his organization's Web site* this week, Rifkin says MAS offers all the advantages of new genomic science without what he calls the great risks to human health and the environment posed by GM crops. Instead of transferring genes from one species to another, MAS simply speeds and improves traditional plant breeding. Researchers search through maps of a plant's genome for sequence markers that are consistently associated with desired traits such as improved yield or disease resistance. Those markers can then be used to screen breeding stock and the progeny of traditional crosses even before they are grown or planted in the field.

Rifkin touts MAS as a path toward cheaper organic food and more sustainable agriculture. And to ensure that all reap its benefits, he advocates that MAS be used in a patent-free, or "open source," system in which the genetic information and techniques used to assist breeding are freely exchanged. "It's not enough to know what you're against. … This paper is my effort to try to frame an opportunity to move into a new age for agriculture," says Rifkin, whose immediate goal is to "open a conversation" with scientists, industry, and policymakers about the future of MAS.

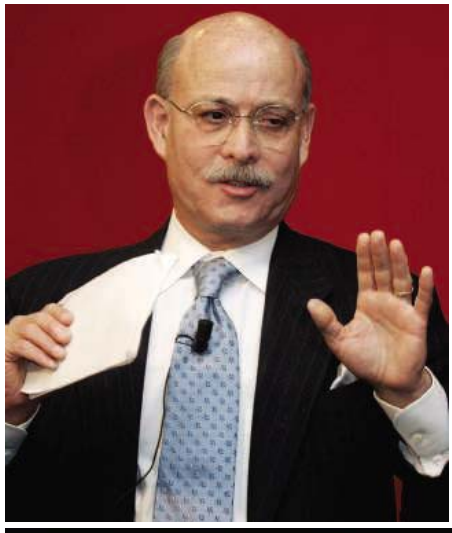

Advocate. To some researchers' surprise, a new report by Jeremy Rifkin endorses genomics for crop breeding, as shown here with soybean DNA.

Greenpeace and other advocacy groups, which have already come out in favor of MAS, say they welcome the move. But many scientists suspect that Rifkin's newfound enthusiasm for MAS is just a subterfuge for another attack on transgenic modification of crops. "This tract is typical Rifkin material," says Alan McHughen of the University of California, Riverside. "He still twists information to fit his agenda." Rifkin does indeed argue that GM crops should be phased out. He claims that few crops have been improved by transgenic modification—"it's primitive science" he says—and, to make matters worse, contamination of wild relatives by transgenes may complicate the process of MAS, he warns.

As Rifkin describes it, his conversion was gradual. After following MAS for some time, he says he realized last year that it had eclipsed transgenic technology in its potential. MAS certainly has provided an enormous boost to breeders, and the pace has accelerated as ever more DNA is sequenced and as genetic screens have become cheaper and faster. Although scientists and companies share Rifkin's enthusiasm for MAS and predict it will become even more powerful, they disagree that transgenic technology has failed or that MAS has somehow rendered it obsolete. "To say that marker-assisted breeding will replace biotech is simply wrong," says Roger Beachy, who directs the Donald Danforth Plant Science Center in St. Louis, Missouri. That's because of the enormous task facing plant breeders, says Mike Gale, an emeritus cereal geneticist at the John Innes Centre in Norwich, U.K.: "If we are going to produce enough food to feed the world, we need every tool in the toolbox."

McCouch agrees that gene splicing remains a crude approach—like adjusting an intricate watch with a sledgehammer. Yet, she and others say, it is the only way forward in some cases—for instance, if a gene for a particular trait can't be found in a crop or its wild relatives. The classic example is Bt, a toxin from a soil bacterium that was added to corn to provide broad and powerful protection against lepidopteran insects. Now companies are working to add genes for omega-3 fatty acids into soybean, to make the oil more healthful. "Those genes don't exist in soybeans at all," says David Fischoff, head of technology strategy and development at the Monsanto Co. in St. Louis, Missouri.

Nor is transgenic technology inherently risky, scientists say. "It is the gene and the management of the crop that make the difference and not the technology used to develop them," says Les Firbank of the Centre for Ecology and Hydrology in Lancaster, U.K.

Rifkin's concerns aren't just biological. He couples his endorsement of MAS with a few caveats about policy, as well. He wants to be sure the technology is used in a way that meets his broader goals of sustainable agriculture and open-source technology—in other words, no patents. "We've seen too much how the patent system restricts the ▶

* www.foet.org

CREDITS (TOP TO BOTTOM): PIERRE VERDY/AFP/GETTY IMAGES; PIONEER HI-BRED INTERNATIONAL INC.

cooperative nature in science," he says. Charles Benbrook, a scientist with the Organic Center in Enterprise, Oregon, agrees that tight constraints on intellectual property are a concern, as ever more technology and markers are locked up in company labs. "I worry that marker-assisted breeding is not going to be able to deliver on its potential."

Although Rifkin stops short of calling for an overhaul of patent law, he predicts that genetic technology and genomic information will eventually make it so easy and cheap to produce germ plasm that companies will have to make profits by selling agroecological consulting to farmers. Rifkin says he plans to start actively hawking his message on the lecture circuit and in his advice to business leaders and governments. "This is what I'm going to hammer away on: MAS should be phased in on the condition of an agroecological approach and open source."

Rifkin's pleas aside, Monsanto and other agribusiness companies contacted by *Science* don't plan to drop their GM research or stop seeking patents. And several in the scientific community say they don't need Rifkin's help promoting a field that's already flourishing. "Having the endorsement of Jeremy Rifkin means nothing," says Martina Newell-McGloughlin, director of the University of California's Biotechnology Research and Education Program in Davis. She and others doubt that any conversation with Rifkin would be productive. "Let's just ignore the man," says Gale. "Let's get on with the job we have, which is to feed the world." But whether or not Rifkin succeeds in opening the conversation he desires, he no doubt will keep talking.

–ERIK STOKSTAD

PALEONTOLOGY

Fossil Embryos Hint at Early Start for Complex Development

Evidence of the earliest animals on Earth dates back about 700 million years. But the arrival time of more complex animals—those with mirror symmetry and digestive tracts, known as bilaterians—has remained a mystery.

Now, on page 1644, an international team of paleontologists says it has isolated hundreds of fossil embryos that resemble those of modern bilaterians such as annelids and mollusks. If they check out, it could mean that a wide array of complex animals existed tens of millions of years before the "Cambrian explosion"—the time when paleontologists think hard-bodied animals proliferated as their ecosystems took shape. Precambrian animals have been notoriously difficult to find and study because their fragile bodies likely did not fossilize well. "I'm delighted to see a paper like this because it suggests there's more to look for out there," says Rudolf Raff of Indiana University in Bloomington.

Two years ago, Jun-Yuan Chen of Nanjing University in China and colleagues described fossils with bilaterian features in *Science* (9 July 2004, p. 218). The find, uncovered in 580-million- to 600-million-year-old rocks in the Doushantuo deposit in China's Guizhou Province, drew fire from paleontologists who suggested that the small, almost featureless "fossils" were actually layers of minerals. The latest discovery comes from the same rocks, but this time Chen's team has unearthed what appear to be fossil embryos bearing hallmarks of bilaterian embryos. If they are bilaterians, says Jon Mallatt of Washington State University in Pullman, it would mean these complex animals existed 40 million years earlier than current evidence suggests.

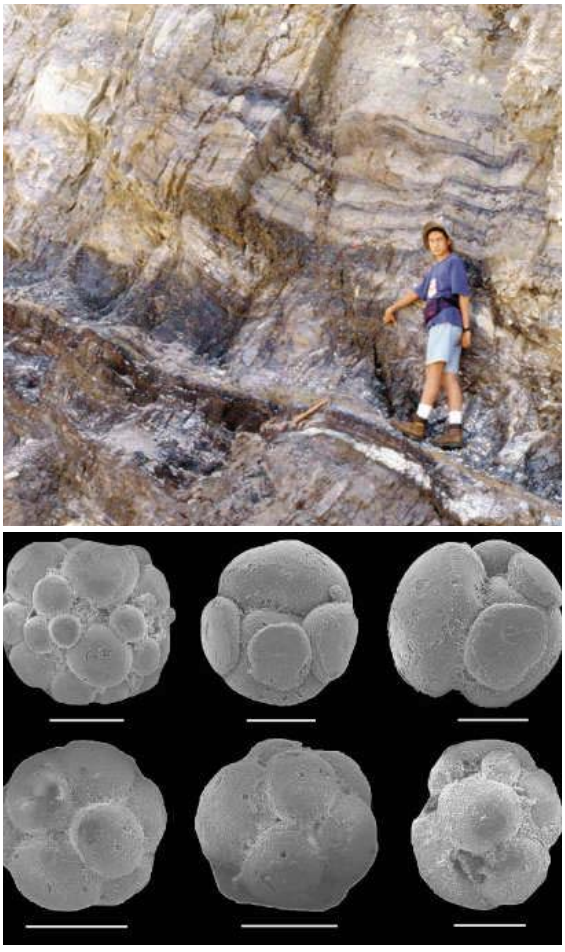

Lumps of life. Lobed fossils removed from Precambrian rocks in China suggest that complex life forms evolved earlier than previously thought. (Scale bar: 250 micrometers.)

CREDITS: JUN-YUAN CHEN

The researchers say the fossil embryos sport so-called polar lobes, asymmetrical bulges that allow bilaterian embryos to form different tissues in adults. The fossil embryos appear to be in different stages of development: Some have three lobes and some five; some have lobes of equal shape, and some are more lopsided. Chen and colleagues isolated the fossils by dissolving away surrounding rock with acid, then examined them under a scanning electron microscope. The researchers say the relative volumes of the spherical lobes are too regular for the fossils to be unrelated embryos or inorganic lumps of rock stuck together.

Some scientists are reluctant to give the fossils their unequivocal endorsement. Nicholas Holland, an invertebrate zoologist at the University of California, San Diego, notes that the specimens show a few "slightly bothersome" differences from other bilaterian embryos. "A lot of critters that make polar lobes have reasonably small eggs, around 200 microns," says Holland, whereas many of the Doushantuo embryos are as much as five times bigger.

Douglas Erwin of the National Museum of Natural History in Washington, D.C., cautions that the embryos' small size makes it hard for scientists to tell organic structures from mineral deposits and other preservation-related artifacts. "If you have a dinosaur bone, it's easy to tell what's bone or what's not," he says. "The closer you look, the harder it is to tell what the original bone structure is." The fossils also lack some characteristics of known annelids and mollusks, Erwin says, although the embryos could represent an extinct lineage of bilaterian.

Just knowing that complex animals existed 580 million years ago would help scientists better understand biodiversity before the Cambrian Period, says Ronald Jenner of the University of Bath in the United Kingdom. If the bilaterians were there, then the "basic branches of the animal kingdom [had] already been established at this point," Jenner says, as indirect evidence from modern animals' genes has suggested.

–KATHERINE UNGER

Planetary scientists are looking for a safe but interesting place to land the next Mars rover, but their track record lately is only one for two in finding both safety and the desired science

In Search of the Red Planet's Sweet Spot

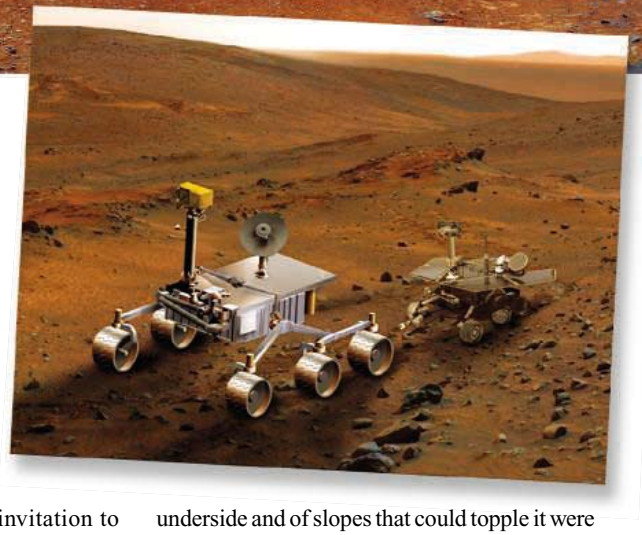

PASADENA, CALIFORNIA—The first time scientists landed a spacecraft on Mars, it was—by necessity—pretty much a matter of throwing darts. Who knew in 1977 where it would be safe, much less scientifically fruitful, for Viking to set down? Five safe landings and terabytes of new data later, planetary scientists gathered here at the end of May* to begin the search for the next martian landing site. This time, they're shooting for the bull's-eye: a single spot where a record of a warm, watery, and habitable Mars has been preserved for billions of years. With luck, they could find traces of early martian life as well.

So far, Mars researchers have a perfect record of identifying safe landing sites. Knowing where the most interesting geology lies has been another matter. In 2004, a "mineralogical beacon" found in data from an orbiting spectrograph drew the Opportunity rover to the flat expanses of Meridiani Planum, where it found the remnants of ancient salty lakes. But Opportunity's sister rover Spirit, landing on what to many researchers looked like an ancient lakebed, found instead a barren lava flow.

When selecting a landing site by "combining geomorphology [terrain features] and mineralogy, you get a slam dunk," planetary geologist James Rice of Arizona State University in Tempe told the workshop, "but that's hard to do on Mars." So hard, said planetary mapper Timothy Parker of the Jet Propulsion Laboratory (JPL) here in Pasadena, that, despite redoubled efforts to get it right this time, "our preconceived notions may be completely wrong when we get to the ground."

To avoid such an unpleasant surprise when the $1.5 billion roving Mars Science Laboratory (MSL) lands in 2010, workshop attendees helped begin a 3-year process to select a safe and scientifically productive landing site. More than 120 researchers responded—most at their own expense—to the agency's open invitation to the first of four workshops for community input. To judge by the 35 sites they proposed and initially ranked in this round, experts disagree drastically about the best sort of place to invest NASA's $1.5 billion. Three years won't be too long to whittle 35 down to one.

Mixed record

Participants started by reviewing the track record of past site selections. In the earliest Mars missions, all agreed, scientists choosing where to land enjoyed a fair measure of luck. They picked spots for the two Viking landers on the basis of the relatively fuzzy images being returned by the two Viking orbiters; it was a matter of "the blind leading the blind," said planetary geologist Matthew Golombek of JPL, co-chair of NASA's Landing Site Steering Committee. Predictions of the number and size of unseen rocks that could crush a lander's underside and of slopes that could topple it were "incorrect in every regard," said Golombek.

By the time NASA's Mars Pathfinder mission touched down in 1997, far more abundant observations made site selection a more rational process; lander observations bore out scientists' safety-related predictions for the first time. On the science side, researchers found their rock-strewn floodplain seen from orbit, the same sort of terrain the Vikings had landed on. Unfortunately, the rocks were more monotonous and less informative than hoped.

When it came time for the Mars Exploration Rover (MER) mission—Opportunity and Spirit—"predictions for safety were right on the mark," said Golombek, but that "was not necessarily the case for the science." Opportunity found water-formed hematite, as predicted from orbital spectroscopy. But contrary to what many experts expected, the hematite had formed not on a lake bottom conducive to life but in briny,

CREDITS: NASA/JPL-CALTECH

* First Landing Site Workshop for the 2009 Mars Science Laboratory, 31 May–2 June, sponsored by the NASA-appointed Landing Site Steering Committee and the MSL Project.

Finally. The MSL rover (*left*) will be the first one able to land within striking distance of rugged outcrops. The smaller MER rover (*inset*, with MSL) had less dramatic targets.

highly acidic groundwaters. Water had flowed on the surface at times, but for the most part, that area of Mars more than 3 billion years ago was salty dune after salty dune. Still, most researchers regard the Opportunity site selection as a complete success; they went looking for signs of water on early Mars, and they found them.

Not so the selection of Gusev crater for Spirit. Out of 155 sites on the original list, most proved fatally flawed: too windy for landing, too dusty to do geology, too many big rocks, not enough space to land, and on and on. The final four sites included an ultrasafe backup site considered by many to be too boring for words and another with little promise of the sought-after signs of water (*Science*, 10 May 2002, p. 1006). Gusev, however, looked like a plum. Orbital imaging convinced many experts that floodwaters had once gushed through the crater rim to fill a lake several hundred meters deep.

On Spirit's arrival, however, the crater floor proved achingly boring: in the words of one team member, a "basalt prison" of impact-pulverized lava that for eons had seen no more than a touch of dampness (*Science*, 9 April 2004, p. 197). When the long-lived Spirit gained the nearby Columbia Hills, it did find a jumble of water-altered volcanic or impact rock, but that rock's story has proved so complex it has yet to be deciphered.

The MSL solution

With MSL, researchers are intent on avoiding another Gusev. Last time, "we had the luxury of two rovers," noted Rice. "We've only got one shot with this one." That's because NASA is going for broke with a single massive rover capable not only of assessing formerly wet environments but also of recognizing markers of past life, such as organic matter containing a distinctive mix of isotopes. The mission will focus on "habitability," the potential of an environment to support life, past or present. MSL will carry 16 times the instrument payload of Opportunity or Spirit, including everything from a subsurface-ice detector to a rock-zapping laser for analyzing elements from afar.

MSL is also dramatically more capable than the MER rovers in getting where its makers really want it to go. The MER rover entry capsules smashed into the martian atmosphere like bullets, slowing until a parachute could be opened to ease the rest of the descent. With such uncontrolled entry and descent, engineers had to assume the lander could end up anywhere in a narrow 100-kilometer-long landing ellipse on the surface. The solar-powered MER rovers were designed to last 90 days, during which they would travel at least 600 meters each.

MSL, on the other hand, will have the time and energy to explore much farther afield and even investigate "go-to" targets beyond its landing zone. Its entry capsule will sense any high-altitude buffeting and adjust course, shrinking the landing ellipse to a 20-kilometer circle. Once on the ground, a radioisotope thermoelectric generator—unlike MER solar panels, a steady, predictable energy source—will power MSL to a design lifetime of 2 years and a range of at least 20 kilometers. It could thus land in a small, safe landing zone and drive off at top speed to a target too rugged for landing. In addition, it can land in the thin air of higher altitudes and operate at much higher, colder latitudes than the MER rovers could.

Where to?

So, exactly where should NASA send its souped-up rover? Scientists at the workshop saw prospects for habitability in a bewildering array of geologic settings, from valleys, canyons, and gullies to craters, plains, and basins. Usually, signs that water had shaped the landscape or altered the rock drew them to a site. If the rock were layered—presumably sediments laid down by water a layer at a time—all the better. And, of course, the site should be safe for landing or at least reachable from a safe landing zone.

A half-dozen speakers favored sites on or around Meridiani Planum, the plain where the Opportunity rover is still driving on top of an 800-meter-thick stack of layered, sulfate-rich sediments laid down by wind and water about 4 billion years ago. These Meridiani strata presumably record changing environmental conditions over a sizable chunk of martian time and space. But Opportunity has inspected only the top 10 meters of the 800 meters of record where it was exposed in a smallish impact crater. By roving up the plateau's sides hundreds of kilometers from Opportunity, MSL has "the potential to tell a much bigger-picture story" than if it visits smaller, layered deposits, said planetary geologist Michael Malin of Malin Space Science Systems in San Diego, California.

Meridiani clearly would satisfy the stratum lust of any red-blooded geologist, but some still had reservations. "We've been there," says Rice. "Let's go somewhere new." One minus was Meridiani's geologic history.

A hit. The MER Opportunity rover (here inserted into an image of Burns Cliff) found layered deposits laid down by wind and water, as predicted from orbital spectroscopic data.

Acid brine would not have been the friendliest habitat for life, and on Earth, rocks left behind by evaporated saltwater tend to harbor little organic matter. Some Meridiani sites also looked dusty enough to cloak any interesting geochemistry. When attendees voted to give high, medium, or low priorities for targeting orbital observations in the coming year, only one Meridiani site—just outside the northern margin of the plateau—made the top 10, coming in at number eight.

A more popular destination proved to be light-toned layered deposits: banded, presumably sedimentary deposits exposed in canyons, craters, and other protected depressions. Researchers suspect that at least some such deposits formed beneath standing water, and orbital spectroscopy has shown that some are composed of water-related sulfates or clays.

In 160-kilometer Gale crater just south of the equator, the layers form a mound in the middle of the crater floor. The Gale mound was a popular proposed MER target, but engineers could not fit a landing ellipse on the adjacent crater floor. Now some scientists—including planetary scientist James Bell of

A miss. On landing, the MER Spirit rover found a pulverized lava flow, not the hoped-for lakebed.

CREDITS: NASA/JPL-CALTECH/CORNELL

Cornell University—want to try again. The 5-kilometer-high stack of 10-meter beds "is one pretty enigmatic feature," Bell said. Whatever process formed the mound "permeates all of Mars studies," he added. "It's an enigma in our present understanding."

Skeptics, however, wonder whether Gale might be too scientifically risky. "You use 'enigma' a lot," said Carlton Allen, curator of astromaterials at NASA's Johnson Space Center in Houston, Texas. "This is a one-shot, billion-dollar mission, and you're talking about going to a place [that] we have severe questions about how it formed." Bell conceded that no one "knows for sure" whether the Gale mound deposits are lake sediments, volcanic ash fall, or windblown dust. In the priority voting, curiosity won out over caution. Gale came in sixth, and three other light-toned deposits ranked in the top 10.

Certain water

Toward the safe end of the science-risk spectrum fall ancient crater lakes such as Eberswalde crater in the southern subtropical latitudes. There, an irrefutable river delta pushes into the crater complete with meandering channels and oxbow river bends. "Eberswalde is *the* science target" for MSL, says Rice, because a delta means water—and sediment—flowed into standing water in the crater. Any clayey sediments of the delta would have acted like magnets for the much-sought-after organic matter. But even Eberswalde's advocates were quick to point out that there isn't much room for even a 20-kilometer landing zone in Eberswalde. Two other proposed craters—Holden and Terby—show less dramatic evidence of having held lakes but offer more room for a safe landing.

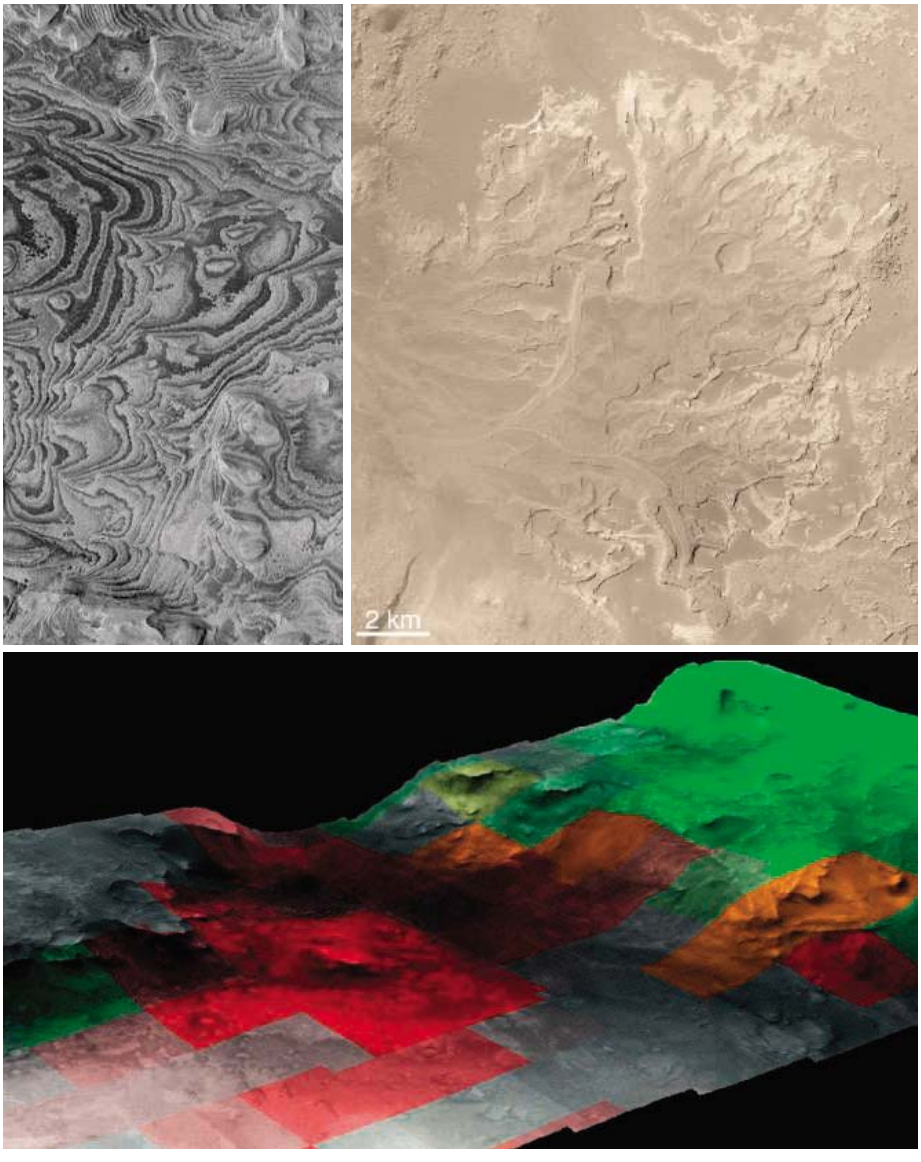

So many choices. Questions linger over selection of the MSL landing site. Did water lay down the light-toned layered terrain (*upper left*)? What is the Eberswalde crater's river delta (*upper right*) made of? Are the winds over Nili Fossae trough's clays (red) too high for a safe landing?

Craters in general, however, suffer from a serious drawback: wind. At the workshop, atmospheric modelers Scot Rafkin and Timothy Michaels of Southwest Research Institute in Boulder, Colorado, reported on their preliminary modeling of winds around Mars. "Mars is a windy place," said Rafkin. "There are good parts of Mars that won't be usable."

In planning for the MER mission, engineers had to eliminate some otherwise attractive sites—such as Melas Chasma, a side canyon to the great Valles Marineris—when computer simulations predicted that overlying winds could be too fast for a safe descent. Gusev just squeaked by. Craters and canyons, Rafkin said, can create small-scale winds fierce enough to overwhelm larger-scale winds. "So it's going to be like MER," said Rafkin. That was bad news, responded planetary geologist Jeffrey Moore of NASA's Ames Research Center in Mountain View, California. He called the MER selection "the slaughter of the landing sites." Undaunted, voters at the workshop put all three proposed craters in the top five.

The right water

Once-watery craters might be fine for geologists, but spectroscopists in the crowd—who think about composition before geology—argued that mineralogical composition should be getting more attention. Spectroscopist Jean-Pierre Bibring of the University of Paris–South in Orsay made a pitch for targeting minerals that have been altered by water. "We have to go to hydrated minerals," he said. They show that water didn't just pass by but lingered long enough to alter mineral chemistry.

And not just any water-bearing minerals will do. Bibring, who heads the OMEGA spectrometer team on the European Mars Express orbiter, argued from OMEGA observations that life-friendly clays had formed before the acid-generated sulfates of Meridiani and elsewhere. If life ever appeared on Mars, he said, the clay era would be the likeliest time for it. But clays haven't shown up in deltas yet, so MSL should be targeted where clays are found: in the walls of Nili Fossae trough or in Marwth Vallis, although both may be liable to high winds. The two clayey sites finished tied for first and fourth, respectively.

All 35 proposed sites will eventually get a close look during the next 16 months. Glacierlike features in the extreme south, dust-smothered outcrops, and seemingly barren rock piles will be targeted by the Mars Reconnaissance Orbiter (MRO), which is now trimming its orbit for a November start of operations. MRO will be able to image the smallest of the dangerous rocks and detect even small areas of interesting minerals. Mars Express may also join in. It can refine the steepness of slopes that MSL must deal with. Come the next community workshop in October 2007, researchers must be ready to slash their wish list to the top dozen.

–RICHARD A. KERR

CREDITS: (TOP LEFT AND RIGHT) NASA/JPL/MALIN SPACE SCIENCE SYSTEMS; OMEGA/ESA AND THEMIS PUBLIC DATA RELEASE

ORNITHOLOGY

Vulture Research Soars as the Scavengers' Numbers Decline

A catastrophic die-off of vultures in South Asia and recent sharp declines in some populations in Africa have focused research on this often reviled but majestic bird

BRITS, SOUTH AFRICA—Awkwardly flapping their injured wings, a half-dozen rescued vultures hunch their long necks and cower in a corner when a visitor walks into their enclosure. "They may look mean, but they are gentle and intelligent birds," says Director Kerry Wolter of the Vulture Unit at the De Wildt Cheetah and Wildlife Centre in South Africa's North West Province. "Just keep your fingers away from their beaks."

It's hard to warm to vultures, quintessential scavengers that gorge themselves on carrion and are the butt of office jokes and Gary Larsen cartoons. But these particular African white-backed vultures—all victims of power-line collisions—have earned a place in scientists' hearts. Following a drastic die-off of vultures in South Asia over the past decade, the birds here have served as sentinels in a research project that aims to shed new light on the crisis in Asia and help prevent similar losses in Africa. "This pool of research birds—injured vultures that could not be reintroduced into the wild—is crucial to the project," says University of Pretoria veterinary pharmacologist Gerald E. Swan.

Two years ago, scientists reported that an anti-inflammatory drug used in cattle called diclofenac was responsible for most of the vulture deaths in Asia, but not before about 97% of three species in the region had been lost. The crisis has, however, sparked a renaissance in the study of vultures. Scientists are investigating the birds' habits, physiology, and vulnerabilities to chemicals, as well as their role in transmitting infectious diseases. In West Africa, investigators are trying to determine the extent of vulture killings for traditional medicine and food. In Israel, researchers use satellite tracking to monitor vultures' movements. In Namibia, experts want to determine the role of vultures in the transmission of anthrax. Spanish researchers are counting vultures killed by wind-energy turbines. And conservationists in Africa, Asia, the Middle East, and part of Europe are establishing sanctuaries, "vulture restaurants," and monitoring campaigns.

There is much to admire about vultures. They are as graceful in the air as they are awkward on the ground, soaring in rising air currents to astonishing heights (one jet collided with a vulture at 10,000 meters) over a wide-ranging territory, and they use their sharp eyesight to spot any sign of carcasses far below. For millennia, vultures and humans have had a love-hate relationship. The ancient Egyptians worshipped the birds, pastoralist tribes revered them for finding dead cattle, and shamans attribute the sharp-eyed scavengers with clairvoyance. Members of the Parsee religion in India do not believe in burying or burning their dead; instead, they leave them out for vultures to consume. For others, vultures' prompt arrival at scenes of death, and their enthusiasm for decaying meat only causes revulsion.

Despite this human ambivalence, the sudden death of large numbers of birds in Asia caused alarm. Munir Virani, a Nairobi-based conservation biologist who coordinates the Peregrine Fund's Asian Vulture Population Project, says, "Three of the five breeding colonies of the Oriental white-backed vultures in Pakistan are now extinct," with only about 75 breeding pairs in the remaining two colonies, as compared to 3500 pairs just 6 years ago.

Although diclofenac was fingered as the culprit 2 years ago (*Science*, 8 October 2004, p. 223), India did not immediately ban its use. Swan helped lead a study to find an alternative cattle drug, and earlier this year his team and colleagues in India and the United Kingdom reported that the substitute drug, meloxicam, does not harm white-backed vultures (*Science*, 3 February, p. 587). India banned the manufacture and sale of diclofenac last month; Pakistan, however, has yet to follow suit. Pretoria researchers are now investigating the impact of other veterinary drugs on vultures, as well as diclofenac's mechanism in killing the birds.

Fetishes and poison

Although the African vulture situation is not as bad as South Asia's, populations of some species are dropping sharply. "Vultures are at the top of the food chain, so if their numbers are declining, it is a sign that something is off balance," says "vulturephile" ornithologist Mark D. Anderson, who is based in Kimberley, South Africa, and is editor of *Vulture News*. He says that the use of anti-inflammatory drugs in livestock is far less common in Africa than in South Asia, but he worries that other drugs and poisons may be killing vultures and other scavengers.

The biggest problem is in West Africa, where ornithologist Guy Rondeau says, "We are seeing vulture declines comparable to South Asia." A 2005 survey supported by the Critical Ecosystem Partnership Fund in Washington, D.C., found that vulture populations in rural areas of eight West African countries had decreased by about 95% since the early 1970s. In his work for the conservation group Africa

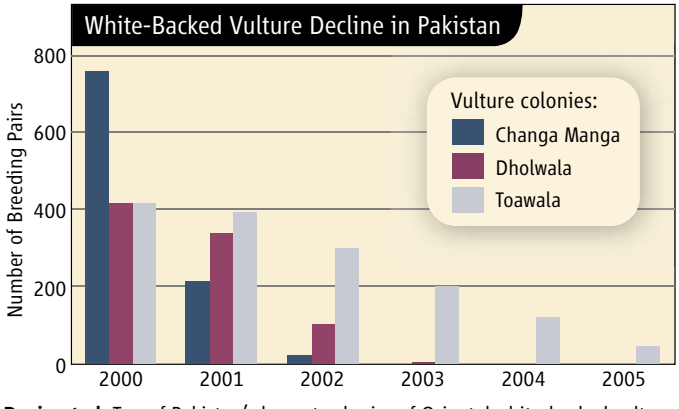

Decimated. Two of Pakistan's largest colonies of Oriental white-backed vultures (Changa Manga and Dholwala) have been wiped out since 2000.

CREDITS (TOP TO BOTTOM): R. KOENIG; SOUCE: THE PEREGRINE FUND

Nature International in Côte d'Ivoire, Rondeau is helping organize vulture sanctuaries in the few areas that still have significant vulture populations, including sites in Mali and Guinea.

The causes of the decline in Africa are many. Some farmers, aiming to control other scavengers and predators such as jackals and hyenas, lay out deliberately poisoned carcasses, and vultures become the unintended victims. "One poisoned carcass can kill a huge number of vultures," says Virani, citing a Kenyan case in which 187 vultures perished after feeding on a cow carcass and four poisoned hyenas.

Other than that, Rondeau says, the main threats in West Africa are "hunting for fetishism, *muti* [traditional medicines], and, more recently, for meat." Stalls in some African markets sell desiccated vulture parts—heads, talons, feathers, eyes, and hearts—for traditional medicine or fetishes. In other areas, smoked vulture meat is traded, and live vultures are exported abroad. In parts of South Africa, a similar vulture trade has flourished with the advent of the National Lottery, because some parts are considered lucky charms, says Steve McKean, an ecologist with KwaZulu-Natal province's wildlife department.

Dried out. A market in Mali offers desiccated vulture heads and feet for sale. Some Africans believe vultures have powers of clairvoyance.

To help find better ways to protect vultures, researchers are trying to get to know them better. In Namibia, Maria Diekmann of the Rare and Endangered Species Trust has used satellite tracking to follow the path of vultures. "One of them flew more than 500 kilometers a day, ranging over four different countries," she says. Namibia's population of Cape vultures, estimated at 2000 in the 1950s, was down to 25 birds this spring, including 13 "repopulated" from South Africa.

The satellite-tracking technology came from scientists in Israel, who have been monitoring that nation's dwindling vulture population since the 1980s. Ohad Hatzofe, an avian ecologist with Israel's Nature and National Parks Protection Authority in Jerusalem, says, "It took only one Griffon vulture with a VHF tag to open our eyes to how ignorant we and the scientific community were" about vulture habits. The telemetry data helped scientists learn the birds' movement patterns and decide where to establish vulture feeding sites; it also gave insight into the factors that are endangering local and migrating vultures.

At the Vulture Unit, Wolter employs cellphone transmitters and a new wing-tag system to track Cape vultures (also known as Cape Griffons) released into the wild. The numbered yellow tags are part of a wider monitoring project coordinated by the Endangered Wildlife Trust's Birds of Prey Working Group in Parkview, managed by raptor conservationist André Botha. On a recent morning in the Magaliesberg mountains, Botha squinted into a telescope lens toward a Cape vulture colony on the rock ledges above, counting each occupied vulture nest and marking them on a laminated photo of the cliff's face. "These colonies have been getting smaller over the years," says Botha.

A hundred kilometers to the north, the Kransberg colony—once the world's largest for Cape vultures—has lost more than 300 nesting pairs over the last 2 decades and is now down to about 650 pairs, says Patrick Benson, who conducts research for the University of the Witwatersrand in Johannesburg. He has compiled a large collection of vulture bones and is completing an analysis of skeletal abnormalities that might give hints to the reasons why so many vultures are dying. He attributes the decline mainly to a loss of food sources, the deliberate poisoning of carcasses, and contact with poorly insulated wires. Other South African scientists are studying whether the growing elephant population in Kruger National Park is driving away vultures by destroying their nesting trees.

The continent's most threatened vulture species is the African bearded vulture, an uncharacteristically beautiful scavenger that inhabits mountainous areas. Kenya's population was down to three bearded vultures last year, and a survey by the South African province of KwaZulu-Natal's wildlife department indicated that its bearded vulture population is declining in the birds' main habitat, the Drakensberg mountains.

Disease carriers?

Some would see fewer vultures as a blessing. But Peter Mundy, a Zimbabwean ornithologist who wrote *The Vultures of Africa*, argues that the scavengers help prevent the spread of animal diseases, such as anthrax, by quickly devouring carcasses. Vultures can eat anthrax-infected flesh without apparent harm, studies have shown, but scientists are also looking into whether they distribute anthrax spores and other disease agents adhering to their feathers and feet over long distances, possibly resulting in the periodic spread of the disease.

Microbiologist Peter Turnbull is trying to learn whether and exactly how vultures are involved. After studying the ecology and epidemiology of anthrax outbreaks in Namibia's Etosha National Park for a quarter-century, Turnbull is now examining vulture blood serum to determine whether the birds spread the anthrax bacterium from one area to another "by dint of actually getting infected or only through mechanical carriage of spores" on their feathers and feet. Because it usually takes many spores to infect an animal with anthrax, he says, "it seems probable that spores deposited by vultures only rarely result in a case of the disease in another animal."

With vultures receiving so much scientific attention, some southern African bird groups are cautiously optimistic that the threatened populations will stabilize in the coming years. Conservation biologist Gerhard Verdoorn, who directs BirdLife South Africa, says fewer farmers are poisoning carcasses, and the birds are feeding at 200 vulture restaurants. South Africa's electric company is marking power lines and improving insulation in areas where vultures fly or roost. Verdoorn says the African white-back and some other vulture species seem to be holding their own for now but warns that "one carcass poisoning can wipe out an entire colony of vultures."

One factor that may bode well for the vultures' future is their dedication to parenthood. "They mate for life, they lay only one egg per year, and the mother and father share the nest duties," says Wolter, who cares for 77 vultures at the De Wildt sanctuary. "They are phenomenal parents."

–ROBERT KOENIG

CREDIT: GUY RONDEAU/AFRICA NATURE INTERNATIONAL

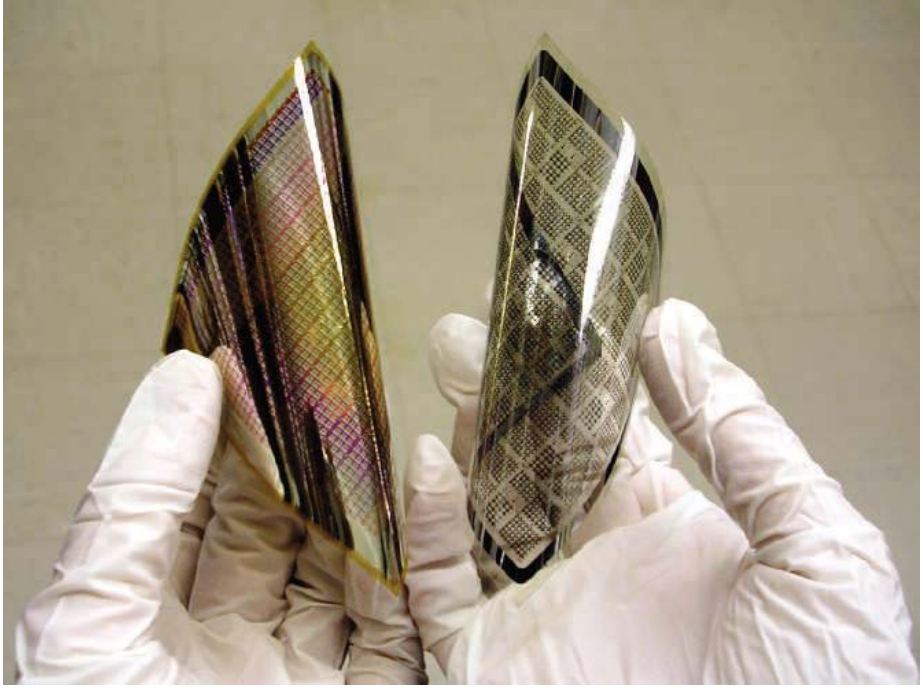

MATERIALS SCIENCE

Inorganic Electronics Begin to Flex Their Muscle

A dark-horse technology bids to overtake plastics in the race to make circuits that can twist and stretch

Like a desert mirage, the promise of organic electronics seems to shimmer always on the horizon. Plastic and other types of organics can form the backbone of electronic components that are cheap, thin, lightweight, and flexible, a combination that makes them sought after for applications as diverse as cheap solar cells and roll-up displays. Yet despite a few commercial successes such as small mobile phone displays, organic electronics have had trouble overcoming nagging problems, such as the slow speed at which electrical charges move through the devices and the fact that exposure to air often degrades their performance. Now, organics have something else to worry about: competition from more traditional inorganic electronics now being made to work on top of flexible materials.

In recent years, several research teams have shown that by making inorganic devices thin enough and layering them on flexible sheets of metal or plastic, they can create circuits that bend and flex much like organics. That approach has enabled researchers to take advantage of the high speed and reliability of inorganic devices and the decades of manufacturing experience that has made them the bedrock of the electronics industry. Now, the two technologies are poised to battle for new electronics applications, such as outfitting robots and medical prostheses with a human-like "skin" complete with flexible temperature and touch sensors. The number of researchers trying to marry inorganic electronic devices with flexible substrates remains a fraction of the crowd working on organic circuitry. "But it's picking up steam," says John Rogers, a flexible-electronics expert at the University of Illinois, Urbana-Champaign (UIUC).

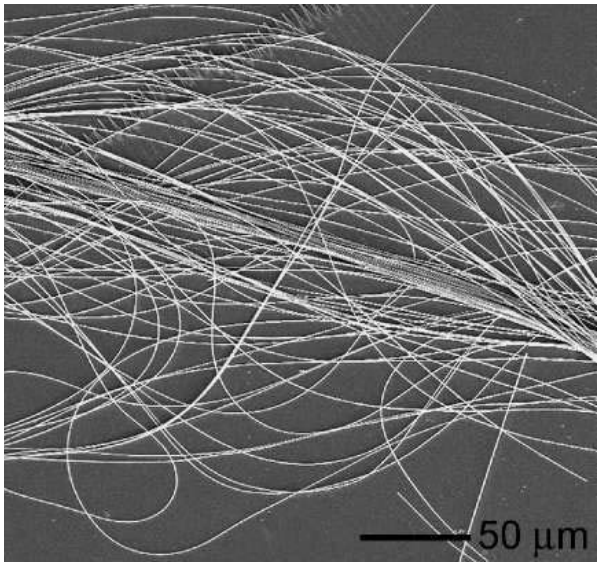

Bend me, shape me. Semiconducting wires from inorganic compounds such as gallium arsenide can form the heart of high-performance circuitry atop flexible substrates.

Researchers worked on thin inorganic electronic devices decades before organic electronics presented a challenge. Labs in the United States first made thin-film inorganic transistors in the 1960s, and today the devices are found everywhere from flat-panel televisions to solar cells. But the devices are still typically deposited on top of glass and other rigid substrates. When organic electronics first entered the picture 30 years ago, the new technology captured the imagination of many groups hoping to create devices atop curved surfaces as well as give electronics the ability to flex and bend. "In the late 1990s, there was a notion by materials and chemical companies that it would be easiest to go with all organics," says Sigurd Wagner, an electrical engineer at Princeton University. But although many successful prototype products have been developed, organics have proven challenging to turn into a robust and reliable manufacturing technology. "There are so many problems, [people] are returning to an inorganic transistor technology used in industry," Wagner says.

Not everybody is returning, of course, and those who make the switch have faced major hurdles. But several groups have recently been showcasing the kinds of things that can be done by putting inorganic electronics on flexible substrates.

The first challenge was to make a workable device at all. To lay down successive atom-thin layers of material, standard semiconductor technology starts by heating slabs of material to a vapor at several hundred degrees Celsius. The white-hot vapor then condenses atop the substrate at temperatures far higher than most flexible materials, such as plastics, can handle. To create usable circuits, researchers had to find ways to deposit those thin organic layers at temperatures only slightly above the boiling point of water.

In 2003, for example, Charles Lieber and colleagues at Harvard University reported in *Nano Letters* that they had deposited a 100-nanometer thin layer of conducting indium tin oxide (ITO) atop a plastic substrate and then patterned an initial set of "gate" electrodes in the ITO using either photolithography or electron beam lithography. The researchers then flowed a solution containing silicon nanowires over the electrodes, depositing the nanowires atop the electrodes when the solvent evaporates. Finally, another lithography step enabled them to pattern the additional metal electrodes needed to create thin-film transistors with a performance comparable to those grown atop crystalline silicon. That same year, Xiangfeng Duan and colleagues at

CREDITS (TOP TO BOTTOM): I-CHUN CHENG/PRINCETON UNIVERSITY; UIUC

the nanotechnology start-up company Nanosys in Palo Alto, California, reported in *Nature* a similar scheme for suspending inorganic silicon nanowires and cadmium-selenide nanoribbons in a solution and patterning them into thin-film transistors perched atop plastics and other flexible substrates. The speed of charges in those devices and the voltages at which they switched on and off easily outperformed organic devices.

More recently, researchers have started taking larger strides. Rogers and colleagues at UIUC and Wright-Patterson Air Force Base in Ohio, for example, reported in the 1 May issue of *Applied Physics Letters* that they had created ultrahigh-speed gallium arsenide (GaAs) transistors on cheap, flexible plastic substrates. To do so, the Illinois researchers initially fabricated GaAs wires from an inorganic wafer using conventional semiconductor manufacturing techniques. They then applied a thin layer of glue beneath the devices and used a stamping technique to place them atop a plastic film, with additional lithographic steps to create the needed electrodes. The final devices, Rogers's team reported, could switch on and off more than 1 billion times a second, far faster than organic devices and a speed that makes them candidates for use in high-speed communications equipment.

The newfound prowess of inorganic flexible electronics is also making them attractive for other potentially lucrative markets, such as displays that conform to car dashboards and other contoured surfaces. In December, for example, Wagner and former postdoctoral candidate Stephanie Lacour reported at the International Electron Devices Meeting in Washington, D.C., that they had fabricated amorphous silicon-based circuitry atop tiny islands of rigid silicon nitride. They placed the devices on a flexible substrate of silicone rubber and connected them with ultrathin flexible gold wires. Because both the substrate and the wires between the devices could flex, the researchers could use them to create the flexible equivalent of the electronic "backplane" that controls current liquid-crystal flat-screen displays.

Rogers and his Illinois team report a similar feat in this month's *IEEE Electron Device Letters*. They fabricated their circuitry out of ultrathin bendable single-crystalline silicon ribbons. They initially created the ribbons atop a rigid support called "silicon on insulator" (SOI). They then etched away the underlying support and used a printing technique to transfer the silicon ribbons to a flexible polyimide substrate. Finally, they used low-temperature computer chip patterning techniques to lay down the additional layers of metal and insulators needed to complete their circuitry. The result: circuits that performed nearly as well on a flexible substrate as those grown atop crystalline silicon wafers.

Rogers and his Illinois team also recently detailed an approach that could make inorganic electronics not only fast and flexible, but cheap as well. They set out to bring down the high cost of relying on wafers made from SOI, which can cost $300 each. In the 22 May issue of *Applied Physics Letters*, the Illinois researchers showed how to carry out the same process using standard bulk crystalline silicon wafers that cost only one-tenth as much as SOI wafers. Marrying conventional crystalline silicon with a flexible substrate "allows us to think about ways to put single-crystal silicon in places you couldn't before," Rogers says.

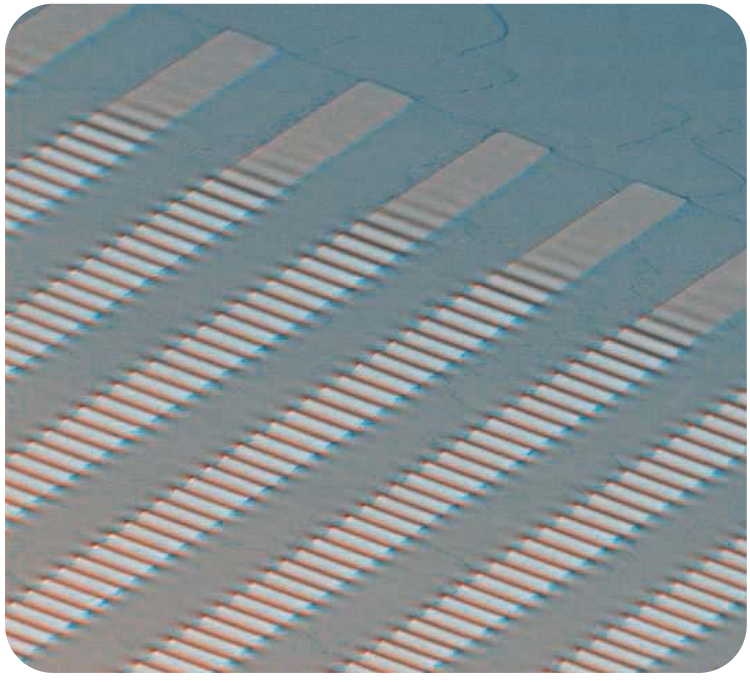

Next wave. Undulating ribbons of silicon atop a flexible substrate can be stretched without damage. Such stretchable semiconductors could pave the way for high-speed flexible circuitry in fabrics.

One of those new places could be in fabrics that not only flex but also stretch, a particularly challenging environment for electronics. Earlier this year, Rogers and a team of Illinois colleagues reported in *Science* (13 January, p. 208) that they had laid down thin silicon ribbons atop a stretched-out plastic sheet. When they then released the tension on the plastic, the sheet snapped back to its original shape, causing the silicon ribbons to buckle in regular waves. When the researchers then stretched the plastic back out again, the silicon ribbons elongated and continued to function normally as transistors. "It's a very powerful approach," says Lacour, who is now at Cambridge University in the United Kingdom. Since publication of their *Science* paper, Rogers says, the team has vastly increased the amount of stretching their devices can tolerate, extended the work to other types of inorganic materials, and allowed materials to stretch in all directions instead of just one.

Wagner and colleagues have also been looking to take inorganic electronics in new directions, such as integrating them with biological systems. Chunks of rocklike semiconductors aren't typically thought of as biocompatible. But the way they work can make them an ideal choice, Wagner explains. That's because unlike many organic devices, silicon and other standard inorganic semiconductors can be used to make devices that turn on and off with tiny amounts of applied voltage. That's critical, Wagner says, because when large voltages have to be applied they invariably dissipate power as heat. "You can't put them close to biological tissue because that raises the temperature too much," Wagner says.

In November, Wagner and colleagues at Princeton and at Columbia University reported at the IEEE Sensors Conference in Irvine, California, that they had made an array of stretchable silicon transistors atop a plastic substrate capable of recording the activity of brain neurons in vitro. The immediate goal of this ongoing project is to understand how neurons respond to rapid stretching, a petri dish analogy to what happens during a car crash or other types of brain trauma.

But Lacour is already planning to take the next step. At Cambridge, she is helping direct an effort to use flexible circuitry in regenerating severed nerves of accident victims. When nerves are severed, Lacour explains, they quickly die unless they receive consistent electrical inputs, as they would from sensory cells. So Lacour has created flexible gold electrodes on plastic that she hopes to use to integrate with regrowing tissue. By integrating transistors and sensors onto such circuitry, researchers may even be able to create prostheses that communicate touch and temperature to the body's nervous system much as a real limb does, Lacour says. With the progress in flexible inorganic electronics, it's a vision that's beginning to look more real all the time.

–ROBERT F. SERVICE

CREDIT: JOHN ROGERS/UIUC

EDITED BY YUDHIJIT BHATTACHARJEE

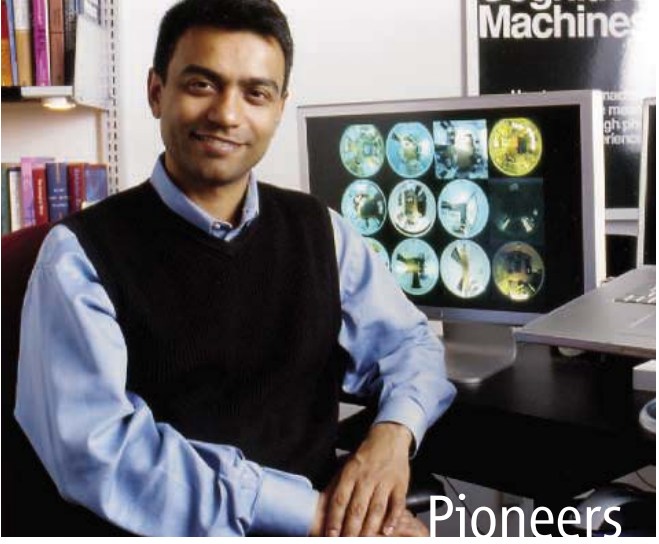

BABY CAM. Even the most doting parent would be put to shame by the amount of video and audio recordings that cognitive scientist Deb Roy (left) of the Massachusetts Institute of Technology in Cambridge is collecting on his 10-month-old son. But it's all in the name of science. Roy wants to understand how the boy acquires language, and he's rigged up 11 fisheye video cameras and 14 microphones at his home to monitor every sound and motion.

"We're primarily capturing the environment of the baby so we can feed that into a learning system on the computer," Roy says. The plan is to model how early words and grammar are learned.

Linguist Ray Dougherty of New York University worries that the amount of information generated by the project might be too much to analyze. "Children learn language on the basis of the smallest amount of data," he notes. The key is to figure out which pieces of data are important, he says.

AWARDS

KYOTO PRIZE. A Japanese mathematician, a U.S. immunologist, and a Japanese designer have won the 2006 Kyoto Prizes from the Inamori Foundation.

Hirotugu Akaike, 78, a researcher at the Institute of Statistical Mathematics in Tokyo, wins the basic sciences prize for work leading to the development of statistical models used in forecasting economic trends and natural phenomena. Leonard Herzenberg, 74, an immunologist and geneticist at Stanford University in California, receives the advanced technology prize for the flow cytometer, an instrument developed in the early 1970s for sorting different types of cells that has been a boon for regenerative medicine. Japan's Issey Miyake, 68, is the winner of the arts and philosophy prize for creating clothes that don't lose form while allowing unrestricted body movement.

Each winner will take home a gold medal and $446,000.

MOVERS

CHANGE AT WOODS HOLE. Robert Gagosian is stepping down as head of the Woods Hole Oceanographic Institution (WHOI) in Massachusetts. The 61-year-old marine geochemist, who has led WHOI since 1994, plans to devote himself to raising the "visibility of the ocean sciences, nationally and internationally."

Since 2000, Gagosian has helped create four ocean institutes, launched a new coastal research vessel, got funding to replace WHOI's 42-year-old research submarine *Alvin*, and raised $150 million.

Executive vice president James Luyten will take over as acting director when Gagosian steps down next month.

A LIFE IN SCIENCE

THE VALUE OF RESEARCH. Molecular biologist Anita Roberts, who studied the role of TGF-β in the progression of cancer and wound healing, died of gastric cancer at her home in Bethesda, Maryland, on 26 May. She was 64.

A researcher at the National Cancer Institute, Roberts wrote extensively about her experiences as a patient (www.anitaroberts.net/blog). She offered this insight in an interview for the spring 2006 issue of *CR*, a publication of the American Association of Cancer Research: "When I was first diagnosed with this cancer, I was so angry about my research. I thought: 'What have I been doing for 25 years? Who cares what compound binds to what piece of DNA?' That lasted about a week. Then I realized we now have drugs based on what we understand from our basic research."

They Said It

"I haven't done any conquering, per se."
—University of Miami, Florida, accounting professor Thomas Robinson, quoted in the *Miami Herald* last week after a British gene-testing company identified him as a descendent of the Mongolian warrior Genghis Khan.

Got a tip for this page? E-mail people@aaas.org

Three Q's >>

Simon "Pete" Worden, the new director of NASA's Ames Research Center at Moffett Field, California, was once called Darth Vader for his advocacy of missile defense as an Air Force colonel. He also championed the Pentagon's successful Clementine mission to the moon before retiring from the Air Force in 2003. An astronomer by training, the 56-year-old Worden is an old friend of NASA chief Michael Griffin.

Q: How can Ames survive a shrinking budget?
We must find new ways of doing things in space and forge new partnerships—particularly with the private sector.

Q: Name one radical idea you would like to pursue.
I think we can build a small lunar lander for under $50 million in less than 2 years, in collaboration with private companies. We can start sending several of these landers to the moon.

Q: What will space look like a century from now?
Besides [having] my final resting place be some asteroid we diverted to save Earth, I would expect the first human colonies on planets discovered by Ames's missions to be thriving.

CREDITS (TOP TO BOTTOM): MIT; NATIONAL CANCER INSTITUTE; TOM TROWER/ARC/NASA

No one understands your laboratory and research needs more than Sigma-Aldrich, because no one listens harder.

By appreciating your individual requirements, our customized approach delivers highly innovative solutions in order to ensure your expectations are always met.

Renowned for providing the highest levels of service and science, we also understand the need to control costs and maintain quality.

With a product line extending from the most frequently used solvents and reagents to the rarest chemical and biological specialties – you can count on us.

By listening to you, Sigma-Aldrich has changed. Why not hear how we can better meet your needs?

SIGMA-ALDRICH

www.sigma-aldrich.com/listening3

Qs & AAAs

www.sciencedigital.org/subscribe

For just US$99, you can join AAAS TODAY and start receiving *Science* Digital Edition immediately!

Qs & AAAs

www.sciencedigital.org/subscribe

For just US$99, you can join AAAS TODAY and start receiving *Science* Digital Edition immediately!

LETTERS

edited by Etta Kavanagh

Veterinary Virologists Share Avian Flu Data

AVIAN INFLUENZA INFECTIONS CAUSED BY VIRUSES OF THE ASIAN HPAI H5N1 subtype have spread from East and Southeast Asia to Europe, the Middle East, and Africa. The virus is occurring in new ecosystems and infecting new hosts, resulting in novel host-pathogen interactions and genetic modifications. There is a lack of information on how the virus spreads across and within continents, including the role of wild birds. This hampers research into avian influenza, which is causing significant food security issues in developing countries, in addition to its pandemic potential.

Veterinary virologists have been working on avian influenza viruses for many years, and our collections of influenza virus isolates could be of great value to the international scientific community.

Within the Scientific Committee of OFFLU (the World Organization of Animal Health/United Nations Food and Agriculture Organization Network of Expertise on Avian Influenza), we have initiated the FLU-ID project. We will make available for genome nucleotide sequencing H5N1 contemporary isolates from several countries and relevant historical strains. This will be achieved in collaboration with the NIH Influenza Genome Project, and the full genetic sequences will be available in GenBank.

The Asian HPAI H5N1 virus is spreading very quickly. Real-time availability of genetic information is now possible and is essential for timely monitoring of viral evolution. These data will increase our knowledge of this pathogen and will help the appropriate selection of viral candidates for experimental studies, thus avoiding duplication of efforts and waste of resources.

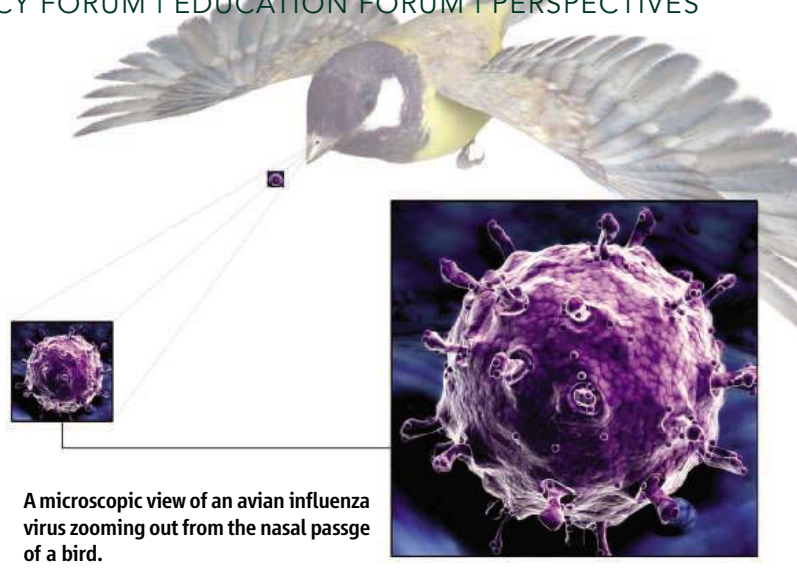

A microscopic view of an avian influenza virus zooming out from the nasal passge of a bird.

We firmly believe that knowledge of the genetic profile of avian influenza viruses from animals is a prerequisite to understanding a complex disease that has already killed hundreds of millions of birds worldwide and that is threatening human lives. We are convinced that this initiative will contribute substantially to the efforts that are being carried out worldwide, and we invite other medical and veterinary virologists to join us.

ILARIA CAPUA,[1] IAN BROWN,[2] MICHAEL JOHNSON,[3] DENNIS SENNE,[4] DAVID SWAYNE[5]

[1]Istituto Zooprofilattico delle Venezie, Viale dell'Università 10, 35020 Legnaro, Padova, Italy. [2]Veterinary Laboratories Agency-Weybridge, Addlestone, Surrey, UK. [3]Australian Animal Health Laboratory, CSIRO Livestock Industries, Private Bag 24, Geelong 3220, Australia. [4]National Veterinary Services Laboratories, Post Office Box 844, Ames, IA 50010, USA. [5]Southeast Poultry Research Laboratory, USDA/ARS, 934 College Station Road, Athens, GA 30605, USA.

Investigating a Second Thymus in Mice

IN THE REPORT "EVIDENCE FOR A FUNCTIONAL second thymus in mice" (14 Apr., p. 284; published online 1 Mar.), G. Terszowski *et al.* provide definitive evidence that, as in a number of other species, the mouse has a cervical thymus in addition to the conventional thoracic one. In this regard, it is useful to remember what Law told us at a meeting held in 1964 (*1*):

"The completeness of thymectomies was always checked at necropsy by inspection with a dissecting microscope and by histologic sections taken from the upper mediastinum. Nevertheless many mice, particularly those of the BALB/c strain, developed normally, after a transient loss in weight and lymphopenia; at necroscopy remnants of the thymus tissue were not found. Since it is known that ectopic thymus tissue may be found within the thyroid, serial sections of the thyroid were often made, and thymus tissue was found in the region of the parathyroid area." (*2*).

Law's group did not have the sophisticated technical tools to prove that the ectopic cervical thymus produced lymphocytes in the same way as the thoracic thymus. But a close look at the picture they published does show lymphocytes and a demarcation between medulla and cortex, suggesting that the cervical thymus could at least function in organizing itself as the thoracic one. In my early work with neonatally thymectomized mice, I found that mice of the Balb/c strain were not as adversely affected by neonatal thoracic thymectomy as mice of other strains (*2*). As Law suggested, this could well have been due to the existence of an ectopic cervical thymus—indirect evidence that such an ectopic tissue was indeed functional. Although this may be so, I have never believed that neonatal thoracic thymectomy could be associated with a complete absence of all thymus-derived lymphocytes (now known as T cells).

Thoracic thymectomy at 4 to 6 weeks of age prevented leukemia induced by x-irradiation in C57BL mice and by carcinogenic hydrocarbons in DBA/2 mice (*3*). In my own leukemia work, thoracic thymectomy at 4 to 5 weeks of age completely prevented leukemia in C3Hf mice that had been inoculated at birth with the Gross virus, and grafting neonatal thoracic thymus tissue as late as 6 months after thymectomy restored leukemia development in inoculated mice (*4*–*6*). From these findings, one might surmise that the cervical thymus is not susceptible to leukemogenesis. A more likely possibility, however, is that

CREDIT: GETTY IMAGES

for leukemia development, the cervical thymus is too small to be relevant. Here it is worth noting that T cell export from the thoracic thymus is proportional to the total thymic mass (*7*) and that according to Terszowski *et al.*, the cellularity of the cervical thymus is only 1/500th of that of the thoracic thymus.

J. F. A. P. MILLER

Walter and Eliza Hall Institute of Medical Research, Melbourne Hospital, Royal Parade, Melbourne, Victoria 3050, Australia.

References

1. L. W. Law, T. B. Dunn, N. Trainin, R. H. Levy, in *The Thymus*, V. Defendi, D. Metcalf, Eds. (Wistar Institute Press, Philadelphia, 1964), p. 106.
2. J. F. A. P. Miller, *Proc. R. Soc. London Ser B.* **156B**, 415 (1962).
3. J. F. A. P. Miller, *Adv. Cancer Res.* **6**, 291 (1961).
4. J. F. A. P. Miller, *Nature* **183**, 1069 (1959).
5. J. F. A. P. Miller, *Nature* **184**, 1809 (1959).
6. J. F. A. P. Miller, *Nature* **187**, 703 (1960).
7. R. G. Scollay, E. C. Butcher, I. L. Weissman, *Eur. J. Immunol.* **10**, 210 (1980).

Response

WE THANK MILLER FOR THE INTERESTING POINTS he raises and his historical perspective. Miller claims that a meeting report from 1964 by Law *et al.* (*1*) provided "indirect evidence that such an ectopic tissue was indeed functional." Law *et al.* presented a histological section from a mouse neck described as "thymus tissue located at the site of the parathyroid gland" (*1*). A histological section cannot provide conclusive evidence that the observed tissue was a T cell–producing thymus.

In hindsight, for contemporary immunologists, the Law *et al.* data could have presented a worthwhile starting point to conclusively address the possibility that mice have functional thymus in their neck. "Tools to prove that the ectopic cervical thymus produced lymphocytes in the same way as the thoracic thymus" have been available for more than 20 years. We were, however, unaware of the histological section reported in 1964. A simple explanation for why cervical thymus tissue was ignored for more than 40 years is that it was considered nonfunctional. Now, Miller writes that "it had been known for decades that BALB/c mice have an ectopic cervical thymus" (*2*). This is a surprisingly late statement given that, throughout the years, thoracic thymectomy was a major tool to study the role of the thymus in immunology, and given the possibility that cervical thymi were not restricted to BALB/c mice.

We are less concerned about the possibility that T cells can be generated prior to thoracic thymectomy. It is the issue of the de novo generation of T cells after thoracic thymectomy that is relevant in the light of cervical thymi. Many investigators have been concerned about the completeness of the surgical removal of the thoracic thymus. As a result, the thoracic cavity is often reexamined at the end of the experiments [e.g., (*3*)]. We have suggested that functional cervical thymus may provide an alternative explanation for ongoing thymopoiesis after thoracic thymectomy.

With regard to leukemogenesis, Miller proposes that the cervical thymus is not susceptible, or too small to be relevant for leukemia development. While this may be the case, the primary function of the thymus is to support the body with immunologically functional T cells, and, as far as we can tell, the cervical thymus is not too small to do that.

Notably, further differences exist comparing Miller's view and our own data. First, the anatomical positions of neck thymi throughout the ventral region of the mouse neck (fig. 1R in our Report) are quite distinct from the exclusive location in the vicinity of the parathyroid. Second, cervical thymi are not restricted to BALB/c mice. Third, the cervical thymus, although in major aspects a "pocket version" of the chest thymus, shows some special features such as its developmental delay until after birth and a different ratio of mature to immature thymocytes. Further experiments will be required to fully elucidate the role of the bona fide neck thymus in mice.

H.-R. RODEWALD

Immunology Department, Ulm University, Albert-Einstein-Allee 11, D-89070 Ulm, Germany. E-mail: hans-reimer.rodewald@uni-ulm.de

References

1. L. W. Law, T. B. Dunn, N. Trainin, R. H. Levy, in *The Thymus*, V. Defendi, D. Metcalf, Eds. (Wistar Institute Press, Philadelphia, 1964), pp. 105–120.
2. J. F. Miller, *Nat. Immunol.* **7**, 3 (2006).
3. F. Lambolez *et al.*, *Nat. Immunol.* **7**, 76 (2006).

BDNF in Anxiety and Depression

ADAPTING THE SOCIAL DEFEAT PARADIGM DEVELoped by one of our groups (*1*), O. Berton and colleagues comprehensively evaluated the role of brain-derived neurotrophic factor (BDNF) in mouse social stress ("Essential role of BDNF in the mesolimbic dopamine pathway in social defeat stress," Reports, 10 Feb., p. 864). Although their molecular data convincingly link chronic social defeat to activated mesolimbic BDNF, their behavioral and pharmacological data might benefit from some reconsideration.

For example, social avoidance in 10-day stressed mice that lose BDNF (interpreted by Berton *et al.* as depression) more correctly resembles "social anxiety" in the original model, where evident depression developed only after 20 days of social stress (*1*). Unaltered anxiety (versus depression) cannot be confirmed by 2.5 mg/kg chlordiazepoxide, a dose insufficient to affect anxiety in most published studies using C57BL/6 mice (*2*, *3*). Moreover, reduced avoidance produced by chronic administration of antidepressants is not specific to depression, but is more likely due to their well-known anxiolytic effects in animals and humans (*4*, *5*).

Indeed, other data implicate BDNF in animal and human anxiety (*6*–*9*). Consistent with this, we have recently shown that loss of one BDNF gene allele increases anxiety in serotonin transporter (SERT) knockout mice (*10*). Implying that both BDNF and serotonergic systems interact in modulation of anxiety, these data may explain anxiogenic effects of social defeat corrected by SERT-modulating drugs. In addition, BDNF signaling improves both short-term and long-term memory (*6*, *9*)—a phenomenon that may also contribute to the learned social aversion reported by Berton *et al.*

Finally, although Berton *et al.* suggest that BDNF inactivation leads to antidepressant effects, there are numerous data on opposite, antidepressant effects of BDNF in brain (*11*–*13*). Clearly, further studies are necessary to examine the role of BDNF in stress responses. Modeling transitions from anxiety to depression (*1*), use of longer social and nonsocial stressors, and specific targeting of neuromediatory systems beyond dopamine may help further elaborate BDNF's important role in brain stress-related disorders.

ALLAN V. KALUEFF,[1] DAMIRA F. AVGUSTINOVICH,[2] NATALIA N. KUDRYAVTSEVA,[2] DENNIS L. MURPHY[1]

[1]Laboratory of Clinical Science, National Institute of Mental Health, Bethesda, MD 20892, USA. [2]Institute of Cytology and Genetics, Novosibirsk 630090, Russia.

References

1. N. N. Kudryavtseva, D. F. Avgustinovich, *Aggress. Behav.* **24**, 271 (1998).
2. G. Griebel *et al.*, *Behav. Pharmacol.* **4**, 637 (1993).
3. R. J. Rodgers *et al.*, *Genes Brain Behav.* **1**, 242 (2002).
4. P. S. Masand, S. Gupta, *Expert Opin. Drug. Saf.* **2**, 486 (2003).
5. S. C. Poltronieri *et al.*, *Behav. Brain Res.* **147**, 185 (2003).
6. F. Cirulli *et al.*, *Hippocampus* **14**, 802 (2004).
7. M. Rios *et al.*, *Mol. Endocrinol.* **15**, 1748 (2001).
8. U. E. Lang *et al.*, *Psychopharmacology* **180**, 95 (2005).
9. E. Koronen *et al.*, *Mol. Cell. Neurosci.* **26**, 166 (2004).
10. R. Ren Patterson *et al.*, *J. Neurosci. Res.* **78**, 756 (2005).
11. K. Hashimoto *et al.*, *Brain Res. Rev.* **45**, 104 (2004).
12. Y. Dwivedi *et al.*, *Neuroscience* **139**, 1017 (2006).
13. R. S. Duman, *Neuromol. Med.* **5**, 11 (2004).

Response

KUDRYAVTSEVA AND HER COLLEAGUES HAVE made significant contributions in developing the social defeat paradigm in mice (*1*). Our work was also influenced by earlier research demonstrating that social defeat in mice induces lasting submissiveness or social avoidance upon sensory exposure to a nonaggressive animal (*2*). We essentially repeated these earlier findings and went on to show that social avoidance, induced by repeated social defeat, is an extremely durable phenomenon, which can be normalized by chronic, but not acute, treatment with antidepressants. We agree with Kalueff *et al.* that the duration of the chronic social defeat, which was not addressed in our study, is a critical dimension for future investigations.

Kalueff *et al.* raise an important point concerning the human syndrome to which social defeat paradigms have the most relevance. The

persistent social avoidance induced by chronic social defeat stress could be relevant to several human syndromes, including depression, social phobia (anxiety), and post-traumatic stress disorder. The distinction between anxiety and depression is not well understood (*3*): Anxiety and depression syndromes share several overlapping symptoms. Our demonstration that chronic antidepressant administration reverses the persistent social avoidance induced by social defeat could be consistent with any of these clinical syndromes, all of which show some responsiveness to antidepressants. We also showed that chlordiazepoxide, given acutely or chronically, does not reverse this social avoidance, but this finding does not clarify the distinction between anxiety and depression because benzodiazepines are ineffective for the long-term treatment of any of these syndromes. Much more work is needed in humans to identify bona fide etiologic and pathophysiologic subtypes of these syndromes before we can appreciate with any confidence which syndrome is closest to social defeat in mice.

It should not be surprising that a molecule like BDNF, and many others, exert different or even opposite effects on behavior depending on the neural circuitry in question. There is indeed considerable evidence for antidepressant-like effects of BDNF in hippocampal circuits (*3*–*6*), but also growing evidence for prodepression-like effects in the mesolimbic dopamine system [our Report; (*7*, *8*)]. This underscores the importance of establishing the molecular underpinnings of complex behavior within the context of carefully delineated neural circuits in the brain. The selective knockout of BDNF within the mesolimbic dopamine circuit, accomplished in our study by use of viral-mediated expression of Cre recombinase within a highly discrete brain region, provides one exciting tool with which to accomplish this critical task for psychiatric neuroscience.

OLIVIER BERTON, VAISHNAV KRISHNAN, ERIC J. NESTLER*

Department of Psychiatry and Center for Basic Neuroscience, The University of Texas Southwestern Medical Center, 5323 Harry Hines Boulevard, Dallas, TX 75390–9070, USA.

*To whom correspondence should be addressed. E-mail: eric.nestler@utsouthwestern.edu

References

1. D. F. Avgustinovich, I. L. Kovalenko, N. N. Kudryavtseva, *Neurosci. Behav. Physiol.* **35**, 917 (2005).
2. B. Siegfried, H. R. Frischknecht, P. G. Waser, *Behav. Neural Biol.* **42**, 91 (1984).
3. O. Berton, E. J. Nestler, *Nat. Rev. Neurosci.* **7**, 137 (2006).
4. R. S. Duman, *Biol. Psychiatry* **56**, 140 (2004).
5. L. M. Monteggia *et al.*, *Proc. Natl. Acad. Sci. U.S.A.* **101**, 10827 (2004).
6. N. M. Tsankova *et al.*, *Nat. Neurosci.*, in press (available online).
7. A. J. Eisch *et al.*, *Biol. Psychiatry* **54**, 994 (2003).
8. E. J. Nestler, W. A. Carlezon Jr., *Biol. Psychiatry*, in press (available online).

Stardust Mission Results: Hot in Cold

THE NEWS OF THE WEEK ARTICLE "MINERALS point to a hot origin for icy comets" by R. A. Kerr (17 Mar., p. 1536) highlighted the recent results from the Stardust mission, which sampled dust from comet Wild 2. The subsequent finding that a major portion of the dust was crystalline and had formation temperatures in excess of 1400 K appears to be surprising, because comets are icy objects that formed some 5 to 40 Astronomical Units (AU) from the sun and were never exposed to such temperatures.

This "hot" in "cold" structure suggests that some solar nebula material was processed in the hot, innermost regions of the solar nebula and transported to the cooler outer regions. Supporting evidence for this idea is provided by observations of young stellar objects (YSOs), which indicate that similar crystalline dust is formed in the inner disk regions, within 1 or 2 AU of a star (*1*).

It was first suggested in 1990 (*2*) that crystalline olivine dust could have formed in an early solar bipolar outflow and was then transported to other regions of the solar nebula. These high-speed jets are produced from and flow perpendicular to the inner regions of the disks that surround young stars. They may exist for millions of years and typically eject about 10% of the material that accretes onto a star (*3*). A solar mass ($M_\odot$) YSO will subsequently eject around 0.1 $M_\odot$ of material of which 10^{-3} $M_\odot$ will probably be "rock-like." If only 10% of this rock-like material falls back to the nebula, then we have 10^{-4} $M_\odot$ of high-temperature, processed material in the solar nebula, an amount that is approximately equal to the total rock mass of the Solar System (*4*). This argument (*5*) plus other lines of evidence suggest that a significant portion of the dust in the solar nebula may have been processed by a solar jet (*6*, *7*).

The Stardust results are consistent with this jet flow model, which may provide a potentially coherent and predictive framework for understanding the formation and transport of rocky material in the solar nebula.

KURT LIFFMAN

Centre for Fluid Dynamics, CSIRO/MIT, Post Office Box 56, Highett, VIC 3190, Australia. E-mail: Kurt.Liffman@csiro.au

References

1. R. van Boekel *et al.*, *Nature*, **432**, 479 (2004).
2. W. R. Skinner, *Lunar Planet. Sci.* **XXI**, 1166 (1990).
3. N. Calvet, in *Herbig-Haro Flows and the Birth of Low Mass Stars* (IAU Symp. 182), B. Reipurth, C. Bertout, Eds. (Kluwer, Dordrecht, Netherlands, 1997), pp. 417–432.
4. W. B. Hubbard, M. S. Marley, *Icarus* **78**, 102 (1989).
5. K. Liffman, M. Brown, *Icarus* **116**, 275 (1995).
6. K. Liffman, M. J. I. Brown, in *Chondrules and the Protoplanetary Disk*, R. Hewins, R. H. Jones, E. R. D. Scott, Eds. (Cambridge Univ. Press, Cambridge, 1996), pp. 285–302.
7. F. Shu, H. Shang, T. Lee, *Science* **271**, 1545 (1996).

AFFYMETRIX
WORKSHOP SERIES
GENOTYPING
SUMMER 2006
Register to receive print and video interviews on whole-genome and targeted genotyping association studies, including:

DISCOVERIES

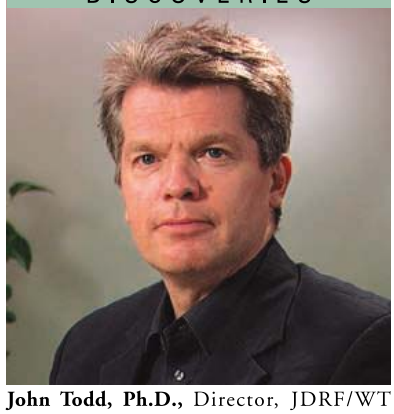

John Todd, Ph.D., Director, JDRF/WT Diabetes and Inflammation Laboratory, Cambridge University. *Drs. Todd and Jason Cooper discuss the discovery of a new type 1 diabetes (T1D) locus identified through a genome-wide scan of ~6,000 nonsynonymous SNPs of thousands of case/control samples.*

Luc Smink, Ph.D., Head of Bioinformatics, JDRF/WT DIL, Cambridge University. *Dr. Smink discusses T1DBase, a community database and web resource for T1D researchers, a joint project with Dr. Nathan Goodman (ISB, Seattle). T1DBase is used at the DIL to integrate, visualize and analyze genomics and genetics data, from different sources.*

SERVICES & TOOLS

Jay Kaufman, Director, DNA Analysis, Affymetrix. *Mr. Kaufman discusses targeted genotyping and SNP discovery services offered through Affymetrix' service lab.*

REGISTER TODAY
www.affymetrix.com/genotyping

AFFYMETRIX®

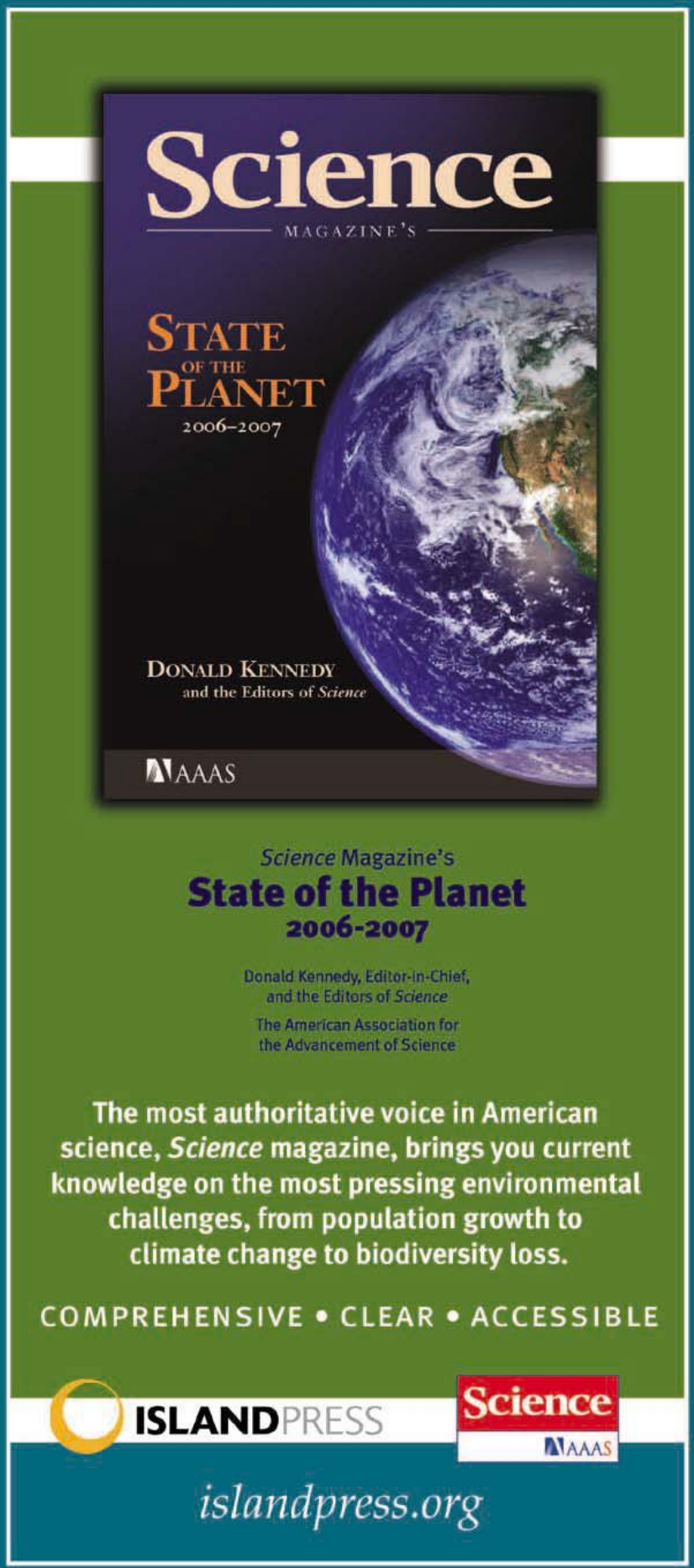

Show Me the Dog

THE NEWS FOCUS ARTICLE "NEW SIGNS OF ANcient life in another martian meteorite?" (R. A. Kerr, 31 Mar., p. 1858) repeats the allegation that the 1911 Nakhla meteorite fall in Egypt killed a dog. Kevin Kichinka argues persuasively that this is more likely fiction than fact (*1*). The essence of the argument is that there is no corroboration of the "dog" story and that the stones fell around the town of El Nakhla el Baharia and none fell on Denshal, where the dog is reported to have been struck. So, no dog, no tail—er, tale.

FRITZ KLEINHANS

Department of Physics, Indiana University–Purdue University Indianapolis, Indianapolis, IN, 46202, USA. E-mail: fkleinha@iupui.edu

Reference

1. K. Kichinka, *The Art of Collecting Meteorites* (Bookmasters, Mansfield, OH, 2005).

CORRECTIONS AND CLARIFICATIONS

News of the Week: "Genomes throw kinks in timing of chimp-human split" by E. Pennisi (19 May, p. 985). Contrary to what was stated in the article, Innan's analysis neither supported nor refuted hybridization between chimp and human ancestors.

Reports: "Chronology for the Aegean Late Bronze Age 1700–1400 B.C." by S. W. Manning *et al.* (28 Apr., p. 565). There was an error in the acknowledgment note (*47*). The correct full name for NERC is the Natural Environmental Research Council.

Special Section on Influenza: Perspectives: "Predictability and preparedness in influenza control" by D. J. Smith (21 Apr., p. 392). In reference (*8*), the journal is incorrect. The reference should read "C. E. Mills, J. M. Robins, C. T. Bergstrom, M. Lipsitch, *PLoS Med.* **3**, e135 (2006)."

Research Articles: "Atomic description of an enzyme reaction dominated by proton tunneling" by L. Masgrau *et al.* (14 Apr., p. 237). There was an error in Fig. 2C. The intermediate labeled as "VI" should have been labeled "VII."

2005 Visualization Challenge: "Photography" by C. Gramling (23 Sept. 2005, p. 1991). The First Place image "Autumn Color, Estonian Bog" should also have been credited to Susan W. Aber of Emporia State University. (This credit has been corrected in the HTML version of the article on *Science* Online.)

Research Articles: "Integration of spatial and temporal information during floral induction in *Arabidopsis*" by P. A. Wigge *et al.* (12 Aug. 2005, p. 1056). The ArrayExpress accession number was incorrect. It should be E-TABM-21.

Letters to the Editor

Letters (~300 words) discuss material published in *Science* in the previous 6 months or issues of general interest. They can be submitted through the Web (www.submit2science.org) or by regular mail (1200 New York Ave., NW, Washington, DC 20005, USA). Letters are not acknowledged upon receipt, nor are authors generally consulted before publication. Whether published in full or in part, letters are subject to editing for clarity and space.

BIOGRAPHY

Best and Brightest of His Generation

Ellis L. Yochelson

In the midst of the American Civil War, Clarence King graduated from Yale with the first class at the Sheffield Scientific School and then migrated west. He joined the California Geological Survey, initially as a volunteer, and explored the Sierra Nevada. He organized and led the Geological Exploration of the 40th Parallel (1867–1879), which mapped a 100-mile-wide strip across Nevada, Utah, and Wyoming. He recognized the Pleistocene lakes of the Great Basin, discovered the first known glaciers in the United States, and exposed the Great Diamond Hoax (an 1872 attempt to trick investors into buying land that had been salted with diamonds and other gems). In 1876, King was elected to the National Academy of Sciences (as its youngest member). He served as the first director (1879–1881) of the U.S. Geological Survey (USGS) before returning to private practice as an economic geologist and mining engineer. King's intriguing life and adventures are the subject of two recent books, *The Explorer King* and *King of the 40th Parallel*.

These books arrive from two different traditions. Robert Wilson is a writer and editor of *The American Scholar*, who after reading Patricia O'Toole's account of the circle of friends comprising the historian Henry Adams and his wife Clover, John Hays (Theodore Roosevelt's Secretary of State) and his wife Clara, and King (*1*) became interested in learning more of King's life. James Moore is a geologist, who for part of his career worked in the Sierras where King first made his mark and became so involved with King that he convinced the USGS to designate its main library as the Clarence King Library. Both books are well written, both have strong points, and each stands on its own merits. My buts will come later.

King near Uinta Lake, Utah.

CREDIT: TIMOTHY O'SULLIVAN/U.S. GEOLOGICAL SURVEY LIBRARY

Wilson's book is shorter and in a smaller format. Its penultimate chapter on the diamond swindle is slightly more that 20 pages. Moore's chapter concerned with the same event runs to 30 pages, although half are devoted to other matters. If one knows something of the career of King, Wilson offers a little more insight as to his character. Moore has a better understanding of the geography and geology, and he has included new material concerning topographer James Gardner, King's right-hand man.

Moore's volume has numerous period illustrations, including excellent images from the photographer Timothy O'Sullivan. Other lithographs and sketches also supplement the text. The difference in style between the books may be epitomized by a lithograph included by Moore, whose caption begins "Miners waiting to descend in two lifts into the depth of the Savage Mine on the Comstock Lode" and continues for eight additional lines about the dangers of a ride in the lift either descending or ascending. Wilson does not present this illustration, which was published in the first-completed volume (III, *Mining Industry*) of the King Survey's reports (*2*). Rather, he devotes half a paragraph to analyzing the image. "Does it suggest these are men going about their business, however risky in a calm and orderly way? It is an image that reassures the reader … Or does the image, of men standing at the top of lighted shafts surrounded by darkness … undercut the study [King's report] that follows, or warn the reader of its inadequacies?"

Wilson's book concludes with a 10-page epilogue, which moves from King's death to his debts and his secret 1888 marriage to a black woman (to whom he revealed his true name only on his deathbed), briefly touches on the 40th Parallel Survey, and concentrates on his 1877 speech at the Sheffield Scientific School. In that, King espoused catastrophism (abrupt change) as more significant than uniformitarianism (gradual change through processes observable today). Moore devotes about one-third of his book to the King Survey. He then briefly mentions F. V. Hayden, J. W. Powell, the founding of the civilian-run USGS, and King's role as director for 22 months. His 20-page epilogue concentrates on King's trip to Spain in the early 1880s (during which King searched for the legendary helmet of Mandrino at La Mancha) and a summary of the later lives of some of the folks who were with King during his earlier days. There is more meat in Moore's treatment than in Wilson's.

Now for my buts. In 1958, Thurman Wilkins wrote a 441-page biography of King (*3*). Thirty years later, a revised edition (*4*), enlarged to 524 pages, critically discussed the literature on King's significance that appeared in the intervening years. This is the book to read if you want to know about King's life. He soared to the heights in completing the territorial survey, surmounting difficulty after difficulty and getting its findings published. It is still being argued as to how much his brief tenure influenced the course of the USGS. The rest of his career—as mining speculator, expert witness, and profligate spender—deserves to be weighed against his accomplishments. Although Wilkins does not dwell on the incident, when Powell ran afoul of Congress in the early 1890s, King showed up in Washington, hinting that he was available in case Powell wanted to leave the USGS directorship. Powell did not resign until 1894, and by then even if King had supporters in Washington, most USGS geologists wanted no part of him.

It is difficult to write a biography of King, for the original material invariably is to a greater or lesser extent incomplete—and King's own accounts may not be accurate. It is even harder to replow the same ground, and perhaps Wilson and Moore were wise to concentrate on the young, golden King, rather than what he was when older. Regardless, King must have been a charmer, for his close friends stood by him and, after his death, paid his debts and provided for his secret wife and children.

The Explorer King
Adventure, Science, and the Great Diamond Hoax—Clarence King in the Old West

by Robert Wilson

Scribner, New York, 2006. 317 pp. $26, C$36. ISBN 0-743-26025-2.

King of the 40th Parallel
Discovery in the American West

by James G. Moore

Stanford University Press, Stanford, CA, 2006. 411 pp. $55. ISBN 0-8047-5222-2. Paper, $21.95. ISBN 0-8047-5223-0.

The reviewer is at the Department of Paleobiology, National Museum of Natural History, Washington, DC 20013–7012, USA. E-mail: yochelsone@si.edu

References

1. P. O'Toole, *The Five of Hearts: An Intimate Portrait of Henry Adams and His Friends, 1880–1918* (Potter, New York, 1990).
2. *Report of the Geological Exploration of the Fortieth Parallel Made By Order of the Secretary of War…* (Government Printing Office, Washington, DC, 1870–1880).
3. T. Wilkins, *Clarence King: A Biography* (Macmillan, New York, 1958).
4. T. Wilkins, *Clarence King: A Biography* (Univ. New Mexico Press, Albuquerque, NM, 1988).

10.1126/science.1130690

SCIENCE COMMUNITY

Scientific Diasporas

Béatrice Séguin,[1] Peter A. Singer,[1,2] Abdallah S. Daar[1,3,4*]

Scientists from the developing world who work in more developed countries are often underutilized resources and should be cultivated for the benefit of their countries of origin.

In Canada, as in other industrialized countries, a high percentage of foreign-born residents are from the developing world (*1*). Some of these migrants are highly skilled scientists and engineers who constitute a "brain drain" from their countries of origin (COs), but also represent a scientific diaspora with enormous potential. Scientific diasporas have been defined as "self-organized communities of expatriate scientists and engineers working to develop their home country or region, mainly in science, technology, and education" (*2*). Unfortunately, many of these diaspora networks depend on a few champions for sustainability, and there has been evidence of Web site inactivity (*3*) and ineffectiveness (*4*, *5*).

We believe scientific diasporas may represent part of the solution to the often crippling economic and social effects of emigration on the developing world (*5*). However, systematic, qualitative research into the needs and perceptions of the diasporas themselves regarding assisting their COs is lacking. Such information is essential to success of any future policies aimed at engaging them.

Using previously described qualitative research methods (*6*–*8*), we studied life science researchers and entrepreneurs during 2005 in three Canadian cities (Vancouver, Toronto, and Montreal) that represent strong science hubs. Participants in academic research centers and biotechnology companies were recruited by posting a study notice in which they were asked to identify themselves as originating from developing countries and to share their views about or experiences with contributing to development and innovation in their COs. Anonymity of participants has been maintained, as information on the national origin of individuals at the workplace is considered confidential. This method addressed concerns about potential harms of stigmatization that scientists from developing countries might face as a result of being identified by origin. Sixty participants were included, of whom 48 were from academia and 12 from the biotechnology industry. Participants were asked open-ended semistructured questions during face-to-face interviews. Questions focused on three areas: linkages to the CO, barriers experienced or expected when forming linkages to the CO, and interest in participating in science and technology (S&T) capacity-building through an organized mechanism.

As might be expected, given the self-selection of participants, the general sentiment expressed by study participants was that of a feeling of moral responsibility or need to "give back" to their CO. Despite observing country-specific differences in the level of trust held by study participants toward their CO's government, about two-thirds of all participants felt positively about working directly with the scientific communities that would benefit from their contributions.

Among the 60 participants, there was very little systematic S&T interaction with their COs. The participants could be divided into three broad categories: interested and/or concerned, leaders, and those who had experienced networks.

Forty-one individuals fell into the category of interested and/or concerned, of whom 25 had a strong desire to "help" but were not aware of any ready vehicles through which to offer assistance. When we asked why they had not initiated formal linkages, participants listed reasons such as lack of time, financial barriers, lack of infrastructure in their CO, or they said that no one, including their CO, had asked for their contributions. Some scientists said they were at a disadvantage because they were still in the process of building their careers in Canada. In one scientist's words "I do not have the freedom (to initiate linkages) because I am not a principal investigator." Other participants echoed this sentiment and said that even if they tried to initiate collaborations with their CO, they would not have credibility unless they held a high-profile position in the developed world. Finally, a common response among these participants was to look at the study notice as a "call for help," and although the notice made no mention of this, they hoped they were being recruited for an existing program.

Nine individuals were actively engaged in projects in or with their COs. They have contributed to S&T capacity-building in various ways such as serving a scientific advisory role in academic institutions, organizing joint research projects, organizing "traveling expert panels," forming a transnational life-science company spanning Canada and the CO, and partnering with a Canadian company to help it enter his CO's market. Among these leaders was an executive officer of a biotechnology firm, principal investigators in academic research centers, and a Ph.D. student. One of these participants was contacted by a diaspora initiative based in his CO. However, he said he received few e-mails from this organization, and his evaluation was that "things start but they don't finish."

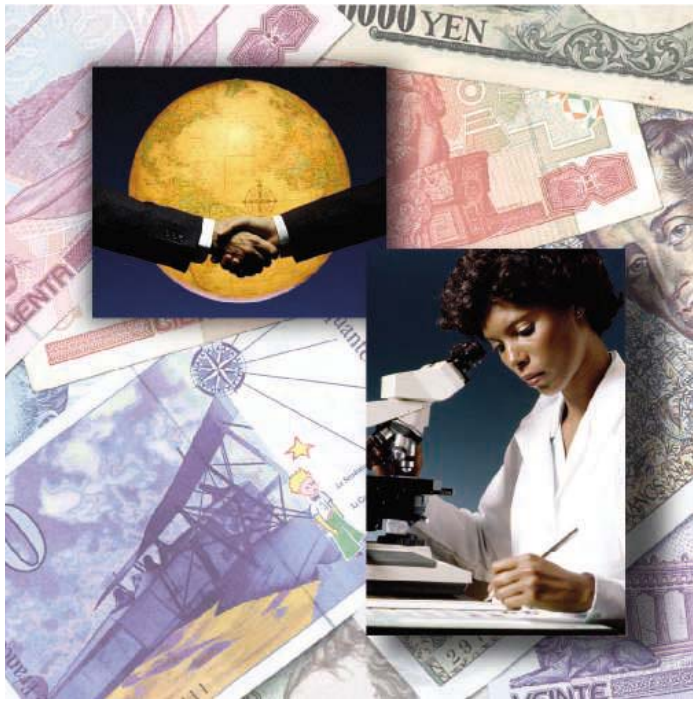

PHOTO CREDITS (INSERTS): PHOTOS.COM

Ten individuals considered themselves to be members of an organized network. Four individual participants were part of two networks with S&T linkages to their CO. However, the networks described by six participants were new and undefined or not related to S&T capacity-building (i.e., had humanitarian or job market goals). One of these networks, AHEAD, has a mission "to explore, solicit, acquire and deliver educational materials that help advance education in Ethiopian universities and colleges" (*9*). Another, the Society of Chinese Bioscientists of America, has as part of its mission "to

[1]Canadian Program on Genomics and Global Health, University of Toronto, and Joint Centre for Bioethics, 88 College Street, Toronto, Canada M5G 1L4. [2]Department of Medicine, University of Toronto, and the University Health Network, Toronto, Canada M5G 2C4. [3]Department of Public Health Sciences, University of Toronto, Toronto, Canada M5T 3M7. [4]McLaughlin Centre for Molecular Medicine, Toronto, Canada M5G 1L4.

*Authors for correspondence. E-mail: a.daar@utoronto.ca (A.S.D.); beatrice.seguin@utoronto.ca (B.S.)

establish a spirit of fraternity and international cooperation" (*10*). One of the members of this network said: "right now, we do this because of personal connections … we are mainly focused on science exchange."

A common belief was that Canada's position in international aid is well respected and that a government-backed diaspora effort would provide credibility when trying to make connections. More than half of our participants (32 out of 60) expressed a desire for some form of external support (financial and/or organizational), guidance, and credibility. When asked about how a hypothetical diaspora program could be most effective, participants indicated a need for (i) a platform that would allow them to participate in short-term visits to developing countries where they could provide "hands-on" science or entrepreneurial training; (ii) access to technology for "virtual" teaching (Web-based educational vehicles); (iii) grant-writing advice and mentoring; (iv) a mechanism to facilitate biomedical business partnerships between the diaspora in Canada and COs; (v) funding mechanisms for joint research projects between Canadian and developing country researchers; and (vi) policies that would help postdoctoral fellows spend time in their CO without harming their careers.

Recommendations

Scientific diasporas represent an untapped resource for their COs and their host countries, and both must become involved with the diasporas. The report of the Global Commission on International Migration concluded that COs should "establish an inventory of the skills base within the diaspora; develop programmes that facilitate the transfer of skills and knowledge from the diaspora to their COs" (*11*).

Developing-world awareness of the potential of the diasporas does exist. For example, political leaders in India and China have made national calls for their diasporas to assist in S&T capacity-building and have supported these calls with concrete incentives. In India, some of these incentives include provision of dual citizenship; recognition of persons of Indian origin (PIOs) through the creation of a special ministry; an annual celebration and conference for PIOs; and a Research Scientists Scheme, which aims to bring back Indian nationals working overseas to teach in Indian universities. China has committed U.S. $25 million over a 15-year period to set up a Web site and center to assist permanently and temporarily returned overseas Chinese scholars (*5*). In 2005, during his keynote address at a Nigerian diaspora conference in which more than 250 scientists from North America participated, the Nigerian president said, "let this conference serve as the beginning of an enduring symbiotic relationship between our peoples in the science and technology sector abroad and those at home that would put in place the necessary structures for the technological transformation of our country" (*12*). National Diaspora Day is an annual event in Nigeria.

Because industrialized countries benefit from brain drain, their governments should play a key role in establishing institutional mechanisms to help diasporas contribute to development and innovation in their COs (*5*). If the Group of Eight "G8" countries make engaging scientific diaspora a priority, this would foster innovation in developing countries, which could create long-term health and economic benefits (*13*).

This recommendation can be achieved by creating Diaspora Business Initiatives and a National Science Corps in industrialized countries. The Diaspora Business Initiatives would provide institutional support and funding to enable partnerships (investment, trade) in the life sciences between business and entrepreneurial communities of industrialized countries and those in COs. The National Science Corps would provide funding for diaspora scientists to travel to S&T institutions in their COs. It would require identification of members of scientific diasporas who are qualified and willing to travel to these institutions in their COs. These National Science Corps could be modeled on the Global Science Corps (GSC), a new initiative that focuses on sending American scientists (not restricted to diasporas) to prequalified institutions in developing countries for 1 to 2 years (*14*). Initiatives facilitating the return of expatriate professionals for short periods, such as TOKTEN (*15*), and recent scientific diaspora pilot projects (*16*) are also models that should be encouraged and evaluated.

Given the increased interest in the scientific diaspora, and the lack of communication and coordination between different initiatives, a stakeholder dialogue between scientific diasporas in industrialized countries, S&T research and biotechnology communities, governments, and nongovernmental organizations in both industrialized and developing countries should be undertaken to determine the best way to harness the human capital of scientific diasporas.

The newly elected government in Canada identified as a priority the creation of an agency to assess the credentials of professionals immigrating to Canada so as to facilitate their entry in their respective fields (*17*).This could represent an excellent starting point from which to gather information and to begin to build a Diaspora Knowledge Network. The former Canadian Prime Minister said in 2004, "our long-term goal as a country should be to devote no less than 5% of our [research and development] investment to a knowledge-based approach to develop assistance for less fortunate countries" (*18*). Immigration, innovation, aid, and trade policies are interdependent. Therefore, the new government has a special opportunity to build on its own commitment to recognize foreign credentials by also creating formal mechanisms to enable diaspora scientists in Canada to give back to their COs.

In addition to skills and resources, scientific diasporas have strong emotional connections toward their COs. Although they may have individual connections, a more organized structure would allow them to be more effective. As one participant said, "if the Canadian government created an organization, provided us with a nucleus, made the initial effort, I think there would be so many people who would join." This sentiment applies to many industrialized countries, and should be turned into benefits for the developing world.

References and Notes

1. Migration Policy Institute (www.migrationinformation.org/GlobalData/countrydata/country.cfm).
2. R. Barre, V. Hernandez, J. B. Meyer, D. Vinck, "Scientific diasporas: How can developing countries benefit from their expatriate scientists and engineers?" (Institut de Recherche pour le Développement, Paris, 2003).
3. B. L. Lowell, S. G. Gerova, "Diasporas and economic development: State of knowledge" (World Bank, Washington, DC, 2004).
4. L. Ravenhill, National Research Foundation, South African Network of Skills Abroad (SANSA), electronic survey 2 March to 19 April 2005, results collation document (National Research Foundation, Pretoria, South Africa, 2005).
5. B. Seguin, L. State, P. A. Singer, A. S. Daar, *Int. J. Biotechnol.* **8**, 78 (2006).
6. H. Thorsteinsdóttir, U. Quach, D. K. Martin, A. S. Daar, P. A. Singer, *Nat. Biotechnol.* **22** (suppl.), DC3 (2004).
7. F. Salamanca-Buentello *et al.*, *PLoS Med* **2**, e97 (May 2005).
8. A. Strauss, J. Corbin, *Basics of Qualitative Research: Techniques and Procedures for Developing Grounded Theory*, P. Labella, Ed. (Sage, Thousand Oaks, CA, ed. 2, 1998), pp. 101–162.
9. Association for Higher Education and Development (AHEAD) (www.aheadonline.org/).
10. (www.scba-society.org/Chapters.html#toronto)
11. "Migration in an interconnected world: New directions for action" (Global Commission on International Migration, Geneva, 2005) (www.gcim.org/en/finalreport.html).
12. (http://nigeriaworld.com/articles/2005/aug/303.html).
13. C. Juma, L. Yee-Cheong, *Innovation: Applying Knowledge in Development* (Millennium Project, United Nations Development Programme, London, 2005).
14. (www.globalsciencecorps.org).
15. Transfer of Knowledge Through Expatriate Nationals (TOKTEN) (www.unvolunteers.org).
16. (www.elysee.fr/elysee/elysee.fr/francais/salle_de_presse/communiques_du_conseil_des_ministres/2003/octobre/communique_du_conseil_des_ministres_du_08_10_2003.137.html).
17. Conservative party of Canada Federal Election Platform 2006, p. 38.
18. (www.pcobcp.gc.ca/default.asp?Page=sftddt&Language=E&doc=sftddt2004_1_reply_e.htm).
19. (www.geneticsethics.net).

20. We are grateful to our participants for sharing their views and experiences. The Canadian Program on Genomics and Global Health is primarily supported by Genome Canada through the Ontario Genomics Institute and the Ontario Research and Development Challenge Fund. Matching partners are listed at (*19*). A.S.D. is supported by the McLaughlin Centre for Molecular Medicine. P.A.S. is supported by a Canadian Institutes of Health Research Distinguished Investigator award. We thank A. Dabu for her comments on earlier versions of this manuscript. D. B. Watters and D. Brook have helped to develop the concept of the National Scientific Disapora Initiatives, Disapora Business Initiatives, and National Science Corps.

Supporting Online Material

www.sciencemag.org/cgi/content/full/312/5780/1602/DC1

10.1126/science.1126325

NEUROSCIENCE

Neurons Find Strength Through Synchrony in the Brain

Although critical for brain function, sensory information enters the cortex of the brain through just a few weak synapses. The key to this paradox seems to be that their strength is multiplied by synchrony of the different inputs.

Jose-Manuel Alonso

For any touch, sound, or image to be perceived, our senses have to activate neurons at the very center of the brain, in the thalamus. In turn, thalamic neurons must activate neurons in the cerebral cortex, where most complex brain functions take place. One would think that, given their role in sensory processing, the connections between the thalamus and cortex would be strong and reliable. After all, the primate brain is able to detect a skin indentation of less than 20 μm and the reflection of just a few photons in the darkness. How could our senses be so remarkably sensitive if thalamocortical connections linking these two regions were weak? Well. . . they are weak, and on page 1622 of this issue, Bruno and Sakmann (*1*) provide the first intracellular measurements in an intact brain to prove it.

Bruno and Sakmann focused on layer 4 of the mouse sensory cortex, a main target for thalamic inputs. By using an impressive and extremely difficult technical approach, the authors were able to measure the excitatory electrical activity generated in a single cortical neuron by a single thalamic neuron. They noted that the median amplitude of the thalamocortical excitatory potential was 0.5 mV (range 0.1 to 4.1 mV), which is smaller by a factor of 30 than the average synaptic potential generated by a sensory stimulus in the cortex (~15 mV).

Neurons connect with each other through small junctions called synapses. On average, a layer 4 neuron receives 20% of inhibitory synapses and 80% of excitatory synapses from other neurons. Surprisingly, most of the excitatory synapses do not originate in the thalamus but in the cortex itself (see the figure). In layer 4 neurons of the mouse somatosensory cortex, only 10 to 23% of the excitatory synapses are formed with thalamic neurons (*2*), and similar percentages (5 to 25%) have been found in layer 4 neurons of the cat visual cortex [the similar percentages hold if the estimates from different research groups are taken as opposite ends of a common range instead of opposite views of thalamocortical function (*3*)]. This remarkable intracortical predominance in synapse number led to the idea that the input from thalamic neurons is not strong enough to elicit, or "drive," neuron activity in the cortex. Therefore, it's been thought that thalamic inputs need to be amplified by recurrent intracortical connections (*4*).

Even though layer 4 intracortical connections can be relatively strong, estimates obtained from cortical slices indicate that thalamocortical connections are stronger, if fewer in number. According to these estimates, thalamic synapses are not only larger in size (and have more active zones where neurotransmitter molecules are released) than intracortical synapses, they are also more effective at driving the cortex by a factor of 4.8 (*5*). Although measurements in the intact brain using techniques such as cross-correlation analysis (*6*, *7*) or single-axon current source density analysis (*8*) are consistent with the idea of a dominant thalamic input to the cortex, a crucial piece of information has been missing: We have not known the amplitude of the thalamocortical postsynaptic potential in an active and intact brain.

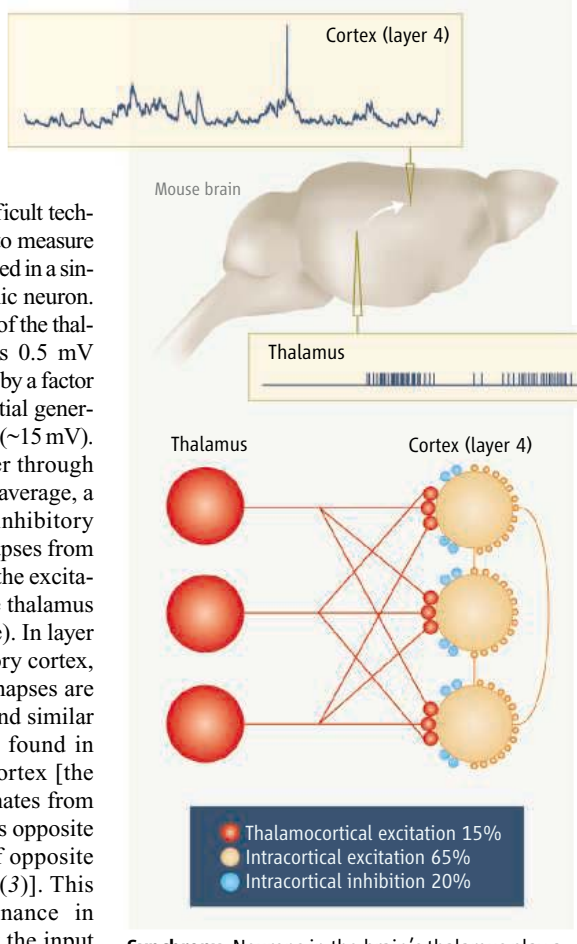

Synchrony. Neurons in the brain's thalamus play a crucial role in transmitting information from sensory stimuli, such as touch and light, to the cortex. The connections between the thalamus and cortex are weak, but as shown by new electrical recordings from the intact mouse brain, they become strong by operating in synchrony.

Bruno and Sakmann now provide this measurement and show that the input from a single thalamic neuron, in isolation, cannot activate a single cortical neuron, because it generates a postsynaptic potential usually smaller than 1 mV, which is below the threshold needed for neuronal activation. On the basis of this finding, the authors conclude that thalamocortical connections are weak—a conclusion that is very consistent with the anatomy. For example, whereas a single retinal neuron makes more than 100 synapses per thalamic target [one of the strongest connections within the visual pathway (*9*)], a thalamic neuron makes fewer than eight synapses per cortical neuron (*10*). Even if thalamocortical connections are weak, they are unlikely to be weaker than intracortical connections (*5*). Unfortunately, there are no measurements of intracortical connections in the intact sensory cortex that could serve as comparison, despite heroic attempts to obtain them (*11*).

Regardless of the differences at the level of single connections, a major conclusion from Bruno and Sakmann is that thalamic inputs do not need a "cortical amplifier" to reach threshold. Although any thalamic input in isolation is weak, thalamic inputs are strong as a group. A group of just 30 synchronized inputs (out of 85 inputs available) will generate a postsynaptic potential very similar to the one generated by a sensory stimulus such as a light touch. Groups of thalamic neurons can generate many synchronized electrical discharges, or spikes, in response to sensory stimulation, and these synchronized spikes are very effective at driving cortical cells to threshold (*12*). Consistently, it has now been reported, in at least three different sensory systems (*7*), that the response properties of layer 4 cortical neurons are largely explained by the response properties of the thalamic inputs (*1*).

The experiments from Bruno and Sakmann will surely raise an old question: What are all the intracortical synapses doing in layer 4 neurons? The answer may not be far from the cortical amplifier idea (*4*). In recent years, it has become clear that intracortical inhibition plays

CREDIT: P. HUEY/SCIENCE

The author is in the Department of Biological Sciences, State University of New York College of Optometry, New York, NY 10036, USA. E-mail: jalonso@sunyopt.edu

a major role in normalizing the gain of intracortical responses while keeping stimulus selectivity constant (*13*). Like intracortical inhibition, intracortical excitation may provide gain adjustments that are far more specific and sophisticated than what we can currently imagine (*14*). In the meantime, the thalamocortical connections seem to be doing their job just fine, leaving the cortical amplifier available for other interesting functions that remain to be discovered.

References

1. R. M. Bruno, B. Sakmann, *Science* **312**, 1622 (2006).
2. G. Benshalom, E. L. White, *J. Comp. Neurol.* **253**, 303 (1986).
3. A. Peters, B. R. Payne, *Cereb. Cortex* **3**, 69 (1993).
4. R. J. Douglas, C. Koch, M. Mahowald, K. A. Martin, H. H. Suarez, *Science* **269**, 981 (1995).
5. Z. Gil, B. W. Connors, Y. Amitai, *Neuron* **23**, 385 (1999).
6. R. M. Bruno, D. J. Simons, *J. Neurosci.* **22**, 10966 (2002).
7. J. M. Alonso, H. A. Swadlow, *J. Neurophysiol.* **94**, 26 (2005).
8. H. A. Swadlow, A. G. Gusev, T. Bezdudnaya, *J. Neurosci.* **22**, 7766 (2002).
9. J. E. Hamos, S. C. Van Horn, D. Raczkowski, D. J. Uhlrich, S. M. Sherman, *Nature* **317**, 618 (1985).
10. T. F. Freund, K. A. Martin, P. Somogyi, D. Whitteridge, *J. Comp. Neurol.* **242**, 275 (1985).
11. I. Lampl, I. Reichova, D. Ferster, *Neuron* **22**, 361 (1999).
12. J. M. Alonso, W. M. Usrey, R. C. Reid, *Nature* **383**, 815 (1996).
13. T. Z. Lauritzen, K. D. Miller, *J. Neurosci.* **23**, 10201 (2003).
14. Y. Yoshimura, J. L. Dantzker, E. M. Callaway, *Nature* **433**, 868 (2005).

10.1126/science.1129705

GEOCHEMISTRY

The Pathway of Carbon in Nature

A complex web of reactions leads from primary biological products to the organic debris found in sediments and rocks. A new study shows that abiotic reactions play an important role.

John M. Hayes

Late in his exceptional career, well after he had received the Nobel Prize in 1961 for elucidating the pathway of carbon in photosynthesis, Melvin Calvin turned his attention to organic geochemistry. The progression was logical: from the pathway of carbon in a cell to the pathway of carbon in nature. In the former, there is an array of precise, enzymatic catalysts. The latter is actually a web of reactions that leads from primary biological products to the organic debris accumulating in Earth's crust. What mechanisms control the flow of carbon within this web? The answer is worth knowing because, among other things, these mechanisms modulate Earth's levels of CO_2 and O_2. On page 1627 of this issue, Hebting *et al.* (*1*) provide striking new information about one of the web's most general features.

Enhanced online at www.sciencemag.org/cgi/content/full/312/5780/1605

In his book *Chemical Evolution* (*2*), Calvin discusses "molecular paleontology" and makes a key point: Hydrocarbons are particularly long-lived. Petroleum is a key example. In contrast, proteins, carbohydrates, and nucleic acids—the abundant and information-rich components of biomass—are rarely preserved for more than a few million years (*3*). Clues about ancient biochemistry must therefore be extracted from sedimentary hydrocarbons derived mainly from lipids and other aliphatic products .

The rocks contain cholestane rather than cholesterol, carotane rather than carotene. The structural relationships are unmistakable, but the molecules are very different. Somehow, carbon skeletons are preserved, double bonds and functional groups are lost, and a saturated hydrocarbon survives to carry the root of its precursor's name with an "-ane" suffix.

Natural sulfide. Cracked open, a clump of gelatinous mud from the seaside is seen to be rich in black iron sulfide. Any hydrogen sulfide that does not react with iron is available to react with organic matter. The sulfide is produced by bacteria that oxidize organic matter at the expense of sulfate, which is abundant in seawater. The process occurs only after molecular-oxygen supplies have been exhausted. The light-colored margin of the clump marks the depth to which molecular oxygen can diffuse in the mud.

How does all this happen? The hydrocarbons—called biomarkers if their structures are distinct enough—are produced by reaction pathways within sediments. For years, organic geochemists have been disentangling those pathways, just as Calvin, Benson, and their co-workers determined the photosynthetic route from CO_2 to carbohydrates.

The time scales differ markedly, however. In photosynthesis, the problem was to stop reactions quickly so that the earliest products could be observed. In sediments, even the faster reactions require decades to produce readily analyzable quantities. Moreover, if a system is manipulated—to speed it up or to add a tracer—the pathways are likely to change. The most useful results have been based on analyses of natural materials at identifiable points in the pathway.

Sterols, which are abundant in oceanic algae and for which structurally related steranes can be found in marine sediments and petroleum, have been favored as tracers within the web of reactions (*4*). Even within particles that have not yet sunk to the seafloor, we find hydrogenated products, stanols, rather than the original algal products. Evidence for microbial catalysis of this process is strong (*5*). Double bonds within the ring system are the first to go, and the process is stereoselective. If the process were abiotic, all double bonds, not just those in the ring system, should be attacked, and there would be no stereoselectivity.

The hydrogenated products are more abundant in environments that are deficient in oxygen (such as interiors of particles or poorly ventilated waters). Apparently, microorganisms are extending their oxidative metabolism by using unsaturated lipids as electron acceptors. Microorganisms also dehydrate sterols to produce conjugated steradienes (*6*). In the dehydration of carotenoids, formation of an acetylenic intermediate that would not be favored in abiotic processes also suggests microbial catalysis (*7*). As such results have accumulated, a new conventional wisdom has emerged: If the temperature is not too high and a reaction could be microbially catalyzed, it probably is.

Or is it just hard to prove that a low-temperature, organic-chemical alteration is abiotic? It's not as if sedimentary environments are chemically benign. Concentrations of hydrogen sulfide (H_2S), a potential reductant, can be appre-

The author is in the Department of Geology and Geophysics, Woods Hole Oceanographic Institution, Woods Hole, MA 02543, USA. E-mail: jhayes@whoi.edu

ciable. The figure provides visual evidence. Supplies of H_2S are often so large that reactive metals cannot consume it all. The excess is available to react with any organic molecules that might be present. Carotenoid pigments, which are rich in double bonds, would be particularly reactive. And here is the difficulty. The range of reduction products found in sediments is huge. One can look at it and say "it's a mess, it must be abiotic." But that does not eliminate the possibility of varying degrees of microbial alteration.

Hebting *et al.* work closely with natural-products organic chemists. This expertise has helped them to separate the components of the "mess." Using a formidable array of spectroscopic techniques, they have elucidated molecular structures. Wherever it has been possible to pin down the stereochemistry at chiral centers, the results show that the hydrogenations were not stereoselective and, therefore, not microbially catalyzed.

Must the conventional wisdom be revised, at least for hydrogenations? Probably. The proven microbial hydrogenations are quite specific, whereas the pathway now demonstrated is general. And practically every aerobic-anaerobic boundary includes a sulfide-rich zone. In fact, the present group was one of those (*8*, *9*) who showed earlier that formation of sulfide bridges—a sort of natural vulcanization—is an important process by which reactive organic molecules are immobilized by attachment to insoluble macromolecules in sediments.

A second phase of the present work is therefore important. In laboratory experiments, Hebting *et al.* (*1*) have demonstrated hydrogenation of double bonds in carotenoids and steroidal ketones incubated at 50° to 90°C in saturated solutions of H_2S. Yields are low, but, as the authors say, the results, and observation of the expected intermediates in some natural sediments, support a hypothetical, two-step process: addition of H_2S to a polyene to yield an allylic thiol, followed by reduction of the thiol. If a double bond is conjugated with a carbonyl group rather than another olefinic bond, initial sulfurization is apparently not required, and a different mechanism applies.

Without doubt, this report erects a new, and highly significant, milepost on the pathway of carbon in nature.

References

1. Y. Hebting *et al.*, *Science* **312**, 1627 (2006); published online 11 May 2006 (10.1126/science.1126372).
2. M. Calvin, *Chemical Evolution* (Oxford Univ. Press, New York, 1969).
3. G. Eglinton, G. A. Logan, *Philos. Trans. R. Soc. London B* **333**, 315 (1991).
4. A. S. Mackenzie, S. C. Brassell, G. Eglinton, J. R. Maxwell, *Science* **217**, 491 (1982).
5. J. A. Beier, S. G. Wakeham, C. H. Piskaln, S. Honjo, *Nature* **351**, 642 (1991).
6. R. B. Gagosian, J. W. Farrington, *Geochim. Cosmochim. Acta* **42**, 1091 (1978).
7. D. J. Repeta, N. Frew, *Org. Geochem.* **12**, 469 (1988).
8. M. E. L. Kohnen, J. S. Sinninghe Damsté, H. L. ten Haven, J. W. de Leeuw, *Nature* **341**, 640 (1989).
9. P. Adam *et al.*, *Geochim. Cosmochim. Acta* **57**, 3395 (1993).

Published online 11 May 2006;
10.1126/science.1128966
Include this information when citing this paper.

IMMUNOLOGY

Discriminating Microbe from Self Suffers a Double Toll

The autoimmune disease lupus is caused by immune cells that secrete antibodies to the patient's own antigens. A mouse version of the disease reveals two genes that lead to this disregulation.

Christopher C. Goodnow

Sensing microbial infection and countering it with a vigorous immune reaction is a double-edged challenge facing all multicellular organisms. Mobilizing a swift immune response to viruses and bacteria is often a critical survival advantage. However, many microbial components are chemically similar to constituents of our own cells, and failure to tell the two apart leads to devastating autoimmune reactions against self. The fine line that the immune system treads between antimicrobial immunity and autoimmunity is highlighted in reports by Pisitkun *et al.* on page 1669 of this issue (*1*) and by Kumar *et al*. on page 1665 (*2*). The groups have identified alterations in two mouse genes that illuminate the pathogenesis of a particularly sinister group of autoimmune diseases affecting 46 out of 100,000 people: systemic lupus erythematosus, Sjogren's syndrome, scleroderma, and polymyositis, where antibodies are secreted against DNA, RNA, and the associated proteins of our own cells.

Why chromatin self components—nucleic acids and associated proteins in the cell nucleus—so frequently recur as targets of systemic autoimmunity has been a long-standing mystery. The findings by Pisitkun *et al*. cap off an impressive body of evidence for "the Toll hypothesis" (*3*–*7*) that these autoimmune diseases stem from imperfect discrimination of microbe from self by an ancient receptor system for detecting microbial DNA and RNA. In plants and animals, a diverse set of leucine-rich repeat receptors sense unique chemical constituents (antigens) of microbes and trigger innate immune reactions to counter these infections (*8*–*10*). The Toll-like receptor (TLR) subfamily of transmembrane proteins is especially crucial in invertebrates and vertebrates.

TLR7 and TLR9 highlight the fine line distinguishing microbial and self-constituents, because they sense nucleic acids that are common to all living things. TLR9 best triggers immune reactions in the presence of bacterial DNA sequences with multiple CpG nucleotides. On a molar basis, mammalian DNA is a much less potent stimulator of TLR9 because it contains fewer such motifs, and these are mostly "masked" by methylation (*10*). TLR7 also shows preference for single-stranded viral genome RNA that is rich in G/U nucleotides and lacks mammalian-specific methylation and other modifications (*11*). A second level of specificity for the nucleic acid–sensing Toll-like receptors is their residence within intracellular endosomal vesicles, and dependence upon endosomal acidification to trigger immune responses (*10*, *12*). Many viruses and bacteria use receptor-mediated trafficking to acidified endosomes as a route to invade cells. In the small volume of an endosome, the single-stranded RNA genome contained in a single virion can release micromolar concentrations of TLR7 ligands. In contrast, self nucleic acids have limited access to this compartment because they are rapidly degraded when released into the extracellular fluid. Nevertheless, mammalian DNA and RNA can become potent stimulators of TLR9 and TLR7, respectively, if they are captured by receptors on the surface of immune cells (such as B cell receptors; see the figure) and concentrated in endosomes (*3*, *4*, *13*).

Plants and invertebrates display a modest repertoire of innate immune responses, and this probably limits the damage when immune reactions are inadvertently triggered by self. Vertebrates, however, have evolved adaptive immune responses that exploit the immunoglobulin domain as a platform to build an infinitely diverse array of microbial receptors—antibodies and T cell receptors. Through a combination of

The author is in the John Curtin School of Medical Research and Australian Phenomics Facility, The Australian National University, Post Office Box 334, Canberra, ACT 0200, Australia. E-mail: chris.goodnow@anu.edu.au

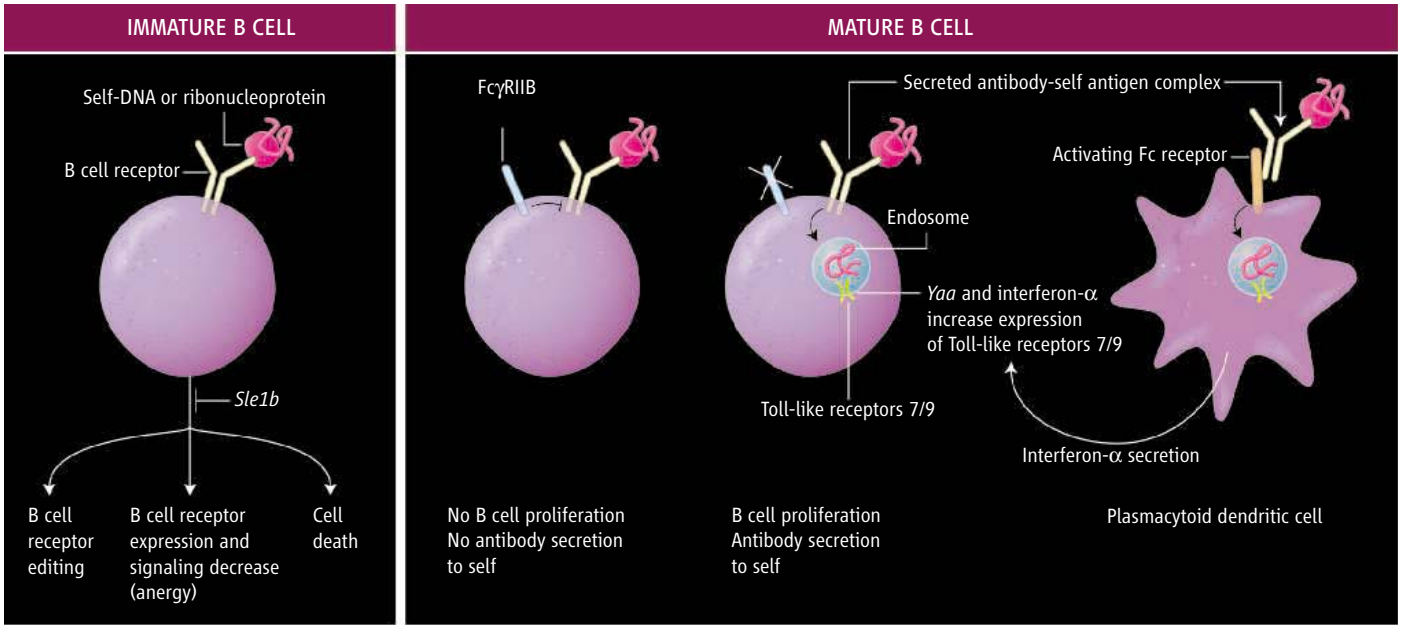

Pathogenesis of lupus autoantibodies. (Left) Binding of self-DNA or ribonucleoproteins to B cell receptors on an immature B cell transmits signals that edit the receptor genes and inhibit B cell survival, proliferation, and maturation. These signals are diminished by the *Sle1b* variant of the gene *Ly108*. **(Right)** In mature B cells, the inhibitory receptor (FcγRIIB) normally opposes signals for proliferation that are generated when the B cell receptor binds antigen. FcγRIIB deficiency, coupled with failure to eliminate immature self-reactive B cells due to *Sle1b*, allows self-reactive B cell receptors in mature B cells to signal proliferation and to capture nucleic acids and associated proteins, delivering them to TLR7 or TLR9 in endosomes. This promotes self-reactive B cell proliferation and antibody secretion. *Yaa* duplication of the *TLR7* gene and increased expression of *TLR7* by interferon-α that is secreted from dendritic cells increase this effect. Secreted antibodies complexed with self-DNA or ribonucleoproteins trigger TLR7- or TLR9-expressing dendritic cells to release more interferon-α, creating a potential positive-feedback loop.

somatic gene conversion, DNA rearrangements, and somatic hypermutation of immunoglobulin variable domains in B cells, the mammalian adaptive immune response tailors antibodies with extraordinary affinity and—under normal conditions—exquisite specificity against microbial and not self-antigens.

As indicated in the current studies (*1*, *2*), lupus autoimmunity arises from a conjunction between imperfect self-microbe discrimination by the Toll-like receptor and the antibody systems. When antibodies are formed in immature B cells by random somatic immunoglobulin-gene rearrangement, many are polyreactive and bind charged microbial and self-components—notably DNA, RNA, and their associated highly charged proteins (*14*). These self-binding antibodies are selected against by an ordered series of checkpoints that allow only B cells displaying (as a membrane-bound receptor) nonself-reactive antibodies to proliferate and mature into antibody-secreting cells (*15*). Binding of a self-antigen, such as ribonucleoprotein or chromatin, transmits intracellular selection signals that cause these cells either to die, "edit" the B cell receptor with a second round of gene rearrangement, or become weak (clonal anergy) such that their potential to proliferate decreases (see the figure). Cells that pass these checkpoints can be activated into cell division and antibody secretion when their B cell receptor binds a microbial antigen in lymph nodes or spleen.

The work by Kumar *et al*. culminates a two-decade effort tracking down the many chromosomal loci contributing to inherited lupus in certain mouse strains. One gene locus, *Sle1b*, has been isolated to a small region of chromosome 1 containing the SLAM family of lymphocyte adhesion receptors. Kumar *et al*. show that inherited differences in splicing of messenger RNA encoding one family member, *Ly108*, are sufficient to alter signaling by the B cell receptor. The product of the lupus-susceptible allele lowers the ability of self-reactive B cell receptors to signal clonal anergy and editing, thus increasing the number of self-reactive B cells in the lymph nodes and spleen.

The findings by Pisitkun *et al*. complete an equally long genetic detective story tracking lupus susceptibility in mice to a Y chromosome–linked "autoimmune accelerator" locus dubbed *Yaa*. Like many human and animal quantitative trait loci, the phenotypic effect of *Yaa* is graded and either suppressed or enhanced through complex interactions with other genes. For example, the combination of *Yaa* with *Sle1b* or with a deficiency in a second lupus susceptibility gene, *FcγRIIB* [encoding a B cell receptor for immunoglobulin G (IgG)] dramatically increases the onset and severity of lupus in an inbred strain of mice (C57BL/6) (*16*, *17*). Even though there are few genes on the Y chromosome, the nature of the *Yaa* gene has remained obscure. Pisitkun *et al*. show that *Yaa* is not due to a mutation in a normal Y-chromosome gene but rather is due to a duplication of a segment of X-chromosomal DNA that has been transposed to the Y. This effectively doubles the *TLR7* gene dosage and the responsiveness of B cells to TLR7 ligands. In conjunction with the lupus allele of *FcγRIIB*, this increases the incidence and severity of autoimmunity and redirects it from DNA to an RNA-associated pattern of autoantibodies. From a genetic perspective, the finding has broad significance because variation in copy number is emerging as a major potential source of inherited variation: Almost 4% of the human genome comprises recently duplicated segments, and a substantial fraction is transposed to other chromosomes (*18*).

Elucidation of *Yaa* and its interaction with *Sle1b* and *FcγRIIB*, coupled with evidence that TLR7 and TLR9 signaling deficiency prevents formation of lupus autoantibodies in mice (*3*–*7*), provides a compelling explanation for the pathogenesis of lupus. Breakdown of self-tolerance develops by a succession of defects in the checkpoints that normally control self-reactive cells, much like cancer arises through defects in multiple checkpoints of the cell cycle. One defect is an increase in the fraction of B cells bearing self-reactive B cell receptors. These cells have escaped clonal deletion, anergy, and editing caused by *Sle1b* (*2*), combined with other susceptibility genes in the C57BL/6 mouse strain (*19*). Furthermore, failure of inhibitory receptor signals that normally oppose B cell receptor signaling of proliferation compounds these problems, as exemplified by loss of FcγRIIB function (*1*, *17*).

CREDIT: P. HUEY/*SCIENCE*

Another pivotal step is breakdown in Toll-like receptor discrimination between microbial and self–nucleic acids, which occurs not only in B cells but also in collaborating dendritic cells of the immune system. B cells and plasmacytoid dendritic cells express TLR7 and TLR9, and signaling by these receptors synergizes with either signals from the B cell receptor to activate B cell proliferation (*3*, *4*, *7*, *20*) or with signals from the receptor for IgG on dendritic cells to activate secretion of the cytokine, interferon-α (*13*, *21*, *22*). When B cells bearing B cell receptors against self-RNA, self-DNA, or associated proteins escape deletion, editing, anergy, as well as the inhibitory effects of FcγRIIB, their B cell receptors not only signal proliferation directly but also efficiently capture and deliver self-RNA or self-DNA to endosomal compartments containing TLR7 or TLR9. The combination of B cell receptor and TLR signals provides a T cell–independent self-stimulus for B cell proliferation and autoantibody secretion. The potential for B cell self-stimulation is magnified by the increased sensitivity to TLR7 activation in B cells caused by the *Yaa* gene duplication. Interferon-α produced by plasmacytoid dendritic cells also increases B cell expression of TLR7 and its intracellular signaling adaptor, myd88 (*23*). Initially, the stimulus for interferon production might be a viral infection, but once IgG autoantibodies to ribonucleoproteins or chromatin have begun to be secreted, these circulating immune complexes will sustain and elevate interferon production by plasmacytoid dendritic cells and in turn promote further B cell activation in a positive-feedback cycle.

Toll-driven pathogenesis of lupus now seems firmly established in mice, but it also explains many clinical mysteries: the induction of lupus by drugs (procainamide) that block CpG DNA methylation or mercury compounds that bind to RNA; the therapeutic effect of chloroquine, which blocks TLR7 and TLR9 signaling; the evidence for robust interferon production in some lupus patients; and the observation that attacks of lupus can be precipitated by single-stranded RNA viral infections such as influenza or by ultraviolet light (which induces cell death and the consequential release of self-RNA and self-DNA). Given the fine line that Toll-like receptors tread between microbial and self-stimulation, it will be important to define mechanisms and regulators of TLR7 and TLR9 signaling. These almost certainly will reveal targets for new drugs to specifically treat lupus and candidate genes whose variation in copy number or sequence, like the TLR7 duplication, push the risk of self-stimulating this pathway over the precipice in different people with lupus.

References

1. P. Pisitkun *et al.*, *Science* **312**, 1669 (2006); published online 18 May 2006 (10.1126/science.1124978).
2. K. R. Kumar *et al.*, *Science* **312**, 1665 (2006).
3. E. A. Leadbetter *et al.*, *Nature* **416**, 603 (2002).
4. C. M. Lau *et al.*, *J. Exp. Med.* **202**, 1171 (2005).
5. S. R. Christensen *et al.*, *J. Exp. Med.* **202**, 321 (2005).
6. D. A. Martin, K. B. Elkon, *J. Exp. Med.* **202**, 1465 (2005).
7. M. Ehlers, H. Fukuyama, T. L. McGaha, A. Aderem, J. V. Ravetch, *J. Exp. Med.* **203**, 553 (2006).
8. N. Inohara, M. Chamaillard, C. McDonald, G. Nunez, *Annu. Rev. Biochem.* **74**, 355 (2005).
9. B. Beutler, *Nature* **430**, 257 (2004).
10. S. Akira, S. Uematsu, O. Takeuchi, *Cell* **124**, 783 (2006).
11. K. Kariko, M. Buckstein, H. Ni, D. Weissman, *Immunity* **23**, 165 (2005).
12. G. M. Barton, J. C. Kagan, R. Medzhitov, *Nat. Immunol.* **7**, 49 (2006).
13. H. Vallin, A. Perers, G. V. Alm, L. Ronnblom, *J. Immunol.* **163**, 6306 (1999).
14. H. Wardemann *et al.*, *Science* **301**, 1374 (2003).
15. C. C. Goodnow, J. Sprent, B. F. de St Groth, C. G. Vinuesa, *Nature* **435**, 590 (2005).
16. L. Morel *et al.*, *Proc. Natl. Acad. Sci. U.S.A.* **97**, 6670 (2000).
17. S. Bolland, Y. S. Yim, K. Tus, E. K. Wakeland, J. V. Ravetch, *J. Exp. Med.* **195**, 1167 (2002).
18. M. C. Zody *et al.*, *Nature* **440**, 1045 (2006).
19. D. R. Sekiguchi *et al.*, *J. Immunol.* **176**, 6879 (2006).
20. L. Rui, C. G. Vinuesa, J. Blasioli, C. C. Goodnow, *Nat. Immunol.* **4**, 594 (2003).
21. F. J. Barrat *et al.*, *J. Exp. Med.* **202**, 1131 (2005).
22. J. Vollmer *et al.*, *J. Exp. Med.* **202**, 1575 (2005).
23. I. B. Bekeredjian-Ding *et al.*, *J. Immunol.* **174**, 4043 (2005).

10.1126/science.1129797

ANTHROPOLOGY

Autonomous Cultivation Before Domestication

Early Near Eastern crop cultivation was a trial-and-error process. Some crops continued until full domestication, while others were abandoned and later adopted independently by distant societies.

Ehud Weiss, Mordechai E. Kislev, Anat Hartmann

It is widely believed that the primary domesticated crops of the Neolithic—namely, einkorn wheat, emmer wheat, barley, lentil, pea, chick pea, and flax—appeared initially in a core area from which they spread throughout the Middle East (*1*, *2*). Recent archaeobotanical data, however, indicate that predomestication cultivation of some of these species was carried out autonomously in very early sites of the Near Eastern PPNA (Pre-Pottery Neolithic A; ~11,500 to 10,300 calendar years before present). Moreover, the data also suggest that some of these crops did not develop into fully domesticated species because their cultivation was abandoned by the local populations.

E. Weiss and A. Hartmann are in the Martin (Szusz) Department of Land of Israel Studies and Archaeology and Faculty of Life Sciences, Bar-Ilan University, 52900 Ramat-Gan, Israel. M. E. Kislev is in the Faculty of Life Sciences, Bar-Ilan University, 52900 Ramat-Gan, Israel. E-mail: eweiss@mail.biu.ac.il

Human domestication of plants can be divided into three stages: "gathering," in which people gathered annual plants from wild stands; "cultivation," in which wild plant genotypes were systematically sown in fields of choice; and "domestication," in which mutant plants with desirable characteristics were raised. Cultivation is the essential stage, as the repetitive cycle of sowing, collecting, and sowing of wild plants gives rise to genotype accumulation that leads to domestication. Given the prevailing view that human selection of domesticated plants was not carried out intentionally, agro-evolution would have to take place over hundreds of years (*3*). The novel characteristics distinguishing domesticated from wild plants are by necessity species-specific. In the Neolithic primary domesticates, these include nonarticulating ears and plump grains in the cereals, pods that do not spontaneously release their seeds (indehiscence), and nondormant seeds in the pulses (i. e., peas, beans, lentils, and other legumes).

Archaeobotanical evidence indicates that different Near Eastern communities throughout prehistory cultivated various local species. Some of these early communities abandoned their plants, which represents a local dead end on the road to domestication. Thus, the initiation of agriculture in one place does not imply that the successfully grown plants would be continuously cultivated, an idea commonly recorded in the literature (*1*). Consequently, the location of the germ plasm of wild-plant founder stocks genetically associated with a particular fully domesticated plant (*1*) are, in reality, just the stocks that led ultimately to the domesticated plant. There might indeed have been earlier predomestication efforts—with different wild stocks—that were abandoned by the ancient society.

Two criteria identify cultivation in PPNA archaeobotanical assemblages. The first is the presence of a conspicuous quantity of seeds in greater amounts than would have been yielded

by harvesting local natural stands of the wild plant (*4*). If such an amount exceeds the yield of local wild stands, it eliminates the possibility that the local human community gathered it in the wild. The other criterion is the presence of predomesticated seeds that are mixed with plant seeds that grow as weeds in contemporary fields (*5*, *6*). This link could only have been established after humans started to manage fields, allowing weed plants to adapt to human-induced environmental conditions. Therefore, their coexistence indicates sowing rather than collecting of wild stands.

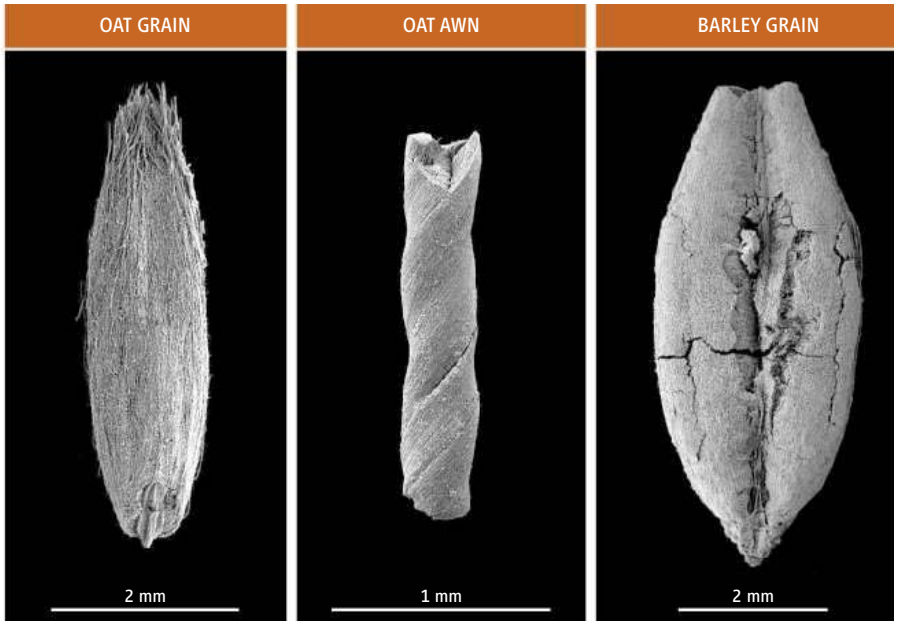

Early grains. Wild oat (*Avena sterilis*) from a PPNA granary in house 11, Gilgal, Jordan Valley: (**left**) grain, (**middle**) fragment of the spiral part of an awn—the specialized, drill-type, dispersal unit of the wild species, and (**right**) wild barley grain. These finds, representative of 120,000 wild oat and 260,000 wild barley grains at the Gilgal site, indicate that the inhabitants sowed these wild crops and were engaged in predomestication cultivation even in the PPNA.

On the basis of these criteria, we have identified several Near Eastern communities that cultivated plants that are among the early PPNA crops, which we term "pioneer crops." Each represents a special course in the transmigration of the wild variety into its domesticated form.

1) Wild barley (*Hordeum spontaneum*), the progenitor of domesticated barley (*H. vulgare*). A huge PPNA (~11,400 to 11,200 calendar years before present) granary, containing more than 260,000 wild barley grains combined with some 120,000 wild oat (*Avena sterilis*) grains, was uncovered in house 11 at Gilgal in the Jordan Valley (*7*) (see the figure). The only plausible explanation for such a large stash of seeds would be predomestication cultivation. Our field observations indicate that the local environment around the site does not support the gathering of these quantities without cultivation; no cereals grow in the vast saline deposits to the east of the site, and only moderate amounts can be collected in good years in the wadi-floodplains to the west. Within a few years, permanent settlement would deplete local plant resources by overexploitation. Humans would then have to abandon the site or start cultivating. Indeed, genetic studies have recently determined that barley was domesticated in the Israel-Jordan area (*8*). Moreover, a cache of 1000 oat grains was found in the layer just below that of the wild barley granary in house 11 (*7*). Taking into account the site's short occupation and that both finds are wild types, we have the first evidence for the rate of change in human mindset from "gathering" in the site's early stage to "cultivation" in the latter. Large quantities of wild barley grains were found also in the adjacent PPNA (~11,300 to 10,900 calendar years before present) site Netiv Hagdud (*9*).

In any case, the domesticated form of oats appeared initially in Europe during the second and first millennia B.C.E. (*2*). Thus, evidence from Gilgal suggests that the early collection or planting of a wild species in one place did not necessarily lead to its domestication, which occurred much later in a faraway region.

2) Rye (*Secale cereale*), a plant with a temporally and spatially fragmented history of domestication. The first signs of rye management—the appearance of domesticated-like grains but with no tough rachises (the ears' axis)—were found in late Natufian (~12,500 calendar years before present) Abu Hureyra in northern Syria (*10*). Domesticated rye grains, along with tough rachises, appeared at PPNB (~8600 calendar years before present) Can Hasan III in south-central Anatolia. Four millennia later, a granary of pure, plump, domesticated rye grains was established in Bronze Age Alaca Höyük, north-central Anatolia (*2*, *11*). Apparently, these three instances of potential and full domestication were local and brief, because present-day rye was independently domesticated in central Europe in the Iron Age (from about the sixth to the first century B.C.E.) (*2*, *12*).

3) Wild lentil (*Lens orientalis*), the progenitor of *L. culinaris*. Two hundred and sixty-seven and 205 seeds of wild lentils were found, respectively, in PPNA (~11,000 calendar years before present) Jerf el Ahmar, Syria, and in Netiv Hagdud (*9*, *13*). Wild lentil is a low (5 to 25 cm), inconspicuous plant, yielding a meager 10 ± 9 seeds per plant. In addition, it is characterized by 90% seed dormancy—that is, only 10% of the seeds germinate readily after sowing. Lentil domestication includes two stages: loss of dormancy and development of pod indehiscence, each governed by a single mutation (*2*, *14*). Because of seed dormancy and poor yield, cultivating wild lentil is implausible, as the expected harvest would equal the number of seeds sown (out of 10 sown seeds, 1 germinates and produces 10 seeds). Therefore, only after the seed dormancy-free mutation occurred could lentils be cultivated (*14*). If so, these PPNA finds may represent mutant forms that belong to the first stage of lentil domestication.

Moreover, because Jerf el Ahmar lies in the heart of the suggested genetic stock origin of *L. orientalis* in southeastern Turkey and northern Syria (*15*), these finds indicate that the first stage of lentil domestication—loss of dormancy—occurred there and quickly spread south to the Jordan Valley. In fact, obsidian objects found at Netiv Hagdud were transported along this well-known trade route (*16*).

The second mutation—and final stage of domestication—is represented by the huge ~1.4 million–seed *L. culinaris* hoard in PPNB (8800 calendar years before present) Yiftah'el, near Nazareth, Israel, some 600 km southwest of Jerf el Ahmar. Moreover, the domesticated state of the Yiftah'el hoard is enforced by its contamination with fruits of *Galium tricornutum*, a well-known weed in present-day lentil fields (*4*).

The beginning of agriculture is framed by both time and stage of plant domestication. Before the onset of the PPNA (~11,500 calendar years before present), humans were involved in "gathering," and from the PPNB (~10,300 calendar years before present) onward, they cultivated domesticated plants (*2*). This frame assigns the progression from wild to domesticated species to the short PPNA, ~1200 years. It also agrees with our data indicating Gilgal's early PPNA transition from "gathering" to "cultivation" and the several hundred years for the "cultivation" to "domestication" process (*3*).

Evidence already gathered shows that at least one PPNA pioneer crop, namely lentil,

CREDIT: Y. LANGZAM/BAR-ILAN UNIVERSITY, ISRAEL

may have been domesticated some hundreds, or even thousands, of kilometers away from the center of its founder-stock germ plasm. Thus, the location of founder germ plasm stocks without supplemental evidence cannot be used for confident reconstruction of the locale of final domestication.

Increasing archaeobotanical evidence indicates that the beginning of agriculture, as well as of crop domestication, was not necessarily a single event but a process of trial and error. For oats and rye, for example, the beginnings of cultivation and subsequent domestication are separated by millennia and great distances. For the Near East, current data suggest that at least three or four species can be considered as early pioneer crops, which predate the seven well-recognized species of founder crops. Because two of these pioneer species—barley and lentil—belong to the group of founder crops as well, our understanding of the domestication of these species must be revised. In the PPNA, Near Eastern human groups in two regions already possessed and applied agricultural knowledge: In the north, they planted lentil and perhaps rye; and in the south, they raised barley and probably oat, together with imported lentil. Although this early barley and lentil was eventually domesticated in the region, two of the crops raised or gathered there—rye and oats—were abandoned.

The transition to food production in eastern North America shows a notable similarity to the Near East. There, indigenous plants—chenopod (*Chenopodium berlandieri* subsp. *jonesianum*), marsh elder (*Iva annua* var. *macrocarpa*), squash (*Cucurbita pepo* subsp. *ovifera*), and sunflower (*Helianthus annuus* var. *macrocarpus*)—became domesticants under indigenous group management between 5000 and 4000 years before the present. In contrast, the cereal-like erect knotweed (*Polygonum erectum*), little barley (*Hordeum pusillum*), and maygrass (*Phalaris caroliniana*), though clearly of economic importance as cultivated crops by about 2500 to 2200 years before present, never became morphological domesticates. With the shift to maize-centered agriculture about 900 C.E. and the arrival of the common bean (*Phaseolus vulgaris*) several centuries later, local eastern crops became less important, and by 1800 C.E., only sunflower and squash were still being grown (*17*).

Thus, both in the Near East and early eastern North America, the first stage of agriculture was cultivating annual wild plants; the second stage was cultivating both wild types and domesticants; and the last stage was the cultivation of domesticants alone. Finally, the recent discovery of PPNA fig domestication (*18*) raises the question of whether, in worldwide locales of agriculture origin, fruit trees were domesticated contemporaneously with the annuals.

References

1. F. Salamini, H. Özkan, A. Brandolini, R. Schäfer-Pregl, W. Martin, *Nat. Rev. Genet.* **3**, 429 (2002).
2. D. Zohary, M. Hopf, *Domestication of Plants in the Old World* (Oxford Science, Oxford, ed. 3, 2000).
3. M. Kislev, *Isr. J. Bot.* **50**, S85 (2002).
4. Y. Garfinkel, M. Kislev, D. Zohary, *Isr. J. Bot.* **37**, 49 (1988).
5. W. van Zeist, J. A. H. Bakker-Heeres, *Palaeohistoria* **26**, 151 (1984).
6. S. Colledge, in *The Origins of Agriculture and Crop Domestication of Crop Plants in the Near East*, A. B. Damania *et al.*, Eds. (FAO/IPGRI/GRCP/ICARDA, Aleppo, Syria, 1998).
7. A. Hartmann, unpublished data.
8. A. Badr *et al.*, *Mol. Biol. Evol.* **17**, 499 (2000).
9. M. E. Kislev, in *An Early Neolithic Village in the Jordan Valley*, Part 1, *The Archaeology of Netiv Hagdud*, O. Bar-Yosef, A. Gopher, Eds. (Peabody Museum of Archaeology and Ethnology, Harvard Univ., Cambridge, MA, 1997), pp. 209–236.
10. G. C. Hillman *et al.*, *Holocene* **11**, 383 (2001).
11. G. C. Hillman, *Anatolian Stud.* **28**, 157 (1978).
12. K.-E. Behre, *Veg. Hist. Archaeobot.* **1**, 141 (1992).
13. G. Willcox, *Veg. Hist. Archaeobot.* **11**, 55 (2002).
14. G. Ladizinsky, *Econ. Bot.* **41**, 60 (1987).
15. G. Ladizinsky, *Genet. Resour. Crop Evol.* **46**, 115 (1999).
16. J. Yellin, in *An Early Neolithic Village in the Jordan Valley*, Part 1, *The Archaeology of Netiv Hagdud*, O. Bar-Yosef, A. Gopher, Eds. ((Peabody Museum of Archaeology and Ethnology, Harvard Univ., Cambridge, MA, 1997), pp. 193–196.
17. B. D. Smith, *Rivers of Change* (Univ. of Alabama Press, Tuscaloosa, AL, ed. 3, 2006).
18. M. E. Kislev, A. Hartmann, O. Bar-Yosef, *Science* **312**, 1372 (2006).

10.1126/science.1127235

ASTRONOMY

A Key Molecular Ion in the Universe and in the Laboratory

T. R. Geballe and T. Oka

The molecular ion H_3^+ is abundant in interstellar clouds and presents many interesting puzzles in the laboratory. A recent conference explored the current knowledge about this species and its implications for astrophysics.

The protonated hydrogen molecule, H_3^+ is the most abundant molecular ion in the universe and plays a pivotal role in interstellar chemistry. As the simplest of all polyatomic molecules, H_3^+ is fascinating to both physicists and chemists, but lately research in astronomy has been an important driver of both laboratory work and theory. Interstellar clouds are almost entirely molecular hydrogen, and anything that causes ionization of H_2 in them should lead to the production of H_3^+. On 16 to 18 January 2006, researchers from different fields in which H_3^+ plays a major role met in London, at the Royal Society and at University College London, to discuss this fundamental molecular ion from a variety of perspectives. A similar meeting on H_3^+ took place in 2000, but since then many exciting developments related to this ion and its deuterated species, both in the laboratory and in space, made a new discussion meeting a necessity.

H_3^+ was discovered in 1911 by J. J. Thomson (*1*). First observed as an "evanescent" trace product of a discharge in H_2, its abundance was soon found to exceed that of both H^+ and H_2^+ in most hydrogen plasmas, demonstrating both its ease of formation and stability. It was realized that H_3^+ was being formed by the efficient reaction, $H_2^+ + H_2 \rightarrow H_3^+ + H$ (*2*). H_3^+ is highly reactive, happily donating a proton to almost every atom and molecule it encounters. In astrophysical environments, the principal seed is cosmic rays, which, as they traverse interstellar clouds, leave trails of H_2^+ ions in their wakes, which are rapidly converted to H_3^+ by the aforementioned reaction. The importance of H_3^+ for interstellar chemistry was recognized in 1973 in two seminal papers (*3*, *4*), both of which demonstrated that H_3^+ is the base of a tree of ion-molecule reactions that produce many of the molecules found in space.

Although the presence of H_3^+ in dense clouds could be inferred, direct detection of H_3^+ proved to be elusive. The only method of observing the molecule in space is via the ν_2 vibration-rotation band whose fundamental occurs near a wavelength of 4 μm. This spectrum was observed in the laboratory in 1980 (*5*). It took 16 additional years before H_3^+ was detected in interstellar space (*6*).

The 2000 Discussion Meeting took place less than 4 years after this detection, and roughly a decade after the ion had been found in the aurorae of Jupiter, Saturn, and Uranus (*7*–*9*). At that time it was already clear that there was a problem in understanding the interstellar data. Although the abundance of H_3^+ in dense clouds was roughly as expected, it was more than an order of magnitude higher than predicted in diffuse clouds where abundant electrons destroy H_3^+ (*10*). That difference has only become more striking in subse-

T. R. Geballe is at the Gemini Observatory, Hilo, HI 96720, USA. T. Oka is in the Department of Chemistry and the Department of Astronomy and Astrophysics, University of Chicago, Chicago, IL 60637, USA. E-mail: tgeballe@gemini.edu (T.R.G.), t-oka@uchicago.edu (T.O.)

quent years as unexpectedly large amounts of H_3^+ have been found in additional diffuse clouds (*11*). Now a combination of measurements in the laboratory and at the telescope have shown that the difference is likely a result of the cosmic-ray ionization rate being much larger in diffuse clouds than in dense clouds (*12*). Although the reason for this is not completely understood, it is well established observationally that, contrary to initial expectations, the abundance of H_3^+ relative to all forms of hydrogen is 10 times higher in diffuse clouds than in dense clouds, and the total amount of H_3^+ is much higher as well. H_3^+ has thus emerged as a unique and powerful astrophysical probe to study the diffuse interstellar medium.

An inspiring example of this is the recent discovery of a vast amount of high-temperature and low-density gas in the Central Molecular Zone of the Milky Way, a region of radius ~200 pc at the Galactic center (*13*). The physical state of the gas in that region, as clearly revealed by spectroscopy of three lines of H_3^+ and one line of carbon monoxide (see the figure), is unique in the Galaxy. The locations along the 8 kpc–long line of sight to the Galactic center where most of the narrow absorption components are formed were already well known from previous radio and infrared observations. However, because the two molecules probe different types of clouds (CO is much more abundant in dense clouds than in diffuse clouds, whereas the opposite is true for H_3^+), in combination they allow one to discriminate between cloud types. The new measurements strongly constrain the amount of dense molecular gas in the center. Together with other gaseous components in the nucleus observed at radio, infrared, and x-ray wavelengths, the H_3^+ measurements provide information vital for understanding the complex energetics of the Galactic center. H_3^+ has also been detected for the first time in an external galaxy (*14*), opening up a new and potentially fruitful area of study.

A remarkable manifestation of the fundamental role H_3^+ plays in interstellar chemistry has recently been revealed in the extremely high deuterium fractionation in the cold cores of dark clouds, where multiply deuterated molecules such as D_2CO, ND_3, and CD_3OH have been discovered. In these clouds the usual destroyers of H_3^+ such as CO are frozen onto dust particles, and HD becomes the principal agent for removal of H_3^+, through the reaction $H_3^+ + HD \rightarrow H_2D^+ + H$. This reaction and similar ones producing more deuterated species proceed efficiently due to the low temperature. For some cases model calculations predict that, despite the extremely low abundance of deuterium, the abundance of H_3^+ isotopomers is in the order $H_3^+ < H_2D^+ < D_2H^+ << D_3^+$ (*15*). Recent detections of H_2D^+ and D_2H^+ support this prediction (*16*).

Studies of H_3^+ are yielding new and exciting results in planetary astronomy. Since its discovery in the jovian ionosphere in 1989, H_3^+ has been used to study plasmas in planetary ionospheres from ground-based observatories. Now it is becoming increasingly clear that H_3^+ also plays a major role in the dynamics of giant planets through both its efficient emission and ion-neutral coupling (*17*).

Although the new astronomical observations spearhead much of the progress in H_3^+ science, during the same period theoretical and laboratory progress in understanding H_3^+ has been no less exciting. Perhaps the most drastic change from the last meeting is the advent of the badly needed full-fledged theory of dissociative recombination. An extensive theoretical calculation that fully takes into account the multidimensionality of the process, including the Jahn-Teller effect (*18*), has given a value for the dissociative recombination rate that is more than two orders of magnitude higher than the one obtained in 2000 and is close to the experimental result. Measurements with rotationally cooled H_3^+ have also been performed (*11*). After decades of uncertainty, a reliable rate of dissociative recombination, which is of overwhelming importance for understanding the chemistry of the diffuse interstellar medium, appears to have been determined.

Interplay between theory and experiment has been the cornerstone of H_3^+ spectroscopy, and the past two decades have seen several theoretical groups competing to achieve a rigorous theory and the experimental groups vying to extend the observations to higher energy. Theoretical efforts have now reached the level where a first-principles calculation based only on natural constants gives spectroscopic accuracy of better than 1 cm^{-1} for states up to 12,500 cm^{-1} above ground (*19*). This may be likened to what the theory for H_2 had achieved in 1975. Theories of H_3^+ in the triplet state and asymptotic vibrational states near the dissociation limit have also been developed.

Meanwhile, laboratory spectroscopy of overtone and combination bands of H_3^+ has reached the visible region, probing high vibrational levels that exceed the barrier to linearity (the vigorously vibrating molecule is on average still an equilateral triangle, but instantaneously linear) (*20*). The higher the energy, the weaker the spectrum, but increases in sensitivity by many orders of magnitude afforded by various new techniques more than compensate. A new method of action spectroscopy, utilizing the ion-neutral reaction of H_3^+ with Ar, has been introduced. With the aforementioned discoveries of high deuterium fractionation in cold interstellar clouds, spectroscopy of deuterated species has been greatly developed (*21*). The new method of lowering the velocity of H_3^+ by sympathetic cooling with laser-cooled ultracold atomic ions (*22*) is noteworthy because it opens the path to ultrahigh-resolution spectroscopy of H_3^+ and its deuterated species.

Understanding the amazingly high interstellar deuterium fractionation has also required detailed information on the reaction rate of H_3^+ and HD and other similar reactions. In addition, the observation of high-temperature gas in the Galactic center

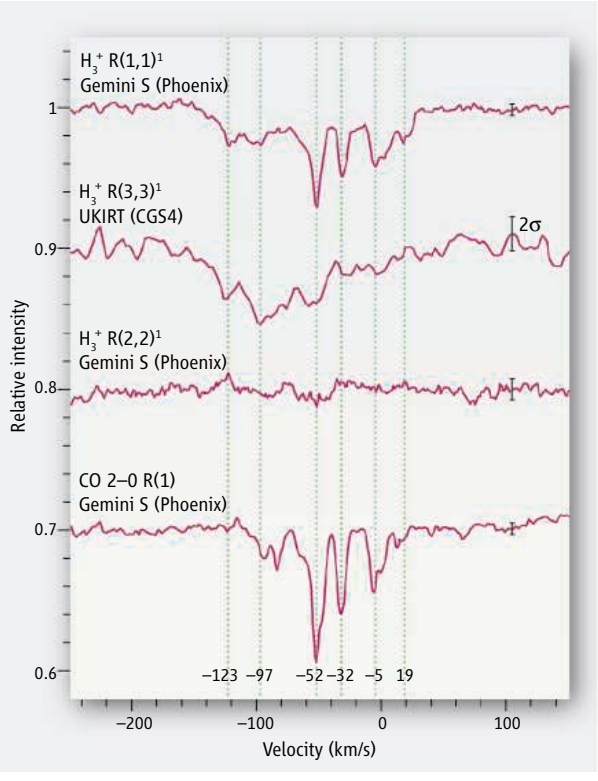

Telltale molecules. Spectra of three lines of H_3^+ at 3.5 to 3.7 μm and one line of CO at 2.34 μm toward the galactic center source GCS 3-2, observed at the Gemini South Telescope on Cerro Pachon, Chile, and the United Kingdom Infrared Telescope on Mauna Kea, Hawaii (*13*). The spectra are offset and are magnified by different factors. The sharp absorption components seen in the H_3^+ R(1,1)^1 and CO lines arise in dense clouds, mostly in spiral arms between the Sun and the center but some very close to the center. The broad absorption profile seen in the H_3^+ R(3,3)^1 line and overlying the sharp features in the H_3^+ R(1,1)^1 profile is thought to arise in gas within 200 pc of the nucleus. The presence of the H_3^+ R(3,3)^1 line demonstrates that the gas is warm and the absence of the H_3^+ R(2,2)^1 line shows that it is diffuse.

requires detailed information on the state-specific collision rate and ortho-to-para conversions of H_2, H_3^+, and isotopomers. Such information is being provided by means of an ingenious temperature-variable cryogenic ion trap (*23*)

The Discussion Meeting contained many other exciting reports on H_3^+ and its deuterated species, as well as the related species, H_3, H_3^-, H_3^{++}, H_5^+, $H_3^+(H_2)_n$, etc. (*24*). With the 100th anniversary of the discovery of H_3^+ only 5 years away and research forging ahead on many fronts, it is likely that a centennial Discussion Meeting on this most interesting and important molecular ion and its relatives will be timely.

References

1. J. J. Thomson, *Philos. Mag*. **21**, 225 (1911).
2. T. R. Hogness, E. G. Lunn, *Phys. Rev*. **26**, 44 (1925).
3. E. Herbst, W. Klemperer, *Astrophys. J.* **185**, 505 (1973).
4. W. D. Watson, *Astrophys. J.* **183**, L17 (1973).
5. T. Oka, *Phys. Rev. Lett*. **45**, 531 (1980).
6. T. R. Geballe. T. Oka, *Nature* **384**, 334 (1996).
7. P. Drossart, *et al*., *Nature* **340**, 539 (1989).
8. T. R. Geballe, M.-F. Jagod, T. Oka, *Astrophys. J.* **408**, L109 (1993).
9. L. M. Trafton *et al*., *Astrophys. J.* **405**, 761 (1993).
10. T. R. Geballe *et al*., *Astrophys. J.* **510**, 251 (1999).
11. B. J. McCall *et al*., *Astrophys. J.* **567**, 391 (2002).
12. B. J. McCall *et al*., *Nature* **422**, 500 (2003).
13. T. Oka *et al*., *Astrophys. J.* **632**, 882 (2005).
14. T. R. Geballe *et al*., http://arxiv.org/abs/astro-ph/0603041.
15. H. Roberts, E. Herbst, T. J. Millar, *Astrophys. J.* **591**, L41 (2003).
16. C. Vastel, T. G. Phillips, H. Yoshida, *Astrophys. J.* **606**, 127 (2004).
17. S. Miller, A. Aylward, G. Millward, *Space Sci. Rev.* **116**, 319 (2005).
18. V. Kokoouline, C. H. Greene, *Phys. Rev*. **A68**, 012703 (2003).
19. P. Schiffels, A. Alijah, J. Hinze, *Mol. Phys*. **101**, 189 (2003).
20. J. L. Gottfried, B. J. McCall, T. Oka, *J. Chem. Phys*. **118**, 10890 (2003).
21. T. Amano, T. Hirao, *J. Mol. Spectrosc*. **233**, 7 (2005).
22. P. Blythe *et al*., *Phys. Rev. Lett.* **95**, 183002 (2005).
23. D. Gerlich, E. Herbst, E. Roueff, *Planet. Space Sci.* **50**, 1275 (2002).
24. Proceedings of the 2006 Discussion Meeting on the Physics, Chemistry, and Astronomy of H_3^+, *Philos. Trans. R. Soc*., in press.

10.1126/science.1126279

CLIMATE CHANGE

Permafrost and the Global Carbon Budget

Climate warming will thaw permafrost, releasing trapped carbon from this high-latitude reservoir and further exacerbating global warming.

Sergey A. Zimov, Edward A. G. Schuur, F. Stuart Chapin III

The carbon content of Earth's atmosphere has increased from ~360 gigatons (Gt)—mainly as CO_2—during the last glacial maximum to ~560 Gt during preindustrial times and ~730 Gt today. These changes reflect redistributions among the main global carbon reservoirs. The largest such reservoir is the ocean (40,000 Gt, of which 2500 Gt is organic carbon), followed by soils (1500 Gt) and vegetation (650 Gt). There is also a large geological reservoir, from which ~6.5 Gt of carbon are released annually to the atmosphere by burning fossil fuels.

Permafrost (permanently frozen ground) is an additional large carbon reservoir that is rarely incorporated into analyses of changes in global carbon reservoirs. Here we illustrate the importance of permafrost carbon in the global carbon budget by describing the past and potential future dynamics of frozen loess (windblown dust, termed yedoma in Siberia) that was deposited during the glacial age, covering more than 1 million km^2 of the north plains of Siberia and Central Alaska to an average depth of ~25 m.

The frozen yedoma represents relict soils of the mammoth steppe-tundra ecosystem that occupied this territory during glacial times (*1*). As windblown or river-borne materials accumulated on the soil surface, the bottom of the previously thawed soil layer became incorporated into permafrost. These sediments contain little of the humus that characterizes modern ecosystems of the region, but they comprise large amounts of grass roots (see the figure) and animal bones, resulting in a carbon content that is much higher than is typical of most thawed mineral soils. Frozen yedoma deposits across Siberia and Alaska typically have average carbon contents from 2% to 5%—roughly 10 to 30 times the amount of carbon generally found in deep, nonpermafrost mineral soils.

Using an overall average carbon concentration for yedoma of ~2.6%, as well as the typical bulk density, average thickness, and ice-wedge content of the yedoma, we estimate the carbon reservoir in frozen yedoma to be ~500 Gt (*2*). Another ~400 Gt of carbon are contained in nonyedoma permafrost (excluding peatlands) (*3*), and 50 to 70 Gt reside in the peatbogs of western Siberia (*4*). These preliminary estimates indicate that permafrost is a large carbon reservoir, intermediate in size between those of vegetation and soils.

Our laboratory incubations and field experiments show that the organic matter in yedoma decomposes quickly when thawed, resulting in respiration rates of initially 10 to 40 g of carbon per m^3 per day, and then 0.5 to 5 g of carbon per m^3 per day over several years. These rates are similar to those of productive northern grassland soils. If these rates are sustained in the long term, as field observations suggest, then most carbon in recently thawed yedoma will be released within a century—a striking contrast to the preservation of carbon for tens of thousands of years when frozen in permafrost.

Some local thawing of yedoma occurs independently of climate change. When permafrost ice wedges thaw, the ground subsides (thermokarst), forming lakes. The abundant thermokarst lakes on yedoma territory migrate across the plains as thawing and subsidence occur along their margins. During the Holocene (the past 10,000 years), about half of the yedoma thawed beneath these migratory lakes and then refroze when the lakes had moved on.

The yedoma carbon beneath the thermokarst lakes is decomposed by microbes under anaerobic conditions, producing methane that is released to the atmosphere primarily by bubbling (*5*). Near eroding lake shores, methane bubbling is so high that channels through the lake ice remain open all winter. During a thaw/freeze cycle associated with lake migration, ~30% of yedoma carbon is decomposed by microbes and converted to methane. As a potent greenhouse gas, this methane contributes to climate warming.

In response to climate warming, permafrost sediments have already begun to thaw (*6*), with extreme projections that almost all yedoma will thaw by the end of the 21st century (*7*). What would happen to the carbon derived from permafrost if high-latitude warming continues?

The unique isotopic signature of permafrost carbon provides clues from past warming episodes, such as the transition from the last glacial maximum to the Holocene. The $^{13}C/^{12}C$ isotope ratio of the permafrost reservoir is similar to that of soil, vegetation, and

S. A. Zimov is at the North-East Scientific Station, Pacific Institute for Geography, Russian Academy of Sciences, Cherskii, Republic of Sakha 678830, Russia. E-mail: szimov@cher.sakha.ru E. A. G. Schuur is in the Department of Botany, University of Florida, Gainesville, FL 32611, USA. F. S. Chapin III is at the Institute of Arctic Biology, University of Alaska, Fairbanks, AK 99775–7000, USA.

marine biota. Unlike these reservoirs, however, permafrost carbon is depleted in radiocarbon (^{14}C). Methane, CO_2, and dissolved organic carbon released from thawing yedoma have a radiocarbon age reflecting the time when the yedoma was formed in the glacial age, differentiating the permafrost carbon signal from emissions from other reservoirs that have a modern radiocarbon age.

For example, the release of a large pool of radiocarbon-depleted carbon from permafrost could have contributed to declines in atmospheric radiocarbon during two strong warming events that occurred during the last deglaciation. These radiocarbon changes have previously been attributed to an assumed increase in deep- and mid-ocean venting, because no terrestrial pool that could readily release ancient carbon (such as permafrost carbon) was included in the analysis (*8*).

Carbon loss from permafrost may also have contributed to past changes in atmospheric CO_2 concentrations. During the last glacial maximum, permafrost extended south to 45°N in Europe and to 40°N in North America. About 4 m of yedoma-like soils accumulated across 3 million km^2 in the steppe-tundra ecosystems of Europe and south of West Siberia toward the end of the glacial age and thawed in the early Holocene (*9*, *10*). If this frozen loess initially had a carbon concentration similar to the average for yedoma (2.6% C) and decreased to the carbon concentration of the current soils (0.15% C), it would have released about 500 Gt of permafrost carbon at the beginning of the Holocene. Additional carbon was presumably released by thawing of nonloess permafrost (river-borne, slope, and glacial sediments).

Most researchers assume that the terrestrial carbon reservoir declined by 300 to 700 Gt at the last glacial maximum as a result of ice sheet formation and a decline in forest area. This terrestrial carbon was assumed to have been transferred to the oceans (*11*). However, these estimates ignore the soils and peat buried in frozen moraines beneath glaciers (380 Gt) (*12*) and assume that the broad expanses (~24 million km^2) of steppe-tundra had a carbon content typical of polar deserts (4 to 40 Gt) (*13*, *14*). The assumed soil carbon content for steppe-tundra in Siberia was only 0.1 kg m^{-2} (*13*).

We can now provide a more accurate estimate of the carbon content of the steppe-tundra based on direct measurements. The carbon content of lowland steppe-tundra soils in Siberia and Alaska is ~2.6% with an active-layer depth of about 1 m, yielding ~42 kg of carbon per m^2. In mountains, the carbon content is about 50% less, giving an average carbon content for the steppe-tundra biome of ~30 kg per m^2 and a total carbon content of ~720 Gt. Taking into account frozen loess (500 Gt), steppe-tundra soils (720 Gt), sediments beneath ice sheets (380 Gt), and other frozen sediments, we hypothesize that the total terrestrial carbon reservoir did not decrease in glacial times but instead may have even absorbed several hundred gigatons of carbon from the atmosphere and ocean.

The decline in the $^{13}C/^{12}C$ ratio in marine dissolved inorganic carbon, recorded in shells of foraminifera, in glacial times is usually taken as strong evidence of transfer of terrestrial carbon to the ocean (*11*). However, the size and isotopic composition of the marine reservoir of organic carbon are similar to those on land (*15*), making it difficult to identify changes in the relative sizes of marine and terrestrial organic reservoirs. A decline in marine productivity (perhaps associated with reduced vertical mixing and reduced illumination under ice) might lead to a net release of depleted ^{13}C from marine organic carbon reservoirs that could instead have caused the decreased foraminifera isotope ratio. Recent reanalysis of data from marine sediment cores shows that biological productivity and carbon export to ocean sediments were substantially reduced at the middle of the last glacial cycle in all oceans. At the last glacial maximum, biological productivity in the Atlantic Ocean increased, but in the much larger Pacific Ocean it decreased (*16*). Independent of carbon transfers between land and ocean, the reduction in alkalinity associated with the lower atmospheric CO_2 concentration at the last glacial maximum could also explain the reduced $^{13}C/^{12}C$ ratio of foraminifera (*17*). Given this estimate of permafrost carbon storage on land, the redistribution of carbon during glacial periods is a fertile area for reassessment.

Permafrost is a globally significant carbon reservoir that responds to climate change in a unique and very simple way: With warming, its spatial extent declines, causing rapid carbon loss; with cooling, the permafrost reservoir refills slowly, a dynamic that mirrors the past atmospheric record of CO_2. In a warmer climate, permafrost carbon is thus likely to become part of more actively cycling carbon reservoirs. Factors inducing high-latitude climate warming should be mitigated to minimize the risk of a potentially large carbon release that would further increase climate warming.

CREDIT: S. A. ZIMOV

Ancient soils. (**Left**) Exposed carbon-rich soils from the mammoth steppe-tundra along the Kolyma River in Siberia. The soils are 53 m thick; massive ice wedges are visible. (**Right**) Soil close-up showing 30,000-year-old grass roots preserved in the permafrost.

References and Notes

1. A. V. Sher *et al.*, *Quat. Sci. Rev.* **24**, 533 (2005).
2. In our calculation, we assumed a bulk density of 1.65 tons per m^3, a yedoma thickness of 25 m, and an ice-wedge content of 50%.
3. Arctic Climate Impact Assessment, *Impacts of a Warming Arctic* (Cambridge Univ. Press, Cambridge, 2005).
4. L. C. Smith *et al.*, *Science* **303**, 353 (2004).
5. S. A. Zimov *et al.*, *Science* **277**, 800 (1997).
6. V. E. Romanovsky *et al.*, *Tohoku Geophys. J.* **36**, 224 (2001).
7. D. M. Lawrence, A. G. Slater, *Geophys. Res. Lett.* **32**, L24401 (2005).
8. K. A. Hughen *et al.*, *Science* **290**, 1951 (2000).
9. A. L. Washburn, *Geocryology. A Survey of Periglacial Processes and Environments* (Edward Arnold, London, 1979).
10. A. A. Velichko, *Prirodnyi Process v Pleistocene* (Nauka, Moscow, 1973).
11. M. I. Bird *et al.*, *Nature* **371**, 566 (1994).
12. N. Zeng, *Adv. Atmos. Sci.* **20**, 677 (2003).
13. J. M. Adams *et al.*, *Nature* **348**, 711 (1990).
14. P. Friedlingstein *et al.*, *J. Geophys. Res.* **100**, 7203 (1995).
15. V. Brovkin *et al.*, *Geochem. Geophys. Geosyst.* **3**, 1027 (2002).
16. K. E. Kohfeld *et al.*, *Science* **308**, 74 (2005).
17. H. J. Spero et al., *Nature* **390**, 497 (1997).

10.1126/science.1128908

Positive Natural Selection in the Human Lineage

P. C. Sabeti,[1,2*] S. F. Schaffner,[1*†] B. Fry,[1] J. Lohmueller,[1,3] P. Varilly,[1] O. Shamovsky,[1] A. Palma,[1] T. S. Mikkelsen,[1] D. Altshuler,[1,4,5] E. S. Lander[1,6,7,8]

Positive natural selection is the force that drives the increase in prevalence of advantageous traits, and it has played a central role in our development as a species. Until recently, the study of natural selection in humans has largely been restricted to comparing individual candidate genes to theoretical expectations. The advent of genome-wide sequence and polymorphism data brings fundamental new tools to the study of natural selection. It is now possible to identify new candidates for selection and to reevaluate previous claims by comparison with empirical distributions of DNA sequence variation across the human genome and among populations. The flood of data and analytical methods, however, raises many new challenges. Here, we review approaches to detect positive natural selection, describe results from recent analyses of genome-wide data, and discuss the prospects and challenges ahead as we expand our understanding of the role of natural selection in shaping the human genome.

Homo sapiens, like all species, has been shaped by positive natural selection. As first articulated by Darwin and Wallace in 1858, positive selection is the principle that beneficial traits—those that make it more likely that their carriers will survive and reproduce—tend to become more frequent in populations over time (*1*). In the case of humans, these beneficial traits likely included bipedalism, speech, resistance to infectious diseases, and other adaptations to new and diverse environments. Understanding the traits (and genes underlying them) that have undergone positive selection during human evolution can provide insight into the events that have shaped our species, as well as into the diseases that continue to plague us today.

Until very recently, the only practical way to identify cases of positive selection in humans was to examine individual candidate genes. Allison noted in 1954 that the geographical distribution of sickle cell disease was limited to Africa and correlated with malaria endemicity (*2*); this observation led to the identification of the sickle cell mutation in the *Hemoglobin-B* gene (*HBB*) as having been the target of selection for malaria resistance (*3*, *4*). Since then, approximately 90 different loci have been proposed as possible targets for selection (table S1 provides a review of this literature).

Some of the proposed candidates for selection, like *HBB*, have strong support in the form of a functional mutation with an identified phenotypic effect that is a likely target of selection. In the case of *HBB*, the selected mutation creates a glutamate to valine amino acid change, but the target of selection need not be in the protein-coding region of a gene. For example, the Duffy antigen (*FY*) gene encodes a membrane protein used by the *Plasmodium vivax* malaria parasite to enter red blood cells. A mutation in the promoter of *FY* that disrupts protein expression confers protection against *P. vivax* malaria and was proposed to be selected for in regions of Africa where *P. vivax* malaria has been endemic (*5*). Another example is a mutation in a regulatory region near the gene for lactase (*LCT*) that allows lactose tolerance to persist into adulthood. This particular variant was apparently selected in parts of Europe after the domestication of cattle (*6*).

Often, however, the functional target of selection is not known. In some cases, candidate genes gain support because they lie in functional pathways, such as spermatogenesis and the immune response, that are known to be frequent targets for selection in other species. One example is protamine 1 (PRM1), a sperm-specific protein that compacts sperm DNA (*7*, *8*). Such cases, however, are the exception. Most proposed candidates lack compelling biological support. Rather, the argument for selection has relied solely on comparative and population genetic evidence.

Despite its great potential to illuminate new biological mechanisms, identification of selected loci by genetic evidence alone is fraught with methodological challenges. Studies based on comparisons between species suffer from limited power to detect individual incidents of selection, whereas studies based on human genetic variation have suffered from difficulties with assessing statistical significance. The evidence for positive selection has traditionally been evaluated by comparison with expectations under standard population genetic models, but the model parameters (especially those relating to population history) have been poorly constrained by available data, leading to large uncertainties in model predictions. One solution would be to assess significance by comparing empirical results from different studies, but this has been challenging because of the varied statistical tests, sizes of genomic region, and population samples used (see table S2 for examples).

The advent of whole-genome sequencing and increasingly complete surveys of genetic variation represent a turning point in the study of positive selection in humans. With these advances, humans can now join model organisms such as *Drosophila* (*9*) at the forefront of evolutionary studies. Newly available tools allow systematic survey of the genome to find the strongest candidate loci for natural selection, as well as to reevaluate previously proposed candidate genes, in comparison with genetic variation in the genome as a whole (the genome-wide empirical distribution). Although they permit us to make progress even while working out remaining theoretical issues, they also bring analytical challenges of their own, because they represent imperfect samples of genetic variation.

Here, we review genetic methods for detecting natural selection, discuss initial results about positive selection based on recent whole-genome analyses, and outline the potential and the challenges ahead in going from candidates of selection to proven examples of adaptive evolution.

Methods for Detecting Selection

When alleles (genetic variations) under positive selection increase in prevalence in a population, they leave distinctive "signatures," or patterns of genetic variation, in DNA sequence. These signatures can be identified by comparison with the background distribution of genetic variation in humans, which is generally argued to evolve largely under neutrality (*10*). This is in accord with the neutral theory, which proposes that most observed genetic variation, both within and between species, is neutral (i.e., has no effect on an individual's fitness), so that its population prevalence changes over time by chance alone (so-called "genetic drift") (*11*). A great challenge for population genetics–based signatures (sections ii to v below) is determining whether a signature is due to selection or to the confounding effects of population demographic history, such as bottlenecks (periods of reduced population size), expansions, and subdivided populations.

[1]Broad Institute of MIT and Harvard, Cambridge, MA, USA. [2]Harvard Medical School, Boston, MA, USA. [3]Brown University, Providence, RI, USA. [4]Departments of Genetics and Medicine, Harvard Medical School, Boston, MA, USA. [5]Department of Molecular Biology, Center for Human Genetic Research, and Diabetes Unit, Massachusetts General Hospital, Boston, MA, USA. [6]Department of Biology, MIT, Cambridge, MA, USA. [7]Whitehead Institute for Biomedical Research, Cambridge, MA, USA. [8]Department of Systems Biology, Harvard Medical School, Boston, MA, USA.

*These authors contributed equally to this work.
†To whom correspondence should be addressed. E-mail: sfs@broad.mit.edu

Many specific statistical tests have been proposed to detect positive selection (table S3 provides a review), but they are all based broadly on five signatures. Below, we describe the nature of each signature, an estimate of the window of evolutionary time in which it can be used to detect moderately strong selection in humans (Fig. 1), and its strengths and weaknesses in human studies. Several excellent reviews (*12*–*18*) provide more information, as well as background on coalescent modeling and on other types of selection (e.g., purifying selection and balancing selection). It should be noted that many instances of selection are likely not detectable by any currently proposed method—for example, if the selective advantage is too small or selection acts on an allele that is already at an appreciable frequency in the population (*19*).

(*i*) *High proportion of function-altering mutations* (*age, many millions of years*). Genetic variants that alter protein function are usually deleterious and are thus less likely to become common or reach fixation (i.e., 100% frequency) than are mutations that have no functional effect on the protein (i.e., silent mutations). Positive selection over a prolonged period, however, can increase the fixation rate of beneficial function-altering mutations (*20*, *21*), and such changes can be measured by comparison of DNA sequence between species. The increase can be detected by comparing the rate of nonsynonymous (amino acid–altering) changes with the rate of synonymous (silent) or other presumed neutral changes, by comparison with the rate in other lineages, or by comparison with intraspecies diversity. One extreme example of this kind of signature is found in the gene *PRM1*, mentioned earlier, which has 13 nonsynonymous and 1 synonymous differences between human and chimpanzee (*7*, *8*) (Fig. 2). Statistical tests commonly used to detect this signature include the Ka/Ks test, relative rate tests, and the McDonald-Kreitman test (*20*–*22*). Similar tests can also be applied to other functional sites, such as noncoding regulatory sequences, and their development is an area of active research (*23*, *24*).

This signature can be detected over a large range of evolutionary time scales. Moreover, it focuses on the beneficial alleles themselves, eliminating ambiguity about the target of selection. Its power is limited, however, because multiple selected changes are required before a gene will stand out against the background neutral rate of change. It is thus typically possible to detect only ongoing or recurrent selection. In practice, when the human genome is surveyed in this manner, few individual genes will give statistically significant signals, after correction for the large number of genes tested. However, the signature can readily be used to detect positive selection across sets of multiple genes (*25*). For example, genes involved in gametogenesis clearly stand out as a class having a high proportion of nonsynonymous substitutions (*25*–*27*).

(*ii*) *Reduction in genetic diversity* (*age <250,000 years*). As an allele increases in population frequency, variants at nearby locations on the same chromosome (linked variants) also rise in frequency. Such so-called "hitchhiking" leads to a "selective sweep," which alters the typical pattern of genetic variation in the region. In a complete selective sweep, the selected allele rises to fixation, bringing with it closely linked variants; this eliminates diversity in the immediate vicinity and decreases it in a larger region. New mutations eventually restore diversity, but these appear slowly (because mutation is rare) and are initially at low frequency. Positive selection thus creates a signature consisting of a region of low overall diversity, with an excess of rare alleles.

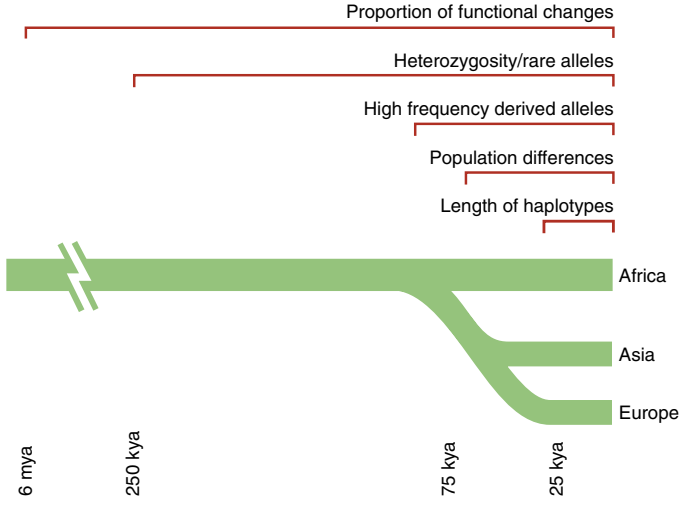

Fig. 1. Time scales for the signatures of selection. The five signatures of selection persist over varying time scales. A rough estimate is shown of how long each is useful for detecting selection in humans. (See fig. S1 for details on how the approximate time scales were estimated).

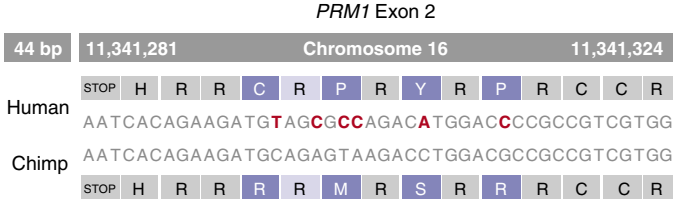

Fig. 2. Excess of function-altering mutations in *PRM1* exon 2. The *PRM1* gene exon 2 contains six differences between humans and chimpanzees, five of which alter amino acids (*7*, *8*).

Unlike excess functional changes, which involve differences between species, selective sweeps are detected in genetic variation within a species. The most common type of variant used is the single-nucleotide polymorphism (SNP). As an example, Akey *et al*. identified a 115-kb region containing four genes including the Kell blood antigen, which showed an overall reduction in diversity and more rare alleles in Europeans than expected under neutrality (Fig. 3) (*28*). Statistical tests commonly used to detect this signal include Tajima's D, the Hudson-Kreitman-Aguadé (HKA) test, and Fu and Li's D* (*29*–*32*).

Reduction in genetic diversity can be particularly useful because it persists longer than other population genetic signatures. The characteristic time for new mutations to drift to high frequency under neutral evolution in the human population is ~1 million years. This means that statistically significant signals of selection can persist for several hundred thousand years, long enough to encompass the origins of modern humans.

The size of the genome region affected by a sweep depends on the strength of positive selection and, thus, the speed at which the selected allele reached high frequency. That is, rapid sweeps affect large regions. If an allele confers a selective advantage of 1% (considered moderately strong selection), the modal size of the affected genomic region has been estimated to be roughly 600,000 base pairs (600 kb) (*27*). Such a large size facilitates detection, although it also makes the subsequent task of identifying the causal variant more difficult. Another challenge is that the signature may be difficult to distinguish from effects of demographic history, e.g., an expanding population increases the fraction of rare alleles.

(*iii*) *High-frequency derived alleles* (*age <80,000 years*). Derived (that is, nonancestral) alleles arise by new mutation, and they typically have lower allele frequencies than ancestral alleles (*33*). In a selective sweep, however, derived alleles linked to the beneficial allele can hitchhike to high frequency. Because many of these derived alleles will not reach complete fixation (as a result of an incomplete sweep or recombination of the selected allele during the sweep), positive selection creates a signature of a region containing many high-frequency derived alleles. A good example of this kind of

signature is the 10-kb region around the Duffy red cell antigen (*FY*), which has an excess of high-frequency derived alleles in Africans, thought to be the result of selection for resistance to *P. vivax* malaria (Fig. 4) (*34*, *35*). The most commonly used test for derived alleles is Fay and Wu's H (*36*).

Tests based on derived alleles require knowledge of the ancestral allele. In practice, the ancestral allele is inferred from the allele present in closely related species, with the assumption that mutation occurred only once at this position and that it occurred after the two species diverged (*36*). Determination of the ancestral allele in humans is facilitated by the availability of the chimpanzee genome sequence and by the growing data from additional primate genomes. The derived-alleles signature differs from the rare-allele signature discussed above in two important ways. First, different demographic effects are potential confounders [for example, population expansion is a major confounder for rare-alleles tests but not for derived-alleles tests (*36*), whereas population subdivision is more of a problem for the latter (*37*)]. Second, the signature persists for a shorter period (*37*) because high-frequency derived alleles rapidly drift to or near fixation.

(*iv*) *Differences between populations* (*age <50,000 to 75,000 years*). When geographically separate populations are subject to distinct environmental or cultural pressures, positive selection may change the frequency of an allele in one population but not in another. Relatively large differences in allele frequencies between populations (at the selected allele itself or in surrounding variation) may therefore signal a locus that has undergone positive selection. For example, the *FY*O* allele at the Duffy locus is at or near fixation in sub-Saharan Africa but rare in other parts of the world, an extreme case of population differentiation (Fig. 5) (*34*, *38*). Similarly, the region around the *LCT* locus demonstrates large population differentiation between Europeans and non-Europeans, reflecting strong selection for the lactase persistence allele in Europeans (*6*). Commonly used statistics for population differentiation include F_{ST} and p_{excess} (*39*–*41*).

Population differentiation can only arise when populations are at least partially isolated reproductively. For humans, it thus pertains largely to events that occurred after the major human migrations out of Africa some 50,000 to 75,000 years ago (Fig. 1). As with other population genetic signatures, distinguishing between genuine selection and the effect of demographic history, especially population bottlenecks, on genetic variation can be difficult.

(*v*) *Long haplotypes* (*age <30,000 years*). Under positive selection, a selected allele may rise in prevalence rapidly enough that recombination does not substantially break down the association with alleles at nearby loci on the ancestral chromosome. Such a collection of alleles in a chromosomal region that tend to occur together in individuals is termed a haplotype. Selective sweeps can produce a distinctive signature that would not be expected under neutral drift—namely, an allele that has both high frequency (typical of an old allele) and long-range associations with other alleles (typical of a young allele). The long-range associations are seen as a long haplotype that has not been broken down by recombination. For example, the lactase persistence allele at the *LCT* locus lies on a haplotype that is common (~77%) in Europeans but that extends largely undisrupted for more than 1 million base pairs (1 Mb) (Fig. 6) (*6*), much farther than is typical for an allele of that frequency. This signature can be detected with the long-range haplotype (LRH) test, haplotype similarity, and other haplotype-sharing methods (*42*–*45*). Developing such tests is an area of vigorous current investigation (*46*, *47*).

Long haplotypes are useful for detecting partial selective sweeps, with allele frequencies as low as ~10%. Tests for this signature are relatively robust to the choice of genetic markers used (ascertainment bias), an important issue in practical applications. Another advantage of this test is that it can identify a narrow candidate region, even a single gene. One limitation of the test is that long-range haplotypes persist for relatively short periods of time, because recombination rapidly breaks down the haplotype. After 30,000 years, a typical chromosome will have undergone more than one crossover per 100 kb, leaving fragments that are too short to detect. A critical issue with this kind of signature is accurate control for variation in recombination rate; evidence that recombination rates may vary between haplotypes is a concern (*48*).

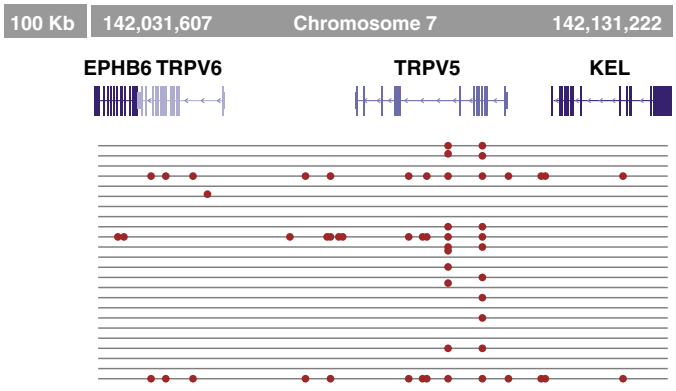

Fig. 3. Low diversity and many rare alleles at the Kell blood antigen cluster. On the basis of three different statistical tests, the 115-kb region (containing four genes) shows evidence of a selective sweep in Europeans (*28*).

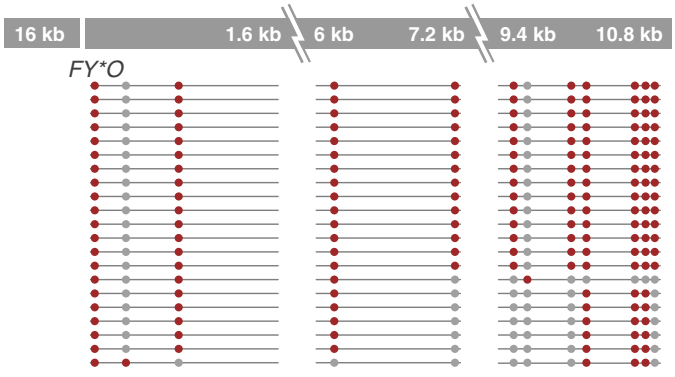

Fig. 4. Excess of high-frequency derived alleles at the Duffy red cell antigen (*FY*) gene (*34*). The 10-kb region near the gene has far greater prevalence of derived alleles (represented by red dots) than of ancestral alleles (represented by gray dots).

Genome-Wide Studies

Genome-wide studies of positive selection in humans have recently become possible because of the availability of (i) a near-complete sequence of the human genome (*49*, *50*), together with an increasing number of genome sequences for other species such as chimpanzee (*27*), mouse (*51*), and dog (*52*), and (ii) large catalogs of human genetic variation, such as those created by the SNP consortium (*53*), International Haplotype Map (HapMap) Project (*54*), and Perlegen Sciences (*55*). The current data are still limited. Additional closely related species are needed, and the polymorphism data are incomplete and not fully representative of human genetic variation. Nonetheless, the data are expanding rapidly: Sequencing of macaque and orangutan is far along, and sequencing of gorilla is beginning. The HapMap project has completed data collection for its second phase, with a SNP density higher by a factor of 4 that will include more than a third of all the estimated 10 to 12 million common human SNPs.

These data sets, although still limited, have already enabled initial genome-wide empirical studies of natural selection in the human genome. Seven large-scale studies of positive selection have recently been published, including

four surveys of amino acid–altering mutations in the human lineage and three surveys of human genetic diversity; more studies will likely be in print by the time of this publication (*46*, *47*). They provide a first look into the genome-wide distribution of diversity, identify high-priority candidates for natural selection without regard to previous biological hypotheses, and allow us to begin to re-evaluate earlier reports. These new studies also reveal the challenges ahead in extracting a coherent picture of adaptive selection in humans from the flood of new information.

Function-altering mutations in the human lineage. Four studies have examined natural selection in the ancient human lineage by considering amino acid–altering mutations. Each of the studies used one of two basic approaches: two-way comparison of human and chimpanzee orthologs (genes in multiple species evolved from a common ancestor) (*25*–*27*) or three-way comparison of human, chimpanzee, and murid (mouse or rat) orthologs (*27*, *56*). The advantage of the latter strategy is that it can distinguish between events that occurred in the human or chimpanzee lineage, but the use of a distant species for comparison limits the number of genes that can be studied (~7000 versus 11,000 to 14,000 genes for the two-way comparison). One of these studies (*26*) also used human polymorphism data to provide additional information about expected rates of change in different parts of the genome.

These analyses offer preliminary insights into the evolution of various functional classes of genes. In particular, they suggest that ongoing positive selection on humans has been strongest for genes related to immune response, reproduction (especially spermatogenesis), and sensory perception (especially olfaction). The studies are not completely consistent with each other (e.g., of two studies, using largely the same data, one found strong evidence for selection in spermatogenesis-related genes and the other did not) (*25*, *56*), but the overall picture is consistent with studies in other mammals, and the results seem plausible in terms of evolutionary predictions.

The studies also found that X-linked genes are significantly overrepresented among rapidly evolving genes (*25*, *27*). Much of the increased selection seen on the X chromosome likely arises from the larger number of sperm- and testis-associated genes (*25*), which are frequent targets of selection, on the chromosome. In addition, the hemizygosity of the X chromosome in males exposes recessive alleles to selective pressure, which may promote rapid evolution (*57*).

The great majority of genes identified in these studies as candidates for positive selection are novel, with the potential to illuminate previously unsuspected biological mechanisms. They include several genes with testis-specific expression (*USP26*, *C15orf2*, and *HYAL3*), several involved in immune regulation (e.g., *CD58*, *APOBEC3F*, and *CD72*), several tumor antigens (e.g., *SAGE1* and *MAGEC2*), and many more with as-yet-unknown functions (e.g., *FLJ46156I*, *ABHD1*, and *LOC389458*) (*25*, *26*). Because power to detect selection at any single gene (as compared to categories of genes) is limited using this approach, false positives are a concern, but one study was able to demonstrate that the candidate genes as a group had significant evidence for selection (*25*).

Interestingly, of 39 previously reported candidates based on function-altering mutations, only 4 were in the top 1% of candidates for selection in these genome-wide empirical studies (table S4). These four genes encode two sperm-related proteins [*PRM1* and *PRM2*, with the former being the strongest candidate for selection in one of the studies (*25*)], one antiviral enzyme (*APOBEC3G*), and an Rh blood antigen (*RHCE*). Of the remaining 35 genes, some had missing or incomplete data and a few had weaker but suggestive evidence for selection (e.g., *SEMG1*, *VIRL1*, and *SRY*). However, some may well be false positives due to previously insufficient knowledge of gene variation across the genome under neutrality.

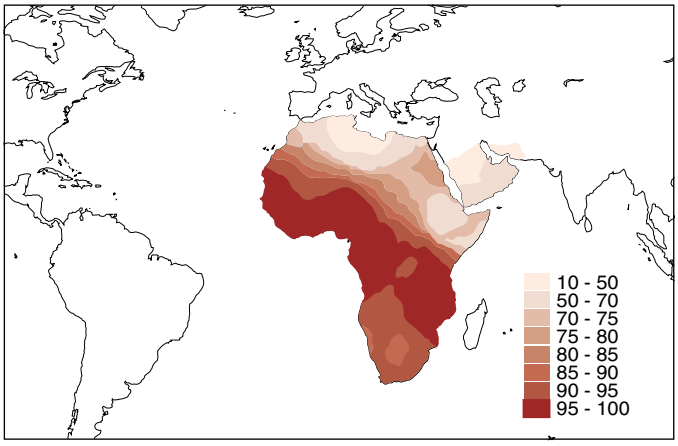

Fig. 5. Extreme population differences in *FY*O* allele frequency. The *FY*O* allele, which confers resistance to *P. vivax* malaria, is prevalent and even fixed in many African populations, but virtually absent outside Africa (*38*).

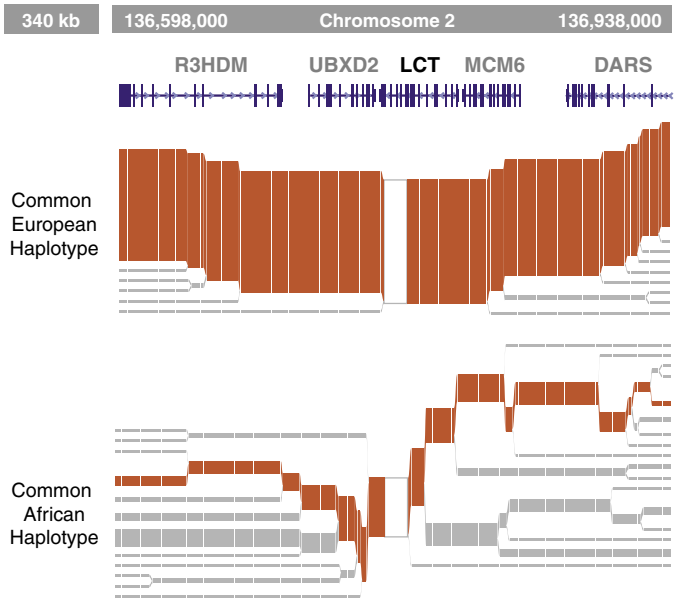

Fig. 6. Long haplotype surrounding the lactase persistence allele. The lactase persistence allele is prevalent (~77%) in European populations but lies on a long haplotype, suggesting that it is of recent origin (*6*).

The increasing number of genome sequences of closely related species will greatly expand the set of genes that can be studied by multiple-species comparison. These new data should also improve estimates of the neutral substitution rate (the rate at which fixed differences between species accumulate under neutral evolution). Humans and chimpanzees show an average of only 4.5 synonymous differences per gene (a number often used to estimate the neutral substitution rate); 10 times that number can be expected between human and macaque. The power of these studies will also be increased by better ways to recognize likely functional changes. These could come from both a greater understanding of the effect of specific mutations on protein structure and function and from a clearer understanding of the noncoding regulatory regions of the genome.

Genetic variation within human populations. Three published genome-wide surveys have used human genetic variation data to study recent selective sweeps (up to ~250,000 years ago). One of these (*27*) identified regions of the human genome with unusually low diversity, with subsequent confirmation by testing for an excess of high-frequency derived alleles. A second study (*54*) used the HapMap data to examine three signatures of selection: population differentiation, allele frequency spectrum, and long haplotypes. The

third investigation (*58*) searched for regions with rare alleles in the Perlegen data and examined high-frequency derived alleles for confirmation.

The three surveys used data that were not developed primarily for the purpose of studying selection. Thus, potential biases in the choice of genetic markers studied (ascertainment biases) had to be taken into account in their analyses (*59*, *60*). For example, the procedure for selecting SNPs in the HapMap data was biased toward high-frequency derived alleles; the analysis of the HapMap data therefore avoided tests based on frequencies of derived alleles and focused instead on tests of overall diversity. Only subsequent work with truly unbiased data sets will reveal how successfully these studies succeeded in avoiding ascertainment bias.

The statistical power of these studies to detect selective events is limited by the still-incomplete nature of current SNP catalogs and by the limited number of individuals genotyped. Greater SNP density will permit more complete dissection of haplotypes, with finer granularity and increased power, particularly for frequency-based measures (as much as 50% greater for older sweeps, simulations suggest). Genotyping of more individuals will be essential for detecting partial sweeps at low-frequency alleles.

Despite these limitations, the initial analyses are striking and will fuel much additional research. The majority of strong candidates for selection found in these surveys were novel. These included the *LARGE*, *ALMS1*, and *SLC24A5* genes and several gene clusters that include the genes *CD36*, *ITGAE*, *FAF1*, *SYT1*, and *GRAP2* (*54*). Interestingly, some high-scoring regions contained no known genes at all, which may reflect selection on noncoding sequences (*27*, *54*).

Also notable is that fewer than half of loci previously identified as targets of positive selection ranked among the top candidates in the empirical genome-wide analyses. When 81 previously proposed candidate genes were reexamined in the genome-wide data, using seven different tests for selection, only 25 were in the top 1% of the genome on at least one test (Fig. 7 and table S4). For the remaining genes, which include well-known cases like *FOXP2*, *G6PD*, and *MC1R*, the genome-wide evidence is weaker or absent.

Why have many earlier results fared poorly in genome-wide studies? In some cases the explanation is insufficient power, either because of the tests employed in the new studies or because of inadequate coverage of some genomic regions. An example of the latter effect may be *G6PD*, which scores in the top 3% of loci but is not an extreme outlier, despite having an established association with malaria resistance (*43*, *61*). This may be because the locus lies in a genomic region (Xq28) with low SNP density in HapMap data, although it may also indicate that the locus has a relatively modest effect. The possibility that these tests could miss some signals is illustrated by the Duffy locus. The role of selection there is well established, but the genetic signal is completely invisible under most of the tests used in the genome-wide surveys [the exception being a single-marker population differentiation test, in which the signal is clearly observed (table S4)]. For other loci, a signal might be missed by all of the tests (*62*).

Based on these genome-wide empirical comparisons, however, some previous claims of association may well represent false positives. That is, it is now clear that some signals that stood out in comparison to simple population genetic models do not stand out relative to the genome-wide distribution of diversity. For example, haplotypes that span relatively short distances (e.g., tens of kilobases) and long haplotypes around rare alleles (e.g., the *CCR5*-Δ*32* mutation) can now be seen to be common features in the genome (*47*, *63*, *64*) and not particularly suggestive of selection. As understanding of the genome-wide landscape improves, the precision of these tests will undoubtedly improve as well.

On the other hand, many of the most well-studied and convincing cases for selection [e.g., *LCT*, *HBB*, *FY*, and the major histocompatibility complex (MHC)] are clear outliers in the empirical distributions. Many of these are genes already associated with adaptive evolu-

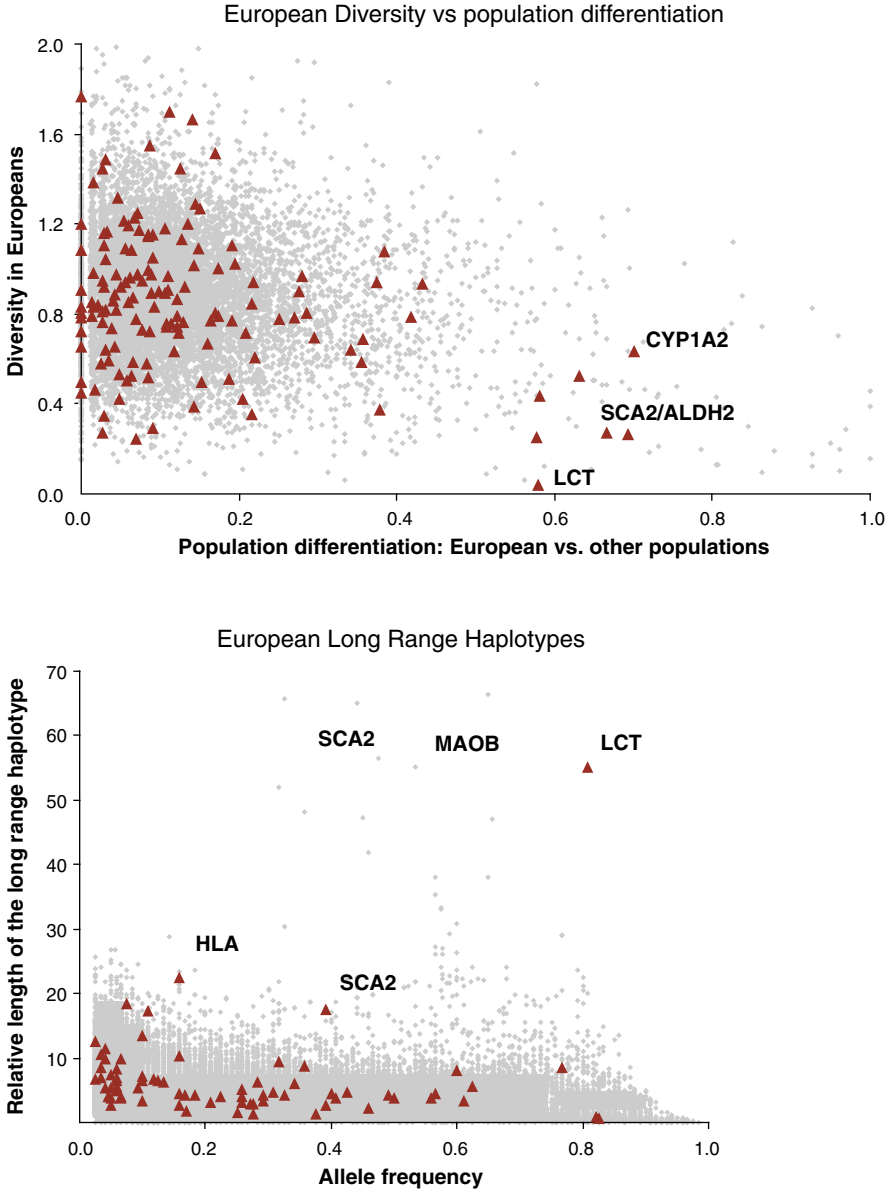

Fig. 7. The previous candidates for selection (red triangles), identified by limited empirical data, in comparison with the newly available genome-wide empirical data sets (gray diamonds). The results are presented here for a European sample for three signatures: diversity, population differentiation, and long-range haplotypes. More detailed results are presented in table S4 and fig. S2.

tion, such as those involved in resistance to malaria (*HBB*, *CD40L*, *FY*, and newly identified *CD36*) or other infectious diseases (MHC). This reinforces the notion that infectious diseases, and specifically malaria, have been among the strongest selective pressures in recent human history. Other previously identified candidates found in the survey data included LCT in Europeans (found by long haplotype and diversity/frequency tests), *DMD* and the *SCA2*/*ALDH2* cluster (long haplotypes), and the *CYP3A4*/*CYP3A5* cluster, *ALDH2*, and immunoglobulin A (diversity/frequency tests).

As with the surveys of amino acid–altering mutations, the studies based on human genetic variation found an excess of candidates on the X chromosome: 10 of 33 candidates in the HapMap-based study lie on the X chromosome, which comprises only 5% of the genome. Although it is prudent to withhold judgement (a higher rate of false positives on the X chromosome could arise from stronger effects of bottlenecks, given the smaller number of X chromosomes than autosomes in the population), it is plausible that this reflects a different impact of selection on the X chromosome. Reassuringly, a similar excess is seen in a population that has experienced major recent bottleneck effects (Europeans) and in a population that has not (West Africans).

The transition to using empirical, rather than purely theoretical, distributions as the basis for selecting candidates represents real progress and lays the foundation for fruitful work to come. It should be remembered, however, that the demonstration that a gene is a clear outlier does not definitively prove that it is the target of selection. Because we do not know the underlying proportion of loci that have experienced positive selection, we cannot calculate a precise posterior probability of selection. In the end, convincing proof will require an understanding of biological function.

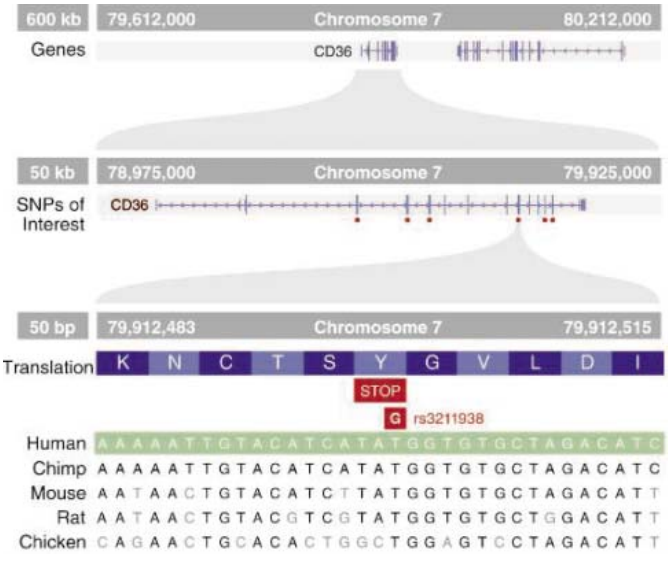

Fig. 8. Identification of functional polymorphism associated with a signature of selection at *CD36*. An allele at *CD36* identified to be under selection by the LRH test (*42*, *53*) has been associated with differential susceptibility to *P. falciparum* cerebral malaria. An animated version of the browser by B. Fry to scan the selected region for functional variations is available at www.broad.mit.edu/mpg/pubs/sabeti-science2006.

From Candidate to Function

True understanding of the role of adaptive evolution will require both better constrained models of neutral evolution (which can be derived in part from the same new data sets discussed here) and detailed, case-by-case analysis of candidate loci to identify those with biological evidence for selection. The latter, which will also help inform estimates of how common positive selection has been in humans, is the real goal, because it is the selected traits themselves that are of the most interest.

Identifying and understanding the traits that have been targets of selection will be a major challenge. Consideration of *HBB* sickle cell, one of the earliest successful dissections of adaptive evolution, demonstrates the depth of work required for this pursuit. Forty years of constant effort, by a succession of researchers including Pauling, Ingram, Allison, and Perutz, were required to unravel the association with malaria and the biochemical properties of the sickle cell mutation (*2*, *65*, *66*). Even now, there is still work to be done to understand exactly how the sickle state inhibits malaria infection.

Dissecting selection at a specific locus can be approached from two directions: finding a DNA change with functional molecular consequence or finding an association to a phenotypic difference in the human population. The first approach begins with good genetic annotation of the region, including both coding and regulatory regions, and will be enhanced by ongoing advances in comparative genomics. Depending on the kind of event under study, the functional changes might be found through comparisons between species, between populations, or between haplotypes. Such clues can be the basis of diverse means of biological experimentation. The second approach, which is only possible if the selected variant is still polymorphic in humans, usually depends on knowledge of the underlying biology of the region. The associated phenotype might be measured in human populations (for example, malaria resistance) or in cell lines (for example, protein function or expression).

The easier end of the spectrum of individual cases is illustrated by a candidate locus discovered among the HapMap data, the gene *CD36* (*54*). A *CD36* haplotype present in Africa and absent elsewhere showed evidence for recent selection by the LRH test. Closer inspection showed that this haplotype contains a nonsense mutation (amino acid changed to a stop codon), T188G, that has been associated with differential susceptibility to *P. falciparum* cerebral malaria (Fig. 8) (*67*, *68*).

A somewhat harder case is the *LARGE* gene. A haplotype residing entirely within this gene shows evidence for selection in West Africans, simplifying the issue of identifying the causal gene (*54*). However, the associated phenotype is a mystery. The function of *LARGE* (it encodes a member of the N-acetylglucosaminyltransferase gene family) is not well understood, although a mutation in it is known to cause muscular dystrophy. (Curiously, *DMD*, another gene with mutations causing muscular dystrophy, also shows evidence for selection in the same population.)

More difficult still are cases in which a causal gene has not been identified. For example, a 0.5-Mb region in chromosome 2q11.1 shows low diversity and an excess of rare alleles in the West African data (*54*). The region contains four known and two putative genes, with no indication as to which was responsible for selection. A very strong candidate region on chromosome 4 suffers from the opposite problem (*27*, *54*): It contains no known genes, although the region has been associated with severe obesity (*69*, *70*). In these cases, the best prospect is to narrow the candidate region and identify all the functional changes (both coding and regulatory) contained therein.

In many cases, comparative genomics and population-based association studies can be extremely helpful. For example, one of the genes showing strong population differentiation in HapMap data was one of unknown function, *SLC24A5* (*54*). Independently, Lamason *et al*. identified a mutation in the Zebrafish homolog of this gene that is responsible for a pigmentation phenotype (*71*). Guided by the two findings, the investigators demonstrated that a human variant in the gene explains roughly one-third of the variation in pigmentation between Europeans and West Africans and that the European variant had likely been a target of selection. In this case, the combination of biological data from a model system and genome-wide polymorphism data rapidly established a plausible link between natural selection and a human trait.

The most difficult case arises when selected alleles have risen to fixation in the modern

human population, so that no phenotypic variation remains. Such cases include some candidates identified by virtue of low diversity in population genetic data, although most are revealed by interspecies studies. Dissection of these events, some of them crucial steps in the development of modern *H. sapiens*, will require better understanding of the biological role played by the genes. For example, there is suggestive genetic evidence for positive selection at the gene *FOXP2* but no relevant variation in the modern human population; the only clue as to what the selected trait might have been is the observation that rare mutations in this gene lead to speech defects (*72*, *73*).

Conclusions

The advent of genome-wide sequence and variation data has dramatically expanded approaches to identifying possible sites of natural selection. Much work still needs to be done to create unbiased data sets of genetic variants and to refine analytical techniques. Still, we have caught a first glimpse of a vast new landscape. We now see that only a small fraction of loci with evidence for positive selection were found by previous approaches, suggesting that many more examples are likely to be found in the coming years. With an even deeper inventory of human variation, it should soon be realistic to generate a catalog of the human loci with signals for selection above a given threshold.

The field is expanding rapidly, as evidenced by the continual flood of papers claiming new regions as candidates for selection and reporting new methods for detecting selection. It will be a challenge to interpret this new information, working toward a coherent picture of human evolution. A set of community standards for reporting and interpreting data will help advance the field and are beginning to emerge. Three key components will be (i) clear demonstration of the utility of new statistical tests, (ii) more rigorous demonstration of evidence for natural selection, and (iii) the inclusion of functional evidence for candidate loci, where possible.

First, new statistical tests will continue to be introduced, both to improve existing methods and to address characteristics of particular data sets (e.g., genotype rather than sequence data). Such methods should be evaluated by direct comparison with published methods—an obvious step, but one too seldom taken. The power, robustness to demographic history, and utility for varied data sets should all be assessed by simulation studies done under a range of demographic scenarios. Application to empirical data, justification for statistical thresholds, and control for multiple testing should be clearly described.

Second, evidence for selection at new candidate loci should be evaluated both relative to theoretical model distributions (ideally, tailored to empirical data) and by comparison to empirical, genome-wide distributions. Good theoretical models are needed to interpret the significance of genome-wide outliers. Whatever a theoretical model might suggest, however, it is also crucial to report where a locus falls in the empirical distribution. In cases where the exact genome-wide distribution is not yet available for a particular test (as in the case of resequencing data), attempts should be made to provide sufficient data for empirical comparison.

Third, genetic evidence for selection is considerably enhanced by functional evidence. This is important because the actual extent of positive selection in the human lineage is unknown, making it hard to define thresholds for genetic evidence of selection. The functional evidence might take many forms, e.g., correlation of the selected allele with human phenotypic variation, model system, or in vitro laboratory studies of the selected allele. The strongest evidence would include both identification of a functional variant in humans and evidence for the advantage that the trait provides.

The quest to identify selected traits is driven not just by curiosity about the past but also by concern for human health. Positive selection, in many cases, represents a response to pathogens or other causes of illness, or to new diet and environmental conditions. Many of these forces are still present today. Moreover, positive selection has wrought changes to human biology, to which the rest of the genome may not yet have had time to adapt. As a result, polymorphic alleles at loci that have undergone recent selection may also be good candidates for risk factors for modern disease.

References and Notes

1. C. Darwin, A. R. Wallace, *Proceedings of Linnean Society of London* **3**, 45 (1858).
2. A. C. Allison, *Br. Med. J.* **4857**, 290 (1954).
3. M. Currat *et al.*, *Am. J. Hum. Genet.* **70**, 207 (2002).
4. J. Ohashi *et al.*, *Am. J. Hum. Genet.* **74**, 1198 (2004).
5. M. T. Hamblin, A. Di Rienzo, *Am. J. Hum. Genet.* **66**, 1669 (2000).
6. T. Bersaglieri *et al.*, *Am. J. Hum. Genet.* **74**, 1111 (2004).
7. A. P. Rooney, J. Zhang, *Mol. Biol. Evol.* **16**, 706 (1999).
8. G. J. Wyckoff, W. Wang, C. I. Wu, *Nature* **403**, 304 (2000).
9. R. R. Hudson, K. Bailey, D. Skarecky, J. Kwiatowski, F. J. Ayala, *Genetics* **136**, 1329 (1994).
10. I. Hellmann, I. Ebersberger, S. E. Ptak, S. Paabo, M. Przeworski, *Am. J. Hum. Genet.* **72**, 1527 (2003).
11. M. Kimura, *Nature* **217**, 624 (1968).
12. D. L. Hartl, A. G. Clark, *Principles of Population Genetics* (Sinauer Associates, Sunderland, Mass., 2nd ed., 1989).
13. E. J. Vallender, B. T. Lahn, *Hum. Mol. Genet.* **13 Spec No 2**, R245 (October 1, 2004).
14. J. Ronald, J. M. Akey, *Human Genomics* **2**, 113 (2005).
15. R. Nielsen, *Annu. Rev. Genet.* (August 31, 2005).
16. M. Kreitman, *Annu. Rev. Genomics Hum. Genet.* **1**, 539 (2000).
17. A. M. Bowcock *et al.*, *Proc. Natl. Acad. Sci. U.S.A.* **88**, 839 (1991).
18. M. Bamshad, S. P. Wooding, *Nat. Rev. Genet.* **4**, 99 (2003).
19. M. Przeworski, G. Coop, J. D. Wall, *Evolution Int. J. Org. Evolution* **59**, 2312 (2005).
20. W. H. Li, C. I. Wu, C. C. Luo, *Mol. Biol. Evol.* **2**, 150 (1985).
21. A. L. Hughes, M. Nei, *Nature* **335**, 167 (1988).
22. J. H. McDonald, M. Kreitman, *Nature* **351**, 652 (1991).
23. P. Andolfatto, *Nature* **437**, 1149 (2005).
24. M. V. Rockman *et al.*, *PLoS Biol.* **3**, e387 (2005).
25. R. Nielsen *et al.*, *PLoS Biol.* **3**, e170 (2005).
26. C. D. Bustamante *et al.*, *Nature* **437**, 1153 (2005).
27. Chimpanzee Sequencing and Analysis Consortium, *Nature* **437**, 69 (2005).
28. J. M. Akey *et al.*, *PLoS Biol.* **2**, e286 (2004).
29. F. Tajima, *Genetics* **123**, 585 (1989).
30. M. Nei, *Molecular Evolutionary Genetics* (Columbia Univ. Press, New York, 1987).
31. R. R. Hudson, M. Kreitman, M. Aguade, *Genetics* **116**, 153 (1987).
32. Y. X. Fu, W. H. Li, *Genetics* **133**, 693 (1993).
33. G. A. Watterson, H. A. Guess, *Theor. Popul. Biol.* **11**, 141 (1977).
34. M. T. Hamblin, E. E. Thompson, A. Di Rienzo, *Am. J. Hum. Genet.* **70**, 369 (2002).
35. A. A. Escalante *et al.*, *Proc. Natl. Acad. Sci. U.S.A.* **102**, 1980 (2005).
36. J. C. Fay, C. I. Wu, *Genetics* **155**, 1405 (2000).
37. M. Przeworski, *Genetics* **160**, 1179 (2002).
38. L. L. Cavalli-Sforza, P. Menozzi, A. Piazza, *The History and Geography of Human Genes* (Princeton Univ. Press, Princeton, NJ, 1994).
39. J. M. Akey, G. Zhang, K. Zhang, L. Jin, M. D. Shriver, *Genome Res.* **12**, 1805 (2002).
40. J. Hastbacka *et al.*, *Cell* **78**, 1073 (1994).
41. R. C. Lewontin, J. Krakauer, *Genetics* **74**, 175 (1973).
42. C. Toomajian, R. S. Ajioka, L. B. Jorde, J. P. Kushner, M. Kreitman, *Genetics* **165**, 287 (2003).
43. P. C. Sabeti *et al.*, *Nature* **419**, 832 (2002).
44. Y. Kim, R. Nielsen, *Genetics* **167**, 1513 (2004).
45. N. A. Hanchard *et al.*, *Am. J. Hum. Genet.* **78**, 153 (2006).
46. E. T. Wang, G. Kodama, P. Baldi, R. K. Moyzis, *Proc. Natl. Acad. Sci. U.S.A.* **103**, 135 (2006).
47. B. F. Voight, S. Kudaravalli, X. Wen, J. K. Pritchard, *PLoS Biol.* **4**, e72 (2006).
48. C. L. Yauk, P. R. Bois, A. J. Jeffreys, *EMBO J.* **22**, 1389 (2003).
49. E. S. Lander *et al.*, *Nature* **409**, 860 (2001).
50. J. C. Venter *et al.*, *Science* **291**, 1304 (2001).
51. R. H. Waterston *et al.*, *Nature* **420**, 520 (2002).
52. K. Lindblad-Toh *et al.*, *Nature* **438**, 803 (2005).
53. D. Altshuler *et al.*, *Nature* **407**, 513 (2000).
54. International HapMap Consortium, *Nature* **437**, 1299 (2005).
55. D. A. Hinds *et al.*, *Science* **307**, 1072 (2005).
56. A. G. Clark *et al.*, *Science* **302**, 1960 (2003).
57. S. F. Schaffner, *Nat. Rev. Genet.* **5**, 43 (2004).
58. C. S. Carlson *et al.*, *Genome Res.* **15**, 1553 (2005).
59. A. G. Clark, M. J. Hubisz, C. D. Bustamante, S. H. Williamson, R. Nielsen, *Genome Res.* **15**, 1496 (2005).
60. G. McVean, C. C. Spencer, R. Chaix, *PLoS Genet.* **1**, e54 (2005).
61. S. A. Tishkoff *et al.*, *Science* **293**, 455 (2001).
62. K. M. Teshima, G. Coop, M. Przeworski, *Genome Res.,* 10 May 2006, in advance of print.
63. N. Mekel-Bobrov *et al.*, *Science* **309**, 1720 (2005).
64. P. C. Sabeti *et al.*, *PLoS Biol.* **3**, e378 (2005).
65. V. M. Ingram, *Biochim. Biophys. Acta* **36**, 402 (1959).
66. L. Pauling *et al.*, *Science* **110**, 543 (1949).
67. T. J. Aitman *et al.*, *Nature* **405**, 1015 (2000).
68. A. Pain *et al.*, *Lancet* **357**, 1502 (2001).
69. R. Arya *et al.*, *Am. J. Hum. Genet.* **74**, 272 (2004).
70. S. Stone *et al.*, *Am. J. Hum. Genet.* **70**, 1459 (2002).
71. R. L. Lamason *et al.*, *Science* **310**, 1782 (2005).
72. J. Zhang, D. M. Webb, O. Podlaha, *Genetics* **162**, 1825 (2002).
73. W. Enard *et al.*, *Nature* **418**, 869 (2002).

74. P.C.S. is funded by the Damon Runyon Cancer Fellowship and the L'Oreal for Women in Science Award. We thank C. Bustamante, R. Nielsen, J. Akey, Y. Gilad, and C. Carlson for providing information from their previous publications. We also thank F. Steele, D. Reich, D. Hartl, R. Neilsen, D. Richter, C. Langley, M. Przeworski, A. Clark, J. Fay, S. Myers, T. Farhadian, T. Herrington, A. Foster, P. Sabeti, and four anonymous referees for careful review of our manuscript.

Supporting Online Material

www.sciencemag.org/cgi/content/full/312/5780/1614/DC1
Figs. S1 and S2
Tables S1 to S4

10.1126/science.1124309

The Age of the Taklimakan Desert

Jimin Sun* and Tungsheng Liu

The Taklimakan Desert, located in the Tarim Basin (Fig. 1A), is the world's second largest shifting sand desert. It covers an area of 337,000 km^2, and as much as 85% of it consists of shifting sand dunes. There are many different opinions about the age of the Taklimakan Desert, ranging from 3.5 million years ago (Ma) (*1*) to the middle Pleistocene (*2*). These debates are due either to the difficulties in finding thick stratigraphic records or to the lack of a well-constrained chronology.

In the southern marginal Tarim Basin, thick Cenozoic deposits were shed into the basin, providing great potential for understanding the relationships between mountain building, sediment deposition, and aridification history. The studied section is located at Sanju (37°11′N, 78°29′E) (Fig. 1A and fig. S1); the well-exposed outcrop has a thickness of 1626 m. The deposits can be divided into three units (fig. S2): the lowest part consists of alternatively deposited gravels and reddish fluvial siltstone (Pakabulake Formation), the middle part consists of gravels and interbedded light yellow silt (Artux Formation, Fig. 1B), and the uppermost part is dominated by gravels (Xiyu Formation).

We examined the surface microtexture and particle size of the interbedded light yellow silt from the Xiyu and Artux Formations. Quartz grains show rounded grain shapes, with typical dish-shaped depressions (Fig. 1C), suggesting the grains have an eolian origin. Additionally, the size distributions of the studied samples are compared with that of modern eolian loess in the northern Kunlun Mountains (fig. S3), and the similarity between them also suggests that the intercalated light yellow silty layers are windblown silt.

The measured magnetic polarity at Sanju was compared with the geomagnetic polarity timescale (GPTS) of Cande and Kent (Fig. 1D) (*3*). The age range of the measured sequence is between 6.5 and 2 Ma. The exposed Xiyu Formation at Sanju spans 3 to 2 Ma. The Artux Formation was accumulated between 5.3 and 3 Ma, which is consistent with the suggested Pliocene age based on Ostracoda biostratigraphy (*4*).

The studied section provides stratigraphic evidence for the onset of dune building in the Tarim Basin. Investigations in the Taklimakan Desert indicate that the dominant direction of sand dune movement is northeasterly (Fig. 1A). Under prevailing near-surface northeasterly winds, dust entrained from the desert can not be moved out of the basin but accumulates on the windward slopes of the Kunlun Mountains. In this sense, there is a close link between windblown silt accumulation and desert formation. Figure 1D indicates that initiation of windblown silt accumulation at Sanju occurred at 5.3 Ma, suggesting shifting sand dunes prevailed in the Tarim Basin by at least 5.3 Ma ago, as they do today.

Two factors probably initiated the formation of the Taklimakan Desert. First, at 5.6 to 5.3 Ma, tectonic activity combined with marine regression resulted in the isolation of the Mediterranean Sea, known as the Messinian Salinity Crisis (MSC) (*5*). The MSC reduced world ocean salinity by 6%, which would have enabled sea-ice formation at higher latitudes. The high latitude cooling that followed this event would have intensified the Siberian High, modifying climate in Mongolia and China. Secondly, the studied deposits at Sanju are piedmont molasse deposits derived from the Kunlun Mountains. Our study indicates that the tectonic uplift continued during the late Cenozoic. Therefore, although the recent study suggested that central Tibet had an elevation of about 4 km by at least 35 Ma (*6*), the growth of Tibet in different parts is not synchronous. Different stages of growth of the plateau could have different climatic effects, and the uplifted height of the northern Tibet around 5.3 Ma could have modified atmospheric circulation patterns, partially accounting for the arid climate in the Tarim Basin.

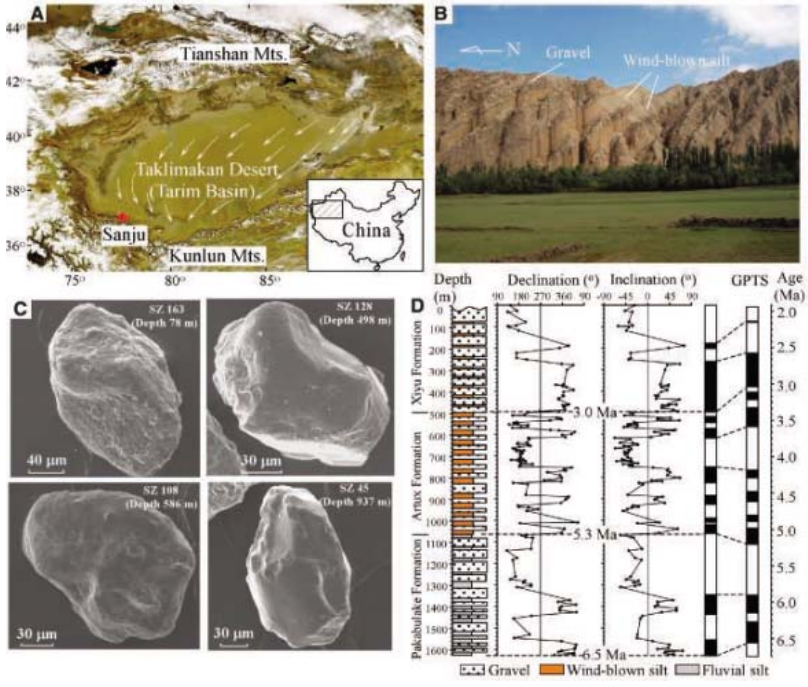

Fig. 1. (**A**) Map showing the Taklimakan Desert. The arrows show near-surface wind directions. (**B**) Photo shows the Artux Formation. (**C**) Microfeatures of quartz grains. (**D**) Magnetostratigraphy of the Sanju section and correlation with the GPTS of Cande and Kent (*3*).

References and Notes

1. H. B. Zheng, H. Z. Chen, J. J. Cao, *Chin. Sci. Bull.* **47**, 226 (2002).
2. Z. D. Zhu, Z. Wu, S. Liu, X. M. Di, *An Outline on Chinese Deserts* (Science Press, Beijing, 1980).
3. S. C. Cande, D. V. Kent, *J. Geophys. Res.* **100**, 6093 (1995).
4. Z. Y. Zhou, P. J. Chen, *Biostratigraphy and Geological Evolution in the Tarim Basin* (Geological Press, Beijing, 1990).
5. W. Krijgsman, F. J. Hilgen, I. Raffi, F. J. Sierro, D. S. Wilson, *Nature* **400**, 652 (1999).
6. D. B. Rowley, B. S. Currie, *Nature* **439**, 677 (2006).

7. We thank R. X. Zhu for helpful discussions and two anonymous reviewers for constructive reviews. Supported by the Chinese Academy of Sciences grant KZCX2-SW-133 and the Natural Science Foundation of China grants 40021202, 40125009, and 40231011.

Supporting Online Material

www.sciencemag.org/cgi/content/full/312/5780/1621/DC1
Figs. S1 to S3

4 January 2006; accepted 17 April 2006
10.1126/science.1124616

State Key Laboratory of Lithospheric Evolution, Institute of Geology and Geophysics, Chinese Academy of Sciences, Post Office Box 9825, Beijing 100029, China.

*To whom correspondence should be addressed. E-mail: jmsun@mail.igcas.ac.cn

Cortex Is Driven by Weak but Synchronously Active Thalamocortical Synapses

Randy M. Bruno* and Bert Sakmann

Sensory stimuli reach the brain via the thalamocortical projection, a group of axons thought to be among the most powerful in the neocortex. Surprisingly, these axons account for only ~15% of synapses onto cortical neurons. The thalamocortical pathway might thus achieve its effectiveness via high-efficacy thalamocortical synapses or via amplification within cortical layer 4. In rat somatosensory cortex, we measured in vivo the excitatory postsynaptic potential evoked by a single synaptic connection and found that thalamocortical synapses have low efficacy. Convergent inputs, however, are both numerous and synchronous, and intracortical amplification is not required. Our results suggest a mechanism of cortical activation by which thalamic input alone can drive cortex.

The thalamocortical (TC) projection has been intensely studied because the thalamus is part of the primary pathway by which information from the outside world is transmitted to the neocortex. Primary sensory nuclei of the thalamus contain cells whose axons project to the cortex, where they synapse mainly on dendrites of neurons in layer 4 (L4). L4 neurons respond to stimulation of the sensory periphery with large postsynaptic potentials (*1*–*3*). As these responses are initiated by direct monosynaptic inputs from the thalamus, TC axons have consequently been thought to comprise one of the most powerful "projection" systems in the brain (*4*, *5*). Paradoxically, thalamocortical synapses account for less than 15% of all synapses onto L4 spiny neurons (*6*).

The relative sparseness of thalamocortical synapses initially led to the assumption that the direct excitation provided by the thalamus is weak and requires amplification to activate the cortex (*5*, *7*, *8*). According to the "amplifier model," recurrent excitatory intracortical connections within L4 provide positive feedback during sensory stimuli and enhance the responses of cortical neurons. Computational models have demonstrated the feasibility of this hypothesis (*7*, *9*). It remains to be shown, however, that TC synapses actually require amplification simply because corticocortical synapses outnumber them.

High-efficacy TC synapses could alternatively ensure the strength of the TC projection. In vitro recordings from cortical neurons in acute (fresh) brain slices combined with minimal electrical stimulation of TC fiber tracts suggest that individual thalamocortical synapses are stronger and more reliable than corticocortical connections (*4*, *5*). Dual recordings could be used to explore this "strong-synapse model." Recording TC pairs, however, has not been feasible in vitro, because long-range connections are usually truncated during preparation of a cortical slice. Furthermore, the nature of the slice preparation prohibits the simultaneous study of functional properties, such as sensory-evoked responses.

These limitations could be overcome by dual recordings in the intact brain. Monosynaptic connections between cells in anesthetized animals have been putatively identified by recording extracellular action potentials (APs) and assessing the statistical probability with which "presynaptic" APs influence "postsynaptic" ones (*10*–*14*). Correlation analysis has additionally suggested an alternative "synchrony model," in which closely timed TC inputs are summed to strongly excite cortical cells directly (*15*). Extracellular AP recordings are limited, however, to inferring the presence of connections and cannot directly measure unitary excitatory postsynaptic potentials (EPSPs). Also, recorded cells are usually not identified in such experiments.

We present a new technique for measuring individual synaptic connections in vivo that overcomes such limitations. APs emitted by presynaptic thalamic cells are recorded extracellularly, while PSPs in postsynaptic cortical cells are simultaneously recorded intracellularly. The average EPSP is then determined by estimating and subtracting the contribution of unrecorded inputs.

Identification of monosynaptic connections in vivo. The TC projection in many sensory systems and species is organized topographically (*16*). The rodent whisker-barrel system is suited to studies where topographic alignment is critical. Rats have a stereotypical pattern of large facial whiskers, each of which drives neural activity in topographically aligned brain regions (*17*). The thalamic ventral-posterior medial (VPM) nucleus is subdivided into "barreloids" representing individual whiskers. L4 neurons in somatosensory cortex are similarly clustered into "barrels," which receive input predominantly from the corresponding barreloid (*16*, *18*, *19*).

Membrane potential (V_m) was recorded from a cortical neuron in an anesthetized or sedated rat [see Supporting Online Material (SOM)], while APs of a topographically aligned thalamic neuron were simultaneously recorded extracellularly (Fig. 1A). A synaptic connection between two neurons in vitro produces a small fluctuation (<4 mV) in postsynaptic V_m after each presynaptic AP (*5*, *20*, *21*). In vivo, however, barrages of thalamic and cortical postsynaptic potentials continuously generate much larger V_m fluctuations—up to 40 mV (Fig. 1A, upper trace; fig. S1). These obscure the EPSP evoked by any single thalamic AP (Fig. 1A, middle). This background "noise" can be overcome by averaging cortical V_m at the time of occurrence of each thalamic AP.

A simple average of V_m might be confounded by spontaneous APs discharged by near-synchronous thalamocortical neurons. In addition, collecting thousands of spontaneous APs to trigger an average would often exceed feasible recording times. Sensory stimuli have been thought to engage different degrees of synchrony among thalamic neurons (*22*, *23*), an idea that we exploited to evoke large numbers of APs while maintaining low levels of thalamic synchrony (see below and SOM). The synchrony of the afferent network was kept at a low level by deflecting the principal whisker (PW) with a small sinusoidal waveform (Fig. 1A, bottom trace). An AP- or "spike-triggered average" of cortical V_m was computed for periods of sinusoidal stimulation (Fig. 1B, top trace). The contribution of other inputs to V_m was estimated by shifting the records of V_m by one stimulus presentation and computing a new average V_m (Fig. 1B, middle trace). Subtraction of this new average from the first yields the average postsynaptic potential (aPSP) that a single thalamic AP evokes in the cortical cell (Fig. 1B, bottom trace; see Methods, SOM). An aPSP with short onset latency (2.4 ms) and typical rising and falling time courses of EPSPs at glutamatergic synapses (20 to 80% rise time 1.1 ms, decay 20 ms) is shown in Fig. 1C.

We also made a second test of connectivity in a subset of paired recordings. Hyperpolarizing current pulses were applied to the putative presynaptic thalamic neuron to evoke high-frequency AP bursts (Fig. 1E, lower traces), mediated by low-threshold voltage-dependent calcium channels. V_m of the cortical cell was then averaged with respect to the first AP in the burst (Fig. 1E, upper trace). The burst-triggered

Department of Cell Physiology, Max Planck Institute for Medical Research, Jahnstrasse 29, 69120 Heidelberg, Germany.

*To whom correspondence should be addressed. E-mail: bruno@mpimf-heidelberg.mpg.de

average (BTA) is several times larger than the aPSP (Fig. 1D), because each AP in the burst produces an aPSP that is summed with the others. Both tests of connectivity classified 10 out of 10 pairs equivalently (three out of three connected, seven out of seven unconnected).

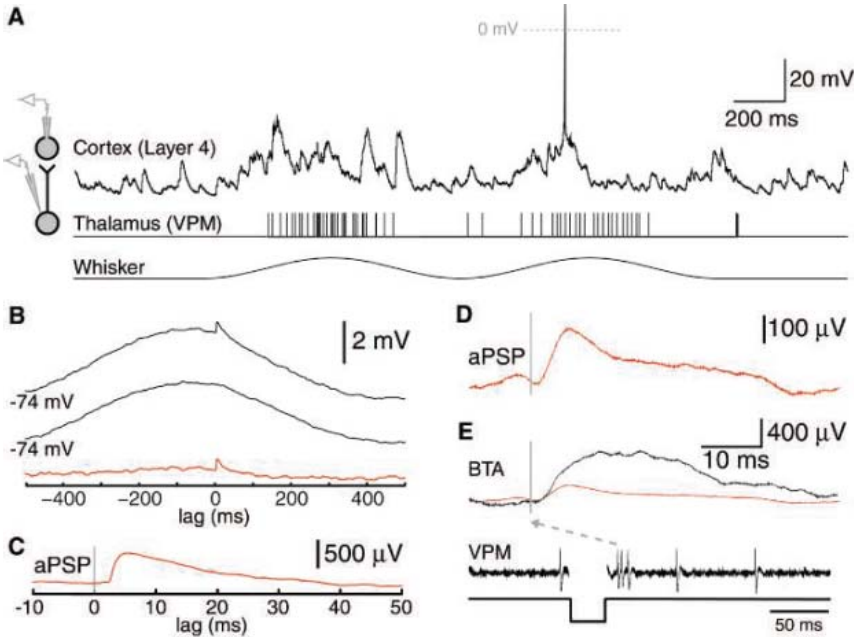

Fig. 1. Unitary connections are measurable in vivo. (**A**) Simultaneous intracellular recording of a cortical L4 neuron (Cortex) and extracellular recording of a somatotopically aligned thalamic neuron (Thalamus) during whisker stimulation (Whisker). (**B**) TC synapse onto an L4 spiny stellate. Top to bottom, Spike-triggered average, stimulus-induced correlation, difference giving aPSP (thalamic APs, $n = 1526$). (**C**) Expanded view of aPSP. (**D**) Example of one of the smallest aPSPs observed (thalamic APs, $n = 9900$). A star pyramid, 720 μm from the pia. (**E**) Electrical tests (black; n bursts = 460) for the same pair that produced the aPSP (red) in (D).

Probability and strength of TC connections. Thalamic neurons established direct monosynaptic connections onto L4 excitatory cells of all known morphologic types (Fig. 2). Spiny stellates have dendritic arbors that are confined to a barrel and lack an apical process (Fig. 2A). Spiny stellates are distinct from star pyramid cells, which have short apical dendrites that extend into layer 2/3 but do not reach layer 1 (Fig. 2B). Barrel star pyramids and spiny stellates received TC inputs with equal probability (10 out of 24 and 7 out of 11, respectively; five additional barrel neurons were spiny but not unambiguously star or stellate). No difference in aPSP amplitudes was observed between the two cell classes ($n = 9$ and $n = 7$, respectively, one connection BTA only, $P = 0.48$).

Monosynaptic connections onto excitatory L4 barrel neurons were frequently observed (17 out of 40 pairs, Fig. 3A). Onset latency, 20 to 80% rise time, and decay times were 1.72 ± 0.73, 3.38 ± 1.79, and 22.5 ± 24.7 ms (mean ± SD), respectively. The connections had small aPSP amplitudes (pooled over all animals: mean 950 μV ± 1.1 SD, median 550 μV, range 165 μV to 4.16 mV). TC-L4 synapses have previously been estimated on the basis of minimal stimulation in vitro to evoke larger EPSPs [mean 1.96 mV, range 0.39 to 5.89 mV (*5*)]. On the assumption that the number of release sites per connection and the efficacy of individual quanta of transmitter cannot be smaller in vivo, our data suggest that the TC

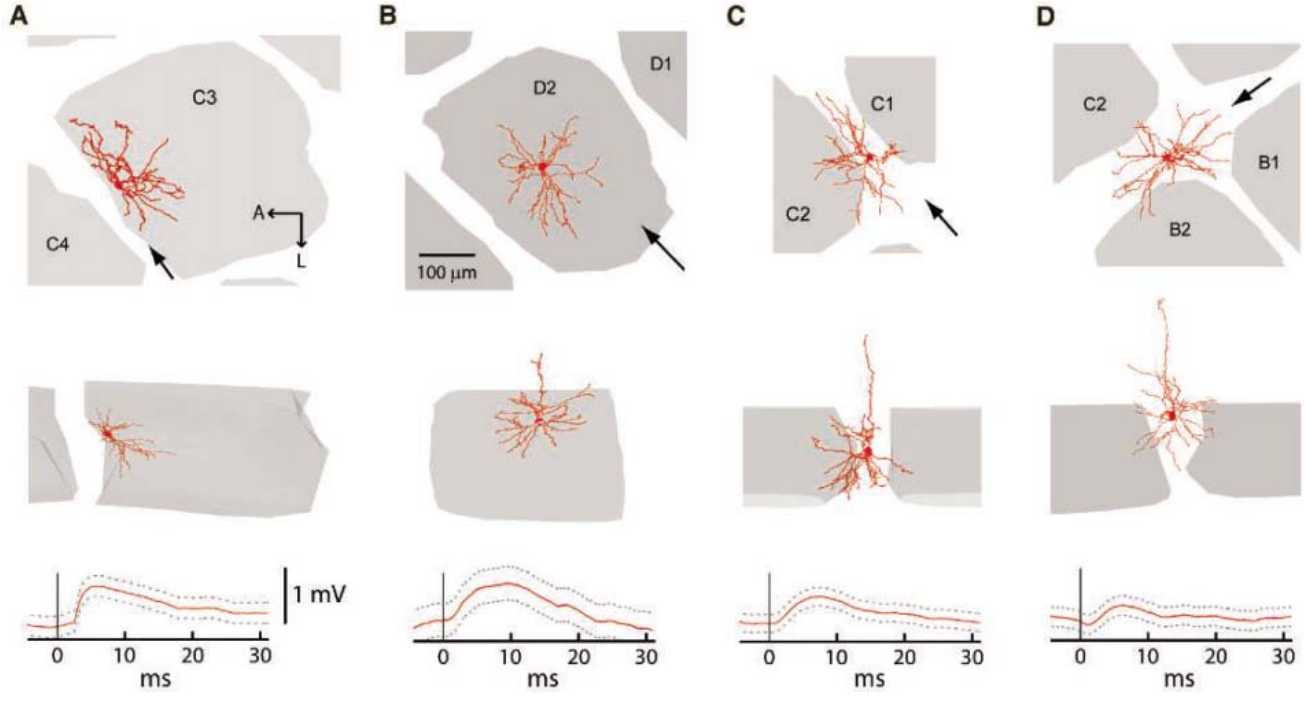

Fig. 2. TC synapses are made directly onto all types of excitatory L4 neurons. Upper row, tangential projections of 3-D reconstructions of four examples of connected cortical cells. Middle row, radial projection. Lower row, corresponding aPSP evoked by a paired thalamic neuron. Large arrows, approximate viewing angle for radial projection. *A*, anterior; *L*, lateral. Dashed lines, pointwise 99% confidence intervals. (**A**) Spiny stellate. (**B**) Star pyramid. (**C**) Interrow septum neuron. (**D**) Interarc septum neuron.

synapse in vivo may have a probability of release much lower than observed in vitro (*4*).

One possible explanation for a drop in release probability is that, in acute brain slices, thalamic axons are almost completely inactive. TC neurons have, however, substantial spontaneous AP rates in both the anesthetized and sedated rats used here (medians 1.0 and 5.4 Hz, respectively) as in the awake rat (*24*). Such high firing rates are likely to cause TC synapses to be continuously depressed in vivo (*25*, *26*). Consistent with this hypothesis, aPSPs of TC-barrel neuron connections were smaller during sedation (median 0.24, range 0.17 to 1.57, mean 0.49 ± 0.13 mV, $n = 11$; $P = 0.028$) than during anesthesia (median 1.3, range 0.25 to 4.16, mean 1.94 ± 0.67 mV, $n = 5$). Depression is also observable when estimating aPSPs from APs divided into subsets by the preceding interspike interval (Fig. 3C). Thus, as thalamic activity increases, TC efficacy decreases. The dependency of aPSP size on ongoing presynaptic AP rate likely explains why strong adaptation of sensory responses seen under anesthesia (*27*) are almost absent in the awake rat (*28*). Thus, individual thalamocortical synapses in the awake animal may be no more effective than typical corticocortical synapses.

Pairs of thalamic and topographically unaligned L4 cells were unconnected, as were pairs involving layer 2/3 cells (Fig. 3A), consistent with the known sparse lemniscal pathway projection to these regions (*18*). We also investigated pairs in which cortical cells were located in the neighboring "septum," interbarrel regions innervated by relatively few VPM axons and thought to be part of the paralemniscal system (*18*, *29*). Surprisingly, septum cells are as likely as barrel neurons to receive input from VPM, which belongs to the lemniscal system (6 out of 14 pairs; Fig. 3A). During sedation, strengths of TC connections onto septum neurons (Fig. 3B; mean 0.40 ± 0.05 mV, $n = 4$) did not differ from those onto barrel neurons (0.49 ± 0.13 mV, $n = 11$, $P = 0.85$), although their similarity may have been due to the small sample size. Monosynaptic connections were observed for septum neurons between both arcs (Fig. 2C) and rows (Fig. 2D). Our observations are consistent with the known morphology of septum neurons (*30*), which extend dendrites into barrels (Fig. 2, C and D). These data suggest that the septum, like other regions (*20*), integrates lemniscal and paralemniscal pathways.

Cortical neurons are known to fluctuate between depolarized ("up") and hyperpolarized ("down") states (*1*, *31*). In the anesthetized animal, we observed typical up and down states in cortical neurons. Such obvious bistability is not seen in L4 neurons in the sedated animal (Fig. 1A) or in the awake animal (fig. S5A). Nevertheless, cortical V_m still fluctuates between depolarized and hyperpolarized levels (Fig. 1A). Thus, the efficacy of single TC synapses may depend on the variable conductance state of the recipient neuron. This possibility was examined by computing aPSPs separately for thalamic APs occurring when a barrel neuron was already "depolarized" or "hyperpolarized," defined here as having a V_m greater or less, respectively, than the median. Figure 3D1 shows an example in which aPSP amplitude during hyperpolarized V_m is three times that seen in a depolarized V_m. An aPSP for a given connection tended, on average, to be larger during hyperpolarized V_m (Fig. 3E, mean increase 0.34 ± 0.19 mV, $n = 22$, $P = 0.03$), but some connections exhibited no difference between states or even the reverse. A similar analysis using electrically evoked thalamic bursts was therefore made for the pair shown in Fig. 3D2. BTAs for this connection were similar during hyperpolarization and depolarization (Fig. 3D2), which indicates that observations lacking a difference between states are not simply due to noise in aPSP estimation. These exceptions may be due to one or more of the following: (i) V_m differences between the soma and the distal dendrites where TC synapses are located, (ii) anomalously rectifying voltage-gated channels, or (iii) dendritic shunting (*32*).

Synchronous subnetworks. What do individual TC connections contribute to the subthreshold activity of cortical cells? Numerous thalamocortical and intracortical axons contact any given L4 neuron and generate compound excitatory and inhibitory PSPs. Combined, they produce spontaneous and stimulus-evoked changes in cortical V_m (Fig. 1A). For example, Fig. 4C shows average net PSPs evoked in a L4 spiny stellate by deflection of its PW in each of eight directions (gray zones). The largest net excitatory PSPs to deflection onset were observed for only a limited range of stimulus directions. Deflections in opposite directions evoked the largest stimulus-offset PSPs (e.g., 45° to 135°). Sustained depolarization is also seen between onset and offset for 180° and 225°. This cortical cell received a monosynaptic connection from the thalamic neuron whose stimulus-evoked APs are shown as peristimulus time histograms (PSTHs) (Fig. 4A).

The excitation that this individual thalamic neuron contributes to the cortical cell's responses can be estimated by convolving the PSTHs of thalamic APs with the aPSP of the single connection (Fig. 4B). Despite the thalamic cell's substantial spontaneous and evoked activity, its total excitatory contribution to the cortical cell is, at all times, less than 1 mV. Possible synaptic dynamics, which could only further decrease this value, were not modeled.

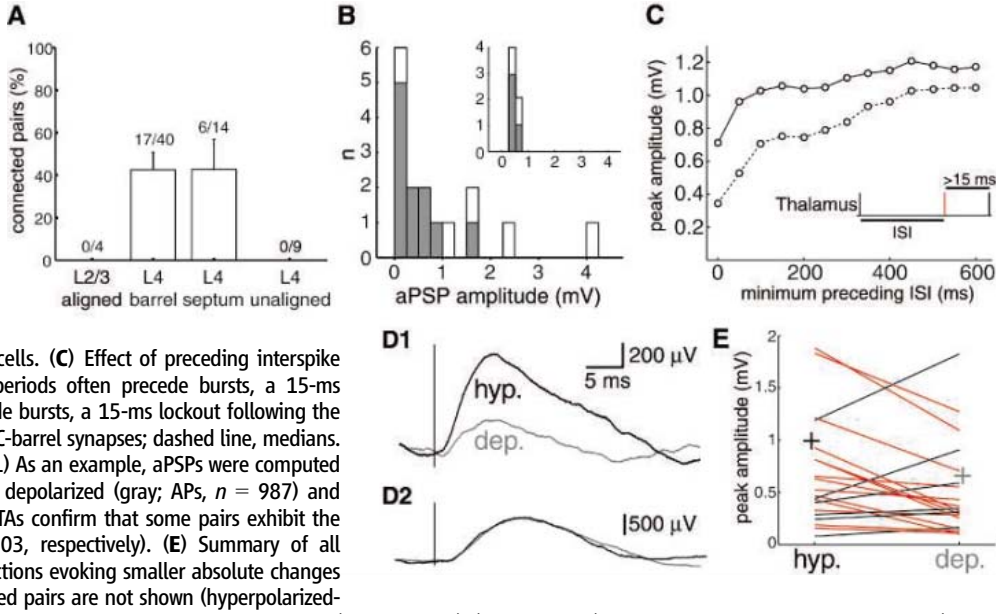

Fig. 3. TC synapses are numerous but weak. (**A**) Proportion of connected pairs involving thalamic cells and spiny cortical cells in various locations (aligned layer 2/3, aligned barrels, septum neighboring aligned barrels, and unaligned L4). Standard error bars calculated for a binomial distribution. (**B**) Amplitude distribution for pairs involving spiny barrel neurons. One connection was studied only by BTAs and, therefore, had no measurable aPSP. The histogram is divided into subsets according to preparation: filled, sedation; white, anesthesia. Inset, Same for septum cells. (**C**) Effect of preceding interspike interval (ISI) on amplitude. Because quiet periods often precede bursts, a 15-ms successor interval was also imposed. To exclude bursts, a 15-ms lockout following the AP was applied (inset). Solid line, means for TC-barrel synapses; dashed line, medians. (**D**) aPSPs are modulated by cortical state. (D1) As an example, aPSPs were computed for APs occurring when the cortical cell was depolarized (gray; APs, $n = 987$) and hyperpolarized (black; APs, $n = 821$). (D2) BTAs confirm that some pairs exhibit the reverse or no effect (APs, $n = 483$ and 503, respectively). (**E**) Summary of all connections, analyzed as in (D1). Red, connections evoking smaller absolute changes during depolarization. For visualization, two red pairs are not shown (hyperpolarized-depolarized values: 6.15 and 2.1 for one, 2.25 and 2.20 for the other, respectively). Plus signs (+) are means (hyperpolarized, 0.99; depolarized, 0.66).

Thus, even for stimulus-evoked AP trains, cortical excitation produced by any individual connection is relatively small. Nevertheless, the overall time course and directional tuning of the single thalamic input (Fig. 4B) and net cortical excitation produced by multiple inputs (Fig. 4C) are remarkably similar. Not all inputs to the cortical neuron are identical: The single TC input contributes nothing to the robust cortical onset response at 315°, which is evoked by other inputs.

We compared the tuning curves of the thalamic and cortical cell populations. Polar plots of the total AP response to each direction of whisker movement were constructed for every thalamic neuron, aligned to their preferred angles, and averaged (Fig. 4D). Thalamic neurons exhibited substantial directional tuning, and the average polar plot of PSPs in cortical cells mirrors this degree of tuning (compare Fig. 4D with Fig. 4F, red). Tuning at the level of APs is sharpened by the spike threshold (Fig. 4F, blue, and fig. S4) as previously found (*33*). No overall directional bias was observed for the cortical neuron population (Fig. 4E; $P = 0.73$ for caudorostral axis; $P = 0.45$ ventrodorsal; $n = 44$ cells). Thus the strong correspondence between thalamic AP output and cortical EPSP input cannot be due to a directional bias in the trigeminal pathway. Rather, their correspondence suggests that a select and potentially synchronous subpopulation of thalamic neurons converges on any given excitatory L4 cell. If this were not the case, the directional tuning of the L4 population would be significantly broader.

Therefore, we quantified the similarity of directional tuning of pairs by calculating correlation coefficients for corresponding thalamic and cortical polar plots. Examples with varying degrees of similarity are shown in Fig. 5A to C. Pairs of connected cells were similarly tuned (Fig. 5D; mean 0.37 ± 0.13, $P = 0.01$). Pairs without connection were both of similar or dissimilar tuning (Fig. 5E; mean –0.07 ± 0.17, $P = 0.7$). Consistent with extracellular findings in the somatosensory (*11*), auditory (*14*), and visual systems (*12*), converging TC inputs onto excitatory neurons are similarly tuned, likely thereby endowing the target cortical neuron with similar tuning.

Previous studies of VPM, using averages of local field potentials (*23*) and population PSTHs of sequentially recorded single units (*22*), suggested that relatively high-velocity whisker stimuli, such as those used here, on average evoke strong synchrony among thalamic inputs. To directly assess near-synchronous discharge of thalamic inputs on a trial-by-trial basis, we made simultaneous extracellular recordings of multiple VPM neurons (Fig. 6, A and B), either on one electrode or two different electrodes in the same barreloid. To be included in analyses, cells recorded on the same electrode were required to have nonoverlapping AP waveform distributions (see SOM). For each pair, cross-correlation histograms were made separately for spontaneous and stimulation periods (Fig. 6, C and D), and the number of near-synchronous events on the time scale of an EPSP was quantified by using a simple measure that normalizes for the firing rates of the two neurons (see SOM).

Weak synchrony is sometimes observed during spontaneous activity (Fig. 6C and fig. S6). For the same thalamic pair, high-velocity whisker stimulation noticeably enhances thalamic synchrony (Fig. 6D). Across the 28 pairs recorded, thalamic synchrony was typically

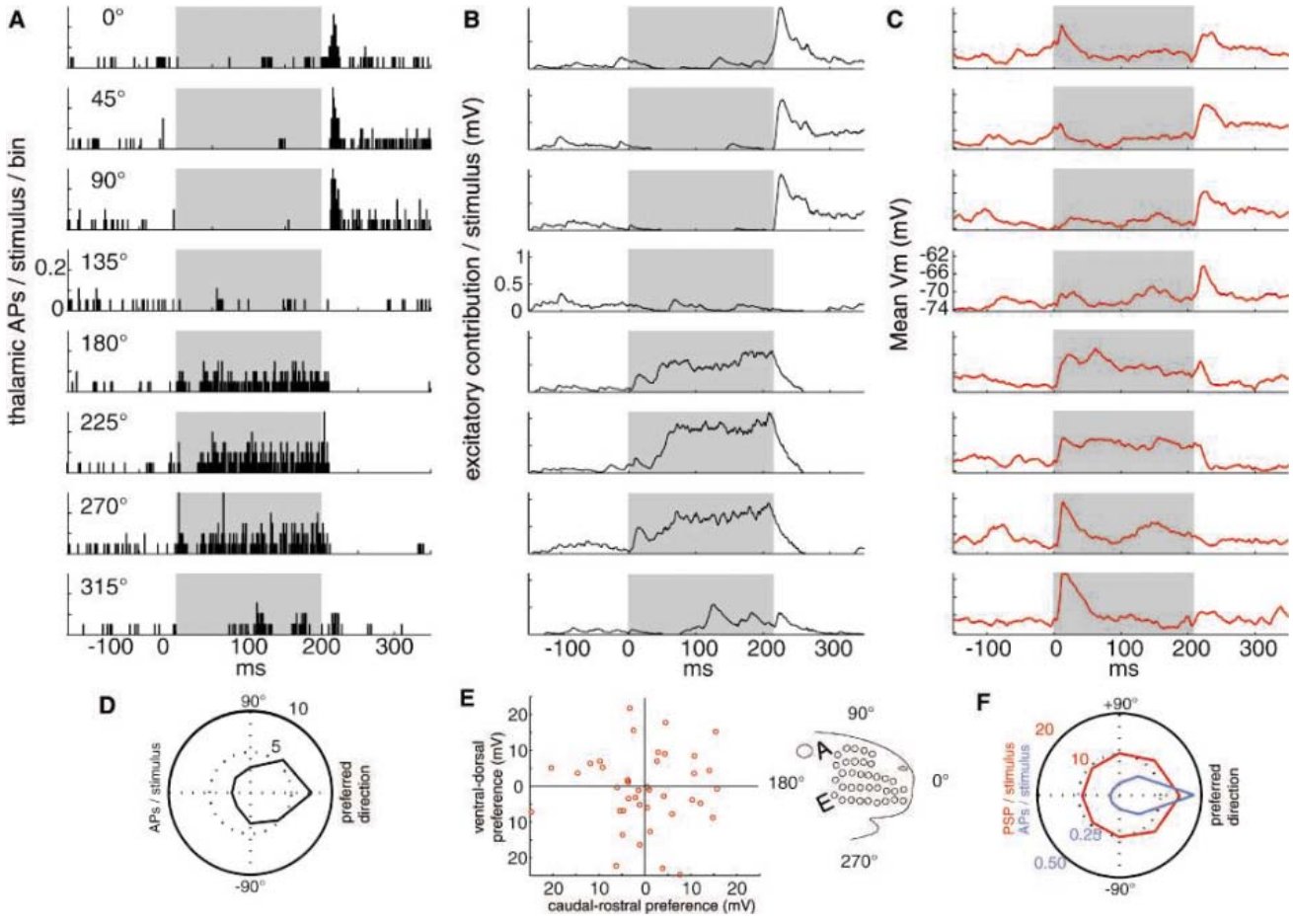

Fig. 4. Net synaptic inputs to a cortical cell closely resemble a single thalamic input. (**A**) PSTHs of APs of a thalamic neuron in response to 20 whisker deflections (gray) in each of 8 directions. (**B**) Excitation provided by the neuron in A. (**C**) PSP responses of a cortical cell postsynaptic to this thalamic cell. (**D**) Average tuning curve for thalamic cell population ($n = 21$) during 200 ms following stimulus onset. (**E**) Scatter plot of cortical cell directional preferences. Layout of rat facial whiskers (rows A to E) with regard to polar plots. (**F**) Same as (D) but for cortical cells ($n = 40$). Red, PSPs; blue, APs.

increased by the high-velocity stimulus (Fig. 6E; paired t test, $P < 10^{-4}$). In contrast, the low-velocity sinusoid used to evoke thalamic APs during aPSP estimation did not increase synchrony (fig. S6C; $P = 0.28$, $n = 19$). Results were equivalent for subsets of the data containing only pairs recorded on the same or different electrodes (see SOM). In conclusion, at the level of individual presentations, sensory stimulation can induce synchronous discharge of thalamic neurons.

Architecture of the thalamocortical pathway. The typical aPSP measures 490 μV whereas the average subthreshold response of a barrel neuron to a preferred stimulus is ~15 mV. Interestingly, field potentials averaged with regard to spontaneous thalamic discharges and sensory stimuli exhibit a similar ratio (*34*). If one considers only TC–spiny barrel neuron connections, then a minimum of 30 thalamic cells could account for stimulus-evoked cortical responses. However, because of additional contributions of feed-forward inhibition (*11*, *13*, *35*) and feedback excitation/inhibition (*3*, *21*, *36*), 30 thalamic inputs is likely an underestimate. Our method suggests a TC convergence ratio of ~0.43, consistent with paired extracellular estimates (*11*), but slightly higher, perhaps because of better sensitivity to weak connections. Therefore, given ~200 thalamic cells per barreloid (*16*, *37*), a L4 cell would on average receive ~85 TC connections (200 cells × 0.43 connections/cell).

About 65% of the roughly 2800 total spines on dendrites of an excitatory L4 neuron are contacted by axons originating from other L4 cells (*8*), which leaves slightly fewer than 1000 spines available for other inputs, such as TC axons. Each TC axon is thought to contribute on average about seven active synaptic contacts (*4*). Our estimate of 85 TC connections per cell suggests that, on average, 600 spines would be contacted by TC axons. This is well within the range of the 1000 spines not associated with axons originating within L4.

Our approach demonstrates that cross-correlation analysis of extracellular data, a technique introduced 40 years ago (*10*) and since used in a variety of systems, can correctly infer monosynaptic connections. Interestingly, paired extracellular recordings find correlogram peaks having latencies of ~2 ms—the same as that of EPSPs here and in vitro (*4*, *5*). This suggests that cortical APs are triggered on the EPSP rising phase rather than at the peak, consistent with reports that neurons are sensitive to the rate of V_m change, as well as absolute V_m (*33*, *38*). Overall time course of aPSPs is slower than that of EPSPs in vitro, perhaps because of jitter during averaging, weaker driving force in vivo, and/or larger contributions of *N*-methyl-D-aspartate receptors in vivo.

Individual TC synapses in vivo appear to be weaker than previously thought from slice studies. This difference may reflect inadvertent activation of multiple axons during "minimal stimulation" in vitro. A more likely explanation is that driving force is reduced in vivo, lessening the impact of any individual TC synapse. Additionally, the relatively high firing rates of thalamic neurons persistently depress TC synapses in vivo, as previously indicated by electrical thalamic stimulation (*25*, *26*). Our measurements demonstrate such depression at the level of unitary EPSPs. Cortical neurons in vivo, however, have lower spontaneous and evoked firing rates than thalamic neurons (*1*, *11*, *17*, *39*), and corticocortical synapses may consequently be less depressed than TC synapses. If this is the case, they may have strengths similar to those observed here. Somatosensory corticocortical connections have not yet been measured in vivo. One study in monkey motor cortex (*40*) observed similar unitary corticocortical connections (mean 226 μV), but a unitary EPSP

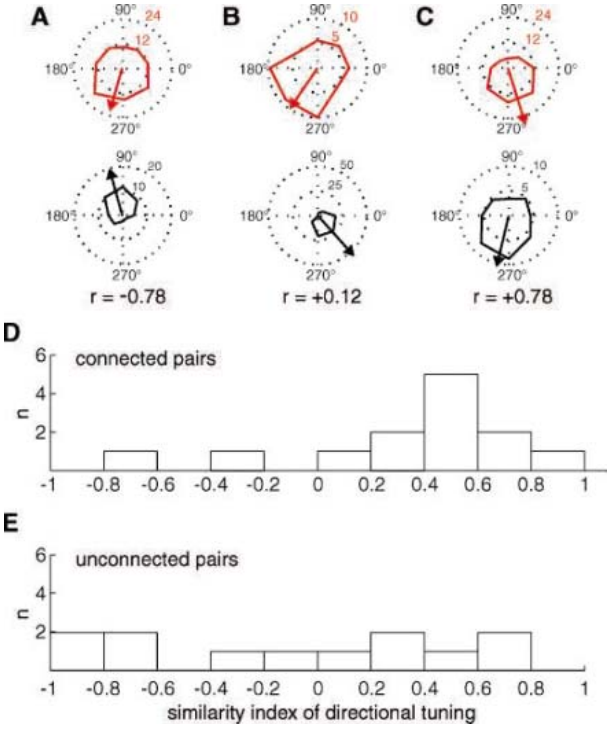

Fig. 5. Converging TC inputs have similar directional tuning. (**A** to **C**) Polar plots of example connected pairs having varying degrees of directional tuning similarity. Red, mean cortical PSP amplitudes (mV); black, mean thalamic spikes per stimulus. *r*, correlation of the polar plots. (**D**) Distribution of directional tuning similarity for connected pairs. (**E**) Distribution for unconnected pairs.

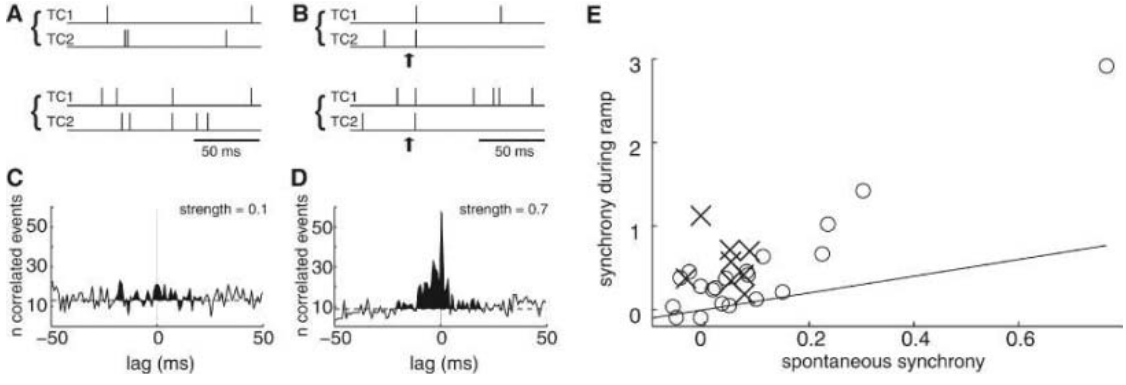

Fig. 6. High-velocity stimuli synchronize TC neurons. (**A**) Spontaneous APs from two TC neurons (*TC1*, *TC2*) recorded simultaneously on two electrodes in the same barreloid during sedation. Braces, simultaneously recorded APs. (**B**) Same pair during whisker stimuli (arrows). (**C** and **D**) Cross-correlation histograms of pair during spontaneous (C) and sensory-evoked (D) activity (trigger events, n = 419 and 395, respectively; 1-ms bins). Long dash, baseline; shading, events above baseline in ±20-ms window. (**E**) Synchrony during high-velocity stimuli is stronger than during spontaneous periods. Line, unity; circle, pair recorded on same electrode; X, pair recorded on two separate electrodes.

could not be determined for 90% of pairs, as it was not possible to estimate and subtract out other synaptic inputs as we did.

Layer 4 networks have been thought to amplify the output of a weak thalamocortical pathway (*5*, *7*, *8*). Although individual TC connections are indeed relatively weak and alone are unable to drive cortical activity, each cortical cell in L4 is the target of substantial numbers of converging TC synapses. Strong sensory stimulation elicits a near-synchronous pattern of APs among the majority of these converging inputs. Such an input pattern affords strong feed-forward excitation on the order of 10s of millivolts, which exceeds the size of the net sensory-evoked PSPs observed here and previously for L4 neurons (*1*–*3*). Recurrent excitatory connections in L4 are, therefore, not required to account for such large PSPs.

References and Notes

1. M. Brecht, B. Sakmann, *J. Physiol.* **543**, 49 (2002).
2. D. Ferster, S. Chung, H. Wheat, *Nature* **380**, 249 (1996).
3. M. Wehr, A. M. Zador, *Nature* **426**, 442 (2003).
4. Z. Gil, B. W. Connors, Y. Amitai, *Neuron* **23**, 385 (1999).
5. K. J. Stratford, K. Tarczy-Hornoch, K. A. Martin, N. J. Bannister, J. J. Jack, *Nature* **382**, 258 (1996).
6. G. Benshalom, E. L. White, *J. Comp. Neurol.* **253**, 303 (1986).
7. R. J. Douglas, C. Koch, M. Mahowald, K. A. Martin, H. H. Suarez, *Science* **269**, 981 (1995).
8. J. Lübke, V. Egger, B. Sakmann, D. Feldmeyer, *J. Neurosci.* **20**, 5300 (2000).
9. H. Suarez, C. Koch, R. Douglas, *J. Neurosci.* **15**, 6700 (1995).
10. D. H. Perkel, G. L. Gerstein, G. P. Moore, *Biophys. J.* **7**, 419 (1967).
11. R. M. Bruno, D. J. Simons, *J. Neurosci.* **22**, 10966 (2002).
12. R. C. Reid, J. M. Alonso, *Nature* **378**, 281 (1995).
13. H. A. Swadlow, A. G. Gusev, *Nat. Neurosci.* **5**, 403 (2002).
14. L. M. Miller, M. A. Escabi, H. L. Read, C. E. Schreiner, *Neuron* **32**, 151 (2001).
15. J. M. Alonso, W. M. Usrey, R. C. Reid, *Nature* **383**, 815 (1996).
16. P. W. Land, S. A. Buffer Jr., J. D. Yaskosky, *J. Comp. Neurol.* **355**, 573 (1995).
17. D. J. Simons, G. E. Carvell, *J. Neurophysiol.* **61**, 311 (1989).
18. S. M. Lu, R. C. Lin, *Somatosens. Mot. Res.* **10**, 1 (1993).
19. P. B. Arnold, C. X. Li, R. S. Waters, *Exp. Brain Res.* **136**, 152 (2001).
20. D. Feldmeyer, A. Roth, B. Sakmann, *J. Neurosci.* **25**, 3423 (2005).
21. D. Feldmeyer, V. Egger, J. Lübke, B. Sakmann, *J. Physiol.* **521**, 169 (1999).
22. D. J. Pinto, J. C. Brumberg, D. J. Simons, *J. Neurophysiol.* **83**, 1158 (2000).
23. S. Temereanca, D. J. Simons, *J. Neurophysiol.* **89**, 2137 (2003).
24. E. E. Fanselow, M. A. Nicolelis, *J. Neurosci.* **19**, 7603 (1999).
25. M. A. Castro-Alamancos, *Prog. Neurobiol.* **74**, 213 (2004).
26. C. E. Boudreau, D. Ferster, *J. Neurosci.* **25**, 7179 (2005).
27. S. Chung, X. Li, S. B. Nelson, *Neuron* **34**, 437 (2002).
28. M. A. Castro-Alamancos, *Neuron* **41**, 455 (2004).
29. E. Ahissar, R. Sosnik, S. Haidarliu, *Nature* **406**, 302 (2000).
30. D. J. Simons, T. A. Woolsey, *J. Comp. Neurol.* **230**, 119 (1984).
31. J. Anderson, I. Lampl, I. Reichova, M. Carandini, D. Ferster, *Nat. Neurosci.* **3**, 617 (2000).
32. J. Waters, F. Helmchen, *J. Neurosci.* **24**, 11127 (2004).
33. W. B. Wilent, D. Contreras, *J. Neurosci.* **25**, 2983 (2005).
34. H. A. Swadlow, A. G. Gusev, T. Bezdudnaya, *J. Neurosci.* **22**, 7766 (2002).
35. L. Gabernet, S. P. Jadhav, D. E. Feldman, M. Carandini, M. Scanziani, *Neuron* **48**, 315 (2005).
36. D. J. Pinto, J. A. Hartings, J. C. Brumberg, D. J. Simons, *Cereb. Cortex* **13**, 33 (2003).
37. C. Varga, A. Sik, P. Lavallee, M. Deschenes, *J. Neurosci.* **22**, 6186 (2002).
38. R. Azouz, C. M. Gray, *Proc. Natl. Acad. Sci. U.S.A.* **97**, 8110 (2000).
39. M. Brecht, B. Sakmann, *J. Physiol.* **538**, 495 (2002).
40. M. Matsumura, D. Chen, T. Sawaguchi, K. Kubota, E. E. Fetz, *J. Neurosci.* **16**, 7757 (1996).

41. Thanks to C. de Kock, D. Feldmeyer, D. Haydon-Wallace, M. Helmstaedter, P. Krieger, P. Medini, P. Osten, and H. Spors for comments on the manuscript; M. Kaiser, R. Roedell, K. Schmidt, and E. Stier for outstanding technical assistance; and B. Gaertner, V. Hotz, M. Maerz, R. Masionyte, S. Tokur, and S. Wiegert for morphological reconstructions. Support provided by the Max Planck Society.

Supporting Online Material

www.sciencemag.org/cgi/content/full/312/5780/1622/DC1
Materials and Methods
SOM Text
Figs. S1 to S7
References

4 January 2006; accepted 5 May 2006
10.1126/science.1124593

Biomarker Evidence for a Major Preservation Pathway of Sedimentary Organic Carbon

Y. Hebting,[1]* P. Schaeffer,[1] A. Behrens,[1] P. Adam,[1] G. Schmitt,[1] P. Schneckenburger,[1] S. M. Bernasconi,[2] P. Albrecht[1]†

Hydrogenation processes leading from biomolecules to fossil biomarkers in anoxic sediments are crucial for the preservation of organic matter. However, these processes are still poorly understood. The present identification of several reduced carotenoids in recent sediments attests that these processes operate at the earliest stages of diagenesis without structural or stereochemical specificity, implying a nonbiological reduction pathway. Sulfur species (e.g., H_2S) are the hydrogen donors involved in such reduction, as demonstrated with laboratory experiments. These reactions allow the preservation of abundant organic carbon in the rock record.

High sedimentation rates, sorption onto mineral surfaces, humification reactions, and intrinsic resistance to biodegradation of naturally occurring biopolymers are important factors associated with the preservation of organic carbon in sediments, depending upon the environment (*1*). In organic-rich marine sediments, which are usually associated with oxygen-depleted depositional environments and which eventually lead to major petroleum deposits by thermal evolution (*2*), enhanced preservation is attributed mainly to efficient reduction processes and sulfurization (*3*, *4*).

The reduction reactions, generally referred to incorrectly as "hydrogenation," have been invoked as being responsible for the defunctionalization of biological lipids, leading to biomarker hydrocarbons present in fossil organic matter. The most classical examples are the widespread occurrence in the geosphere of biomarker hydrocarbons such as β-carotane, phytane, steranes, and hopanes deriving, respectively, from β-carotene, phytol-related terpenoids, steroids, and hopanoids present in various organisms of mainly algal and bacterial origin. The role of late diagenetic or catagenetic thermal processes in the formation of sedimentary hydrocarbons through a sequence of cracking and hydrogen transfer reactions is well described (*5*), leading to petroleum, gases, and graphitized material. In contrast, only a few studies have been devoted to the effective reductive alteration of sedimentary organic carbon during early diagenesis, despite the major role that this process certainly plays in the transformation and preservation of organic material in the geosphere.

It has been proposed that biological processes intervene in the reductive transformation undergone by sedimentary organic carbon at the first stages of sedimentation, as is the case of the conversion of sterols to stanols (*6*, *7*). However, such transformations might also result from purely chemical, abiotic reactions, although this has not been clearly established, except for in some xenobiotics, which are reduced in natural environments (*8*).

We investigated this problem on a molecular basis by studying the reductive transformations undergone by carotenoids as precursors in recent sediments deposited in the lake of Cadagno (Switzerland), an ideally suited model system of sulfide-rich, anoxic environment (*9*, *10*). In addition, we developed laboratory experiments demonstrating that the sulfides formed by bacterial sulfate reduction are most likely to be the reducing agents responsible for the reduction affecting decaying carotenoids and other lipids in the water column and within the sediment.

[1]Laboratoire de Géochimie Bioorganique, Unité Mixte de Recherche 7509 du CNRS, Université Louis Pasteur, Ecole de Chimie, Polymères, Matériaux de Strasbourg, 25 rue Becquerel, 67200 Strasbourg, France. [2]Geologisches Institut, ETH Zürich, CH-8092 Zürich, Switzerland.

*Present address: Department of Earth, Atmospheric, and Planetary Sciences, Massachusetts Institute of Technology, 77 Massachusetts Avenue, Cambridge, MA 02139, USA.
†To whom correspondence should be addressed. E-mail: albrecht@chimie.u-strasbg.fr

These results enabled us to unveil a mechanism responsible for the preservation of organic matter in anoxic sediments.

Reduced carotenoids in recent sediments. Carotenoids are commonly occurring tetraterpenoid pigments that are widespread in living organisms such as algae, bacteria, and higher plants. The most common components are β-carotene **1** (bold numbers refer to structures shown in Scheme 1), which is widely distributed in terrestrial and marine plants, and fucoxanthin **2**, which is often found in planktonic organisms such as diatoms and dinoflagellates. Although highly sensitive to oxidation, the carotenoid structures may be preserved intact in recent or even in immature ancient sediments deposited under strictly anaerobic conditions (*11*). They occur more generally in fossil organic matter as fully or significantly reduced equivalents. Only a few, such as β-carotane **3** and the aromatic carotenoids **4** to **8**, are characterized structurally (*12*–*17*).

Gas chromatography–mass spectrometry (GC-MS) analysis (*18*) of aromatic and polar fractions of the solvent-extractable organic matter from recent sediments of Lake Cadagno revealed that numerous partly reduced carotenoid derivatives were present and thus that "hydrogenation" already operates during the earliest stages of diagenesis. Given their high relative abundance, three could be isolated in order to determine their stereochemistry. Formation of chiral center(s) would indicate reduction through biologically mediated reactions, whereas an abiotic process would lead to mixtures of enantiomers or diastereomers.

After catalytic hydrogenation (H_2, PtO_2) of fractions containing partly reduced carotenoids, we identified six hydrogenated counterparts with GC-MS using authentic standards: β-carotane **3**, isorenieratane **4**, chlorobactane **9**, β-isorenieratane **10**, as well as two novel hydrocarbons, **8** and **11**, related to okenone **12** and β-renierapurpurin **13**, respectively (*17*).

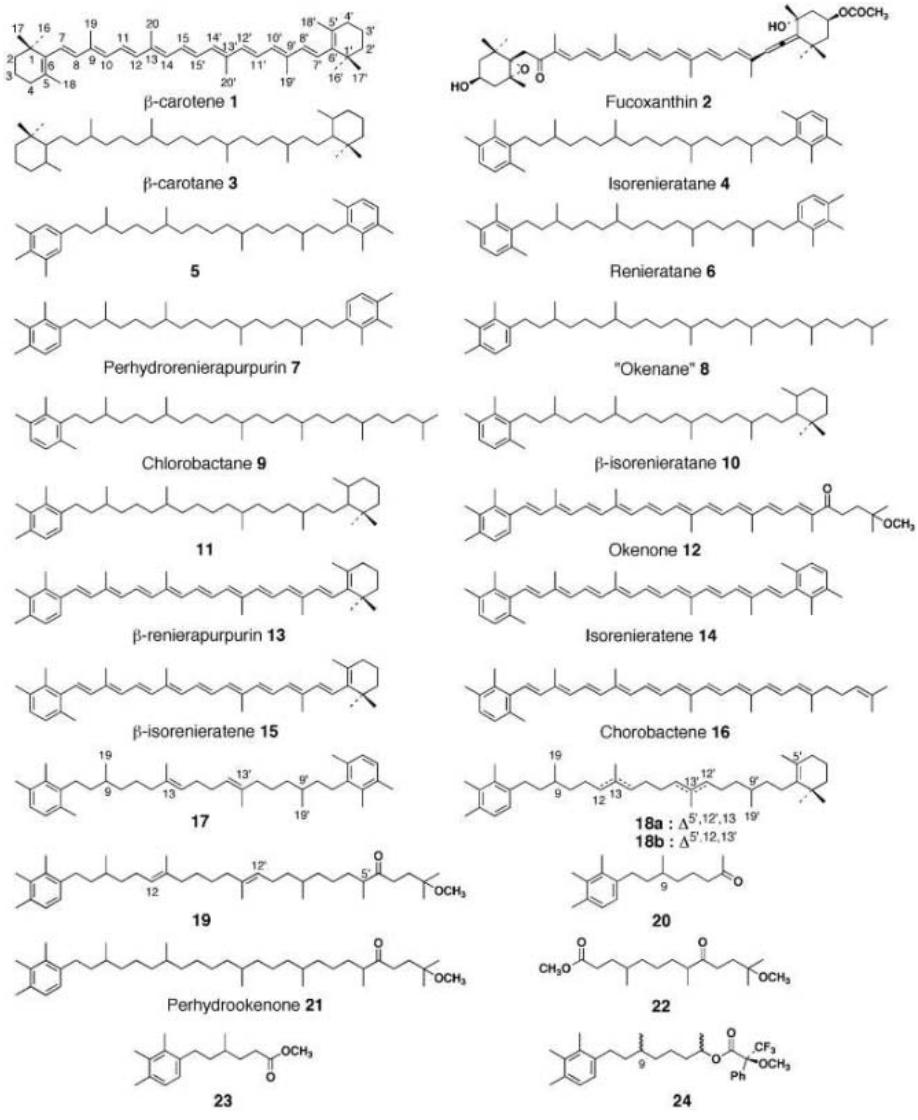

Scheme 1.

The presence of intact parent carotenoids such as β-carotene **1**, okenone **12**, isorenieratene **14**, β-isorenieratene **15**, and chlorobactene **16** among the predominant carotenoids from these sediments (*17*, *19*) implies that the partly reduced derivatives, for which up to ten double bonds have been reduced, must be diagenetic transformation products of the former. Determination of their stable carbon isotopic composition using GC-isotope ratio monitoring MS (GC-irmMS) confirmed that compounds **4**, **9**, and **10** derive from carotenoids **14** to **16** biosynthesized by *Chlorobiaceae* (*20*, *21*). On the other hand, compounds **8** and **11** show $\delta^{13}C$ values close to that of okenone **12**, the major carotenoid from *Chromatiaceae*, which represent the prominent sulfur phototrophic bacteria in the water column of Lake Cadagno [see supporting online material (SOM) text] (*20*, *22*).

Structural identifications. We isolated three partly reduced C_{40} carotenoid hydrocarbons with two unsaturations remaining on the isoprenoid chain (**17** to **19**) and one C_{18} carotenoid ketone moiety **20** (Fig. 1), which is likely to be a diagenetic transformation product of a C_{40} precursor. They were obtained in milligram amounts using multiple step liquid chromatography and reverse phase high-performance liquid chromatography (HPLC) from the solvent extract (*18*).

The structure of compound **17** could be unambiguously established with nuclear magnetic resonance (NMR) as $\Delta^{13,13'}$-tetradecahydroisorenieratene (table S1). The presence of nuclear Overhauser effects (nOes) between H12/H14 and H12′/H14′ indicates a trans geometry for both double bonds. No conclusion based on NMR data could however be drawn as to the presence of diastereomers at positions 9 and 9′ (Fig. 1).

The NMR results reveal that compound **18** must be a mixture of two compounds (2:1 ratio; unresolved with HPLC and GC), the predominant and the minor compounds most likely corresponding to $\Delta^{5',12',13}$ and $\Delta^{5',12,13'}$ tetradecahydro-β-renierapurpurin (**18a** and **18b**), respectively, as indicated by the splitting of almost all signals observed in the distortionless enhancement by polarization transfer (DEPT) and 1D-^{13}C spectra (table S2). However, the possibility of diastereoisomers differing by their stereochemistry at the two asymmetric centers at C9 and C9′ cannot be excluded. The tiny amounts of the compound did not allow us to pursue further structural studies.

Comparison between the mass spectrum of perhydrookenone **21** obtained by catalytic hydrogenation of okenone **12** with that of the isolated carotenoid **19** (*18*) indicates a very similar mass fragmentation pattern characterized by a fragment with a mass-to-charge ratio (*m/z*) = 133 atomic mass units (amu), typical of a trimethyl substituted aromatic ring at one end of the molecule, and an ion at *m/z* = 562 corresponding to the loss of a methoxy group $(M\text{-}CH_3OH)^+$. For compound **19**, the molecular ion M^+ at *m/z* = 594 revealed the probable

presence of two double bonds as compared with perhydrookenone **21**. Finally, NMR data enabled us to identify compound **19** as hexadecahydrookenone (table S3). However, because there were some uncertainties left on the exact location of the double bonds, ozonolysis of **19** was carried out (*18*) and yielded mainly, after esterification, the products **22** and **23**, which confirmed that the two double bonds are at positions 12 and 12′ (fig. S1).

Selectivity of the reduction processes. In the ^{1}H-NMR spectra of **19** measured in both $CDCl_3$ and C_6D_6, the signals from the $CH_3$19 and $CH_3$19′ appear with the shape of triplets, whereas that of $CH_3$18 shows up as a doublet. Similarly, the DEPT and 1D ^{13}C spectra show that some ^{13}C signals are split in two, suggesting that compound **19** must correspond to a mixture of diastereomers differing at least by the stereochemistry at position 5′ (enol position), known to be easily isomerized during early diagenesis (*23*). Because no further splitting was observed for the $CH_3$18, $CH_3$19, or $CH_3$19′ groups, no conclusions could be drawn as to whether positions 9 or 9′ were epimerized.

Structural elucidation of the C_{18} aromatic ketone **20** was established by comparing the isolated compound with a reference compound prepared as a racemic mixture by synthesis (fig. S2). The isolated compound is presumably a degradation product of carotenoid precursors from purple sulfur photosynthetic bacteria formed by diagenetic transformation (e.g., oxidative cleavage of a double bond, followed by reduction of several remaining double bonds). Attempts to use chiral stationary phases in GC and HPLC, or chiral shift reagents in NMR, all failed to distinguish the two enantiomers at C9 in the racemic synthetic compound. However, reduction of the ketone to the alcohol and transformation of the latter into its Mosher ester **24** was successful and led to the distinction using NMR spectroscopy of four diastereomers occurring in equal amounts. Similarly, the Mosher ester derivative **24** obtained by derivatization of the geochemical compound led to the conclusion that the naturally-occurring ketone **20** is present as a racemic mixture, demonstrating that the latter had undergone a nonstereoselective reduction at C9.

An early diagenetic process. Our results document the partly reduced carotenoid derivatives occurring in this recent sediment. These compounds, which derive from pigments of *Chromatiaceae* and *Chlorobiaceae* that are widely present in Lake Cadagno, are already abundant in the surface sediment, showing that the processes that have produced them must be operative in the water column or during the first stages of sedimentation.

β-carotene derivatives (of mainly phytoplanktonic origin, as shown using irmMS) and other C_{40} reduced aromatic compounds, with 1 to 10 reduced double bonds on the isoprenoid chain, have also been characterized using probe MS, GC-MS, and GC-irmMS. Moreover, for a given molecular mass, several compounds are present, indicating the probable occurrence of cis, trans, and/or positional isomers (Fig. 2). The different origins of these compounds and the wide variety of their extent of reduction rule out a direct biosynthetic origin of the partly reduced counterparts, which have never been reported to occur in living organisms (SOM text). Furthermore, their formation by (microbial) reutilization of carotenoids from decaying organic matter can be excluded because such a process is unlikely to lead to the complex isomeric mixtures observed or inferred from our NMR and GC-MS studies. Our results suggest that the reduction of the double bonds proceeds via a nonbiological process, as opposed to stereoselective, enzyme-mediated reactions. This conclusion immediately raises the question of the nature of the reducing agent(s) and the chemical mechanism(s) involved in this reduction.

Reduction by H_2S. An indirect mechanism of hydrogen transfer has been proposed, in which carotenoids first become linked into a macromolecular network by reaction with inorganic sulfur species before being released as partly reduced counterparts under thermal stress during burial (*24*). However, such a

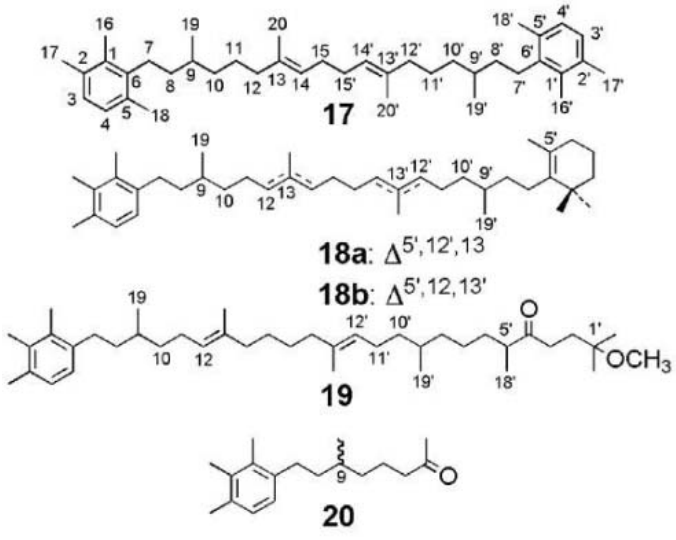

Fig. 1. Structures of novel reduced carotenoid derivatives **17** to **20** identified using NMR spectroscopy after isolation from a recent lacustrine sediment (Lake Cadagno, Switzerland). For details of the isolation procedure and ^{1}H and ^{13}C NMR data, see (*18*).

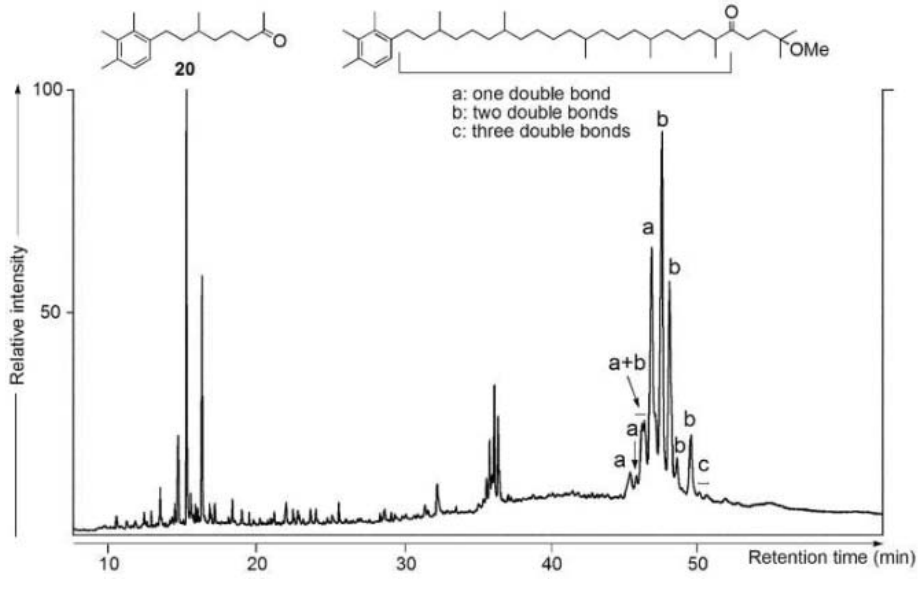

Fig. 2. Gas chromatogram total ion current of a fraction isolated from the solvent extract of the recent sediment from Lake Cadagno using a multiple step chromatographic sequence composed of column and thin layer chromatography on silica gel. This fraction contains the ketone **20** as well as a complex mixture of reduced okenone derivatives having one, two, or three remaining double bonds on the isoprenoid chain. GC-MS conditions: Finnigan Mat TSQ 700 (EI, 70eV), HP5-MS (30 m × 0.25 mm × 0.1 μm film thickness). Temperature program: 80°C (1 min), 80° to 200°C (10°C min^{-1}), 200° to 300°C (3°C min^{-1}), isothermal at 300°C. Carrier gas: helium (constant flow: 1.7 mL min^{-1}).

hypothesis cannot be operative in the case of recent deposits that have never been submitted to elevated temperature. We therefore propose another purely chemical process involving the reducing potential of sulfides. These are produced by bacterial sulfate reduction and are abundant in the anoxic part of the water column and in the sediments of Lake Cadagno (*9*, *10*), as well as in many other settings (mostly marine) in which reduced counterparts of biological molecules are widespread.

Sulfides or thiols have been shown to be effective as reducing agents in synthetic chemistry for the reduction of diketones to ketones (*25*) or of activated double bonds (*26*). This role has also been observed in the conversion of nitroaromatic pollutants taking place in anaerobic soils and sediments (*27*). Furthermore, sulfides act as electron-transferring species in the reduction of carbonyls to thiols in natural environments (*28*).

Laboratory experiments. In order to test our hypothesis that sulfides are able to reduce double bonds under geochemically relevant conditions, we developed laboratory chemical experiments involving β-carotene **1**, as well as an unsaturated ketone (cholesta-4,6-dienone) in the presence of hydrogen sulfide (*18*).

In the case of β-carotene **1**, the formation of derivatives with one and two reduced double bonds was observed, as shown with probe-MS experiments (M^+ = 538 and 540, from M^+ 536 for parent β-carotene; 1% yield). These findings demonstrate that H_2S/HS^- is able to hydrogenate double bonds from the carotenoid polyenic system, yielding partly reduced counterparts. Because these compounds are highly sensitive to oxidation, their isolation for NMR structural studies was not feasible. The observed reduction most likely proceeds via a two-step reaction sequence (Fig. 3A). The first would involve the addition of H_2S to double bonds on the polyenic system, leading notably to a complex mixture of allylic thiols as a result of the high number of possibly reactive double bonds. This hypothesis is supported by the detection using probe-MS of β-carotene derivatives having incorporated one, two, or three H_2S molecules (M^+ = 570, 604, and 638 respectively). Unfortunately, the multiplicity of isomers prevented their isolation and study using NMR spectroscopy. The second step involves the reduction of the allylic thiols, leading to the corresponding counterparts with hydrogenated double bonds, and it is likely to operate via a single electron transfer reaction involving H_2S/HS^- as electron donor. Under similar conditions, cis and trans phyt-2-ene-1-thiols (or, more generally, allylic thiols) undergo reductive desulfurization via a single electron transfer process involving intermediate free radical species (*29*), leading to an isomeric mixture of phytenes (*18*) in the same relative proportions as those found in various recent sulfur-rich sediments (Fig. 3B). Furthermore, the plausible intermediates between phytol and phytenes, cis and trans phyt-2-ene-1-thiols, were identified in the same sulfur-rich sediments, which include lacustrine environments (Lake Cadagno), brackish environments (Siders Pond, MA, USA), and upwelling marine settings (Walvis Bay, Namibia) (*30*).

In the case of polyenic substrates such as carotenoids, iteration of the same two-step mechanism (i.e., addition of H_2S followed by reductive desulfurization; Fig. 3A) results in the reduction of several double bonds. The geochemical relevance of such a process is further supported by the co-occurrence in sediments, notably in those from Lake Cadagno, of partly reduced carotenoids, of their polyunsaturated precursors, and of sulfurized carotenoids bound to macromolecular constituents of the organic matter. The latter are shown by the release of carotenoid hydrocarbons upon Raney nickel desulfurization of polar macromolecular fractions isolated from the organic extract (*18*).

The laboratory experiment involving cholesta-4,6-dienone yielded cholest-4-en-3-one and 5α(H)- and 5β(H)-cholestan-3-one (Fig. 3C) under the same mild conditions (*18*), showing that H_2S and/or HS^- are able to reduce directly double bonds conjugated to carbonyl groups without an initial sulfurization of the double bond (*18*). Consequently, another mechanism of reduction, which can operate in parallel, can be proposed in the case of oxygenated carotenoids (i.e., xanthophylls) such as okenone **12**. In addition to the naturally occurring xanthophylls, carbonyl functions necessary to trigger this type of reduction reaction may be introduced into carotenoids by biological or abiotic oxidation (e.g., **20**) during early diagenesis in the sediment or within the water column.

An ongoing preservation pathway. The laboratory experiments confirm that reduction processes can be ascribed to the reducing power of inorganic sulfur species. Such abiotic reactions are likely to play a key role in the preservation of sedimentary organic matter, an ongoing process occurring throughout geologic history, by transforming labile, oxygen-sensitive lipids into their more stable reduced counterparts (*31*, *32*). This phenomenon can explain the widespread occurrence of saturated carotenoid derivatives in billion-year-old rocks (*14*). In prebiotic chemistry, such sulfur reduction might have played a role in the chemical processes occurring in the sulfide-rich environments of hydrothermal vents, which have been postulated as possible sites for the first steps of organic chemical evolution (*33*, *34*).

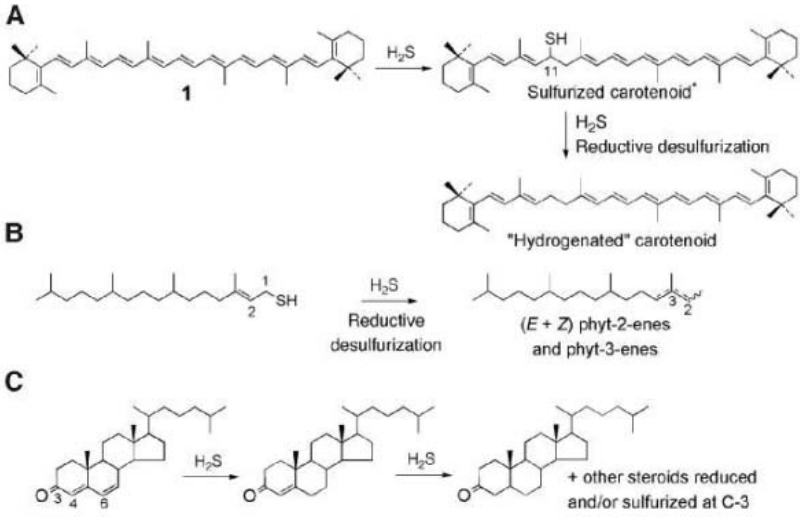

Fig. 3. Reduction products obtained by reaction of hydrogen sulfide under aqueous conditions with (**A**) β-carotene **1**, (**B**) phyt-2-ene-1-thiol, and (**C**) cholesta-4,6-dien-3-one. For experimental conditions, see (*18*). The asterisk indicates that the location of the sulfur incorporation at C11 has been chosen arbitrarily.

References and Notes

1. J. I. Hedges *et al.*, *Nature* **409**, 801 (2001).
2. K. E. Peters, C. C. Walters, J. M. Moldowan, *The Biomarker Guide* (Cambridge Univ. Press, Cambridge, ed. 2, 2005).
3. J. S. Sinninghe Damsté, W. I. C. Rijpstra, A. C. Kock-Van Dalen, J. W. de Leeuw, P. A. Schenck, *Geochim. Cosmochim. Acta* **53**, 1343 (1989).
4. P. Adam *et al.*, *Geochim. Cosmochim. Acta* **57**, 3395 (1993).
5. J. M. Hunt, *Petroleum Geochemistry and Geology* (W.H. Freeman and Company, New York, ed. 2, 1996), pp. 60–140.
6. M. Nishimura, *Geochim. Cosmochim. Acta* **42**, 349 (1978).
7. S. G. Wakeham, *Nature* **342**, 787 (1989).
8. M. Elsner, R. P. Schwarzenbach, B. Haderlein, *Environ. Sci. Technol.* **38**, 799 (2004).
9. The mountain lake of Cadagno, located in the Swiss Alps, displays many similarities with restricted marine deposits, because it has highly mineralized waters enriched in sulfate and carbonate (*10*) coupled to a high productivity, allowing extensive sulfate reduction to occur. This results in the formation of sulfide-rich anoxic bottom waters (*10*) extending up to the photic zone within which populations of purple and green sulfur photosynthetic bacteria (i.e., *Chromatiaceae* and *Chlorobiaceae* respectively) thrive.
10. C. Del Don, K. W. Hanselmann, R. Peduzzi, R. Bachofen, *Aquat. Sci.* **63**, 70 (2001).
11. A. Putschew, P. Schaeffer, C. Schaeffer-Reiss, J. R. Maxwell, *Org. Geochem.* **29**, 1849 (1998).
12. M. T. J. Murphy, A. McCormick, G. Eglinton, *Science* **157**, 1040 (1967).

13. J. Schaeflé, B. Ludwig, P. Albrecht, G. Ourisson, *Tetrahedron Lett.* **41**, 3673 (1977).
14. J. J. Brocks *et al.*, *Nature* **437**, 866 (2005).
15. W. A. Hartgers, J. S. Sinninghe Damsté, M. P. Koopmans, J. W. de Leeuw, *J. Chem. Soc. Chem. Commun.* **1993**, 1715 (1993).
16. W. A. Hartgers *et al.*, *Org. Geochem.* **22**, 703 (1994).
17. P. Schaeffer, P. Adam, P. Wehrung, P. Albrecht, *Tetrahedron Lett.* **38**, 8413 (1997).
18. Materials and methods are available as supporting material on *Science* Online.
19. H. Züllig, *Schweiz. Hydrol.* **47**, 87 (1985).
20. Determination of the stable carbon isotopic composition of individual compounds by GC-irmMS allows a link to be established between biomarkers and their biological precursors. In the sediments from Lake Cadagno, carotenoid derivatives from green sulfur photosynthetic bacteria using the reverse tricarboxylic acid cycle for carbon fixation (*21*) show $\delta^{13}C$ values of ~–27 per mil (‰), whereas those from purple sulfur bacteria have a clearly distinct, much lighter, isotopic signature of ~–45‰ (SOM text). $\delta^{13}C = 10^3(R_x - R_s/R_s)$, where R=$^{13}C/^{12}C$, x: sample, s: Pee Dee Belemnite (PDB) standard, and $R_s = 0.0112372$.
21. L. Quandt, G. Gottschalk, H. Ziegler, W. Stichler, *FEMS Microbiol. Lett.* **1**, 125 (1977).
22. M. Tonolla, R. Peduzzi, D. Hahn, *Appl. Environ. Microbiol.* **71**, 3544 (2005).
23. R. Y. P. Burhan *et al.*, *Geochim. Cosmochim. Acta* **66**, 4085 (2002).
24. M. P. Koopmans, J. W. de Leeuw, J. S. Sinninghe Damsté, *Org. Geochem.* **26**, 451 (1997).
25. R. Mayer, M. Nitzschke, J. Jentzsch, *Angew. Chem.* **21**, 1011 (1963).
26. J. W. G. Meissner, A. C. Van der Laan, U. K. Pandit, *Tetrahedron Lett.* **35**, 2757 (1994).
27. R. P. Schwarzenbach, R. Stierli, K. Lanz, J. Zeyer, *Environ. Sci. Technol.* **24**, 1566 (1990).
28. P. Schneckenburger, P. Adam, P. Albrecht, *Tetrahedron Lett.* **39**, 447 (1998).
29. Y. Hebting, P. Adam, P. Albrecht, *Org. Lett.* **5**, 1571 (2003).
30. P. Adam, P. Schneckenburger, P. Schaeffer, P. Albrecht, *Geochim. Cosmochim. Acta* **64**, 3485 (2000).
31. C. D. Watts, J. R. Maxwell, *Geochim. Cosmochim. Acta* **41**, 493 (1977).
32. J. S. Sinninghe Damsté, M. P. Koopmans, *Pure Appl. Chem.* **69**, 2067 (1997).
33. M. J. Russell, A. J. Hall, *J. Geol. Soc. (London)* **154**, 377 (1998).
34. G. D. Cody *et al.*, *Science* **289**, 1337 (2000).
35. Dedicated to Professor Guy Ourisson on the occasion of his 80th birthday. We thank the donors of The Petroleum Research Fund, administrated by the American Chemical Society, for partial support of this research. We thank R. Graff and J. D. Sauer for NMR spectroscopy and P. Wehrung and E. Mastio-Motsch for mass spectrometry.

Supporting Online Material

www.sciencemag.org/cgi/content/full/1126372/DC1
Materials and Methods
SOM Text
Figs. S1 and S2
Tables S1 to S3
References

17 February 2006; accepted 26 April 2006
Published online 11 May 2006;
10.1126/science.1126372
Include this information when citing this paper.

Measurement of Forces Inside a Three-Dimensional Pile of Frictionless Droplets

J. Zhou,[1] S. Long,[2] Q. Wang,[2] A. D. Dinsmore[1]*

We present systematic and detailed measurements of interparticle contact forces inside three-dimensional piles of frictionless liquid droplets. We measured long-range chainlike correlations of the directions and magnitudes of large forces, thereby establishing the presence of force chains in three dimensions. Our correlation definition provides a chain persistence length of 10 mean droplet diameters, decreasing as load is applied to the pile. We also measured the angles between contacts and showed that the chainlike arrangement arises from the balance of forces. Moreover, we found that piles whose height was comparable to the chain persistence length exhibited substantially greater strain hardening than did tall piles, which we attributed to the force chains. Together, the results establish a connection between the microscopic force network and the elastic response of meso- or macroscopic granular piles. The conclusions drawn here should be relevant in jammed systems generally, including concentrated emulsions and piles of sand or other heavy particles.

The response of disordered materials to applied stresses is a fascinating but difficult problem in nonequilibrium statistical mechanics, with applications in transporting and storing disordered materials. Examples of such materials include powders, gels, concentrated emulsions, and piles of large and heavy particles such as sand grains, whose thermal motions are negligible. Measurements of the contact forces among these grains have exposed some possibly universal trends that might point the way to a general understanding of the static stresses in granular systems (*1*, *2*). Earlier approaches include numerical simulations (*3*–*7*) and experimental force measurements in two dimensions (*8*–*10*) and on surfaces of three-dimensional (3D) bulk (*1*, *2*, *11*–*14*). These studies showed that the magnitudes of the contact forces follow probability distributions with common features and notably that the largest forces might be arranged in a chainlike architecture that bears no resemblance to the arrangement of the grains themselves (*1*, *10*). To date, however, these "force chains" have eluded quantitative definition and there is not an accepted intuitive model to explain their spontaneous appearance. In describing the macroscopic stress response, simulations show an inhomogeneous, nonelastic response to a point force at small length scales, although at larger length scales the response can be described by linear elasticity theory (*15*–*17*). In the absence of tangential forces (without static friction), the inhomogeneous behavior persists to longer length scales in the simulations; frictionless granular systems therefore provide an important model with which to understand force correlations or chains (*6*, *18*). The challenge remains, however, to define and measure this characteristic length in three dimensions and understand intuitively how it arises.

We provide a comprehensive set of measurements of frictionless 3D piles and show how force chains arise from the architecture of the force network and the force-balance constraint. We also show how the force correlation length determines the macroscopic response to stress. We used frictionless liquid droplets in a pile with no Brownian motion (effectively at zero temperature) that was subjected to uniaxial stress in the linear response regime. 3D images were obtained by means of confocal fluorescence microscopy (Fig. 1). High resolution was achieved by labeling only the droplet surfaces with a monolayer of fluorescent nanoparticles [4-nm of trioctylphosphine oxide (TOPO)-CdSe (*19*)] or 30-nm *N*,*N*,*N*′,*N*′-tetramethyl rhodamine (TMR)–modified cowpea mosaic virus (CPMV) (*20*). To obtain the contact forces, we measured the sizes of the contact regions between adjacent droplets and the droplet radii from the confocal images (Fig. 1, B and C). The contact force, f_{ij}, between droplets i and j is given by $f_{ij} = A_{ij}\gamma(R_i + R_j)/(R_iR_j)$, where γ is surface tension, $R_{i,j}$ are the droplet radii, and A_{ij} is the contact area (*21*). As evidence of the absence of static friction (as expected for liquid droplets), we found that the calculated net force on each droplet approached zero. We imaged ~10^3 droplets near the bottom of the piles (containing on the order of 10^7 droplets, which was substantially more than in typical

[1]Department of Physics, University of Massachusetts, Hasbrouck Laboratory 411, 666 North Pleasant Street, Amherst, MA 01003, USA. [2]Department of Chemistry and Biochemistry, University of South Carolina, 631 Sumter Street, Columbia, SC 29208, USA.

*To whom correspondence should be addressed. E-mail: dinsmore@physics.umass.edu

simulations) and obtained 10^3 to 10^4 contact forces in each sample. Here we report three data sets: one derived from a monodisperse pile and two derived from a polydisperse pile subjected to different loads (one load with its own weight and the other with a Teflon disk immersed in fluid and resting atop the droplet pile).

Chainlike spatial correlations of the contact forces are clearly present in the experimentally derived force map (Fig. 2A), in which all of the measured forces in the polydisperse sample were greater than a cutoff value (f_{cut}) of $1.6\langle f\rangle$, where $\langle f\rangle$ is the mean of all forces f in the imaged volume. These large forces were not spatially random, and chainlike arrangements were prevalent. In this map, the longest chain was $12\langle d\rangle$ in length, where the mean droplet diameter $\langle d\rangle$ was ~30 μm. To quantify the chains, we focused on their key geometric property, which is the tendency to align forces along the chain axis. We computed the correlation of the directions and magnitudes of forces, $C_{\mathbf{f}\cdot\mathbf{r}}$. Specifically, we computed $C_{\mathbf{f}\cdot\mathbf{r}}(r; f_{cut})$ by first isolating all contact forces greater than f_{cut}, choosing pairs of forces separated by length r, and then finding their normalized correlation function (see the legend of Fig. 2B). The principal result was a robust, long-range correlation that decayed exponentially with a characteristic length, l_f or chain correlation length. The degree of chainlike correlation was quantified by extrapolating the exponential decay to $r = 0$; we defined this correlation magnitude as $\alpha(f_{cut})$. α is a rapidly increasing function of f_{cut} (Fig. 2C), indicating that the largest forces are more highly correlated (for example, $\alpha = 0.3$ for $f_{cut} = 1.6\langle f\rangle$; larger values of f_{cut} were subjected to greater statistical uncertainty). When $f_{cut} = 1.6\langle f\rangle$, the value of l_f for this pile was $10\langle d\rangle$, which is close to the maximum chain length in the force map. We interpreted l_f as the persistence length of a force chain, which is analogous to the persistence length of a polymer; the chains might in fact be longer but are tortuous (Fig. 2A). We found no substantial long-range correlations of coordination number (the number of contacts on a droplet, Z), magnitudes of forces f, or droplet positions, in agreement with previous experiments (*11*, *22*) and simulations (*5*). A recent two-dimensional experiment measured the spatial correlation of the total force on a disk, but no long-range correlation was found under isotropic compression (*10*).

With addition of a compressive load at the top of the polydisperse pile, $\langle f\rangle$ increased by 16%, l_f decreased to $\sim 7\langle d\rangle$, and α increased slightly. This trend is consistent with the proposal that the lowest density jammed state (the J point) is a critical point and that moving away from this point should lead to a shortening of a previously unidentified correlation length (*6*) and possibly to an increase of α. In a droplet pile, the J point corresponded to minimal load; the loads produced by the droplets' weight and the Teflon disk moved the sample progressively farther from the J point. We anticipate that the directional correlation defined here will provide useful characterization of many jammed systems.

The chains arise from the tendency of the two largest forces on a droplet to oppose one another. To see how this tendency occurs, we characterized the geometry of the contact-force network. For each droplet, we measured θ, the angle between each pair of contact forces on the droplet [there are $Z(Z-1)/2$ such pairs]. The directions of individual contact forces are random, as are the θ values [the probability of θ per unit solid angle is nearly flat (Fig. 3A)], except for a strong suppression at $\theta < 60°$ owing to the finite droplet size. The monodisperse sample presents the same trend, with an additional peak at $\theta = 60°$ owing to short-range in-plane order. By contrast, the probability distribution of the angle (per unit solid angle) between the two largest forces on each droplet, θ_{lf}, exhibits a peak at 180° (Fig. 3B), demonstrating that the largest forces prefer a straight propagation. We next considered only droplets whose two largest forces exceed f_{cut}. Using the same f_{cut} value as in Fig. 3A ($1.6\langle f\rangle$), we found that the peak of the probability distribution P for θ_{lf} near 180° was more prominent than that for

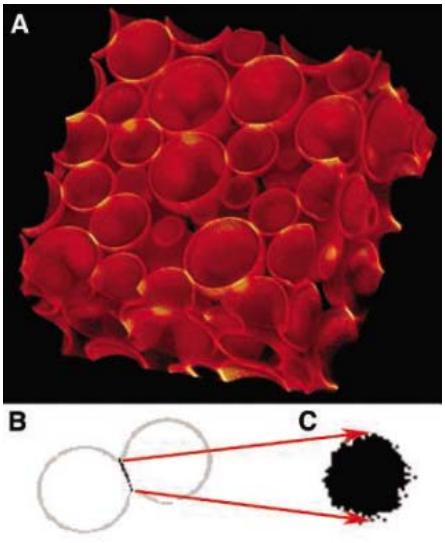

Fig. 1. (**A**) The projection of a 3D image of a small part (80 μm by 80 μm by 30 μm) of a pile shows the fluorescence from the surfaces of the liquid droplets. Droplets of a mixture of perfluorodecalin and α,α,α-trifluorotoluene were formed in refractive-index–matched K-phosphate–aqueous buffer with fluorescent TMR-CPMV particles. Droplets were piled in a 5.7-mm-diameter cylindrical tube to a depth of 6 mm and imaged with a confocal microscope (Zeiss Laser Scan Microscope model 510, 40× objective with a numerical aperture of 1.3). (**B**) A cross section shows the surfaces of two adjacent droplets in the pile. The surfaces were isolated by means of intensity gradients in the 3D image. (**C**) Voxels shared by two adjacent droplets were identified (black); a projection of the contact area defines a circular shape of area A.

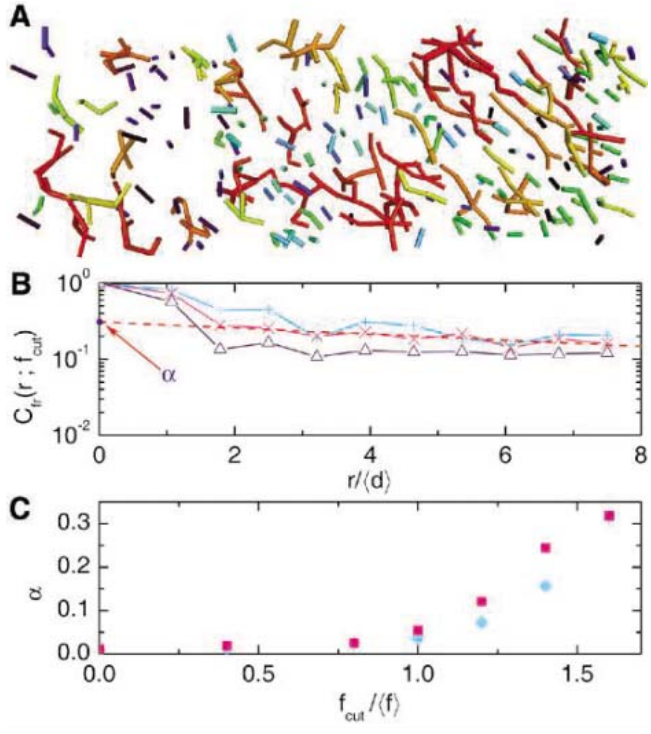

Fig. 2. (**A**) A perspective view of contact forces greater than $1.6\langle f\rangle$ for the polydisperse sample (670 μm by 220 μm in the plane of the image; 110 μm in the direction of gravity, pointing into the plane). Contiguous forces are drawn as cylinders of the same color whose diameters are proportional to the force magnitude f. (**B**) The correlation $C_{\mathbf{f}\cdot\mathbf{r}}(r; f_{cut})$ in the same sample for $f_{cut}/\langle f\rangle$ values of 1.4, 1.6, and 1.8 (Δ, ×, and +, respectively). $C_{\mathbf{f}\cdot\mathbf{r}}(\boldsymbol{r}_{ij})$ is defined as the correlation of $|\boldsymbol{f}_i\cdot\boldsymbol{e}_{ij}|$ with $|\boldsymbol{f}_j\cdot\boldsymbol{e}_{ij}|$, where $\boldsymbol{f}_i$ refers to the force vector of the ith interdrop contract, $\boldsymbol{r}_{ij}$ is the vector connecting the two contacts, and $\boldsymbol{e}_{ij} = \boldsymbol{r}_{ij}/|\boldsymbol{r}_{ij}|$. In the equation $C_y(r) = \langle(y_i - \langle y\rangle)(y_j - \langle y\rangle)\rangle/\sigma_y^2$, $y_i = |\boldsymbol{f}_j\cdot\boldsymbol{e}_{ij}|$, σ_y is the standard deviation of y, and $\langle..\rangle$ defines an average over all force pairs with separation between r and $r + dr$. The dashed line shows an exponential fit to $\alpha\cdot\exp(-r/l_f)$ for $r > 2\langle d\rangle$ and $f_{cut} = 1.6\langle f\rangle$. (**C**) The likelihood of appearing in a chain, α, increases with $f_{cut}/\langle f\rangle$. The polydisperse sample with extra load (squares) tends to have larger values of α than the same sample under its own weight (diamonds).

the entire ensemble of droplets (Fig. 3C), although $P(\theta)$ was unchanged (the same value as that in Fig. 2A). The parallel alignment of the largest forces qualitatively explains the emergence of the long-range chainlike correlations for large values of f_{cut}. By Newton's third law, a force also acts on the adjacent droplet; the largest forces thus tend to propagate along a line (*i.e.*, form chains). From the measured probability that θ_{lf} lies between 120° and 180°, we estimate the distance over which the probability of having nearly parallel, large contact forces drops by 1/*e*. Again, this length is comparable to the measured persistence length of the force chain and decreases with added load.

Further understanding of the statistics of the contact-force network is achieved by postulating that individual droplets are statistically identical and that the contact forces on each droplet are drawn from a common distribution (Fig. 4) (*1*, *23*–*25*). To support the possibility of statistical independence of droplets, we note that the mean force on each droplet, $\langle f \rangle_{drop}$, follows an approximate Gaussian probability distribution (Fig. 4, inset) and $\langle f \rangle_{drop}$ has no long-range spatial correlations. We propose a simple model that accurately incorporates the force-balance constraint with purely repulsive forces and assumes isotropic compression (*26*). The distribution of θ that was determined numerically from our model was consistent with that of the measurement (Fig. 3A). The model also successfully described $P(\theta_{lf})$ measured for large-force droplets (Fig. 3C). From the qualitative agreement of the experimental data and the single-droplet model, we conclude that the angles of the largest-force droplets and hence the chains arise from the force-balance constraint at the scale of individual particles.

Long-range correlations of the force network might be expected to stiffen piles whose dimension is on the order of the chain persistence length. We measured the modulus by immersing Teflon disks of various thicknesses atop droplet piles and finding the compressive strain ε (fig. S1). In a 5-mm-tall pile, the modulus was ~750 Pa [as expected from $\gamma/\langle d \rangle$ (*27*)]. Strain hardening was observed when $\varepsilon > 0.15$. For a short pile, 300 μm or $20\langle d \rangle$ in height, marked strain hardening occurred even with ε as small as 0.08. We attribute this enhanced nonlinear response to the longer force-chain persistence length. This trend is analogous to the reduction of ε for strain hardening in biological gels as the persistence length of the filaments composing the gel is increased (*28*). We thereby establish a connection among the microscopic contact-force network, its mesoscopic-scale correlations, and the elastic response of jammed materials.

Our measurements show chainlike correlations of forces in static 3D granular piles. These correlations arise from the tendency of the two largest forces on a droplet to oppose one another to achieve mechanical stability (zero net force). A simple model that incorporates this force-balance constraint confirms that large forces oppose one another, which leads to formation of chains. As a pile is compressed, l_f decreases and α increases. When tangential forces are present (e.g., from static friction), the tendency of parallel alignment of the two largest forces ($\theta_{lf} \approx 180°$) might be reduced because a large f can be balanced by tangential forces at any θ. Hence, friction should reduce chainlike correlations, which would explain the earlier finding (*17*) that adding friction makes granular solids behave like ordinary elastic media over a broader range of length scales. Finally, our data show a connection between the correlation length and the modulus of piles; when the correlation length approaches the sample size, the nonlinear response is enhanced. We thus show how force-balance in a frictionless system with a discrete number of contacts leads to correlations at the mesoscopic scale and determines the collective stress response.

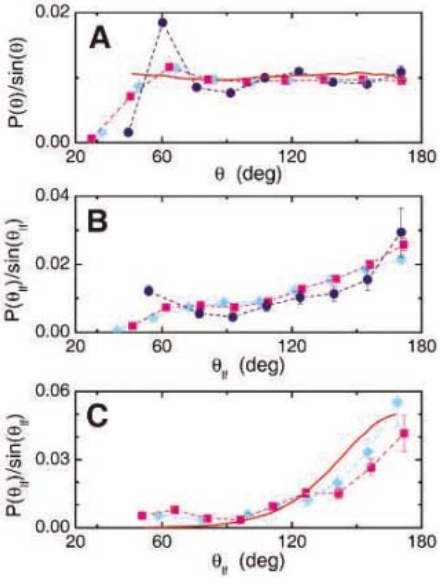

Fig. 3. (**A**) The distribution of angles between all pairs of forces on each droplet per unit solid angle [$P(\theta)/\sin(\theta)$]. The dashed curves show experimental data for the polydisperse sample (diamonds), the polydisperse sample with extra load (squares), and the monodisperse sample (circles). The distribution of θ_{lf} (**B**) for every droplet and (**C**) only for droplets whose two largest forces exceed $1.6\langle f \rangle$. In (A) and (C), similar trends arise from the numerical solution of our model (solid curves). Error bars in (B) and (C) are calculated from the square root of the number of measurements.

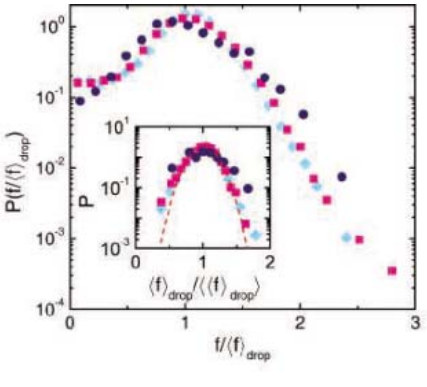

Fig. 4. The measured probability distribution P of the contact forces on each drop normalized by the mean force on the drop, $\langle f \rangle_{drop}$. The symbols are the same as those in Fig. 3. (**Inset**) Distribution of values of $\langle f \rangle_{drop}$, normalized by the sample mean, $\langle\langle f \rangle_{drop}\rangle$. The dashed curve is a Gaussian fit to the polydisperse sample.

References and Notes

1. C. Liu *et al.*, *Science* **269**, 513 (1995).
2. H. M. Jaeger, S. R. Nagel, R. P. Behringer, *Rev. Mod. Phys.* **68**, 1259 (1996).
3. S. Ouaguenouni, J. N. Roux, *Europhys. Lett.* **39**, 117 (1997).
4. C. S. O'Hern, S. A. Langer, A. J. Liu, S. R. Nagel, *Phys. Rev. Lett.* **86**, 111 (2001).
5. L. E. Silbert, G. S. Grest, J. W. Landry, *Phys. Rev. E* **66**, 061303 (2002).
6. C. S. O'Hern, L. E. Silbert, A. J. Liu, S. R. Nagel, *Phys. Rev. E* **68**, 011306 (2003).
7. S. Ostojic, E. Somfai, B. Nienhuis, *Nature* **439**, 828 (2006).
8. A. Drescher, G. de Josselin de Jong, *J. Mech. Phys. Solids* **20**, 337 (1972).
9. J. F. Geng, G. Reydellet, E. Clément, R. P. Behringer, *Physica D* **182**, 274 (2003).
10. T. S. Majmudar, R. P. Behringer, *Nature* **435**, 1079 (2005).
11. D. M. Mueth, H. M. Jaeger, S. R. Nagel, *Phys. Rev. E* **57**, 3164 (1998).
12. H. A. Makse, D. L. Johnson, L. M. Schwartz, *Phys. Rev. Lett.* **84**, 4160 (2000).
13. D. L. Blair, N. W. Mueggenburg, A. H. Marshall, H. M. Jaeger, S. R. Nagel, *Phys. Rev. E* **63**, 041304 (2001).
14. J. M. Erikson, N. W. Mueggenburg, H. M. Jaeger, S. R. Nagel, *Phys. Rev. E* **66**, 040301(R) (2002).
15. C. Goldenberg, I. Goldhirsch, *Phys. Rev. Lett.* **89**, 084302 (2002).
16. C. Goldenberg, I. Goldhirsch, *Granular Matter* **6**, 87 (2004).
17. C. Goldenberg, I. Goldhirsch, *Nature* **435**, 188 (2005).
18. M. van Hecke, *Nature* **435**, 1041 (2005).
19. Y. Lin, H. Skaff, T. S. Emrick, A. D. Dinsmore, T. P. Russell, *Science* **299**, 226 (2003).
20. J. T. Russell *et al.*, *Angew. Chem. Int. Ed. Engl.* **44**, 2420 (2005).
21. H. M. Princen, *J. Colloid Interface Sci.* **91**, 160 (1983).
22. G. Løvoll, K. J. Måløy, E. G. Flekkøy, *Phys. Rev. E* **60**, 5872 (1999).
23. S. N. Coppersmith, C. Liu, S. Majumdar, O. Narayan, T. A. Witten, *Phys. Rev. E* **53**, 4673 (1996).
24. J. Brujić, S. F. Edwards, I. Hopkinson, H. A. Makse, *Physica A* **327**, 201 (2003).
25. J. H. Snoeijer, T. J. H. Vlugt, M. van Hecke, W. van Saarloos, *Phys. Rev. Lett.* **92**, 054302 (2004).
26. Materials and methods are available as supporting material on *Science* Online.
27. T. G. Mason, J. Bibette, D. A. Weitz, *Phys. Rev. Lett.* **75**, 2051 (1995).
28. C. Storm, J. J. Pastore, F. C. MacKintosh, T. C. Lubensky, P. A. Janmey, *Nature* **435**, 191 (2005).

29. We thank N. Menon and R. A. Guyer for valuable comments, H. Skaff and T. Emrick for providing CdSe nanoparticles, and the Central Microscopy Facility of University of Massachusetts Amherst (NSF-Biological, Behavioral, and Social Sciences) for use of the confocal microscope. This work was supported by NSF-Division of Materials Research (J.Z. and A.D.D.) and U.S. Department of Defense–Multidisciplinary University Research Initiative (DOD-MURI) grants (S.L. and Q.W.).

Supporting Online Material

www.sciencemag.org/cgi/content/full/312/5780/1631/DC1
Materials and Methods
Fig. S1

19 January 2006; accepted 3 May 2006
10.1126/science.1125151

Bidirectional Counting of Single Electrons

Toshimasa Fujisawa,[1,2]* Toshiaki Hayashi,[1] Ritsuya Tomita,[1,2] Yoshiro Hirayama[1,3,4]

A bidirectional single-electron counting device is demonstrated. Individual electrons flowing in forward and reverse directions through a double quantum dot are detected with a quantum point contact acting as a charge sensor. A comprehensive statistical analysis in the frequency and time domains and of higher order moments of noise reveals antibunching correlation in single-electron transport through the device itself. The device can also be used to investigate current flow in the attoampere range, which cannot be measured by existing current meters.

Photon counting has been shown to be useful for detecting a faint light and for characterizing nontrivial photon statistics (*1*). Similarly, electron counting is expected to provide a sensitive ammeter and deep insights into correlated transport (*2*, *3*). In contrast to photon counting, in which only incoming photons are considered, electron transport involves the frequent occurrence of backscattering events, which makes bidirectional counting essential for a full understanding of its statistics.

Conventional current noise measurements are successful for characterizing correlated transport (*3*, *4*), such as the sub-Poissonian statistics in single-electron tunneling (*5*) and the fractional quantum Hall effect (*6*, *7*). However, the second-order noise measurements are restricted to strongly nonequilibrium conditions where transport can be considered unidirectional. In addition, these measurements cannot determine correlations of a few electrons, because existing current meters require the movement of millions of electrons. Recently, individual single-electron transport through a quantum dot has been investigated in real time with the use of an integrated charge detector (*8*–*11*), but single-dot charge detection cannot determine the direction of the transport.

We demonstrate a bidirectional single-electron counting (B-SEC) device in which individual electrons tunneling through a double quantum dot (DQD) are detected with a charge sensor made of a quantum point contact (PC). Statistical analysis of forward and reverse tunneling events allows us to determine all parameters that describe the system. We find that two forward tunneling events never occur consecutively; this phenomenon reveals antibunching correlation in the single-electron transport. The third-order noise is insensitive to thermal fluctuations, which allows us to extract the correlation effect even in a nearly equilibrium condition. These statistical methods can also be used to investigate extremely small currents from an external test device.

The operation of our B-SEC device is based on charge detection in a DQD in the Coulomb blockade regime, where higher order tunneling processes can be safely neglected (*12*). The device consists of a DQD (dots L and R) and a PC for charge detection (Fig. 1A). The PC is asymmetrically coupled to the dots (stronger to dot L), so that the current through the PC, I_{PC}, depends differently on the respective electron numbers (n,m) in dots L and R (*13*, *14*). The current through the DQD results in temporal changes in the electron numbers (n,m), which appear as fluctuations in the PC current (Fig. 1B). By observing transitions between (1,0) and (0,1) states, we can regard the current across the central barrier, I_C, as a train of single-electron pulses (Fig. 1C).

A scanning electron micrograph (SEM) of a B-SEC device fabricated in an AlGaAs/GaAs heterostructure is shown in Fig. 1D. The application of appropriate negative voltages on metal gates (gold regions) depletes conductive electrons nearby and forms the integrated device in a desired action (*8*). The PC is adjusted in the tunneling regime, where I_{PC} is sensitive to the charge distribution around the PC. The current, $\langle I_{PC} \rangle \approx 12$ nA on average at an excitation voltage $V_{PC} = 0.8$ mV, changes by a few percent depending on the charge state of the DQD. The charge state (n,m) of the DQD can be controlled by voltages V_L and V_R, respectively, applied to gates G_L and G_R; the average current $\langle I_{PC} \rangle$ shown in Fig. 2A indicates four discrete values depending on (n,m). Clear separation of (0,0) and (1,1) domains indicates an electrostatic coupling energy of ~200 μeV for the DQD (*15*). Similar patterns are observed in a wide range of the V_L-V_R plane, and we select a specific region where all the tunneling rates of the DQD are within the bandwidth (~10 kHz) of the current amplifier used to measure I_{PC}. Then, individual tunneling events can be clearly visible in the time domain, as shown in Fig. 2B. The three-level fluctuation observed at charge triple points E and H (denoting electron-like and hole-like transport, respectively), the two-level fluctuation between (1,0) and (0,1) at M (the middle), and the absence of fluctuation in blockade region B are consistent with expectations.

We record I_{PC} traces over a period $T_p = 1.3$ s with a time resolution of $t_0 = 20$ μs and digitize the current into four values, corresponding to the (n,m) states of interest, with an appropriate filtering and threshold. If required, a group of many (up to 50) traces are used to obtain reliable statistics. All information needed for characterizing the transport can be obtained from the statistics. The residence time $T_{res}^{(n,m)}$, defined as how long the QD stays in a particular charge state (n,m) before changing to another state (as in Fig. 1B), is a stochastic quantity and takes a random value every time (Fig. 2C). The data are taken in the nonlinear conductance regime at a positive bias voltage $V_S = 300$ μV. The exponential distribution is observed for all charge

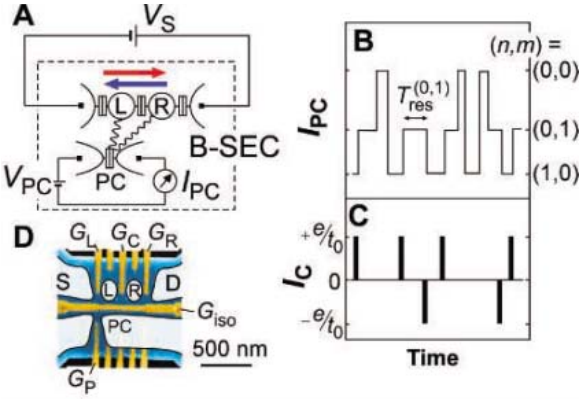

Fig. 1. B-SEC device. (**A**) The B-SEC device consists of a double dot (L and R) and a charge detector (PC). The double boxes represent tunneling barriers; wavy lines illustrate Coulomb interaction and red and blue arrows indicate forward and reverse electron transport, respectively. (**B**) Schematic fluctuation of detector current, I_{PC}, which corresponds to charge state (n,m) with n and m excess electrons, respectively, in dots L and R. (**C**) Pulsed current across the central barrier, I_C. Each current pulse with height e/t_0 and time resolution t_0 of the measurement represent transport of elementary charge e. (**D**) Colored SEM image (blue and black, unetched and etched semiconductor surface, respectively; gold, metal gates; white, conductive regions) of a control device fabricated by standard lithographic techniques. The double dot (L and R) and PC are formed by applying negative voltages to the gates. All measurements were performed at 35 mK at zero magnetic field.

[1]NTT Basic Research Laboratories, NTT Corporation, 3-1 Morinosato-Wakamiya, Atsugi 243-0198, Japan. [2]Tokyo Institute of Technology, 2-12-1 Ookayama, Meguro-ku, Tokyo 152-8551, Japan. [3]Solution Oriented Research for Science and Technology (SORST), Japan Science and Technology Agency, 4-1-8 Honmachi, Kawaguchi 331-0012, Japan. [4]Department of Physics, Tohoku University, Sendai, Miyagi 980-8578, Japan.

*To whom correspondence should be addressed. E-mail: fujisawa@nttbrl.jp

states, indicating a random Poisson process characterized by a single lifetime $\tau_{nm} = \langle T_{res}^{(n,m)} \rangle$ (*8*, *16*), which is related to the sum of all possible tunneling rates $\Gamma_{nm \to ij}$ from (n,m) to (i,j)—that is, $\tau_{nm}^{-1} = \sum_{i,j} \Gamma_{nm \to ij}$. One can also count the number of transition events $N_{nm \to ij}$ from (n,m) to (i,j), which should be proportional to the rates by the relation $N_{nm \to ij} = p_{nm}^0 \Gamma_{nm \to ij} T_p$, where p_{nm}^0 is the occupation probability for (n,m) in a steady condition. By solving these relations, all relevant rates $\Gamma_{nm \to ij}$ and populations p_{nm}^0 can be determined.

Figure 2D shows $N_{nm \to ij}$ obtained from the same data set. The transport is dominated by a cyclic transition (shown by red arrows) from (1,1) through (1,0) to (0,1) and back to (1,1), which carries an electron from the left to the right. Note that non-negligible reverse processes (blue arrows) are also revealed in the present measurements. The very small counting rate [< 30 cps for the transitions involving the (0,0) state] is attributed to noise in the PC current (dark counting) and should thus be disregarded; transitions between (0,0) and (1,1) are unphysical in the sequential tunneling regime. Because of the finite bandwidth, our measurement fails to count very fast successive transitions within 100 μs. These effects are all minor and do not affect our analysis. The obtained rates $\Gamma_{nm \to ij}$ are summarized in Fig. 2E.

We performed similar analyses at various points in the V_L-V_R plane and investigated how the forward and reverse tunneling rates change. We first examined dot-lead tunneling across the left barrier by comparing $\Gamma_{01 \to 11}$ and $\Gamma_{11 \to 01}$. These are plotted in Fig. 2F as a function of the electrochemical potential, $\mu = E_{01} - E_{11}$, where E_{nm} is the total energy of the (n,m) state (*15*). The dependence can be well fitted with solid lines by considering the Fermi distribution in the electrode with an electron temperature of T_e = 130 mK in the lead (*17*). The behaviors of the forward and reverse rates are almost symmetric with respect to $E_{10} = E_{11}$ (dashed line). The small difference (factor of ~1.5) between the maximum saturated rates for the forward and reverse tunneling may be related to spin degeneracy; a factor of 2 difference is expected for transitions between different charge states having total spins of 0 and ½ (*18*). The dot-lead tunneling shows detailed balancing in which the ratio of forward and reverse rates is determined by the electrochemical potential, $\Gamma_{01 \to 11}/\Gamma_{11 \to 01} = \exp[\mu/(kT_e)]$ (where k is the Boltzmann constant), up to degeneracy. In contrast, the interdot tunneling rates $\Gamma_{01 \to 10}$ and $\Gamma_{10 \to 01}$ measure how frequently the system absorbs or emits energy from or to the environment (*19*). As shown in Fig. 2G, the rates deviate from the symmetric dependence in the whole range across some peaks (indicated by arrows) associated with alignments of discrete energy levels in the dots. Violation of detailed balancing implies strong nonequilibrium excitation under back action from the PC detector (*20*).

Although each tunneling process characterized by $\Gamma_{nm \to ij}$ is Poisson random, Coulomb interaction prohibits double occupancy in a small island and correlates the overall electron transport. Charge transport in the sequential tunneling regime can be described by the rate equation $(d/dt)\mathbf{p}(t) = \mathbf{M}\mathbf{p}(t)$, where $\mathbf{p}(t)$ is an array of time-dependent occupation probabilities $\{p_{nm}(t)\}$ (*21*). The matrix $\mathbf{M}$ describes the transition rates consisting of diagonal and off-diagonal terms $-\tau_{nm}^{-1}$ and $\Gamma_{nm \to ij}$, respectively. Because we have already obtained $\mathbf{M}$ as in Fig. 2E, we can calculate the expected average current, noise spectrum (*21*), and higher order moments of noise (*22*), which are more suitable for describing the correlated transport. These statistics can be obtained by analyzing the pulsed current (conserved quantity), which is more versatile even when complete information, such as $\mathbf{M}$, is not available.

We next define three pulsed currents, I_L, I_C, and I_R, which exhibit B-SEC at the left, central, and right barriers, respectively. They are obtained by considering the corresponding tunneling processes as discussed for I_C in Fig. 1C. The average currents obtained for a long period, T_p = 1.3 s, always coincide with each other (i.e., $\langle I_L \rangle = \langle I_C \rangle = \langle I_R \rangle$) as a result of current conservation. The average current $\langle I \rangle$ in the V_L-V_R plane is shown in Fig. 3A. The triangular conductive regions around E and H with a resonant tunneling peak on one side of the triangles are consistent with the energetics for transport through a DQD (*15*).

Noise power spectra S_L, S_C, and S_R (Fig. 3B, top) are obtained from numerical Fourier transforms of the corresponding pulsed currents. The spectra are qualitatively the same as those calculated from $\mathbf{M}$ (Fig. 3B, bottom) (*21*), indicating the validity of our statistical analysis. The enhanced spectrum in the high-frequency part (>1 kHz, the characteristic frequency set by $\mathbf{M}$) is related to how frequently an electron experiences backscattering across the barrier. The low-frequency part, identical for the three spectra, is almost flat except for excess dark-counting noise below 10 Hz. Background charge fluctuation (1/*f* noise), which often dominates low-frequency noise, is suppressed by the digitizing

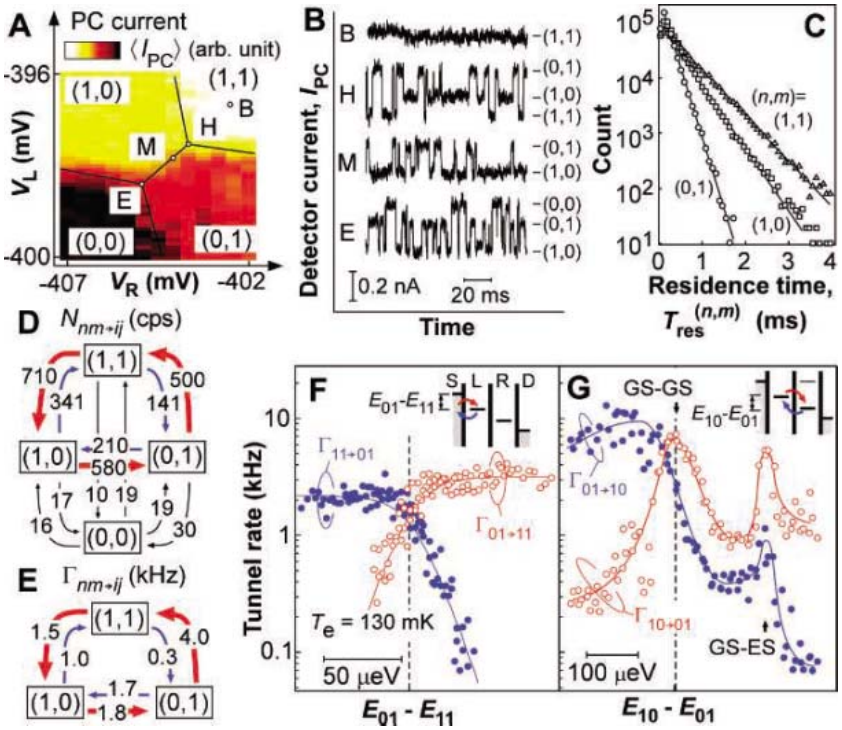

Fig. 2. Statistics of charge fluctuation in a DQD. (**A**) Color plot of the averaged PC current, $\langle I_{PC} \rangle$, in the V_L-V_R plane measured at V_S = 0 and V_{PC} = 0.8 mV, with a stability diagram (n,m) of the DQD. An appropriate linear function of V_L and V_R is subtracted from the raw data to remove electrostatic coupling from the gates. (**B**) Fluctuation of I_{PC} measured at some points shown in (A). Typically, $\langle I_{PC} \rangle \approx 12$ nA. (**C**) Distribution of the residence time T_{res} for (0,1), (1,0), and (1,1) states. (**D**) An example of the number of transition events $N_{nm \to ij}$. (**E**) An example of tunneling rates $\Gamma_{nm \to ij}$. The same data set measured at V_S = 300 μV around point α in Fig. 3A is used for (C), (D), and (E). (**F** and **G**) Forward and reverse rates across left (F) and central (G) barriers. Insets show energy diagrams of the DQD with corresponding tunnel processes. Obtained rates at V_S = 300 μV and various V_L and V_R points are plotted as a function of chemical potential, $E_{01} - E_{11}$ in (F) and $E_{10} - E_{01}$ in (G). Solid lines in (F) are fitted with T_e = 130 mK; solid lines in (G) are guides for the eye. Arrows in (G) represent resonances of the ground state (GS) of one dot to the ground and excited states (ES) of the other dot.

process. The noise level in the 10 to 100 Hz range is suppressed below full shot noise $2e\langle I\rangle$ (dashed line), indicating correlated transport (*5*). In fact, we find that B-SEC provides better statistics that identify the antibunching correlation directly. The distribution of the time interval, t_{++}, between two successive forward current pulses (Fig. 3C) is no longer a simple exponential, and suppression of consecutive forward pulses at $t_{++} \approx 0$ (antibunching) is directly identified, consistent with a rate-equation calculation (solid curve). Note that the broad peak in the distribution indicates quasi-periodic current as a precursor of single-electron tunneling oscillations (*10*).

We can extract other statistics often used in quantum optics, such as electron (photon) number distribution (*1*, *2*, *23*). The third-order moment of the distribution, which is called skewness, is of particular interest for its insensitivity to thermal distribution (*24*–*26*) and is considered to be a new tool for investigating correlated transport, valid even for near-equilibrium conditions. Gustavsson *et al.* used charge detection measurement on a single quantum dot to identify correlated transport from its second- and third-order noise (*11*). Taking advantage of bidirectional counting in our device, we have shown that the third-order noise is insensitive to the thermal noise (supporting online text).

The reverse problem of identifying unknown correlation would be useful in many cases. The top part of Fig. 4A illustrates a circuit for counting electrons from a test device. Although it is impossible to obtain all information about the test device, one can obtain useful information by means of time, frequency, and momentum analyses with a B-SEC device. For this purpose, the impedance of the B-SEC device should be smaller and its correlation time shorter than that of the test device (*27*). Our B-SEC device can be applied to investigate extremely small current from a high-impedance test device, and this is precisely what conventional electronics cannot cover. In Fig. 4A we show how our device performs as a current meter, using another single quantum dot as a test device. The average current $\langle I\rangle$ obtained from the B-SEC device reasonably depends on two gate voltages, V_A and V_B, of the test device (Fig. 4B), indicating that the observed Coulomb blockade peaks are associated with the test device. The peak-to-peak noise level in the blockade region is 3 aA for an averaging time of 1.3 s, which is about three orders of magnitude smaller than that in conventional current meters.

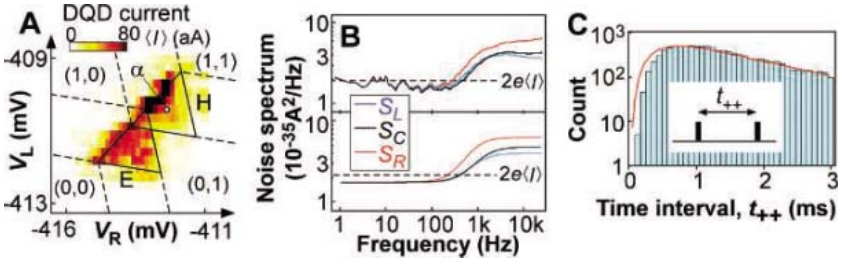

Fig. 3. Statistics of current at the left, central, and right barriers. (**A**) Average current $\langle I\rangle$ in the V_L-V_R plane at V_S = 300 μV. Triangles E and H define conductive regions. (**B**) Noise power spectra, S_L, S_C, and S_R, of the corresponding currents. The upper panel shows the power spectrum of the pulsed current; the lower panel shows the spectrum of the correlation function derived by solving rate equations. The dashed line denotes full shot noise $2e\langle I\rangle$. (**C**) Distribution of the time interval between successive forward tunneling events in I_C. The solid curve shows calculated occurrence of the conditional event derived from the corresponding rate equations. The inset illustrates the time interval, t_{++}. The data set used for (B) and (C), as well as for Fig. 2, C to E, was taken in the nonlinear conductance regime [point α in (A)].

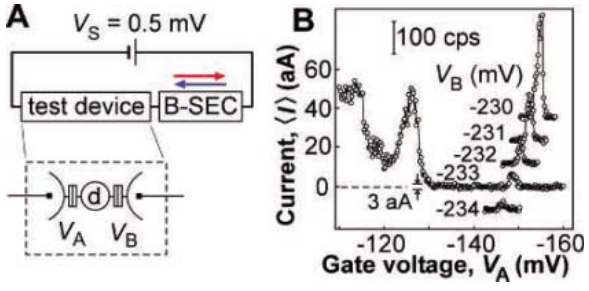

Fig. 4. Single-electron counting for an external test device. (**A**) Measurement diagram with a QD (d) test device fabricated with the same technique as the B-SEC device. Tunneling rates of the two barriers on both sides of the QD can be controlled with voltages V_A and V_B. The net electron flow rate (current) is obtained by subtracting the reverse counting rate (blue arrow) from the forward rate (red arrow). (**B**) Average current obtained from the B-SEC device. Current ranging from −10 to 50 aA can be measured with a voltage drop of ~200 μV across the present B-SEC device. The observed Coulomb blockade peak changes with V_B. Each trace is offset for clarity.

The demonstrated B-SEC device enables the use of various statistical analyses to characterize the correlation, and it is also useful for investigating extremely small currents. Integration with other mesoscopic electron devices, such as beam splitters or interferometers, would lead to various techniques for exploring nontrivial intensity correlation and entanglement in mesoscopic electron systems (*28*).

References and Notes

1. R. Loudon, *The Quantum Theory of Light* (Oxford, New York, 1973).
2. L. S. Levitov, H. Lee, G. B. Lesovik, *J. Math. Phys.* **37**, 4845 (1996).
3. Yu. V. Nazarov, Ed., *Quantum Noise in Mesoscopic Physics*, Vol. 97 of *NATO Science Series II* (Kluwer, Dordrecht, Netherlands, 2003).
4. Ya. M. Blanter, M. Büttiker, *Phys. Rep.* **336**, 1 (2000).
5. H. Birk, M. J. M. de Jong, C. Schönenberger, *Phys. Rev. Lett.* **75**, 1610 (1995).
6. L. Saminadayar, D. C. Glattli, Y. Jin, B. Etienne, *Phys. Rev. Lett.* **79**, 2526 (1997).
7. R. de Picciotto *et al.*, *Nature* **389**, 162 (1997).
8. T. Fujisawa, T. Hayashi, Y. Hirayama, H. D. Cheong, Y. H. Jeong, *Appl. Phys. Lett.* **84**, 2343 (2004).
9. W. Lu, Z. Ji, L. Pfeiffer, K. W. West, A. J. Rimberg, *Nature* **423**, 422 (2003).
10. J. Bylander, T. Duty, P. Delsing, *Nature* **434**, 361 (2005).
11. S. Gustavsson *et al.*, *Phys. Rev. Lett.* **96**, 076605 (2006).
12. H. Grabert, M. H. Devoret, Eds., *Single Charge Tunneling: Coulomb Blockade Phenomena in Nanostuctures* (Plenum, New York, 1991), chap. 3.
13. M. Field *et al.*, *Phys. Rev. Lett.* **70**, 1311 (1993).
14. J. R. Petta *et al.*, *Science* **309**, 2180 (2005); published online 1 September 2005 (10.1126/science.1116955).
15. W. G. van der Wiel *et al.*, *Rev. Mod. Phys.* **75**, 1 (2003).
16. N. G. van Kampen, *Stochastic Processes in Physics and Chemistry* (Elsevier, Amsterdam, 1992).
17. D. H. Cobden, B. A. Muzykantskiĭ, *Phys. Rev. Lett.* **75**, 4274 (1995).
18. D. H. Cobden, M. Bockrath, P. L. McEuen, A. G. Rinzler, R. E. Smalley, *Phys. Rev. Lett.* **81**, 681 (1998).
19. T. Fujisawa *et al.*, *Science* **282**, 932 (1998).
20. R. Aguado, L. P. Kouwenhoven, *Phys. Rev. Lett.* **84**, 1986 (2000).
21. S. Hershfield, J. H. Davies, P. Hyldgaard, C. J. Stanton, J. W. Wilkins, *Phys. Rev. B* **47**, 1967 (1993).
22. D. A. Bagrets, Yu. V. Nazarov, *Phys. Rev. B* **67**, 085316 (2003).
23. M. Ueda, *Phys. Rev. A* **40**, 1096 (1989).
24. L. S. Levitov, M. Reznikov, *Phys. Rev. B* **70**, 115305 (2004).
25. B. Reulet, J. Senzier, D. E. Prober, *Phys. Rev. Lett.* **91**, 196601 (2003).
26. Yu. Bomze, G. Gershon, D. Shovkun, L. S. Levitov, M. Reznikov, *Phys. Rev. Lett.* **95**, 176601 (2005).
27. C. W. J. Beenakker, M. Kindermann, Yu. V. Nazarov, *Phys. Rev. Lett.* **90**, 176802 (2003).
28. P. Samuelsson, E. V. Sukhorukov, M. Büttiker, *Phys. Rev. Lett.* **92**, 026805 (2004).

29. We thank L. S. Levitov, K. Muraki, Yu. V. Nazarov, Y. Tokura, M. Ueda, and Y. Yamamoto for valuable comments. Supported by the Strategic Information and Communications R&D Promotion Program (SCOPE) from the Ministry of Internal Affairs and Communications of Japan, and by a grant-in-aid for scientific research from the Japan Society for the Promotion of Science.

Supporting Online Material

www.sciencemag.org/cgi/content/full/312/5780/1634/DC1
SOM Text
Figs. S1 and S2
References

28 February 2006; accepted 27 April 2006
10.1126/science.1126788

The Role of πσ* Excited States in the Photodissociation of Heteroaromatic Molecules

M. N. R. Ashfold,* B. Cronin, A. L. Devine, R. N. Dixon, M. G. D. Nix

High-resolution measurements of the kinetic energies of hydrogen atom fragments formed during ultraviolet photolysis of imidazole, pyrrole, and phenol in the gas phase confirm that N(O)–H bond fission is an important nonradiative decay process from their respective $^1\pi\sigma^*$ excited states. The measurements also reveal that the respective cofragments (imidazolyl, pyrrolyl, and phenoxyl) are formed in very limited subsets of their available vibrational states. Identification of these product states yields uniquely detailed insights into the vibronic couplings involved in the photoinduced evolution from parent molecule to ultimate fragments.

Imidazole, pyrrole, and phenol are key components of the long-wavelength chromophores in nucleobases and aromatic amino acids, such as histidine, tryptophan, and tyrosine, which dominate the ultraviolet (UV) absorption spectra of many biological molecules. $\pi^* \leftarrow \pi$ transitions are responsible for this strong UV absorption, but these heteroaromatics also have excited states formed via $\sigma^* \leftarrow \pi$ electron promotions. Absorption to the $^1\pi\sigma^*$ states is much weaker, but these states can nonetheless be populated by direct photoexcitation (in imidazole and pyrrole) or by radiationless transfer from the $^1\pi\pi^*$ state (in phenol). Sobolewski *et al.* (*1*) suggested that N(O)–H bond fission should be an important contributor to the nonradiative decay of such heteroaromatics in their $^1\pi\sigma^*$ states.

The experiments described here validate such predictions for all three of our target molecules and show the resulting imidazolyl, pyrrolyl, and phenoxyl cofragments to be formed in remarkably limited subsets of their available vibrational state density. Such mode-specific product formation after photoexcitation of medium-sized organic molecules would, until recently, have been considered very unusual. Traditionally, such fragmentations would be assumed to proceed via nonradiative transfer [internal conversion (IC)] to high vibrational levels of the ground (S_0) state, and by subsequent dissociation after randomization of the internal energy among the various vibrational degrees of freedom. The product branching ratios were expected to be dictated by statistical considerations, favoring slow (low energy) H atoms (with internally excited radical cofragments) and alternative molecular elimination products. However, recent studies are causing a paradigm shift in our understanding of organic molecular photochemistry. Vibrational mode-specific dynamics is now recognized as one signature of ultrafast radiationless transfer enabled by conical intersections (CIs) between potential energy surfaces (PESs). As we show, identifying the active product vibrations can provide uniquely detailed insights into the specific parent modes that promote the photoexcitation and/or the subsequent radiationless couplings, and thus the fragmentation process.

Figure 1 shows sections through multidimensional, diabatic PESs for the ground and first excited $^1\pi\sigma^*$ and $^1\pi\pi^*$ states of bare pyrrole and phenol molecules, plotted, respectively, against the N–H and O–H internuclear distances R_{N-H} and R_{O-H} (*1*). Their respective S_0 potentials correlate with an excited electronic state of the radical. The $^1\pi\pi^*$ states are bound with respect to $R_{N(O)-H}$, but the $^1\pi\sigma^*$ states are repulsive; their energetic ordering in pyrrole [or imidazole (*2*)] is reversed in phenol (*1*). The diabatic $^1\pi\sigma^*$ potential correlates with ground state products and thus exhibits a CI with the S_0 PES at planar geometries and extended $R_{N(O)-H}$ (Fig. 1). Direct excitation to the $^1\pi\sigma^*$ state, or radiationless transfer to it after excitation to a $^1\pi\pi^*$ state, may thus constitute efficient photoinduced decay routes for these heteroaromatics. Indeed, it has been speculated (*1*) that such processes may have conferred biological advantage by minimizing the population of long-lived excited states that could participate in alternative, and potentially more dangerous, photoreactions in living cells.

High-resolution time-of-flight (TOF) spectra of H atoms formed by photolysis of the title molecules, at various UV wavelengths (λ_{phot}), have been obtained by H (Rydberg) photofragment translational spectroscopy (PTS) methods (*3*–*5*). Total kinetic energy release (TKER) spectra are derived by rebinning measured TOF spectra using the relationship (*6*)

$$\mathrm{TKER} = \frac{1}{2} m_H \left(1 + \frac{m_H}{m_R}\right)\left(\frac{d}{t}\right)^2 \qquad (1)$$

Energy and momentum conservation arguments then enable the determination of the population distribution among the internal states of the cofragment at each λ_{phot}.

Figure 2A shows the H atom TOF spectrum measured after 234-nm photoexcitation of imidazole, with the polarization vector (ε_{phot}) aligned at $\theta = 90°$ to the TOF axis. The $\theta = 0°$ spectrum has a similar profile but is much weaker, showing that photolysis involves a perpendicular excitation ($^1A'' \leftarrow {}^1A'$, C_s point group) and subsequent prompt dissociation (*7*, *8*). The associated TKER spectrum (Fig. 2B) displays a short progression of peaks, indicating that the imidazolyl cofragment is formed in just a few vibrational (v) states. The peak intensities reflect the branching probabilities into the active H + imidazolyl (v) product channels, and their narrowness indicates that the products carry little rotational excitation. The active product vibrations are assigned by reference to the (calculated) frequencies of the fundamental vibrations of the ground state imidazolyl radical (*9*). Most imidazolyl products are formed in levels with 0, 1, or 2 quanta in ν_6, the C–C stretching vibration. Comparing the calculated minimum energy structures for the ground states of imidazole and imidazolyl provides a rationale for such state-specific product formation. H atom loss from N1 (*10*) triggers a rearrangement of the electron density involved in ring bonding, an elongation of C4–C5 and N1–C2, and a concurrent reduction of the N1–C5 and N3–C4 bond lengths. The C4–C5 bond length changes the most (>7%) and is the principal nuclear motion associated with product mode ν_6. Franck-Condon considerations thus account for its dominance in the measured spectra.

TKER spectral analysis confirms that the cofragments are ground state imidazolyl radicals and that most of the photon energy (E_{phot}) above that required to break the N−H bond is released as product translation. This and the observed recoil anisotropy indicate that dissociation involves prompt N–H bond fission on a $^1\pi\sigma^*$ PES with topology similar to that illustrated in Fig. 1A. Analysis also provides a direct determination of the N−H bond strength, D_0(imidazolyl–H), via the relation

$$E_{phot} + E_{int}(\text{imidazole}) = D_0(\text{imidazolyl–H}) + \mathrm{TKER}_{v=0} \qquad (2)$$

E_{int}(imidazole), the average internal energy of the jet-cooled precursor, is negligible, and $\mathrm{TKER}_{v=0}$ is the kinetic energy (KE) of the H + imidazolyl (v = 0) fragment peak. Plotting $\mathrm{TKER}_{v=0}$ versus E_{phot} (Fig. 2C) yields a straight line of unit slope; extrapolating to $\mathrm{TKER}_{v=0} = 0$ yields D_0(imidazolyl–H) = 33240 ± 40 cm^{-1}, in good accord with the value derived from photoelectron studies of the imidazolide anion (*11*).

In pyrrole, the $^1\pi\sigma^*(S_1)$ state also lies below the $^1\pi\pi^*(S_2)$ state. Pyrrole has higher (C_{2v}) symmetry, and its $S_1(^1A_2) \leftarrow S_0(X^1A_1)$ excitation is electric dipole forbidden. Weak $S_1 \leftarrow S_0$ absorption is observed, however, because the

School of Chemistry, University of Bristol, Bristol, BS8 1TS UK.

*To whom correspondence should be addressed. E-mail: mike.ashfold@bris.ac.uk

$^1\pi\sigma^*$ state can be populated by a vibronically induced transition (*12*, *13*). H atom TOF spectra measured after excitation to the pyrrole (S_1) state show structure that is attributable to population of selected vibrational levels of the ground state pyrrolyl radical (*5*). The $TKER_{v=0}$ peak is discernable in all spectra, enabling determination of D_0(pyrrolyl–H) = 32850 ± 40 cm^{-1}. Replacing one CH moiety in the five-membered ring (pyrrole) by N (imidazole) thus has little effect on the N–H bond strength. All other peaks in the TKER spectra are attributable to pyrrolyl fragments with one or more quanta of vibration in nonsymmetric skeletal modes. Different H + pyrrolyl (v) product channels display different recoil anisotropies, and their relative showings vary with λ_{phot}, but the overall distribution remains centered at TKER ~ 7000 cm^{-1} (*5*).

These observations indicate a remarkable degree of vibrational adiabaticity in the dissociation of pyrrole (S_1) molecules. Recall that the $S_1 \leftarrow S_0$ transition acquires intensity through vibronic interaction. The photoexcited S_1 level(s) will thus involve one or more quanta of the mode(s) promoting the vibronic transition, with the requirement that the overall combination mode be nonsymmetric. Each such level will constitute a lifetime-broadened vibronic resonance within the overall $S_1 \leftarrow S_0$ absorption, and thus be populated with a λ_{phot}-dependent efficiency. The identities of the product states formed at any given λ_{phot}, and their state-specific recoil anisotropies can be rationalized by assuming that the skeletal mode(s) that promote the $S_1 \leftarrow S_0$ absorption are largely conserved during the pyrrole (S_1) → product evolution and thus acting simply as spectators to the N–H bond fission. The mean TKER of products arising via such vibrationally adiabatic dissociations should be ~δE, the decrease in potential energy on passing from the barrier region to the dissociation asymptote (Fig. 1A). δE can be estimated from the difference between the energetic threshold for parent absorption and D_0(pyrrolyl–H); the value so derived (~7000 cm^{-1}) matches the mean of the fast H atom distribution in all measured TKER spectra (*5*, *14*–*16*). H + pyrrolyl products recoiling with TKER > δE (of which the v = 0 products are the most extreme example) arise from vibrational to translational energy transfer in the exit channel, e.g. from modes involving N–H motion which disappear as R_{N-H} increases.

In contrast to imidazole and pyrrole, the S_1 state of phenol is a bound $^1\pi\pi^*$ state. The $S_1 \leftarrow S_0$ origin band shows resolvable rovibronic structure, analysis of which has established the $^1A' \leftarrow X^1A'$ transition symmetry, the wavelength of the band origin (275.11 nm) (*17*), and the excited state lifetime (≤2 ns) (*18*). Time-resolved pump-probe studies confirm IC to the S_0 state as the dominant nonradiative decay pathway for phenol (S_1, v = 0) molecules (*19*). Replacing the OH hydrogen by deuterium causes a ~100-fold reduction in the nonradiative decay rate, implying a dominant role for O−H vibrations as acceptor modes in the IC process (*20*).

The higher lying $S_2(^1\pi\sigma^*)$ state has $^1A''$ symmetry, a much smaller transition moment from the S_0 state (*21*), and is dissociative with respect to extending R_{O-H}. Its PES thus exhibits CIs with both the S_1 and S_0 states (Fig. 1B) (*1*, *22*, *23*). Given the weakness of the $S_2 \leftarrow S_0$ transition, we assume that the S_2 state is populated by radiationless transfer from the optically prepared $S_1(^1\pi\pi^*)$ state or, at higher energies, from another $^1\pi\pi^*$ state that dominates the absorption at $\lambda < 220$ nm (*24*). Other experimental evidence for O−H bond fission after UV excitation of phenol comes from a

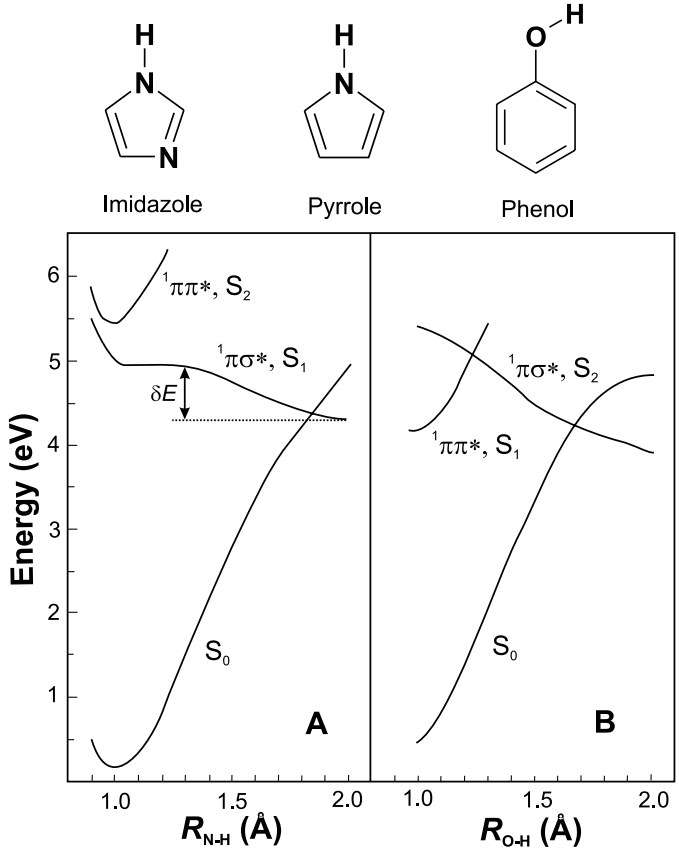

Fig. 1. Structural formulas of imidazole, pyrrole, and phenol, together with schematic PE profiles for the ground and first excited $^1\pi\pi^*$ and $^1\pi\sigma^*$ states of (**A**) pyrrole and (**B**) phenol, plotted against the N−H and O−H stretch coordinates, R_{N-H} and R_{O-H}, respectively [adapted from (*1*)].

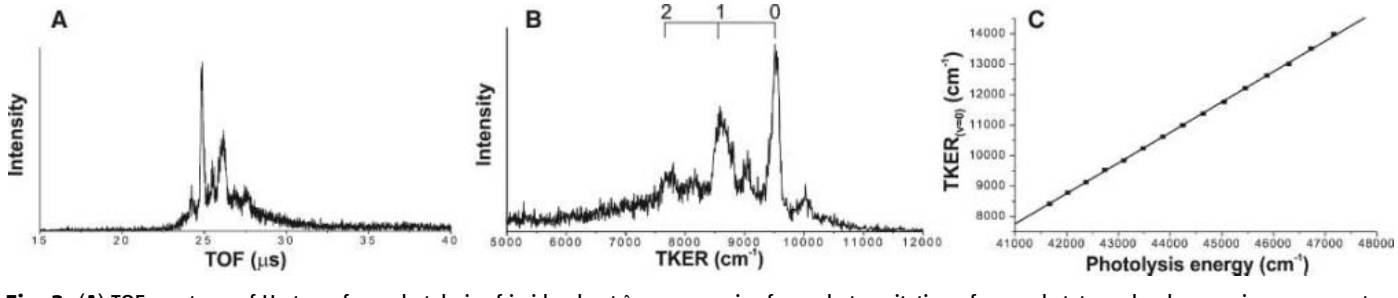

Fig. 2. (**A**) TOF spectrum of H atoms from photolysis of imidazole at λ_{phot} = 234 nm. (**B**) TKER spectrum obtained from the data in (A) using Eq. 1 and m_R = 67.07 dalton. Peaks due to population of the v = 0 and ν_6 = 1 and 2 states of imidazolyl are labeled; the weak satellites appearing at higher TKER arise from photoexcitation of ground state molecules carrying one quantum of N–H out-of-plane bending vibration, ν_{21}. (**C**) Plot showing variation of $TKER_{v=0}$ with photon energy (both in cm^{-1}). The intercept gives D_0(imidazolyl–H) = 33240 ± 40 cm^{-1}.

PTS study of the H + C_6H_5O products formed after excitation at 248 nm (*25*) and from photofragmentation studies of phenol-$(H_2O)_n$ and phenol-$(NH_3)_n$ complexes, where n is an integer, which indicate H atom transfer from the phenolic OH group to the adduct in the excited state complex (*26*, *27*).

The KE resolution afforded by H (Rydberg) atom PTS enables far greater insights into the role of the $^1\pi\sigma^*$ state and the detailed fragmentation dynamics. The TKER spectrum shown in Fig. 3A, obtained at λ_{phot} = 275.11 nm (the $S_1 \leftarrow S_0$ origin), shows resolved peaks on an underlying background. This fast component persists in spectra taken at shorter λ_{phot}, but the structure within it gradually merges into an unresolved shoulder on a larger, slower component (Fig. 3B) (λ_{phot} = 244 nm). These spectra are insensitive to the relative alignment of ε_{phot} and the detection axis. Another faster, structured component appears once $\lambda_{phot} \leq$ 240 nm (Fig. 3C) (λ_{phot} = 228 nm). Polarization-dependent studies show that the formation of these fast H atoms involves a perpendicular parent excitation and subsequent prompt dissociation.

Comparing the observed peak separations with fundamental vibrational frequencies of the ground state phenoxyl radical (*9*) leads to the following internally consistent sets of mode assignments. No peak attributable to H + phenoxyl (v = 0) fragments is observed at any λ_{phot}. All peaks evident in the TKER spectra recorded at wavelengths near the $S_1 \leftarrow S_0$ origin are attributable to phenoxyl modes with a″ vibrational symmetry; the structure in Fig. 3A involves progressions in the out-of-plane vibration $\nu_{16a}(a'')$, built on either zero or one quantum of $\nu_{18b}(a')$, such that the combination mode has a″ vibrational symmetry (*28*). The analysis implies that D_0(phenoxyl–H) = 30015 ± 40 cm^{-1}. The fast peaks observed in the $\lambda_{phot} \leq$ 240 nm TKER spectra are attributable to a progression in the in-plane C–C–O bending mode $[\nu_{18b}(a')]$ but, to satisfy the D_0(phenoxyl–H) value, this progression must be built on one quantum of $\nu_{16b}(a'')$, the out-of-plane ring-puckering mode.

We explain these findings using the schematic PE curves shown in Fig. 4. The S_0 and S_1 states both have A′ electronic symmetry but, in the (C_{2v}) limit when the O–H bond lies along the C_2 axis, the electronic transition moment of the ring-centered $\pi^* \leftarrow \pi$ transition is B_2 (i.e., perpendicular to the O–H bond). The $S_2(^1\pi\sigma^*)$ state has A″ symmetry (B_1 in C_{2v}). Given the calculated oscillator strengths (*21*), we assume that photoexcitation is to the $S_1(^1\pi\pi^*)$ state and that the appearance of the fast structure in TKER spectra recorded at $\lambda_{phot} \leq$ 240 nm indicates the onset of a nonradiative pathway between the S_1 and S_2 ($^1\pi\sigma^*$) states (pathway A in Fig. 4). Such coupling must be vibronically induced, because the S_1 and S_2 states have different electronic symmetries, and must be efficient, given the observed (perpendicular) recoil anisotropy of the H atom photofragments. The deduction that the phenoxyl cofragments carry one quantum of $\nu_{16b}(a'')$ suggests that the corresponding parent mode provides the dominant coupling at the CI between the S_1 and S_2 PESs. Such a conclusion should enable extension of recent time-dependent wave packet analyses of O–H bond fission in phenol (*23*), which invoked the CCOH dihedral angle as the S_1/S_2 coupling coordinate. Earlier calculations revealed an antibonding interaction in the σ* orbital, between the hydroxyl H atom and the nearest C–H bond at short R_{O-H}, which has the effect of repelling the C–O bond away from what would be the C_2 axis in the phenoxyl group (*22*). Thus we conclude that $\nu_{16b}(a'')$ provides the dominant S_1/S_2 coupling and that, upon sampling the S_2 PES, the C–C–O bond angle starts to deviate from 120° concurrent with the extension of R_{O-H}. However, the minimum energy geometry of phenoxyl is C_{2v}, so the configuration point describing the dissociating molecule should execute a slalom-like trajectory, in which the available energy is partitioned between product translation and C–C–O in-plane bending motion.

O–H bond fission also occurs at longer λ_{phot}, even for phenol (S_1, v = 0) molecules. Such excitation energies fall below the S_1/S_2 CI. Dissociation thus requires two successive radiationless transitions: an initial, rate limiting, S_1 to S_0 IC (*19*) followed by S_0/S_2 coupling. The structured part of the TKER spectrum in Fig. 3A can be understood in terms of IC to that subset of the S_0 vibrational state density that has sufficient energy in the O–H stretching coordinate (*20*) to sample the S_0/S_2 CI [presumably with $\nu_{16a}(a'')$ as the parent coupling mode] during its first excursion to large R_{O-H}, and thereby dissociate (scheme B in Fig. 4). Such a mechanism accounts for the isotropic product recoil velocity distributions, and the unusually selective product state distributions. Conversely, phenol (S_1) molecules that convert to S_0 levels with more vibrational energy in modes other than the O–H stretch have insufficient energy to access the S_0/S_2 CI on the first R_{O-H} extension and thus return to explore more of the S_0 PES before dissociation. Much of the unresolved background signal in Fig. 3A may be attributable

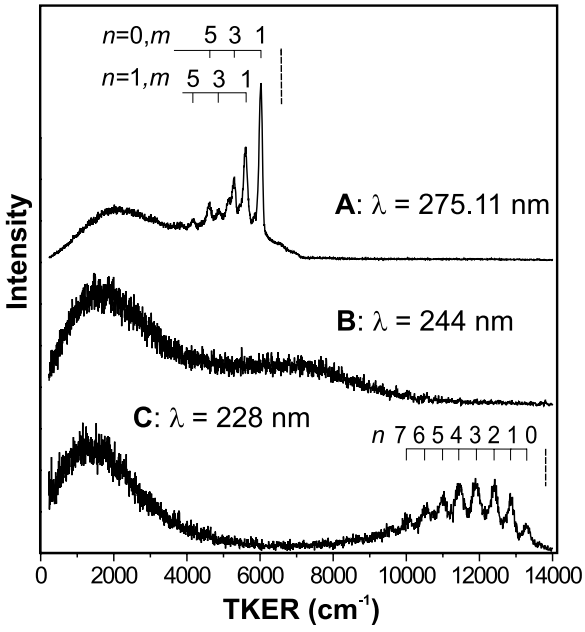

Fig. 3. TKER spectra of the H + phenoxyl fragments arising in the photolysis of phenol at (**A**) 275.11 nm, (**B**) 244 nm, and (**C**) 228 nm, with peaks associated with population of specific vibrational states of phenoxyl labeled according to $\nu_{16a} = m$, $\nu_{18b} = n$ in (A), and $\nu_{16b} = 1$, $\nu_{18b} = n$ in (C). The dashed vertical lines in (A) and (C) indicate the TKER predicted for H + phenoxyl (v = 0) products.

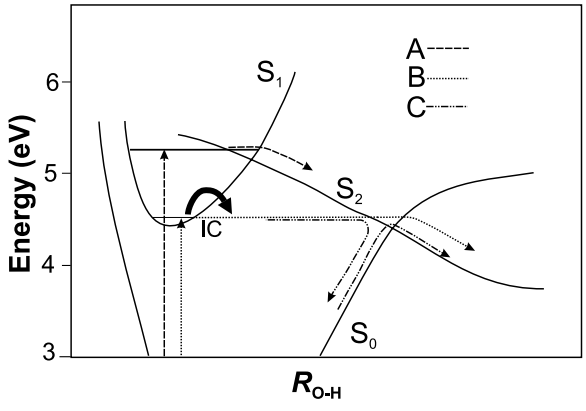

Fig. 4. Schematic PE profiles for the S_0, $S_1(^1\pi\pi^*)$, and $S_2(^1\pi\sigma^*)$ states of phenol, plotted versus R_{O-H}. The fragmentation pathway for phenol (S_1) molecules prepared at $\lambda_{phot} \leq$ 240 nm is shown as route A (long dashes), whereas schemes B (short dashes) and C (dot-dashed line) illustrate direct and indirect fragmentation pathways for molecules excited at wavelengths close to the $S_1 \leftarrow S_0$ origin and which decay after IC to high vibrational levels of the S_0 state.

to such indirect dissociations, which is indicated as Scheme C in Fig. 4.

The prediction (*1*) that N(O)–H bond fission after photoexcitation to the $^1\pi\sigma^*$ state represents an efficient nonradiative decay pathway for heteroaromatics like imidazole, pyrrole, and phenol in the gas phase is thus confirmed, irrespective of whether the $^1\pi\sigma^*$ state is populated by direct photoexcitation as in imidazole or pyrrole, or indirectly, by radiationless transfer from a photoprepared $^1\pi\pi^*$ state, as in phenol. The quantum yield for H atom production after UV excitation of pyrrole in the wavelength ranges discussed in this work is estimated to be near unity. Due to the similarity in the PESs for pyrrole and imidazole, we can also assume a high quantum yield for the H atom production in this case. The picture is less clear for phenol, but the fast H atoms formed by the S_1/S_2 coupling at $\lambda <$ 240 nm show anisotropic recoil distributions, implying fast and efficient fragmentation. Further, the recent PTS study of phenol photolysis at 248 nm (*25*) reports no fragmentation channels other than H + C_6H_5O at that wavelength. The available evidence thus suggests that H atom loss is a major process after UV excitation of these gas phase molecules. Future challenges include the following: (i) extending such high-resolution PTS studies to larger, less volatile biomolecules like adenine, histidine, tyrosine, and tryptophan, and (ii) exploring whether such photoinduced prompt N(O)–H bond fission processes also operate in the condensed phase.

References and Notes

1. A. L. Sobolewski, W. Domcke, C. Dedonder-Lardeux, C. Jouvet, *Phys. Chem. Chem. Phys.* **4**, 1093 (2002).
2. L. Serrano-Andrés, M. P. Fülscher, B. O. Roos, M. Merchán, *J. Phys. Chem.* **100**, 6484 (1996).
3. Imidazole, pyrrole, and phenol were obtained commercially (Aldrich, Gillingham, UK, 98%). Pyrrole, at its room temperature vapor pressure (~11 torr) and diluted in 700 torr of Ar, was introduced into the photolysis region in the form of a pulsed, skimmed molecular beam. For imidazole and phenol, solid samples were packed in the tube leading to the same pulsed molecular beam source and heated to ~100°C (imidazole) or 60°C (phenol), and the resulting vapor entrained in 700 torr of Ar before expansion into the interaction region.
4. L. Schnieder, W. Meier, K. H. Welge, M. N. R. Ashfold, C. M. Western, *J. Chem. Phys.* **92**, 7027 (1990).
5. B. Cronin, M. G. D. Nix, R. H. Qadiri, M. N. R. Ashfold, *Phys. Chem. Chem. Phys.* **6**, 5031 (2004).
6. m_H and m_R in Eq. 1 are the masses of the H atom (m_H = 1.0079 dalton) and of the partner fragments (imidazole, pyrrolyl, and phenoxyl, with respective masses m_R = 67.07 dalton, 66.08 dalton, and 93.11 dalton), d = 0.368 m is the length of the flight path, and t is the measured H atom TOF.
7. The angular variation of the product yield is characterized by the beta (β) parameter. Photoexcitation preferentially selects molecules that are aligned so that their transition moment ($\boldsymbol{\mu}$) is parallel to $\boldsymbol{\varepsilon}_{phot}$. Direct dissociation occurs on a time scale that is much shorter than a classical rotational period. The resulting fragments will recoil along the axis of the breaking bond in the photoexcited molecule, i.e., they will display a spatial anisotropy that reflects the original $\boldsymbol{\mu}\cdot\boldsymbol{\varepsilon}$ interaction. The photofragment angular distribution is given by $I(\theta) = [1 + \beta P_2(\cos\theta)]/4\pi$, where θ is the angle between the fragment recoil velocity vector $\mathbf{v}$ and the TOF axis, and $P_2(x) = (3x^2 - 1)/2$ is the second-order Legendre polynomial. β takes limiting values of +2 in the case of prompt dissociation after excitation via a parallel transition (i.e., $\boldsymbol{\mu}$ lies along the breaking bond) and −1 in the case of a perpendicular transition. Less anisotropic fragment recoil distributions (i.e., with β closer to 0) are observed in the case of predissociations (i.e., where the excited state lifetime is comparable to, or longer than, the rotational period of the parent molecule).
8. R. N. Zare, *Angular Momentum. Understanding Spatial Aspects in Physics and Chemistry* (Wiley, New York, 1988).
9. Equilibrium structures and vibrational frequencies discussed in this work were calculated using Gaussian 03 (Revision B.04, M. J. Frisch *et al*., Gaussian, Inc., Pittsburgh, PA, 2003), B3LYP, with a 6-311G(d,p) basis set.
10. Convention identifies the N atom involved in the N−H bond in imidazole as atom 1, and the other heavy atoms in the ring labeled by counting in a clockwise direction in the case of the structure depicted in Fig. 1, i.e., C2, N3, etc.
11. A. J. Gianola *et al.*, *J. Phys. Chem. A* **109**, 11504 (2005).
12. Vibronic coupling is an example of a breakdown of the Born-Oppenheimer separation, which applies when the vibrational and electronic degrees are coupled sufficiently strongly that they cannot be factored. In the case of an electric dipole forbidden transition, inclusion of a quantum of a nonsymmetric vibration changes the overall (vibronic) symmetry and permits the transition (with an intensity that depends on the degree of mixing of the vibrational and electronic wave functions).
13. B. O. Roos, P.-A. Malmqvist, V. Molina, L. Serrano-Andres, M. Merchan, *J. Chem. Phys.* **116**, 7526 (2002).
14. D. A. Blank, S. W. North, Y. T. Lee, *Chem. Phys.* **187**, 35 (1994).
15. J. Wei, A. Kuczmann, J. Riedel, F. Renth, F. Temps, *Phys. Chem. Chem. Phys.* **5**, 315 (2003).
16. J. Wei, J. Riedel, A. Kuczmann, F. Renth, F. Temps, *Faraday Disc* **127**, 267 (2004).
17. H. D. Bist, J. C. D. Brand, D. R. Williams, *J. Mol. Spectrosc.* **24**, 402, 413 (1967).
18. C. Ratzer, J. Kupper, D. Spangenberg, M. Schmitt, *Chem. Phys.* **283**, 153 (2002).
19. A. Sur, P. M. Johnson, *J. Chem. Phys.* **84**, 1206 (1986).
20. R. J. Lipert, S. D. Colson, *J. Phys. Chem.* **93**, 135 (1989).
21. J. Lorentzon, P.-A. Malmqvist, M. Fülscher, B. O. Roos, *Theor. Chim. Acta* **91**, 91 (1995).
22. A. L. Sobolewski, W. Domcke, *J. Phys. Chem. A* **105**, 9275 (2001).
23. Z. Lan, W. Domcke, V. Vallet, A. L. Sobolewski, S. Mahapatra, *J. Chem. Phys.* **122**, 224315 (2005).
24. K. Kimura, S. Nagakura, *Mol. Phys.* **9**, 117 (1965).
25. C.-M. Tseng, Y. T. Lee, C.-K. Ni, *J. Chem. Phys.* **121**, 2459 (2004).
26. S. Ishiuchi *et al.*, *J. Chem. Phys.* **117**, 7077 (2002).
27. K. Daigoku, S. Ishiuchi, M. Sakai, M. Fujii, K. Hashimoto, *J. Chem. Phys.* **119**, 5149 (2003).
28. Two alternative numbering schemes for the normal mode vibrations of benzene and benzene derivatives are commonly found in the scientific literature (the so-called Wilson and Herzberg assignments). We consistently use the former. To assist readers familiar with the latter, the Herzberg labels for the modes of phenol discussed in this work are: $\nu_{16a} \rightarrow \nu_{16}$, $\nu_{16b} \rightarrow \nu_{21}$, $\nu_{18b} \rightarrow \nu_{33}$.

29. We are grateful to the Engineering and Physical Sciences Research Council UK for financial support via the Portfolio Partnership LASER and to K. N. Rosser for his outstanding practical support of this work.

26 January 2006; accepted 24 April 2006
10.1126/science.1125436

A Nearly Modern Amphibious Bird from the Early Cretaceous of Northwestern China

Hai-lu You,[1] Matthew C. Lamanna,[2]* Jerald D. Harris,[3]* Luis M. Chiappe,[4] Jingmai O'Connor,[4] Shu-an Ji,[1] Jun-chang Lü,[1] Chong-xi Yuan,[1] Da-qing Li,[5] Xing Zhang,[6] Kenneth J. Lacovara,[7] Peter Dodson,[8] Qiang Ji[1]

Three-dimensional specimens of the volant fossil bird *Gansus yumenensis* from the Early Cretaceous Xiagou Formation of northwestern China demonstrate that this taxon possesses advanced anatomical features previously known only in Late Cretaceous and Cenozoic ornithuran birds. Phylogenetic analysis recovers *Gansus* within the Ornithurae, making it the oldest known member of the clade. The Xiagou Formation preserves the oldest known ornithuromorph-dominated avian assemblage. The anatomy of *Gansus*, like that of other non-neornithean (nonmodern) ornithuran birds, indicates specialization for an amphibious life-style, supporting the hypothesis that modern birds originated in aquatic or littoral niches.

Neornithean (modern) birds are the most diverse extant tetrapods, comprising ~10,000 species (*1*). Neornitheans, plus the predominantly Late Cretaceous Hesperornithes and *Ichthyornis dispar*, constitute the Ornithurae, a clade that, along with a few other Cretaceous taxa, comprises the Ornithuromorpha (*2*). Previously reported, alleged Early Cretaceous ornithurans are either fragmentary (*3*, *4*), of debatable age (*5*), or have received only limited examination (*6*–*8*). Furthermore, they are rare compared to members of the extinct clade Enantiornithes (*9*, *10*). Consequently, the early evolution of the Ornithuromorpha and the phylogenetic, temporal, and paleoecological contexts of ornithuran (and ultimately neornithean) origins remain obscure. One of the first Early Cretaceous birds discovered was *Gansus yumenensis*, based on an isolated partial left pelvic limb from the Lower Cretaceous (?Aptian-Albian, ~115 to 105 million years ago; see supporting online material) Xiagou Formation near Changma, Gansu Prov-

ince, northwestern China (*11*) (Fig. 1). *Gansus* was initially recognized as more closely allied to neornithean birds than is *Archaeopteryx*; subsequent discoveries have reinforced this hypothesis (*2*, *12*).

Here we describe five new, tern-sized specimens of *G. yumenensis*, also from the Xiagou Formation near Changma, that collectively represent the entire skeleton except the skull, mandibles, and cranial-middle cervical vertebrae (Fig. 2 and figs. S1 to 6). Unlike many compressed or split avian fossils from the Jehol Group of northeastern China, most of the new *Gansus* specimens consist of three-dimensional, largely uncrushed and undistorted bones, and many include soft tissues. Autapomorphies are difficult to pinpoint in the fragmentary *Gansus* holotype, but the most frequently cited feature is pronounced, distally projecting flexor tubercula separate from, and distal to, the proximoplantar ends of the pedal unguals (*10*, *11*). One of the new specimens has identical pedal morphology (Fig. 2J and fig. S5); skeletal elements of this specimen are indistinguishable from their counterparts in the remaining four skeletons, justifying the referral of all to *G. yumenensis*. Unless otherwise noted, the phylogenetically important characters of *Gansus* discussed below represent apomorphies relative to more basal birds (see also supporting online material).

The caudal cervical and 10 thoracic vertebrae of *Gansus* are plesiomorphically not heterocoelous. The thoracics are excavated by deep, emarginate, craniocaudally elongate, lateral pneumatic fossae. The cranialmost three to four thoracics possess well-developed ventral processes ("hypapophyses") (Fig. 2G and fig. S4). The cranialmost three of the 10 to 11 synsacral vertebrae exhibit dorsally directed costal processes. The tail comprises six to seven free vertebrae, all with poorly developed cranial and caudal zygapophyses, and a pygostyle the length of three caudals. All specimens lack ossified gastralia and uncinate processes.

A tall carina extends the length of the sternum (Fig. 2G and fig. S4). Closely spaced coracoidal articular sulci embay the cranial edge of the element. The thin U-shaped furcula has an ~38° intraclavicular angle. The dorsally convex scapula tapers distally. The strutlike, plesiomorphically apneumatic coracoid possesses well-developed procoracoid and lateral processes (Fig. 2E and fig. S2), a deep circular scapular cotyle, and a humeral articular facet situated well ventral to the acrocoracoid process.

The proximal end of the plesiomorphically apneumatic humerus exhibits a ventral tubercle, capital incisure, and domed articular condyle. The cranially projecting bicipital crest bears a transverse sulcus on its proximoventral surface and a tiny fovea caudodistally. A shallow brachial fossa lies proximal to approximately subequal, cranially developed distal humeral condyles. The ulna is slightly longer than the humerus and displays a prominent bicipital tubercle and a deep narrow brachial impression. The dorsal trochlear surface of the dorsal condyle is developed as a semilunate ridge. The carpal trochlea (semilunate carpal) is completely co-ossified with, and positioned proximal to, major and minor metacarpals that may also be fused distally. The weakly developed extensor process of the alular metacarpal extends cranially just beyond the shelflike phalangeal articular facet. The alular metacarpal does not reach the proximal terminus of the intermetacarpal space. The craniocaudal diameter of the major metacarpal is more than twice that of the minor. The proximal phalanx of the major digit is strongly dorsoventrally compressed, flat caudally, and longer than the second phalanx.

The iliac preacetabular alae extend cranially beyond the synsacrum, overlapping the caudalmost pair of thoracic ribs. A weak, subtriangular preacetabular tuberculum ("pectineal process") is situated cranioventral to the acetabulum. A preacetabular ("cuppedicus") fossa is absent. A well-developed antitrochanter occupies the caudodorsal corner of the acetabulum. The pubis and ischium are seamlessly fused to the ilium at the acetabulum. The pubes are strongly retroverted, nearly parallel to the ischia; their distalmost ~5 to 6% are in contact but not fused. The iliac ("dorsal") process of the ischium, situated approximately at midshaft, broadly contacts, and may be co-ossified with, the caudoventral surface of the ilium, enclosing a craniocaudally elongate ilioischiadic foramen (Fig. 2B and fig. S1).

The femur exhibits a trochanteric crest proximolaterally and a patellar sulcus craniodistally. The lateral gastrocnemial ("ectocondylar") tubercle and condyle form a single distolateral trochlear surface. The conjoined cranial and lateral cnemial crests of the tibiotarsus make up a single, well-developed, proximocranially projected rounded crest (Fig. 2C and fig. S1). A tibiotarsal extensor canal is present as an emarginate groove that plesiomorphically lacks a supratendinal pons. The tarsometatarsal articular surface of the approximately subequal distal condyles extends onto the tibiotarsal caudal surface. The fibula terminates proximal to the ankle. The hypotarsus lacks crests and sulci (Fig. 2H and fig. S4). Plantar displacement of the proximal end of metatarsal III creates a deep dorsal extensor sulcus that contains a pronounced tibialis cranialis tuberosity and one vascular foramen that penetrates to the plantar surface. Metatarsal I is twisted and distally deflected so that its plantaromedial surface is concave proximal to its trochlea. The trochlea of metatarsal II lies proximal to the proximalmost extent of those of metatarsals III and IV. It also exhibits marked plantar offset and lateral rotation and is compressed mediolaterally as compared to those of metatarsals III and IV. Metatarsals III and IV completely

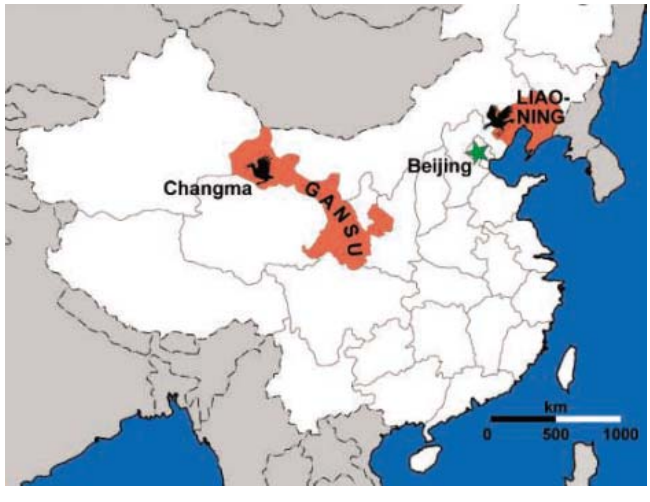

Fig. 1. Map of China (white), with Changma locality in Gansu Province and fossil bird–producing deposits of the Jehol Group in Liaoning Province (~2000 km away) marked by bird silhouettes.

[1]Institute of Geology, Chinese Academy of Geological Sciences, 26 Baiwanzhuang Road, Beijing 100037, People's Republic of China. [2]Section of Vertebrate Paleontology, Carnegie Museum of Natural History, 4400 Forbes Avenue, Pittsburgh, PA 15213–4080, USA. [3]Science Department, Dixie State College, 225 South 700 East, St. George, UT 84770, USA. [4]The Dinosaur Institute, Natural History Museum of Los Angeles County, 900 Exposition Boulevard, Los Angeles, CA 90007, USA. [5]Fossil Research and Development Center, Third Geology and Mineral Resources Exploration Academy of Gansu Province, 1 Langongping Road, Lanzhou, Gansu 730050, People's Republic of China. [6]Provincial Museum of Gansu Province, Nature Department, 3 West Xijin Road, Lanzhou, Gansu 730050, People's Republic of China. [7]Geology and Paleontology Program, Department of Bioscience and Biotechnology, Drexel University, 409 Stratton Hall, 32nd and Chestnut, Philadelphia, PA 19104, USA. [8]Department of Animal Biology, School of Veterinary Medicine, University of Pennsylvania, 3800 Spruce Street, Philadelphia, PA 19104, USA.

*To whom correspondence should be addressed. E-mail: lamannam@carnegiemnh.org (M.C.L); jharris@dixie.edu (J.D.H.)

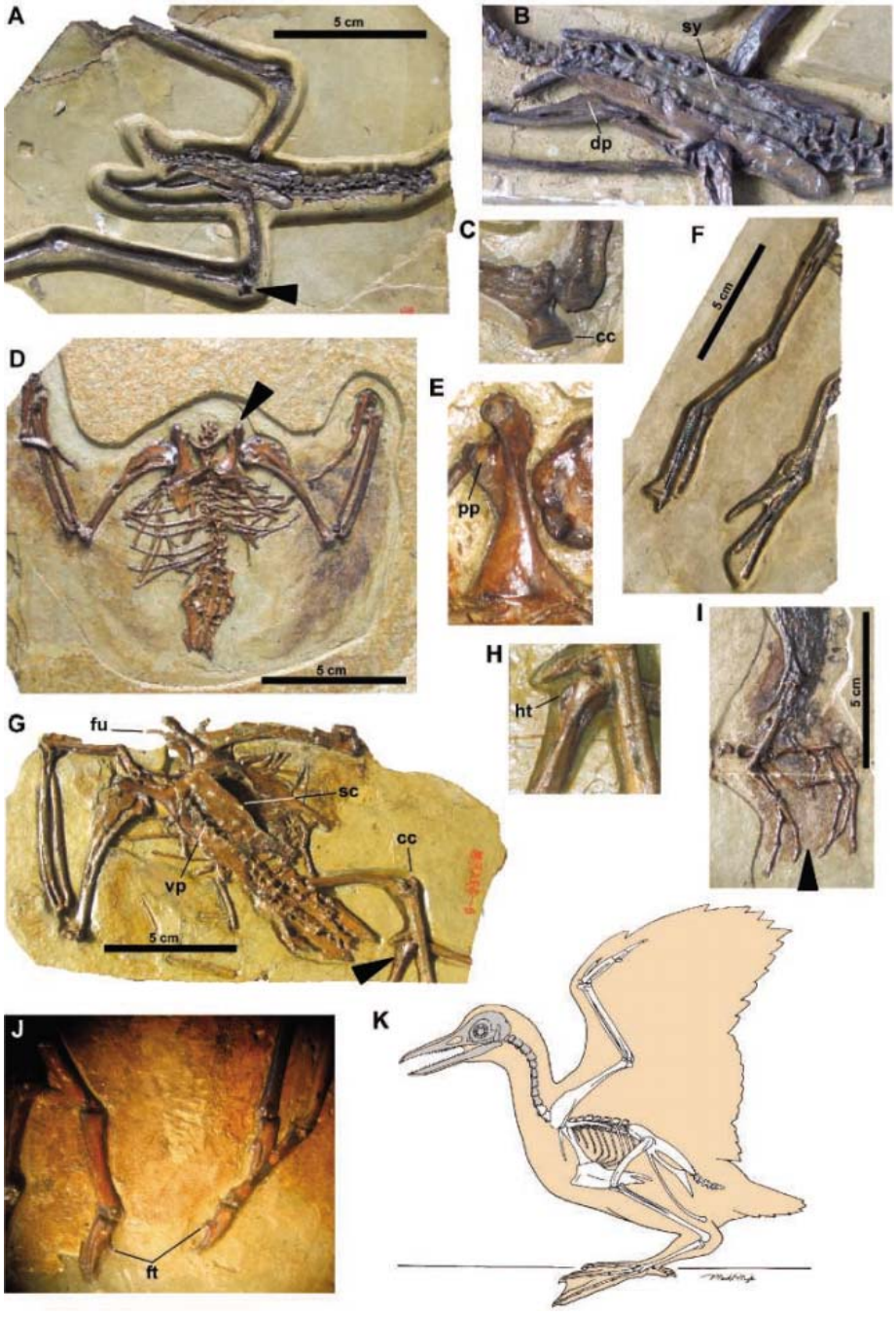

Fig. 2. New specimens of *G. yumenensis* (Chinese Academy of Geological Sciences, Institute of Geology, prefix CAGS-IG-04-). (**A**) CM-002, articulated caudal cervical, thoracic, synsacral, and caudal vertebrae, pelvic girdle, and partial pelvic limbs in right dorsolateral view. (**B**) CM-002, pelvis and synsacrum. (**C**) CM-002, proximal right tibiotarsus [indicated by arrowhead in (A)]. (**D**) CM-004, nearly complete skeleton in ventral view with feathers (dark brown) on thoracic limbs, lacking cranium, cranial-midcervical vertebrae, and both pelvic limbs. (**E**) CM-004, left coracoid in ventral view [indicated by arrowhead in (D)]. (**F**) CM-001, partial right and left pelvic limbs. (**G**) CM-003, nearly complete skeleton in ventral view, lacking cranium, cervical vertebrae, distal left thoracic limb, and right and distal left pelvic limbs. (**H**) CM-003, proximal tarsometatarsus [indicated by arrowhead in (G)]. (**I**) CM-008, partial pelvic limbs with soft-tissue preservation. (**J**) CM-008, tubercular soft tissue preserved around toes [indicated by arrowhead in (I)]. (**K**) Reconstruction of *G. yumenensis* based on new specimens. Elements shaded gray remain unknown. Abbreviations in figure are as follows: cc, cnemial crests; ft, flexor tubercula; dp, dorsal process of ischium; fu, furcula; ht, hypotarsus; pp, procoracoid process; sc, sternal carina; sy, synsacrum; vp, ventral processes of cranial thoracic vertebrae.

enclose a large, proximodistally elongate, distal vascular foramen. The first phalanges of all pedal digits are longer than any of their respective distal phalanges; all unguals are small, short, and unrecurved.

Wing feathers preserved with one specimen (Fig. 2D and fig. S2) are asymmetrical and virtually identical to those of volant modern birds. Semiplumes or down also appear to be present.

Most Early Cretaceous bird species have been recovered from northeastern China and Spain and are primarily non-ornithuromorphs (enantiornitheans plus more basal taxa) (*8*, *10*, *13*). However, most of nearly 50 bird specimens recovered from Changma appear to pertain to *Gansus*. Thus, the Xiagou Formation preserves the oldest known avian assemblage dominated by ornithuromorphs, possibly indicating the first stages of the rise of ornithuromorphs to diversity-based dominance over enantiornitheans (supporting online material).

Despite pectoral and alar features that indicate powered flight, *Gansus* pelvic limb elements exhibit specializations that are characteristic of amphibious (*14*) birds. Osteologically, these include the prominent, proximally projecting cnemial crests on the tibiotarsus; proximal position of the trochlea of metatarsal II; elongate pedal digits [III and IV each longer than the tarsometatarsus (tables S1 and S2)] with elongate proximal phalanges (all longer than any penultimate phalanges); and unrecurved unguals with large flexor tubercula. Except the last, these features predominantly occur elsewhere in undoubted foot-propelled divers such as *Hesperornis*, loons (Gaviidae), and grebes (Podicipedidae) (*15*); the cnemial crests are more elongate in *Gansus* than in the slightly younger hesperornithean *Enaliornis* (*5*). Similar flexor tubercula characterize some extant shorebirds (Charadriiformes) (*3*), herons (Ardeidae), and diving ducks (Anatidae) (*16*). Moreover, one new *Gansus* specimen preserves tubercular skin surrounding the pedal digits (Fig. 2J and fig. S5) that indicate interdigital telae (webbing) extending at least to the proximal ends of the unguals. The presence of web-footed birds in the Early Cretaceous is supported by footprints elsewhere in Asia (*17*). *Gansus* has typically been considered a sandpiper (Scolopacidae) analog (*3*, *11*), implying that it was not amphibious (that is, it lacked fully webbed feet and did not dive) but instead waded and probed nearshore sediments for food (*1*). Its anatomy, however, demonstrates that it was more similar to, but not as adept as, foot-propelled diving birds such as grebes, loons, and diving ducks.

In all consensus trees from a phylogenetic analysis (see supplementary online material for methods and details), *Gansus* occurs with-

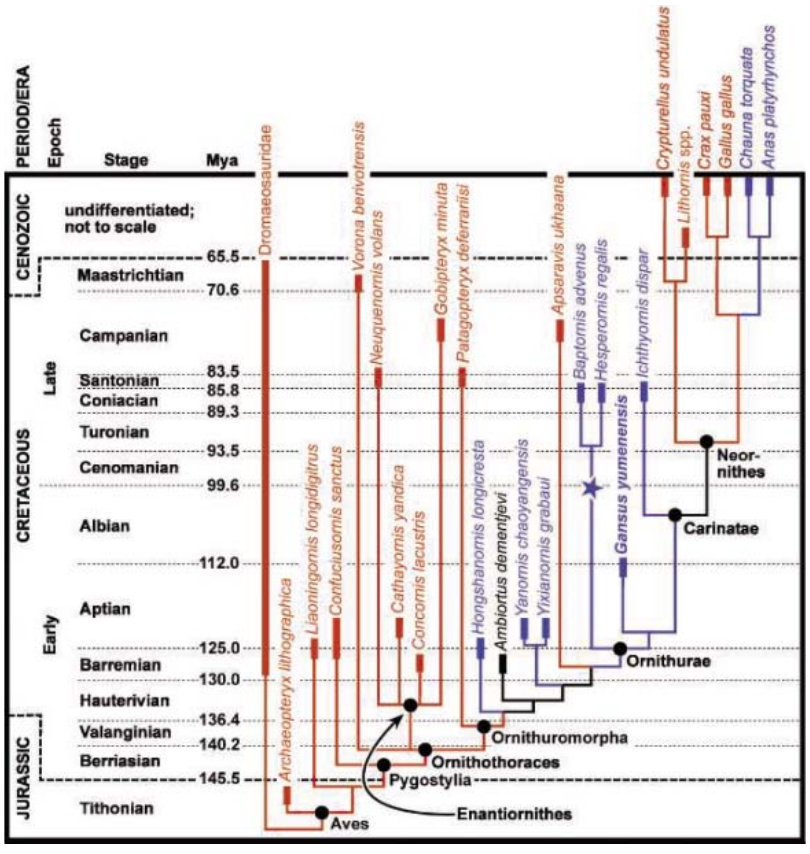

Fig. 3. Phylogenetic position of *G. yumenensis* (50% majority-rule consensus tree) based on holotype and new referred specimens; time scale is per (*28*). Thin line segments represent ghost lineages; thick line segments represent known ranges of terminal taxa. Clades are denoted by black circles (see supporting online material for clade definitions). The star represents the temporal position of *Enaliornis* spp. Colors indicate known or inferred ecologies as follows: brown, terrestrial/arboreal; blue, aquatic/amphibious; black, equivocal. Note the sequence of amphibious taxa basal to the Neornithes. Depicted divergence times are intended as approximations only, based on the oldest occurrence of an included species and subsequent divergences. Mya, million years ago.

in the Ornithurae (Fig. 3). This position is considerably more derived than that of all known birds from the Jehol Group of northeastern China. *Gansus* predates other, later Cretaceous ornithurans that are considered to exhibit amphibious features [such as hesperornitheans] or are thought to have occupied water-based niches [such as *Ichthyornis*] (*5*, *12*, *18*–*23*). Some younger yet more basal ornithuromorphs, including *Apsaravis ukhaana* (*24*) and *Patagopteryx deferrariisi* (*25*), occupied fully terrestrial niches, as did some later purported neornitheans (*12*, *20*, *24*). *Ichthyornis* and *Gansus* are recovered as proximal outgroups to the Neornithes, consistent with the hypothesis that neornitheans originated in an aquatic habitat (*26*). Thus (Fig. 3), the most basal ornithuromorphs appear to have evolved in a terrestrial/arboreal context (*25*) but rapidly shifted to an aquatic ecology (*8*) (Fig. 3).

Before the end of the Cretaceous, some non-ornithuran ornithuromorphs must have reverted to a terrestrial life-style (*24*). The Cretaceous existence of members of basal neornithean clades [Anseriformes and possibly Gaviiformes (*19*, *20*, *22*)] implies that representatives of the neornithean clades Galliformes and more basal Palaeognathae, all known fossil and extant members of which are terrestrial, must also have existed during the Cretaceous (*27*). Thus, although neornitheans may have originated in aquatic niches, some basal neornitheans apparently re-radiated into terrestrial niches before the Cretaceous/Paleogene extinction event. Consequently, contrary to recent hypotheses, adaptation to an aquatic ecology appears to have played little part in the survival of birds across the K/P boundary (*27*).

References and Notes

1. F. B. Gill, *Ornithology* (Freeman, New York, ed. 2, 1995).
2. L. M. Chiappe, in *Mesozoic Birds: Above the Heads of Dinosaurs*, L. M. Chiappe, L. M. Witmer, Eds. (Univ. of California Press, Berkeley, CA, 2002), pp. 448–472.
3. L. Hou, *Mesozoic Birds of China* (Feng-huang-ku Bird Park, Taiwan, 1997) (in Chinese).
4. E. N. Kurochkin, *Smithson. Contrib. Paleobiol.* **89**, 275 (1999).
5. P. M. Galton, L. D. Martin, in *Mesozoic Birds: Above the Heads of Dinosaurs*, L. M. Chiappe, L. M. Witmer, Eds. (Univ. of California Press, Berkeley, CA, 2002), pp. 317–338.
6. C. Yuan, *Acta Geol. Sin.* **78**, 464 (2004) (in Chinese with English summary).
7. Z. Zhou, F. Zhang, *Chin. Sci. Bull.* **46**, 1258 (2001).
8. Z. Zhou, F. Zhang, *Proc. Natl. Acad. Sci. U.S.A.* **102**, 18998 (2006).
9. L. Hou, Z. Zhou, F. Zhang, Y. Gu, *Mesozoic Birds from Western Liaoning in China* (Liaoning Science and Technology Publishing House, 2002) (in Chinese).
10. Z. Zhou, L. Hou, in *Mesozoic Birds: Above the Heads of Dinosaurs*, L. M. Chiappe, L. M. Witmer, Eds. (Univ. of California Press, Berkeley, CA, 2002), pp. 160–183.
11. L. Hou, Z. Liu, *Sci. Sin. Ser. B* **27**, 1296 (1984).
12. S. Hope, in *Mesozoic Birds: Above the Heads of Dinosaurs*, L. M. Chiappe, L. M. Witmer, Eds. (Univ. of California Press, Berkeley, CA, 2002), pp. 339–388.
13. J. L. Sanz, B. P. Pérez-Moreno, L. M. Chiappe, A. D. Buscalioni, in *Mesozoic Birds: Above the Heads of Dinosaurs*, L. M. Chiappe, L. M. Witmer, Eds. (Univ. of California Press, Berkeley, CA, 2002), pp. 209–229.
14. V. de Buffrénil, J.-M. Mazin, in *Secondary Adaptations of Tetrapods to Life in Water*, J.-M. Mazin, V. de Buffrénil, Eds. (Friedrich Pfeil, Munich, Germany, 2001), pp. 91–93.
15. J. Cracraft, *Syst. Zool.* **31**, 35 (1982).
16. R. W. Shufeldt, *N.Y. State Mus. Bull.* **130**, 5 (1909).
17. J.-D. Lim, Z. Zhou, L. D. Martin, K.-S. Baek, S.-Y. Yang, *Naturwissenschaften* **87**, 256 (2000).
18. O. C. Marsh, *Prof. Pap. Eng. Dept. U.S. Army* **18**, 1 (1880).
19. E. N. Kurochkin, G. J. Dyke, A. A. Karhu, *Am. Mus. Novit.* **3386**, 1 (2002).
20. S. Chatterjee, in *Proceedings of the 5th Symposium of the Society of Avian Paleontology and Evolution, Beijing, 1-4 June 2000*, Z. Zhou, F. Zhang, Eds. (Science Press, Beijing, China, 2002), pp. 125–155.
21. D. C. Parris, S. Hope, in *Proceedings of the 5th Symposium of the Society of Avian Paleontology and Evolution, Beijing, 1-4 June 2000*, Z. Zhou, F. Zhang, Eds. (Science Press, Beijing, China, 2002), pp. 113–124.
22. J. A. Clarke, C. P. Tambussi, J. I. Noriega, G. M. Erickson, R. A. Ketcham, *Nature* **433**, 305 (2005).
23. G. J. Dyke *et al.*, *Naturwissenschaften* **89**, 408 (2002).
24. J. A. Clarke, M. A. Norell, *Am. Mus. Novit.* **3387**, 1 (2002).
25. L. M. Chiappe, in *Mesozoic Birds: Above the Heads of Dinosaurs*, L. M. Chiappe, L. M. Witmer, Eds. (Univ. of California Press, Berkeley, CA, 2002), pp. 281–316.
26. A. Feduccia, *Trends Ecol. Evol.* **18**, 172 (2003).
27. D. S. Robertson, M. C. McKenna, O. B. Toon, S. Hope, J. A. Lillegraven, *Geol. Soc. Am. Bull.* **116**, 760 (2004).
28. F. M. Gradstein, J. G. Ogg, A. Smith, *A Geologic Time Scale 2004* (Cambridge Univ. Press, Cambridge, 2004).

29. We thank Z.-c. Bai. and C. Peng and their field crew for excavation and collection of the specimens; G.-h. Cui and Y.-q. Zhang for specimen preparation; B. Livezey, Z.-x. Luo, and R. Mulvihill for discussion; S. Yu for translating (*6*); M. Klingler for Fig. 2K; and anonymous manuscript reviewers. Funding was provided by the Discovery Quest program for The Science Channel to H.-l.Y., M.C.L., and J.D.H.; the Carnegie Museum of Natural History to M.C.L.; Dixie State College to J.D.H.; the Chinese Geological Survey of the Ministry of Land and Resources of China and the Ministry of Science and Technology of China (973 Project) to H-l.Y. and Q.J.; and the Gansu Bureau of Geology and Mineral Resources to D.-q.L.

Supporting Online Material

www.sciencemag.org/cgi/content/full/312/5780/1640/DC1
Materials and Methods
SOM Text
Figs. S1 to S6
Tables S1 and S2
References

17 February 2006; accepted 19 April 2006
10.1126/science.1126377

Phosphatized Polar Lobe–Forming Embryos from the Precambrian of Southwest China

Jun-Yuan Chen,[1*] David J. Bottjer,[2] Eric H. Davidson,[3] Stephen Q. Dornbos,[4] Xiang Gao,[1] Yong-Hua Yang,[1] Chia-Wei Li,[5] Gang Li,[6] Xiu-Qiang Wang,[1] Ding-Chang Xian,[6] Hung-Jen Wu,[5] Yeu-Kuang Hwu,[7] Paul Tafforeau[8,9]

In developing embryos of some extant spiralian animals, polar lobe formation is one of the symmetry-breaking mechanisms for segregation of maternal cytoplasmic substances to certain blastomeres and not others. Polar lobe formation leads to unique early cleavage morphologies that include trilobed, J-shaped, and five-lobed structures. Fossil embryos similar to modern lobe-forming embryos are recognized from the Precambrian Doushantuo Formation phosphates, Weng'an, Guizhou Province, China. These embryos are abundant and form a developmental sequence comparable to different developing stages observed in lobe-forming embryos of extant spiralians. These data imply that lobe formation is an evolutionarily ancient process of embryonic specification.

The Weng'an fossil fauna from Precambrian Doushantuo phosphates in Weng'an, Guizhou Province, China contains likely fossil representatives of the oldest known metazoans (*1*, *2*). The fossil-bearing interval of the Doushantuo has been dated as at least 580 million years old (*3*, *4*). Previous studies have presented fossil evidence of sponges (*5*), cnidarians (*6*, *7*), and possible bilaterians (*8–10*) in this formation. In addition, a large number of embryos (*11–13*) display a variety of developmental patterns and different morphological types, implying that metazoans may have been diverse 40 million years before the Cambrian (*1*). The affinities of these embryos, however, remain enigmatic. We present fossil evidence of developing embryos that resemble the different developmental stages of lobe-forming embryos, which in modern fauna are found in spiralians including many extant mollusks and some annelids (*14*, *15*).

We studied material from the gray facies of the Weng'an Phosphate Member of the upper Doushantuo Formation at Wusi, Baisaikang, and Nanbao quarries, Weng'an county, Guizhou (*1*). Rock samples were treated with a 10% acetic acid solution for removal of specimens from the matrix. Fossil embryos were recovered from the acid residues, coated with gold, and observed and photographed with a Hitachi S2600N scanning electron microscope (SEM); we identified 248 embryos with morphological characters like those of lobe-forming embryos common in many modern mollusks (*16–18*). A few selected samples were examined by synchrotron radiation microtomography (SR-μCT) at both the European Synchrotron Radiation Facility (ESRF) and the Taiwan Synchrotron Radiation Research Center (NSRRC).

Lobe formation is a sequential process of dynamic change, which occurs by the protrusion and then absorption of a cytoplasmic lobe called a polar lobe. The lobe protrudes from the vegetal pole of the embryo at each round of cytokinesis, leading to the formation of dumbbell, three-fold (trefoil), J-shaped, and five-lobed morphologies (Fig. 1). The polar lobe (PL) superficially resembles a blastomere, but the lobe is anucleate and is connected to the CD or D blastomere by a deep constricted neck. Fossil PLs can be recognized by their size and connecting necks and by the complementary relation between their size and that of the CD or D blastomere from which they arose.

In the modern mud snail (*Nassarius obsoletus*) the first PL is protruded soon after fertilization, leading to the formation of a calabash-shaped structure: a large ball attached to a small one (*16*). Similar structures occur in many of our samples from the Weng'an. In *N. obsoletus*, the fertilized eggs at the first-lobe stage bear a superficial resemblance to unequally cleaving two-cell embryos, but they differ in that the embryo consists of a rather large uncleaved fertilized egg with a smaller anucleate lobe. After first cleavage, the larger blastomere (CD cell) in the lobe-forming two-cell embryos protrudes a lobe from its vegetal pole, forming a trilobed structure as seen in modern mollusks (termed a trefoil stage). A total of 94 specimens with similar structures are recognized in the Weng'an fossil assemblage. A large number of them are encased partially or

Table 1. Measurements of the volume of AB cells, CD cells, and PLs of the embryos illustrated in Fig.2, with relative volumes of different combinations of these components.

Sample	AB cell (mm^3)	CD cell (mm^3)	PL (mm^3)	CD + PL/AB	PL/CD + PL (%)	PL/AB (%)	CD/AB (%)
Embryos with equal division							
1 (Fig. 2J)	0.035	0.033	0.006	1.1	15%	17%	94%
2 (Fig. 2I)	0.018	0.014	0.004	1.0	22%	22%	78%
3 (Fig. 2F)	0.064	0.050	0.020	1.1	29%	31%	78%
4 (Fig. 2G)	0.050	0.035	0.015	1.0	30%	30%	70%
5 (Fig. 2E)	0.006	0.004	0.002	1.0	33%	33%	67%
6 (Fig. 2A)	0.022	0.016	0.010	1.2	38%	45%	73%
7 (Fig. 2D)	0.006	0.004	0.003	1.1	39%	42%	65%
8 (Fig. 2C)	0.033	0.020	0.014	1.0	41%	42%	60%
9 (Fig. 2B)	0.082	0.042	0.036	1.0	46%	43%	51%
10 (Fig. 2H)	0.050	0.025	0.025	1.0	50%	50%	50%
11 (Fig. 2K)	0.012	0.007	0.007	1.2	50%	58%	58%
Embryos with unequal division							
12 (Fig. 2M)	0.020	0.030	0.008	1.9	21%	40%	150%
13 (Fig. 2R)	0.008	0.011	0.004	1.9	27%	50%	138%
14 (Fig. 2T)	0.028	0.034	0.016	1.8	32%	57%	121%
15 (Fig. 2N)	0.004	0.006	0.003	2.2	32%	70%	150%
16 (Fig. 2V)	0.019	0.027	0.014	2.2	34%	74%	142%
17 (Fig. 2U)	0.022	0.028	0.017	2.0	38%	77%	127%
18 (Fig. 2Q)	0.012	0.015	0.011	2.2	42%	92%	125%
19 (Fig. 2P)	0.026	0.027	0.021	1.8	44%	81%	104%
20 (Fig. 2S)	0.030	0.030	0.026	1.9	46%	87%	100%
21(Fig. 2L)	0.067	0.064	0.063	1.9	48%	93%	95%
22 (Fig. 2O)	0.024	0.025	0.023	2.0	48%	96%	104%

[1]Nanjing Institute of Geology and Paleontology, Institute of Evo/Developmental Biology, and State Key Laboratory of Pharmaceutical Biotechnology, Nanjing University, Nanjing 210093, China. [2]Department of Earth Sciences, University of Southern California, Los Angeles, CA 90089, USA. [3]Division of Biology, 156-29, California Institute of Technology, Pasadena, CA 91125, USA. [4]Department of Geosciences, University of Wisconsin, Milwaukee, WI 53201, USA. [5]Department of Life Science, National Tsing Hua University, Hsinchu 300, Taiwan, China. [6]Institute of High Energy Physics, Beijing 100049, China. [7]Institute of Physics, Academia Sinica, Taipei, Taiwan, China. [8]European Synchrotron Radiation Facility, F-38043 Grenoble, France. [9]Laboratoire de Géobiologie, Biochronologie et Paléontologie Humaine, UMR CNRS 6046, F-86022 Poitiers, France.

*To whom correspondence should be addressed. E-mail: chenjy@nju.edu.cn, chenjunyuan@163.net

entirely within an envelope, rendering unlikely the possibility that the interpreted PLs are merely adventitious extrusions of cytoplasm due to damage (*19*). The diameter of the Weng'an eggs ranges from 0.2 to 1.2 mm. The inferred fossil embryos show variable arrangements with the blastomere and PL in loose contact in many specimens and in tight contact in other specimens.

On the basis of the nature of cleavage, two different groups of embryos are recognized: equal division (Fig. 2, A to K) and unequal division (Fig. 2, L to V). The CD cell (plus PL) in equal-division embryos is the same size or slightly larger than the AB cell, whereas in unequal-division embryos it is typically twice as large as the AB cell (Table 1 and Fig. 3). This implies the existence of at least two different groups of organisms within which there may have been more than one species.

The three lobes are noticeably different in size in these specimens. SR-μCT examination of the trefoil fossils displaying equal (Fig. 2, A and B) and unequal division (Fig. 2L) suggests that these three lobes are homologous with the CD cell, AB cell, and PL of trefoil embryos, respectively. Among the three lobes in the equal-division embryos (Fig. 2, A and B), the second largest one is interpreted as the CD cell because it is separated completely from the likely AB cell (the largest lobe) by a thin membrane but is connected to the likely PL (smallest lobe) by a narrow cytoplasmic neck (Fig. 2, A′, B′, and B″). In Fig. 2A, the PL, AB cell, and CD cell volumes are 0.01 mm^3, 0.022 mm^3, and 0.016 mm^3, respectively; in Fig. 2B these volumes are 0.036 mm^3, 0.082 mm^3, and 0.042 mm^3, respectively (Table 1).

The relative sizes of the PL and CD cells differ among the embryos, but measurements from the specimens illustrated in Fig. 2 and listed in Table 1 reveal a complementary relationship between the volumes of the PL and CD cells (Fig. 3). In different specimens of a given species of PL embryo at the trefoil stage, the volume of the lobe plus the CD cell (PL + CD) should bear a constant relation to the volume of the AB cell, whether the lobe is just beginning to be protruded, is fully extended, or is in the process of retraction. For the analysis in Fig. 3, we normalized the size data for the different embryos by plotting the volumetric ratios PL/AB versus PL/(PL + CD) for each embryo.

The results show that the sum (PL + CD) has a constant relationship to the size of AB. This is expected because in a lobe-forming embryo, the AB blastomere is not affected by PL extrusion. There are two populations of fossil embryos in our study: those in which PL/AB = PL/(CD + PL), and those in which PL/AB = 2PL/(CD + PL)—that is, the equal and unequal embryo types referred to above. The high correlation coefficients for the two curves demonstrate that each is a statistically robust relation that could not have resulted from the random aggregation of three spheroidal bodies developmentally unrelated in origin. The complementary relation of the PL with the CD volumes directly supports the homology of the three lobes in these fossils with the PL, the CD cell, and the AB cell, respectively, of modern trefoil

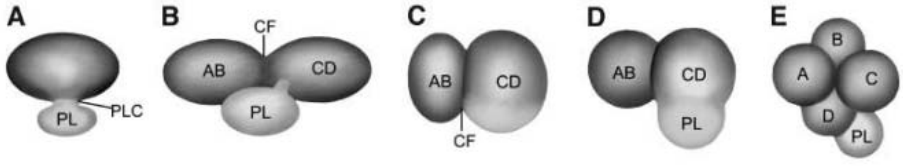

Fig. 1. Schematic diagrams showing changes in shape of the fertilized egg before cleavage and embryos during cleavage of the PL-forming species in some extant mollusks and annelids. (**A**) Egg with the first lobe; (**B**) trefoil stage; (**C**) two-cell stage; (**D**) J-shaped embryo; (**E**) five-lobed embryo.

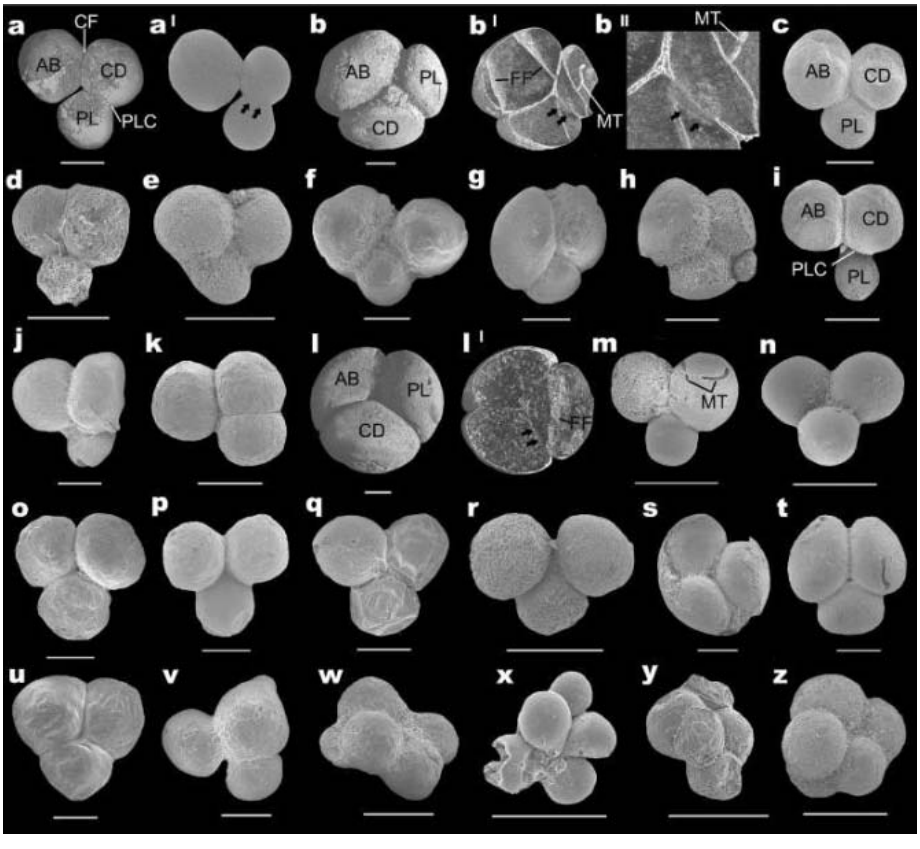

Fig. 2. Lobe-forming embryos from the Precambrian Doushantuo Formation. (**A** to **K**) Lobe-forming embryos with equal division both in trefoil stage [(A) to (H)] and J-shaped stage [(I) to (K)]. (**L** to **V**) Lobe-forming embryos with unequal division in trefoil stage [(L) to (U)] and J-shaped stage (V). (**W** to **Z**) Five-lobed embryos. Panels (A′), (B′), and (L′) are dissecting images of (A), (B), and (L), respectively, showing preservation of a connected neck (black arrow); (B″) is a magnified image of (B′). Abbreviations: MT, biogenetic microtunnel; FF, diagenetic fissure filling. Images are SEM [(C) to (K), (M) to (Z)] or SR-μCT [(A), (B), and (L)]. Scale bar, 250 μm.

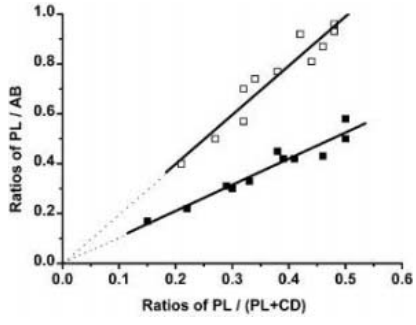

Fig. 3. Values of the ratios PL/AB (*y* axis) plotted against values of PL/(PL + CD) (*x* axis) from the measurements in Table 1. The data were fit by linear least squares, with the result that the upper plot of points (open squares) from unequal-division embryos fits 1.9706 (±0.0046), with a correlation coefficient of 0.9173; the lower plot of points (solid squares) from equal-division embryos fits 1.0472 (±0.0013), with a correlation coefficient of 0.933.

embryos. The constant relationship between PL + CD and AB volumes implies that the PL volume is a dynamic variable, as required for a cytoplasmic lobe undergoing active protrusion and resorption.

As first cleavage is completed in modern lobe-forming embryos, the neck of the PL rapidly increases in diameter, leading to the formation of a J-shaped embryo until the CD cell finally absorbs the PL. About 39 J-shaped lobe-forming embryos can be identified on the basis of fossil shape. These are represented mainly by two different groups related to equal (Fig. 2, I to K) and unequal trefoil embryos (Fig. 2V), respectively. The smallest among the three parts of each embryo typically represents the PL. It can also be recognized by the presence of the PL constriction (PLC), which is relatively deeper than the cleavage furrow (CF) (Fig. 2I). The fully protruded lobe (Fig. 2K) is nearly equal in size to the CD cell.

During second cleavage of modern lobe-forming embryos, the last phase of lobe protrusion leads to the formation of a five-lobed morphology, which comprises the first four blastomeres of equal or subequal size and a PL protruding from the D cell. About 17 embryos are recognized to be fossil representatives of such five-lobed embryos (Fig. 2, W to Z). The lobes in these embryos are mostly uncompacted and nearly equal, with the smallest one corresponding possibly to the PL.

Lobe formation and retraction constitutes a symmetry-breaking device for the segregation of polar material to only one blastomere, an alternative to asymmetric cleavage. This mechanism is used today in disparate groups of mollusks including polyplacophorans, gastropods, scaphopods, and bivalves (*14*, *20*–*22*), as well as a few types of annelids (*Chaetoplerus*) (*14*). The PL appears also in polyclad turbellarian flatworms (*Hoploplana inquilina*) (*23*, *24*), which are widely accepted as a basal group of spiralians. In spiralian embryogenesis, the constituents of PL are required for specification of mesodermal structures and secondarily of other embryonic parts that are induced by mesoderm (*15*). That is, the blastomeres that receive the PL cytoplasm become mesoderm founder cells.

These fossil embryos may not be spiralians or spiralian ancestors, and indeed none of the later cleavage forms that have been recovered in the same deposits convincingly display the characteristic patterns of spiral cleavage (*1*, *8*, *11*). The most widespread and basal mode of embryogenesis in bilaterians operates by means of cleavage stage specification of blastomere fate, followed immediately by establishment of differential gene expression in the cell lineages descendant from these blastomeres (*25*, *26*). The diverse territories of the embryo then soon express specific gene batteries generating a mosaic of differentiated cell types. This general mechanism is used in both direct and indirect developing bilaterian forms. PL formation is only one of a great variety of mechanisms whose essential function is the asymmetric delivery of maternal components of regulatory importance to specific blastomeres (*25*, *26*). In the case of the lobe-forming embryos studied here, the second cleavage lobe indicates that these embryos will specify one particular blastomere out of four that will be distinct in subsequent regulatory states. Only bilaterian embryos proceed in such a manner, but this is a typical bilaterian strategy of early development. Thus, these fossils imply that lobe formation is an ancient evolutionary device, and that the general strategy of precocious blastomere specification still used in most bilaterian groups was extant at least 40 million years before the Cambrian.

References and Notes

1. J.-Y. Chen, *The Dawn of Animal World* (Publishing House of Jiangsu Science & Technology, Nanjing, 2004).
2. X.-L. Yuan *et al.*, *Doushantuo Fossils: Life on the Eve of Animal Radiation* (Publishing House of Univ. of Science & Technology, Heifei, 2002).
3. D. Condon *et al.*, *Science* **308**, 95 (2005); published online 24 February 2005 (10.1126/science.1107765).
4. G. H. Barfod *et al.*, *Earth Planet. Sci. Lett.* **201**, 203 (2002).
5. C.-W. Li, J.-Y. Chen, T. Hua, *Science* **279**, 879 (1998).
6. J.-Y. Chen *et al.*, *Dev. Biol.* **248**, 182 (2002).
7. S. H. Xiao, X.-L. Yuan, A. H. Knoll, *Proc. Natl. Acad. Sci. U.S.A.* **97**, 13684 (2000).
8. J.-Y. Chen *et al.*, *Science* **305**, 218 (2004); published online 3 June 2004 (10.1126/science.1099213).
9. S. Bengtson, G. Budd, *Science* **306**, 1291a (2004).
10. J.-Y. Chen, P. Oliveri, E. Davidson, D. J. Bottjer, *Science* **306**, 1291b (2004).
11. J.-Y. Chen *et al.*, *Proc. Natl. Acad. Sci. U.S.A.* **97**, 4457 (2000).
12. S.-H. Xiao, Y. Zhang, A. H. Knoll, *Nature* **391**, 553 (1998).
13. S.-H. Xiao, A. H. Knoll, *J. Paleontol.* **74**, 767 (2000).
14. D. B. Conn, *Atlas of Invertebrate Reproduction and Development* (Wiley, Hoboken, NJ, ed. 2, 2000).
15. S. F. Gilbert, A. M. Raunio, Eds., *Embryology: Constructing the Organism* (Sinauer, Sunderland, MA, 1997).
16. G. W. Conrad *et al.*, *J. Cell Biol.* **59**, 228 (1979).
17. E. W. MacBride, *Text-Book of Embryology* (Macmillan, London, 1914).
18. L. W. Browder, C. A. Erickson, W. R. Jeffery, *Developmental Biology* (Saunders, Philadelphia, ed. 3, 1991).
19. See supplementary material on *Science* Online. The cleavage cells and the PLs in these embryos are either spherical or in compacted spherical form. The compacted form is regularly rounded in top view but has a relatively shorter radius in the distal-proximal direction. Cleavage cell and PL volumes were calculated as $^4/_3\pi R^3$ in spherical forms (R, radius) and as $^4/_3\pi R_1^2 R_2$ in compacted forms (R_1, noncompacted radius; R_2, compacted radius). The volumetric data of the embryos examined with SR-μCT (Fig. 2, B and I) were calculated precisely from the pixel number; each pixel bears a volume of 0.343 μm^3.
20. A. C. Giese, J. S. Pearse, Eds., *Reproduction of Marine Invertebrates: Molluscs: Gastropods and Cephalopods* (Academic Press, New York, 1977).
21. A. C. Giese, J. S. Pearse, Eds., *Reproduction of Marine Invertebrates: Molluscs: Pelecypods and Lesser Classes* (Academic Press, New York, 1979).
22. A. S. Tompa, N. H. Verdonk, J. van den Biggelaar, Eds., *The Mollusca: Reproduction* (Academic Press, New York, 1984).
23. B. C. Boyer, *Int. J. Invertebr. Reprod. Dev.* **9**, 243 (1986).
24. B. C. Boyer, *Int. J. Invertebr. Reprod. Dev.* **13**, 157 (1988).
25. E. H. Davidson, *Gene Activity in Early Development* (Academic Press, Orlando, FL, 1986).
26. E. H. Davidson, *Genomic Regulatory Systems: Development and Evolution* (Academic Press, San Diego, CA, 2001).

27. Supported by Chinese Academy of Science grant KZCX3-SW-141; National Science Foundation of China grants 42432006, 40302004, 10490190, 60172042, and 10490194; 111 Project and 985-2 Project of Nanjing University, LPS of Nanjing Institute of Geology & Paleontology, NASA/Ames grant NAG2-1541, and an NSC grant. We thank the European Synchrotron Radiation Facility, Taiwan NSRRC, and Beijing Synchrotron Radiation Facility and Photon Factory for provision of synchrotron radiation facilities.

Supporting Online Material

www.sciencemag.org/cgi/content/full/312/5780/1644/DC1
Fig. S1

8 February 2006; accepted 27 April 2006
10.1126/science.1125964

Element Partitioning: The Role of Melt Structure and Composition

M. W. Schmidt,[1]* J. A. D. Connolly,[1] D. Günther,[2] M. Bogaerts[1]

We segregated coexisting gabbroic and granitic melts by centrifuging them at high pressures and temperatures and measured the trace element compositions of the melts by laser ablation inductively coupled plasma mass spectrometry. Our results demonstrate that the effect of melt structure contributes about one order of magnitude to crystal/melt partition coefficients. Partitioning of alkali and alkaline earth elements strongly depends on field strength: Amphoteric and lone pair electron elements partition into the polymerized granitic melt; and rare earth, transition, and high field strength elements coordinated by nonbridging oxygens partition remarkably similar into the gabbroic melt. A regular solution model predicts these effects.

Element partitioning between magmas and crystals is essential to the differentiation of the Earth. Early work on trace element partitioning related mineral/melt partition coefficients, $D^{crystal/melt}$, to the relative ionic radii of the trace and major elements (*1*, *2*) and to melt composition (*3*, *4*). The melt compositional term was simplified by normalizing to the partitioning of a major cation (*3*). By ascribing ideal mixing to the mineral component, which

expresses the behavior of the major cation in the melt, trace element partitioning can be formulated in terms of the lattice strain model (*2*, *5*). This model defines a parabolic relationship between cation radius and partition coefficients that is specified by the effective Young's modulus, E, the partition coefficient, D_0, and the cation radius, r_0, relevant to the strain-free state. Although D_0 is dependent on melt composition, melt composition itself is not an explicit variable. Attempts to explicitly include melt composition in the lattice strain model were limited to specific compositional parameters such as H_2O content (*6*) and Fe/Mg ratio (*7*). Studies of coexisting silicate melts (*8*, *9*) and mineral-melt systems suggest a strong dependence of crystal-melt partitioning on melt composition (*10*–*15*), but a general model for this dependence remains to be formulated.

In this study, we investigated partitioning of 45 elements between coexisting gabbroic and granitic K_2O-FeO-Al_2O_3-SiO_2 melts (*16*, *17*) to isolate the effect of melt composition and structure from crystallographic effects. We used an experimental apparatus consisting of a piston cylinder mounted in a centrifuge that can achieve pressure and temperature conditions of 1.8 GPa and 1600°C, respectively, under an acceleration of 3000 g. Centrifuging is necessary to segregate coexisting silicate melts into pools large enough for measurement by laser ablation techniques, which permit simultaneous measurement of a large number of elements at trace-level concentrations [<200 parts per million (ppm)]. The centrifuging piston cylinder itself consists of a 42-kg integrated single-stage piston cylinder (*18*) with a 14-mm bore and 36-mm furnace length, allowing for capsules with an outer diameter of 4 mm and a length of 6 mm. The piston cylinder is mounted on a rotating 860-kg table with a 1.4-m diameter. With the sample at a radius of 32 cm, maximal acceleration of 3000 g is reached at 2850 revolutions per minute (rpm); at this frequency, the outer table rim travels at 753 km hour^{-1}.

Our experiments consisted of two steps: chemical equilibration (*19*) at the temperatures and pressures of interest (1100° to 1240°C and 0.3 to 0.7 GPa) at static conditions for 12 to 24 hours and physical segregation of the equilibrated melts by centrifuging for 3 to 14 hours at 600 to 1000 g. The experiments generated coexisting granitic and ferrogabbroic melts (Table 1). Additionally quartz, fayalite, or wuestite were sometimes present depending on composition and physical conditions. Centrifuging at 1000 g for >8 hours completely separated the melts (Fig. 1A) when crystals were absent; calculated density (*20*) differences between coexisting melts ranged from 0.45 to 0.95 g cm^{-3}. In experiments at 600 to 800 g, a segregated gabbroic melt layer formed (Fig. 1B) with occasional quench fayalite or homogeneously distributed quench microdroplets (≤0.5 μm). In these experiments, the granitic melt, which is free of quench phases, contained quartz and gabbroic blobs, but blob- and quartz-free areas were large enough (up to 100 μm diameter) for laser ablation techniques. Large-diameter microprobe (10 μm) and laser ablation inductively coupled plasma mass spectrometry (LA-ICP-MS) analyses [20 to 40 μm spot size (*18*)] yielded homogeneous major and trace element compositions for the segregated gabbro and granite. In contrast, droplets that had not been segregated were heterogeneous (Fig. 1C) and composed of zones of internal droplets, fayalite needles with typical quench textures, and in some samples wuestite or Cr spinel. The internal droplets were <1 μm in size and may represent equilibrium inclusions of granitic melt or melt that exsolved during quenching.

The temperature range for segregation is limited by the critical temperature of the solvus at ~1200°C (*21*) and by abundant crystallization of fayalite and quartz at ≤1130°C. Although melt compositions that may be investigated are restricted to those on the miscibility gap, our melts are good proxies for gabbroic- and dacitic-to-granitic melts (Table 1). The network modifier Fe^{2+} in our synthetic system is an analog for the network modifiers Mg^+ Ca^+ Fe^{2+} in natural melts. Our experimental design ensures that all Fe is present as ferrous iron (*18*), thereby eliminating uncertainties that might arise from the presence of ferric iron, a network former. Trace elements are assumed to be present predominantly in their reduced form (i.e., Mn^{2+}, V^{3+} and V^{4+}, $Cr^{2+} > Cr^{3+}$, $Mo^{4+} > Mo^{5+}$, Sn^{2+}, Pb^{2+}, Ga^{3+}, As^{3+}, and Sb^{3+}).

The measured partition coefficients span two orders of magnitude (Fig. 2). Most amphoteric elements and heavy alkalis partition into the polymerized melt, with the lowest partition coefficient, $D^{gabbro/granite}$, values near 10^{-1} (Cs, As, and Pb). Most other metal cations concentrate in the depolymerized gabbroic melt, with the highest $D^{gabbro/granite}$ above 10 [rare earth elements (REE), U, and P]. On the basis of partitioning behavior, three groups of elements can be distinguished: (i) Alkalis and earth alkalis (except Mg), which have the lowest Pauling electronegativities (*22*) and field strengths (*23*, *24*) of all elements investigated and form dominantly ionic bonds. This group shows a strong increase in $D^{gabbro/granite}$ with an increase

Table 1. Melt composition and polymerization of coexisting melts and comparison to natural melts. Z10 and Z18a represent the maximum and minimum width of the immiscibility gap at which segregation was achieved. Z10 pressure and temperature values were 0.7 GPa and 1180°C, respectively; for Z18a, they were 0.35 GPa and 1150°C. The difference in polymerization for the melt-pair of Z10 is similar to that of a primitive basaltic and a dacitic melt. The magnitude of D values measured in this study is thus representative of the span of melt compositions as to be expected in natural fractionation processes. NBO/T polymerization calculated after (*27*). x(NBO) is the molar fraction of nonbridging oxygens. x_{MO_n} is the molar fraction of major network-modifying component MO_n in our model. Picritic basalt is a representative for typical weakly polymerized mantle melt (*33*), whereas average granite is a representative for highly polymerized crustal melt (*34*). Dashed entry indicates oxide component is not present.

	Z10		Z18a		Natural picrobasalt	Natural alkaligranite
	Gabbroic	Granitic	Gabbroic	Granitic		
SiO_2	37.1	72.2	48.5	67.0	48.9	70.13
TiO_2	0.95	0.19	—	—	0.50	0.30
Al_2O_3	3.57	8.00	3.50	5.83	11.40	7.97
Fe_2O_3	—	—	—	—	1.3	2.77
FeO	51.4	11.5	45.0	21.1	8.8	5.27
MgO	—	—	—	—	14.7	0.07
CaO	—	—	—	—	10.3	0.55
Na_2O	—	—	—	—	1.84	7.46
K_2O	1.66	7.40	2.72	5.83	1.18	4.24
P_2O_5	1.77	0.21	0.10	0.03	0.25	0.26
Si*	2.236	3.320	2.719	3.234	2.392	3.239
$\Sigma(Fe^{3+} + Al)$*	0.254	0.433	0.231	0.332	0.705	0.495
$\Sigma(M^{2+})$*	2.594	0.442	2.107	0.852	1.979	0.278
$\Sigma(K+Na)$*	0.128	0.435	0.195	0.340	0.248	0.917
NBO/T	2.246	0.252	1.416	0.485	1.146	0.271
x(NBO)	0.699	0.118	0.522	0.216	0.443	0.127
x_{MO_n}	0.745	0.307	0.723	0.479	0.721	0.233
$x_{(NBO)}^{gabbro}/x_{(NBO)}^{granite}$	4.23		2.137		4.80	

*Atoms per eight oxygens.

[1]Institut für Mineralogie und Petrologie, Department of Earth Sciences, [2]Department of Chemistry, Eidgenössische Technische Hochschule (ETH), 8092 Zürich, Switzerland.

*To whom correspondence should be addressed. E-mail: max.schmidt@erdw.ethz.ch

in electronegativity, field strength, or ionization potential ($D_{Cs} < D_{Rb} < D_K < D_{Na} < D_{Li} < D_{Ba} < D_{Sr} < D_{Ca}$), with Cs through Na partitioning into the polymerized melt. (ii) Amphoteric and lone electron pair elements (Ga, Ge, Sn^{2+}, Pb^{2+}, As^{3+}, Sb^{3+}, and Bi^{3+}) with electronegativities of 1.8 to 2.2. This group, which also includes Si and Al, substitutes into network-forming tetrahedra or has oxygen coordination numbers ≤ 4 (table S1) and partitions into the polymerized melt. (iii) RE, transition, and high field strength elements partitioning into the depolymerized melt with surprisingly uniform $D^{gabbro/granite}$ values (Fig. 2). Members of this group (Mg, Mn, Co, REE, Y, Sc, Ti, Th, U, Zr, Hf, V, Mo, and P) have coordination numbers ≥ 5 (table S1) except for Mo^{5+} and P^{5+}, which are predominantly fourfold coordinated but have two shells of nonbridging oxygens (NBOs) (*25*, *26*), explaining their strong partitioning into the depolymerized melt. Among NBO-coordinated elements, rare earths exhibit the highest affinity for the depolymerized melt, and Zn, Zr, and Hf exhibit the lowest. REE have the highest (six- or sevenfold), and the mildly amphoteric element Zn the lowest, oxygen coordination numbers (fourfold), suggesting that coordination number influences partitioning behavior. Although the partitioning for the NBO-coordinated elements is similar, differences in geochemically similar elements such as Nb-Ta and Zr-Hf are systematic (Figs. 2 and 3B), elements with higher electronegativities exhibiting a preference for the depolymerized melt. The differences in Nb-Ta and Zr-Hf partitioning can cause relative enrichments, by fractionation, within these pairs by a factor of up to 1.6, an effect that would be substantial in geochemical modeling (*11*, *13*, *14*).

The partitioning behavior of the three element groups is explained by the different oxygen bonding environments in silicate melts (*27*). Bridging oxygens (BOs) shared by two network forming tetrahedra constitute the network of tetrahedrally coordinated cation sites occupied by Si and Al. Both Si and Al concentrate in the granitic melt, and elements coordinated by tetrahedral oxygens are consequently also concentrated into the granitic melt. Among these, Ga^{3+} has the highest $D^{gabbro/granite}$, reflecting its relatively large ionic radius and its presence in both four- and sixfold coordination. Oxygens belonging to tetrahedra occupied by Al are charge-deficient and obtain charge compensation through alkalis and, to a lesser extent, by earth alkalis. Our data demonstrate that the elements with the highest degree of ionic bonding are preferred for this charge-compensating role. The affinity within the alkali and earth alkali groups for the depolymerized melt increases regularly with decreasing atomic number and radius. For these two groups, the effect of melt composition influences both the position and shape of the lattice strain parabola. The largest divalent cations, Ba and Pb, have, for different reasons, the lowest $D^{gabbro/granite}$ with respect to other divalent cations. Because of their extreme size, these elements exert a strong influence on the definition of the divalent cation lattice strain parabola. Apart from the alkalis and alkalis earth, coordination with charge-deficient tetrahedral oxygens may also influence the behavior of amphoteric elements Pb^{2+}, Sn^{2+}, As^{3+}, and Sb^{3+}, contributing to their preference for the polymerized melt. Lastly, the third group of elements, with oxygen coordination numbers ≥ 4 and that partition into the depolymerized melt, is controlled by the abundance of nonbridging oxygens, which permit cations to form their preferred coordination polyhedra. Field strength does not play an important role for the elements partitioning into NBO-coordinated sites, in contrast to interpretations from early melt-melt partitioning studies (*8*, *9*) but in agreement with the data on the limited number of elements that were measured in both earlier data sets.

Values of the partition coefficients depend on the solvus width. Previous descriptions of melt-melt element partitioning used a two-

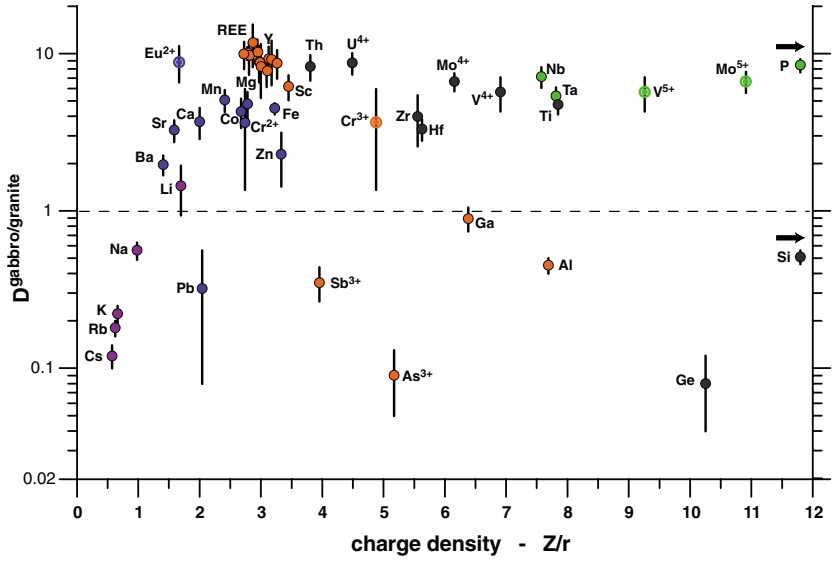

Fig. 2. Nernst partition coefficients, $D^{gabbro/granite}$, between gabbroic and granitic melt versus field strength (*Z*/*r*) for the experiment at 1180°C and 0.7 GPa (Z10). P (*Z*/*r* = 34.6) and Si (*Z*/*r* = 15.4) are off the scale. Cations that may have two major oxidation states are given with both values; the predominant oxidation state has a solid symbol.

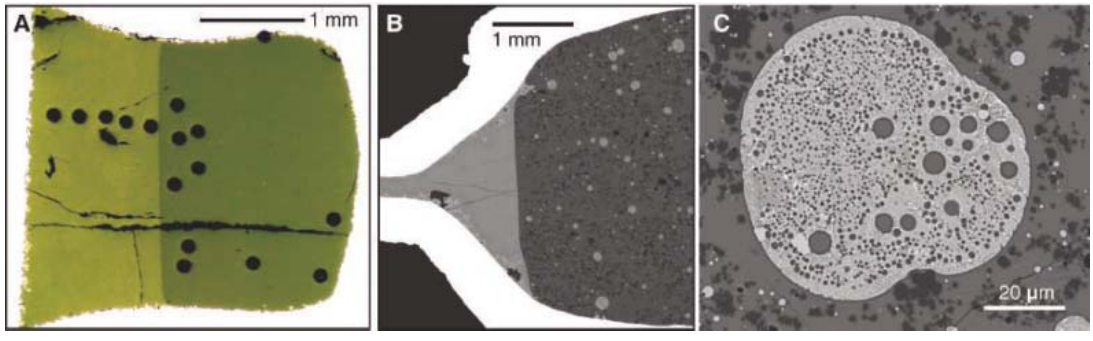

Fig. 1. Textures of segregated and nonsegregated coexisting silicate melts. (**A**) Full segregation at 1150°C, 0.3 GPa, 12 hours static, and 9 hours at 1000 g (Z18a) for Mo in Pt double capsule. The bright left side is Fe-rich gabbroic, the dark side granitic melt. (**B**) Partial segregation at 1180°C, 0.7 GPa, 12 hours static, and 3 hours at 900 g (Z10) for AuPd capsule. Droplets of gabbroic melt are present in the granitic matrix. Black crystals are quartz; bright crystals in gabbro, wuestite [also in (C)]. (**C**) Unsegregated composite droplet of gabbroic melt from a static experiment (1140°C, 0.7 GPa, and 12 hours). The droplet has two generations of internal granitic droplets. Most of the droplet is composed by fayalite quench crystals; to the left, it has a single small homogeneous area of gabbroic melt.

lattice site model (*8*, *28*), in which major cations are replaced by trace cations in a tetrahedral network-forming site or in a cation site coordinated by NBOs. This model precludes mixing between the two lattices and thus fails to explain the dependence of partition coefficients on the composition of melt pairs (*28*). Therefore, to rationalize and extrapolate the observed trace element partitioning, we formulate a model (*18*) for the melts as a mixture of a major network-modifying component, MO_n, a trace network-modifying component, BO_m, and a major polymerized component, C_oO_p. Melt excess energy is included at lowest order approximation (regular binary interactions). For our experimental system, MO_n is identified with FeO, whereas C_oO_p is taken to be a combination of $KAlO_2$ and SiO_2 so as to satisfy mass balance constraints. Optimization of the stoichiometric factor p to match the solvus symmetry required by the regular solution model yields a value of 5.96 ± 0.05, approximated here as $p = 6$. Assuming excess energy arises only through the interaction of the network-modifying components with the polymerized component, the molar trace element partition coefficient is

$$Q_{BO_m}^{\text{gabbro/granite}} = \exp\left[\left(1 - 2x_{MO_n}^{\text{granite}}\right) W'_{BO_m\text{-}C_oO_p}\right] \quad (1)$$

where $x_{MO_n}^{\text{granite}}$ is the mole fraction of MO_n in the granitic melt and $W'_{BO_m\text{-}C_oO_p} = W_{BO_m\text{-}C_oO_p}/RT$ is the dimensionless interaction parameter for BO_m-C_oO_p melt (*18*). The parameter $W'_{BO_m\text{-}C_oO_p}$ can be expressed in a more physically meaningful way as $W'_{BO_m\text{-}C_oO_p} = 2/T'_{BO_m\text{-}C_oO_p}$, where $T'_{BO_m\text{-}C_oO_p}$ is the homologous temperature measured relative to the critical temperature of the BO_m-C_oO_p solvus. Thus, Eq. 1 predicts trace element partitioning as a function of $T'_{BO_m\text{-}C_oO_p}$ and major element chemistry. The $x_{MO_n}^{\text{granite}}$-$Q_{BO_m}$ trends calculated from the mean BO_m-C_oO_p critical temperatures inferred from Eq. 1 are consistent with the experimental trends (Fig. 3A), confirming the model dependence of trace element partition coefficients on the width of the miscibility gap. Additionally, the inferred BO_m-C_oO_p critical temperatures are comparable to, but less than those of, the BO_m-SiO_2 solvii, a result consistent with the expectation that alumina in the C_oO_p component increases melt miscibility.

The effect of melt composition on trace element crystal-melt distribution predicted by the lattice strain model can be assessed by considering a generalized exchange reaction

$$BO_m + \text{M crystal} = \frac{m}{n}MO_n + \text{B crystal} \quad (2)$$

where M and B crystal represent the pure major and trace element limiting compositions of the crystalline phase, chosen so that a formula unit of pure B crystal contains 1 mol of B. In the context of our model (*18*), the trace element distribution coefficient is

$$Q_{BO_m}^{\text{crystal/melt}} = a_{\text{M-crystal}} \frac{\gamma_{BO_m}}{a_{MO_n}^{m/n}} \exp\left(-\frac{\Delta G_{\text{strain}}}{RT}\right) \quad (3)$$

where a_i and γ_i denote the thermodynamic activity and the activity coefficient, respectively, of species i and ΔG_{strain} is derived from the lattice strain model (*5*, *7*). The second factor in Eq. 3 is the correction to the lattice strain model due to melt chemistry (Fig. 3C) and is expressed in terms of major element chemistry as

$$\frac{\gamma_{BO_m}}{a_{MO_n}^{m/n}} = \exp\left[(1 - x_{MO_n})\left\{W'_{BO_m\text{-}C_oO_p} - W'_{MO_n\text{-}C_oO_p}\left[(1 - x_{MO_n})\frac{m}{n} + x_{MO_n}\right]\right\}\right] / x_{MO_n}^{m/n} \quad (4)$$

where $W'_{MO_n\text{-}C_oO_p}$ and $W'_{BO_m\text{-}C_oO_p}$ are known functions of the experimental observables $x_{MO_n}^{\text{granite}}$ and $Q_{BO_m}^{\text{gabbro/granite}}$. Taking x_{MO_n} as a proxy for the NBO/T ratio of silicate melts (Fig. 3) and noting that the nonlinearity arising from $m \neq n$ is weak for the oxides of interest, Eq. 4 implies, in the ideal limit and the limits $x_{MO_n} \to 0$ and $x_{MO_n} \to 1$, that the correction factor for melt composition is $x_{MO_n}^{-m/n}$ and that the correction factor will usually be less than the ideal value if $W'_{MO_n\text{-}C_oO_p} > W'_{BO_m\text{-}C_oO_p}$ (i.e., if BO_m partitions less strongly than MO_n into the more polymerized melt). Thus, although melt composition can cause a 10-fold increase in partition coefficients [e.g., Zr and Hf (Fig. 3C)], nonideality can also lead to situations in which the uncorrected lattice strain model is valid over most of the range of natural melt compositions [e.g., Zn (Fig. 3C)].

In our model, partition coefficients depend on the width of the MO_n-C_oO_p solvus and the BO_m-C_oO_p solvus critical temperature. Certain minor elements, notably P and Ti, increase the width of silicate liquid solvi (*8*, *29*) but are not explicitly accounted for in the model. The model

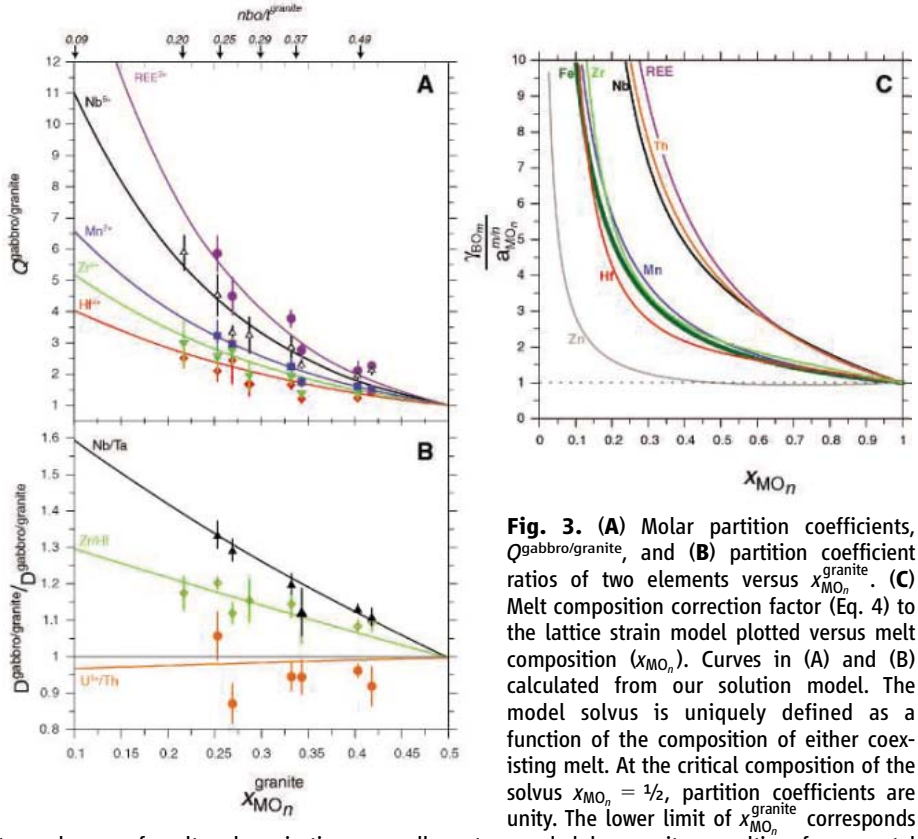

Fig. 3. (**A**) Molar partition coefficients, $Q^{\text{gabbro/granite}}$, and (**B**) partition coefficient ratios of two elements versus $x_{MO_n}^{\text{granite}}$. (**C**) Melt composition correction factor (Eq. 4) to the lattice strain model plotted versus melt composition (x_{MO_n}). Curves in (A) and (B) calculated from our solution model. The model solvus is uniquely defined as a function of the composition of either coexisting melt. At the critical composition of the solvus $x_{MO_n} = ½$, partition coefficients are unity. The lower limit of $x_{MO_n}^{\text{granite}}$ corresponds to a degree of melt polymerization normally not exceeded by granites resulting from crystal fractionation processes. Thus, intercept values for partition coefficients on the vertical axis represent the maximum effect of melt composition during magma crystallization processes, reaching $Q_{REE}^{\text{granite/gabbro}} = 16.4$ for REE, which corresponds to $D_{REE}^{\text{granite/gabbro}} \approx 30$. Significant fractionation between the geochemical pairs Nb/Ta and Zr/Hf is obtained as a function of melt composition, but not for other pairs such as U^{4+}/Th. The values plotted along the upper axis are melt polymerization as expressed by the commonly used fraction of nonbridging oxygens over tetrahedra (NBO/T) in the granite, calculated after (*27*). Natural melt compositions (x_{MO_n}) in fractionation and partial melting processes are in the range from 0.1 to 0.7.

reproduces the observed distribution coefficients in both P-rich and P-poor experiments. This behavior implies that phosphorous, at least at geologically relevant concentration levels, does not influence partition coefficients through complexing with trace cations, as proposed by (*28*), but rather influences partitioning indirectly by affecting NBO/BO ratios. Specifically, elements such as P with high coordination numbers lower the melt NBO/BO ratio and decrease the configurational entropy of the melt, an effect that widens the MO_n-C_oO_p solvus and increases melt-melt partition coefficients. Within the di- and trivalent cations, such a tendency is observable in our data; i.e., partition coefficients decrease with decreasing coordination number.

Our data imply that a significant change in the shape of the lattice-strain model parabola will result for the alkalis. To quantify this effect, we used data sets of $D^{cpx/basalt}$ (*30*, *31*) for basalts analogous to the gabbroic melt of experiment Z10 and combine $D^{cpx/basalt}$ with our $D^{basalt/granite}$. The site parameters for monovalent cations calculated from $D^{cpx/granite}$ with respect to $D^{cpx/basalt}$ are characterized by a Young's modulus decreased by 16 to 35% and by a strain-free partition coefficient D_0 increased by a factor of 2. This softening of the site is attributed to the effect of melt composition. For the cations coordinated to NBOs, the effect of melt composition will increase $D^{crystal/melt}$, D_o, and hence the position of the parabola with respect to the D coordinate (*1*, *5*) by one order of magnitude when changing from basaltic to granitic melt compositions. This effect acts in concert with the changes in crystal composition that occur as a consequence of the change in melt composition. Melt composition will play a key role for elements whose crystal/melt partition coefficients are close to unity, because they may change from compatible to incompatible as a function of melt composition. Because of the relative uniformity of partition coefficients for traces of Ca, Mg, RE, transition, and high field strength elements, melt composition does not strongly affect the relative partition coefficients of these elements. The latter are in general well characterized by models describing relative crystal-melt partition coefficients solely in terms of crystal lattice strain, but to quantify individual partition coefficients an explicit melt compositional term such as in Eq. 4 is necessary. Gross exceptions to the above generality are Pb (Fig. 2), for which $D^{gabbro/granite}$ is as much as two orders of magnitude different from other divalent cations, and to a lesser extent Ba, Zn, and Sn. Among the NBO-coordinated cations, variations of $D^{basalt/granite}$ up to a factor of 2 exist, a nonnegligible effect in the context of geochemical melting models.

References and Notes

1. N. Onuma, H. Higuchi, H. Wakita, H. Nagasawa, *Earth Planet. Sci. Lett.* **5**, 47 (1968).
2. J. C. Brice, *J. Cryst. Growth* **28**, 249 (1975).
3. S. Banno, Y. Matsui, *Chem. Geol.* **11**, 1 (1973).
4. M. J. Drake, D. F. Weill, *Geochim. Cosmochim. Acta* **39**, 689 (1975).
5. J. D. Blundy, B. J. Wood, *Nature* **372**, 452 (1994).
6. B. J. Wood, J. D. Blundy, *Geochim. Cosmochim. Acta* **66**, 3647 (2002).
7. B. J. Wood, J. D. Blundy, *Contrib. Mineral. Petrol.* **129**, 166 (1997).
8. E. B. Watson, *Contrib. Mineral. Petrol.* **56**, 119 (1976).
9. F. J. Ryerson, P. C. Hess, *Geochim. Cosmochim. Acta* **42**, 921 (1978).
10. B. O. Mysen, D. Virgo, *Geochim. Cosmochim. Acta* **44**, 1917 (1980).
11. R. L. Linnen, H. Keppler, *Geochim. Cosmochim. Acta* **66**, 3293 (2002).
12. B. O. Mysen, E. V. Dubinsky, *Geochim. Cosmochim. Acta* **68**, 1617 (2004).
13. M. W. Schmidt, A. Dardon, G. Chazot, R. Vannucci, *Earth Planet. Sci. Lett.* **226**, 415 (2004).
14. S. Klemme, S. Prowatke, K. Hametner, D. Günther, *Geochim. Cosmochim. Acta* **69**, 2361 (2005).
15. I. V. Veksler, C. Petibon, G. A. Jenner, A. M. Dorfman, D. B. Dingwell, *J. Petrol.* **39**, 2095 (1998).
16. E. Roedder, *Geochim. Cosmochim. Acta* **42**, 1597 (1978).
17. W. Visser, A. F. K. VanGroos, *Am. J. Sci.* **279**, 70 (1979).
18. Material and methods are available as supporting material on *Science* Online.
19. Previous studies (*8*, *9*) have shown that 14 hours are sufficient to reach chemical equilibrium in this temperature range; we thus generally doubled this run time.
20. R. L. Lange, I. S. E. Carmicheal, *Rev. Mineral.* **24**, 25 (1990).
21. At 1180°C, the two melts have SiO_2 contents of 72.2 and 37.1 weight %; at 1210°C, the immiscibility gap is closed, which is in excellent agreement with (*16*, *17*).
22. Electronegativities are from (*32*).
23. R. D. Shannon, *Acta Cryst.* **A32**, 751 (1976).
24. Ionic radii are those for the dominant coordination number as listed in table S1.
25. L. Galoisy *et al.*, *Mineral. Mag.* **64**, 409 (2000).
26. F. J. Ryerson, P. C. Hess, *Geochim. Cosmochim. Acta* **44**, 611 (1980).
27. B. O. Mysen, *Structures and Properties of Silicate Melts,* vol. 4 of *Developments in Geochemistry* (Elsevier, Amsterdam, 1988).
28. A. J. G. Ellison, P. C. Hess, *Geochim. Cosmochim. Acta* **53**, 1965 (1989).
29. W. Visser, A. F. K. VanGroos, *Am. J. Sci.* **279**, 970 (1979).
30. J. D. Blundy, J. Dalton, *Contrib. Mineral. Petrol.* **139**, 356 (2000).
31. R. A. Brooker *et al.*, *Nature* **423**, 738 (2003).
32. R. D. Lide, Ed., *The Handbook of Chemistry and Physics* (CRC Press, Boca Raton, FL, ed. 85, 2005), table 9-74.
33. W. R. H. Ramsey, A. J. Crawford, J. D. Fodon, *Contrib. Mineral. Petrol.* **88**, 386 (1984).
34. H. Sorenson, Ed., *The Alkaline Rocks* (Wiley, Letchworth, UK, 1974), p. 117.

35. We thank N. Baker from *g-max* for building the centrifuge and K. Hametner for help with the LA-ICP-MS analyses. M.W.S. acknowledges Swiss National Science Foundation grant no. 2-77182-02 for financing part of the centrifuge.

Supporting Online Material

www.sciencemag.org/cgi/content/full/312/5780/1646/DC1
Materials and Methods
SOM Text
Table S1
References

24 February 2006; accepted 25 April 2006
10.1126/science.1126690

p53 Regulates Mitochondrial Respiration

Satoaki Matoba,[1] Ju-Gyeong Kang,[1] Willmar D. Patino,[1] Andrew Wragg,[1] Manfred Boehm,[1] Oksana Gavrilova,[2] Paula J. Hurley,[3] Fred Bunz,[3] Paul M. Hwang[1]*

The energy that sustains cancer cells is derived preferentially from glycolysis. This metabolic change, the Warburg effect, was one of the first alterations in cancer cells recognized as conferring a survival advantage. Here, we show that p53, one of the most frequently mutated genes in cancers, modulates the balance between the utilization of respiratory and glycolytic pathways. We identify Synthesis of Cytochrome c Oxidase 2 (SCO2) as the downstream mediator of this effect in mice and human cancer cell lines. SCO2 is critical for regulating the cytochrome c oxidase (COX) complex, the major site of oxygen utilization in the eukaryotic cell. Disruption of the *SCO2* gene in human cancer cells with wild-type p53 recapitulated the metabolic switch toward glycolysis that is exhibited by p53-deficient cells. That SCO2 couples p53 to mitochondrial respiration provides a possible explanation for the Warburg effect and offers new clues as to how p53 might affect aging and metabolism.

Cancer is a genetic disease caused by the dysregulation of various cellular pathways that orchestrate cell growth and death (*1*). It is clear that some of these pathways must modulate cellular metabolism. As described by Otto Warburg in 1931, cancer cells preferentially utilize glycolytic pathways for energy generation while down-regulating their aerobic respiratory activity (*2*). A number of mechanisms have been proposed to explain the Warburg effect (*3*–*7*), but there have not been any reports of a genetically defined pathway that couples a tumor suppressor gene to mitochondrial aerobic respiration.

Critical to aerobic life is the cytochrome c oxidase (COX) complex in the mitochondrion, where most of the molecular oxygen is consumed in the eukaryotic cell. In cancer cells mitochondrial respiratory activity is decreased in association with changes in the expression levels of COX complex subunit proteins, but the genetic mechanisms that underlie their modulation are unclear (*8*, *9*). We reasoned that because the metabolic alterations of cancer cells are

so widespread, an explanation for this phenomenon must lie, at least in part, in a pathway that is commonly altered in cancer cells. We therefore examined whether alteration of p53, the gene most commonly mutated in human cancer, might affect COX complex assembly and activity.

Aerobic respiration was assessed in liver mitochondria preparations from mice with wild-type (+/+), heterozygous (+/−), or homozygous (−/−) disruption of *TP53*. There was a significant decrease in oxygen consumption that closely correlated with p53 deficiency ($p53^{+/+}$ versus $p53^{-/-}$, $P < 0.001$) (Fig. 1A). We confirmed a similar p53-dependent reduction (~25%) in cellular oxygen consumption using isogenic human colon cancer HCT116 cells with a targeted disruption of *TP53* (Fig. 1A) (*10*). Direct measurement of COX enzymatic activity showed a comparable reduction of 25 ± 3% in the $p53^{-/-}$ cells (fig. S1). To estimate the relative contributions of glycolysis and aerobic respiration, we calculated total adenosine 5′-triphosphate (ATP) generated by measuring whole-cell lactate production and oxygen consumption, respectively (*11*). The total amount of ATP measured was similar in all three genotypes, but the p53-deficient cells produced significantly higher levels of lactate, indicating a change in the mode of energy production to one favoring glycolysis (Fig. 1B). The ratio of ATP produced by glycolysis versus ATP produced by aerobic respiration increased with p53 deficiency: $p53^{+/+}$, 0.81 ± 0.12; $p53^{+/-}$, 1.04 ± 0.20; and $p53^{-/-}$, 1.72 ± 0.16 (Fig. 1B).

Our results indicated that $p53^{-/-}$ mice exhibit decreased mitochondrial respiration, which could translate into a decrease in functional aerobic capacity. The general appearance and behavior of $p53^{+/+}$ and $p53^{-/-}$ mice were indistinguishable, as previously observed (*12*), and their body mass and composition were essentially identical (Fig. 1C). However, the endurance of $p53^{-/-}$ mice was reduced, as measured by a swimming stress test (Fig. 1D) (*13*).

Because p53 is a transcriptional activator, we reasoned that a gene regulated by p53 might mediate this effect on mitochondrial respiration. We examined a serial analysis of gene expression (SAGE) database of potential p53 target genes (*14*) that may influence mitochondrial function. SCO2 (Synthesis of Cytochrome c Oxidase 2) was induced in a p53-dependent manner in HCT116 cells, as evidenced by a ninefold increase in transcripts. On the basis of more recent genetic and biochemical studies (*15*, *16*), we reasoned that SCO2 could potentially mediate the effect of p53 on aerobic respiration. SCO2 is required for the assembly of mitochondrial DNA-encoded COX II subunit (*MTCO2* gene) into the COX complex, and inactivating mutations of this gene in humans result in fatal cardioencephalomyopathy due to aerobic respiratory failure (*17*).

To confirm that SCO2 transcription is directly transactivated by p53, we used human colon cancer DLD1 cell lines with either inducible wild-type (WT) or mutant (MUT) p53 for expression studies (*18*). SCO2 mRNA expression increased within 3 to 18 hours of induced WT p53 expression but was not affected by mutant p53 (Fig. 2A and fig. S2). We also measured the mRNA expression level of SCO1, another COX assembly factor. SCO1 mRNA expression remained unchanged with induced p53 expression, serving as a negative control and demonstrating the specificity of the observed SCO2 mRNA increase (Fig. 2A).

The time course of SCO2 transcription and the presence of p53 DNA-binding consensus sequence in intron 1 (−322 to –302 from the start codon) suggested that SCO2 may be directly transactivated by p53. We tested this hypothesis by cloning a ~1.1-kb fragment of the SCO2 gene containing the p53-binding sequence into a luciferase reporter plasmid. To control for the nonspecific effects of endogenous p53, we used the $p53^{-/-}$ HCT116 cell line to express the reporter and exogenous p53 plasmids. As predicted for a specific p53 binding site, we observed increases in luciferase activity that were dependent on the dose of exogenous WT p53 (pCMV-p53) but not mutant p53 (pCMV-p53mt135) (Fig. 2B). When the p53 binding sequence in the reporter construct was mutated, the transcriptional activation by exogenous WT p53 was abrogated, establishing its in vitro specificity (Fig. 2B).

Antibodies against SCO2 were generated and used to determine the expression of SCO2. SCO2 protein expression decreased in both p53-deficient mouse liver mitochondria and human cell lines, whereas the amount of mitochondrial anion transporter (voltage-dependent anion channel, or VDAC) remained constant (Fig. 2C). Although p53 transactivates SCO2, the amounts of SCO2 protein detected in the $p53^{-/-}$ mice and human cells indicate that p53-independent pathways exist for its regulation, as is the case for other p53-target genes (Fig. 2C) (*19*). In contrast to SCO2 expression, the level of SCO1 protein was unaffected by p53 genotype status, consistent with transcriptional data (Fig. 2C and fig. S2). These results suggested a direct interaction between p53 and SCO2 to regulate mitochondrial aerobic respiration.

Expression of WT SCO2 cDNA in $p53^{-/-}$ HCT116 cells increased mitochondrial oxygen consumption within 48 hours in a dose-dependent manner (Fig. 3A). The amount of SCO2 protein needed to rescue the deficit in mitochondrial respiration of the $p53^{-/-}$ cells corresponded well to the physiological levels observed in the $p53^{+/+}$ cells (Fig. 3A). Oxygen consumption also increased with SCO2 expression in human colon cancer cell lines with naturally occurring p53 mutations (DLD1 and

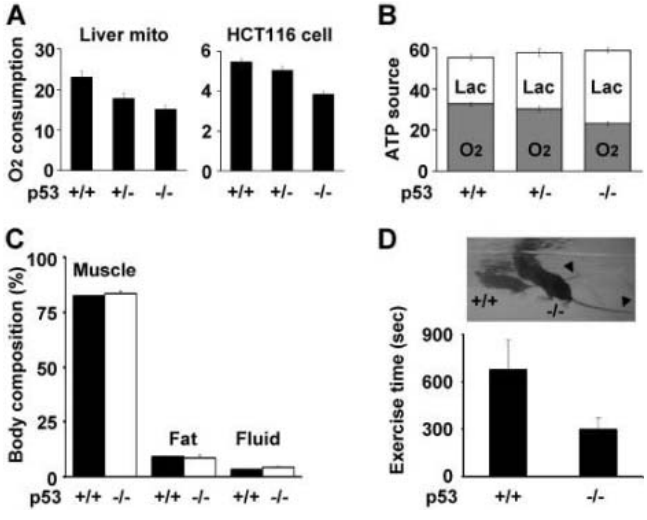

Fig. 1. Dependence of aerobic respiration, glycolysis, and exercise capacity on p53. (**A**) Oxygen consumption (mean ± SD, nmol min^{-1} mg^{-1} protein) was measured by a Clark-type oxygen microelectrode in mouse liver mitochondria preparations and in HCT116 cells with three *TP53* genotypes: wild-type (+/+), heterozygous (+/−), and homozygous disruption (−/−). (**B**) The amount of ATP (mean ± SD, nmol min^{-1} mg^{-1} protein) produced by aerobic respiration (gray bars, O_2) and glycolysis (light bars, Lac) was calculated by measuring oxygen consumption and lactate production in the three different *TP53* genotypes of HCT116 cells. (**C**) Body mass composition of muscle, fat, and free fluid (percentage of total) was determined in nonanesthetized age- and sex-matched mice using a nuclear magnetic resonance analyzer. Body mass (mean ± SD) for the $p53^{+/+}$ and $p53^{-/-}$ mice was 20.4 ± 1.2 g and 20.1 ± 1.9 g, respectively. p53 genotypes indicated for wild-type (+/+) (dark bars, $n = 5$) and homozygous knockout (−/−) (light bars, $n = 5$) mice. (**D**) Maximum duration of swimming exercise measured in a temperature-controlled adjustable-current tank. Exercise time (mean ± SD, s) to the point of exhaustion, as indicated by inability to stay afloat, is shown for each genotype ($P = 0.008$, $n = 5$ for each group). Note that the $p53^{-/-}$ mouse (foreground) assumes a more vertical posture consistent with early fatigue, in contrast to the wild-type mouse (background) with horizontal body and tail positions (arrowheads) (*13*).

[1]Cardiology Branch, National Heart, Lung, and Blood Institute, [2]Diabetes Branch, National Institute of Diabetes and Digestive and Kidney Diseases, National Institutes of Health, Bethesda, MD 20892, USA. [3]Department of Radiation Oncology and Molecular Radiation Sciences, The Sidney Kimmel Comprehensive Cancer Center, The Johns Hopkins School of Medicine, Baltimore, MD 21231, USA.

*To whom correspondence should be addressed. E-mail: hwangp@mail.nih.gov

SW480 cells), suggesting that SCO2 expression can generally rescue oxygen consumption in p53-deficient cells (Fig. 3A).

To rule out the possibility that decreased mitochondrial respiration in the $p53^{-/-}$ HCT116 cells may result from chronic metabolic or other unrelated genetic changes that may have occurred during clonal selection, we examined oxygen consumption after reducing p53 expression by small interfering RNA (siRNA). Decreased p53 expression in parental HCT116 cells resulted in decreased SCO2 protein expression and reduced oxygen consumption within 48 hours, phenocopying the p53-deficient cells (Fig. 3B).

To genetically test whether p53 regulates mitochondrial respiration through SCO2, we disrupted the *SCO2* locus by homologous recombination in the human HCT116 cell line. Elimination of one of the two *SCO2* alleles could phenocopy the p53-deficient cells through the direct reduction of SCO2 expression. A targeting vector was designed to remove about 500 base pairs of SCO2 coding sequence upon homologous recombination into the *SCO2* locus. This construct was assembled into a recombinant adeno-associated virus (rAAV) (*20*). After viral transduction and screening of 1200 drug-selected clones, we identified three independently derived clones that gave the appropriately sized knockout (KO) polymerase chain reaction (PCR) product, indicating successful disruption of the *SCO2* allele (Fig. 4A). The amounts of SCO2 protein in each of the three $SCO2^{+/-}$ (H1 to H3) knockout clones were reduced relative to that in the WT parental (P) and sister clones (S1 and S2) that had also undergone parallel viral transduction and selection processes (Fig. 4A). Cell viability and growth rates were similar for the WT and $SCO2^{+/-}$ clones. However, the $SCO2^{+/-}$ cells displayed decreased oxygen consumption (O_2) and increased glycolytic activity (Lac) compared to WT cells, whereas total ATP concentrations remained the same, similar to the results for p53-deficient cells (Fig. 4B).

The direct regulation of aerobic respiration by p53 has important implications for understanding tumorigenesis. To date, much of the research on cellular processes driven by oncogenes and tumor suppressor genes has focused on the regulation of cell birth and death (*1*). Our study identifies a direct transcriptional target of p53 that modulates aerobic respiration and, by its haploinsufficiency, recapitulates the Warburg effect. It also defines a genetic pathway, not involving cell cycle regulation, by which the inactivation of p53 may promote tumorigenesis by decreasing cellular dependence on oxygen, potentially permitting growth in

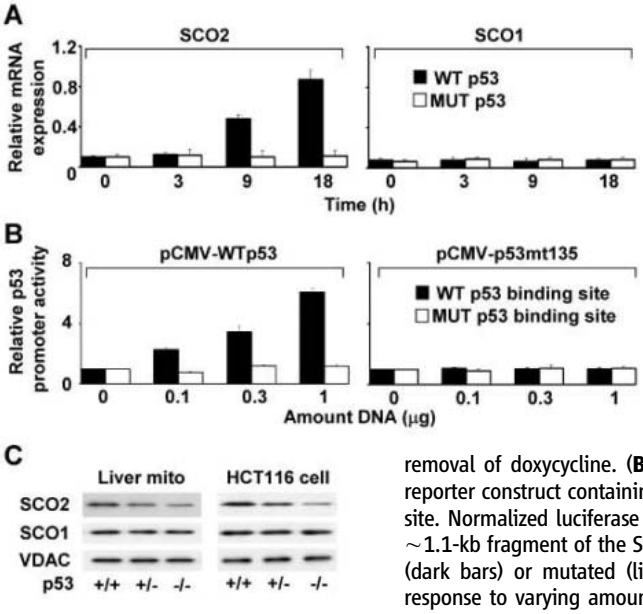

Fig. 2. Dependence of SCO2 mRNA transactivation and protein levels on p53. (**A**) SCO2 and SCO1 transactivation by wild-type (WT, dark bar) or mutant (MUT, light bar) p53 were measured using a modified tetracycline-inducible system in human colon cancer DLD1 cell line. mRNAs were quantified by real-time reverse transcription (RT)–PCR and normalized to a control gene *EIF3S5* (mean ± SD, relative value). Time (in hours) indicates induction by removal of doxycycline. (**B**) p53 transactivates luciferase reporter construct containing the *SCO2* gene p53 binding site. Normalized luciferase activity under the control of a ~1.1-kb fragment of the SCO2 gene containing wild-type (dark bars) or mutated (light bars) p53 binding site in response to varying amounts of wild-type (pCMV-p53) or mutant (pCMV-p53mt135) p53 transfection. (**C**) Dependence of SCO2 protein expression levels on p53 gene dosage in mouse liver mitochondria and HCT116 cells. Western blot analyses were done with specific antibodies against SCO2, SCO1, and VDAC proteins in mouse liver mitochondria and human HCT116 cell lines.

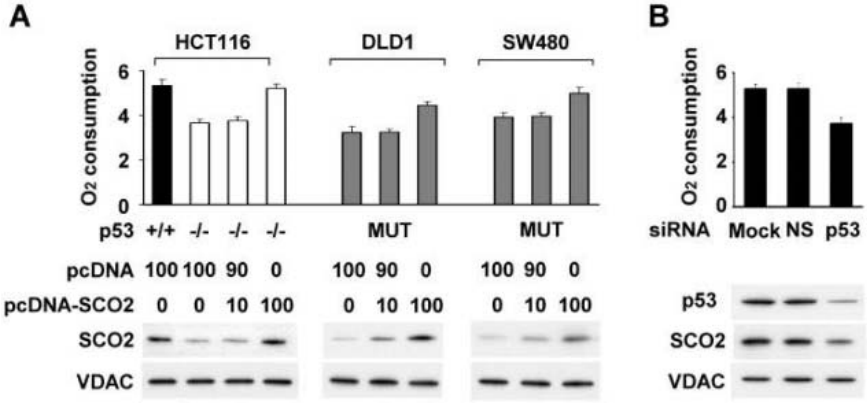

Fig. 3. Expression of SCO2 rescues alterations in mitochondrial respiration. (**A**) Transient transfection of SCO2 (pcDNA-SCO2, ng of DNA) into $p53^{-/-}$ HCT116 cells (light bars) increased SCO2 protein expression and oxygen consumption (mean ± SD, nmol min^{-1} mg^{-1} protein) to $p53^{+/+}$ (dark bar) levels. Control empty vector (pcDNA, ng of DNA) had no effect. Oxygen consumption was increased to wild-type HCT116 levels by SCO2 in p53-mutant (MUT) cell lines DLD1 and SW480 (gray bars). (**B**) Transient knockdown of p53 in wild-type HCT116 cells by sequence-specific siRNA (p53) decreases SCO2 protein and oxygen consumption (mean ± SD, nmol min^{-1} mg^{-1} protein). Mock (no siRNA) and nonspecific (NS) siRNA transfections had no effect.

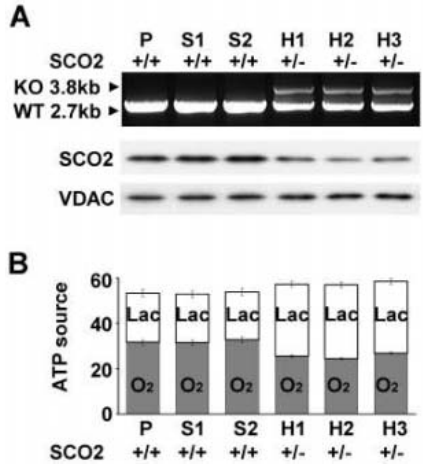

Fig. 4. Targeted disruption of one *SCO2* allele reproduces the p53-deficient metabolic phenotype. (**A**) Three clones (H1 to H3) with heterozygous disruption of *SCO2* were identified by the appearance of the 3.8-kb KO band accompanied by a decrease in the intensity of the 2.7-kb WT band. P is the parental cell line, and S1 and S2 are two sibling clones without SCO2 disruption. SCO2 protein expression levels were assessed by Western blotting. (**B**) The amount of ATP (mean ± SD, nmol min^{-1} mg^{-1} protein) produced by aerobic respiration (gray bars, O_2) and glycolysis (light bars, Lac) was calculated by measuring oxygen consumption and lactate production in the three wild-type (+/+) and three *SCO2* heterozygous (+/−) knockout clones.

more hypoxic environments. Two recent studies have implicated p53 in the control of glycolysis by its negative regulation of phosphoglycerate mutase (PGM) and Akt (*6*, *7*, *21*). Interestingly, despite the marked increase in glycolysis stimulated by Akt expression, cellular oxygen consumption remained stable, reflecting the tight homeostatic controls governing mitochondrial respiration (*22*). Additional functions of the *TP53* gene continue to be uncovered (*23*), and the effect of p53 status on exercise tolerance suggests that it has global functions that extend beyond processes related to cell birth and death (*24*). The COX complex is critical for aerobic eukaryotes, and *SCO2* and *MTCO2* (COX II) are ancient genes conserved in organisms as diverse as yeast and humans. The regulation of mitochondrial genome-encoded COX II by p53 suggests that our observations pertain to a fundamental control point in metabolism. Recent studies have implicated p53 as a mediator of senescence and aging (*25*–*27*), although specific aspects of this model remain controversial (*28*, *29*). Given the mounting evidence supporting a role for metabolism and oxidative stress in aging (*30*, *31*), the functional relationship between p53 and the COX complex assembly may underlie some aspects of organismal aging. In filamentous fungus, the genetic disruption of COX II markedly increases life-span (*32*). Future studies examining the role of p53 in mitochondrial regulation may clarify how a tumor suppressor gene can have such diverse and global effects on cellular and organismal functions.

References and Notes

1. B. Vogelstein, K. W. Kinzler, *Nat. Med.* **10**, 789 (2004).
2. O. Warburg, *Science* **124**, 269 (1956).
3. G. L. Semenza *et al.*, *Novartis Found. Symp.* **240**, 251 (2001).
4. N. C. Denko *et al.*, *Oncogene* **22**, 5907 (2003).
5. J. W. Kim *et al.*, *Mol. Cell. Biol.* **24**, 5923 (2004).
6. H. Kondoh *et al.*, *Cancer Res.* **65**, 177 (2005).
7. D. R. Plas, C. B. Thompson, *Oncogene* **24**, 7435 (2005).
8. P. C. Herrmann *et al.*, *Proteomics* **3**, 1801 (2003).
9. S. Zhou, S. Kachhap, K. K. Singh, *Mutagenesis* **18**, 287 (2003).
10. F. Bunz *et al.*, *Science* **282**, 1497 (1998).
11. S. Sariban-Sohraby, I. T. Magrath, R. S. Balaban, *Cancer Res.* **43**, 4662 (1983).
12. L. D. Attardi, L. A. Donehower, *Mutat. Res.* **576**, 4 (2005).
13. K. Matsumoto, K. Ishihara, K. Tanaka, K. Inoue, T. Fushiki, *J. Appl. Physiol.* **81**, 1843 (1996).
14. P. M. Hwang *et al.*, *Nat. Med.* **7**, 1111 (2001).
15. E. A. Shoubridge, *Am. J. Med. Genet.* **106**, 46 (2001).
16. P. Pecina, H. Houstkova, H. Hansikova, J. Zeman, J. Houstek, *Physiol. Res.* **53** (Suppl. 1), S213 (2004).
17. L. C. Papadopoulou *et al.*, *Nat. Genet.* **23**, 333 (1999).
18. J. Yu *et al.*, *Proc. Natl. Acad. Sci. U.S.A.* **96**, 14517 (1999).
19. B. Vogelstein, D. Lane, A. J. Levine, *Nature* **408**, 307 (2000).
20. M. Kohli, C. Rago, C. Lengauer, K. W. Kinzler, B. Vogelstein, *Nucleic Acids Res.* **32**, e3 (2004).
21. A. J. Levine, Z. Feng, T. W. Mak, H. You, S. Jin, *Genes Dev.* **20**, 267 (2006).
22. R. L. Elstrom *et al.*, *Cancer Res.* **64**, 3892 (2004).
23. L. J. Hofseth, S. P. Hussain, C. C. Harris, *Trends Pharmacol. Sci.* **25**, 177 (2004).
24. U. Wisloff *et al.*, *Science* **307**, 418 (2005).
25. S. D. Tyner *et al.*, *Nature* **415**, 45 (2002).
26. B. Maier *et al.*, *Genes Dev.* **18**, 306 (2004).
27. J. Campisi, *Cell* **120**, 513 (2005).
28. I. Garcia-Cao *et al.*, *EMBO J.* **21**, 6225 (2002).
29. M. V. Poyurovsky, C. Prives, *Genes Dev.* **20**, 125 (2006).
30. L. Bordone, L. Guarente, *Nat. Rev. Mol. Cell Biol.* **6**, 298 (2005).
31. R. S. Balaban, S. Nemoto, T. Finkel, *Cell* **120**, 483 (2005).
32. S. W. Stumpferl, O. Stephan, H. D. Osiewacz, *Eukaryot. Cell* **3**, 200 (2004).

33. We thank S. Nemoto, C. Mcleod, I. Pagel, C. Rago, and O. Mian for technical advice and assistance, and T. Finkel, M. N. Sack, N. Epstein, R. S. Balaban, and B. Vogelstein for helpful suggestions and critical reading of this manuscript. The p53-disrupted HCT116 cell lines, tetracycline-inducible p53 DLD1 cell lines, and plasmid constructs were gifts from B. Vogelstein and B. H. Park. This research was supported by the Division of Intramural Research, National Heart, Lung, and Blood Institute, NIH.

Supporting Online Material

www.sciencemag.org/cgi/content/full/1126863/DC1
Materials and Methods
Figs. S1 and S2
References and Notes

1 March 2006; accepted 17 May 2006
Published online 25 May 2006;
10.1126/science.1126863
Include this information when citing this paper.

The *Xist* RNA Gene Evolved in Eutherians by Pseudogenization of a Protein-Coding Gene

Laurent Duret,[1]* Corinne Chureau,[2] Sylvie Samain,[3] Jean Weissenbach,[3] Philip Avner[2]

The *Xist* noncoding RNA is the key initiator of the process of X chromosome inactivation in eutherian mammals, but its precise function and origin remain unknown. Although *Xist* is well conserved among eutherians, until now, no homolog has been identified in other mammals. We show here that *Xist* evolved, at least partly, from a protein-coding gene and that the loss of protein-coding function of the proto-*Xist* coincides with the four flanking protein genes becoming pseudogenes. This event occurred after the divergence between eutherians and marsupials, which suggests that mechanisms of dosage compensation have evolved independently in both lineages.

Mammalian X and Y chromosomes evolved from a pair of autosomes shortly after the divergence of mammals from other amniotes (*1*). In eutherians and in marsupials, the desiquilibrium in gene dosage between XY males and XX females is compensated for by silencing one of the X chromosomes in females (*2*–*4*). In eutherians, this silencing involves the *Xist* gene, which is located in the X inactivation center (*Xic*) and encodes a long untranslated RNA (*5*). *Xic* is located on the long arm of the human X chromosome, which corresponded to the proto–X chromosome in the mammalian cenancestor (last common ancestor) (*6*, *7*). This observation is consistent with the hypothesis that X-chromosome inactivation might have emerged contemporaneously with the chromosomal sex-determining mechanism, early in mammalian evolution (*8*).

To study the evolution of X inactivation, we searched for homologs of *Xist* in 14 vertebrate genomes (*9*). We found *Xist* in all eutherians (Fig. 1), which demonstrates that *Xist* was already present in the eutherian cenancestor. With BLAST, we failed to detect significant sequence similarity to *Xist* in noneutherian vertebrates.

In humans, the genomic region surrounding the *Xist* gene contains three protein-coding genes (*Cdx4*, *Chic1*, and *Xpct*) that have orthologs in all vertebrate classes (table S1). The linkage between these genes is conserved in chicken and in *Xenopus* (Fig. 2A). We will hereater refer to the genomic interval between *Chic1* and *Xpct* in noneutherian species as the *XicHR* (*Xic* homologous region). In eutherians, besides *Xist*, the *Xic* region contains two RNA genes (*Jpx* and *Ftx*) and two protein-coding genes (*Tsx* and *Cnbp2*) (*10*) (Fig. 2A). *Cnbp2* is a retrotransposed gene that is specific to eutherians (*9*). We failed to detect any homolog of *Tsx*, *Jpx*, or *Ftx* genes in noneutherian vertebrates. In both chicken and *Xenopus*, the *XicHR* contains five protein genes (*Fip1l2*, *Lnx3*, *Rasl11c*, *UspL*, and *Wave4)* that have no detectable orthologs in eutherian genomes (table S1). The gene content, order, and orientation of the *XicHR* is perfectly conserved between chicken and *Xenopus* (Fig. 2A), which indicates that the chicken *XicHR* (on an autosome) corresponds to the ancestral state in the tetrapod cenancestor.

To search for possible vestiges of *XicHR* genes in eutherians, we compared the chicken genomic sequence to its counterpart from four species representative of different eutherian orders

[1]Laboratoire de Biométrie et Biologie Evolutive (UMR 5558), CNRS and Université Lyon 1, 16 rue Raphaël Dubois, 69622 Villeurbanne Cedex, France. [2]Unité de Génétique Moléculaire Murine, URA CNRS 1947, Institut Pasteur, 75015 Paris, France. [3]Genoscope, Centre National de Séquençage and CNRS UMR8030, Case Postale 5706, 91057 Evry Cedex, France.

*To whom correspondence should be addressed: E-mail: duret@biomserv.univ-lyon1.fr

(human, mouse, dog, and cow) (*9*). The *XicHR* covers 162 kb in chicken (998 kb in human), of which 5% (2%) consists of exons and 3% (59%) of repeat sequences. Comparison of human and chicken sequences revealed 22 alignments in nonrepeated sequences. Although these alignments are short (on average 62 base pairs with 72% identity), eight of them overlap with known exons in chicken, of which five also correspond to exons in human. The probability that such alignments would occur by chance is extremely low ($P < 10^{-7}$ in each species) (*9*), indicating that they correspond to homologous regions, conserved between human and chicken. Overall, we detected 63 distinct fragments in chicken, covering 3.4 kb, that align with at least one of the four eutherian species, with 12 of these alignments overlapping with chicken exons (from *Fip1l2*, *Lnx3*, and *Rasl11c*) (table S2).

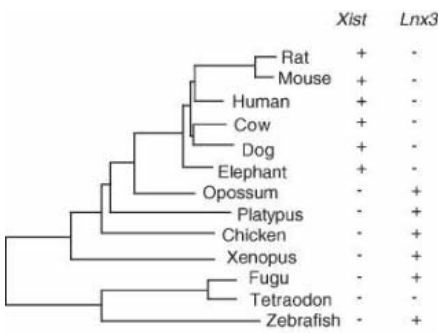

Fig. 1. Phylogenetic distribution of *Xist* and *Lnx3* within vertebrate species for which whole-genome sequence data are available. The phylogenetic tree was adapted from references (*16*, *17*). We searched for homologs of *Xist* within genomic sequences with BLASTN. The presence of a significant hit homologous to *Xist* is indicated by a plus sign (+). We searched for homologs of *Lnx3* with BLASTP against Ensembl protein predictions and with TBLASTN against genome assemblies, except for the platypus, for which we used whole-genome shotgun sequences. Phylogenetic analyses were conducted to distinguish *Lnx3* from its paralogs (fig. S2). The presence of a *Lnx3* ortholog is indicated by a plus sign (+).

There are six exons of *Fip1l2* that show homology with the human or mouse sequence. Three of them correspond to exons of *Tsx* (Fig. 2B). The protein alignment revealed that the mouse *Tsx* is a truncated gene, encoding a protein orthologous to the N-terminal end of *Fip1l2*. *Tsx* is functional (transcribed and translated) in mouse and rat, but is evolving very rapidly (*11*). *Tsx* is a pseudogene in human (*10*), as it is in dog and cow. We identified the four exons of the *Rasl11c* gene in cow and dog (one in human, none in mouse), but in all these species, *Rasl11c* has become a pseudogene. Two exons of *Lnx3* are homologous to *Xist* (Fig. 2C). The first corresponds to *Xist* exon h4/m4, which is well conserved in eutherians (Fig. 3A and fig. S1). The second corresponds to the exon h5/m6, which, although conserved in human and mouse, is more divergent in dog and cow (Fig. 3B). The probability that, by chance, two independent alignments overlap exons in both species is extremely low (5×10^{-5}), which indicates that these exons of the *Xist* RNA gene are homologous to the *Lnx3* protein gene.

In marsupials, the *XicHR* is located on the X chromosome (*7*, *12*). We have sequenced an opossum genomic clone including *Rasl11c* and the 5′ end of *Lnx3*, and we have sequenced the *Lnx3* mRNA (*9*). We have identified *Wave4* in sequence databases (Fig. 2A and table S1). Phylogenetic analyses indicate that these three genes are functional in the opossum (see fig. S2 for details on *Lnx3*). Thus, the loss of protein-coding function of *Lnx3* occurred in the eutherian lineage and was concomitant with the pseudogenization of at least two of the four other *XicHR* genes.

Lnx3 is conserved in all vertebrate classes and is highly similar to its paralogs *Lnx1* and *Lnx2* (*13*). The exons conserved in *Xist* correspond to two PDZ motifs, and both contain frameshift mutations (Fig. 3). By screening databases of expressed sequence tags, we found that in both chicken and *Xenopus*, *Lnx3* is transcribed in varied tissues and developmental stages. In the

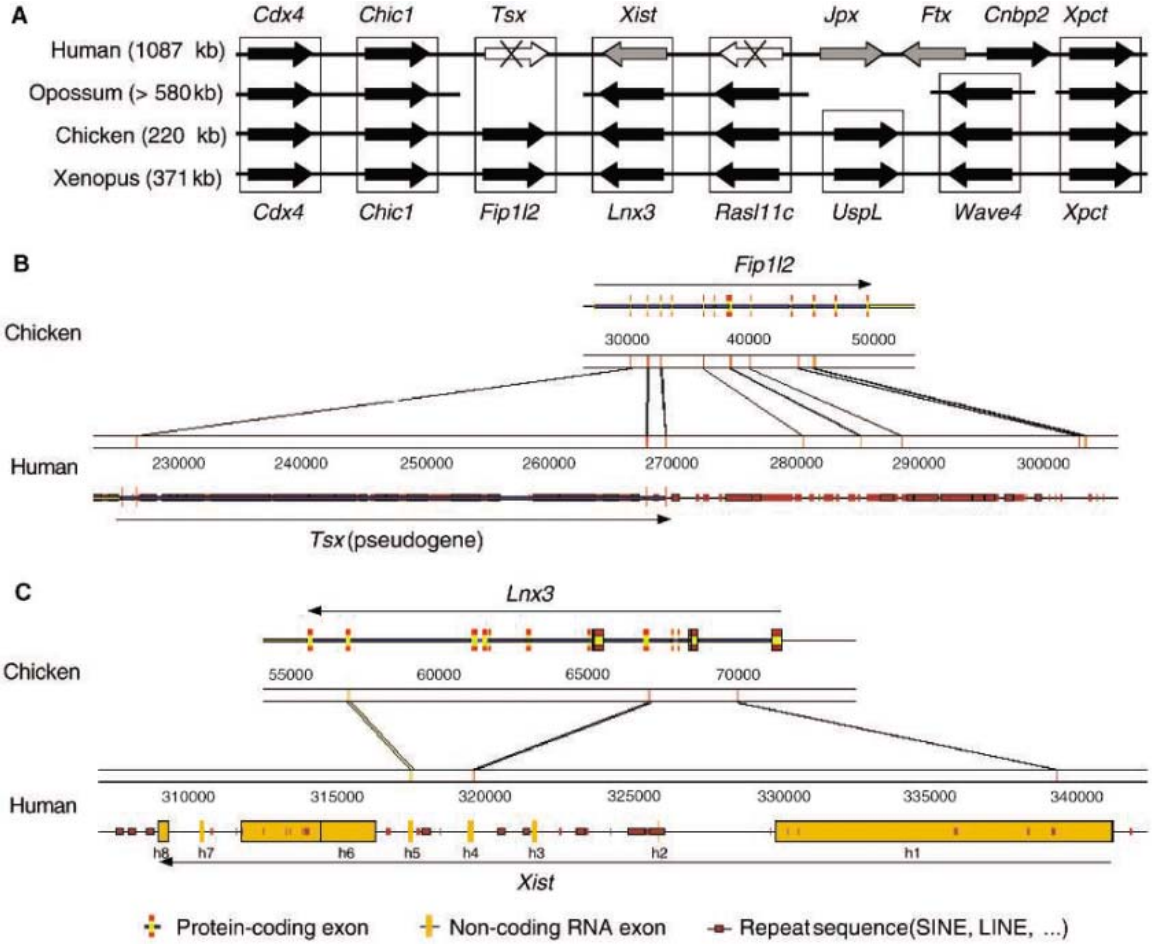

Fig. 2. Comparison of the human *Xic* region and of its orthologous region in opossum, chicken, and *Xenopus*. (**A**) Genomic map. Protein-coding genes are indicated in black, RNA-genes in gray, and pseudogenes in white. Groups of genes for which there is evidence of homology are surrounded by a rectangle. The assembly of the opossum genome is incomplete, and the order and orientation of contigs (thick black lines) is therefore not known. (**B**) Alignment of the chicken *Fip1l2* genomic region with the human *Tsx* region. (**C**) Alignment of the chicken *Lnx3* genomic region with the human *Xist* region. The numbering of *Xist* exons corresponds to the nomenclature proposed by reference (*10*). Positions are indicated as base pairs.

opossum, *Lnx3* is expressed both in males and females, a behavior very different from that of *Xist* in eutherians. In mice, although *Xist* exon h4/m4 (which is homologous to *Lnx3*) is dispensable for X inactivation (*14*), the exon has been shown to affect the transcription and/or processing of *Xist* RNA (*14*). This suggests that *Xist* might have retained some regulatory elements of the *Lnx3* transcription unit.

Our results show that two exons of *Xist* derive from *Lnx3*. However, *Lnx3* and *Xist* contain, respectively, 11 and 6 other exons, for which we failed to detect significant similarities. Notably, we did not detect homology to the *Xist* A-repeat, which is a discrete sequence element implicated in X-silencing function (*15*). This lack may be because RNA genes and protein genes are subject to very different selective constraints and may rapidly diverge. It is also possible that the first exons of *Xist* are not homologous to *Lnx3* and derive from the insertion of a sequence (e.g., a transposable element) that was recruited to form a proto-*Xist* gene. We analyzed the opossum genomic interval between *Rasl11c* and *Lnx3* to search for hallmarks of a potential proto-*Xist* gene, but failed to detect any significant similarity with *Xist,* even using the most accurate alignment software (*9*). Given that *Xist* exons are highly conserved among eutherians, the lack of similarity with the opossum strongly suggests that marsupials do not contain any proto-*Xist* gene at this locus and, hence, that *Xist* is specific of eutherians.

The mechanisms of dosage compensation in marsupials and eutherians both involve chromosomewide X inactivation (XCI), but with some significant differences. In marsupials, it is always the paternal X-chromosome that is inactivated, and the inactivation, which is incomplete and tissue-specific, does not seem to involve DNA methylation (*4*). Our results, moreover, indicate that in marsupials, XCI does not involve *Xist*. In monotremes, the *XicHR* has been translocated to an autosome, which indicates that dosage compensation does not require this locus (*6*). There is, therefore, no evidence that the processes of dosage compensation in eutherian, marsupial, and monotremes are homologous. It is possible that *Xist*-independent XCI existed in the mammalian cenancestor and that *Xist* overtook this mechanism in eutherians. However, it should be stressed that in the earliest stages of the divergence of the X and Y chromosomes, most of the X-linked genes still had an active Y homolog and so did not need dosage compensation. It is only after the Y chromosome had lost a large number of genes that it might become advantageous to achieve dosage compensation by inactivation of the whole X chromosome. We, therefore, propose that the emergence of XCI might be a late event in the evolution of sexual chromosomes.

A *Xist* exon h4/m4:

```
Chicken-Lnx3    TTTTTTCTCTTTGATTTCCACCATCAGATGTTCCTC-AGAGAGCTAGCCCTGTGGCTGAA
Human-Xist      ---TTTTTCTTTTATCTCTTTT--CAGATCTTCCTC-AGAAGAATAGGCTTGTTGTTTTA
Mouse-Xist      TGGCTTTTCTTTCACCTCTTTT-CCAGATCTCCCCCCAGAATTGTGGGCTTGCTGCTTTG
Dog-Xist        TTATTTTTCTTTGATCTCTTCT-CCAGATGTTCCTC-AGAAGAATAGGCTTGTTGCTCTA
Cow-Xist        TTATTTTTCTTTTATCTCTTTT-CCAGATCTACCTC-AAAAGAATAGGCCTGTTGCTTTA
                :  :** ***** *: **      ***** * **:* *:*    *:* * **: *:*  :
                                        <- exon start

Chicken-Lnx3    ACGAGCACAATAGAAATTCACCGAGAAGATCCAGAGGAAGAGCTTGGG-ATGAGAATAGT
Human-Xist      CAGTGTTAGTGATCCATTCCCTTTGACGATCCCTAGGTGGAGATGGGGCATGAGGATCCT
Mouse-Xist      CAGTGCTGGCGACCTATTCCCTTTGACGATCCCTAGGTGGAGATGGGGCATGAGGATCCT
Dog-Xist        CAGTGTTAGTGACCCGTTCCCTTTGACGATCCCTAGGTGGAGATGGGGCATGAGGATCCT
Cow-Xist        CAGTGTTAGTGACCCATTCCCTTTGACGATTCCTAGGTGGAGATGGGGCATGAGGATCCT
                  * *      *   :*** *   ** ***:*  ***  *** * *** ***** **  *

Chicken-Lnx3    T--GGGGGTAAGGACACG-CCACTAGGAAACA
Human-Xist      CCAGGGGAAAAGCTCACTACCACTGGGCAACA
Mouse-Xist      CCAGGGGAATAGCTCACCACCACTGGGCAACA
Dog-xist        CCAGGGGAAAAGCTCACTACCACTAGGCAACA
Cow-Xist        CCAGGGGAAAGATTCACTACCACTGAGCAACA
                   ****  :::  ***  ***** :* ****
```

B *Xist* exon h5/m6:

```
Chicken-Lnx3    TCTTTGCAGCTACCTTCACTG----------CTGTCAAGATATTGTCCTTAGCAAAGGCA
Human-Xist      TTTTTATAGCTCTTCATTGTTCC-----TATCTGCCAAATCATTATACTTCCTACAAGCA
Mouse-Xist      --TTTGTAGTGCC---------------ATCTACCAAAT-ATTACCCTTCCCCAAAGCA
Dog-Xist        TTTTTATAGCTCCTGATTGTTCCCTTTTTATCTACCAAATCATTGTC--TCCCAAAAGCA
Cow-Xist        CTTTTGTAGCTCCTGGTTGTTCCCTTCATATTTGCCAAATCATTATCTTTCCCTGAAGTA
                  ***  **                    :*  ***   *** :: :*  :  * *:*
                       <- exon start

Chicken-Lnx3    ACCAGGAAAGCTGGGGCTTCAGCATTGTTGGAGGCTTTGAGGAGAGCAAAGGAAACCAGC
Human-Xist      GTGCAGAGAGCTGAGTCTTCAGCAGGTCCAAGAAATTTGAACACACTGAAGGAAGTCAGC
Mouse-Xist      GCACAGAAAACTGGGTCTTCAGCGTGATCAAGCAATGTGAACACACAAAAGGAAGGCAGC
Dog-Xist        GTGCAGAGGGC-----------------AAGAAAGTGGAACATATCAAAG---------
Cow-Xist        GTGCAAAGAGC-----------------AAGAAATGTGAACACACC-AAG---------
                     :*  :*                  : :**  * *   ***

Chicken-Lnx3    CCTTCT----TCATCAAAACCATCGTGCCTGGGACGCCTGCC-TGCCGCAGCGCAAGGCT
Human-Xist      CTTCCC----ACCTGAAGATCAACATGCCTGGCACTCTAGCA-CTTGAGGATAGCTGAAT
Mouse-Xist      TTTATAAATGACCCGAGGATCAACATGCCTG--ACTGCAGCATCTTAAAAGCAATAGAAT
Dog-Xist        --------------GAAGATCAACATGCCTGGCATGCTAGCA-TTTTAGAACATCAGAAT
Cow-Xist        --------------GAAGATCAACATGCCTGCAATGCTAGCA-TTTTAGAATAGCAGAAT
                              *: * ** * ******  *  :  **        :      *  *

Chicken-Lnx3    GAAGTGAGT
Human-Xist      GAAGTAAGT
Mouse-Xist      GAGGTAAGT
Dog-Xist        GAAGTAAGT
Cow-Xist        GAAGTAAGT
                **:** ***
          exon end ->
```

Fig. 3. Alignment of the two homologous regions of chicken *Lnx3* and eutherian *Xist*. (**A**) Sequence alignment [computed with MUSCLE (*18*)] of the 5′ part of *Xist* exon h4/m4 and of *Lnx3* exon 3 (Ensembl transcript ENSGALT00000012483). (**B**) Alignment of the entire *Xist* exon h5/m6 and *Lnx3* exon 9. Exon boundaries are indicated in bold. Sites that are conserved in all species or in four out of five species are indicated respectively by an asterisk (*) and a colon (:).

References and Notes

1. M. Kohn, H. Kehrer-Sawatzki, W. Vogel, J. A. Graves, H. Hameister, *Trends Genet.* **20**, 598 (2004).
2. B. Charlesworth, *Proc. Natl. Acad. Sci. U.S.A.* **75**, 5618 (1978).
3. M. T. Ross *et al.*, *Nature* **434**, 325 (2005).
4. F. Grutzner, J. A. Graves, *Curr. Opin. Genet. Dev.* **14**, 642 (2004).
5. J. C. Chow, Z. Yen, S. M. Ziesche, C. J. Brown, *Annu. Rev. Genomics Hum. Genet.* **6**, 69 (2005).
6. P. D. Waters *et al.*, *Chromosome Res.* **13**, 401 (2005).
7. J. A. Graves, M. Westerman, *Trends Genet.* **18**, 517 (2002).
8. H. S. Chandra, *Proc. Natl. Acad. Sci. U.S.A.* **82**, 6947 (1985).
9. Methods and other details are described in Supporting Online Material.
10. C. Chureau *et al.*, *Genome Res.* **12**, 894 (2002).
11. D. B. Cunningham, D. Segretain, D. Arnaud, U. C. Rogner, P. Avner, *Dev. Biol.* **204**, 345 (1998).
12. E. Koina *et al.*, *Chromosome Res.* **13**, 687 (2005).
13. D. S. Rice, G. M. Northcutt, C. Kurschner, *Mol. Cell. Neurosci.* **18**, 525 (2001).
14. M. L. Caparros, M. Alexiou, Z. Webster, N. Brockdorff, *Cytogenet. Genome Res.* **99**, 99 (2002).
15. A. Wutz, T. P. Rasmussen, R. Jaenisch, *Nat. Genet.* **30**, 167 (2002).
16. W. J. Murphy *et al.*, *Nature* **409**, 614 (2001).
17. E. H. Margulies *et al.*, *Proc. Natl. Acad. Sci. U.S.A.* **102**, 3354 (2005).
18. R. C. Edgar, *Nucleic Acids Res.* **32**, 1792 (2004).

19. This work was supported by the CNRS, the Institut Pasteur, the Genoscope, the European Union Epigenome Network of Excellence, and the Mission de la Recherche et de la Technologie. We thank the Broad Institute for making the opossum sequences publicly available. Sequences have been deposited in EMBL (accession numbers AM230659 and AM230660).

Supporting Online Material

www.sciencemag.org/cgi/content/full/312/5780/1653/DC1
Materials and Methods
SOM Text
Figs. S1 and S2
Tables S1 and S2
References and Notes

16 February 2006; accepted 17 May 2006
10.1126/science.1126316

Neuronal Pathway from the Liver Modulates Energy Expenditure and Systemic Insulin Sensitivity

Kenji Uno,[1,2*] Hideki Katagiri,[2*†] Tetsuya Yamada,[1*] Yasushi Ishigaki,[1] Takehide Ogihara,[2] Junta Imai,[1,2] Yutaka Hasegawa,[1,2] Junhong Gao,[1,2] Keizo Kaneko,[1,2] Hiroko Iwasaki,[2] Hisamitsu Ishihara,[1] Hironobu Sasano,[3] Kouichi Inukai,[4] Hiroyuki Mizuguchi,[5] Tomoichiro Asano,[6] Masakazu Shiota,[7] Masamitsu Nakazato,[8] Yoshitomo Oka[1]

Coordinated control of energy metabolism and glucose homeostasis requires communication between organs and tissues. We identified a neuronal pathway that participates in the cross talk between the liver and adipose tissue. By studying a mouse model, we showed that adenovirus-mediated expression of peroxisome proliferator–activated receptor (PPAR)–γ2 in the liver induces acute hepatic steatosis while markedly decreasing peripheral adiposity. These changes were accompanied by increased energy expenditure and improved systemic insulin sensitivity. Hepatic vagotomy and selective afferent blockage of the hepatic vagus revealed that the effects on peripheral tissues involve the afferent vagal nerve. Furthermore, an antidiabetic thiazolidinedione, a PPARγ agonist, enhanced this pathway. This neuronal pathway from the liver may function to protect against metabolic perturbation induced by excessive energy storage.

The incidence of obesity, insulin resistance, hyperlipidemia, and hypertension, collectively referred to as the metabolic syndrome, is increasing at an alarming rate in Western cultures (*1*). Secreted humoral factors, including leptin (*2*), convey information about energy storage from adipose tissue to the central nervous system (CNS). As in adipose tissues, fat storage in the liver is dynamically changed by overall energy balance, but our understanding of how the liver transmits metabolic signals to other tissues remains incomplete. Studies of mouse models created by tissue-specific genetic engineering (*3*, *4*) or adenoviral gene transfer (*5*, *6*) have shown the importance of cross talk between tissues in the regulation of energy metabolism. Mice with tissue-specific knockout of peroxisome proliferator–activated receptor γ (PPARγ) provide an example of such intertissue communication (*7*). PPARγ activates genes involved in lipid storage and metabolism (*8*). Although PPARγ expression in the liver is low compared with that in adipose tissues (*9*), hepatic expression of PPARγ (*10*, *11*), especially that of PPARγ2 (*12*), is functionally enhanced in a number of obesity models. In addition, liver-specific disruption of PPARγ in obese (ob/ob) mice prevents hepatic steatosis but increases peripheral adiposity and decreases insulin sensitivity in muscle and fat (*13*). Thus, hepatic PPARγ2 plays important roles not only in the development of liver steatosis but also in the regulation of peripheral lipid storage and insulin sensitivity.

To investigate the mechanism by which hepatic PPARγ2 expression affects metabolism in peripheral tissues, we overexpressed PPARγ2 in the livers of C57BL/6 mice using adenoviral gene transfer. After being fed a high-fat diet for 4 weeks, the mice developed obesity-associated diabetes (*14*). The PPARγ2 adenovirus vector was then administered intravenously to mice (PPARγ2 mice). Control mice given the LacZ adenovirus (LacZ mice) showed no alterations in blood glucose levels, food intake, or plasma lipid parameters after virus administration (*14*). Systemic infusion of the PPARγ2 adenovirus into mice resulted in expression of the transgene primarily in the liver (Fig. 1A), without increased expression in peripheral tissues, including white adipose tissue (WAT) (Fig. 1B).

The livers of PPARγ2 mice were pale and enlarged as compared with those of control mice (fig. S1A). Liver weights were significantly increased (Fig. 1C) because of increased triglyceride content (Fig. 1D). Histological analysis of PPARγ2 mice revealed an abundance of large lipid droplets in the livers, without apparent inflammation or structural change (fig. S1B). Thus, hepatic PPARγ2 expression induced severe hepatic steatosis. Hepatic PPARγ2 expression enhanced the expression of lipogenesis-related genes (fig. S2), suggesting that increased uptake and synthesis of fatty acids induce severe steatosis.

In contrast, WAT in PPARγ2 mice was notably diminished in size (fig. S1A); for example, epididymal fat weight was decreased by 46.6% in PPARγ2 mice versus controls (Fig. 1E). Cell diameters in WAT and brown adipose tissue (BAT) were also markedly decreased in PPARγ2 mice (fig. S1C). The increases in body weights induced by a high-fat diet were suppressed in PPARγ2 mice (Fig. 1F). Resting oxygen consumption was increased by 29.4% in PPARγ2 mice (Fig. 1G), whereas food intake did not differ from that of LacZ mice (Fig. 1H).

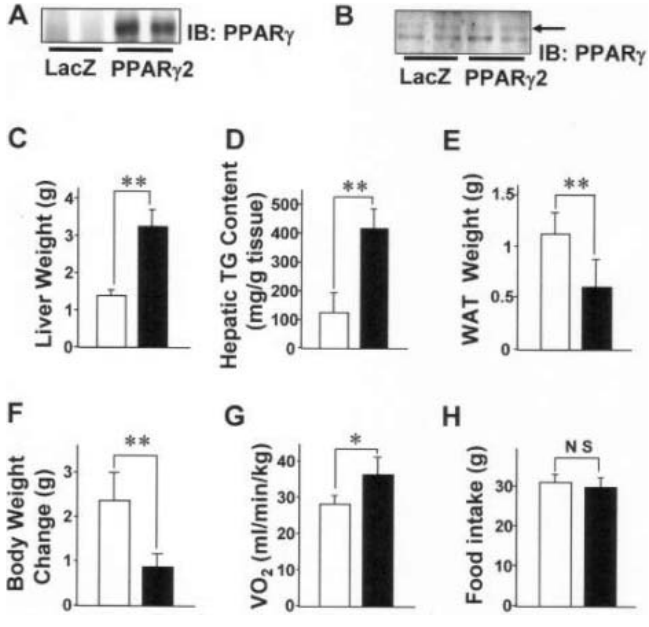

Fig. 1. Hepatic PPARγ2 expression aggravates hepatic steatosis but diminishes peripheral adiposity. (**A** and **B**) Immunoblotting (IB) with an antibody to PPARγ of liver (A) and epididymal fat (B) extracts. Liver weight (**C**), triglyceride (TG) content (**D**), and epididymal fat tissue (WAT) weights (**E**) are shown. Experiments in (A) to (E) were performed on day 7 after adenoviral administration. (**F**) Body weight changes during the 7 days after adenoviral administration. (**G**) Resting oxygen consumption (VO_2) was measured on day 3 after adenoviral injection. (**H**) Total food intake was measured for 7 days after adenoviral administration. In (C) to (H), white and black bars indicate results from LacZ mice and PPARγ2 mice, respectively. Significance as compared to LacZ mice is indicated (**$P < 0.01$ and *$P < 0.05$) by an unpaired *t* test. NS, not significant.

[1]Division of Molecular Metabolism and Diabetes, [2]Advanced Therapeutics for Metabolic Diseases, Center for Translational and Advanced Animal Research, [3]Department of Pathology, Tohoku University Graduate School of Medicine, Sendai 980–8575, Japan. [4]The Fourth Department of Internal Medicine, Saitama Medical School, Moroyama, Iruma-gun, Saitama 350–0495, Japan. [5]Laboratory of Gene Transfer and Regulation, National Institute of Biomedical Innovation, Osaka 567–0085, Japan. [6]Department of Physiological Chemistry and Metabolism, University of Tokyo, Tokyo 113–8655, Japan. [7]Department of Molecular Physiology and Biophysics, Vanderbilt University Medical Center, Nashville, TN 37232, USA. [8]Third Department of Internal Medicine, Miyazaki Medical College, University of Miyazaki, Kiyotake, Miyazaki 889–1692, Japan.

*These authors contributed equally to this work.
†To whom correspondence should be addressed E-mail: katagiri@mail.tains.tohoku.ac.jp

Thus, hepatic PPARγ2 expression increased systemic energy expenditure, thereby suppressing high-fat diet–induced weight gain.

Control mice were hyperglycemic, hyperinsulinemic, and hyperleptinemic in response to a 5-week-long high-fat diet. Hepatic PPARγ2 expression decreased fasting blood glucose and insulin levels (Fig. 2A), indicating markedly improved systemic insulin sensitivity. As shown in Fig. 2B, PPARγ2 mice also showed a 79% reduction in serum leptin levels. Although serum adiponectin levels were similar to those in control mice, tumor necrosis factor–α (TNF-α) levels were significantly decreased in PPARγ2 mice. These findings are consistent with a reduction in peripheral adiposity.

Glucose tolerance (Fig. 2C) and insulin tolerance (Fig. 2D) tests showed that hepatic expression of PPARγ2 markedly improved insulin sensitivity and glucose tolerance. Furthermore, improved insulin sensitivity in muscle (fig. S3A) and epididymal fat tissue (fig. S3B) was confirmed by enhanced tyrosine phosphorylation of the insulin receptor and insulin receptor substrate–1 in response to insulin administration. Thus, hepatic PPARγ2 expression clearly exerts remote beneficial effects on insulin sensitivity in muscle and WAT. Although insulin sensitivity in the liver was impaired (fig. S3C), hepatic PPARγ coactivator (PGC)–1α and hepatic phosphoenolpyruvate carboxykinase (PEPCK) expression was decreased (Fig. 2E), suggesting decreased hepatic glucose output.

To further examine insulin sensitivity and endogenous glucose production in PPARγ2 mice, we performed hyperinsulinemic euglycemic clamp experiments. Basal glucose production in PPARγ2 mice was decreased by 22% as compared with that in LacZ mice, whereas insulin's ability to suppress endogenous glucose production was severely blunted in PPARγ2 mice (Fig. 2F). In addition, glucose infusion rates in PPARγ2 mice were markedly increased (Fig. 2G). Thus, hepatic PPARγ2 expression improved insulin sensitivity in the periphery and decreased glucose output from the liver despite hepatic insulin resistance.

Serum free–fatty-acid (FFA) levels were markedly increased in PPARγ2 mice (fig. S4A), suggesting that hepatic PPARγ2 expression promotes hydrolysis of triglycerides stored in adipose tissues. Increased expression levels of the uncoupling protein (UCP)–1 (*15*), PGC1α (*16*), and hormone-sensitive lipase (*17*) in BAT (fig. S4B) and WAT (fig. S4C) indicate high tonus of the sympathetic nerves innervating these adipose tissues. In addition, the administration of bupranorol, a pan–β-adrenergic blocker (*18*), decreased serum FFA in PPARγ2 mice but had no effect in LacZ mice (fig. S4D), confirming that the β-adrenergic nerve function enhances lipolysis in adipose tissues of PPARγ2 mice.

To examine whether afferent nerves originating in the liver mediate the remote effects, we dissected the hepatic branch of the vagus nerve. Seven days after selective hepatic vagotomy (HV), we administered recombinant adenovirus encoding LacZ or PPARγ2 to mice. Hepatic PPARγ2 expression similarly altered liver weights, hepatic triglyceride content, and PEPCK expression in mice subjected to HV and sham operation (SO) (Table 1). In contrast, selective HV completely blocked the decreases in WAT weights and brown adipocyte size as well as the increases in serum FFA, resting oxygen consumption, and WAT UCP1 expression in PPARγ2 mice (Table 1), indicating that the hepatic vagus mediates the remote effects of hepatic PPARγ2 expression.

HV involves dissection of both afferent and efferent vagal branches innervating the liver. To determine whether the remote effects of hepatic PPARγ2 expression are mediated by the afferent vagus, we applied a specific afferent neurotoxin, capsaicin, to the hepatic branch of the vagus of diet-induced obese male Sprague-Dawley (SD) rats. Seven days after perivagal application of capsaicin or vehicle, we administered recombinant adenovirus encoding LacZ or PPARγ2. Expression of calcitonin gene–related peptide, a sensory neuropeptide, was markedly decreased in the capsaicin-treated vagal nerve, whereas immunoreactivity for S100 proteins was similar in vehicle- and capsaicin-treated nerves (fig. S5A). Furthermore, transmission electron microscopic analyses (fig. S5B) revealed selective degradation of unmyelinated fibers in the vagal hepatic branch. In addition, application of capsaicin to this branch did not affect the esophageal branch of the posterior vagal trunk (fig. S5). These observations indicate selective deafferentation of the hepatic branch of the vagus. Under these conditions, perivagal capsaicin treatment completely blocked the hepatic PPARγ2 expression–induced decrease in WAT weight (Table 1). When taken together, these findings strongly suggest that afferent vagal nerve ac-

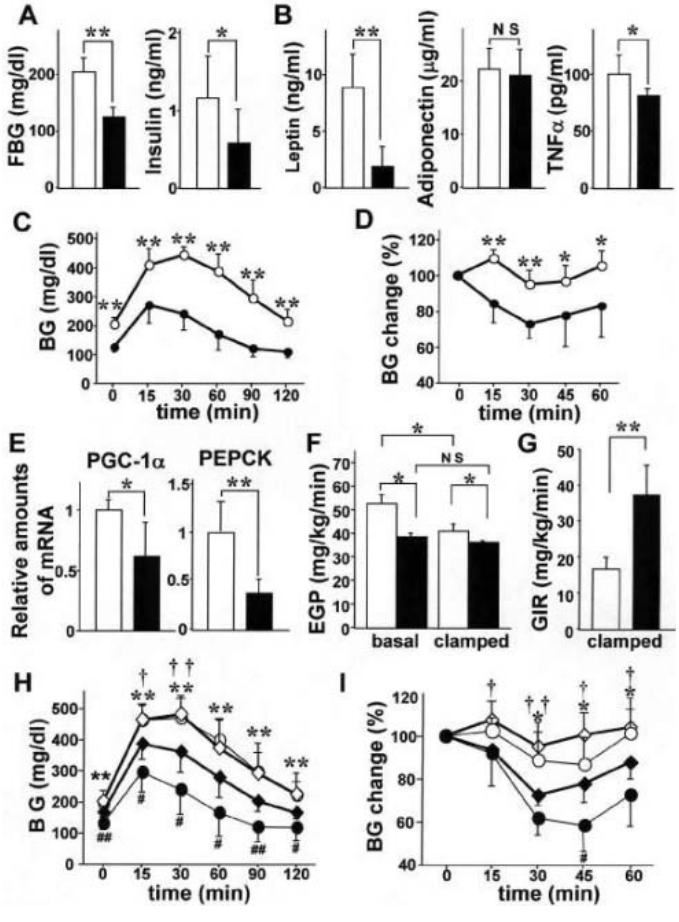

Fig. 2. Hepatic PPARγ2 expression improves peripheral insulin resistance. Fasting blood glucose (FBG) and serum insulin (**A**) and adipocytokines (**B**) were measured in LacZ mice (white bars) and PPARγ2 mice (black bars) on day 7 after adenoviral administration. These serum parameters were measured after a 10-hour fast. (**C** and **D**) LacZ mice (open circles) and PPARγ2 mice (solid circles) were subjected to glucose tolerance (C) and insulin tolerance (D) tests. BG, blood glucose. (**E**) Relative amounts of PGC-1α and PEPCK mRNA in the liver were measured by quantitative reverse transcriptase polymerase chain reaction. (**F** and **G**) Metabolic variables during hyperinsulinemic euglycemic clamp. Endogenous glucose production (EGP) in basal and clamped states (F) and rates of glucose infusion (GIR) were required to maintain euglycemia during the clamp study (G). Experiments in (A) to (G) were performed on day 7 after adenoviral administration. In (A), (B), and (E) to (G), white and black bars indicate results from LacZ mice and PPARγ2 mice, respectively. Significance as compared to LacZ mice is indicated (**$P < 0.01$ and *$P < 0.05$) by an unpaired t test. NS, not significant. (**H** and **I**) HV or SO was performed 7 days before the administration of LacZ or PPARγ2 adenovirus. Mice were subjected to glucose tolerance (H) and insulin tolerance (I) tests on day 7 after adenoviral administration. Open and solid circles indicate SO LacZ mice and SO PPARγ2 mice, respectively. Open and solid diamonds indicate HV LacZ mice and HV PPARγ2 mice, respectively. Data are presented as mean ± SD. **($P < 0.01$) and *($P < 0.05$) indicate significance in SO LacZ mice versus SO PPARγ2 mice, ††($P < 0.01$) and †($P < 0.05$) indicate significance in HV LacZ mice versus HV PPARγ2 mice, and ##($P < 0.01$) and #($P < 0.05$) indicate significance in HV PPARγ2 mice versus SO PPARγ2 mice, by unpaired t tests.

tivation originating in the liver mediates the remote effects of hepatic PPARγ2 expression on peripheral lipolysis.

We next examined the effects of HV on glucose (Fig. 2H) and insulin (Fig. 2I) tolerance test results in PPARγ2 mice. In SO mice, glucose tolerance and insulin sensitivity were improved by hepatic PPARγ2 expression, but these improvements were partially suppressed by hepatic branch vagotomy. These findings suggest that hepatic PPARγ2 expression improved glucose tolerance and systemic insulin sensitivity via both improved peripheral insulin sensitivity and decreased hepatic glucose output; the former requires afferent vagal and efferent sympathetic nerves, whereas the latter does not.

Next, to determine whether the neuronal system, consisting of afferent vagal and efferent sympathetic nerves, functions in the physiological setting of enhanced endogenous PPARγ2 expression in the liver, we examined the effects of an antidiabetic thiazolidinedione (TZD, a PPARγ agonist) using db/db mice, which are a murine model of genetic obesity and diabetes. In db/db mice, endogenous expression of PPARγ2, at both the mRNA (Fig. 3A) and the protein (fig. S6A) levels, is markedly enhanced in the liver. To eliminate the secondary effects of body weight changes, troglitazone, a TZD derivative, was given to db/db mice for 2 days, followed by an evaluation of acute effects. The TZD administration did not alter body weights (Fig. 3B) but did increase resting oxygen consumption (Fig. 3C) and UCP1 expression in BAT (Fig. 3D) and WAT (Fig. 3E), suggesting activation of sympathetic nerves to BAT and WAT. Dissection of the hepatic branch of the vagus 7 days before TZD administration reversed the increases in resting oxygen consumption (Fig. 3C) as well as UCP1 expression in BAT (Fig. 3D) and WAT (Fig. 3E). These findings indicate that the neuronal pathway originating in the liver is also involved in the acute systemic effects of TZDs, under conditions in which hepatic PPARγ expression is upregulated, such as in obese subjects.

To further examine whether endogenous PPARγ in the liver affects energy metabolism, we knocked down hepatic PPARγ in db/db mice. Administration of recombinant adenovirus expressing short hairpin RNA for PPARγ (*19*) 7 days before TZD treatment substantially decreased endogenous PPARγ expression in the liver (fig. S6B) as well as hepatic triglyceride content (fig. S6C) and sterol regulatory element binding protein–1c expression (fig. S6D), indicating functional knockdown of hepatic PPARγ (*20*). Under these conditions, TZD-enhanced energy expenditure was partially but significantly suppressed (fig. S6E). Thus, endogenous PPARγ in the liver regulates acute energy metabolism in vivo. TZD treatment reportedly alleviates insulin resistance in adipose-tissue–ablated mice (*10*) and adipose-specific-PPARγ–deficient mice (*21*), which may involve the aforementioned hepatic-PPARγ–induced neuronal activation in addition to a muscle PPARγ contribution (*22*).

We have shown that a neuronal pathway, consisting of the afferent vagus from the liver and efferent sympathetic nerves to adipose tissues, is involved in the regulation of energy expenditure, systemic insulin sensitivity, glucose metabolism, and fat distribution between the liver and the periphery. Because hepatic PPARγ expression is physiologically associated with obesity, the liver may convey information regarding excess energy balance to the CNS via the afferent vagus. This neuronal system may underlie chronic adaptive thermogenesis, resulting in protection against metabolic perturbation induced by excessive energy storage. There are two avenues of communication between the

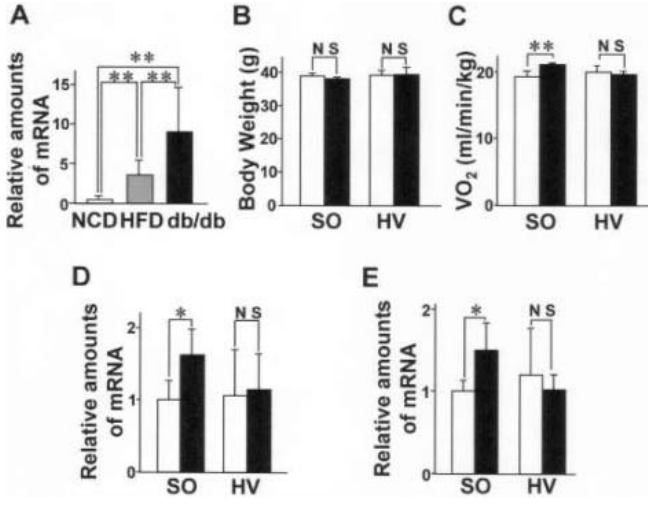

Fig. 3. HV inhibits TZD-enhanced energy expenditure in obese mice. (**A**) Relative amounts of PPARγ2 mRNA in the livers of normal chow diet–fed (NCD) C57BL/6 mice, high-fat diet–fed (HFD) C57BL/6 mice, and normal chow diet–fed db/db (db/db) mice. (**B** to **E**) db/db mice were subjected to HV or SO 7 days before the 2-day administration of TZD (black bars) or vehicle (white bars), after which body weights (B) and resting oxygen consumptions (C) were measured. Relative amounts of UCP1 mRNA in BAT (D) and epididymal fat tissue (E) from mice fed ad libitum. Data are presented as mean ± SD. Significance as compared to control mice is indicated (**$P < 0.01$ and *$P < 0.05$) by an unpaired t test. NS, not significant.

Table 1. Afferent vagal activation from the liver is involved in remote effects of hepatic PPARγ2 expression. (Upper section) Mice were subjected to HV or SO 7 days before administration of LacZ or PPARγ2 adenovirus. Resting oxygen consumption (VO_2) was measured on day 3 after adenoviral injection. Mice were killed after a 10-hour fast on day 7 after adenoviral injection. (Lower section) Male SD rats with high-fat diet–induced obesity were subjected to application of capsaicin or vehicle to the vagal hepatic branch 7 days before administration of LacZ or PPARγ2 adenovirus. Seven days after adenoviral administration, epididymal fat weights were determined. Significance as compared to LacZ mice is indicated (P values) by an unpaired t test. LW, liver weight; HTG, hepatic TG content; P, PEPCK; CD, cell diameter; NS, not significant.

	SO			HV		
	LacZ	PPARγ2	P	LacZ	PPARγ2	P
LW (g)	1.11 ± 0.13	2.30 ± 0.39	<0.001	1.12 ± 0.07	2.07 ± 0.32	<0.001
HTG (mg/g tissue)	78.71 ± 46.50	171.26 ± 43.90	0.008	62.02 ± 24.92	215.09 ± 75.78	<0.001
P mRNA (liver)	1.00 ± 0.21	0.50 ± 0.17	0.003	1.356 ± 0.460	0.54 ± 0.22	0.002
WAT weight (g)	1.13 ± 0.13	0.85 ± 0.14	<0.001	1.04 ± 0.26	1.06 ± 0.19	NS
BAT CD (μm)	11.55 ± 4.45	7.69 ± 2.09	<0.001	10.63 ± 3.38	10.55 ± 3.93	NS
FFA (μEq/l)	556.14 ± 87.33	860.47 ± 206.04	0.005	533.14 ± 59.50	558.38 ± 151.58	NS
VO_2 (ml/min/kg)	30.25 ± 2.38	34.38 ± 3.03	0.015	32.73 ± 4.54	31.98 ± 4.05	NS
UCP1 mRNA (WAT)	1.00 ± 0.24	2.36 ± 0.77	0.019	2.05 ± 0.64	1.82 ± 1.15	NS
	Vehicle			Capsaicin		
WAT weight (g)	8.95 ± 0.99	7.06 ± 1.32	0.024	8.70 ± 1.14	8.85 ± 1.71	NS

brain and other tissues: humoral factors and neuronal pathways. Leptin, a humoral factor from adipocytes, is a mediator of metabolic information from adipose tissue to the hypothalamus (*2*). In addition, circulating nutrients reportedly affect food intake and alter hepatic glucose production via the efferent vagal pathway (*23*, *24*). An afferent vagal signal originating in the liver is likely to be another metabolic information pathway. In this way, the brain may integrate information obtained from several tissues and organs via both humoral and neuronal pathways. When the brain receives information regarding excess energy storage, the sympathetic nervous system is activated to enhance energy expenditure and lipolysis, thereby maintaining energy homeostasis. Disturbance of the control system is implicated in the development of the metabolic syndrome (*25*). Targeting of this neuronal pathway is a potential therapeutic strategy for treating the metabolic syndrome.

References and Notes

1. J. S. Flier, *Cell* **116**, 337 (2004).
2. J. M. Friedman, J. L. Halaas, *Nature* **395**, 763 (1998).
3. Y. Minokoshi, C. R. Kahn, B. B. Kahn, *J. Biol. Chem.* **278**, 33609 (2003).
4. T. Kitamura, C. R. Kahn, D. Accili, *Annu. Rev. Physiol.* **65**, 313 (2003).
5. J. An *et al.*, *Nat. Med.* **10**, 268 (2004).
6. T. Yamada *et al.*, *Cell Metab.* **3**, 223 (2006).
7. O. Gavrilova *et al.*, *J. Biol. Chem.* **278**, 34268 (2003).
8. V. Bocher, I. Pineda-Torra, J. C. Fruchart, B. Staels, *Ann. N.Y. Acad. Sci.* **967**, 7 (2002).
9. L. Fajas *et al.*, *J. Biol. Chem.* **272**, 18779 (1997).
10. C. F. Burant *et al.*, *J. Clin. Invest.* **100**, 2900 (1997).
11. L. Chao *et al.*, *J. Clin. Invest.* **106**, 1221 (2000).
12. R. Rahimian *et al.*, *Mol. Cell. Biochem.* **224**, 29 (2001).
13. K. Matsusue *et al.*, *J. Clin. Invest.* **111**, 737 (2003).
14. Y. Ishigaki *et al.*, *Diabetes* **54**, 322 (2005).
15. I. Nagase *et al.*, *J. Clin. Invest.* **97**, 2898 (1996).
16. J. Gomez-Ambrosi, G. Fruhbeck, J. A. Martinez, *Mol. Cell. Endocrinol.* **176**, 85 (2001).
17. Y. Hatakeyama, Y. Sakata, S. Takakura, T. Manda, S. Mutoh, *Am. J. Physiol. Regul. Integr. Comp. Physiol.* **287**, R336 (2004).
18. A. Wellstein, D. Palm, G. G. Belz, *J. Cardiovasc. Pharmacol.* **8** (suppl. 11), S36 (1986).
19. T. Hosono *et al.*, *Gene* **348**, 157 (2005).
20. S. Herzig *et al.*, *Nature* **426**, 190 (2003).
21. W. He *et al.*, *Proc. Natl. Acad. Sci. U.S.A.* **100**, 15712 (2003).
22. A. L. Hevener *et al.*, *Nat. Med.* **9**, 1491 (2003).
23. A. Pocai, S. Obici, G. J. Schwartz, L. Rossetti, *Cell Metab.* **1**, 53 (2005).
24. T. K. Lam *et al.*, *Nat. Med.* **11**, 320 (2005).
25. M. W. Schwartz, D. Porte Jr., *Science* **307**, 375 (2005).

26. We thank M. Kaji, T. Takai, Y. Sato, H. Yawo, T. Hashikawa, M. Kanzaki, Y. Minokoshi, and M. Tominaga for advice and discussions. Supported by grants-in-aid from the Ministry of Education, Science, Sports, and Culture of Japan (H.K.), a grant-in-aid from the Ministry of Health, Labor, and Welfare of Japan (Y.O.), and the 21st Century Center of Excellence Programs (H.K. and Y.O.).

Supporting Online Material

www.sciencemag.org/cgi/content/full/312/5780/1656/DC1
Materials and Methods
SOM Text
Figs. S1 to S6
Table S1
References

9 February 2006; accepted 8 May 2006
10.1126/science.1126010

Synaptic Amplifier of Inflammatory Pain in the Spinal Dorsal Horn

Hiroshi Ikeda,* Johanna Stark, Harald Fischer, Matthias Wagner, Ruth Drdla, Tino Jäger, Jürgen Sandkühler†

Inflammation and trauma lead to enhanced pain sensitivity (hyperalgesia), which is in part due to altered sensory processing in the spinal cord. The synaptic hypothesis of hyperalgesia, which postulates that hyperalgesia is induced by the activity-dependent long-term potentiation (LTP) in the spinal cord, has been challenged, because in previous studies of pain pathways, LTP was experimentally induced by nerve stimulation at high frequencies (~100 hertz). This does not, however, resemble the real low-frequency afferent barrage that occurs during inflammation. We identified a synaptic amplifier at the origin of an ascending pain pathway that is switched-on by low-level activity in nociceptive nerve fibers. This model integrates known signal transduction pathways of hyperalgesia without contradiction.

Inflammation of peripheral tissues causes spontaneous pain and hyperalgesia. Amplification of pain-related information in the spinal dorsal horn lamina I contributes to inflammatory pain (*1*–*6*). Inflammation causes release of neuromodulators, including substance P and glutamate in spinal dorsal horn (*7*, *8*), potentially leading to Ca^{2+}-dependent LTP. In all previous studies, spinal LTP was induced by brief (1 s), high-frequency (100 Hz) burstlike stimulation (HFS) of afferent nerve fibers. High-frequency bursts do not, however, resemble the continuous low-frequency afferent barrage that occurs during inflammation. Low-frequency presynaptic activity normally fails to induce LTP but rather induces synaptic long-term depression (LTD) (*9*). The LTP model of inflammatory hyperalgesia thus may be questioned. Here, we evaluated the effect of low-frequency afferent barrage on synaptic transmission in ascending pain pathways and asked if synaptic plasticity is differentially induced in distinct ascending pain tracts. We labeled lamina I projection neurons by retrograde fluorescent marker DiI (1,1′-dioctadecyl-3,3,3′,3′-tetramethylindocarbocyanine perchlorate), injected into either of two major projection areas of spinal lamina I neurons: the parabrachial (PB) area or the periaqueductal gray (PAG) (*10*, *11*) (Fig. 1, A and B). To circumvent confounding developmental factors, we used only juvenile or adult rats in this study. Transverse spinal cord slices with long dorsal roots attached were prepared 3 to 4 days after DiI injections to allow whole-cell recordings from identified projection neurons in 21- to 28-day-old rats (*10*). In the presence of tetrodotoxin, bath application of substance P (2 μM) induced transient inward currents in 21 out of 27 spino-PB and in 9 out of 12 spino-PAG neurons (Fig. 1C), confirming the expression of functional neurokinin 1 receptors (NK1Rs). Spinal release of substance P following electrical stimulation of primary afferents at C-fiber strength was assessed by the internalization of NK1R in lamina I neurons. HFS parameters (100-Hz bursts) similar to all previously used conditioning stimulation protocols to induce classical LTP in pain pathways, or low-frequency stimulation (LFS, 2 Hz), was used. Both types of stimulation elicited substantial NK1R internalization in 89 ± 1% and in 78 ± 4% of 150 neurons evaluated in three rats per group (Fig. 1D). We then used these stimulation protocols for conditioning.

Conditioning HFS induces LTP at synapses between C-fibers and lamina I neurons that project to the PB (*12*). We confirmed these results by showing LTP of monosynaptically evoked excitatory postsynaptic currents (EPSCs) to 172 ± 15% of the control value at 30 min after conditioning ($n = 8$) (Fig. 2A). However, conditioning electrical stimulation within the typical frequency band of C-fibers during inflammation (2 Hz) (*13*) did not change synaptic strength in any of the spino-PB neurons tested (108 ± 19% of control, $n = 7$) (Fig. 2C). LFS, however, did modify synaptic strength in spinal lamina I neurons with a projection to the PAG. In all spino-PAG neurons tested, LFS induced a robust LTP of monosynaptic C-fiber–evoked EPSCs [to 262 ± 30% of the control value at 30 min after stimulation ($n = 18$) and to 346 ± 33% at 60 min ($n = 8$)] (Fig. 2D). In all seven lamina I neurons with a projection to the PAG, conditioning stimulation at high frequency was ineffective (98 ± 10%, $n = 7$) (Fig. 2B). Monosynaptic, A-fiber–evoked

Department of Neurophysiology, Center for Brain Research, Medical University of Vienna, Vienna, Austria.

*Present address: Department of Human and Artificial Intelligence Systems, University of Fukui, 3-9-1 Bunkyo, Fukui 910-8507, Japan.

†To whom correspondence should be addressed. E-mail: juergen.sandkuehler@meduniwien.ac.at

EPSCs were not affected by conditioning LFS at C-fiber strength (113 ± 5% of the control value in four spino-PAG neurons tested).

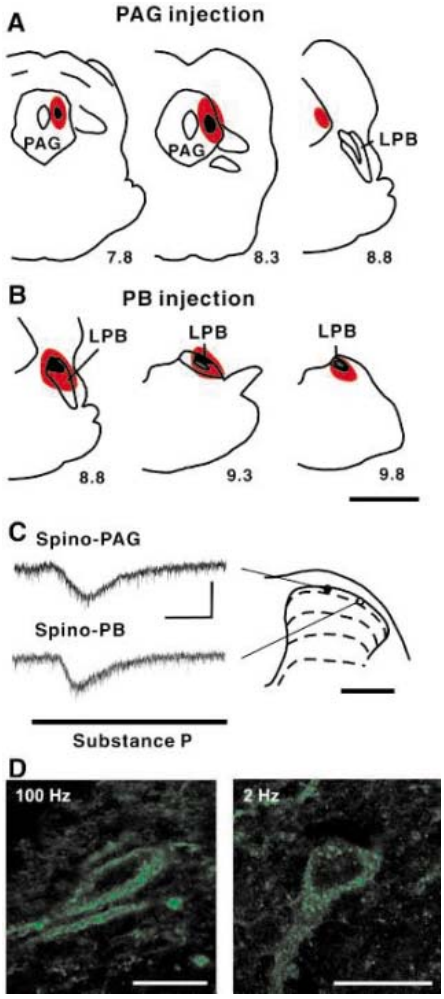

Fig. 1. Properties of lamina I projection neurons that express N1KRs. Retrograde, fluorescent marker DiI (30 to 50 nl, 2.5%) was injected into either the PAG (**A**) or the PB (**B**) of 18- to 24-day-old rats. Shown are representative injection sites of two different animals on coronal sections. Black spots represent tissue damage due to the injections and red areas distribution of the dye. The distance from bregma is given in mm below each section; bar: 3 mm. LPB: lateral parabrachial area. (**C**) Recording sites of two lamina I neurons in lumbar spinal cord of two rats with a projection to the PAG (filled circle) or the PB (open circle) on a representative sketch of spinal dorsal horn (right-hand site; bar: 500 μm). Both neurons responded with a transient inward current to bath application of substance P (horizontal bar: 2 μM; V_{hold} = –60 mV, left-hand site). Calibration bars: 30 s/20 pA. (**D**) Internalization of NK1Rs in spinal lamina I neurons following HFS (three bursts of 100 Hz, each given for 1 s at 10-s intervals) or LFS (2 Hz, 2 min) of sciatic nerve at C-fiber strength in intact, adult rats. Confocal images of representative transverse sections through the ipsilateral lumbar enlargement are shown. NK1R immunoreactivity is shown in green. Bars: 20 μm.

We next explored whether signal transduction pathways that are known to lead to hyperalgesia in vivo are also relevant for the induction of spinal LTP in vitro. In behaving animals, inflammatory hyperalgesia is prevented by spinal blockade of *N*-methyl-D-aspartate receptors (NMDARs), NK1Rs, or low-threshold, T-type voltage-gated calcium channels (VGCCs) (*14*, *15*). Here, induction of LTP by conditioning LFS also required activation of NK1Rs, NMDAR channels, and T-type VGCCs (fig. S1, A to C). This synergistically triggers a rise in postsynaptic cytosolic free Ca^{2+} concentration ($[Ca^{2+}]_i$) and activation of phospholipase C (PLC), protein kinase C (PKC), and calcium-calmodulin–dependent protein kinase II (CaMKII), which

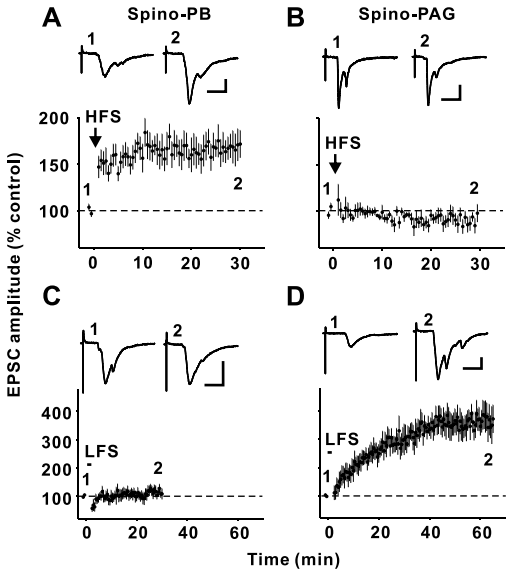

Fig. 2. Contrasting forms of LTP are expressed in distinct groups of spinal lamina I projection neurons. (**A** and **B**) Time courses of mean amplitudes (± SEM) of C-fiber–evoked EPSCs in lamina I neurons with a projection to the PB (n = 8) or the PAG (n = 7). Conditioning HFS induced LTP in all spino-PB neurons tested but was ineffective in spino-PAG neurons. (**C** and **D**) Conditioning LFS induced LTP in all 18 spino-PAG neurons tested but was ineffective in 7 spino-PB neurons. $V_{hold} \approx -50$ mV; current-clamp mode was used during conditioning stimulation in all groups. Above the graphs are shown original, representative EPSCs recorded just before and 30 or 60 min after HFS or LFS, respectively. Calibration bars: 20 ms/200 pA.

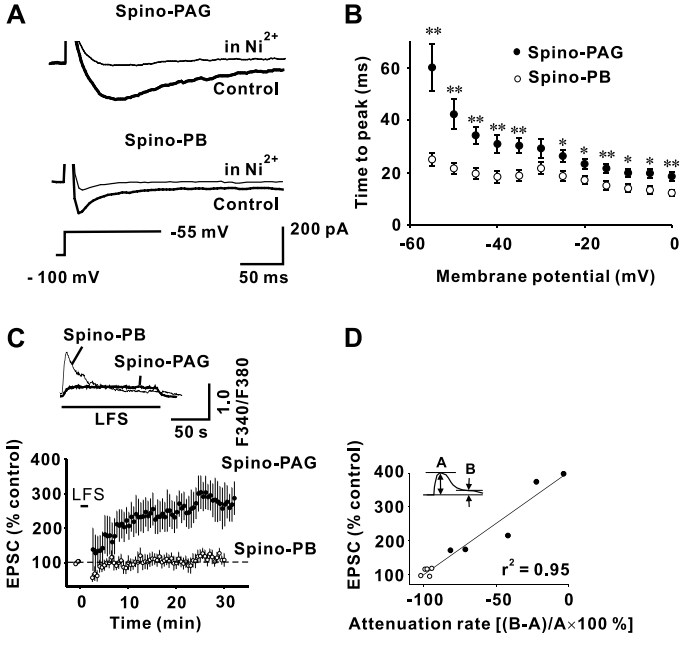

Fig. 3. LFS-induced LTP in spino-PAG neurons requires sustained influx of Ca^{2+} into the cell. (**A**) Representative current traces evoked in a spino-PAG or a spino-PB neuron in response to a voltage step (bottom trace) and under control conditions (thick lines). Downward deflection (inward current) was sensitive to bath application of 100 μM Ni^{2+} and had slower kinetics in spino-PAG than in spino-PB neurons (thin lines). (**B**) Activation kinetics of Ca^{2+} currents as determined from voltage-current curves. The mean time to peak (±SEM) of activation kinetics are plotted against test membrane potential and reveal slower activation kinetics for spino-PAG neurons (n = 15, filled circles) as compared to spino-PB neurons (n = 15, open circles). *$P < 0.05$, **$P < 0.01$ as compared to spino-PB neurons. (**C**) Upper traces indicate Ca^{2+} signals of one spino-PAG neuron and one spino-PB neuron during LFS. The ratio of the intensities of fluorescence measured at 340 nm and 380 nm (F340/F380) is plotted against time. Graphs below show mean time courses of EPSC amplitudes (in percent of control values) in spino-PAG neurons or spino-PB neurons before and after LFS at time zero (n = 5 in each group). In this group of neurons, Ca^{2+} imaging was performed in parallel with EPSC recordings. (**D**) A linear correlation exists between the change of EPSC amplitude (in percent of controls) and the attenuation rate. The attenuation rate of the Ca^{2+} signal varies for spino-PAG neurons but clusters around −100% for spino-PB neurons. Open circles, spino-PB neurons; filled circles, spino-PAG neurons.

are all necessary for the full development of inflammatory hyperalgesia. Block of a Ca^{2+} rise in lamina I spino-PAG neurons (fig. S1D) or bath application of blockers of PLC, PKC, or CaMKII all abolished induction of LTP by LFS (fig. S1, E to G). Blockade of inositol-1,4,5-trisphosphate receptors (IP_3Rs) converted LTP into LTD (fig. S1H).

A rise in $[Ca^{2+}]_i$ may also activate nitric oxide synthase (NOS), which is essential for mediating inflammatory hyperalgesia in behaving animals (*16*). We therefore examined whether NO is essential for induction of LTP and which NO substrate is involved. Inhibition of NOS abolished LTP induction by LFS (fig. S2A). Soluble guanylyl cyclase (sGC), which is a major substrate for NO, was indispensable for LTP induction (fig. S2B). Immunohistochemically, we have identified sGC, but not NOS, in spino-PAG lamina I neurons (*17*), suggesting that NO has to cross the extracellular space to reach its target. Bath application of an NO scavenger effectively blocked LTP induction in spino-PAG neurons (fig. S2C).

The level and the time course of the $[Ca^{2+}]_i$ rise in postsynaptic neurons determine the expression and polarity of synaptic plasticity (*9*, *18*–*20*). We compared Ca^{2+} currents induced by depolarizing voltage steps from a holding potential (V_{hold}) of −100 mV in spino-PAG and spino-PB neurons in voltage-clamp experiments. Calcium currents in both groups had low activation thresholds (≈ −60 mV from a V_{hold} of −90 mV) and inactivation thresholds (≈ −75 mV) and were abolished by Ni^{2+} (Fig. 3A), suggesting the contribution of T-type VGCCs. The time to peak of activation kinetics was longer in spino-PAG neurons than in spino-PB neurons (Fig. 3B). We next used Ca^{2+} imaging to evaluate activity-dependent Ca^{2+} gradients. LFS applied to dorsal root induced a slower rise and fall in $[Ca^{2+}]_i$ in spino-PAG neurons as compared to spino-PB neurons (Fig. 3C). The attenuation rate of $[Ca^{2+}]_i$ was inversely correlated with the magnitude of LTP (Fig. 3D).

Presynaptic activity at low frequencies consistently fails to induce LTP unless the rise in postsynaptic $[Ca^{2+}]_i$ is facilitated by removal of the voltage-dependent Mg^{2+} block of the NMDAR channel (*9*, *18*–*21*). However, the induction of inflammatory hyperalgesia in vivo is triggered by irregular, asynchronous, low-frequency discharges in primary afferent C-fibers impinging on dorsal horn neurons, which are subject to considerable pre- and postsynaptic inhibition (*14*, *22*). Thus, one might question whether a natural afferent barrage during inflammation or trauma can induce a sufficiently strong rise in $[Ca^{2+}]_i$ in spinal neurons to trigger LTP in vivo. To address this key question, we monitored Ca^{2+} gradients in lamina I neurons during LFS or inflammation in vivo.

In 25- to 29-day-old intact rats, two-photon laser-scanning microscopy was used to quantify neuronal Ca^{2+} gradients in response to sensory stimulation (*10*). LFS of the sciatic nerve at C-fiber but not at A-fiber intensity induced a strong and sustained rise in Ca^{2+} concentration in all 27 lamina I neurons tested, including 7 neurons with an identified projection to the PAG (fig. S3, A and B). We next investigated whether natural, low-frequency irregular and nonsynchronous discharges in a subset of nociceptive C-fibers can also raise Ca^{2+} concentrations in spinal lamina I neurons in vivo. Subcutaneous injection of capsaicin activates transient receptor potential vanilloid 1 receptor ion channels in a subset of nociceptive C-fiber afferents, leading to intense burning pain for a few minutes, followed by hyperalgesia for hours (*7*). Hyperalgesia evoked by capsaicin is commonly used to study the central mechanisms of pain amplification (*7*, *23*). Here, capsaicin induced a strong rise in $[Ca^{2+}]_i$ in 15 lamina I neurons tested (fig. S3C).

We then asked if conditioning stimuli that trigger sustained Ca^{2+} gradients in nociceptive lamina I neurons also amplify synaptic strength in vivo. We recorded C-fiber–evoked field potentials in the superficial spinal dorsal horn of adult, deeply anesthetized rats, with spinal cords intact (*10*). Capsaicin induced a slowly developing LTP to 173 ± 9% of the control value (n = 5) 60 min after injection (Fig. 4A). Subcutaneous injection of diluted formalin is a model of chemically induced inflammation and leads to long-lasting, low-frequency discharges in C-fibers and biphasic pain behavior in animals. Here, formalin injections induced a slow-onset LTP (to 172 ± 16% of the control value at 60 min, n = 6) (Fig. 4B). To exclude the possibility that ongoing activity in C-fibers contributed to the enhanced responses in spinal cord, we cooled the afferent nerve by a Peltier-element distal to the stimulation electrode 60 min after formalin injection. The nerve block did not affect maintenance of LTP in any of the three animals tested. Electrical LFS of sciatic nerve at C-fiber but not at A-fiber intensity (101 ± 1% of control, n = 3) also induced a robust LTP in vivo (to 274 ± 21% of the control value at 120 min and to 228 ± 20% at 300 min, n = 28) (Fig. 4C), which lasted up to 10 hours. In line with the in vitro results, LFS-induced LTP in vivo also required coactivation of NMDARs and NOS (Fig. 4, D and E). A-fiber–evoked field potentials were not potentiated by LFS at C-fiber strength in any of the eight animals tested.

We have identified a synaptic pain amplifier in the spinal cord that is turned on in mature animals by natural, asynchronous and irregular, low-rate discharge patterns in nociceptive C-fibers at synapses with spino-PAG neurons, a distinct subgroup of lamina I projection neurons (*24*–*26*). In contrast to other, rare forms of low frequency–induced LTP in the central nervous system, the synaptic plasticity described in this work can be induced under physiological conditions and in the presence of tonic pre- and postsynaptic inhibition. Our results suggest that during low-level presynaptic activity, multiple sources of Ca^{2+} are recruited simultaneously by activation of NMDARs, VGCCs, and NK1R and mobilization of Ca^{2+} from intracellular stores to achieve a sufficient rise of Ca^{2+} in the

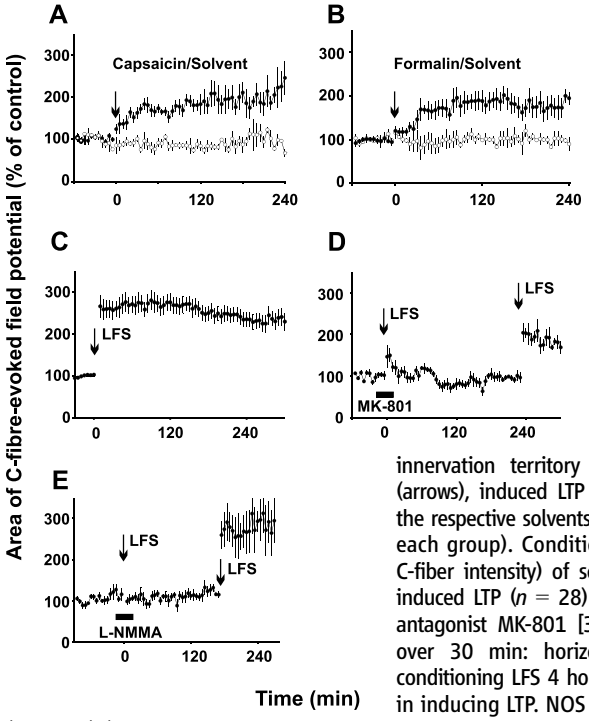

Fig. 4. LTP can be induced by natural, low-frequency afferent barrage evoked by inflammation of peripheral tissue in vivo. Mean time courses of C-fiber–evoked field potentials recorded extracellulary in superficial spinal dorsal horn in response to electrical stimulation of left sciatic nerve of deeply anesthetized adult rats with spinal cords and afferent nerves intact. Subcutaneous injections of transient receptor potential vanilloid 1 channel agonist capsaicin (1%, 100 μl, n = 5) (**A**) or formalin (5%, 100 μl, n = 6) (**B**) into the glabrous skin at the ipsilateral hind paw, within the innervation territory of the sciatic nerve at time zero (arrows), induced LTP (closed circles), whereas injections of the respective solvents (open circles) had no effect (n = 3 in each group). Conditioning electrical LFS (2 Hz, 2 min at C-fiber intensity) of sciatic nerve at time zero (arrow) also induced LTP (n = 28) (**C**), which was prevented by NMDAR antagonist MK-801 [3 mg kg^{-1}, intravenous (iv) infusion over 30 min: horizontal bar, n = 5) (**D**). A second conditioning LFS 4 hours later (arrow) was partially effective in inducing LTP. NOS inhibitor NG-monomethyl-L-arginine (L-NMMA) (100 mg kg^{-1} $hour^{-1}$, iv infusion: horizontal bar, n = 5) (**E**) also blocked LTP induction. This block was fully reversible, as shown by a second LFS 3 hours later (arrow).

postsynaptic neuron. This then leads to activation of calcium-dependent protein kinases and NOS, which causes amplification of pain-related information at the first synapse in pain pathways. Blockade of IP_3Rs unmasked LTD of synaptic strength in C-fibers induced by LFS. This suggests that LFS may simultaneously induce synaptic plasticity of opposite polarity involving divergent signal transduction pathways. Hyperalgesia in human (*27*) and in animal studies (*7*, *28*, *29*) and the synaptic pain amplifier described in this work share induction mechanisms, relevant neuron populations in spinal cord, pharmacological profile, and signal transduction pathways. This strongly suggests that LTP at the first synapse in pain pathways between nociceptive C-fibers and spinal lamina I projection neurons is a cellular key mechanism of inflammatory hyperalgesia and perhaps other forms of low-level afferent-induced hyperalgesia (*30*, *31*).

References and Notes

1. C. J. Woolf, *Nature* **306**, 686 (1983).
2. J. L. K. Hylden, R. L. Nahin, R. J. Traub, R. Dubner, *Pain* **37**, 229 (1989).
3. D. A. Simone *et al.*, *J. Neurophysiol.* **66**, 228 (1991).
4. S. G. Khasabov *et al.*, *J. Neurosci.* **22**, 9086 (2002).
5. A. J. Todd *et al.*, *J. Neurosci.* **22**, 4103 (2002).
6. A. D. Craig, *J. Comp. Neurol.* **361**, 225 (1995).
7. W. D. Willis, *Ann. N.Y. Acad. Sci.* **933**, 142 (2001).
8. S. P. Hunt, P. W. Mantyh, *Nat. Rev. Neurosci.* **2**, 83 (2001).
9. M. Cavazzini, T. Bliss, N. Emptage, *Cell Calcium* **38**, 355 (2005).
10. Materials and methods are available as supporting material on *Science* Online.
11. A. J. Todd, M. M. McGill, S. A. S. Shehab, *Eur. J. Neurosci.* **12**, 689 (2000).
12. H. Ikeda, B. Heinke, R. Ruscheweyh, J. Sandkühler, *Science* **299**, 1237 (2003).
13. S. Puig, L. S. Sorkin, *Pain* **64**, 345 (1996).
14. W. D. Willis Jr., R. E. Coggeshall, *Sensory Mechanisms of the Spinal Cord. Primary Afferent Neurons and the Spinal Dorsal Horn* (Kluwer Academic/Plenum, New York, ed. 3, 2004), pp. 1–560.
15. T. L. Yaksh, X. Y. Hua, I. Kalcheva, N. Nozaki-Taguchi, M. Marsala, *Proc. Natl. Acad. Sci. U.S.A.* **96**, 7680 (1999).
16. S. T. Meller, G. F. Gebhart, *Pain* **52**, 127 (1993).
17. R. Ruscheweyh, A. Goralczyk, G. Wunderbaldinger, A. Schober, J. Sandkühler, *Neuroscience,* in press.
18. I. Ismailov, D. Kalikulov, T. Inoue, M. J. Friedlander, *J. Neurosci.* **24**, 9847 (2004).
19. R. C. Malenka, B. Lancaster, R. S. Zucker, *Neuron* **9**, 121 (1992).
20. S. N. Yang, Y. G. Tang, R. S. Zucker, *J. Neurophysiol.* **81**, 781 (1999).
21. J. Lisman, *Philos. Trans. R. Soc. London B Biol. Sci.* **358**, 829 (2003).
22. E. R. Perl, in *Handbook of Physiology*, Section 1, *The Nervous System*, vol. 3, I. Darian-Smith, Ed. (American Physiological Society, Bethesda, MD, 1984), pp. 915–975.
23. H. E. Torebjörk, L. E. Lundberg, R. H. LaMotte, *J. Physiol.* **448**, 765 (1992).
24. R. C. Spike, Z. Puskár, D. Andrew, A. J. Todd, *Eur. J. Neurosci.* **18**, 2433 (2003).
25. R. Ruscheweyh, H. Ikeda, B. Heinke, J. Sandkühler, *J. Physiol.* **555**, 527 (2004).
26. Because most lamina I spino-PAG neurons have collaterals to the parabrachial area, they constitute a subgroup of about one-third of the spino-PB population. Nevertheless, they have been shown to differ from other spino-PB neurons, e.g., with respect to NK1R expression and active and passive membrane properties. See (*24*, *25*) for further discussion.
27. T. Klein, W. Magerl, H. C. Hopf, J. Sandkühler, R.-D. Treede, *J. Neurosci.* **24**, 964 (2004).
28. P. W. Mantyh *et al.*, *Science* **278**, 275 (1997).
29. M. L. Nichols *et al.*, *Science* **286**, 1558 (1999).
30. F. Cervero, R. Gilbert, R. G. Hammond, J. Tanner, *Pain* **54**, 181 (1993).
31. W. Koppert *et al.*, *Anesthesiology* **95**, 395 (2001).

32. Supported by grant P18129 from the Austrian Science Fund (FWF) to J.S. The Japan Society for the Promotion of Science partially supported H.I. We thank R.-D. Treede and A. H. Dickenson for reading an earlier version of the manuscript.

Supporting Online Material

www.sciencemag.org/cgi/content/full/312/5780/1659/DC1
Materials and Methods
Figs. S1 to S3
References

9 March 2006; accepted 10 May 2006
10.1126/science.1127233

Food-Caching Western Scrub-Jays Keep Track of Who Was Watching When

Joanna M. Dally,[1,2] Nathan J. Emery,[1] Nicola S. Clayton[2]*

Western scrub-jays (*Aphelocoma californica*) hide food caches for future consumption, steal others' caches, and engage in tactics to minimize the chance that their own caches will be stolen. We show that scrub-jays remember which individual watched them during particular caching events and alter their recaching behavior accordingly. We found no evidence to suggest that a storer's use of cache protection tactics is cued by the observer's behavior.

Social living is suggested to have selected for increased sociocognitive skills in animals (*1*, *2*). Several species use information about the dominance rank (*3*) and social relationships (*4*) of conspecifics when forming alliances or competing for resources (*5*, *6*). Corvids rely on observational spatial memory to steal others' caches (*7*–*9*), and they engage in a variety of behaviors to reduce cache theft (*10*–*15*). It may be advantageous to remember who was watching during specific caching events, because scrub-jays can only defend caches against subordinates (*16*). Scrub-jays should therefore engage in cache protection when they are caching in view of dominant birds, but might refrain from doing so when watched by their partner, because they often defend their partner's caches and tolerate cache theft by their mate (*16*).

Nine birds (storers) cached in two trays, one near and one far from an observer. Storers cached in the presence of a dominant bird ("dominant"), a subordinate bird ("subordinate"), their partner ("partner"), or when an observer's view was obscured ("in private"). After 3 hours, storers recovered their caches "in private" (*17*). Partnerships and dominance indices were determined before this experiment when the birds were aviary housed (*16*).

The total number of items cached did not differ significantly between conditions [Friedman's analysis of variance (ANOVA), $\chi_3^2 = 2.5$, $P = 0.45$]. Birds cached predominantly in the far tray in the "dominant" (sign test: $S = 7/7$, $P = 0.02$) and "subordinate" condition ($S = 7/7$, $P = 0.02$), but not in the "partner" condition ($S = 5/7$, $P = 0.13$) or "in private" ($S = 3/7$, $P > 0.05$) (table S1).

The proportion of items that were recached at recovery was greatest in the "dominant" condition (Fig. 1A). In the "dominant" and "subordinate" conditions, items were predominantly moved from the near tray. Surprisingly, items were also moved, but from both trays, after the "in private" and "partner" conditions (Fig. 1B). Irrespective of condition, items were always moved to out-of-tray sites around the home cage.

The pattern of caching and recaching suggests that scrub-jays engage in cache protection to combat the specific risk that nonpartners pose to their caches, even though observers did not have the opportunity to pilfer. Specifically, birds cached mainly in the far tray when observed by a nonpartner and recached the few items hidden in the near tray at recovery. It may be difficult for observers to see the location of caches in the far tray, thereby decreasing their ability to use observational spatial memory to facilitate cache pilferage. This strategy was not implemented when the storer's partner was present, perhaps because storers prefer to spend time near to their partner and do not perceive them as a risk to cache safety.

There are three alternate explanations for the preference to cache in the far tray in the "dominant" and "subordinate" conditions.

[1]Sub-department of Animal Behavior, University of Cambridge, Cambridge, CB3 8AA, UK. [2]Department of Experimental Psychology, University of Cambridge, Cambridge, CB2 3EB, UK.

*To whom correspondence should be addressed. E-mail: nsc22@cam.ac.uk

First, being near nonpartners might be aversive. However, in a previous experiment, scrub-jays spent similar amounts of time near and in-view and far and out-of-view of nonpartners during caching (*15*). Second, jays might be predisposed to cache at a distance from nonpartners. Yet our youngest cohort of birds do not discriminate between near [median = 1.5, interquartile range (IQR) = 11.5] and far trays (median = 6.5, IQR = 6.5; Wilcoxon's Z =0.42, P = 0.67) (table S4). Unlike the birds in this experiment (age 10), these young birds (age 3) have not experienced stealing others' caches, an experience that seems essential for the expression of recaching (*10*) and other protective behaviors. Finally, storers might have learned that caching in far sites reduces cache theft. However, storers received a single trial in each caching condition, and, because caches were never stolen, they received no feedback as to the success of their caching strategies. Critically, these explanations cannot explain the differences in the birds' recaching behavior, because cache recovery always occurred "in private." Differences in recaching must therefore be based on a storer's memory for the social status of who watched them cache.

To test whether scrub-jays remember which particular individual was present when they made specific caches, eight birds were given eight trials in which they cached successively in two trays, each in view of a different observer. Consequently, individual A observed the storer caching in one tray, and individual B observed the storer caching in a second tray immediately afterwards (AB trial), or vice versa (BA trial). During each caching period, both trays were placed in the storer's cage, but Perspex strips covered one tray to prevent caching in that tray. Observers therefore saw the storer caching in one (observed tray) but not the other tray. After 3 hours, storers recovered their caches either "in private," in-view of individual A or individual B ("observed" condition), or watched by a "control" bird that had not witnessed the storer caching (*17*). To control for any affect of observer social status on caching behavior, birds of similar rank were used, and storer-observer dominance relationships were counter balanced across trials.

No differences were detected in the number of items cached in the presence of individual A and individual B during AB and BA trials (χ_3^2 = 4.8, P = 0.21). The proportion of caches that were recached at recovery differed significantly between conditions (χ_3^2 = 17.9, P < 0.01) (table S2), and significantly more caches were recached during the "observed" condition relative to the "control" condition (Fig. 2A). A similar proportion of caches were recached from either tray "in private" (S = $^8/_{12}$, P = 0.39), whereas in the "observed" condition, storers recached specifically from the "observed" tray (Fig. 2A). Few items were recached from the "other" tray in the "observed" condition, or from either tray in the "control" condition.

Recaching in the "observed" and "in private" conditions differed in two respects. First, "in private" items were recached in "out-of-

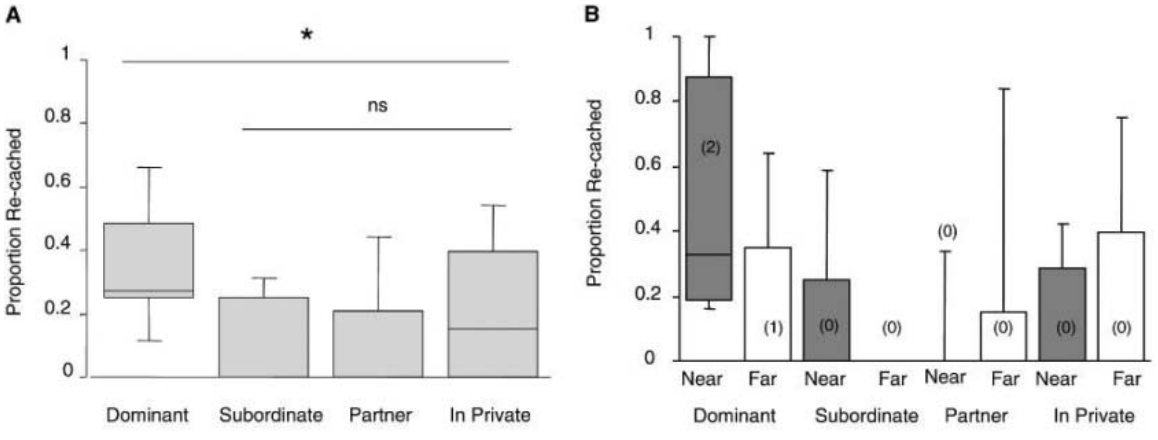

Fig. 1. Median proportion (25th percentile and 75th percentile) of items recached after each caching condition. (**A**) Recaching was greatest after the "dominant" condition (χ_3^2= 9.8, P = 0.02). When the "dominant" condition was removed from the analysis, no significant difference was identified between the remaining conditions (χ_3^2 = 1.4, P = 0.37). The asterisk indicates P < 0.05. ns, not significant. (**B**) The median proportion (25th percentile and 75th percentile) and median number (in parentheses) of items recached from "near" (open bars) and "far" (shaded bars) trays is shown for birds that cached in both trays. The data could not be analyzed statistically, because several birds did not cache in both trays (two in the "dominant" condition, four in the "partner" condition, and two "in private"), and their recovery behavior would therefore be confined to one location.

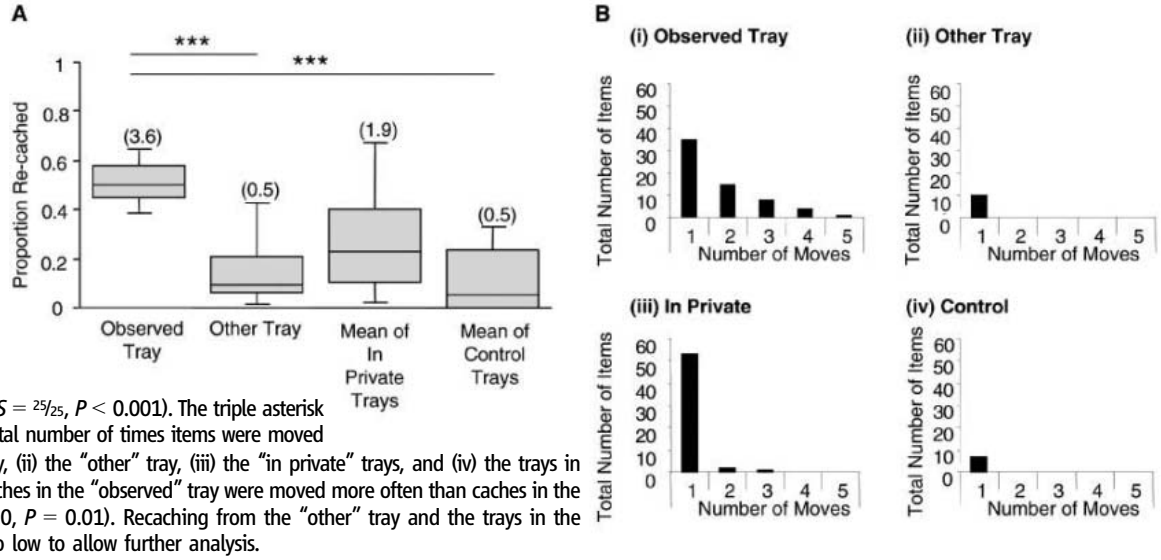

Fig. 2. (**A**) Median (25th percentile and 75th percentile) proportion and median number (in parentheses) of items recached from the "observed" and "other" trays in the "observed" condition, and the mean of trays in the "control" and "in private" conditions (χ_3^2 = 17.3, P = 0.0006). The proportion that was recached from the "observed" and "other" trays differed significantly (S = $^{25}/_{25}$, P < 0.001). The triple asterisk indicates P < 0.001. (**B**) Total number of times items were moved from (i) the "observed" tray, (ii) the "other" tray, (iii) the "in private" trays, and (iv) the trays in the "control" condition. Caches in the "observed" tray were moved more often than caches in the "in private" trays (χ_1^2 = 8.0, P = 0.01). Recaching from the "other" tray and the trays in the "control" condition was too low to allow further analysis.

tray" locations. By contrast, items from the "observed" tray were predominantly moved to cache sites within that tray ($\chi_1^2 = 17.9$, $P < 0.01$) (table S2). Second, caches in the "observed" condition were moved twice as often as those recached "in private" (Fig. 2B). Repeatedly moving items may decrease the accuracy with which potential thieves can relocate caches, because memories for successive locations should interfere with one another. Storing jays have been shown to recover caches they did or did not move multiple times with a comparable degree of accuracy (*14*).

It is possible that in experiment 2, storers were simply reacting to cues provided by the observer (*18*). For example, observers may direct more (or less) attention to trays they have seen a bird caching in. In experiment 3, we repeated the "observed" condition of experiment 2, and contrasted it with an "observer-control" condition (Fig. 3A). The "observer-control" condition was identical to the "observed" condition, except that in the "observed" condition, the observer saw the same bird at caching and recovery, whereas in the "observer-control" condition, the control bird watched a different individual recover its caches from the one it saw caching (*17*).

If cache recovery is mediated by a memory for who was present during caching, the birds' recovery behavior should differ between the "observed" and "observer-control" conditions. Based on experiment 2, storers in the "observed" condition should recache predominantly from the tray in which the observer at recovery had seen them cache ("observed" tray). However, because the control bird was not present when the storer cached, few items should be recached from either tray in the "observer-control" condition. A behavior-cueing account leads to a different prediction. If observers primarily attend to trays in which they have seen caching, and if storers use these cues to guide recovery, then storers should recache specifically from the "observed" tray in both conditions.

The number of items cached in the "observed" and "observer-control" conditions did not differ statistically ($\chi_1^2 = 17.9$, $P = 0.86$), nor was there any preference for caching in either tray ("observed": $S = 7/14$, $P > 0.05$; "observer-control": $S = 7/12$, $P > 0.05$) (table S3). The proportion of caches that were recached at recovery did not differ statistically between conditions ($\chi_1^2 = 0.13$, $P = 0.72$). In the "observed" condition, items were predominantly recached from the "observed" and not from the "other" tray. By contrast, in the "observer-control" condition, items were recached from both trays without selectivity (Fig. 3B). In both conditions, few items were recached in "out-of-tray" sites ($\chi_1^2 = 8.1$, $P = 0.01$) (table S3). Furthermore, in terms of the behavior of the birds that were observing at recovery, there was no evidence that observers and control birds (that saw a different bird at caching and recovery) differed in the amount of time they spent nearest to, or oriented toward, either tray (*17*).

These results suggest that scrub-jays remember who observed them make specific caches, and are not consistent with a behavior-cueing account. In our experiments, observers were never given the opportunity to pilfer the storer's caches. However, in previous studies, the birds not only had their caches pilfered (*10*) but witnessed observers stealing their caches (*19*). The unpredictability of cache safety might have motivated storers to consistently engage in

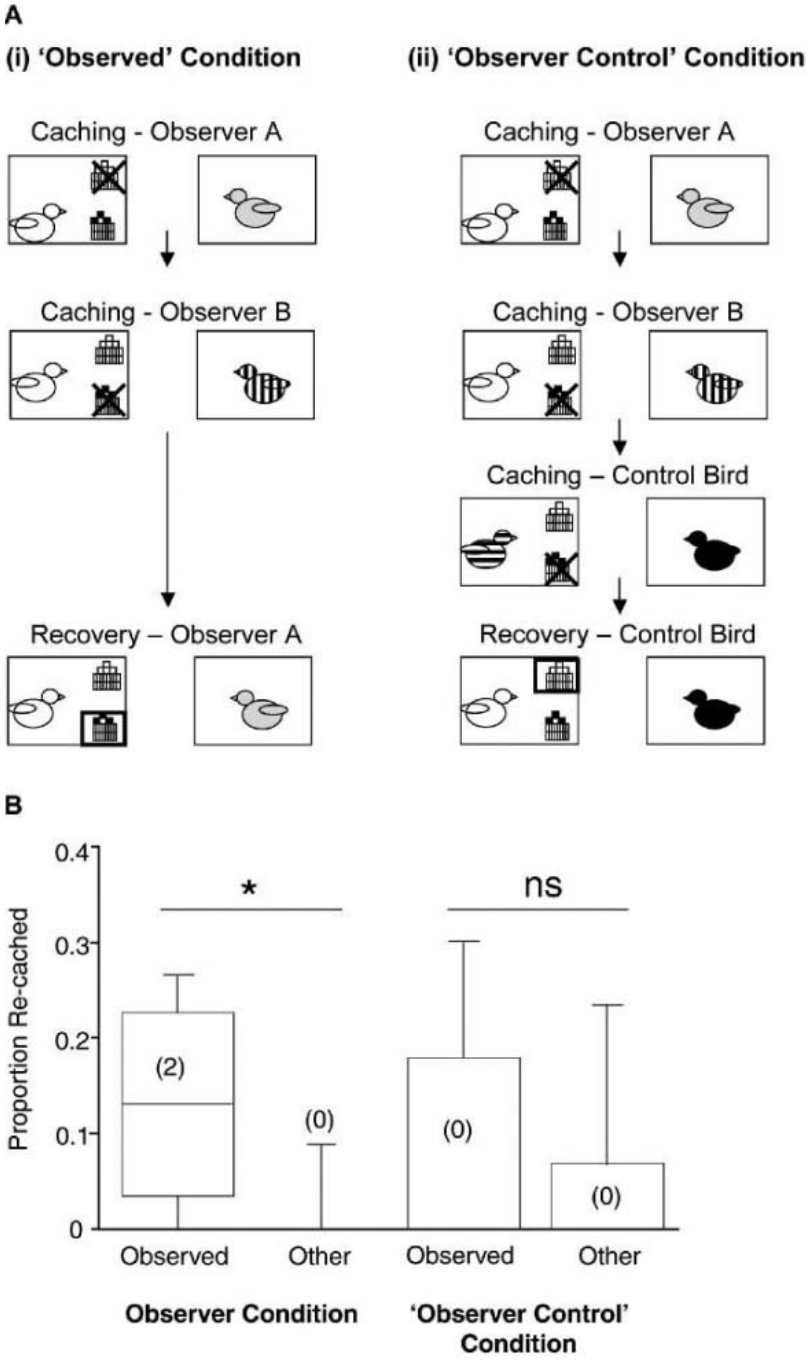

Fig. 3. (**A**) The "observed" and "observer-control" conditions of experiment 3. The clear bird indicates the storer in the "observed" and "observer-control" conditions, the horizontal striped bird indicates an additional storer in the "observer-control" condition, the lightly shaded bird indicates individual A, the vertical striped bird indicates individual B, and the black bird indicates the control bird. The black X indicates Perspex strips, the rectangle indicates the "observed" tray. (**B**) Median (25th percentile and 75th percentile) proportion and median number (in parentheses) of items recached from the "observed" and "other" trays in the "observed" ($S = 6/6$, $P = 0.03$) and "observer-control" conditions ($S = 4/6$, $P = 0.69$). The asterisk indicates $P < 0.05$. ns, not significant.

cache protection. Indeed, it was necessary to use different birds in experiments 2 and 3, because the birds in experiment 2 ceased to cache in the presence of an observer. Cache cessation appeared to be a direct consequence of observer presence as the birds continued to cache "in private," a finding perhaps indicative of a mechanism that acts to reduce caching levels with increased observer presence.

It is possible that scrub-jay caching and recovery behavior might be based on a series of conditional rules, rather than an assessment of risk. That is, jays might form specific associations between particular observers and cache locations. To generate the flexibility demonstrated in these experiments, however, these rules would have to be highly conditional and integrated with the associations between a specific tray and a particular individual.

Scrub-jays encode the "what-where-when" of specific caching episodes (*20*). Our findings suggest that scrub-jays also remember who was present during earlier caching events. This ability need not be based on a humanlike episodic memory, because these what-where-when memories may exist without the jay mentally reconstructing the past (*21*, *22*). Similarly, keeping track of who was watching when need not require a humanlike "theory-of-mind" in terms of attributing unobservable metal states (*18*), but it may result from behavioral predispositions in combination with specific learning algorithms or from reasoning about future risk. The propensity for subordinates to adjust their behavior in response to the presence or absence of a dominant conspecific has been suggested as evidence for knowledge attribution in chimpanzees (*23*) and ravens (*24*). Although the ability of nonhuman animals to reason about another's mind continues to elude definitive study, our study provides evidence to suggest that a nonhuman animal might discriminate between individuals with different knowledge states.

References and Notes

1. N. Humphrey, in *Machiavellian Intelligence: Social Expertise and the Evolution of Intellect in Monkeys, Apes and Humans*, R. Byrne, A. Whiten, Eds. (Clarendon Press, Oxford, 1988), pp. 13–26.
2. R. Byrne, A. Whiten, Eds., Machiavellian Intelligence: Social Expertise and the Evolution of Intellect in Monkeys, Apes and Humans (Clarendon Press, Oxford, 1988).
3. J. Silk, *Anim. Behav.* **58**, 45 (1999).
4. D. Cheney, R. Seyfarth, *Anim. Behav.* **34**, 1722 (1996).
5. A. Engh, E. Siebert, D. Greenberg, K. Holekamp, *Anim. Behav.* **69**, 209 (2005).
6. R. Connor, M. Heithaus, L. Barre, *Proc. R. Soc. London Ser. B* **268**, 263 (2000).
7. P. Bednekoff, R. Balda, *Behaviour* **133**, 807 (1996).
8. P. Bednekoff, R. Balda, *Anim. Behav.* **52**, 833 (1996).
9. N. Clayton, D. Griffiths, N. Emery, A. Dickinson, *Philos. Trans. R. Soc. London Ser. B* **356**, 1 (2001).
10. N. Emery, N. Clayton, *Nature* **414**, 443 (2001).
11. T. Bugnyar, K. Kotrschal, *Anim. Behav.* **64**, 185 (2002).
12. K. Clarkson, S. Eden, W. Sutherland, A. Houston, *J. Anim. Ecol.* **55**, 111 (1986).
13. J. Dally, N. Emery, N. Clayton, *Proc. R. Soc. London Ser. B* **271**, S387 (2001).
14. J. Dally, N. Emery, N. Clayton, *Anim. Behav.* **70**, 1251 (2005).
15. B. Heinrich, J. Pepper, *Anim. Behav.* **56**, 1083 (1998).
16. J. Dally, N. Emery, N. Clayton, *Behaviour* **142**, 961 (2005).
17. Materials and methods are available as supporting material on *Science* Online.
18. D. Povinelli, J. Vonk, *Trends Cogn. Sci.* **7**, 157 (2003).
19. N. Emery, J. Dally, N. Clayton, *Anim. Cogn.* **7**, 37 (2004).
20. N. Clayton, A. Dickinson, *Nature* **395**, 272 (1998).
21. T. Suddendorf, J. Busby, *Trends Cogn. Sci.* **7**, 391 (2003).
22. T. Suddendorf, J. Busby, *Learn. Motiv.* **36**, 110 (2005).
23. B. Hare, J. Call, M. Tomasello, *Anim. Behav.* **61**, 139 (2001).
24. T. Bugnyar, B. Heinrich, *Proc. R. Soc. London Ser. B* **272**, 1641 (2005).

25. N.S.C. received grants from the Biotechnology and Biological Sciences Research Council, Clare College, and the University of Cambridge. N.J.E. was funded by a Royal Society University Research Fellowship. J.M.D. received financial support from Clare College, the University of Cambridge, the Sir Richard Stapeley Educational Trust and the Sefton Educational Trust. We thank T. Dickinson, N. Davies, D. Byrne, S. de Kort, C. Rutte, N. Humphrey, C. Teufel, A. Seed, D. Alexis, A. Miller, and H. Prior for comments and discussion; S. Stevens and S. de Kort for allowing reference to their data; and D. Alexis, C. Teufel, and A. Seed for acting as observers. We are indebted to B. Brown for his statistical expertise.

Supporting Online Material

www.sciencemag.org/cgi/content/full/1126539/DC1
Materials and Methods
Tables S1 to S4
References

22 February 2006; accepted 5 May 2006
Published online 18 May 2006;
10.1126/science.1126539
Include this information when citing this paper.

Regulation of B Cell Tolerance by the Lupus Susceptibility Gene *Ly108*

Kirthi Raman Kumar,[1] Liunan Li,[1] Mei Yan,[1] Madhavi Bhaskarabhatla,[1] Angela B. Mobley,[2] Charles Nguyen,[2] Jill M. Mooney,[3] John D. Schatzle,[2,3] Edward K. Wakeland,[2] Chandra Mohan[1,2]*

The susceptibility locus for the autoimmune disease lupus on murine chromosome 1, *Sle1*^{z}/*Sle1b*^{z}, and the orthologous human locus are associated with production of autoantibody to chromatin. We report that the presence of *Sle1*^{z}/*Sle1b*^{z} impairs B cell anergy, receptor revision, and deletion. Members of the *SLAM* costimulatory molecule family constitute prime candidates for *Sle1b*^{z}, among which the *Ly108.1* isoform of the *Ly108* gene was most highly expressed in immature B cells from lupus-prone B6.*Sle1*^{z} mice. The normal *Ly108.2* allele, but not the lupus-associated *Ly108.1* allele, was found to sensitize immature B cells to deletion and *RAG* reexpression. As a potential regulator of tolerance checkpoints, *Ly108* may censor self-reactive B cells, hence safeguarding against autoimmunity.

Loss of B cell tolerance is the hallmark of systemic lupus erythematosus (SLE), or lupus, an antibody-mediated chronic autoimmune disease affecting multiple organs. However, the precise means by which tolerance is breached in lupus, and the underlying genes and molecules responsible, remain obscure. The origin of lupus in both mice and humans appears to be polygenic, involving more than a dozen potent loci (*1*–*3*), although of these, at least one locus on chromosome 1 appears to be shared by both species. The *z* allele of *Sle1* and its component sublocus *Sle1b*, derived from the lupus-prone NZM2410/NZW strain of mice, are linked to a variety of lupus-related disease phenotypes, including antinuclear antibodies (ANAs), splenomegaly, and glomerulonephritis (*4*, *5*). A locus on human chromosome 1 orthologous to murine *Sle1* has also been implicated in lupus susceptibility (*6*). Located within the *Sle1b*^{z} sublocus, the *SLAM* gene family–encoded costimulatory molecules are among the first candidate genes to be identified as being linked to spontaneous lupus in mice (*7*). Extensive polymorphisms and expression differences were documented in several members of this gene cluster between the normal C57BL/6 (B6) strain and the lupus-prone B6.*Sle1b*$^{z/z}$ congenic mice bearing the *z* haplotype of *SLAM* (*7*).

To determine the mechanisms by which B cell tolerance might be infringed in lupus, the B cell repertoire of B6.*Sle1*$^{z/z}$ congenic mice (*8*) was modified to an essentially monoclonal specificity by breeding onto them a B cell receptor (BCR) transgene specific for lysozyme (HEL) (*9*). In these B6.HEL^{Ig} mice, the HEL^{Ig} BCR transgene leads to a near-uniform pool of HEL-specific B cells bearing a BCR heavy chain of immunoglobulin M^a (IgM^a) allotype and high titers of serum antibodies to HEL of IgM^a allotype (*9*). Developmental exposure of these B cells to a strong cross-linking surrogate

[1]Department of Internal Medicine (Rheumatology), [2]Center for Immunology, [3]Department of Pathology, University of Texas Southwestern Medical Center, Dallas, TX 75390, USA.

*To whom correspondence should be addressed. E-mail: chandra.mohan@utsouthwestern.edu

self-antigen [in the form of cell-membrane–bound HEL (mHEL)], leads to clonal deletion in the bone marrow (*10*). However, when exposed to a weaker surrogate self-antigen [in the form of soluble HEL (sHEL)], the same HEL-specific B cells are censored by an alternate tolerogenic mechanism known as anergy (*9*). To ascertain how *Sle1*^{z} might influence B cell tolerance, B6.*Sle1*$^{z/z}$.HEL^{lg} mice were bred to mHEL or sHEL mice.

B6.*Sle1*$^{z/z}$ mice display several features of systemic autoimmunity (*8*), which are now established as B cell intrinsic (*11*). Whereas B6.*Sle1*$^{z/z}$ mice exhibit increased B cell and T cell activation, splenomegaly, and ANAs, these features were not apparent in B6.*Sle1*$^{z/z}$.HEL^{lg} mice (fig. S1). However, B6.HEL^{lg}.mHEL and B6.*Sle1*$^{z/z}$.HEL^{lg}.mHEL mice showed a comparable loss of transgenic B cells in the spleen and bone marrow, and an absence of IgM^{a} antibodies to HEL in their sera (fig. S2). Thus, *Sle1*^{z} does not impede deletion of B cells upon strong engagement of the surrogate self-antigen, mHEL. This is consistent with previous reports showing that central tolerance of high avidity anti-self B cells is intact in other models of murine lupus (*12*, *13*).

To ascertain whether *Sle1*^{z} influenced anergy induction upon weak engagement by self-antigen, B6.*Sle1*$^{z/z}$.HEL^{lg}.sHEL mice were next examined. A measurable number of B6.*Sle1*$^{z/z}$.HEL^{lg}.sHEL mice beyond 3 months of age, but not B6.HEL^{lg}.sHEL controls, exhibited elevated titers of IgM^{a} antibodies to HEL with levels comparable to that seen in non–lysozyme-exposed B6.HEL^{lg} mice (Fig. 1A and fig. S3). However, neither strain exhibited significant ANA titers (Fig. 1B and fig. S3).

In contrast to spleens from B6.HEL^{lg}.sHEL mice, which show reduced numbers of B cells (*9*), those from B6.*Sle1*$^{z/z}$.HEL^{lg}.sHEL mice exhibited considerable B cell expansion (tables S1 to S3). Coexpression of soluble HEL in the B6 Tg background normally results in an age-dependent increase in the proportion of splenic B cells bearing the endogenous IgM^{b} receptor versus the Tg IgM^{a} (Fig. 1C and tables S1 to S3), possibly as a consequence of active receptor revision in response to HEL or selective expansion of B cells that are not HEL-reactive. However, this proportion of splenic B cells expressing endogenous IgM^{b} heavy chain was considerably reduced in B6.*Sle1*$^{z/z}$.HEL^{lg}.sHEL mice as compared with their B6.HEL^{lg}.sHEL

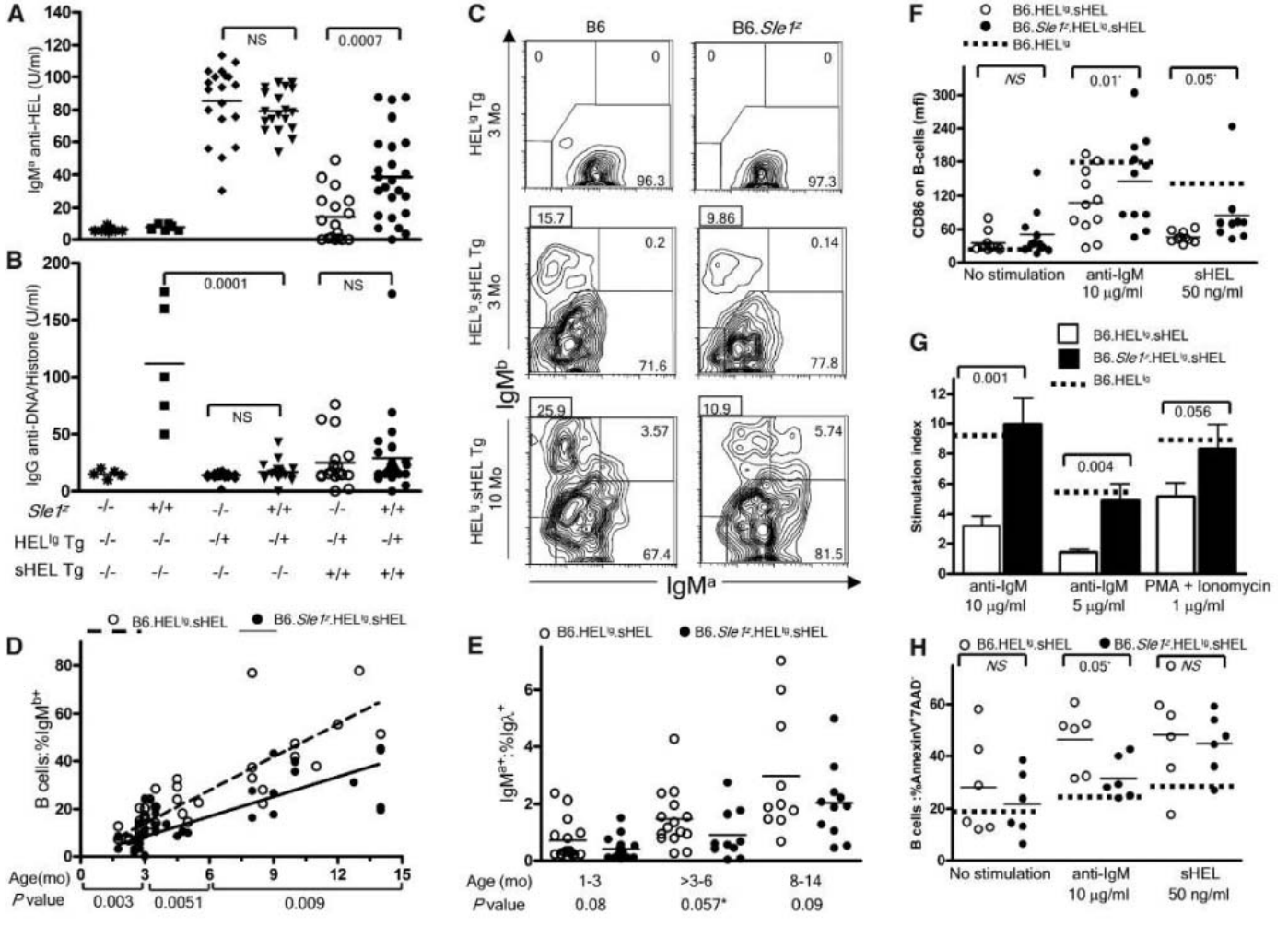

Fig. 1. B6.*Sle1*$^{z/z}$.HEL^{lg}.sHEL mice exhibit breach in B cell tolerance. (**A** and **B**) Levels of IgM^{a} antibodies to HEL (A) and IgG antibodies to DNA/histone (B) in 8- to 14-month-old mice were measured by enzyme-linked immunosorbent assay. (**C** to **E**) Whole splenocytes from B6.HEL^{lg} and B6.HEL^{lg}.sHEL mice, with or without *Sle1*^{z}, were surface-stained for IgM^{a}, IgM^{b}, B220, and Ig-λ and analyzed. (C) Representative contour plots of IgM^{a} versus IgM^{b}, pregated on B220^{+} cells. Boxed numbers at the top left corner indicate percentage IgM^{b+}IgM$^{a\text{-}lo}$ cells. (D) Scatterplot relating the percentage of B cells expressing IgM^{b} to the age of mice. (E) Percentage of IgM^{a+} cells expressing Ig-λ. (**F** to **H**) Whole splenocytes [(F) and (H)] or purified B cells (G) from various strains were stimulated as indicated for 18 hours (F) or 48 hours [(G) and (H)] and assayed for CD86 levels (F), proliferation (G), or apoptosis (H) (*18*). Each dot represents an individual mouse. The solid and dotted horizontal lines indicate group means and B6.HEL^{lg} mean values, respectively. Bars indicate mean + SEM of five to six mice each. The *P* value results of Student's *t* test are indicated. *, Mann-Whitney test (E) or paired *t* test [(F) and (H)]. NS, not significant.

counterparts (Fig. 1, C and D). Furthermore, IgM^{a+} B cells from B6.HEL^{lg}.sHEL spleens exhibited an age-dependent shift toward the use of nontransgenic Ig-lambda light chains, which was attenuated in the presence of *Sle1^{z}* (Fig. 1E). In contrast to the spleen, there was negligible IgM^{b} usage among bone marrow B cells in both strains (fig. S4). Thus, the revision away from transgenic BCR to endogenous BCR usage appears to be a peripheral rather than a central bone marrow B cell event that occurs in response to ongoing exposure to surrogate self-antigen, sHEL.

B6.HEL^{lg}.sHEL B cells have been documented to display reduced functional response to BCR ligation, indicative of efficient tolerization (*14*). Notably, however, B6.*Sle1$^{z/z}$*.HEL^{lg}.sHEL B cells exhibited stronger up-regulation of CD86, and higher proliferation and reduced apoptosis in response to BCR cross-linking, as compared with B6.HEL^{lg}.sHEL B cells (Fig. 1, F to H). Thus, consistent with the in vivo findings, our in vitro studies also indicate that B6.HEL^{lg}.sHEL B cells are inadequately anergized on the B6.*Sle1$^{z/z}$* background.

To examine the functional properties of *Sle1^{z}*-bearing B cells before exposure to self-antigen, B cells from B6.HEL^{lg} and B6.*Sle1$^{z/z}$*.HEL^{lg} mice were compared. Although total splenic B cells from both strains showed similar activation and apoptotic profiles upon BCR cross-linking, B6.*Sle1$^{z/z}$*.HEL^{lg} spleens exhibited a significant expansion of B220^{+}AA4.1^{+}CD21^{-}CD23^{-} (T1) transitional immature B cells, with a resultant increase in the T1:follicular B cell ratio compared with B6.HEL^{lg} controls (Fig. 2A).

Because the *Sle1b^{z}* sublocus accounts for most of the autoimmune phenotypes attributed to the *Sle1^{z}* locus (*5*), B6.*Sle1b$^{z/z}$*.HEL^{lg} mice were next generated and were also found to exhibit a significant expansion in T1 B cells (Fig. 2A). Collectively, these findings suggested a relative block in the transition from T1 to mature B cells in the presence of *Sle1b^{z}*. Potentially, such a block could result from impaired deletion of immature B cells, leading us to examine the function of *Sle1b^{z}*-bearing immature B cells. Bone-marrow–derived immature B cells were cultured in interleukin-7 (IL-7) (fig. S5) (*15*–*18*). After cross-linking of the BCR, immature B cells from B6.*Sle1$^{z/z}$*.HEL^{lg} and B6.*Sle1b$^{z/z}$*.HEL^{lg} mice were seen to flux considerably less calcium (Fig. 2, B and C), underwent cell death less readily, and showed an increase in proliferation, as compared with B6.HEL^{lg} controls (Fig. 2D). These results suggest that the *Sle1b^{z}* allele may impede antigen-triggered death of immature B cells, possibly as a consequence of impaired BCR signaling.

The candidate gene(s) for *Sle1b^{z}* have recently been elucidated to belong to the *SLAM* gene cluster of activation and costimulatory molecules (*7*, *19*). Among these, polymorphic variants of the *Ly108* gene–encoded protein were the most differentially expressed on immature B cells. Compared with B6, B6.*Sle1$^{z/z}$*/*Sle1b$^{z/z}$* immature B cells expressed four times as much Ly108.1 splice isoform but one-fourth as much Ly108.2 (Fig. 2E). To study the influence of these two splice isoforms on immature B cell function, the genes encoding the two *Ly108* isoforms were transfected into the immature B cell line, WEHI-231 (WEHI), which expresses very low levels of endogenous *Ly108* (fig. S6). In line with the findings observed in primary immature

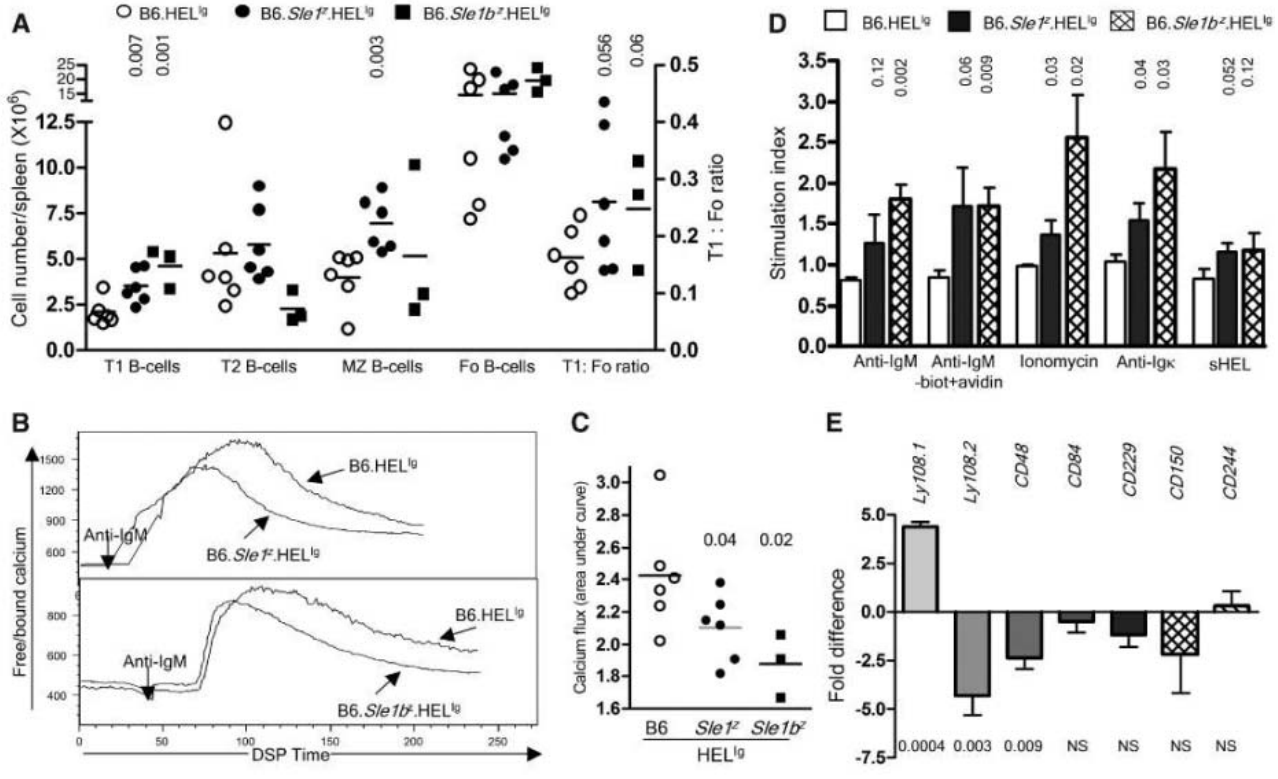

Fig. 2. *Sle1/Sle1b^{z}*-bearing immature B cells have impaired responses to BCR cross-linking. (**A**) Numbers of splenic B cell subsets (left *y* axis) and T1:follicular B cell ratios (right *y* axis) in 6- to 10-week-old B6.HEL^{lg}, B6.*Sle1$^{z/z}$*.HEL^{lg}, and B6.*Sle1b$^{z/z}$*.HEL^{lg} mice are shown. Horizontal lines indicate group means. (**B** and **C**) Displayed are calcium flux responses in IL-7–driven, bone-marrow–derived immature B cells to 20 μg/ml F(ab)′$_2$ antibody to IgM, measured as described (*18*). (B) Representative plots of digital signal processing (DSP) time versus free/bound calcium. (C) Area under calcium-flux curve in the three strains, compiled from two independent experiments. (**D**) Displayed are the mean + SEM (n = 3) stimulation indices of IL-7–driven, bone-marrow–derived immature B cells cultured in triplicate for 48 hours with 25 μg/ml F(ab)′$_2$ antibody to IgM, 10 μg/ml biotin-labeled F(ab)′$_2$ antibody to IgM + 10 μg/ml avidin, 1 μM ionomycin, 25 μg/ml antibody to Igκ, or 2 μg/ml sHEL. Representative data from three independent experiments are shown. (**E**) Real-time polymerase chain reaction analysis of *SLAM* molecules in B6.HEL^{lg} and B6.*Sle1$^{z/z}$*.HEL^{lg} IL-7–driven bone-marrow–derived immature B cells. Bars represent mean + SEM expression levels in B6.*Sle1$^{z/z}$*.HEL^{lg}, relative to B6.HEL^{lg} (n = 6 each), after normalizing against *GAPDH*. (A) to (E) P values pertain to Student's t test comparison of B6.HEL^{lg} to either B6.*Sle1$^{z/z}$*.HEL^{lg} or B6.*Sle1b$^{z/z}$*.HEL^{lg}.

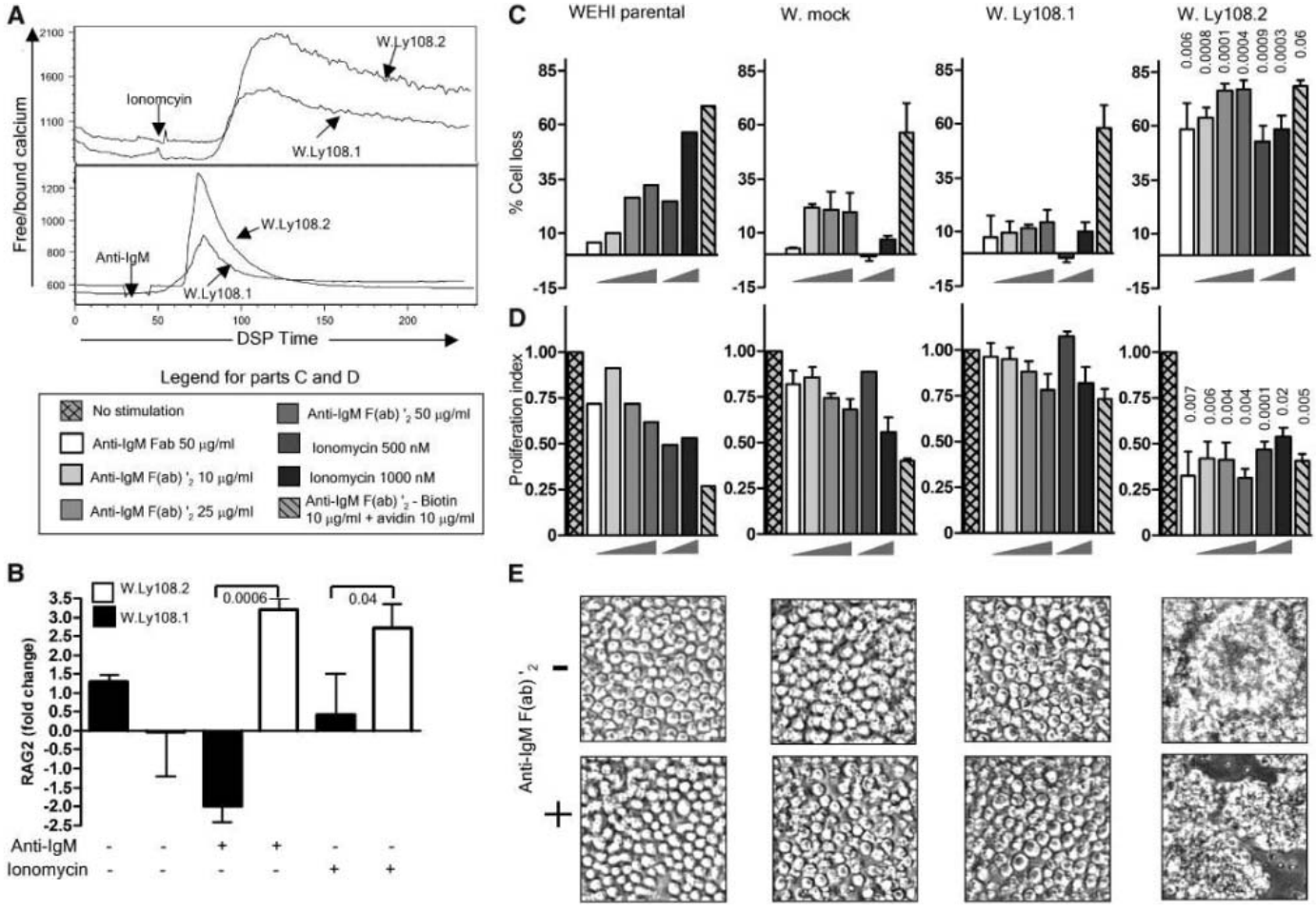

Fig. 3. *Ly108.2* but not *Ly108.1* promotes strong calcium flux, RAG reexpression, and death in immature B cells following BCR ligation. (**A**) Displayed calcium flux responses to 1 μM ionomycin or 20 μg/ml antibody to IgM F(ab)′$_2$ in W.Ly108.1 and W.Ly108.2 stable WEHI-231 transfectants. Data shown are representative of at least two independent experiments and clones. (**B**) WEHI transfectants (n = 4 independent clones each) were stimulated for 36 hours with 25 μg/ml F(ab)′$_2$ antibody to IgM or 1 μM ionomycin. *RAG2* message (mean + SEM) was measured in real time, normalized to *GAPDH*, and expressed relative to the level in unstimulated, untransfected WEHI cells (*18*). (**C** and **D**) Stable WEHI transfectants were stimulated as indicated for 48 hours and assayed for the percentage of apoptotic cell loss (C) and proliferation (D) (*18*). Each bar represents mean + SEM of n = 2 (mock) or n = 4 to 5 each (W.Ly108.1 and W.Ly108.2) independent transfectants, cultured in triplicate. Representative data are shown from three independent experiments. (**E**) Displayed are 200X images of WEHI transfectants grown with or without 10 μg/ml F(ab)′$_2$ antibody to IgM for 72 hours. Images shown are representative of four to five independent stable transfectants of each type. (B) to (D) P values pertain to Student's t test comparison of W.Ly108.1 versus W.Ly108.2.

B cells (Fig. 2, B to D), W.Ly108.1 transfectants exhibited reduced calcium flux (Fig. 3A), reduced RAG reexpression (Fig. 3B), and decreased cell death (Fig. 3, C to E), compared with W.Ly108.2, upon triggering the BCR with a variety of stimuli. In particular, the W.Ly108.2 transfectants bearing the normal B6 allele of *Ly108* were exquisitely sensitive to BCR cross-linking; even monovalent Fabs, low doses of F(ab)′$_2$ antibody to IgM, and ionomycin resulted in a strong calcium flux, RAG reexpression, and near-maximal cell death (Fig. 3).

The above findings indicate that at least some of the genes that cause lupus may function by crippling multiple B cell tolerance mechanisms such as deletion, receptor revision, and anergy induction by tuning down BCR signaling at the immature stage of development. Among the *SLAM* molecules, *Ly108* (and possibly others) may function as molecular rheostats, determining the stringency with which self-reactive B cells are censored during early development. Whether the dramatically different properties of the two *Ly108* isoforms emanate from the dissimilar number of intracellular tyrosine switch motifs they possess warrants further investigation.

Given the present finding that the *Ly108* isoforms influence B cell tolerance in a generalized, non–antigen-specific manner, it is intriguing that the serology in B6.*Sle1*/*Sle1b*$^{z/z}$ mice is chromatin-centric rather than polyclonal (*7*, *8*, *20*). We believe this outcome might relate to the fact that the early B cell repertoire at the pre-B and immature B cell stages may already be nuclear-antigen skewed to begin with, even in normal individuals, as illustrated by recent studies (*21*, *22*). Hence, the emergence of ANAs and the pathognomonic hallmark of lupus, the LE (lupus erythematosus) cells (*23*), may be the consequence of a generalized tolerance defect in immature B cells that already encode nuclear-antigen reactivity following primary immunoglobulin gene rearrangement. Unraveling the molecular cascades through which *Ly108* dictates how immature B cells toggle between life and death is the challenge that lies ahead.

References and Notes

1. D. H. Kono, A. N. Theofilopoulos, *Int. Rev. Immunol.* **19**, 367 (2000).
2. K. Raman, C. Mohan, *Curr. Opin. Immunol.* **15**, 651 (2003).
3. E. K. Wakeland, K. Liu, R. R. Graham, T. W. Behrens, *Immunity* **15**, 397 (2001).
4. L. Morel, U. H. Rudofsky, J. A. Longmate, J. Schiffenbauer, E. K. Wakeland, *Immunity* **1**, 219 (1994).
5. L. Morel, K. R. Blenman, B. P. Croker, E. K. Wakeland, *Proc. Natl. Acad. Sci. U.S.A.* **98**, 1787 (2001).
6. B. P. Tsao *et al.*, *J. Clin. Invest.* **99**, 725 (1997).

7. A. E. Wandstrat *et al.*, *Immunity* **21**, 769 (2004).
8. C. Mohan, E. Alas, L. Morel, P. Yang, E. K. Wakeland, *J. Clin. Invest.* **101**, 1362 (1998).
9. C. C. Goodnow *et al.*, *Nature* **334**, 676 (1988).
10. S. B. Hartley *et al.*, *Nature* **353**, 765 (1991).
11. E. S. Sobel, C. Mohan, L. Morel, J. Schiffenbauer, E. K. Wakeland, *J. Immunol.* **162**, 2415 (1999).
12. C. F. Rubio, J. Kench, D. M. Russell, R. Yawger, D. Nemazee, *J. Immunol.* **157**, 65 (1996).
13. J. C. Rathmell, C. C. Goodnow, *J. Immunol.* **153**, 2831 (1994).
14. M. P. Cooke *et al.*, *J. Exp. Med.* **179**, 425 (1994).
15. D. Melamed, D. Nemazee, *Proc. Natl. Acad. Sci. U.S.A.* **94**, 9267 (1997).
16. R. J. Benschop, D. Melamed, D. Nemazee, J. C. Cambier, *J. Exp. Med.* **190**, 749 (1999).
17. L. E. Tze, K. L. Hippen, T. W. Behrens, *J. Immunol.* **171**, 678 (2003).
18. Materials and methods are available as supporting material on *Science* Online.
19. A. Veillette, S. Latour, *Curr. Opin. Immunol.* **15**, 277 (2003).
20. C. Mohan *et al.*, *J. Clin. Invest.* **103**, 1685 (1999).
21. H. Wardemann *et al.*, *Science* **301**, 1374 (2003).
22. S. Yurasov *et al.*, *J. Exp. Med.* **201**, 703 (2005).
23. H. R. Holman, H. G. Kunkel, *Science* **126**, 162 (1957).
24. We would like to thank K. Hsu, R. Samudrala, X. J. Zhou, A. Satterthwaite, and C. Xie for technical assistance and helpful discussions. This work has been supported by NIH RO1 AR44894 and AI54902 and the Lupus Research Institute.

Supporting Online Material
www.sciencemag.org/cgi/content/full/312/5780/1665/DC1
Materials and Methods
Figs. S1 to S6
Tables S1 to S3
References

7 February 2006; accepted 18 May 2006
10.1126/science.1125893

Autoreactive B Cell Responses to RNA-Related Antigens Due to *TLR7* Gene Duplication

Prapaporn Pisitkun,[1] Jonathan A. Deane,[1] Michael J. Difilippantonio,[2] Tatyana Tarasenko,[1] Anne B. Satterthwaite,[3] Silvia Bolland[1]*

Antibodies against nuclear self-antigens are characteristic of systemic autoimmunity, although mechanisms promoting their generation and selection are unclear. Here, we report that B cells containing the Y-linked autoimmune accelerator (*Yaa*) locus are intrinsically biased toward nucleolar antigens because of increased expression of TLR7, a single-stranded RNA-binding innate immune receptor. The *TLR7* gene is duplicated in *Yaa* mice because of a 4-Megabase expansion of the pseudoautosomal region. These results reveal high divergence in mouse Y chromosomes and represent a good example of gene copy number qualitatively altering a polygenic disease manifestation.

The analysis of genetic modifiers of autoimmune disease provides insight into mechanisms underlying disease susceptibility and possible therapeutic approaches. The *Yaa* genetic modifier, for example, increases severity of systemic lupus erythematosus (SLE) in male mice (*1*). *Yaa* was first identified from a cross between a C57BL/6 (B6) female and a SB/Le male that produced the BXSB hybrid line. BXSB mice develop SLE with much higher incidence and with earlier onset in males compared with females, whereas mice from the reciprocal cross (SB/Le female and B6 male) do not show the same acceleration of disease in males. Thus, this autoimmune-enhancing effect in BXSB males was attributed to the Y chromosome derived from the SB/Le strain and was named *Yaa*, which stands for Y-linked autoimmune accelerator (*2*). In addition to the BXSB strain, the *Yaa* Y chromosome exacerbates disease in a number of lupus-prone strains, but it has not been found to induce autoimmune disease in wild-type B6 male mice (*3*–*5*).

We have analyzed the effect of the *Yaa* genetic modifier in mice deficient in the antibody-binding inhibitory receptor FcγRIIB. With the B6 background, *FcγRIIB*$^{-/-}$ mice develop spontaneous SLE-like disease, characterized by the presence of autoantibodies against chromatin (antichromatin) and development of lethal glomerulonephritis (*6*). Addition of the *Yaa* modifier to the *FcγRIIB*-deficient model by genetic crossing not only aggravates the autoimmune pathology, but it also leads to a switch of specificity from chromatin to nucleolar autoantibodies (*7*). Distinct autoantibody specificities against nuclear antigens are often used in the diagnosis and prognosis of systemic autoimmune disease (*8*). Thus, in humans, chromatin antibodies are considered characteristic of SLE, whereas the presence of nucleolar antibodies often corresponds with systemic sclerosis (*9*). In this study, we aimed to identify the *Yaa* gene product and to understand how *Yaa* modifies autoantibody specificity toward nucleolar antigens.

To determine which cell type instructs the *Yaa* nucleolar antibody specificity, we generated bone marrow chimeras with an equal mix of *FcγRIIB*$^{-/-}$ *Yaa* and *FcγRIIB*$^{-/-}$ cells. For this experiment, the *FcγRIIB* mutation was bred into a congenic B6.*IgH*^{a} strain so that antibodies produced by *FcγRIIB*$^{-/-}$ B cells (a allotype) could be distinguished from the antibodies derived from *FcγRIIB*$^{-/-}$ *Yaa* B cells (b allotype) by using allotype-specific immunofluorescence staining. *RAG*$^{-/-}$ mice reconstituted with the mixed bone marrow contained equivalent numbers of *Yaa* [immunoglobulin M^{b+} (IgM^{b+})] and non-*Yaa* (IgM^{a+}) B cells in peripheral blood 1 month after the transfer (Fig. 1A) and in spleen 4 months after the transfer (table S1). Equal amounts of spontaneous activation of both IgM^{a+} and IgM^{b+} B cells were detected by the expression of the activation marker CD69 (Fig. 1, B and C, and table S1). When tested for antigen specificity by using a standard assay for nuclear antibodies (ANA) on Hep-2 cells (*10*), serum from the mixed chimeras yielded a homogeneous nuclear pattern typical of antichromatin specificities when detecting a-allotype immunoglobulins G (IgGs) (Fig. 1D). In contrast, detection of b-allotype IgGs gave rise to a speckled nucleolar pattern, characteristic of RNA-related specificities (Fig. 1E). This differential pattern was not apparent when detecting a and b allotype–specific IgGs in the control experiment, for which an equal mix of non-*Yaa* *FcγRIIB*$^{-/-}$ *IgH*^{a} and *FcγRIIB*$^{-/-}$ *IgH*^{b} was used to reconstitute irradiated *RAG*$^{-/-}$ mice (Fig. 1, F and G). This suggests that *Yaa* B cells have an intrinsic bias toward the production of antibodies with nucleolar specificity in the context of a general loss of tolerance promoted by genetic factors such as the *FcγRIIB*$^{-/-}$ background. These results validate and further expand the notion, previously suggested by Izui's group, that *Yaa* can activate autoreactive B cells depending on the nature of autoantigens (*11*, *12*).

Besides the intrinsic *Yaa* effect on antibody specificity, we also observed a B cell extrinsic effect of *Yaa* in terms of the extent of B cell activation and autoantibody production. Thus, the presence of the *Yaa* bone marrow in the mixed chimera resulted in increased production of IgG of the a allotype (non-*Yaa*) and elevated numbers of activated cells as compared with the control chimeras where no *Yaa* bone marrow was transferred (table S1).

Hyperactivity of B cells in *Yaa* has been previously suggested by the observation that *Yaa* B cells show increased spontaneous IgM secretion and lack marginal zone B cells (MZBs) (*13*). Such an inverse relationship between the strength of B cell receptor signaling

[1]Laboratory of Immunogenetics, National Institute of Allergy and Infectious Diseases (NIAID), NIH, Rockville, MD 20852, USA. [2]Section of Cancer Genomics, Genetics Branch, Center for Cancer Research, National Cancer Institute (NCI), NIH, Bethesda, MD 20892, USA. [3]Department of Internal Medicine, University of Texas Southwestern, Dallas, TX 75390, USA.

*To whom correspondence should be addressed. E-mail: sbolland@nih.gov

and MZB development has been suggested previously by studies of B cells deficient in Bruton's tyrosine kinase, Btk, which are generally hyporesponsive to antigen stimulation and show increased representation of MZBs (*14*, *15*). We therefore reasoned that the MZB defect in B6.*Yaa* mice might be reversed by mutations that reduce overall B cell responsiveness. To test this, we crossed B6.*Yaa* mice with *Btk*-deficient mice to generate B6.*Yaa Btk*$^{-}$ mice and control B6.*Yaa Btk*$^{+}$ littermates. We observed that, whereas B6.*Yaa Btk*$^{+}$ mice lack MZBs in the spleen, the B6.*Yaa Btk*$^{-}$ double mutant phenotypically resembles B6.*Btk*$^{-}$ mice with restoration of MZBs (Fig. 2, A and B).

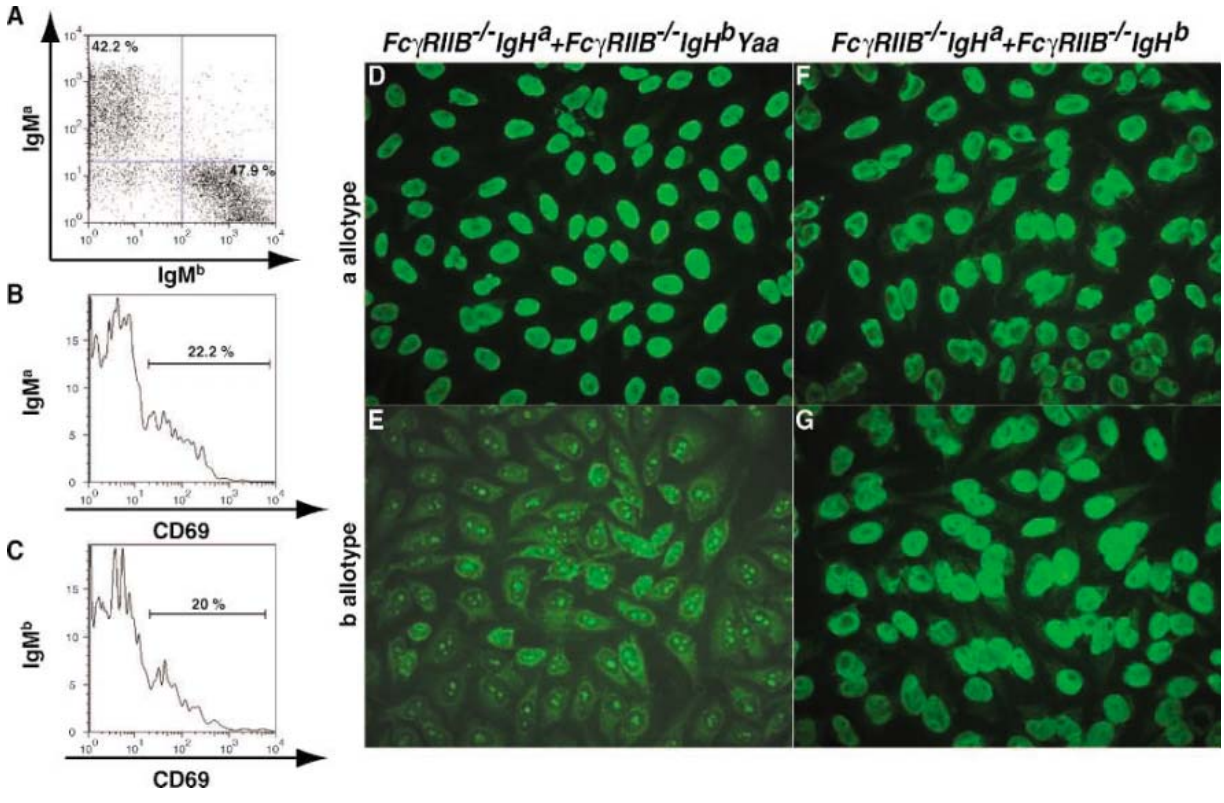

Fig. 1. B cell intrinsic ANA specificity in *FcγRIIB*$^{-/-}$ *Yaa* mice. (**A** to **C**) Flow cytometric analysis of B cells from the blood of *RAG*$^{-/-}$ mice 1 month after reconstitution with *FcγRIIB*$^{-/-}$ (*IgH*^{a}) and *FcγRIIB*$^{-/-}$ *Yaa* (*IgH*^{b}) bone marrow cells. (**D** to **G**) ANA production in serum from the mixed bone marrow chimera 4 to 6 months after reconstitution ($n = 6$).

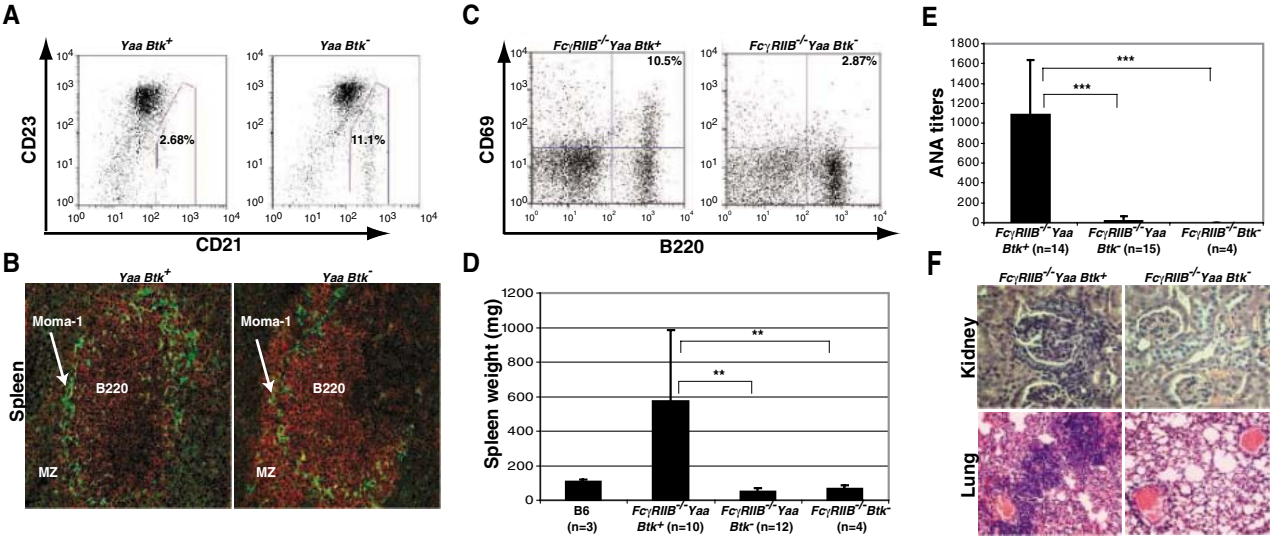

Fig. 2. The Yaa phenotype is Btk-dependent. (**A** and **B**) Btk deficiency restores the MZB population in B6.*Yaa* spleens. (A) Flow cytometric analysis of B220^{+} splenocytes shows percentage of MZBs. (B) Immunofluorescence staining of spleen sections using antibodies to Moma-1 and B220 to identify marginal zone macrophages and B cells, respectively. (**C** to **F**) Btk deficiency prevents autoimmune disease in *FcγRIIB*$^{-/-}$ *Yaa* mice. (C) Flow cytometric analysis shows percentage of activated B cells in the spleen. (D) *Btk* deletion alleviates splenomegaly in *FcγRIIB*$^{-/-}$ *Yaa* mice. ** $P < 0.005$. (E) Titers of serum ANAs in 6-month-old mice. *** $P < 0.001$. Error bars indicate ± SD. (F) Hematoxylin and eosin staining of kidney and lung sections showing membranoproliferative glomerulonephritis and lung infiltration in *FcγRIIB*$^{-/-}$ *Yaa* but not in *FcγRIIB*$^{-/-}$ *Yaa Btk*$^{-}$ mice ($n \geq 3$).

This revealed a genetic and functional interaction between the *Yaa* and *Btk* genes. Moreover, addition of the *Btk* mutation to *FcγRIIB*$^{-/-}$ *Yaa* eliminated the autoimmune phenotype: It resulted in reduced spontaneous B cell activation (Fig. 2C), normal spleen weight (Fig. 2D), and eliminated autoantibody production (Fig. 2E) as well as tissue damage in both kidney and lung (Fig. 2F). Thus, the Btk signaling pathway is required for the loss of tolerance to nucleolar antigens in *FcγRIIB*$^{-/-}$ *Yaa* mice, correlating with what was shown in Btk-deficient human patients (*16*).

In attempt to identify candidate genes for the *Yaa* locus, we compared gene expression in B6 versus B6.*Yaa* by microarray analysis on follicular B cell RNA. Only 26 genes were substantially up-regulated (>1.5-fold) in B6.*Yaa* B cells compared with B6 B cells in three out of four independent experiments (table S2). Of the genes that showed a twofold increase in expression in *Yaa* B cells, four (*Msl31*, *TLR7*, *Tmsb4x*, and *Rab9*) are located in the most distal part of chromosome X, with sequences that are consecutive in the genome. This suggested to us that the genomic region of chromosome X containing these four genes might be duplicated in the *Yaa* genome. To validate this hypothesis, we performed quantitative polymerase chain reaction (PCR) on genomic DNA from B6 and B6.*Yaa*. Probes detecting genes *Msl31*, *TLR7*, *TLR8*, *Tmsb4x*, and *Rab9* showed double the quantity of DNA in B6.*Yaa* male and B6 female cells as compared with wild-type B6 males (table S3). Fluorescence in situ hybridization (FISH) using bacterial artificial chromosome (BAC) probes that span a 4-Mb region at the distal end of the X chromosome (Fig. 3, A to C, and fig. S1) revealed hybridization in the B6.*Yaa* Y chromosome, confirming the genomic duplication and determining its location in the genome. One of these probes (154O12) expands the region that had been reported to include the *Mus musculus* pseudoautosomal region (PAR) (*17*). Indeed, this probe hybridized with the X and Y chromosomes in both B6.*Yaa* and B6 cells, although the Y chromosome signal in B6 was notably weaker in intensity compared with both the X chromosome and the B6.*Yaa* Y chromosome (Fig. 3C). Six other probes located in this distal region hybridized with the chromosome X and Y in B6.*Yaa* cells but only with the chromosome X in B6 cells. Probe 239H22 showed lower amounts of hybridization on the *Yaa* Y chromosome compared with the X chromosome, indicating that the duplicated region begins somewhere within the sequence represented by this BAC clone. Overall this analysis uncovers a 4-Mb expansion of the PAR in *Yaa* males that results in the duplication of at

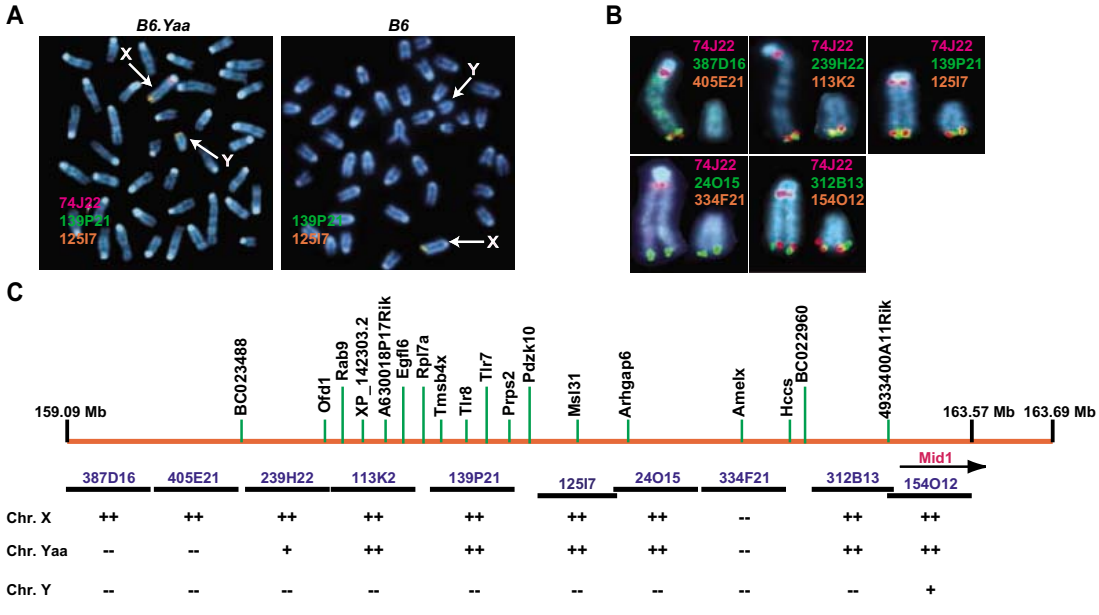

Fig. 3. Expansion of the pseudoautosomal region in the *Yaa* genome. (**A** and **B**) FISH analysis in B6 and B6.*Yaa* embryonic fibroblasts. BAC clone RP23-74J22 (X centromeric–specific, pink) was used with BAC clones listed in (C). (A) Whole chromosomal spread in B6.*Yaa* and B6 cells stained with 139P21 and 125I7 probes. (B) Magnified view of X and Y chromosomes using the indicated fluorescently labeled BAC probes. For purposes of visualization, the Y chromosome signal intensity for clone 239H22 was enhanced. (**C**) Diagram shows genomic location on the X chromosome of BAC DNAs used for hybridization. Hybridization signals are ++ for strong; +, weak; and –, negative.

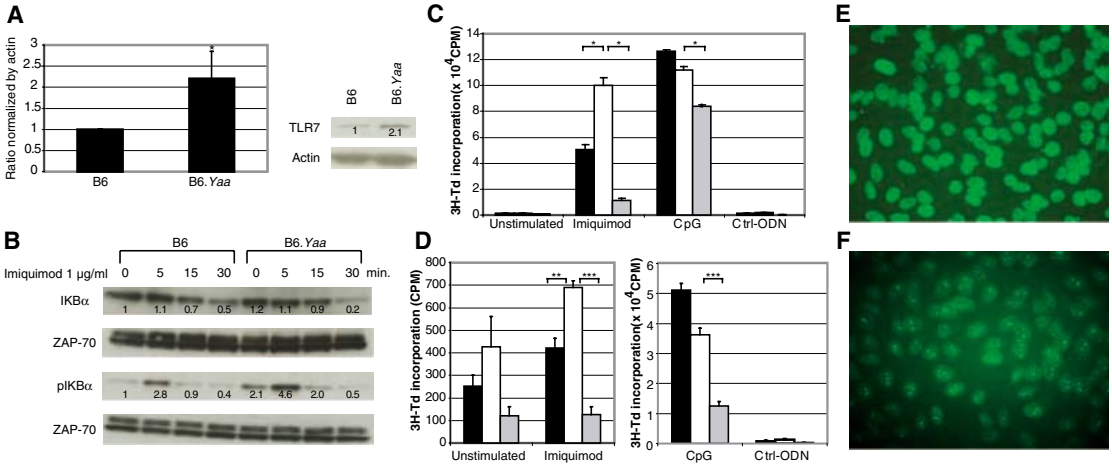

Fig. 4. Increased expression and function of TLR7 in *Yaa* mice. (**A**) TLR7 mRNA and protein levels measured by quantitative PCR on cDNA and Western blot in CD43^{-}CD9^{-} B cells. (**B**) B6 or B6.*Yaa* splenocytes were stimulated with imiquimod for the indicated times and IκBα and pIκBα measured by Western blot. ZAP-70 is a loading control. Proliferative responses of splenocytes (**C**) and follicular B cells (**D**) upon stimulation with imiquimod (1 μg/ml), CpGs (0.1 μg/ml for splenocytes and 1μg/ml for follicular B cells), and control oligodeoxynucleotides (ODNs). Black bar, B6; white bar, B6.*Yaa*; gray bar, B6.*Btk*$^{-}$. ***$P < 0.001$, ** $P < 0.005$, * $P < 0.05$. Error bars indicate ± SD. (**E** and **F**) ANA test of serum from B6.*FcγRIIB*$^{-/-}$ mice before or after treatment with imiquimod. Data are representative of at least three independent experiments ($n \geq 3$).

least 13 known and four unknown genes that in B6 wild-type mice are X chromosome–specific. Duplication of the *TLR7* gene was also confirmed in the BXSB and SB strains from which the *Yaa* Y chromosome was derived (table S3).

Among the genes included in the genomic duplication of *Yaa*, *TLR7* was of most interest to us because it shares several characteristics predicted for the *Yaa* locus: It is expressed in B cells (*18*), it binds Btk, and its ligand is single-stranded RNA (*19*, *20*), which is also a likely component of nucleolar antigens. Quantitative PCR on cDNA and Western blot analysis confirmed that the genomic duplication in *Yaa* resulted in increased TLR7 mRNA and protein in B cells (Fig. 4A). Functionally, stimulation of *Yaa* splenocytes with the TLR7 agonist imiquimod resulted in enhanced phosphorylation of the transcriptional regulator IκBα and increased proliferation compared with wild-type responses (Fig. 4, B and C). Naïve follicular *Yaa* B cells showed a small, but significant, increase in proliferation upon imiquimod stimulation compared with wild-type B6 cells (Fig. 4D). This increased proliferation in response to imiquimod in B cells and total splenocytes was dependent on *Btk*, again confirming the *Btk* requirement for the *Yaa* phenotype revealed in the genetic analysis. In vivo administration of imiquimod was also sufficient to alter the homogenous nuclear pattern seen in sera from *FcγRIIB*$^{-/-}$ mice to a nucleolar pattern (Fig. 4, E and F), demonstrating that enhancing TLR7 signaling induces nucleolar-specific responses. It is nevertheless possible that genes other than *TLR7* included in the PAR expansion promote the acceleration of autoimmune disease observed in *Yaa* males.

Just as TLR9 has been suggested to promote B cell activation by DNA-containing self-antigens (*21*), our data indicate that TLR7 may contribute to autoimmunity by inducing activation of B cells by RNA-containing antigens of nucleolar origin. In vitro B cell activation by RNA-associated autoantigens has been reported (*22*, *23*), but the best confirmation of the model would come from the study of the effect of this pathway on the development of spontaneous autoimmune disease. The results presented here provide strong evidence that naturally occurring differences in expression of the *TLR7* gene as well as environmental factors that induce TLR7 responses may result in increased B cell sensitivity to RNA-containing self-antigens. Thus, the *Yaa* locus represents an excellent example in which qualitative phenotypic differences in disease pathology are derived from a copy number polymorphism, a genetic event that has been shown to be common both in mice and humans (*24*).

References and Notes

1. S. Izui *et al.*, *Immunol. Rev.* **144**, 137 (1995).
2. E. D. Murphy, J. B. Roths, *Arthritis Rheum.* **22**, 1188 (1979).
3. S. Izui, M. Higaki, D. Morrow, R. Merino, *Eur. J. Immunol.* **18**, 911 (1988).
4. L. Morel *et al.*, *Proc. Natl. Acad. Sci. U.S.A.* **97**, 6670 (2000).
5. C. Mary *et al.*, *J. Immunol.* **165**, 2987 (2000).
6. S. Bolland, J. V. Ravetch, *Immunity* **13**, 277 (2000).
7. S. Bolland, Y. S. Yim, K. Tus, E. K. Wakeland, J. V. Ravetch, *J. Exp. Med.* **195**, 1167 (2002).
8. D. Leslie, P. Lipsky, A. L. Notkins, *J. Clin. Investig.* **108**, 1417 (2001).
9. E. S. Weiner *et al.*, *Arthritis Rheum.* **34**, 68 (1991).
10. Materials and methods are available as supporting material on *Science* Online.
11. L. Fossati, M. Iwamoto, R. Merino, S. Izui, *Eur. J. Immunol.* **25**, 166 (1995).
12. T. Moll *et al.*, *J. Immunol.* **174**, 702 (2005).
13. H. Amano *et al.*, *J. Immunol.* **170**, 2293 (2003).
14. W. N. Khan *et al.*, *Immunity* **3**, 283 (1995).
15. A. Cariappa *et al.*, *Immunity* **14**, 603 (2001).
16. Y. S. Ng, H. Wardemann, J. Chelnis, C. Cunningham-Rundles, E. Meffre, *J. Exp. Med.* **200**, 927 (2004).
17. L. Dal Zotto *et al.*, *Hum. Mol. Genet.* **7**, 489 (1998).
18. K. Takeda, T. Kaisho, S. Akira, *Annu. Rev. Immunol.* **21**, 335 (2003).
19. J. M. Lund *et al.*, *Proc. Natl. Acad. Sci. U.S.A.* **101**, 5598 (2004).
20. S. S. Diebold, T. Kaisho, H. Hemmi, S. Akira, C. Reis e Sousa, *Science* **303**, 1529 (2004); published online 19 February 2004 (10.1126/science.1093616).
21. E. A. Leadbetter *et al.*, *Nature* **416**, 603 (2002).
22. C. M. Lau *et al.*, *J. Exp. Med.* **202**, 1171 (2005).
23. J. Vollmer *et al.*, *J. Exp. Med.* **202**, 1575 (2005).
24. J. H. Nadeau, C. Lee, *Nature* **439**, 798 (2006).

25. We are grateful to B. Scott (NIAID) for technical support, T. Myers (NIAID) for assistance in microarray experiments, O. Schwartz and J. Kabat (NIAID) for help with confocal microscopy, and S. Pierce for comments on the manuscript. This research was supported by the Intramural Research Program of the NIH, NIAD, and NCI and by the Lupus Research Institute. A.S. is the Southwestern Medical Foundation Scholar in Biomedical Research.

Supporting Online Material

www.sciencemag.org/cgi/content/full/1124978/DC1
Materials and Methods
Fig. S1
Table S1 to S3
References

17 January 2006; accepted 3 May 2006
Published online 18 May 2006;
10.1126/science.1124978
Include this information when citing this paper.

Extrafollicular Activation of Lymph Node B Cells by Antigen-Bearing Dendritic Cells

Hai Qi, Jackson G. Egen, Alex Y. C. Huang, Ronald N. Germain*

In contrast to naïve T cells that recognize short antigen-derived peptides displayed by specialized antigen-presenting cells, immunoglobulin receptors of B lymphocytes primarily recognize intact proteins. How and where within a lymph node such unprocessed antigens become available for naïve B cell recognition is not clear. We used two-photon intravital imaging to show that, after exiting high-endothelial venules and before entry into lymph node follicles, B cells survey locally concentrated dendritic cells. Engagement of the B cell receptor by the dendritic cell (DC)–associated antigen leads to lymphocyte calcium signaling, migration arrest, antigen acquisition, and extrafollicular accumulation. These findings suggest a possible role for antigen-specific B-DC interactions in promoting T cell–dependent antibody responses in vivo.

Adaptive immunity depends on the activation of rare, antigen (Ag)-specific lymphocytes, which recirculate through blood and secondary lymphoid organs such as lymph nodes (LNs) in search of their Ags. T cell stimulation typically involves dendritic cell (DC) presentation of protein Ag fragments bound to major histocompatibility complex (MHC)–encoded molecules (*1*). In contrast, naïve B cells are thought to respond to intact free Ags that exit the lymph or the blood and enter the LN follicular area, within which most B cells reside. However, the lymph carrying Ags from peripheral tissues to the LN is channeled through sinuses and conduits that lie outside of the follicles and whose structure limits direct access of high molecular weight or particulate material to the LN parenchyma (*2*–*4*).

Given these constraints on antigen access, we considered the possibility that B cell activation may also use a system of active cell-aided Ag delivery. Consistent with this hypothesis, injection of DCs carrying protein, bacterial, or viral Ags leads to the induction of specific antibodies (*5*–*9*). Furthermore, DCs that capture bacteria from the circulation have been shown to interact with and promote activation of splenic marginal zone B cells (*10*), and DCs are known to maintain intracellular pools of undegraded Ags that can be recycled to the cell surface (*5*, *11*–*13*). To test our hypothesis directly, we used the well-studied protein antigen hen egg lysozyme (HEL), which is highly cationic and taken up efficiently into cells through

Lymphocyte Biology Section, Laboratory of Immunology, National Institute of Allergy and Infectious Diseases (NIAID), National Institutes of Health (NIH), Bethesda, MD 20892, USA.

*To whom correspondence should be addressed. E-mail: rgermain@nih.gov

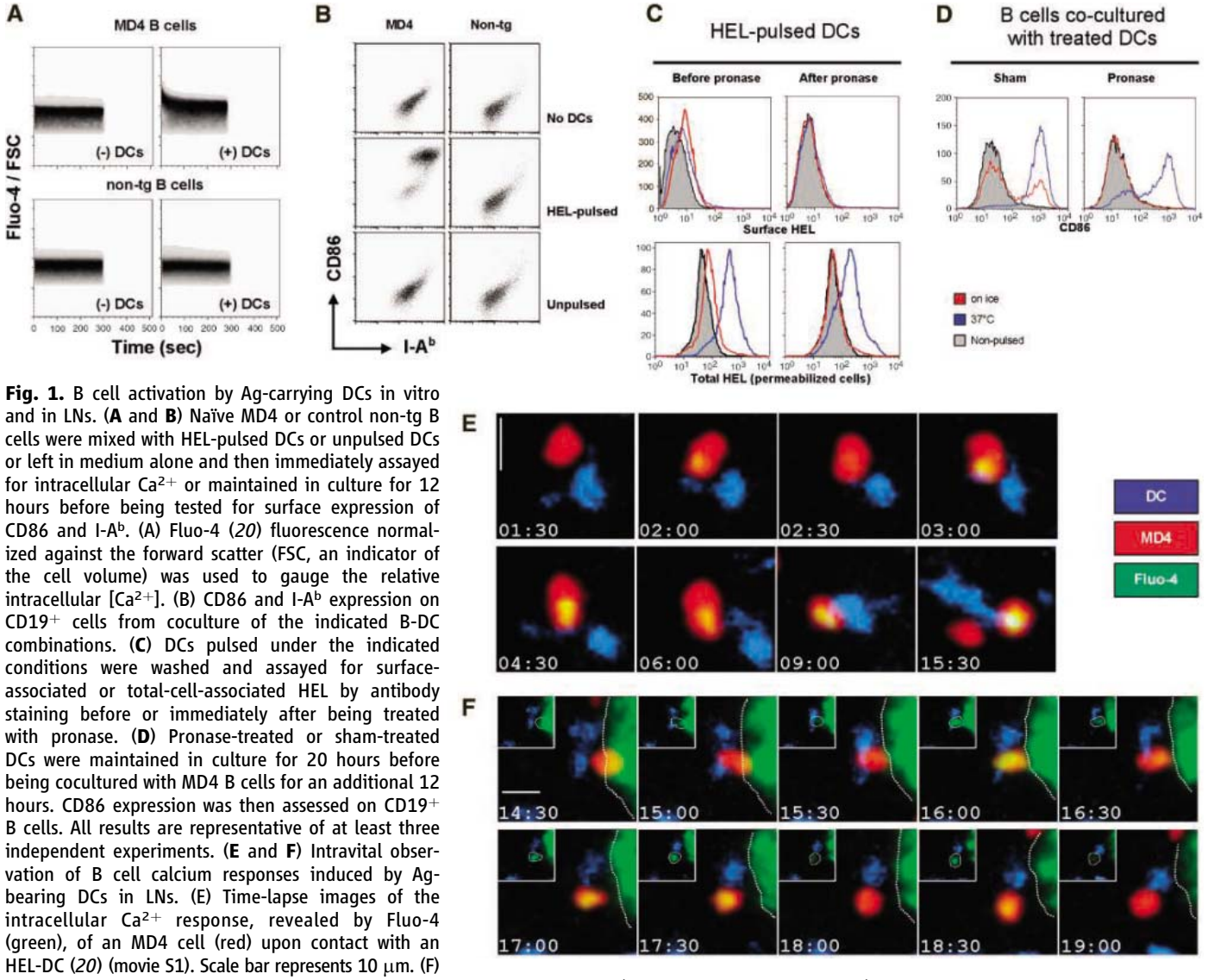

Fig. 1. B cell activation by Ag-carrying DCs in vitro and in LNs. (**A** and **B**) Naïve MD4 or control non-tg B cells were mixed with HEL-pulsed DCs or unpulsed DCs or left in medium alone and then immediately assayed for intracellular Ca^{2+} or maintained in culture for 12 hours before being tested for surface expression of CD86 and I-A^b. (A) Fluo-4 (*20*) fluorescence normalized against the forward scatter (FSC, an indicator of the cell volume) was used to gauge the relative intracellular [Ca^{2+}]. (B) CD86 and I-A^b expression on $CD19^+$ cells from coculture of the indicated B-DC combinations. (**C**) DCs pulsed under the indicated conditions were washed and assayed for surface-associated or total-cell-associated HEL by antibody staining before or immediately after being treated with pronase. (**D**) Pronase-treated or sham-treated DCs were maintained in culture for 20 hours before being cocultured with MD4 B cells for an additional 12 hours. CD86 expression was then assessed on $CD19^+$ B cells. All results are representative of at least three independent experiments. (**E** and **F**) Intravital observation of B cell calcium responses induced by Ag-bearing DCs in LNs. (E) Time-lapse images of the intracellular Ca^{2+} response, revealed by Fluo-4 (green), of an MD4 cell (red) upon contact with an HEL-DC (*20*) (movie S1). Scale bar represents 10 μm. (F) Time-lapse images of an MD4 cell that exited an HEV, came into contact with an HEL-DC, and responded with an elevation of intracellular Ca^{2+}. Dotted lines approximate the HEV border. (Insets) The B cell border (without the cytoplasmic stain) for better differentiation of the B cell-associated Fluo-4 fluorescence from that of the HEV labeled with fluorescein isothiocyanate (FITC)–dextran (movie S2). Scale bar, 10 μm.

electrostatic interactions with anionic surface molecules, thus simulating normal receptor-mediated Ag uptake by DCs. B cells from HEL-specific B cell receptor (BCR) transgenic MD4 mice (*14*) showed rapid elevation of intracellular calcium concentration ([Ca^{2+}]) upon coculture with HEL-pulsed DCs (HEL-DCs) (Fig. 1A) followed by increased surface expression of CD86 and MHC class II molecules (Fig. 1B). Such activation was abrogated if the B cells and DCs were separated by a cell-impermeable membrane (fig. S1), making it unlikely that MD4 B cells had simply been triggered by Ags released from viable or dead DCs. To examine this issue further, we pulsed DCs with HEL at 37°C or on ice and then treated them with pronase to remove surface-associated HEL. Although DCs pulsed at 37°C had a lower amount of surface-associated HEL than those pulsed on ice, they nevertheless acquired a much larger total amount of Ags (Fig. 1C, left), indicating that HEL acquired by DCs at physiological temperature is predominantly intracellular. When pronase was used to remove HEL from the DC surface (Fig. 1C, right), DCs pulsed at 37°C retained the ability to activate MD4 B cells, whereas those pulsed on ice did not (Fig. 1D); again, membrane separation of the cells prevented the response (fig. S1). Thus, HEL endocytosed by DCs can reach the cell surface in a form able to activate B cells in vitro.

Although these data demonstrate that B cell activation can be induced directly by Ag-carrying DCs in culture, in LNs the majority of DCs reside in the T cell zone (*15*), raising the question of how naïve B cells might access DC-associated Ags in vivo. The region surrounding the high-endothelial venules (HEVs) is potentially an ideal place for B cells to scan DC-associated Ags; because this is the first parenchymal location of naïve B cells on their way to the follicle, it is a region rich in migrating Ag-laden DCs (*16*, *17*), and it is also where resident DCs sample Ags arriving via the LN conduits (*18*). Consistent with this idea, LN sections showed that recent immigrant B cells initially concentrated around HEVs before entering follicles (figs. S2 and S3), colocalizing with and physically contacting DCs (fig. S4).

Next, intravital two-photon microscopy (*19*) was used to determine whether these apparent DC-B interactions around HEVs result in B cell activation by DC-associated Ag. To look for an early sign of Ag stimulation, we examined Ca^{2+} responses of MD4 B cells in the LNs of living mice that had been transferred with HEL-DCs or control ovalbumin (OVA)-pulsed DCs (*20*). Upon contact with dendrites extending from HEL-DCs, MD4 B cells exhibited an abrupt increase in intracellular [Ca^{2+}], often

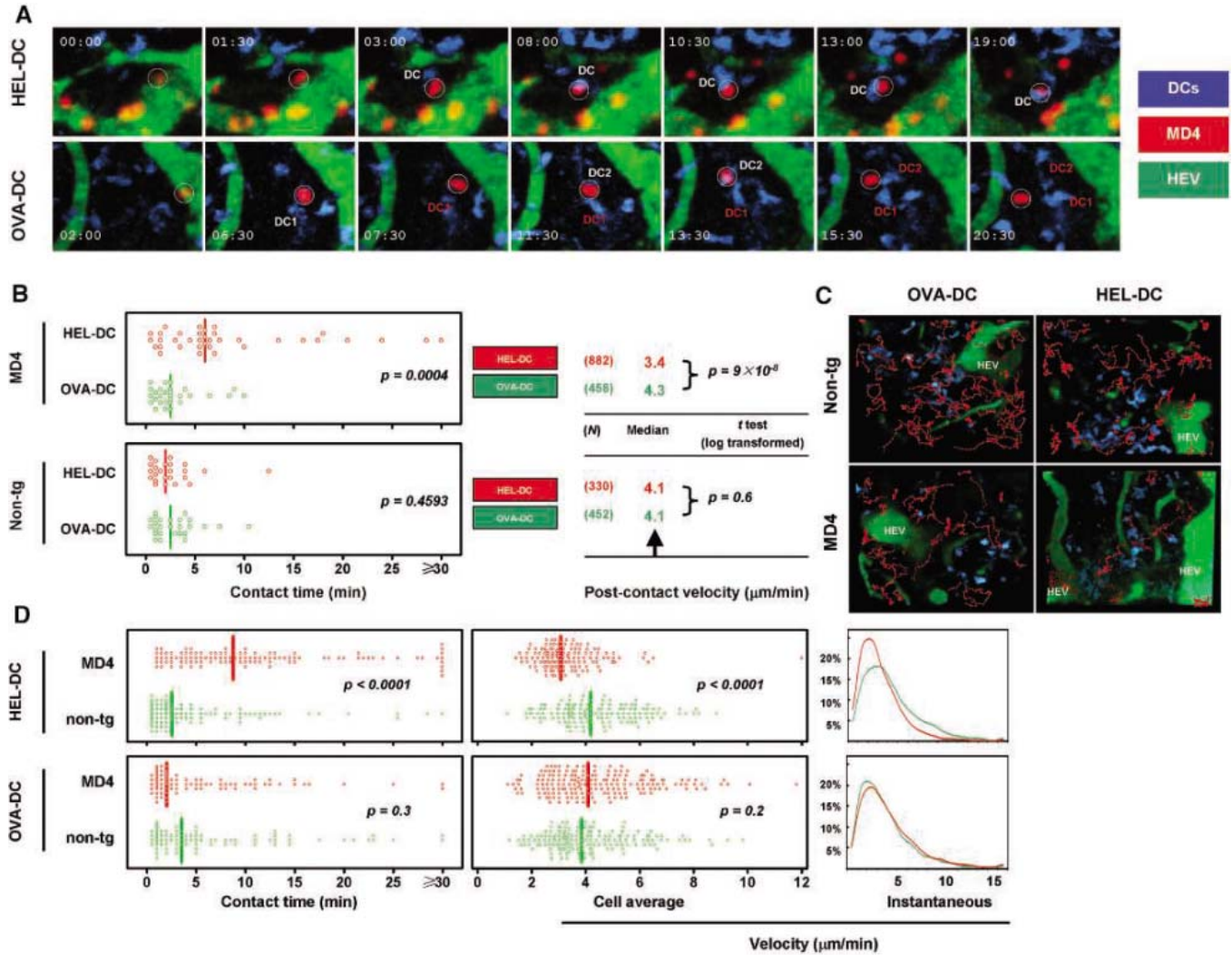

Fig. 2. Contact-dependent, Ag-specific interactions between recent immigrant B cells and Ag-carrying DCs in the peri-HEV region of LNs. (**A**) Time-lapse images of DC interactions with MD4 B cells as the latter exit HEVs. "DC" in white denotes a DC in contact with an MD4 B cell (circle), whereas "DC" in red indicates a DC from which an MD4 cell has disengaged. (**B**) (Left) Scatter plots of the duration of individual DC contacts made by B cells imaged as they leave HEVs. The lines indicate median values. (Right) The median instantaneous velocity of B cells leaving HEV during and after contacts with DCs. *N* is the number of velocity measurements in each category. Data were compiled from more than 30 imaging sessions that captured 33 MD4 B cells as they exited HEV and interacted with DCs (23 with HEL-DCs and 10 with OVA-DCs) and that also captured 20 non-tg B cells imaged under the same conditions (eight with HEL-DCs and 12 with OVA-DCs). (**C**) From these same data sets, typical migration patterns of recent immigrant B cells within and around DC arrays (blue) in the peri-HEV region were examined. Blood vessels are in green. HEV segments were identified on the basis of intravascular attachment of transferred B cells. Migration tracks are highlighted in red, with the actual B cell fluorescence omitted for clarity (movie S7). (**D**) Contact time (left), average cell migration speed (center), and distribution of instantaneous velocities (right) of MD4 and non-tg B cells cotransferred into HEL-DC or OVA-DC recipients. Data were compiled from four independent experiments involving each type of DC recipient, with imaging conducted 4 to 6 hours after B cell transfer. The vertical lines indicate medians.

followed by signal oscillations during an extended period of association (Fig. 1E and movie S1). Coincident with this Ca^{2+} response, B cells typically lost their initial polarized shape, similar to what has been observed with Ag-triggered T lymphocytes (*21*, *22*). Of 159 MD4 cells visualized contacting HEL-DCs, 45 showed detectable elevation of intracellular [Ca^{2+}], a frequency five times higher than that seen when MD4 cells contacted OVA-DCs (8 out of 143; $P < 0.01$). By using covisualization of HEVs, we also documented such Ca^{2+} responses in MD4 cells that exited HEVs and immediately engaged HEL-DCs (Fig. 1F and movie S2). Together, these data indicate that, upon contact with Ag-bearing DCs, receptor-dependent signaling can be triggered in LN B cells shortly after their exit from HEVs and before migration into the follicle.

T cells show prolonged interactions with DCs upon recognition of peptide-MHC ligands in vivo (*23*, *24*), and elevation of intracellular [Ca^{2+}] is linked to reduced migration by receptor-engaged T cells and thymocytes (*22*). We therefore undertook a detailed survey in which the migration behavior of each B cell was documented from the moment of its entry into a LN through an HEV. This analysis revealed that MD4 B cells bound to HEV-proximate HEL-DCs (Fig. 2A and movie S3) for considerably longer periods than they bound to OVA-DCs (Fig. 2A and movie S4). In contrast, immigrating nontransgenic (non-tg) B cells made only brief contact with either HEL- or OVA-DCs, consistent with a lack of specific Ag recognition (movies S5 and S6). Initial MD4 B cell associations with HEL-DCs lasted three times as long as those involving Ag-nonspecific B-DC combinations ($P = 0.0004$) (Fig. 2B). There was also a reduction in the migration speed of MD4 cells interacting with HEL-DCs compared with OVA-DCs or non-tg B cells inter-

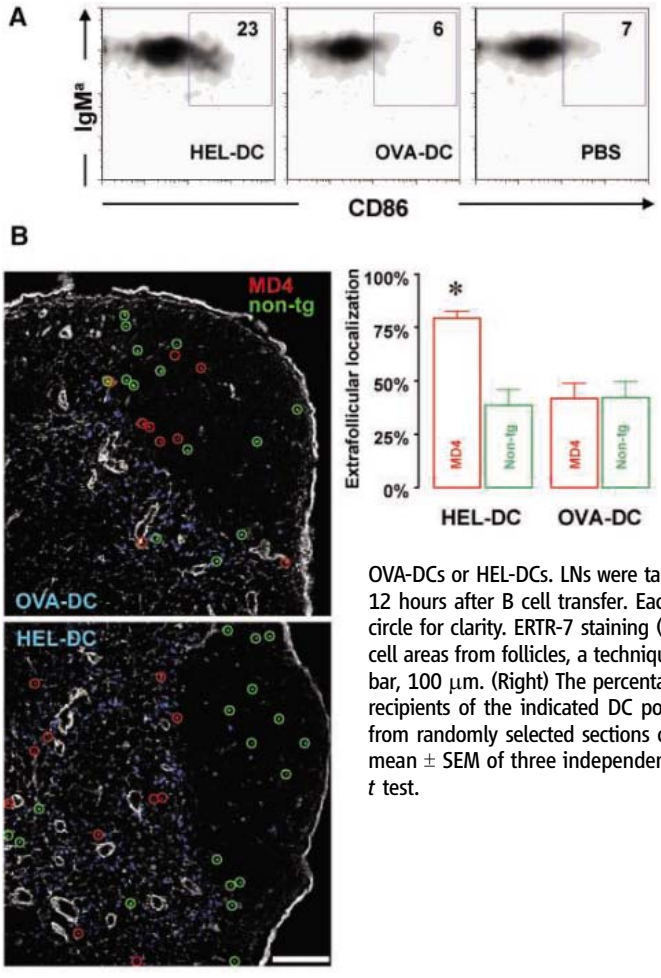

Fig. 3. Follicular exclusion of B cells activated by Ag-carrying DCs. (**A**) Ten to 12 hours after being transferred into mice injected with HEL-DCs, OVA-DCs, or phosphate-buffered saline (PBS), carboxyfluorescein diacetate succinimidyl ester (CFSE)–labeled MD4 B cells were recovered from draining inguinal LNs for fluorescence-activated cell sorting analysis. Data are gated on $CD19^{+}CFSE^{+}$ cells. One of three similar experiments is shown. (**B**) (Left) Distribution of co-transferred MD4 (red) and non-tg B cells (green) on sections of LNs containing OVA-DCs or HEL-DCs. LNs were taken from recipient mice 10 to 12 hours after B cell transfer. Each B cell is highlighted with a circle for clarity. ERTR-7 staining (white) is used to distinguish T cell areas from follicles, a technique established in fig. S1. Scale bar, 100 μm. (Right) The percentage of extrafollicular B cells in recipients of the indicated DC population. Data were collected from randomly selected sections or fields and are presented as mean ± SEM of three independent experiments. * $P < 0.01$ by *t* test.

acting with either HEL- or OVA-DCs (Fig. 2B). MD4 cells that had not interacted with any transferred HEL-DCs moved more rapidly than those that had physically engaged Ag-bearing DCs (median instantaneous velocities of 4.8 versus 3.4 μm/min from 405 versus 882 measurements, $P = 3 \times 10^{-17}$). The velocities of the MD4 cells failing to contact an HEL-DC were comparable to those of non-tg B cells that failed to contact transferred DCs (median instantaneous velocities of 4.8 versus 4.8 μm/min from 405 versus 658 measurements, $P = 0.7$), although the velocities of both B cell types were lower than their respective migration speeds within the follicles of nonimmunized mice, presumably reflecting Ag-nonspecific inflammatory and/or activated DC-related factors influencing B cell motility (fig. S5). Thus, in a LN containing HEL-DCs, immigrating MD4 B cells only showed appreciable motility changes if they directly contacted the Ag-carrying DCs. This implies that DCs released little or no free Ag into the extracellular space of the LN, at least in a form or quantity able to evoke a measurable change in B cell mobility, consistent with the result from the in vitro transwell assays (fig. S1).

We next examined the dynamic behavior of larger populations of recently arriving B cells located within the peri-HEV region. Many MD4 cells in this setting also showed prolonged interactions with HEL-DCs, migrating slowly along short-range tracks near their DC partners (Fig. 2C and movie S7). In contrast, MD4 and non-tg B cells migrated rapidly in and out of perivascular arrays of DCs lacking specific Ags,

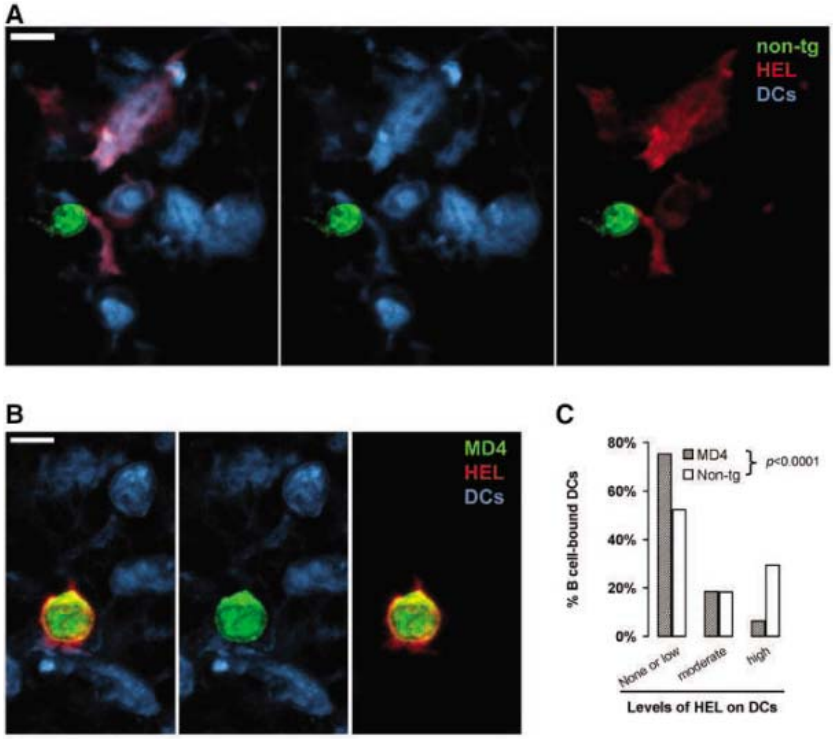

Fig. 4. B cell acquisition of Ags from DCs. (**A** and **B**) Sections were obtained from LNs of HEL-DC recipients taken 3 hours after B cell transfer and stained for HEL. Examples of HEL-pulsed DCs in contact with non-tg (A) or MD4 B cells (B) are shown as overlays of all three colors (left), only transferred DCs and B cells (center) to highlight cell-cell contacts, and only B cells and HEL staining (right) to highlight the difference in Ag distribution. Scale bar, 5 μm. (**C**) 153 HEL-pulsed DCs in contact with MD4 B cells and 157 in contact with non-tg B cells were scored for amounts of HEL in randomly selected fields of four LNs for each condition collected from two independent experiments. The Mann-Whitney rank sum test was used to compare amounts of HEL associated with HEL-pulsed DCs in contact with MD4 cells versus with non-tg B cells.

resulting in the generation of longer-range tracks covering both DC-rich and DC-sparse areas (Fig. 2C and movie S7). Quantitative analysis 3 to 6 hours after transfer showed no measurable differences in contact time or migration speed for MD4 versus non-tg B cells in the presence of control OVA-DCs (Fig. 2D and movie S8). In contrast, MD4 cells, but not non-tg B cells, exhibited a considerable increase in contact time and reduced migration speed in the presence of HEL-DCs (Fig. 2D and movie S9).

Follicular exclusion is a well-established property of Ag receptor–engaged B cells, a phenomenon characterized by the localization of these cells to the outer T cell zone (*25*). Because our results revealed a series of Ag-specific B cell–DC interaction events within the T cell zone that influenced B cell mobility, we tested whether HEL-DCs would prevent or retard follicular entry by MD4 B cells 10 to 12 hours after transfer into mice that had previously received DCs. This was a time point at which many MD4 cells showed phenotypic evidence of activation in the presence of HEL-DCs (Fig. 3A). Although MD4 and non-tg B cells homed to follicles with a similar efficiency after arriving in LNs containing OVA-DCs, MD4 B cells were preferentially retained in the T cell zone in HEL-DC recipients (Fig. 3B). Consistent with this result, the expression of the chemokine receptor CCR7 by MD4 B cells was increased in this situation (fig. S6) (*26*).

A hallmark of specific B lymphocyte activation is BCR-mediated acquisition of Ags. This allows B cell presentation of the MHC molecule–associated peptides required for development of T cell–dependent antibody responses. In accord with the preceding data on activation and migration, a substantial majority of MD4 cells acquired HEL 3 to 4 hours after arriving in a LN containing HEL-DCs (fig. S7). Analysis of the HEL distribution pattern in B-DC pairs on stained LN sections revealed that non-tg B cells failed to acquire HEL from the DCs they contacted, which typically stained for HEL throughout the cell interior (Fig. 4A) and sometimes along dendrites (fig. S8). In contrast, considerably less HEL remained associated with DCs engaged by MD4 cells, and the Ag was instead concentrated in the Ag-specific B cell partner (Fig. 4, B and C). These data indicate that BCR-mediated Ag acquisition occurs during direct B-DC interactions in the T cell zone rather than as a result of the spontaneous release of Ags from the DCs, a conclusion consistent with the migration analysis detailed above (Fig. 2).

The extrafollicular localization of receptor-engaged B cells is likely dictated by the need for cognate T-B interactions in the T cell zone before further development of T-dependent antibody responses (*27*). Here, we used intravital two-photon imaging to document that upon LN entry, B cells survey local Ag-carrying DCs. Specific B cells recognizing their Ags on these DCs are activated and arrested in the T cell zone before their follicular homing (Note S1). These results are not in conflict with the available evidence that diffusing low-molecular-weight Ags may engage specific B cells inside follicles and induce their migration toward the T cell zone (*28*, *29*) (Note S2); rather, they point to a mechanism that, given the wide variety of Ag-capturing mechanisms possessed by DCs, may provide B cells with broader access to Ags, particularly those of large sizes or associated with particulate materials. In addition, presentation of membrane-tethered Ags would also facilitate activation of low-affinity B cells in the naïve repertoire (*30*). Lastly, through presentation of both T cell and B cell epitopes derived from the same Ag, DCs could serve as a cellular platform to facilitate activation, colocalization, and mutual communication of rare Ag-specific T and B cells, whose interaction ultimately leads to antibody responses.

References and Notes

1. J. Banchereau, R. M. Steinman, *Nature* **392**, 245 (1998).
2. C. Drinker, B. Wislocki, M. E. Field, *Anat. Rec.* **56**, 261 (1935).
3. A. O. Anderson, N. D. Anderson, *Am. J. Pathol.* **80**, 387 (1975).
4. J. E. Gretz, C. C. Norbury, A. O. Anderson, A. E. I. Proudfoot, S. Shaw, *J. Exp. Med.* **192**, 1425 (2000).
5. M. Wykes, A. Pombo, C. Jenkins, G. G. MacPherson, *J. Immunol.* **161**, 1313 (1998).
6. C. Berney *et al.*, *J. Exp. Med.* **190**, 851 (1999).
7. B. Ludewig *et al.*, *Eur. J. Immunol.* **30**, 185 (2000).
8. J. Colino, Y. Shen, C. M. Snapper, *J. Exp. Med.* **195**, 1 (2002).
9. H. Wang, M. N. Griffiths, D. R. Burton, P. Ghazal, *Proc. Natl. Acad. Sci. U.S.A.* **97**, 847 (2000).
10. M. Balazs, F. Martin, T. Zhou, J. Kearney, *Immunity* **17**, 341 (2002).
11. A. Bergtold, D. D. Desai, A. Gavhane, R. Clynes, *Immunity* **23**, 503 (2005).
12. A. Chow, D. Toomre, W. Garrett, I. Mellman, *Nature* **418**, 988 (2002).
13. M. B. Lutz *et al.*, *J. Immunol.* **159**, 3707 (1997).
14. C. C. Goodnow *et al.*, *Nature* **334**, 676 (1988).
15. R. M. Steinman, M. Pack, K. Inaba, *Immunol. Rev.* **156**, 25 (1997).
16. M. Bajenoff, S. Granjeaud, S. Guerder, *J. Exp. Med.* **198**, 715 (2003).
17. T. Katakai *et al.*, *Int. Immunol.* **16**, 1133 (2004).
18. M. Sixt *et al.*, *Immunity* **22**, 19 (2005).
19. M. J. Miller, S. H. Wei, M. D. Cahalan, I. Parker, *Proc. Natl. Acad. Sci. U.S.A.* **100**, 2604 (2003).
20. Materials and methods are available on *Science* Online.
21. P. A. Negulescu, T. B. Krasieva, A. Khan, H. H. Kerschbaum, M. D. Cahalan, *Immunity* **4**, 421 (1996).
22. N. R. Bhakta, D. Y. Oh, R. S. Lewis, *Nat. Immunol.* **6**, 143 (2005).
23. S. Stoll, J. Delon, T. M. Brotz, R. N. Germain, *Science* **296**, 1873 (2002).
24. T. R. Mempel, S. E. Henrickson, U. H. Von Andrian, *Nature* **427**, 154 (2004).
25. J. G. Cyster, C. C. Goodnow, *Immunity* **3**, 691 (1995).
26. K. Reif *et al.*, *Nature* **416**, 94 (2002).
27. I. C. MacLennan *et al.*, *Immunol. Rev.* **156**, 53 (1997).
28. P. Garside *et al.*, *Science* **281**, 96 (1998).
29. T. Okada *et al.*, *PLoS Biol.* **3**, e150 (2005).
30. F. D. Batista, D. Iber, M. S. Neuberger, *Nature* **411**, 489 (2001).

31. We are grateful to O. Schwartz at the NIAID Biological Imaging Facility for expert advice on confocal microscopy; I. Ifrim and A. Rinker for research assistance; and R. Casellas, J. Cannons, and P. Schwartzberg for comments on the manuscript. H.Q. and A.Y.C.H. received Cancer Research Institute Postdoctoral Fellowships. H.Q. is particularly in debt to Y. Hong for support, encouragement, and inspiration. This work was supported by funds from the Intramural Program, NIAID, NIH, U.S. Department of Health and Human Services.

Supporting Online Material

www.sciencemag.org/cgi/content/full/312/5780/1672/DC1
Materials and Methods
SOM Text
Figs. S1 to S8
References
Movies S1 to S9

1 February 2006; accepted 17 May 2006
10.1126/science.1125703

Protein Gel Processor

Designed for generating precisely focused two-dimensional (2D) protein gels, the IEF-SYS is a one-tank system designed to save time by allowing users to run 2D gels with both immobilized pH gradient strips and pre-cast acrylamide gels. Scientists can then generate images of their 2D gels using either Syngene's ProteomeScan scanner or Dyversity, a charge-coupled-device–based imager. For the next stage in the proteomics workflow, users can automatically transfer the results into Dymension 2D image analysis software. The software can perform background correction, spot matching, and reporting in minutes.

Syngene For information 800-686-4407 www.syngene.com

Chromogenic Detection

The femto-CHROMO-HRP kit is designed for the chromogenic detection of antibodies labeled with horseradish peroxidase (HRP) on protein immunoblots. It makes use of a single-step chromogenic substrate, modified TMB (3,3′,5,5′-tetramethylbenzidine), which generates a dark blue precipitate in the presence of HRP. With sensitivity greater than 20 ng, the resulting signal is high in reproducibility with minimal fading. To ensure a high signal-to-background ratio, this kit is supplied with an enhanced blocking agent and a concentrated washing buffer.

G-Biosciences/Genotech For information 800-628-7730 www.GBiosciences.com

Soil DNA Extraction

The SoilMaster DNA Extraction Kit enables the recovery of DNA ready for polymerase chain reaction (PCR) from a variety of soils and sediments. This kit makes use of a hot detergent lysis process combined with a simple spin column step that removes PCR inhibitors, such as humic and fulvic acids, which are known to be co-extracted with DNA from soils and sediments.

Epicentre Biotechnologies For information 800-284-8474 www.EpiBio.com

Protein Research Products

New tools are available to streamline protein research. A major challenge facing researchers studying individual cell compartments or organelles is obtaining pure fractions free of contaminating proteins from other compartments. Reproducible separation of mitochondria and cytosolic proteins is notoriously difficult. Qproteome Mitochondria Isolation and Plasma Membrane Protein kits provide high-purity, highly active mitochondria and plasma-membrane protein preparations, virtually free of contaminating proteins from other cell compartments, for apoptosis and cell-signaling assays and cellular localization studies. Mass-Spec-Turbo Chips are ready-to-use targets pre-spotted with up to 1600 homogeneous matrix spots for high-throughput matrix-assisted laser desorption ionization analyses of complex proteomics samples.

Qiagen For information 800-426-8157 www.qiagen.com

Chromogenic Biotinylation Kit

The EZ-Link NHS-Chromogenic Biotinylation Kit contains the essential components for the biotinylation and direct determination of biotin incorporation into antibodies and proteins using an amine-reactive, colorimetric reagent. The kit includes all the reagents required for labeling antibodies, proteins, and other macromolecules containing primary amine groups. In addition to the biotin reagent, the kit includes a reconstitution solvent, a reaction buffer, and spin columns for purifying the labeled molecule. The kit is structured for labeling 1 to 10 mg of protein in a 1-ml reaction, but the procedure can be easily adapted to smaller and larger volumes.

Pierce For information 815-968-0747 www.piercenet.com

Markers for Degenerating Neurons

The Fluoro-Jade C, like its predecessors, Fluoro-Jade and Fluoro-Jade B, stains all degenerating neurons, regardless of the specific insult or mechanism of cell death. The Fluoro-Jade C exhibits superior signal-to-background ratio and the highest resolution of the three dyes. It is suitable for localizing not only degenerating nerve cell bodies, but also distal dendrites, axons, and terminals. It is compatible with virtually all histological processing and staining protocols.

Chemicon International For information 800-437-7500 www.chemicon.com

Human Cell Selection

Several EasySep human positive selection kits are available for use with whole blood. The column-free protocols are designed to minimize sample handling; red blood cell lysis is followed immediately by immunomagnetic cell separation in the same tube. High cell purities (>99%) can be achieved, and the tiny magnetic nanoparticles are compatible with flow cytometry and other downstream applications. Additionally, up to four samples can be processed simultaneously using RoboSep, the automated cell separator. CD3+, CD4+, CD8+, CD15+, CD19+, CD33+, CD66b+, and myeloid selection kits are available now, with CD14+, CD34+, CD56+, and lymphoid selection kits coming soon.

StemCell Technologies For information call 800-667-0322 www.stemcell.com

For more information visit Product-Info, *Science*'s new online product index at *http://science.labvelocity.com*

From the pages of Product-Info, you can:
- Quickly find and request free information on products and services found in the pages of *Science*.
- Ask vendors to contact you with more information.
- Link directly to vendors' Web sites.

Newly offered instrumentation, apparatus, and laboratory materials of interest to researchers in all disciplines in academic, industrial, and government organizations are featured in this space. Emphasis is given to purpose, chief characteristics, and availability of products and materials. Endorsement by *Science* or AAAS of any products or materials mentioned is not implied. Additional information may be obtained from the manufacturer or supplier by visiting www.science.labvelocity.com on the Web, where you can request that the information be sent to you by e-mail, fax, mail, or telephone.

ScienceCareers.org

Classified Advertising

For full advertising details, go to **www.sciencecareers.org** and click on **For Advertisers,** or call one of our representatives.

United States & Canada

E-mail: advertise@sciencecareers.org
Fax: 202-289-6742

JILL DOWNING
(CT, DE, DC, FL, GA, MD, ME, MA, NH, NJ, NY, NC, PA, RI, SC, VT, VA)
Phone: 631-580-2445

KRISTINE VON ZEDLITZ
(AK, AZ, CA, CO, HI, ID, IA, KS, MT, NE, NV, NM, ND, OR, SD, TX, UT, WA, WY)
Phone: 415-956-2531

KATHLEEN CLARK
Employment: AR, IL, LA, MN, MO, OK, WI
Canada; Graduate Programs; Meetings & Announcements (U.S., Canada, Caribbean, Central and South America)
Phone: 510-271-8349

DARYL ANDERSON
(AL, IN, KY, MI, MS, OH, TN, WV)
Phone: 202-326-6543

GABRIELLE BOGUSLAWSKI
(U.S. Recruitment Advertising Sales Director)
Phone: 718-491-1607

Europe & International

E-mail: ads@science-int.co.uk
Fax: +44 (0) 1223-326-532

TRACY HOLMES
Phone: +44 (0) 1223-326-525

HELEN MORONEY
Phone: +44 (0) 1223-326-528

CHRISTINA HARRISON
Phone: +44 (0) 1223-326-510

SVITLANA BARNES
Phone: +44 (0) 1223-326-527

JASON HANNAFORD
Phone: +81 (0) 52-789-1860

To subscribe to *Science*:
In U.S./Canada call 202-326-6417 or 1-800-731-4939
In the rest of the world call +44 (0) 1223-326-515

Science makes every effort to screen its ads for offensive and/or discriminatory language in accordance with U.S. and non-U.S. law. Since we are an international journal, you may see ads from non-U.S. countries that request applications from specific demographic groups. Since U.S. law does not apply to other countries we try to accommodate recruiting practices of other countries. However, we encourage our readers to alert us to any ads that they feel are discriminatory or offensive.

ScienceCareers.org
We know science
AAAS

I want to advance drug development and my career.

You can at AstraZeneca. Discover your potential with a pharmaceutical industry leader who values your contributions, seeks innovation, and rewards success.

At AstraZeneca R&D Boston, in Waltham, MA, we are focused on infectious disease research and discovering life-enhancing drugs for cancer patients. Several positions are currently available:

CELL SCIENCES
Senior Scientist (1772288)
Senior Associate Scientists (1772137 & 1772289)

IN VIVO PHARMACOLOGY
Senior Scientist (1171947)
Scientist (1172611)

MOLECULAR AND PROTEIN SCIENCES
Associate Scientist (1774251)

BIOCHEMISTRY
Senior Scientist (1770886)

DISCOVERY MEDICINE
Principal Pathologist (1772675)

To apply, please visit **www.AstraZenecaCareers.com** and use the reference number(s) provided above to view the specific position details. We are an equal opportunity employer.

www.AstraZenecaCareers.com

AstraZeneca

UNIVERSITY OF SOUTH CAROLINA

ENDOWED CHAIRS
SOUTH CAROLINA CENTERS OF ECONOMIC EXCELLENCE

MUSC
MEDICAL UNIVERSITY OF SOUTH CAROLINA

The University of South Carolina (USC) in Columbia, SC, and the Medical University of South Carolina (MUSC) in Charleston, SC, are jointly seeking applications and nominations for two endowed chairs, sponsored by the statewide South Carolina Centers of Economic Excellence program. One chair will be in the general area of Chemical Biology/Medicinal Chemistry, while the other will be in Cancer Chemotherapy/Mechanisms of Drug Action. For each position, the successful candidate will be an established scientist who has a strong reputation in research, has a productive record of publication and extramural funding, and is qualified for a tenured appointment at the level of Full Professor. Both endowed appointments, as well as the associated laboratory spaces, will be located at USC, with joint appointments at MUSC. The chair holders will play key roles in the growth and development of cancer research and/or drug discovery in the State of South Carolina. They will be expected to participate in professional and graduate education, and to maintain nationally recognized, extramurally funded research programs.

USC has undergone expansion of its biomedical research capabilities, and has developed significant strength in the area of cancer. This has been spearheaded by the Center for Colon Cancer Research, an interdisciplinary unit dedicated to studies of the biology, epidemiology, detection, prevention, and therapy of colorectal cancer. MUSC has several Centers of Economic Excellence, including the Center for Drug Discovery, and is likewise experiencing rapid growth in its research environment, with its extramural funding topping the $170 million mark during the last fiscal year. State-of-the-art core research facilities exist at both institutions, fostering a variety of collaborative research interactions.

Interested candidates should submit curriculum vitae, statements of research interests and accomplishments, and the names of three references to: **Dr. Franklin G. Berger, Director, Center for Colon Cancer Research, University of South Carolina, Columbia, SC 29208 (email: berger@sc.edu), or Dr. Charles Smith, Center for Drug Discovery, Medical University of South Carolina, 280 Calhoun St., POB 250140, Charleston, SC 29425 (email: smithchd@musc.edu)**. Nominations are also welcomed, and can be sent to one or both of these individuals. Review of applications will begin on **August 1, 2006** and will continue until both positions are filled.

The University of South Carolina and the Medical University of South Carolina are Affirmative Action/Equal Opportunity Employers.

Careers in Biotech and Pharma

Where's the Heat?

Rapid advances in biotechnology and pharmaceutical sciences generate some of the hottest careers in science. The industry experts interviewed here describe lifelong opportunities in new fields—such as pharmacogenetics—and more traditional pursuits—such as basic pharmacology. In addition, these experts lay out some softer and harder skills that can make the difference in getting the best job. BY MIKE MAY

The general press often reports ups and downs for both the biotechnology and pharmaceutical industries. Despite all of that, the experts interviewed here expect continuing growth and hiring. Dan Guaglianone, executive director of corporate staffing for research labs at Merck, says, "We're hiring—drug discovery through development and everywhere in between." Many other companies concur.

For example, Ginger Gregory, global head of human resources for Novartis Institutes for BioMedical Research, the research arm of Novartis AG, says, "We work on different therapeutics at different sites, but we are growing at most of those locations." Overall, Novartis sites cover 140 countries and include more than 81,000 employees.

The pharmaceutical industry, in general, requires a wide range of expertise. Steve Arkinstall, vice president of Serono's U.S. research, says, "In the drug industry, we often look for scientists with skills that may be seen as distinct from directly supporting the development of new drugs." For example, people with skills in basic biological research can play fundamental roles in the pharmaceutical industry. Also, Arkinstall says that it's challenging to hire people with some areas of expertise, especially protein engineering, production, and purification. He explains, "Someone who can take cDNA and make large quantities of a protein is fundamental to the success of early stage, biotherapeutic drug discovery programs."

The current needs in biotech and pharma, however, go beyond entirely modern approaches. Many of the experts interviewed here express needs for people trained in traditional pharmacology. The key to future successes in biotech and pharma, however, will surely combine techniques of the past and present. CONTINUED »

AstraZeneca
http://www.astrazeneca.com

KAI Pharmaceuticals
http://www.kaipharmaceuticals.com

Merck
http://www.merck.com

Novartis Institutes for BioMedical Research
http://www.nibr.novartis.com

Roche
http://www.roche.com

Serono
http://www.serono.com

Careers in Biotech and Pharma


AILEEN ALLSOP

Skills in Demand

Today's biotech and pharma industries need people with various skills. For example, Aileen Allsop, vice president of science policy at AstraZeneca, immediately mentions the value of understanding chemistry. She also notes the value of experience in whole animal biology and toxicology, and then adds, "In Europe, we are finding that the numbers of people studying these subjects are decreasing, and the number of academic departments teaching these areas is also declining."

Experts from other companies also see rather specific skills in demand. Jim Tomlinson, senior scientist II, cell biology, at KAI Pharmaceuticals, sees a lack of highly qualified people in bioanalytical areas associated with pharmacokinetics and pharmacodynamics, often known simply as PK and PD, respectively. From Roche, Jeanne Lyon, senior vice president of human resources, provides an even longer list of needs: biomarker knowledge, genetics, genomics, medicinal chemistry, drug metabolism and pharmacokinetics, and neuroscience. She adds, "Increases in regulatory stringency also drive needs for people skilled in safety areas."

Lyon's mention of biomarkers reflects the beliefs of other experts, as well. "As personalized medicine comes closer to reality," says Guaglianone, "there will be more emphasis on the use of biomarkers in the drug development process. There is already lots of energy around identifying biomarkers for potential drug candidates."

Gregory of Novartis says, "We have needs across many disease areas and technologies." For example, she mentions that for all therapeutic areas there is ongoing research in small molecules and increasingly in proteins as well. In thinking of the large molecules, she says, "Experience in biologics is very valuable."

Some of the skills in demand, however, go beyond science. As Corinna Patmore, lead recruitment partner for research and development at AstraZeneca, explains: "We are broadening our portfolio of companies, so we are always looking for people with good commercial skills, such as in-licensing or managing collaborations." Such broadening often increases the global features of a company, too. "People at senior levels," says Patmore, "often need the ability to work in different countries and understand different cultures."


STEVE ARKINSTALL

Is Anybody Hiring?

Jobs do exist. Lyon says, "We've hired more than 70 researchers in the last year." Many of those people were hired in therapeutic areas: autoimmunity, transplantation, neurosciences, and virology.

In the near future, some of these experts expect even more jobs in biotech and pharma. Guaglianone of Merck says, "Our industry is looking at a limited, high skilled, highly educated talent pool, and the jobs outstrip the pool." He adds, "The U.S. educational system is not graduating enough scientists, engineers, and mathematicians." (For more on opportunities for physical scientists, see the accompanying "The Harder Side of Biotech & Pharma.") Guaglianone draws a simple conclusion: "We need a bigger talent pool."


GINGER GREGORY

For current job hunters, though, an inadequate talent pool is good news. Tomlinson says, "KAI is in a major growth phase, increasing in size by greater than 30 percent." With so many positions coming up, Tomlinson says, "it's a seller's market right now."


DAN GUAGLIANONE

Getting a Seller's Edge

How does an aspiring scientist become someone with the right skills for sale? Despite the common advice to gain breadth, it's not always the best approach, according to Allsop of AstraZeneca. "We're seeing a dilution of skills happening in university degree systems," she says. "We often find youngsters from their first degree to have little experience in practical science, and that makes it hard to engage them in industry." To solve that issue of dilution, students should take every opportunity to get more experience in a lab or even find an internship in industry. Also, Allsop recommends a focused first degree over some combination of majors. For example, instead of combining chemistry and finance in a first degree, Allsop says, "a degree in pure chemistry will make the world your oyster. If you want finance too, you can add that later."

For those who do want to mix science and business, many universities offer special M.B.A. programs for scientists who already have a Ph.D. "There is a huge return on investment for companies when employees can bring business concepts and principles to bear on science," says Guaglianone. Someone can bring that perspective to a company by getting a solid background in a specific science and then adding business skills. Guaglianone points out that most Ph.D./M.B.A. students go to the marketing and sales side of industry. "In the future," he says, "I think there will be lots of demand for those people on the science side, primarily in project management"

When it comes to getting hired at Novartis, Gregory says, "We want people who are engaged in cutting-edge science. We seek scientists who are doing extremely high quality work yet also innovating to find novel treatments for patients." Being part of a company that covers so many therapeutic areas and regions of the world, she adds, "our scientists must collaborate well with each other and actively seek opportunities to innovate. We all need to work together to create the best medicine for our patients as quickly as possible."

Arkinstall of Serono looks beyond bench skills. "One thing that is really important across the board is personal leadership skills," he says. "These cannot be underestimated." He adds, "So many times great scientists are unable to communicate to nonscientists outside of their area of expertise. This is an essential skill because drug CONTINUED »

For the latest job postings online visit **www.sciencecareers.org**.

Choosing Roche

We all dream of doing big things.

Solving important problems.
Making a difference.
Improving lives.

Roche is in the midst of one of the most exciting periods in its history. With an array of established products, a healthy line of new products and several exciting launches ahead, Roche is extremely well positioned to be one of the truly preeminent companies that lead the industry into the 21st century. If you want to work in a dynamic, challenging environment that capitalizes on your strengths and abilities, please take a few moments to peruse the following job openings at our Nutley, NJ campus:

Toxicologist, Non-clinical Drug Safety- Req. #3887

The successful candidate will plan, design, and effectively manage and oversee designated toxicology programs necessary to support the selection and timely development of potential drug candidates through close interactions with discovery therapeutic areas, and affiliated non-clinical and clinical development functions as necessary. Candidate will coordinate toxicological/non-clinical safety evaluations of discovery and development candidates locally and internationally within Roche, and externally with contract laboratories, consultants, and development partners. Candidate will be responsible for preparing contributions to internal and regulatory documents (IBs, CTXs, INDs, NDAs, Expert Reports, etc.). The incumbent may oversee a small team of scientists working on a specific issue or program.

Requirements include a DVM, PhD or equivalent advanced degree/experience in toxicology or allied field. Ideal candidates would have a minimum of five years experience in drug development (toxicology), with a demonstrated ability to manage multiple scientific projects and make sound scientific interpretations and assessments. Candidates must have a proficient knowledge of general toxicology and related disciplines with expertise in one or more areas of specialization and proficient understanding of regulatory toxicology and US and international guidelines. Strong interpersonal skills, skills in collaborative problem solving, project management and team interactions are required.

Pharmacokineticist, Research Leader, Nonclincial Drug Safety-Req. #3894

The successful candidate will plan, design, and effectively manage and oversee designated nonclinical pharmacokinetic (PK), pharmacodynamic (PD) and drug metabolism programs necessary to support the selection and timely development of potential drug candidates through close interactions with discovery therapeutic areas, and affiliated nonclinical and clinical development functions as necessary. Candidate will coordinate PK, toxicokinetic (TK), PD and toxicodynamic (TD) evaluations of discovery and development candidates locally and internationally within Roche, and externally with contract laboratories, consultants, and development partners. The candidate will actively participate as a member of Research Development and Life Cycle Project Teams, and provide expert opinions and feedback regarding interpretation and utilization of PK/TK in discovery and development. Candidate will be responsible for preparing contributions to internal and regulatory documents (IBs, CTXs, INDs, NDAs, BLAs, Expert Reports, etc.), and contribute to or lead ongoing process improvement and technology development efforts in the fields of pharmacokinetics, pharmacodynamics and drug metabolism.

Requirements include a PhD or equivalent advanced degree/experience in pharmacokinetics/pharmacodynamics or allied field. Ideal candidates would have a minimum of five years experience in drug development (pharmacokinetics/pharmacodynamics/drug metabolism). Expertise in Modeling and Simulation or another area of specialization is desired. Candidates must be capable in the design, conduct, interpretation, and reporting of PK/TK/PD studies, integration of ADME data, and be able to address and resolve PK/TK and drug metabolism issues arising in drug development programs, and adequately assess the relevance of any findings to human safety. Strong interpersonal skills, demonstrated knowledge of drug discovery and development, and skills in collaborative problem solving and project management required

To apply for these positions, please visit us at **www.rocheusa.com/career**, and refer to the appropriate requisition number.

Hoffmann – LaRoche is an equal opportunity employer.

We Innovate Healthcare
from research to real life

Roche

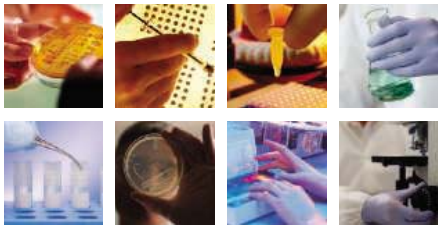

Careers in Biotech and Pharma


JEANNE LYON

development teams are multidisciplinary." That ability to communicate can determine which projects survive. As Arkinstall explains: "Lots of projects that start within companies are very good but can die because they do not have internal champions." Consequently, some projects do not get sold convincingly.

The best career preparation, however, might come from a young scientist's heart. "You've got to be on fire for your subject," says Arkinstall. Virtually any area of biology can be applied to drug discovery and development. "So look at where you are on fire," Arkinstall says, "and then find out how that fits into the biotech or pharma business."


CORINNA PATMORE

Tomorrow's Transitions

Anyone looking toward a career in biotech or pharma should also consider the futures of these fields. Making predictions about future directions, though, proves extremely difficult for anyone outside these industries. Even different experts predict various futures.

From a perspective at Roche, Lyon sees lots of work on biomarkers in the years ahead. But as she looks for people prepared to do that kind of work, she says, "We're not seeing huge numbers of people graduating with the right background to work on biomarkers. It is our challenge to get more young people to pursue those areas."

Many of the experts do point in the same general direction: research that leads to medical advances. "Translational medicine is moving very fast, leading to the demand for new skills and techniques, such as pathway analysis, imaging, and biomarker specialists," says Patmore of AstraZeneca. "However, there will always be an underlying demand for core skills, like synthetic chemistry and biologists with in vivo skills."

Many of those future medical advances will involve pharmacogenetics. Arkinstall thinks this will become a hot topic for many companies. "This will take a good understanding of the theory behind human genetics," he says. "In 10 to 20 years, targeted therapies will demand matching therapeutics with specific patients. Drugs will require such matching as an integral part of development, even starting early in discovery." He adds that his company already delivers lead molecules with a biomarker package. "That way," he says, "we already have endpoints that could be developed for the clinic." Tomlinson of KAI Pharmaceuticals agrees that the future will include an increasing use of targeted therapy. He says, "Scientists will focus on trying to design better clinical studies and trying to understand which compounds can be used more effectively in smaller populations of patients."

Also, biologics—pharmaceuticals made from biological building blocks—will play an increasing role in the future of pharma. "Many big pharmas now have new portfolios of biological molecules," says Allsop. "Some of the skills we require for this are the same as for small molecules, and others are not the same." She adds, "Biologics will be a growth area as an increasing number of them get in development and toward the marketplace."


JIM TOMLINSON

Some very specialized areas also promise lots of opportunities just ahead. Two such areas are M.D.s who specialize in cardiology or oncology. These areas—already called "the hottest out there" by Guaglianone—could get even hotter. "It's the hardest space that we recruit in," he says. "Lots of pharmas are focusing on it. That makes it difficult to find people who can manage clinical trials."

With so many opportunities in biotech and pharma, anyone interested in this field will do best by following Arkinstall's advice: "Listen to your heart and then match that against skills needed in the industry. Only then can you be a leader in it."

The Harder Side of Biotech & Pharma

Today's world of biotech and pharma opens opportunities for many scientists from the physical side. That means that people with backgrounds in computer science, engineering, mathematics, physics, and so on could build productive careers in biotech or pharma. Moreover, the needs for such specialists appear to be growing.

All biotech and pharma companies need experts in the physical sciences for a variety of tasks. "The formulation and delivery of drugs and the development of new devices for distribution are big areas now and will be even bigger in the next five years," says Tomlinson of KAI Pharmaceuticals. "And those areas require engineers." At AstraZeneca, Aileen Allsop and Corinna Patmore both point to the growing value of imaging in pharma. "There has been fantastic progress in using imaging to understand disease and the impact of treatment," says Allsop. "Most big pharmas have imaging groups." Those groups depend on computational scientists, engineers, and physicists.

Several of the experts interviewed for this article also see a growing need for mathematicians. For instance, Allsop says mathematicians prove invaluable in projects related to systems biology. Also, Dan Guaglianone says that Merck "hires a lot of math majors with an emphasis in statistics to analyze clinical trial data."

At the later stages of drug development, biotech and pharma turn to engineers once more. "When we go from clinical trials to full-scale manufacturing," says Guaglianone, "the engineering talent required is crucial." In thinking of the overall needs for engineers, mathematicians, and physicists, Guaglianone says, "There are tremendous opportunities."

Mike May (mikemay@mindspring.com) is a publishing consultant for science and technology based in the state of Minnesota, U.S.A.

Director of Protein Science

Monsanto Company, the worldwide leader in Agricultural Biotechnology, **is looking for a Senior Scientist** to lead our efforts in the field of Protein Science.

MONSANTO imagine

Job Description:

The successful candidate will lead an experienced research team that utilizes cutting edge tools in biophysics, biochemistry and structural biology to design proteins optimized for product performance. The candidate will be responsible for continuing to build on Monsanto's capabilities in x-ray crystallography, protein modeling and bioinformatics, high throughput protein design, and enzymology including the use of advanced assay techniques. He/she will also have responsibilities for spearheading efforts to continue to develop Monsanto's future protein science skill base by identifying and implementing new technologies and fostering outside relationships with key academics and institutions. The successful candidate will have strong technical and leadership skills demonstrated by a proven track record of innovative and creative scientific accomplishments in all aspects of modern protein design including a strong publication record. In addition to science excellence core competencies for this position include written and oral communication, budget management, and people development skills.

2005 BEST places to work INDUSTRY The Scientist

Science 2005 TOP EMPLOYER

OPEN TO

EXPLORE

Each individual brings new possibilities for innovation.
We invite you to join our mission of lifesaving drug discovery.

At the Novartis Institutes' cutting-edge research facilities in Cambridge, MA, we now have multiple openings at all levels (BS/MS/PhD) in areas such as chemistry, biochemistry, in vivo pharmacology, cellular/molecular biology, epigenetics, strategic alliances, communications, and IT, and in the following disease areas: cardiovascular, diabetes & metabolism, oncology, ophthalmology, infectious diseases, and muscle disorders.

To view descriptions of all open positions and to apply, visit www.nibr.novartis.com and follow the links to Careers and Job Opportunities.

Novartis is committed to embracing and leveraging diverse backgrounds, cultures, and talents to achieve competitive advantage. Novartis is an equal opportunity employer. M/F/D/V

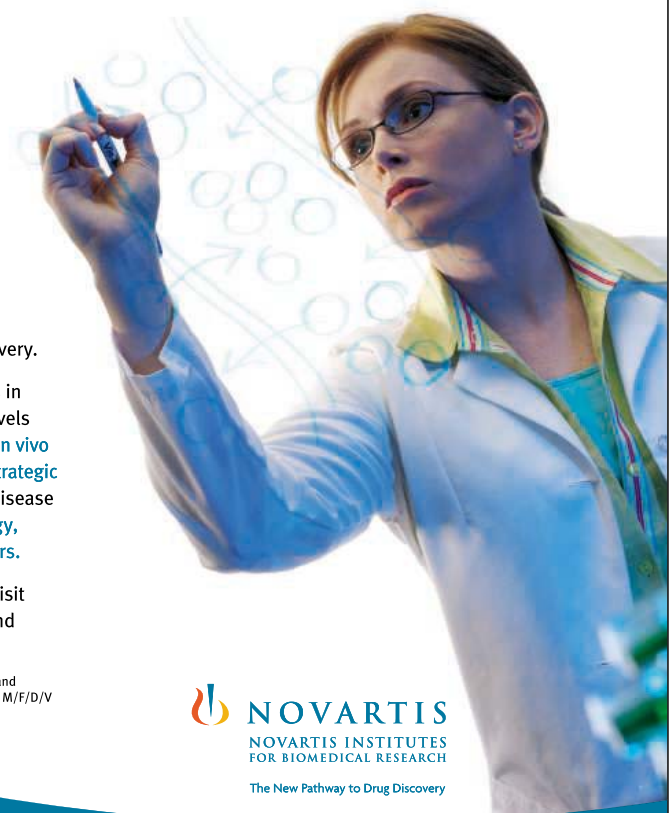

NOVARTIS
NOVARTIS INSTITUTES FOR BIOMEDICAL RESEARCH
The New Pathway to Drug Discovery

www.nibr.novartis.com
©2006 Novartis AG

Giving someone more years of life.

That's a pretty amazing job benefit.

Millennium is focused on developing breakthrough treatments in the areas of oncology and inflammation that will make a real difference in patients' lives. We encourage innovation and seek results through collaboration. If you're looking for a dynamic environment where respect and excellence are core values, learn more about us and the possibilities for you at **www.millennium.com**

We are an equal opportunity employer committed to discovering the individual in everyone.

We currently have openings for the following positions:

QA Specialist II - Commercial Quality Operations; QA Specialist II - Investigational QA; Sr. Software Engineer; Scientist II - Protein Sciences; Scientist I - Analytical Development; Quality Control Analyst I - Commercial Quality Operations; Research Associate - Cancer Pharmacology; Manager, Product Safety - Pharmacovigilance; Scientist II - Analytical Development; Engineer IV - Process Development; Sr. Research Associate - Inflammation Specialists; Lead Specialist, Quality Assurance - Commercial Quality Operations; Research Associate - Biological Assay; Manager II - Commercial Quality Auditing; Scientist I - Structural Biology; Sr. Scientist II - DMPK; Sr. Medical Writer; cGMP Compliance Manager and Auditor - Investigational QA

MILLENNIUM®

Breakthrough science. Breakthrough medicine.

SENIOR RESEARCH SCIENTIST ASSISTANT RESEARCHER

The research project involves the identification of breast cancer biomarkers using proteomic technology including mass spectrometric and affinity-based technologies as well as related bioinformatics. The candidate will be responsible for the study design, performing experiments, data analysis, trouble-shooting and supervision of junior researchers on the project. Ideal candidate will be a Ph.D. in Chemistry, Biochemistry, or Biology with additional 3-5 years of hands-on-research experience in proteomics and mass spectrometry. Candidates must have demonstrated knowledge and experience in mass spectrometry and excellent writing skills. Experience in MALDI-TOF, LC-MS-MS and quantitative proteomics, such as isotope-coded affinity tag (ICAT) technology and Luminex-based bead array technology, is preferred.

The salary/compensation for this position are commensurate to the qualifications of candidates. Career development opportunity is possible. Interested candidates should fax or email CV with a cover letter stating their career goals and research interest and names of three references to: **Helena R. Chang, M.D., Ph.D., Director, Revlon/UCLA Breast Center and Gonda/UCLA Breast Cancer Research laboratory. FAX: 310-206-2982, E-mail: hchang@mednet.ucla.edu**.

VERTEX

Small Molecules. Huge Discoveries.

Vertex Pharmaceuticals Incorporated is a global biotechnology company focused on the discovery, development and commercialization of breakthrough drugs for a range of serious diseases. Our business strategy is to commercialize major new drugs both independently and in collaboration with other pharmaceutical companies. We currently have the following opportunities available:

Biology (Coralville, Iowa)
Research Scientist I/II, 4160-01B

Infectious Diseases (Cambridge, MA)
Research Fellow I/II, 4110-01B

Medicinal Chemistry (Cambridge, MA)
Sr. Research Associate, 4350-01B

We provide a highly stimulating working environment coupled with a high level of professional and intellectual challenge. In addition to competitive salary and benefits, we also offer equity participation and participation in a stock purchase program. No agencies, please. Apply online at: **www.vrtx.com**. EOE

VERTEX

We Enjoy a Big Lead in Small Molecules.

Pfizer

Expect More From Your Career.®

Imagine a career that touches the lives of people everywhere. Imagine an opportunity to reach beyond your area of expertise to make an impact on something greater than the bottom line. Imagine playing a key role in some of the most critical issues facing healthcare today. This is your career at Pfizer – a career unlike any other.

Our St. Louis, MO facility currently has an opportunity for:

Biomarkers Group Leader

Primary responsibilities include providing business-driven input with regard to the strategic direction of the lab consistent with local and global needs; providing both technical and strategic mentoring to project teams by driving scientific excellence in applying immunoassay technology to biomarker discovery, biomarker assay development, and biomarker assay implementation across all St. Louis Therapeutic Areas (TAs); and coordinating, facilitating and tracking all biomarker efforts and progress, independent of technology, for one of the three St. Louis TAs (cardiovascular, inflammation, and respiratory). In addition, actively identify novel opportunities to enhance the biomarker discovery and development process, and increase the impact of biomarkers on drug discovery.

The ideal candidate will have translational pharmacology expertise and drug discovery experience; experience in biomarker assay methods, cell and animal models and PK/PD. Specific experience in disease biology and models of at least one of the three therapeutic areas in Saint Louis is desired (cardiovascular is preferred). Position requires a PhD or MD/PhD in Pharmacology or related field with 5+ years of post-doctoral experience (at least 3 within the pharmaceutical industry) related to translational pharmacology in either cardiovascular, inflammation, or respiratory diseases, with a preference for cardiovascular experience. Record of hands-on technical achievement, commitment to the ongoing identification and sharing of best practices, demonstrated organizational effectiveness, and proven mentoring skills are essential.

We offer competitive compensation, full benefits and talented professional colleagues...some of the best and brightest in the industry. To find out more about this position and submit your resume, visit our website at: **www.pfizer.com/careers** and search by **Req # 53529.**

Pfizer is proud to be an Equal Opportunity Employer and welcomes applications from people with different experiences, backgrounds and ethnicities.

PGRD
Pfizer Global Research & Development

Our work is someone's hope. Join us.

MERCK RESEARCH LABORATORIES
www.MRLpeople.com

At Merck Research Laboratories, we know that there are many rewards inherent in your work, but it's patients that come first. That's why we've devoted decades to the drug discovery process—bringing novel medicines and vaccines in over 20 therapeutic categories to market, and beyond that, making medicines and unbiased health information accessible to everyone.

Working in one of our laboratories, you'll be part of a multidisciplinary project team whose ideas and commitment to science will lead to the selection and optimization of promising compounds. So that someday, diseases such as Cancer, Alzheimer's disease and other health crises like HIV/AIDS might be history. Besides bringing hope to millions the world over, you can infuse your own life and career with new enthusiasm.

Thanks to Merck's renowned training and mentorship programs, innovative approaches to work-life balance and other benefits, you'll be able to devote yourself to all the people who are counting on you.

To learn more about our Scientists and endeavors, or apply on line, please visit www.MRLpeople.com.

Where patients come first MERCK

Merck is an equal opportunity employer—proudly embracing diversity in all of its manifestations. ©2006 Merck & Co., Inc. All rights reserved. Merck and the Merck logotype are registered trademarks of Merck & Co., Inc.

Fulfill your hunger to improve life.

For AB's 25th Year Anniversary, we recognize the values and culture that have allowed us to succeed and grow as a company.

We believe in the power of science to improve the human condition.

Our first responsibility is our customers who use our products to improve the quality of life.

Most importantly, we value our people, our greatest strength.

Applied Biosystems is a leading contributor to life sciences research and development. It has an active intramural research program and a vibrant scientific and engineering community. AB is expanding its postdoctoral fellowship program providing unique opportunities to participate in and contribute to an exciting range of basic and applied research projects. The postdoctoral fellowship program will offer candidates the chance to gain skills that would be difficult to acquire in other environments while at the same time encouraging them to present their work at open scientific meetings and publish in peer-reviewed journals. Competitive salary and benefits will be offered.

Currently, postdoctoral fellow positions are available in the following areas:

- Protein Engineering
- Algorithm Development/Applied Mathematics
- Molecular Biology
- Organic Chemistry

For more information about these opportunities, please visit our website at www.appliedbiosystems.com

Applied Biosystems is an equal opportunity employer.

25 YEARS ADVANCING SCIENCE

AB Applied Biosystems

Career matters.
Life matters.
Health matters.

At the heart of all that matters are people, connected in purpose by career, life, and health. Throughout the world and here at home, sanofi-aventis fights for what is essential to us all – health. Now the world's third-largest pharmaceutical company, we have a superior product portfolio and one of the industry's richest pipelines that will set the course for improving the health of millions worldwide.

Your expertise in your field and your passion to grow professionally will ensure we continue to improve the health of millions…because health matters. We offer a variety of career opportunities in the following areas:

Science & Medical Affairs (R&D)
Pharmacovigilence
Quality & Compliance
Regulatory Affairs

Opportunities are also available in the areas of Finance, Information Technology, Sales & Marketing, and Administration.

Driven by a pioneering spirit, a strong set of core values and a mosaic of talent worldwide, we strive for success – in health. In doing so, we strengthen careers and enrich lives. Discover your future with sanofi-aventis. Apply online today.

www.careers.sanofi-aventis.us

Sanofi-aventis is an **equal opportunity employer** that embraces diversity to foster positive, innovative thinking that will benefit people worldwide. Sanofi-aventis is also committed to employing qualified individuals with disabilities and, where warranted, will provide reasonable accommodation to applicants, as well as its employees.

sanofi aventis
Because health matters

Scientist/Senior Scientist High Content Screening

The High Throughput Drug Screening Facility (HTDSF) uses a combination of robotics, computational tools and small molecule libraries to study biological pathways and to discover novel probes which potentially could be developed as therapies for cancer, infectious diseases, immunology and virology. The Facility develops, validates and performs both chemical (ChemScan) and genomewide (GeneScan) screening on biological assays submitted by the MSKCC investigators.

We are seeking a highly-motivated, multi-discipline trained scientist to join our group to implement all aspects of cell based assay development and screening. This position requires expert knowledge of cell biology and will work closely with MSKCC investigators to develop and validate cell-based assays for high-throughput screening of small molecules and/or siRNAs. The candidate should have experience in signal transduction, phenotypic screens, and/or functional genomics. This position offers a unique opportunity for a talented scientist to work in a dynamic and innovative environment at the heart of basic research and drug discovery and development.

A minimum of 2-4 years of biotech/pharmaceutical experience with an emphasis in cell based assay development and high content screening (we will also consider academics with a strong performance record in similar scientific disciplines). Solid background in the development, troubleshooting of cell-based assays, automated imaging and screening data acquisition and analysis is highly desirable. Candidates should have excellent communication skills, computer skills, meticulous lab technique and recording of findings and must be able to work in a highly collaborative manner.

Interested candidates should send their CV and three letters of references to **djaballh@mskcc.org** EOE/AA.

Memorial Sloan-Kettering Cancer Center
The Best Cancer Care. Anywhere.
www.mskcc.org

Drexel UNIVERSITY

Department Head
Department of Bioscience and Biotechnology
College of Arts and Sciences
Drexel University
Philadelphia, PA

The Department of Bioscience and Biotechnology in Drexel University's College of Arts and Sciences is seeking an outstanding Department Head committed to a balance between research and education at undergraduate and graduate levels.

The successful candidate for this senior position (professor with tenure) will have a proven track record in extramurally funded research in an area of biological sciences as well as experience in managing personnel and budgets. Demonstrated capability for active collaborations on an interdepartmental level and/or with industry and government are major advantages, as is experience in faculty governance. Drexel University is moving toward the first tier of research universities nationwide. The successful candidate is expected to energetically advance the Department as a leader in life sciences.

Applicants are requested to submit a full CV, statements of research and educational interests, and the contact information for at least five references to the **Dean's Office College of Arts and Sciences, Attention: Bioscience Head Search Committee, Drexel University, 4020 MacAlister Hall, 33rd and Chestnut Streets, Philadelphia, PA 19104, Tel: (215) 895-2620**.

The review of the applications will begin **July 5, 2006**, and continue until the position is filled. Details on the department can be found at **www.drexel.edu/bioscience**.

Drexel University is an Equal Opportunity Employer.

POSITIONS OPEN

Assistant/Associate Professor
Molecular Imaging

The Division of Molecular Pharmaceutics, School of Pharmacy, and the Biomedical Research Imaging Center, University of North Carolina at Chapel Hill, are seeking to fill a full time, tenure-track position at the rank of Assistant/Associate Professor. Successful candidates must possess a Ph.D. degree, or equivalent, and appropriate postdoctoral experience in the broad area of molecular imaging. Research using nanotechnology and related sciences is welcome. The person is expected to participate in teaching at both professional and graduate levels in the School of Pharmacy and to establish an outstanding research program that is fundable or already funded by NIH. Please visit the school's website **www.pharmacy.unc.edu** and the website of BRIC: **http://bric.unc.edu**.

Applications including a CV, statement of research interest, and the names and contact information of four references should be submitted to:

Ms. Angela Lyght
Administrative Division Manager
Division of Molecular Pharmaceutics
School of Pharmacy
2316 Kerr Hall, CB# 7360
University of North Carolina
Chapel Hill, NC 27599-7360
or
by email to: **angela_lyght@unc.edu**

The University of North Carolina is an Equal Opportunity/Affirmative Action Employer. Women and members of minority groups are encouraged to apply.

CAREERS IN BIOTECH AND PHARMA

UNIVERSITY of TORONTO

Faculty Positions
Department of Pharmacology

We are accepting applications for two tenure-track faculty positions at the level of Assistant Professor in the Department of Pharmacology at the University of Toronto. We seek outstanding individuals with the potential to develop independently funded research programs as well as to contribute significantly to undergraduate, graduate and professional education in pharmacology. Our goal is to recruit academic scientists with interests and expertise that align with one or more of the Department's central research and education themes, which include neuropharmacology, molecular toxicology, drug metabolism, pharmacogenetics, receptor pharmacology and cellular signaling. The ideal candidate will hold a Ph.D. degree or its equivalent in pharmacology, have significant post-doctoral experience, and demonstrate an emerging record of research achievement with evidence of superior future research potential.

The University of Toronto and its affiliated teaching hospitals and research institutes make up one of the world's largest and most productive biomedical research environments, ranking first among North American public research universities in the number of research publications by its health scientists. Many opportunities for collaboration and interdisciplinary research are available. The city of Toronto is also a vibrant, inviting, safe and multicultural environment in which to live and work.

Interested applicants should forward **electronic** versions – as Microsoft Word or PDF files – of (1) a covering letter of application; (2) a Curriculum Vitae; (3) an overview of current and future research interests; (4) a summary of teaching experience and philosophy; and (5) the names and contact information of at least three referees to: **The Chair, Search Committee, Department of Pharmacology, University of Toronto, at pclsearch@utoronto.ca**. Evaluation of applications will commence on **August 15, 2006**, and applications will be considered until the positions are filled.

The University of Toronto is strongly committed to diversity within its community. The University especially welcomes applications from visible minority group members, women, Aboriginal persons, persons with disabilities, and others who may contribute to further diversification of ideas. All candidates are encouraged to apply; however, Canadians and permanent residents will be given priority.

POSITIONS OPEN

School of Biological Sciences
College of Natural Sciences
Seoul National University

Faculty Position: Developmental Biology

The School of Biological Sciences, Seoul National University, Seoul, Korea, is seeking candidates for a tenure-track faculty position in Developmental Biology. The candidate should have a Ph.D. degree and at least 2 years of post-doc experience. We are particularly interested in the areas of vertebrate developmental biology, but researchers of high quality in other developmental biology areas will be considered as well. Successful candidates will be directly contacted by the Pre-screening Committee shortly after the deadline. Applicants should submit a curriculum vitae and a short description of their research plans (1-2 pages) to:

Faculty Pre-screening Committee
School of Biological Sciences
Seoul National University
56-1 Shillim-dong, Gwanak-gu
Seoul, Korea 151-742

Or via email:
kangsaou@plaza.snu.ac.kr
Application deadline: July 23, 2006

CAREERS IN BIOTECH AND PHARMA

Shanghai Genomics, Inc.

Shanghai Genomics, a GNI Ltd. subsidiary, is a fast-growing global biopharmaceutical company. Located in the dynamic Zhangjiang Hi-Tech Park, Shanghai, China. To further our current research programs of inflammation and cancer, we are looking for enthusiastic individuals to join our growing team. All positions require relocation to Shanghai, China. Speaking Mandarin Chinese is not necessary.

Director/Vice President – Business Development/Marketing
Responsibilities include leading the company's business development effort to expand collaborative research with international partners, screening license-in opportunity, and supervising the marketing program of biomaterials in China. Ideal candidates should have excellent communication skills in English and deep understanding of the uniqueness of Chinese market. A Ph.D./M.S. in life sciences plus many years of related industry experience is required. A M.B.A. Degree is preferred but not required.

Director/Project Leader - Cell and Molecular Biology/Protein Chemistry
Responsibilities include supervising a group of research associates and participating in the overall research plan design and frequent communication with corporate partners. Must have strong problem-solving skills and excellent communication and organizational capability. A Ph.D. and 2-5 years of postdoctoral experience are required. Experience in biochemical kinase assays, cell cycle/apoptosis assays, siRNA assays, and/or recombinant protein expression and purification is highly preferred.

Director - Animal Model Studies
Responsibilities include establishment of cancer and inflammation models in house. A Ph.D. and 2-5 years of postdoctoral experience are required. Must be able to work independently and to train and supervise junior level research associates.

We provide a stimulating working environment, a high level of professional and intellectual challenge, and a very competitive compensation package including stock options. Interested individuals may apply by specifying their job of interest and sending their resumes by e-mail to **bd@shanghaigenomics.com**. For additional information, please go to ***www.shanghaigenomics.com***. Address: 647 Song Tao Road, Building #1, Zhangjiang Hi-Tech Park, Pudong New Area, Shanghai 201203, P. R. China. Tel: 86-21-50802786, Fax: 86-21-50802783.

ScienceCareers.org

CAREERS IN BIOTECH AND PHARMA

LEAD SCIENTIST-
Inorganic

Molecular FOUNDRY
A USER FACILITY FOR NANOSTRUCTURED MATERIALS
MATERIALS SCIENCES DIVISION · LAWRENCE BERKELEY NATIONAL LABORATORY

The Molecular Foundry at Lawrence Berkeley National Laboratory is a national user facility for the design, synthesis, and characterization of materials with nanometer dimensions. One of five such Nanoscale Science Research centers recently established by the U.S. Department of Energy, its charter defines two primary missions: a) conduct outstanding research across the breadth of nanoscience, and b) collaborate with scientists from around the world who visit to use its state-of-the-art instruments and techniques and to take advantage of the expertise of its staff to further their own nanoscience research efforts. [See http://foundry.lbl.gov/]. It houses six facilities: Inorganic Nanostructures; Organic and Macromolecular Synthesis; Nanofabrication; Biological Nanostructures; Theory of Nanostructured Materials; and Imaging and Manipulation of Nanostructures.

Reporting to and working with the Inorganic Nanostructures Facility Director, the Lead Scientist will establish and direct the overall scientific program and long-term strategic plan for the Facility. He/she will personally lead an innovative program of research in the area of the development of novel materials with nanoscale architectures, the development of new nanoscale devices, and the application of nanomaterials and technologies to energy related systems. He/she will also be responsible for the management and operation of the Inorganic Facility. This involves collaborating with users on approved projects, supervision of the approximately six scientific and technical staff of the Facility and their research activities, and the oversight of the user program, maintaining the high level of user research projects undertaken. It also involves responsibility for budget, personnel, reporting, safety, equipment maintenance matters, as well as the technical coordination of the Facility's user program, including assignment of staff to projects and assuring that they are completed. The lead scientist is also expected to maintain the Facility at the forefront of nanoscience by upgrading instrumentation techniques and training staff.

The candidate must have a Ph.D. in Physics, Chemistry, Materials Science, or a related field, with postdoctoral research and/or user facility experience. Ability to conduct creative, independent research and to recommend process improvements will be essential, in conjunction with excellent analytical and interpersonal skills. He/she must have demonstrated ability to lead a team of professional scientists and to interact effectively with a broad range of colleagues. Experience in nanocrystal and nanowire manipulations and analysis, chemical synthesis, and nanoscience is also important. An established record of productive and creative research demonstrated by publications in peer-reviewed journals is required.

Visit **http://foundry.lbl.gov** for a link to the full job description (# 018873) and application procedures. Applicants are requested to submit a CV with a list of publications, a summary of research interests in proposal format, and a list of at least five references, attached as one document.

LBNL is an AA/EEO employer committed to developing a safe and diverse workforce.
www.lbl.gov

Bergen Center for Computational Science
COMPUTATIONAL BIOLOGY UNIT

GROUP LEADER BIOINFORMATICS

University of Bergen

The Computational Biology Unit (CBU) at the University of Bergen, Norway, is seeking a competent bioinformatics scientist to lead a new research group. The bioinformatics environment in Bergen currently consists of seven research groups and about 40 staff and students. Salary and professional resources are internationally competitive.

For more information about the position and about CBU, please refer to **http://www.cbu.uib.no/jobs**, or contact the head of CBU, professor Inge Jonassen (**Inge.Jonassen@bccs.uib.no**). Evaluation of applications commences immediately and continues until a successful candidate has been identified.

PhD STUDENT/POST-DOC POSITIONS available. Deadline of application **August 15th, 2006**.

See: **http://www.cbu.uib.no/jobs/**

CAREERS IN BIOTECH AND PHARMA

THE ULTIMATE SYMBIOTIC RELATIONSHIP.

Focusing on a common goal. Performing your job accurately so that the next person can do theirs. That's how we work together at ICON Clinical Research. Because at ICON, your personal best is the valuable link we need to achieve quality results.

Working with ICON, you'll share in a unique culture of a large company that emphasizes a warm, friendly environment. This is where career possibilities can become realities... where those who look for challenges, embrace the learning and growth opportunities we offer.

ICON Clinical Research is dedicated to providing the pharmaceutical and biotechnology industries with exceptional clinical research and biometrics services, and we're the first international CRO awarded ISO 9001:2000 quality certification across all divisions and functions.

To continue our legacy of excellence at ICON, GloboMax, a dynamic and innovative Product Development Organization committed to helping pharmaceutical and biotech companies bring products through development from early stage to regulatory approval, is now the Strategic Pharmaceutical Development Division of ICON.

- **Clinical Research Associates** - all levels, all locations. Experience required.
- **Clinical Project Managers** - all locations. Experienced required.
- **Clinical Studies Associates** - Wilmington, DE and Nashville, TN
- **Associate Director/Director Medical Affairs (Oncology experience)** - Philadelphia, PA

Come to ICON and you'll enjoy highly competitive benefits in addition to flexible scheduling, relocation assistance, tuition reimbursement, credit union, health club privileges, and many other exceptional advantages.

To apply, or for more information on our opportunities, please visit us at www.iconclinical.com and CLICK ON EMPLOYMENT OPPORTUNITIES. No agencies, please.

ICON Clinical Research is an Equal Opportunity Employer committed to strength in diversity.

ICON
www.iconclinical.com

ICON. we are the right solution.

CHAIRPERSON
DEPARTMENT OF PSYCHOLOGY
UNIVERSITY OF MARYLAND, COLLEGE PARK

The University of Maryland, College Park is the flagship campus of the University System of Maryland. The Psychology Department has undergone dramatic change in recent years. With the full support of the College of Behavioral and Social Sciences and the University administration, it is becoming one of the very best graduate departments of psychology in the country. The administration and the faculty are committed to the department's continued growth and development. Numerous well-funded research programs comprise the scientific core of the Department, with research that spans neural, functional and social levels of analysis, and is at the forefront of both basic science and real-world implementation. You can learn more about the department by visiting **www.psychology.umd.edu**.

The new chair must have an international research reputation in Psychology; as well as demonstrated success in campus leadership, external funding, communications, budgeting and human resource management, and have a record of substantial academic leadership. This appointment is to be made at the full professor level.

Applications should include a curriculum vitae, statement succinctly describing one's experience as related to this position and one's vision for a psychology department at a major research university, and the names and contact information of three references. Applications and inquiries will be kept confidential. Please send all materials by mail to: **Professor Charles Wellford, Chair Search Committee for Psychology Chairperson, 2220 Lefrak Hall, University of Maryland, College Park, MD. 20742**. Review of applications has begun and will continue until the position is filled. For best consideration applications should be received no later than **October 15, 2006**.

The University of Maryland is an Equal Opportunity Affirmative Action Employer with a commitment to racial, cultural, and gender diversity. Women and minorities are encouraged to apply.

UNIVERSITY OF MARYLAND

Industrial Technology Research Institute
Biomedical Engineering Research Laboratories

Innovative Technologies for a Better Future

Biomedical Engineering Research Laboratories (BEL) of Industrial Technology Research Institute(ITRI), the leading biomedical engineering R&D institute in Taiwan, have created exceptional career opportunities for motivated research scientists, and technology and business managers. Positions are open on:

- **Division Director/Program Leader-Orthopedics**

  Ph.D. with technical background and at least 10 years R&D experience in biomaterial & medical device products development. Good communication skill, with strong leadership. Familiar with medical devices related products market.

- **Deputy Division Director**

  Ph.D. with at least 8 years of working experiences in Pharmacology, Biostatistics, Clinical research or related fields, with the global vision and enthusiasm in Biotech development and commercialization and preferably 3 years of managerial experiences preferred.

- **Technical Managers and Project Leaders**

  Ph.D. with at least 5 years of working experiences in one of following fields:
  - Genomics, Proteomics, Biostatistics, and Bioinformatics
  - Drug Lead Optimization and Peptidominetics
  - Pharmacology, Pharmacognosy, and Pharmacokinetics
  - Stem Cell and Biomaterial

- **Business Managers**

  Technical of business background with experience in technical marketing/sales business development or consulting in biotech, pharmaceutical or medical device industries.

ITRI is located in Hsinchu, 45 miles south of Taipei. The Laboratories has 320 research scientists & engineers including about 70 Ph.D.'s and 160 MS's. Adjacent to National Tsing Hua University, National Chiao Tung University and Science-Based Industrial Park, the institute offers an excellent R&D environment and fast growing opportunities for technology innovation and commercialization.

Please indicate the position you are applying for and send your resume to:
E-mail :GraceLai@ itri.org.tw
Tel: 886 3 591-2129
Fax:886 3 591-0098

http://www.itri.org.tw/eng/careers/index.jsp

Medical College of Georgia Cancer Center

Associate/Full Professor Basic and Translational Cancer Research

Medical College of Georgia Cancer Center (MCGCC), a new, state-of-the-art, 167,000 sq ft research facility, invites applications from distinguished investigators and/or physician scientists to lead cancer related basic and/or translational research. Candidates are expected to contribute to and enhance MCGCC's multi-disciplinary programs in basic and translational research in the areas of Cancer Molecular Signaling and Therapeutics, Molecular Immunology, Cancer Genetics and Epigenetics. Applicants should have an MD, MD/PhD, PhD or equivalent degree and an active extramurally supported research program. Candidates are also expected to contribute to graduate and medical education.

MCG offers attractive salary and generous start-up and support packages. Rank and salary are commensurate with experience and prior accomplishments. State-of-the-art microarray, proteomics, genomics, flowcytometry and microscopy are also available as supportive core facilities. The clinical research efforts of the physician scientist will also be supported by clinical research core facilities and nurse/coordinators.

Applicants should submit a letter of interest, curriculum vitae and three references to: **Kapil Bhalla, M.D., c/o Joel Covar, Medical College of Georgia, Department of Operations, AA155, Augusta, GA 30912; Email: jcovar@mail.mcg.edu.**

The Medical College of Georgia is the health sciences campus of the University System of Georgia. It is located in the historic city of Augusta, Georgia with excellent recreational and lifestyle opportunities.

The Medical College of Georgia is an Equal Opportunity and Equal Access Institution. Applications from women and members of under-represented minority groups encouraged.

AA/EEO/Equal Access/ADA Employer.

COLUMBIA UNIVERSITY
IN THE CITY OF NEW YORK

Tenure-Track Faculty in Developmental Neuroscience

The Columbia University Center for Neuroscience Initiatives, in conjunction with the Department of Psychiatry at Columbia and the Department of Developmental Psychobiology at the New York State Psychiatric Institute, is seeking applications for a new tenure-track faculty position in the area of Developmental Neuroscience. Candidates must have an M.D., Ph.D., or equivalent degree. The appointment is open to individuals at the level of Assistant or Associate Professor.

Applicants should have a demonstrated ability to conduct innovative, basic research that has the potential to contribute to translational investigations. Expertise in a broad range of neuroscience methodologies is highly desirable. These can include, but are not limited to, molecular neurobiology, neurogenetics, neuroanatomy, neuropharmacology, and electrophysiology. Areas of particular interest include developmental studies of neural circuits that underlie higher-level brain functions, including the regulation of emotional and/or cognitive states. Interest in genetic and environmental determinants of plasticity in neural systems will also be a useful area of emphasis.

Applicants should send their CV, a statement of research interests, and names of three referees to:

Bradley S. Peterson, M.D.
Columbia University Department of Psychiatry
1051 Riverside Drive, Unit 74, Room 2301
New York, NY 10032

E-mail: PetersoB@childpsych.columbia.edu

Columbia University takes affirmative action to ensure equal employment opportunity.

ScienceCareers.org

Positions @ NIH

The National Institutes of Health

Cell Adhesion and Signal Transduction in Tumor Cell Metastasis

Kenneth Olden, Ph.D. and John D. Roberts, Ph.D.
roberts1@niehs.nih.gov
(919)541-5023, Fax:(919)541-0176
Laboratory of Molecular Carcinogenesis

Intramural Research Training Award (IRTA) post-doctoral position, in the Metastasis Section, Laboratory of Molecular Carcinogenesis, National Institute of Environmental Health Sciences (NIEHS), Research Triangle Park, North Carolina, is available to study signaling pathways and mechanisms of cell adhesion and invasion in human tumor cells. A Ph.D. with a strong background in molecular biology and/or signal transduction is required. Ongoing research emphasizes: 1) protein kinase C, MAP kinase and G protein signaling pathways induced by fatty acids in tumor cells, 2) mechanisms of tumor cell adhesion, migration, and invasion in vitro and in vivo, and 3) modulation of gene expression in metastatic tumor cells by environmental agents. Applicants must have less than five years of postdoctoral experience to qualify for this appointment.

TO APPLY: Mail, fax or e-mail cover letter, curriculum vitae, and the names of three people who could provide letters of references to:

John D. Roberts, Ph.D., Metastasis Section, Laboratory of Molecular Carcinogenesis, NIEHS, P.O. Box 12233, Mail drop D2-05, Research Triangle Park, NC 27709

Intramural Fellow Position in Molecular Regulation of the Cytochrome P450s

The Laboratory of Pharmacology and Chemistry of the National Institutes of Health is recruiting a postdoctoral position in the Human Metabolism Group headed by Dr. Joyce Goldstein. Current projects include transcriptional regulation of the human and murine CYP2C genes by drugs, oxidative stress and physiological changes via multiple nuclear receptors and transcription factors such as PXR, CAR, HNF4, and coregulators.

Minimum qualifications include a doctoral degree and experience in molecular biology and biochemistry emphasizing molecular techniques such as experience in construction and use of luciferase-promoter constructs, gel shift assays, cell culture, expression vectors for nuclear receptors and use of plasmid vectors. Familiarity with cytochrome P450 regulation and experience in identification of nuclear regulators (GST pulldown, ChIP assays) would be helpful. Applicants must have less than five years of postdoctoral experience to qualify for this appointment.

For additional information contact Dr. Joyce Goldstein at 919-541-4495 or goldste1@niehs.nih.gov. For additional information concerning the group projects visit the information on the Human Metabolism group at the following website http://dir.niehs.nih.gov/dirlpc. To apply submit curriculum vitae, bibliography, references (with telephone numbers) preferably via email or mail to:

Dr. Joyce Goldstein, National Institutes of Health, National Institute of Environmental Health Sciences, PO Box 12233, Maildrop A3-02, Research Triangle Park, NC 27709, E-mail: goldste1@niehs.nih.gov

For students, recent graduates, and postdoctoral, research, and clinical fellows.
Your on-line guide to training with the best at the world's largest biomedical research institution.
In Bethesda, Maryland, and at other NIH laboratories.

Office of Intramural Training and Education
Bethesda, Maryland
20892
800.445.8283

opportunity *clicks*

www.training.nih.gov

Department of Health and Human Services
National Institutes of Health
National Heart, Lung, and Blood Institute

NHLBI-Cardiology Branch Postdoctoral Fellowship

The National Heart, Lung, and Blood Institute (NHLBI), Division of Intramural Research seeks to hire a Postdoctoral Fellow to train in the Molecular Biology Section. Research includes examining the molecular mechanisms of mitochondrial function and inflammation in the cardiovascular system. Research topics may also have significant overlap with cancer cell metabolism. Examples of our work include the following references: *Science*, in this issue; *Proc Natl Acad Sci. USA*, 102(9):3423-3428; *Nature Medicine* 7:1111-1117.

The postdoctoral position requires a Ph.D. and/or M.D degree. Qualified applicants should have experience in molecular biology and a history of prior publications in peer reviewed journals. The successful candidate will be offered stipend support commensurate with experience. Please submit a *curriculum vitae*, a statement of future research interests and career goals, along with the names and telephone numbers, postal and e-mail addresses of three references to:

Paul M. Hwang, M.D., Ph.D., Investigator, NHLBI-NIH, 10 Center Drive, MSC 1454, Bldg 10-CRC, 5 East Rm 5-5330, Bethesda, MD 20892-1670, Email: hwangp@mail.nih.gov

WWW.NIH.GOV

National Institutes of Health

Virtual Career Center

at the tip of your mouse

www.training.nih.gov/careers

-EXPLORE CAREER OPTIONS
-CONTINUE YOUR EDUCATION
-SEARCH FOR A JOB

Careers in science, medicine, and beyond at the college, postbaccalaureate, graduate, and postdoctoral levels

Office of Intramural Training and Education
(800) 445-8283

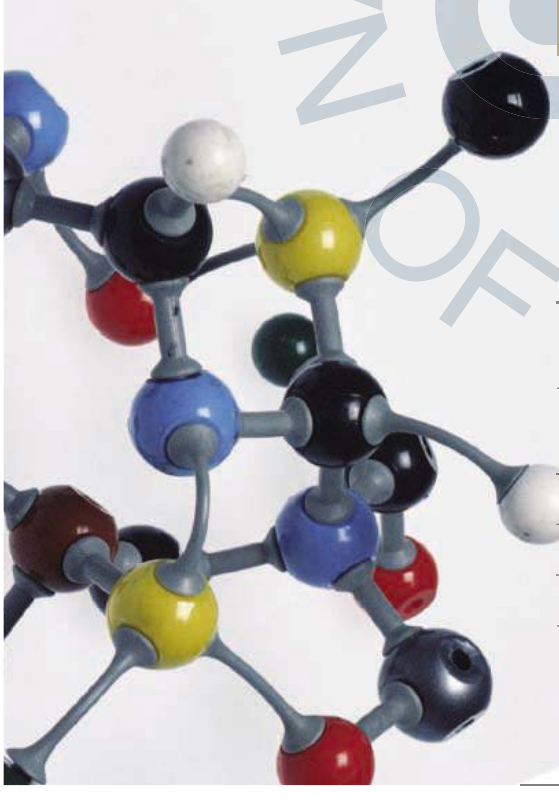

Postdoctoral Research Training at NIH

- Launch a career to improve human health
- Work in one of 1250 of the most innovative and well-equipped biomedical research laboratories in the world
- Explore new options in interdisciplinary and bench-to-bedside research
- Develop the professional skills essential for success
- Earn an excellent stipend and benefits
- Click on www.training.nih.gov

Office of Intramural Training and Education

Science AAAS

Director
Science & Human Rights Program
American Association for the Advancement of Science

Successful candidate will be responsible for directing the Science & Human Rights (SHR) program, an internationally known program that defends the rights of scientists throughout the world and applies scientific knowledge and methods to the promotion and protection of the human rights of all people.

The SHR Program Director is also responsible for developing funding prospects and overseeing grant process including researching and establishing contact, preparing proposals, and allocating and tracking budgets for reporting to funders, and evaluating effectiveness; overseeing and mentoring staff including determining staffing needs, supervising staff, delegating and assigning work, monitoring work progress; conducting performance reviews and recommending changes; monitoring trends, developments, and major issues in science and human rights; managing budget and overseeing financials for SHR; organizing meetings, conferences and symposia, participating in panels, writing articles, and conducting community outreach activities to share information, foster cooperation, and develop and implement mutual programmatic interests; representing and serving as a liaison with both the human rights and scientific communities; acting as a spokesperson on human rights issues; writing project reports, program descriptions and correspondence related to ongoing projects; performing other work related duties as assigned.

Qualifications: Position requires an advanced university or college training leading to a Master's degree (Ph.D preferred) in a field related to science and/or human rights; 7-10 years experience in progressively responsible positions in program development and management; 3-4 years experience supervising others; in-depth knowledge of human rights and the nexus between science and human rights; a collaborative working style; excellent written and oral communication skills; proven track record in fundraising, including experience in working with foundations and charitable organizations; experience working in a nonprofit organization and working with NGO's, intergovernmental organizations and government agencies would be helpful; grant proposal development and financial and personnel management experience is required; computer skills (Microsoft Office, e-mail, Internet) are required.

AAAS, located in downtown Washington, DC, is the world's largest general scientific organization and publisher of the journal *Science*. It offers a competitive salary, an excellent benefits package, and a congenial working environment. For additional information, please see the SHR web site (**http://shr.aaas.org**) and the Science & Policy Programs web site (**http://www.aaas.org/spp**). Please send a resume along with cover letter and salary requirements to: **AAAS, 1200 New York Ave., NW, Suite 100, Washington DC, 20005**, **Attn: Program Director (Requisition #1451); Fax (202) 682-1630 or email to jobs@aaas.org**.

EOE. Non-smoking environment.

NSU NOVA SOUTHEASTERN UNIVERSITY
Beyond the Classroom

ASSISTANT/ASSOCIATE PROFESSOR, OCEANOGRAPHY

The NSU Oceanographic Center (OC) invites application for a 12 month faculty position at the Assistant/Associate Professor level. Candidates must have a doctoral degree and experience (postdoctoral research is desirable). Teaching responsibilities will be undergraduate general microbiology (typically 1 course with 2 lecture sections and associated labs) and one graduate course in the individual's specialty for 75% of annual salary. Extramurally funded research is expected. Research expertise should be within the broad area of marine prokaryotic or eukaryotic microbiology. Salary is commensurate with experience. Please apply online to position **#997182: www.nsu-jobs.com**. Position could begin as early as January 07. NSU offers a comprehensive benefits package including, medical and dental.

Visit our website: **www.nova.edu**.

Nova Southeastern University is an Equal Opportunity/Affirmative Action Employer.

University of BRISTOL

Chair in Statistics
Professorial Grade Salary

The University of Bristol seeks to appoint an outstanding statistical scientist to a new Chair in its Statistics Group. This top-rated group recently won major strategic funding through an EPSRC Science and Innovation award, which will support four new lectureships and eight postdoc positions, and a wide range of research and research training activities. The new Chair will play a major role in leading and developing this initiative, which will focus on innovative theory and methodology, equipping the discipline to meet the challenges of future applications. The successful candidate must demonstrate an excellent record of research achievement and a talent for insightful academic leadership.

For informal enquiries please contact Professor P J Green on (0117) 928 7967 or e-mail p.j.green@bristol.ac.uk

Further details and an application form can be found at www.bristol.ac.uk/vacancies Alternatively you can telephone (0117) 954 6947 or e-mail recruitment@bristol.ac.uk (stating postal address ONLY), quoting reference number 12245.

The closing date for applications is 9.00am, 31st July 2006.

www.bristol.ac.uk

You got the offer you always dreamed of.

Now what?

www.sciencecareers.org

ScienceCareers.org
We know science AAAS

VCU Medical Center
Virginia Commonwealth University

MOLECULAR IMMUNOLOGY

Virginia Commonwealth University's School of Medicine seeks a prominent molecular immunologist to join our faculty in the tenure track as part of a strong programmatic and multidisciplinary expansion of basic biomedical research. Candidates should be at the Associate or Professor level, possess an M.D. and/or Ph.D. degree, and be nationally recognized for achievements and sustained productivity in molecular immunology as demonstrated by extramural funding and publications. The successful candidate will be expected to continue an independent, extramurally funded research program addressing important problems that relate to human immunologic disorders. Current areas of strength at VCU include asthma and hypersensitivity diseases (Departments of Microbiology and Immunology, Internal Medicine and Biology), tumor immunology (Massey Cancer Center and the Departments of Microbiology and Immunology and Surgery) and cell activation and signal transduction (Department of Biochemistry). Substantial resources and endowments are available to support this position. Salary and rank will be based on the applicant's experience.

Interested candidates should send their curriculum vitae, letter of interest indicating their current and future research goals, and names and email addresses of three references to: **Dr. Lawrence Schwartz, Chair, Division of Rheumatology, Allergy, and Immunology, Virginia Commonwealth University, Box 980263, Richmond, VA 23298-0263. E-mail: lbschwar@vcu.edu.**

VCU is an Equal Opportunity/Affirmative Action Employer. Women, minorities, and persons with disabilities are encouraged to apply.

VIB, the Flanders Interuniversity Institute for Biotechnology, is an entrepreneurial research institute, where 900 scientists and technicians in 60 research groups conduct spearhead research in a wide range of life sciences domains. VIB holds long-term perspectives in research and technology transfer of new findings by means of patents and licenses and the creation of new start-up companies.

The VIB Department of ***Molecular and Developmental Genetics,*** *K.U.Leuven is currently looking for a*

Biochemist (m/f)

with expertise in enzymology for our program on gamma-Secretase. This enzyme complex is responsible for the intramembranous cleavage of a range of Type 1 transmembrane proteins. Gamma-Secretase is a pivotal enzyme in several signaling pathways, but is also responsible for the release of the amyloid peptide in Alzheimer's disease and therefore constitutes an important drug target.

References: Nat. 391, 387-390 (1998); Nat. 398, 518-522 (1999); Neuron38, 9-12, (2003); PNAS 102, 1719-1724 (2005).

You will be working in the laboratory of Bart De Strooper, a challenging and interesting environment with the possibility to perform cutting edge research in a multidisciplinary team at the interface of academia and industry. Experience with enzymatic (kinetic) studies, creativity and ambition is required.

We offer a 2 year contract (renewable) and a competitive postdoctoral salary. Start date: as soon as possible.

If you are interested in this position please send your curriculum vitae including references to ***marie-anne.everaerts@med.kuleuven.be.***

For more information please visit http://med.kuleuven.be/cme-mg/LabIntro/BartDeStrooper_en.html.

FELLOWSHIPS

MAX PLANCK INSTITUTE
FOR CHEMICAL ECOLOGY

At the **Department of Evolutionary Neuroethology** we specialize in investigations of olfactory-driven behavior and its underlying neural substrate in insects. Our interests comprise both insect-plant and insect-insect interactions. Processes, from molecular events and single neuron responses to behavior, are investigated using state-of-the-art molecular, neurophysiological, neuroanatomical and ethological techniques.

In this area we offer

Postdoctoral fellowships

in:
- **The evolution of olfaction in Drosophila**
- **The neurobiological background to host plant choice in moths**
- **Spatial and temporal patterns in insect olfactory coding**
- **Pollination systems and their sensory background**

Candidates should preferably have experience from some of these different fields or equivalent skills. The duration of the stipends is two years with a possible extension for another year. Applications should contain a brief CV and a description of previous research experience. In addition, the names of two referees should be provided.

Application deadline is July 15, 2006. Further information can be obtained from:

Prof. Dr. Bill S. Hansson
MPI for Chemical Ecology
Department of Evolutionary Neuroethology
Hans-Knoell-Strasse 8
07745 Jena
Germany

Phone: +49 (0) 3641 571400
Fax: +49 (0) 3641 571402
E-mail: hansson@ice.mpg.de

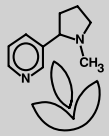

Department of Zoology
UNIVERSITY OF OXFORD

University Lecturership in Zoology in association with Magdalen College

Applications are invited for the above University Lecturership, tenable from 1st October 2006 or as soon as possible thereafter. The Lecturership is associated with a Tutorial Fellowship at Magdalen College. The combined University and College salary will be on a scale up to £47,078 p.a. (under review), and additional College allowances are available.

The University and the College are seeking candidates with a proven record of teaching and research in zoology, and a track record of attracting research funding. The Lecturership will be established at the interface of at least two of the Department's research groupings: behaviour, development, disease, ecology, entomology, evolution, and ornithology.

The appointee will be required to engage in research, which will contribute to the Department's research reputation; to teach, supervise and examine undergraduate and graduate students; and to contribute to administration in the College and Department.

Further particulars are available from http://www.zoo.ox.ac.uk/Current_Vacancies/ http://www.magd.ox.ac.uk/ or from Professor Paul H Harvey FRS, Department of Zoology, South Parks Road, Oxford OX1 3PS, e-mail paul.harvey@zoo.ox.ac.uk to whom applications should be sent for receipt not later than 7th July 2006. Please quote reference number MPS/5/4.

Interviews will be held on a date to be determined.

The University and Magdalen College are Equal Opportunities Employers.

www.ox.ac.uk/jobs

FELLOWSHIPS

UCI
University of California, Irvine

POSTDOCTORAL SCHOLAR FELLOWSHIPS IN STEM CELL BIOLOGY

Stem Cell Research Center

http://stemcell.uci.edu/

UCI's new **Stem Cell Research Center**, directed by Drs. Hans Keirstead and Peter Donovan, has openings for four postdoctoral fellows, to be supported on fellowships funded by the California Institute for Regenerative Medicine. The Program provides training in stem cells, broadly defined, including but not restricted to human embryonic stem cells. Consult the web site for details of the participating faculty and their research interests.

In addition to laboratory training, the program will provide opportunities for formal training in the stem cell curriculum which includes three new courses: Basic Biology of Stem Cells; Clinical Applications of Stem Cells; and Stem Cell Policy and Ethics. Trainees will also have access to intensive short laboratory courses on Human Embryonic Stem Cells, a dedicated workshop on Large-Animal Models, and regular seminars and symposia.

The Stem Cell Research Center includes a Core Facility, equipped entirely through non-federal funds and available for the generation and characterization of new and genetically modified human embryonic stem cells. It also provides related resources including cell culture and cell sorting, fluorescence and confocal imaging, and bioinformatics. Additional research facilities available on campus include multiphoton microscopy, whole-animal bioluminescence imaging, transgenic mouse technology, blastocyst injection, high-throughput molecular biology techniques, and microarray technology. Work with human stem cells is regulated by a campus Stem Cell Oversight Committee.

Excellent salary and benefits are provided. Candidates must contact and be nominated by a proposed mentor from the participating faculty: **http://stemcell.uci.edu/community/researchers.cfm**.

Application materials must include a cv, description of prior research and publications, and letters of recommendation from current and previous research mentors. Appointments are for one year and will be renewed for a second year if recommended by the selection committee. Applications will start being reviewed on **June 30, 2006**. Submit printed applications to:

Dr. Peter J. Bryant
Director, Stem Cell Training Program
Room 4221, Building 503
University of California, Irvine
Irvine, CA 92697

University of California, Irvine is an Equal Opportunity Employer committed to excellence through diversity. It has an active career partner program and an NSF ADVANCE Gender Equity Program.

SCRIPPS INSTITUTION OF OCEANOGRAPHY

THREE RESEARCH SCIENTIST POSITIONS

Scripps Institution of Oceanography (**SIO, http://sio.ucsd.edu/**) invites applications for full time Research positions (9-month academic year appointment) to be funded by extramural research grants and contracts. The appointments may be at the **Assistant, Associate, or Full Research** level with rank and salary depending on qualifications and experience. Associate level appointments receive 25% matching salary support from SIO funds, and Full appointments receive 50% matching salary support for the academic year (subject to availability of institutional funds). Start-up funds and moving expenses may be available.

(1) Oceans and Atmospheres: Candidates with research interests and experience in physical oceanography, meteorology, climate sciences, or closely related fields are invited to apply. Possible research areas include ocean-atmosphere observations and analysis, general circulation modeling, data assimilation, instrumentation for oceanic and atmospheric observations, and geophysical fluid dynamics.

(2) Physical Coastal Oceanography: Candidates with research interests and experience in observational oceanography of inshore waters are invited to apply. Possible research areas include but are not limited to wind-driven flows, mixing, internal waves, coastal and estuarine circulation and sediment transport. Collaborations with chemical and biological oceanographers are encouraged.

(3) Marine Biology/Biological Oceanography: Candidates with research interests and experience in any aspect of marine biology or biological oceanography are invited to apply. Possible research areas include planktonic, pelagic and benthic ecology, systematics, biophysics, and the biochemical, genetic, or physiological bases of adaptations to marine environments.

All candidates will be judged on the basis of research excellence and ability to contribute to the diverse research programs at SIO. Interdisciplinary research is especially encouraged and the search committees will share candidate files when appropriate. Junior candidates should demonstrate outstanding potential to obtain extramural funding for their research; more senior candidates are expected to have a record of such funding. Researchers often obtain lecturer appointments in the SIO Graduate Department and serve as graduate student advisors; participation in SIO/UCSD undergraduate education is also possible.

Interested applicants should send curriculum vitae, statement of research expertise, immigration status, selected reprints, and names and addresses of three suggested referees to:

Chair, Search Committee (Specify position)
c/o Leslie Costi, 0209
Scripps Institution of Oceanography
9500 Gilman Drive
La Jolla, CA 92093-0209

Application review will begin **July 1, 2006** and will continue until position(s) have been filled.

The University of California is an Equal Opportunity and Affirmative Action Employer with a strong institutional commitment to excellence through diversity.

What's your next career move?

Get help from the experts.

www.sciencecareers.org

- Job Postings
- Job Alerts
- Resume/CV Database
- Career Advice from Next Wave
- Career Forum
- Graduate Programs
- Meetings and Announcements

ScienceCareers.org
We know science AAAS

kmc international

ifr

RESEARCH LEADERS

Institute of Food Research, Norwich Research Park, Norwich, UK

World-class research leaders in Systems Biology, Molecular Immunology, Molecular Nutrition, GI Tract Biology are sought to join the premier research organisation in the United Kingdom for the study of the relationship between diet and health, food borne microbial pathogens and food innovation.

- First class post-genomics and other facilities
- Fabulous location with fantastic quality of life alongside international status teaching hospital and university in the Norwich Research Park.

The Institute intends to appoint Research Leaders with outstanding track records of research achievement to build and develop their own research programmes and to enhance existing IFR programmes. In particular, the Institute wishes to build on the synergy between its various activities by developing an integrated programme to understand the gut as a system, using the posts above to help achieve this. Researchers at an earlier stage of their career who can demonstrate strong potential are also welcome to apply.

Consideration would be given to the possibility of a senior researcher to relocate with their existing team.

The Institute would also welcome expressions of interest from scientists with expertise in other areas that are compatible with IFR's science or those whose current research focus is not directly related to IFR's strategic direction, but who wish to redirect their research, including individuals with a clinical background.

The Institute is sponsored by the Biotechnology and Biological Sciences Research Council (BBSRC) and benefits from close collaboration with its sister Institute, the John Innes Centre specialising in plant and microbial science, the University of East Anglia and the Norfolk and Norwich University Hospital.

Further particulars, including instructions on how to apply, may be obtained from: kmc international, Southgate House, 9th Floor West, Wood Street, Cardiff CF10 1EW, by emailing ifr@kmcinternational.com or downloaded from www.kmcinternational.com In all cases please quote reference 992/3.
The closing date for applications is Friday, 18th August 2006.

POSITIVE ABOUT DISABLED PEOPLE

Science Careers Forum

- How can you write a resume that stands out in a crowd?
- What do you need to transition from academia to industry?
- Should you do a postdoc in academia or in industry?

Let a trusted resource like ScienceCareers.org help you answer these questions. ScienceCareers.org has partnered with moderator Dave Jensen and three well-respected advisers who, along with your peers, will field career related questions.

Visit ScienceCareers.org and start an online dialogue.

Bring your career concerns to the table. Dialogue online with professional career counselors and your peers.

ScienceCareers.org
We know science AAAS

ScienceCareers.org

POSITIONS OPEN

FACULTY POSITIONS
Radiology Research

The Department of Radiology at the University of Arkansas for Medical Sciences (UAMS) is inviting applications for three tenure-track faculty positions at the **ASSISTANT, ASSOCIATE,** or **FULL PROFESSOR** rank. The Radiology Department has interests in molecular imaging of cancer and other diseases, nanotechnology-based therapies, gene therapy, radiation biology, ultrasonic biophysics, hyperthermia and thermal ablation, and nuclear medicine. However, exceptional candidates with other research interests that complement those of the current faculty will receive strong consideration.

The Department of Radiology is offering competitive salaries and generous startup funds, in accordance with each candidate's academic experience, publication record, and funding history. Research resources include a CTI MicroPET, a 4.7 T GE MRI, a new cyclotron and nucleosynthesis lab, flow cytometry, an image analysis laboratory, plus research use of clinical imaging instrumentation. Faculty members also have access to: a XENOGEN IVIS-200 optical imaging system, confocal microscopes equipped for fluorescence recovery after photobleaching (FRAP) and fluorescence energy transfer (FRET), genomic and proteomic core facilities, ionizing radiation systems, and more.

Applicants should send curriculum vitae, a summary of their research interests and accomplishments, and the contact information for three references by electronic (in PDF format) or regular mail to: **Michael J. Borrelli, Ph.D., Director of Radiology Research, Department of Radiology, University of Arkansas for Medical Sciences, 4301 West Markham Street, Mail Slot 556, Little Rock, AR 72205 (e-mail: mjborrelli@uams.edu).**

The University of Arkansas for Medical Sciences is an Affirmative Action/Equal Opportunity Employer. Hiring is contingent upon eligibility to work in the United States. Women and minorities are encouraged to apply.

CHAIR, DEPARTMENT OF PHARMACEUTICAL SCIENCES

Midwestern University Chicago College of Pharmacy invites applications for the Chair at the **ASSOCIATE** or **FULL PROFESSOR** level. Requirements: Applicants will have a doctoral degree in the pharmaceutical or biomedical sciences, pharmacology or pharmacodynamics, and a strong commitment to pharmacy education and scholarship. At least five years of academic experience in pharmaceutical education is desirable. Applicants will demonstrate nationally recognized accomplishments in teaching, scholarship, and service. Excellent communication and an ability to think strategically are required. Applicants should send a letter of application, curriculum vitae, the names and contact information of three references, and a brief statement of research and teaching philosophy by electronic or U.S. mail to: **Mary Lee, Pharm.D., BCPS, FCCP, Dean and Professor, Midwestern University Chicago College of Pharmacy, 555 31st Street, Downers Grove, IL 60515, telephone: 630-971-6417, fax: 630-971-6097, e-mail: mleexx@midwestern.edu.** For more information about the Chicago College of Pharmacy, visit our **website: http://www.midwestern.edu/Pages/CCP.html.**

CHIEF MEDICAL OFFICER

Highly intelligent individual with exceptional communication skills sought by prominent Manhattan family to research and coordinate family medical and healthcare issues. Act as liaison with leading medical researchers and consultants in academia and industry, with full responsibility for technical, financial, and administrative functions. Considerable weight given to evidence of unusual academic or other intellectual distinction. Ph.D. or M.D. required, clinical experience a plus but not essential. Possible entrepreneurial opportunities involving delivery of ultrahigh-end medical care to other, similar families. Full-time position. Excellent compensation with significant upside potential and management possibilities. Resume to **e-mail: fmc4@spsfind.com.**

POSITIONS OPEN

University of Michigan Hospitals and Health Centers

TENURE-TRACK FACULTY POSITION
Division of Metabolism, Endocrinology and Diabetes
Department of Internal Medicine
University of Michigan

The Division of Metabolism, Endocrinology and Diabetes, Department of Internal Medicine at the University of Michigan, Ann Arbor, Michigan, seeks applicants for tenure-track **PHYSICIAN SCIENTIST** positions. Candidates should have sufficient experience to establish a cutting-edge, independently funded research program in metabolism, endocrinology or diabetes. All candidates will be evaluated but those applying at the level of Assistant/Associate Professor and Board certified/eligible in endocrinology are preferred.

The Division of Metabolism, Endocrinology and Diabetes currently has 22 primary faculty members with active basic, clinical, and health services research programs in the areas of diabetes, obesity, thyroid, adrenal, pituitary, and neuroendocrine diseases. Candidates with research programs in these or other areas of endocrinology and metabolism are welcome to apply. The Division is home to an NIH-funded Diabetes Research and Training Center and vigorous NIH-funded training programs in basic laboratory and clinical research.

Applicants should forward curriculum vitae and contact information for three references to: **MEND Metabolism, Endocrinology, and Diabetes Search Committee, c/o Dr. Ronald Koenig, University of Michigan, 5560 MSRB-2, 1150 West Medical Center Drive, Ann Arbor, MI 48109-0678.**

The University of Michigan is an Equal Opportunity/Affirmative Action Employer and encourages nominations and applications from women and minority candidates.

POSTDOCTORAL FELLOWSHIPS IN IMMUNOLOGY AND VIROLOGY. Sponsored by the National Institutes of Health Training Grants at the University of Massachusetts Medical School interdepartmental Immunology and Virology Program provides graduate and postdoctoral training in several disciplines, including cellular and molecular immunology, viral immunology, molecular virology and experimental diabetes. For information, see **website: http://www.umassmed.edu/ivp.** *United States citizens or permanent resident* candidates interested in applying for this active, multidisciplinary NIH-supported training program should send curriculum vitae, the names of three references, and a letter stating their research interests and the laboratories in which they would be interested in undertaking training to: **Ms. Janet Zafiris, Department of Pathology, University of Massachusetts Medical Center, 55 Lake Avenue North, Worcester, MA 01655.** *The University of Massachusetts Medical School is an Affirmative Action Employer.*

RESEARCH POSITION
Columbia University
College of Physicians and Surgeons

POSTDOCTORAL or **ASSOCIATE RESEARCH SCIENTIST,** depending upon qualifications, to study the molecular genetics of kidney diseases in humans and animal models. Work will have direct relevance to clinical medicine, particularly to the pathophysiology of renal disease in humans. Requires training in cell or molecular biology at the Ph.D./M.D. level.

Please send curriculum vitae and names of three references to: **Dr. Ali Gharavi, Columbia University, Department of Medicine, Box 84, 630 West 168th Street, New York, NY 10032;** or **e-mail: ag2239@columbia.edu.**

Columbia University is an Affirmative Action/Equal Opportunity Employer.

POSITIONS OPEN

DEAN
School of Veterinary Medicine
Louisiana State University

Applications and nominations are being sought for the position of Dean of the School of Veterinary Medicine (SVM) at Louisiana State University **(website: http://www.vetmed.lsu.edu/).** The successful candidate will have a strong commitment to excellence in research, teaching, and service; implement and update the mission and strategic plan for the school; embrace cultural, ethnic, and gender diversity; and promote the University's Flagship Agenda **(website: http://www.lsu.edu/flagship).** Qualified candidates must possess a D.V.M. or equivalent. A D.V.M./Ph.D. is preferred. Candidates must have demonstrated leadership and administrative skills. A clear vision of the future role of schools of veterinary medicine in education and biomedical research is essential. Additional qualities that we seek include: a strong research record, including a record of extramural support; a commitment to aggressively engage in philanthropic fundraising on behalf of the School; and the ability to establish and maintain relationships with external stakeholders, including alumni, state, and national veterinary professional organizations, and governmental representatives. For more information, see our **website: http://www.lsu.edu/lsucareers.** Women and minorities are encouraged to apply. Review of applications will begin on July 31, 2006, and will continue until an appointment is made. Applications must include both a hard copy and electronic copy via e-mail of the following: (1) a letter of application summarizing the applicant's qualifications, (2) a complete curriculum vitae, and (3) names, addresses, e-mail, and telephone numbers of at least five references. An offer of employment is contingent on a satisfactory pre-employment background check. Applications should be sent to: **Ms. Sandra Donaldson, Dean Search, School of Veterinary Medicine, Louisiana State University, Ref: 000729, Baton Rouge, LA 70803. E-mail: sdonald@vetmed.lsu.edu.**

Louisiana State University is an Equal Opportunity/Equal Access Employer.

RESEARCH SCIENTIST

The Department of Microbiology/Immunology at the University at Buffalo is seeking a research scientist with expertise in microbiology and genomics. This Department of Defense funded position is available immediately and the position will be part of the newly opened Center for Excellence in Bioinformatics and Life Sciences.

Interested candidates must have a Master's degree in basic science or related field with a minimum of one year of supervisory experience in a microbiology or genomics laboratory. Excellent written and verbal communication skills are essential, as is experience in genomic technologies and extensive knowledge of computers. Experience with programming language, including Perl and java is preferred. The duties of this position will include the daily operation, maintenance, and troubleshooting of Applied Biosystems 3130x1 and 454 Life Sciences GS-20 DNA analyzers and Affymetrix GeneChip System. The responsibilities will also include construction of genomic sequencing libraries and synthesis of probes for microarray analysis, experimental design of the daily sequencing schedule, monitoring of quality control, data analysis and sequencing alignment, and supervision of technical laboratory staff in general laboratory maintenance and ordering. The successful candidate will also prepare progress/status reports and communicate with team leaders to discuss project priorities, potential problems, and clientele.

Interested individuals should submit an application letter together with curriculum vitae containing the names and contact information for three references to: **Anthony Campagnari, Ph.D., Department of Microbiology/Immunology, State University of New York (SUNY) at Buffalo, 3435 Main Street, 143 Biomedical Research Building, Buffalo, NY 14214-8024. E-mail: aac@buffalo.edu.** *The State University of New York at Buffalo is an Equal Opportunity/Affirmative Action Employer/Recruiter.*

2006 Career Awards in the Biomedical Sciences

The Burroughs Wellcome Fund has provided $500,000 awards over five years for the following postdoctoral fellows. Congratulations on this achievement!

2006 Career Award Recipients (24 awards)

Derek W. Abbott, M.D., Ph.D.
Harvard Medical School

Karl Mark Ansel, Ph.D.
Harvard Medical School/CBR Institute for Biomedical Research

Thomas G. Bernhardt, Ph.D.
Case Western Reserve University School of Medicine

Michael D. Blower, Ph.D.
University of California-Berkeley

Leah E. Cowen, Ph.D.
MIT/Whitehead Institute for Biomedical Research

Justin L. Gardner, Ph.D.
New York University Faculty of Arts and Science

Levi A. Garraway, M.D., Ph.D.
Harvard Medical School

Matthew C. Gibson, Ph.D.
Harvard Medical School

Ira M. Hall, Ph.D.
Cold Spring Harbor Laboratory

Mondira Kundu, M.D., Ph.D.
University of Pennsylvania School of Medicine

Cheng-Yu Lee, Ph.D.
University of Oregon

Anthony Leonardo, Ph.D.
Harvard University

Stephen B. Long, Ph.D.
Rockefeller University

Aaron W. McGee, Ph.D.
Yale University School of Medicine

Kakoli Mitra, Ph.D.
State University of New York-Albany

Lev Z. Osherovich, Ph.D.
University of California-San Francisco School of Medicine

Stephanie A. Pangas, Ph.D.
Baylor College of Medicine

Margot E. Quinlan, Ph.D.
University of California-San Francisco School of Medicine

Oliver J. Rando, M.D., Ph.D.
Harvard University

Antonina I. Roll-Mecak, Ph.D.
University of California-San Francisco

Pardis C. Sabeti, M.D., D.Phil.
Broad Institute of MIT and Harvard

Sara L. Sawyer, Ph.D.
University of Washington/Fred Hutchinson Cancer Research Center

Benjamin P. Tu, Ph.D.
University of Texas Southwestern Medical Center-Dallas

David M. Weinstock, M.D.
Memorial Sloan-Kettering Cancer Center

BURROUGHS WELLCOME FUND

t 919.991.5100
f 919.991.5160
www.bwfund.org
Post Office Box 13901
21 T. W. Alexander Drive
Research Triangle Park, NC 27709-3901

The Burroughs Wellcome Fund is an independent private foundation dedicated to advancing the biomedical sciences by supporting research and other scientific and education activities. Visit our website to learn about other career development awards—Career Awards for Medical Scientists, Career Awards at the Scientific Interface, Clinical Scientist Awards in Translational Research, and Investigators in Pathogenesis of Infectious Disease.

POSITIONS OPEN

ASSISTANT/ASSOCIATE PROFESSOR
Bioengineering

The Pennsylvania State University invites applications for a tenure-track position in the Department of Bioengineering at its University Park campus. Applicants are expected to have a Ph.D. in bioengineering, biomedical engineering, biophysics, or a related discipline. Postdoctoral research and/or teaching experience is highly desirable. The Department has a 30-year history of multidisciplinary graduate training and solid institutional support to promote faculty growth and development. Current research strengths include cardiovascular bioengineering, cell and molecular biomechanics, biophotonics, biomaterials, biomedical microelectromechanical systems (bioMEMS), biomedical imaging, and neural engineering. Productive interactions between engineering and life science faculty are fostered by well-supported research programs in Penn State's Materials Research Institute, Huck Institutes for Life Sciences, and the Institute for Biomedical Engineering at the Milton S. Hershey Medical Center. For more details, visit **website: http://bioeng.psu.edu.** Research areas of particular interest include experimental/computational analysis of intracellular signaling, cardiovascular tissue engineering, small animal MRI, and all areas that expand current strengths of the Department. Preference will be given to candidates with teaching interests in the areas of physiological systems analysis, biological transport phenomena, and/or biothermodynamics. Send curriculum vitae, statement of research and teaching objectives, and names of three references by September 1, 2006, to: **Dr. Herbert H. Lipowsky, Professor and Head, Department of Bioengineering, The Pennsylvania State University, 205 Hallowell Building, Box E-22535, University Park, PA 16802.** *Penn State is committed to Affirmative Action, Equal Opportunity and the diversity of its workforce.*

FACULTY POSITIONS
Program in Cell Stress and Cancer Nanomedicine
Simmons Comprehensive Cancer Center
University of Texas Southwestern Medical Center at Dallas

Tenure-track faculty positions at the level of **ASSISTANT PROFESSOR** are available to qualified Ph.D. candidates in the area of cancer nanomedicine. Areas of interest include drug/siRNA delivery, imaging probes, nanoparticle self-assembly and trafficking, combinatorial approaches for target screening and identification, biomarker identification and validation, and cancer molecular and cellular imaging. Successful candidates will join a dynamic group of investigators studying molecular stress responses in combination with novel nanomedicine platforms for targeted imaging and therapy. The candidates will also benefit from a growing bioengineering consortium among the University of Texas (UT) Southwestern Medical Center and UT Dallas, and where appropriate, the position will have a joint appointment with UT Dallas. Applicants must submit a cover letter outlining research interests, curriculum vitae, and a list of three references to: **Jinming Gao, Ph.D., Associate Professor of Oncology and Pharmacology, University of Texas Southwestern Medical Center at Dallas, 5323 Harry Hines Boulevard, Dallas, TX 75390.**

UT Southwestern is an Equal Opportunity/Affirmative Action Employer.

One long-term contract **GRADUATE FACULTY POSITION** beginning January 2007. Ph.D. and teaching experience required in gross anatomy and/or medical physiology. Expected to teach graduate students in both lecture and laboratories. Experience in small liberal arts college preferred. Responsibilities include academic advising, committee work, research, writing grants, and publishing. Strong record of teaching excellence and scholarship desirable. Send letter stating interest, complete resume, transcripts, and three letters of reference to: **Sr. John Karen Frei, Dean, School of Natural and Health Sciences, Barry University, 11300 N.E. Second Avenue, Miami Shores, FL 33161** by September 1, 2006.

ASSISTANT PROFESSOR POSITION
Solid-Earth Geophysics
Yale University, Department of Geology and Geophysics

The Department of Geology and Geophysics at Yale University invites applications for an Assistant Professor position in solid-Earth geophysics with an emphasis on mineral physics.

We seek a candidate who can develop a strong research program in the broad areas of the physics and chemistry of minerals that will complement the existing programs at the Department of Geology and Geophysics. One of our focus areas is the dynamics and evolution of Earth and planetary interiors; we are therefore particularly interested in individuals who investigate fundamental problems from the crust to the core.

A successful applicant should have strong potential for developing independent, externally funded research programs, advising students, and facilitating our effort to establish a strong interdisciplinary research program in Solid-Earth Geophysics and Geochemistry.

Applicants should submit a curriculum vitae, a statement of research and teaching interests, and a list of publications, plus the names, addresses, and e-mail addresses for four references to: **Professor Leo Hickey, Chairman, Department of Geology and Geophysics, Yale University, P. O. Box 208109, New Haven, CT 06520-8109. Telephone: 203-432-3161.** Applications that arrive before October 1, 2006, will receive full consideration.

For full information regarding Yale Geology and Geophysics, visit our **website: http://www.yale.edu/geology.** *Yale University is an Equal Opportunity/Affirmative Action Employer. Applications from female and minority-group scientists are strongly encouraged.*

ASSISTANT PROFESSOR. Department of Pharmaceutical Sciences, South Dakota State University (SDSU). A tenure-track academic year appointment with summer support and attractive startup package available. Teach courses in areas of expertise, and develop and maintain an active extramurally funded research program. Earned Ph.D. degree with research experiences in neuropharmacology, behavioral pharmacology, molecular pharmacology and pharmacogenomics, or a related area required. For full list of qualifications, consult **website: http://Jobs.sdstate.edu.** Screening of applicants begins July 5, 2006. Send a letter of interest, curriculum vitae, list of publications, description of teaching philosophy, future research plans, and names and contact information of three professional references to: **Dr. Hesham Fahmy, Chair, Search Committee, Department of Pharmaceutical Sciences, College of Pharmacy, South Dakota State University, Box 2202C, Brookings, SD 57007. Telephone: 605-688-4243, fax: 605-688-5993, e-mail: hesham.fahmy@sdstate.edu. University website: htpp://www.sdstate.edu.** *ADA accommodation available at* **TTY 605-688-4394**. *SDSU is an Affirmative Acion/Equal Employment Opportunity Employer and encourages applications from women and minorities.*

POSTDOCTORAL RESEARCHER
Cancer Immunotherapy and Vaccine Development

The research will focus on the development of recombinant cancer vaccines. Successful candidates will conduct preclinical testing of cancer vaccine and mechanistic investigations including antigen-specific immunity, antigen processing, and immune tolerance. Candidate must have a Ph.D, or M.D./Ph.D. and a strong background in cancer immunology/molecular biology. New Ph.D. graduates in cancer immunology are encouraged to apply.

The salary/compensation for this position are commensurate to the qualifications of candidates. Interested candidates should fax or e-mail curriculum vitae with a cover letter stating their career goals and research interest and names of three references to: **Helena R. Chang, M.D., Ph.D., Director, Revlon/University of California Los Angeles Breast Center and Gonda/UCLA Breast Cancer Research laboratory. Fax: 310-206-2982, e-mail: hchang@mednet.ucla.edu.**

TENURE-TRACK FACULTY POSITION
Faculty Excellence Initiative on AIDS/Drugs of Abuse
University of South Carolina

Applications are invited for a Faculty position at the **ASSISTANT, ASSOCIATE** or **FULL PROFESSOR** level in the Department of Pathology, Microbiology and Immunology, University of South Carolina School of Medicine, to pursue research on HIV/drugs of abuse. A Ph.D., M.D., or equivalent is required. It is expected that the individual will establish a strong, independent, NIH-funded research program. The Department seeks outstanding candidates who will develop translational research in collaboration with clinicians who are treating a large number of HIV/AIDS patients. Applicants for Associate/Full Professor should have extramural funding. The review will begin immediately and will continue until the position is filled. Applicants should submit curriculum vitae, future research plans and three letters of reference to: **Dr. Mitzi Nagarkatti (e-mail: pathmicrohivads@gw.med.sc.edu), Chair, Department of Pathology, Microbiology and Immunology, University of South Carolina, School of Medicine, Columbia, SC 29208.** *The University of South Carolina is an Affirmative Action, Equal Opportunity Institution.*

RESEARCH ASSOCIATE
(ASSISTANT PROFESSOR)

The University of Chicago, The Ben May Institute for Cancer Research is seeking a full-time Research Associate (Assistant Professor) to examine the structural interactions and biological functions of cellular signaling molecules involved in growth control using a range of molecular, cellular, genetic, and /or biophysical approaches. Applicants should have Ph.D. degree, and at least five years of research experience in signal transduction.

Qualified applicants should provide current curriculum vitae and bibliography, statement of research interest and goals, and full names, addresses, telephone/fax numbers, and e-mail addresses of at least three scholars who can provide academic references. Application material should be sent to: **Azisti Dembowski, Executive Administrator, The University of Chicago, The Ben May Institute for Cancer Research, 929 E. 57th Street, CIS, W-421B Chicago, IL 60637.**

The University of Chicago is an Affirmative Action/Equal Opportunity Employer.

POSTDOCTORAL POSITION
Tufts University School of Medicine
Boston, Massacusetts

Projects focus on the development of gene therapy vectors and their application in the rescue of photoreceptor degeneration in models of retinitis pigmentosa and macular degeneration. Send curriculum vitae to **e-mail: rajendra.kumar-singh@tufts.edu**

Find your future here.
ScienceCareers.org
We know science AAAS

MARKETPLACE

Widely Recognized Original & Guaranteed
KlenTaq1
8¢/u
Truncated Taq DNA Polymerase Withstand 99°C
US Pat #5,436,149
Call: Ab Peptides
Fax: 314•968•8988
e-mail: abpeps@msn.com
1•800•383•3362
www.abpeps.com

TaKaRa

CELL BIOLOGY

Accurately Measure Your Toxicity Level

LDH Cytotoxicity Detection Kit

The LDH Cytotoxicity Detection Kit is a simple, sensitive, non-radioactive assay which measures cell viability. It is based upon the measurement of lactate dehydrogenase (LDH) released by damaged cells into the cell culture supernatant. With this kit, LDH present in the culture supernatant participates in a coupled reaction converting yellow tetrazolium salt (INT) into red formazan product. The amount of enzyme activity, measured as absorbance using a microplate reader at 490/492 nm, correlates to the number of damaged cells in the culture.

- **Measures LDH Enzymatic Activity:** from damaged cells.
- **Accurate Correlation:** between the number of damaged cells and kit results.
- **Detects Low Cell Numbers:** (i.e. 0.2-2 x 10^4 cells/wells).

Premix WST-1 Cell Proliferation Assay System

The Premix WST-1 Cell Proliferation Assay System allows fast and easy colorimetric measurement of cell proliferation and viability of cells cultured in 96-well plates. This system provides a non-radioactive and spectrophotometric method of determining cell proliferation and viability without harvesting or washing steps, and can be performed in a single multi-well plate.

- **Convenient:** no washing steps or harvesting.
- **Accurate:** conversion of tetrazolium salt strongly correlates with metabolic activity.
- **Sensitive:** low cell numbers can be used.
- **Fast:** multiple plate reads over several time points.

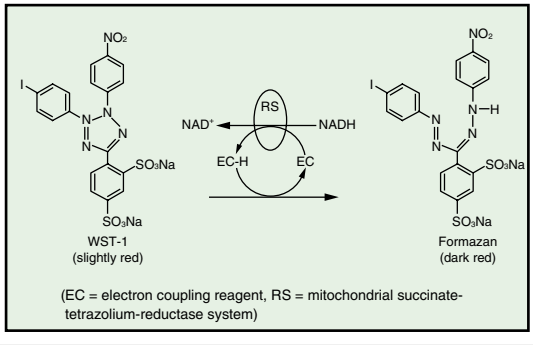

The Premix WST-1 Cell Proliferation Kit uses a colorimetric change from WST1 to Formazan to detect cell proliferation and viability.

EC = electron coupling reagent RS = mitochondrial succinate-tetrazolium-reductase system

TAKARA BIO INC.
The Biotechnology Company™

Otsu, Shiga, Japan
Phone: +81 77-543-7247
Fax: +81 77-543-9254

USA: Takara Mirus Bio Inc. Phone: 888-251-6618 • www.takaramirusbio.com
Europe: Takara Bio Europe S.A.S. Phone: +33 1 3904 6880 • www.takara-bio.eu
Korea: Takara Korea Biomedical Inc. Phone: +82 31 739 3300 • www.takara.co.kr

For more information and a list of Takara distributors worldwide, please visit our website today!

www.takara-bio.com